

Applied Mathematical Sciences

David Holcman
Zeev Schuss

Asymptotics of Elliptic and Parabolic PDEs

and their Applications in Statistical
Physics, Computational Neuroscience,
and Biophysics

Applied Mathematical Sciences

Volume 199

Editors

S. S. Antman, Institute for Physical Science and Technology, University of Maryland, College Park, MD, USA

ssa@math.umd.edu

Leslie Greengard, Courant Institute of Mathematical Sciences, New York University, New York, NY, USA

Greengard@cims.nyu.edu

P. J. Holmes, Department of Mechanical and Aerospace Engineering, Princeton University, Princeton, NJ, USA

pholmes@math.princeton.edu

Advisors

J. Bell, Lawrence Berkeley National Lab, Center for Computational Sciences and Engineering, Berkeley, CA, USA

P. Constantin, Department of Mathematics, Princeton University, Princeton, NJ, USA

R. Durrett, Department of Mathematics, Duke University, Durham, NC, USA

R. Kohn, Courant Institute of Mathematical Sciences, New York University, New York, NY, USA

R. Pego, Department of Mathematical Sciences, Carnegie Mellon University, Pittsburgh, PA, USA

L. Ryzhik, Department of Mathematics, Stanford University, Stanford, CA, USA

A. Singer, Department of Mathematics, Princeton University, Princeton, NJ, USA

A. Stevens, Department of Applied Mathematics, University of Münster, Münster, Germany

S. Wright, Computer Sciences Department, University of Wisconsin, Madison, WI, USA

Founding Editors

Fritz John, Joseph P. LaSalle and Lawrence Sirovich

More information about this series at <http://www.springer.com/series/34>

David Holcman · Zeev Schuss

Asymptotics of Elliptic and Parabolic PDEs

and their Applications in Statistical Physics,
Computational Neuroscience, and Biophysics



Springer

David Holcman
Group of Applied Mathematics
and Computational Biology
École Normale Supérieure
Paris
France

Zeev Schuss
Department of Mathematics,
Tel Aviv School of Mathematical Science
Tel Aviv University
Tel Aviv
Israel

and

Churchill College
Cambridge
UK

ISSN 0066-5452
Applied Mathematical Sciences
ISBN 978-3-319-76894-6
<https://doi.org/10.1007/978-3-319-76895-3>

ISSN 2196-968X (electronic)
ISBN 978-3-319-76895-3 (eBook)

Library of Congress Control Number: 2018934941

Mathematics Subject Classification (2010): 35Q84, 35Q82, 35Q92, 81Q20, 30E25, 35P20, 34E20

© Springer International Publishing AG, part of Springer Nature 2018

This work is subject to copyright. All rights are reserved by the Publisher, whether the whole or part of the material is concerned, specifically the rights of translation, reprinting, reuse of illustrations, recitation, broadcasting, reproduction on microfilms or in any other physical way, and transmission or information storage and retrieval, electronic adaptation, computer software, or by similar or dissimilar methodology now known or hereafter developed.

The use of general descriptive names, registered names, trademarks, service marks, etc. in this publication does not imply, even in the absence of a specific statement, that such names are exempt from the relevant protective laws and regulations and therefore free for general use.

The publisher, the authors and the editors are safe to assume that the advice and information in this book are believed to be true and accurate at the date of publication. Neither the publisher nor the authors or the editors give a warranty, express or implied, with respect to the material contained herein or for any errors or omissions that may have been made. The publisher remains neutral with regard to jurisdictional claims in published maps and institutional affiliations.

Printed on acid-free paper

This Springer imprint is published by the registered company Springer International Publishing AG
part of Springer Nature

The registered company address is: Gewerbestrasse 11, 6330 Cham, Switzerland

Preface

This book is a summary of modern asymptotic methods for the construction of solutions to boundary value problems for partial differential equations (PDEs) arising from modern applications in molecular and cellular biology and in biophysics. The solutions are used to explore the large parameter space of the mathematical models and, in particular, to identify critical parameters. These parameters play a key role, because the physical quantities they represent often diverge to infinity, rendering numerical simulations inefficient. Asymptotic formulas express new biophysical or cellular laws that account for the complex geometry of the phase space and its functional role. Combining numerical simulations and asymptotic methods has been recognized as a fruitful approach for theoreticians interested in computational biology. The book is written for a wide audience of applied mathematicians, engineers, physicists, chemists, or computational neuroscientists looking for analytical methods for solving the boundary value problems of statistical physics or theoretical biophysics where standard methods fail.

Solutions of linear second-order elliptic boundary value problems in bounded domains develop singularities in certain limits. Specifically, this occurs in the singular perturbation limit, when the ellipticity constant vanishes, and in the mixed Neumann–Dirichlet boundary value problem, when the Dirichlet part of the boundary shrinks to zero. In either case, the solution to the inhomogeneous boundary value problem blows up in the singular limit, while the solution of the homogeneous equation with inhomogeneous boundary conditions may develop discontinuities in the domain or on its boundary in this limit. While the former problem has been in mathematical physics for over 100 years, the latter case, called the narrow escape problem, has come to the forefront of applied mathematics with the advent of mathematical theory in molecular and cellular biology. The singular perturbation problem describes rare events, such as the escape of a Brownian particle from an attractor, whereas the mixed boundary value problem for elliptic and parabolic partial differential equations describes its escape from a domain with an impermeable boundary, except for a number of small absorbing windows. The singular perturbation problem is to construct an explicit asymptotic approximation to the solution of the homogeneous and inhomogeneous Dirichlet boundary value

problem in the limit of a vanishing ellipticity constant and to the mixed problem of the Poisson equation in a domain with the Neumann condition imposed on the entire boundary, except for the small windows, where the Dirichlet condition is imposed.

The analytical problems discussed in this book are versed in the context of Brownian motion and more general diffusion of particles. This context keeps the underlying physical picture in the background of the analytical, dynamical, and geometrical problems that are involved in the formulation and analysis of the boundary value problems of the elliptic and parabolic partial differential equations under consideration. Thus, for example, the normal derivative of the solution on the Dirichlet boundary of the domain, which represents the absorption flux density in the boundary of diffusing trajectories, is the reciprocal of the mean first passage time of Brownian trajectories emanating from any point in the domain, to the absorbing boundary (e.g., in a biological cell). When the size of the Dirichlet part of the boundary is much smaller than the Neumann part (the narrow escape limit), the narrow escape problem becomes a singular perturbation problem in the sense that, as the Dirichlet window shrinks to zero, the boundary value problem becomes ill-posed and the solution blows up. The construction of an asymptotic approximation to the solution is called for in this limit.

The narrow escape problem differs from typical singular perturbation problems in elliptic partial differential equations, e.g., from the singular perturbation of a vanishing diffusion coefficient, in that the singular perturbation in the narrow escape problem is in the geometry of the domain, not in the coefficients, a part of whose boundary can disappear in the singular limit, not as in the limit of a vanishing ellipticity constant that causes a change of the equation from second-order elliptic type to a first-order hyperbolic type. For example, a dumbbell domain becomes disconnected in the former limit. This calls for a different analytical approach to the construction of the asymptotic approximation than in the latter singular perturbation limit. However, once the asymptotic method is developed for the elliptic case, it is applied to the parabolic case in a straightforward manner.

It also should be stressed that this book is not about mathematical rigor, but rather about developing new analytic approximations to solutions of singular problems in elliptic boundary value problems that appear in modern applications. The analysis of convergence of the asymptotic approximations in this book lags many years behind the rather formal results presented here. This situation, much like that of J.B. Keller's geometrical diffraction theory at the time, presents a theoretical challenge to the PDE community. Examples in the past of filling such gaps were obtained by the work of Eckhaus, Vasilieva, Freidlin, and many others. But the importance of the explicit analytical approximations in the various areas of applications certainly motivates and justifies such an effort. Thus, all theorems and lemmas should be understood as statements of results obtained by formal calculations specified in the "proofs," without detracting from the sanctity of the term. All sections of the book should be understood in this spirit.

This book is divided into two parts. The first part concerns the asymptotics of singular perturbations of linear second-order elliptic boundary value problems. A chapter is dedicated to the short-time asymptotic of the Fokker–Planck equation. The second part presents traditional and new analytical methods for constructing analytical approximations to the solution of the mixed boundary value problem in the above-mentioned narrow escape limit. The asymptotics of singular perturbation problems include boundary layer expansions, matched asymptotics, the Wentzel–Kramers–Brillouin (WKB) method, and more. The methods break down in the asymptotics of the mixed boundary value problem of the new problems of mathematical physics in molecular and cellular biology. The breakdown occurs in domains with singular boundaries, in the presence of narrow passages in the domain, in the appearance of narrow necks (e.g., dumbbell-shaped domains), and so on. In the last part, we present a new asymptotic solution of Poisson–Nernst–Planck equations, which represent a nonlinear model of electro-diffusion. Finally, a Monge–Ampere type equation is derived and serves to reconstruct two-dimensional surfaces from the projection of stochastic trajectories from the surface to a plane.

Paris, France/Cambridge, UK
Tel Aviv, Israel

David Holcman
Zeev Schuss

Contents

Part I Singular Perturbations of Elliptic Boundary Problems

1 Second-Order Elliptic Boundary Value Problems with a Small Leading Part	3
1.1 Introduction	3
1.2 Application to Stochastic Differential Equations	4
1.3 The Survival Probability and the Eigenvalue Problem	8
1.4 Discussion	9
2 A Primer of Asymptotics for ODEs	11
2.1 The Laplace Expansion of Integrals	12
2.2 The Asymptotics of a First-Order Initial Value Problem	14
2.2.1 Matched Asymptotic Expansions	14
2.2.2 An Application to Stochastic Differential Equations: The Exit Problem in \mathbb{R}^1	17
2.3 Asymptotics of a Second-Order Boundary Value Problem	20
2.4 Asymptotics of a Homogeneous Second-Order Boundary Value Problem	22
2.5 Asymptotics of the Inhomogeneous Boundary Value Problem	24
2.6 Examples and Applications to Stochastic Equations	28
2.6.1 Small Diffusion with the Flow: The Homogeneous Boundary Value Problem	28
2.6.2 Small Diffusion Against the Flow	32
2.6.3 Small Diffusion Against the Flow: The Inhomogeneous Boundary Value Problem	37
2.6.4 The Boundary Value Problem with a Sharp Potential Barrier	38

2.6.5	The Problem for a Smooth Potential Barrier at the Boundary	41
2.6.6	The Second Eigenvalue of the Fokker–Planck Operator	44
2.7	A Diffusion Model of Random Signals	44
2.8	Loss of Lock in a First-Order Phase-Locked Loop in Phase-Modulated Radio Signals	47
2.9	Annotations	48
3	Singular Perturbations in Higher Dimensions	49
3.1	Introduction	49
3.2	The WKB Method	51
3.2.1	The Eikonal Equation	53
3.2.2	The Transport Equation	55
3.2.3	The Characteristic Equations	56
3.2.4	Boundary Layers at Non-characteristic Boundaries	57
3.2.5	Boundary Layers at Characteristic Boundaries in the Plane	60
3.3	The Boundary Value Problem With Non-characteristic Boundaries	63
3.4	The Boundary Value Problem in Planar Domains With Characteristic Boundaries	68
3.5	Loss of Lock in a Second-Order Phase-Locked Loop	70
3.5.1	The Phase Plane of the Reduced Problem	73
3.5.2	The Mean Time to Lose Lock	76
3.5.3	The Boundary Layer Structure of $u_\epsilon(x)$	78
3.5.4	Asymptotic Solution of the Stationary Fokker–Planck Equation	82
3.5.5	The Eikonal Equation for (3.136)	82
3.5.6	The Eikonal on the Separatrix	86
3.5.7	The Transport Equation	89
3.5.8	Derivation of (3.114)	92
3.5.9	Green’s Function for the Boundary Value Problem is the Exit Density	93
3.6	Annotations	94
3.7	An Attractor Inside an Unstable Limit Cycle	97
3.7.1	The Reduced Equation: an Underdamped Forced Pendulum	98
3.7.2	Asymptotics of the Fokker–Planck Equation Near the Limit Cycle	102
3.7.3	The Boundary Value Problem for the Fokker–Planck Equation in Ω_S	108
3.8	Annotations	112

4 Eigenvalues of a Non-self-adjoint Elliptic Operator	115
4.1 Introduction	115
4.2 Eigenvalues and the Survival Probability	117
4.3 The Principal Eigenvalue and the Structure of the Field $a(x)$	118
4.4 The Precise WKB Structure of the Principal Eigenfunction	120
4.4.1 The Eikonal Equation	120
4.4.2 The Transport Equation	121
4.4.3 The Boundary Layer Equation	122
4.4.4 The First Eigenfunction of the Adjoint Problem	125
4.5 Higher-Order Eigenvalues	125
4.6 Oscillatory Escape Time	128
4.7 Spontaneous Activity in the Cerebral Cortex	128
4.8 Numerical Study of Oscillatory Decay	130
4.9 A Model of Up-State Dynamics in a Neuronal Network	130
4.10 The Phase Space of the Model	132
4.11 Brownian Simulations of Oscillation Phenomena in (4.80)	134
4.12 The Exit Density from a Focus Near a Limit Cycle	135
4.12.1 The Mean First Passage Time $\bar{\tau}_\varepsilon(\mathbf{x})$	136
4.12.2 Numerical Study of the Eikonal Equation	140
4.13 Normal Flux on $\partial\Omega$: the Exit Time Density	142
4.14 Computation of the Second Eigenvalue	143
4.15 Brownian Dynamics Simulations	145
4.15.1 A Two-Term Approximation of the Exit-Time Density	145
4.15.2 Exit Time Densities in Three Ranges of Noise Amplitude	146
4.16 Appendices	147
4.16.1 The Density of Exit Points	147
4.16.2 Expansion of the Field Near the Boundary and No Cycling	151
4.16.3 The Jacobian of $b(\zeta)$ at ζ_0	154
4.16.4 The Real Part ω_1	154
4.17 Annotations	156
5 Short-Time Asymptotics of the Heat Kernel	159
5.1 The One-Dimensional Case	162
5.2 The Ray Method for Short Time Asymptotics of Green's Function	166
5.3 The Trace	170
5.3.1 Simply Connected Domains	170
5.3.2 Multiply Connected Domains	176

5.4	Recovering δ_1 from $P(t)$	177
5.5	Discussion	179
5.5.1	Construction of the Short-Time Asymptotic of the Fokker–Planck Equation with a Periodic Potential	182
5.5.2	Annotations	186
Part II Mixed Boundary Conditions for Elliptic and Parabolic Equations		
6	The Mixed Boundary Value Problem	191
6.1	Introduction	191
6.2	Formulation of the Mixed Boundary Value Problem	192
6.2.1	The Narrow Escape Time Problem	193
6.2.2	A Pathological Example	194
6.2.3	The Matched Asymptotics Approach	194
6.2.4	Higher-Order Asymptotics in the Unit Ball	196
6.2.5	The Narrow Escape Time Through Multiple Absorbing Windows	196
6.3	Annotations	199
7	The Mixed Boundary Value Problem in \mathbb{R}^2	201
7.1	A Neumann–Dirichlet Boundary Value Problem	201
7.2	The Neumann Function	203
7.3	The Mixed Boundary Value Problem on a Riemannian Manifold in \mathbb{R}^2	205
7.3.1	Exit through Several Windows	216
7.3.2	The Helmholtz Equation for Two Windows	217
7.3.3	Asymptotic Solution of the Helmholtz Equation	218
7.4	The Mixed Boundary Value Problem for Poisson’s Equation in Dire Straits	222
7.4.1	The Case of a Bottleneck	222
7.4.2	The Case of Several Bottlenecks	228
7.4.3	The Mixed Boundary Value Problem on a Surface of Revolution	230
7.5	A Composite Domain with a Bottleneck	233
7.6	The Narrow Escape Time from Domains in \mathbb{R}^2 and \mathbb{R}^3 with Bottlenecks	236
7.7	The Principal Eigenvalue and Bottlenecks	237
7.7.1	Connecting Head and Neck	238
7.7.2	The Principal Eigenvalue in Dumbbell-Shaped Domains	239

7.8	Diffusion of a Needle in Dire Straits	240
7.8.1	The Diffusion Law of a Needle in a Planar Strip	241
7.8.2	The Turnaround Time $\bar{\tau}_{L \rightarrow R}$	244
7.9	Applications of the Narrow Escape Time	250
7.10	Annotation to the Narrow Escape Time Problem	253
8	Narrow Escape in \mathbb{R}^3	257
8.1	The Neumann Function in Regular Domains in \mathbb{R}^3	257
8.1.1	Elliptic Absorbing Window	261
8.1.2	Second-Order Asymptotics for a Circular Window	265
8.2	The First Eigenvalue for Two Small Dirichlet Windows	267
8.2.1	Multiple Absorbing Windows	269
8.2.2	Higher-Order Expansion of the NET Through Many Small Windows on a Sphere	273
8.2.3	Application to Leakage in a Conductor of Brownian Particles	274
8.3	Activation Through a Narrow Opening	279
8.3.1	The Neumann Function	282
8.3.2	Solution of the Mixed Boundary Value Problem	284
8.3.3	Deep Well – A Markov Chain Model	287
8.4	The Mixed Boundary Value Problem in a Solid Funnel-Shaped Domain	290
8.5	The Mixed Boundary Value Problem with a Dirichlet Ribbon	295
8.6	Selected Applications in Molecular Biophysics	301
8.6.1	Leakage from a Cylinder	301
8.6.2	Applications of the Mixed Boundary Value Problem	305
8.7	Annotations	308
9	Short-Time Asymptotics of the Heat Kernel and Extreme Statistics of the NET	311
9.1	Introduction	311
9.1.1	The pdf of the First Escape Time	311
9.1.2	The pdf of the First Arrival Time in an Interval	313
9.1.3	Asymptotics of the Expected Shortest Time $\bar{\tau}^1$	314
9.1.4	Escape from a Ray	315
9.2	Escape from an Interval $[0, a]$	317
9.3	The FAT in a Bounded Domain in $\mathbb{R}^{2,3}$	320
9.3.1	Asymptotics in \mathbb{R}^3	321
9.3.2	Asymptotics in \mathbb{R}^2	330

9.4	Statistics of the Arrival Time of the Second Particle	335
9.4.1	Poissonian-Like Approximation	336
9.4.2	$\Pr\{\tau^{(2)}\}$ of N Brownian i.i.d. Trajectories in a Segment	337
9.4.3	Applications of the FAT in Biophysics	340
9.4.4	Annotations	340
10	The Poisson–Nernst–Planck Equations in a Ball	341
10.1	Introduction	341
10.2	Synopsis of Results	342
10.3	Poisson–Nernst–Planck Equations in a Ball	342
10.3.1	The Steady-State Solution	344
10.3.2	Existence of Solutions	345
10.3.3	The Distribution of Voltage and Charge in a Dielectric Ball	350
10.3.4	Scaling Laws for the Maximal Number of Charges	351
10.4	Ionic Flux in a Small Window at High Charge	352
10.5	Flow Through a Narrow Window at High Charge	353
10.6	Current in a Voltage-Clamped Dendritic Spine	354
10.6.1	Appendix 1: Reverse Liouville–Gelfand–Bratú Equation	356
10.6.2	Small λ Expansion of $u_\lambda(x)$	358
10.6.3	Numerical Scheme for the Solution of (10.13)	359
10.7	Steady Solution in a Ball with a Cusp-Shaped Funnel	361
10.7.1	Reduced Equations in an Uncharged Cusp-Shaped Funnel	363
10.7.2	Asymptotics of Voltage Between Funnel and Center	369
10.7.3	Poisson–Nernst–Planck Solutions in a 3D Cusp-Shaped Funnel	371
10.7.4	Asymptotic Analysis of the PNP Equations in a Cusp-Shaped Funnel	375
10.7.5	The Potential Drop in Ω_w	380
10.8	Annotations	382
11	Reconstruction of Surface Diffusion from Projected Data	385
11.1	Projection of Diffusion from a Curve to a Line	385
11.1.1	Driftless Diffusion on a Curve	385
11.1.2	The Case of Diffusion with Drift	388
11.1.3	Reconstruction of a Parabola from Projected Diffusion Data	389
11.1.4	Appendix 2	392
11.1.5	Reconstruction of Projected Stochastic Dynamics	393

11.2	Reconstruction of a Surface from Planar Projections of Diffusion Trajectories	396
11.2.1	The Drift Field	396
11.2.2	The Reconstruction Procedure	400
11.3	Annotations	401
12	Asymptotic Formulas in Molecular and Cellular Biology	403
12.1	Introduction	403
12.2	From Molecular to Cellular Description	406
12.3	Flux Through Narrow Passages Identifies Cellular Compartments	406
12.4	Examples of Asymptotic Formulas: Fluxes into Small Targets	407
12.4.1	Formulas in Two Dimensions	407
12.4.2	Narrow Escape Formulas in Three-Dimensions	412
12.4.3	Cusp-Shaped Funnel: Hidden Targets Control Rates in \mathbb{R}^3	414
12.4.4	DNA Repair in a Confined Chromatin Structure in \mathbb{R}^2	415
12.4.5	Asymmetric Dumbbell-Shaped Cell Division	416
12.5	Annotations	418
Bibliography		421
Index		439

Acronyms

AMPA	(AMPAR) α -amino-3-hydroxy-5-methyl-4-isoxazolepropionic acid (receptor)
DNA	Deoxyribonucleic acid
FM	Frequency modulation
FPT	First passage time
MBM	Mathematical Brownian motion
MFPT	Mean first passage time
MSD	Mean square displacement
MTLL	Mean time to lose lock
NET	Narrow escape time
NMDA	N-Methyl-D-aspartate (receptor)
ODE	Ordinary differential equation
Pdf	Probability density function
PDF	Probability distribution function
PLL	Phase-locked loop
PM	Phase modulation
PNP	Poisson–Nernst–Planck
PSD	Post-synaptic density
RNA	Ribonucleic acid
SDE	Stochastic differential equation
SNR	Signal-to-noise ratio
SS	Stochastic separatrix
WKB	Wentzel–Kramers–Brillouin

Symbols

We use interchangeably $\langle \cdot \rangle$ and $\mathbb{E}(\cdot)$ to denote the expectation (average) of a random variable, but $\mathbb{E}(\cdot | \cdot)$ and $\Pr\{\cdot | \cdot\}$ to denote the conditional expectation and conditional probability, respectively.

$A, B \dots$	Matrices—bold upper case letters
A^T	The transpose of A
A^{-1}	The inverse of A
$\delta(x)$	Dirac's delta function (functional)
$\det(A)$	The determinant of the matrix A
$\mathbb{E}(x), \langle x \rangle$	The expected value (expectation) of x
Δ, Δ_x	Greek <i>Delta</i> , the Laplace operator (with respect to x): $\Delta_x = \frac{\partial^2}{\partial x_1^2} + \frac{\partial^2}{\partial x_2^2} + \cdots + \frac{\partial^2}{\partial x_d^2}$
$e(t)$	The estimation error process: $\hat{x}(t) - x(t)$
$n \sim \mathcal{N}(\mu, \sigma^2)$	The random variable n is normally distributed with mean μ and variance σ^2
$N \sim \mathcal{N}(\mu, \Sigma)$	The random vector N is normally distributed with mean μ and covariance matrix Σ
∇, ∇_x	Greek <i>nabla</i> , the gradient operator (with respect to x): $\nabla_x = \left(\frac{\partial}{\partial x_1}, \frac{\partial}{\partial x_2}, \dots, \frac{\partial}{\partial x_d} \right)^T$
$\nabla \cdot J$	The divergence operator $\nabla \cdot J = \frac{\partial J_1(x)}{\partial x_1} + \frac{\partial J_2(x)}{\partial x_2} + \cdots + \frac{\partial J_d(x)}{\partial x_d}$
$\Pr\{event\}$	The probability of <i>event</i>
$p_{\mathbf{X}}^{(x)}$	The probability density function of the vector X
\mathbb{R}, \mathbb{R}^d	The real line, the d -dimensional Euclidean space
V_x	The partial derivative of V with respect to x : $V_x = \partial V / \partial x$
$\bar{\tau}(x)$	Mean first passage time from x to an absorbing target
$\text{Var}(x)$	The variance of x
$w(t), v(t)$	Vectors of independent Brownian motions
$x, f(x)$	Scalars—lower case letters
$\mathbf{x}, f(\mathbf{x})$	Vectors—bold lower case letters

x_i	The i th element of the vector \mathbf{x}
$\mathbf{x} \cdot \mathbf{y}$	Dot (scalar) product of the vectors \mathbf{x} and \mathbf{y} : $\mathbf{x} \cdot \mathbf{y} = x_1y_1 + x_2y_2 + \cdots + x_dy_d$
$ \mathbf{x} ^2 = \mathbf{x} \cdot \mathbf{x}$	L_2 norm of \mathbf{x}
$\dot{\mathbf{x}}(t)$	Time derivative: $\dot{\mathbf{x}}(t) = d\mathbf{x}(t)/dt$

List of Figures

Fig. 2.1	Asymptotic approximations	17
Fig. 2.2	A bistable potential	18
Fig. 2.3	The solution inside and outside the domain of attraction	19
Fig. 2.4	A potential $U(x)$ with two wells	33
Fig. 2.5	Discontinuous drift	34
Fig. 2.6	A potential with stable equilibrium states	48
Fig. 3.1	A typical trajectory of the phase estimation error $e(t)$	72
Fig. 3.2	Exit trajectories in the phase plane	73
Fig. 3.3	The lock domain and characteristics that hit the separatrix	85
Fig. 3.4	The values of the eikonal along the characteristics	85
Fig. 3.5	Blow-up of the graph of the eikonal near the saddle point	86
Fig. 3.6	The eikonal as function of arc length on the separatrix	86
Fig. 3.7	The eikonal and its partial derivatives near the saddle point	87
Fig. 3.8	Partial derivatives of the eikonal on the critical characteristic	87
Fig. 3.9	The exit density on the separatrix at different noise intensities	95
Fig. 3.10	The point of maximal exit density vs noise intensity	95
Fig. 3.11	The washboard potential $U(x) = \cos x - Ix$ for $I = 0.3$	98
Fig. 3.12	The stable running solution	99
Fig. 3.13	The stable running solution disappears to infinity	100
Fig. 3.14	The effective global potential $\Phi(A)$	110
Fig. 4.1	A stable focus within a limit cycle	116
Fig. 4.2	Oscillatory decay of the probability density function	128
Fig. 4.3	Phase-plane dynamics of the Holcman–Tsodyks model	129
Fig. 4.4	Escape from the Up-state and distribution of time	132
Fig. 4.5	Möbius image of the Hopf vector field	133
Fig. 4.6	Exit from an attractor near the characteristic boundary	134
Fig. 4.7	Distribution of exit points	136
Fig. 4.8	The solution of the eikonal equation	140
Fig. 4.9	The eikonal on the boundary	142

Fig. 4.10	Histogram of exit times	146
Fig. 4.11	Peak oscillations	147
Fig. 4.12	Mean first passage time for different focus positions	153
Fig. 5.1	The locus of critical points	169
Fig. 5.2	The second and third eikonals	170
Fig. 5.3	The arclength on the boundary	171
Fig. 5.4	The domain Ω	172
Fig. 5.5	The rays emanating from the boundary	173
Fig. 5.6	Eikonals with two reflections in a circle	175
Fig. 5.7	Eikonals with two reflections in a circle	175
Fig. 5.8	Histogram of increments	185
Fig. 6.1	Escaping Brownian trajectory	191
Fig. 6.2	Receptor movement on the neuronal membrane	193
Fig. 6.3	Composite domains	194
Fig. 6.4	Dumbbell-shaped domain	194
Fig. 7.1	Escape through a funnel	202
Fig. 7.2	Funnel formed by a partial block	202
Fig. 7.3	Small opening near a corner	209
Fig. 7.4	Narrow escape from an annulus	209
Fig. 7.5	Escape near a cusp	210
Fig. 7.6	Escape to the north pole	212
Fig. 7.7	Two holes	220
Fig. 7.8	Mean first passage time vs distance	221
Fig. 7.9	A surface of revolution with a funnel	223
Fig. 7.10	Conformal image of a funnel	225
Fig. 7.11	Drift of a projected Brownian motion	232
Fig. 7.12	Narrow straits formed by a cone-shaped funnel	233
Fig. 7.13	Rod in a strip	242
Fig. 7.14	Conformal image of a rod in a strip	247
Fig. 7.15	Boundary layers	249
Fig. 7.16	Narrow escape time from a domain	252
Fig. 7.17	Organization of the neuronal membrane	254
Fig. 8.1	Cluster of 6 Dirichlet windows	272
Fig. 8.2	Brownian search for a narrow ribbon	296
Fig. 8.3	Conformal mapping	297
Fig. 8.4	Neuronal synapse	302
Fig. 8.5	An idealized model of the synaptic cleft	303
Fig. 8.6	Leak trajectory	303
Fig. 8.7	Probability to exit through a single pump on the neck membrane	304
Fig. 8.8	Exit probability in a synaptic cleft	307
Fig. 8.9	Exit probability in a synaptic cleft	305
Fig. 9.1	Histograms of the arrival times of the fastest particle	314
Fig. 9.2	$\Pr\{\tau^{(1)} = t\}$	319

Fig. 9.3	Extreme statistics of the narrow escape time in dim 3	330
Fig. 9.4	Escape through a narrow opening in a planar disk	335
Fig. 9.5	Histogram of the arrival time of the second fastest particle, obtained from Brownian simulations with Euler's scheme	339
Fig. 10.1	Geometrical representations of dendritic spines.	343
Fig. 10.2	Distribution of a single unscreened ionic specie in a dielectric ball.	345
Fig. 10.3	Asymptotic behavior of the electric potential in a ball	348
Fig. 10.4	Initial value problem for the radial Poisson–Nernst–Planck equation	349
Fig. 10.5	Phase-plane solution of the radial Poisson-Nernst-Planck equation	350
Fig. 10.6	Asymptotics of the potential drop for $d = 1, 2, 3$	350
Fig. 10.7	Potential, charge density, and field in a dielectric ball	352
Fig. 10.8	Conformal image of a funnel	363
Fig. 10.9	Influence of a cusp on the field lines	364
Fig. 10.10	One-dimensional Poisson-Nernst-Planck	369
Fig. 10.11	Numerical solutions of the reduced PNP equations.	372
Fig. 10.12	Three-dimensional ball with a cusp-shaped funnel	373
Fig. 10.13	Decomposition of the domain Ω_w	375
Fig. 10.14	PNP solution in a 3D domain	377
Fig. 11.1	Reconstruction of a surface from projected trajectories	386
Fig. 11.2	Projection on a line of a diffusion process on a curve	386
Fig. 11.3	Estimates of the effective diffusion coefficient and geometric drift	390
Fig. 11.4	Reconstruction of diffusion process on a parabola (constant drift)	391
Fig. 11.5	Reconstruction of an OU process on a parabola	392
Fig. 11.6	Implementation of the reconstruction algorithm	394
Fig. 11.7	Projection of spherical Brownian motion	402
Fig. 12.1	Spines on a dendrite	405
Fig. 12.2	Electron-microscopy of an excitatory synapse.	406
Fig. 12.3	Classification narrow-escape-time formulas.	408
Fig. 12.4	Schematic cusp targets in cell biology	414
Fig. 12.5	Complex molecule	415
Fig. 12.6	Two-dimensional stratification	416
Fig. 12.7	Rod in strip	417
Fig. 12.8	Time-lapse images of mitotic cells	418

Part I

**Singular Perturbations of Elliptic
Boundary Problems**

Chapter 1

Second-Order Elliptic Boundary Value Problems with a Small Leading Part

1.1 Introduction

A typical second-order linear elliptic mixed (Robin) boundary value problem (boundary value problem), which arises in many modern applications, is to solve

$$\varepsilon \Delta u_\varepsilon(\mathbf{x}) + \mathbf{b}(\mathbf{x}) \cdot \nabla u_\varepsilon(\mathbf{x}) = f(\mathbf{x}) \text{ for } \mathbf{x} \in \Omega \quad (1.1)$$

$$\beta(\mathbf{x})u_\varepsilon(\mathbf{x}) + \alpha(\mathbf{x})\frac{\partial u_\varepsilon(\mathbf{x})}{\partial n(\mathbf{x})} = g(\mathbf{x}) \text{ for } \mathbf{x} \in \partial\Omega, \quad (1.2)$$

where Ω is a domain in the Euclidean space \mathbb{R}^d , whose boundary $\partial\Omega$ is sufficiently smooth. Here $\varepsilon > 0$ is a small parameter, in a sense that is made clear below, $\mathbf{n}(\mathbf{x})$ is the unit outer normal at $\mathbf{x} \in \partial\Omega$, the “drift” $\mathbf{b}(\mathbf{x})$ is a vector field in Ω , the coefficients $\alpha(\mathbf{x})$ and $\beta(\mathbf{x})$ are scalar functions defined on $\partial\Omega$, the function $f(\mathbf{x})$ is defined in Ω , and $g(\mathbf{x})$ is defined on $\partial\Omega$. All functions and domains are assumed sufficiently regular to ensure that the boundary value problem (1.1), (1.2) is well posed. The boundary condition reduces to the Dirichlet problem if $\alpha(\mathbf{x}) = 0$ for $\mathbf{x} \in \partial\Omega$ and to the Neumann problem if $\beta(\mathbf{x}) = 0$ for $\mathbf{x} \in \partial\Omega$. When $\alpha(\mathbf{x}) = 0$ on a part $\partial\Omega_\alpha$ of the boundary and $\beta(\mathbf{x}) = 0$ for $\mathbf{x} \in \partial\Omega_\beta$, where $\partial\Omega_\beta = \partial\Omega - \partial\Omega_\alpha$, the boundary value problem is a mixed Dirichlet–Neumann problem.

The boundary value problem (1.1), (1.2) becomes a singular perturbation problem for $\varepsilon \rightarrow 0$, because the reduced problem

$$\mathbf{b}(\mathbf{x}) \cdot \nabla u_0(\mathbf{x}) = f(\mathbf{x}) \text{ for } \mathbf{x} \in \Omega \quad (1.3)$$

$$\beta(\mathbf{x})u_0(\mathbf{x}) + \alpha(\mathbf{x})\frac{\partial u_0(\mathbf{x})}{\partial n(\mathbf{x})} = g(\mathbf{x}) \text{ for } \mathbf{x} \in \partial\Omega, \quad (1.4)$$

is over-determined in the sense that conditions cannot be imposed on $\partial\Omega$, but only on its part. Thus the solution can develop singularities inside the domain and on parts

of its boundary in the limit. Therefore the problem at hand is to construct a uniform asymptotic approximation to $u_\varepsilon(\mathbf{x})$ in Ω in this limit.

Another type of singular perturbation arises in the mixed boundary value problem if the Dirichlet part $\partial\Omega_\alpha$ of the boundary is much smaller than the Neumann part $\partial\Omega_\beta$ in the mixed boundary value problem. More specifically, setting

$$\delta = \frac{|\partial\Omega_\beta|}{|\partial\Omega_\alpha|}$$

and denoting the solution by $u_\delta(\mathbf{x})$, in the limit $\delta \rightarrow 0$ the reduced problem,

$$\varepsilon \Delta u(\mathbf{x}) + \mathbf{b}(\mathbf{x}) \cdot \nabla u(\mathbf{x}) = f(\mathbf{x}) \text{ for } \mathbf{x} \in \Omega \quad (1.5)$$

$$\alpha(\mathbf{x}) \frac{\partial u(\mathbf{x})}{\partial n(\mathbf{x})} = g(\mathbf{x}) \text{ for } \mathbf{x} \in \partial\Omega, \quad (1.6)$$

becomes ill-posed, because the compatibility condition, obtained by integrating (1.5) over Ω , (1.6) over $\partial\Omega$, and applying Green's theorem, requires that

$$\oint_{\partial\Omega} \frac{\partial u(\mathbf{x})}{\partial n(\mathbf{x})} dS = \oint_{\partial\Omega} \frac{g(\mathbf{x})}{\alpha(\mathbf{x})} dS = \int_{\Omega} \frac{f(\mathbf{x}) - \mathbf{b}(\mathbf{x}) \cdot \nabla u(\mathbf{x})}{\varepsilon} d\mathbf{x}, \quad (1.7)$$

which is not necessarily satisfied for every $f(\mathbf{x})$ and $g(\mathbf{x})$. Thus the solution $u_\delta(\mathbf{x})$ blows up in this limit. The singular perturbation problem is to construct an asymptotic expansion of $u_\delta(\mathbf{x})$ for small δ .

1.2 Application to Stochastic Differential Equations

As mentioned in the Preface, the analytical problems discussed in this book are versed in the language of Brownian motion and more general diffusion of particles. This context keeps the underlying physical picture in the background of the analytical, dynamical, and geometrical problems that are involved in the formulation and analysis of the boundary value problems of the elliptic partial differential equations (parabolic partial differential equations) under consideration. Thus, for example, the normal derivative of the solution on the Dirichlet boundary of the domain, which represents the absorption flux density of diffusing trajectories in the boundary, is the reciprocal of the mean first passage time of Brownian trajectories emanating from any point in the domain, to the absorbing boundary (e.g., in a biological cell). More specifically, the elliptic boundary value problems discussed in this book originate in the system of Itô stochastic differential equations of the form [Schuss (2010b)]

$$\dot{\mathbf{x}} = \mathbf{a}(\mathbf{x}) + \sqrt{2\varepsilon} \mathbf{B}(\mathbf{x}) \dot{\mathbf{w}}(t), \quad \mathbf{x}(0) = \mathbf{x}_0, \quad (1.8)$$

where $\mathbf{a}(\mathbf{x})$ is a vector field, $\mathbf{B}(\mathbf{x})$ is a matrix field, both are Lipschitzian in a smooth domain Ω in \mathbb{R}^d , $\dot{\mathbf{w}}(t)$ is a vector of independent δ -correlated Gaussian white noises, and ε is a small parameter. The stochastic differential equation (1.8) is defined by the recursion

$$\mathbf{x}(t + \Delta t) = \mathbf{x}(t) + \mathbf{a}(\mathbf{x}(t)) \Delta t + \sqrt{2\varepsilon} \mathbf{B}(\mathbf{x}(t)) \Delta \mathbf{w}(t), \quad (1.9)$$

where the noise vector $\Delta \mathbf{w}(t) \sim \mathcal{N}((0), \Delta t \mathbf{I})$ (normal vector with covariance $\Sigma = \Delta t \mathbf{I}$). It can be shown [Schuss (2010b)] that the trajectories of the recursion (1.8) converge to a continuous limit with probability 1 as $\Delta t \rightarrow 0$.

The trajectories of (1.8) can be defined in the entire space, or be terminated when they hit the boundary $\partial\Omega$ (an absorbing boundary), or be reflected there according to certain reflection rules, or be terminated (absorbed) on a part $\partial\Omega_a$ and reflected on a part $\partial\Omega_r$ of $\partial\Omega$ (mixed boundary conditions), or behave at $\partial\Omega$ according to a prescribed rule.

The second-order elliptic boundary value problem

$$\sum_{i,j=1}^2 \varepsilon \sigma^{i,j}(\mathbf{x}) \frac{\partial^2 u_\varepsilon(\mathbf{x})}{\partial x^i \partial x^j} + \sum_{i=1}^2 a^i(\mathbf{x}) \frac{\partial u_\varepsilon(\mathbf{x})}{\partial x^i} = f(\mathbf{x}) \text{ for } \mathbf{x} \in \Omega \quad (1.10)$$

$$u_\varepsilon(\mathbf{x}) = g(\mathbf{x}) \text{ for } \mathbf{x} \in \partial\Omega, \quad (1.11)$$

is related to (1.8) and to the boundary behavior of the trajectories in many ways [Schuss (2010b)]. Thus, Green's function of the homogeneous problem ($f(\mathbf{x}) = 0$) represents the probability density function on $\partial\Omega$ of the points where the random trajectories of (1.8) are absorbed in $\partial\Omega$. The vector $\mathbf{a}(\mathbf{x})$ represents the drift field of the noiseless dynamics ($\varepsilon = 0$) the noise matrix $\mathbf{B}(\mathbf{x})$ defines the diffusion tensor as $\boldsymbol{\sigma}(\mathbf{x}) = \frac{1}{2} \mathbf{B}(\mathbf{x}) \mathbf{B}^T(\mathbf{x})$. The solution of the inhomogeneous problem with $f(\mathbf{x}) = -1$ and the homogeneous boundary condition $g(\mathbf{x}) = 0$ for $\mathbf{x} \in \partial\Omega$, is the mean first passage time of a random trajectory from $\mathbf{x} \in \Omega$ to $\partial\Omega$.

The recursion (1.9) is, indeed, a numerical simulation scheme for the stochastic differential equations (1.8). Histograms of various functionals of the simulated trajectories are related to the solution of the boundary value problem (1.10), (1.11) and therefore can be considered numerical solutions of the boundary value problem, as described below.

The *first passage time* (exit time) τ_ε of a trajectory $\mathbf{x}_\varepsilon(t)$ of (1.8) to $\partial\Omega$ is defined as

$$\tau_\varepsilon = \inf\{t > 0 : \mathbf{x}_\varepsilon(t) \in \partial\Omega\}. \quad (1.12)$$

Its conditional probability density function, given $\mathbf{x}_\varepsilon(0) = \mathbf{x}$, can be expressed in terms of the *transition probability density function* $p_\varepsilon(\mathbf{y}, t | \mathbf{x})$ of the trajectories $\mathbf{x}_\varepsilon(t)$ from $\mathbf{x}(0) = \mathbf{x} \in \Omega$ to $\mathbf{y} \in \Omega$ in time t . The probability density function of trajectories that are terminated upon hitting $\partial\Omega$ is the solution of the initial and

homogeneous Dirichlet boundary value problem for the Fokker–Planck equation

$$\begin{aligned}\frac{\partial p_\varepsilon(\mathbf{y}, t | \mathbf{x})}{\partial t} &= L_y p(\mathbf{y}, t | \mathbf{x}) \text{ for } \mathbf{x}, \mathbf{y} \in \Omega \\ p_\varepsilon(\mathbf{y}, t | \mathbf{x}) &= 0 \text{ for } \mathbf{x} \in \partial\Omega, \mathbf{y} \in \Omega, t > 0 \\ p_\varepsilon(\mathbf{y}, 0 | \mathbf{x}) &= \delta(\mathbf{y} - \mathbf{x}) \text{ for } \mathbf{x}, \mathbf{y} \in \Omega,\end{aligned}\quad (1.13)$$

where the *Fokker–Planck operator* L_y is given by

$$L_y u(\mathbf{y}) = \varepsilon \sum_{i,j=1}^2 \frac{\partial^2 [\sigma^{i,j}(\mathbf{y}) u(\mathbf{y})]}{\partial y^i \partial y^j} - \sum_{i=1}^2 \frac{\partial [a^i(\mathbf{y}) u(\mathbf{y})]}{\partial y^i}. \quad (1.14)$$

The *backward Kolmogorov operator*, adjoint to L_y , defined in (1.10), is

$$L_x^* v(\mathbf{x}) = \varepsilon \sum_{i,j=1}^2 \sigma^{i,j}(\mathbf{x}) \frac{\partial^2 v(\mathbf{x})}{\partial x^i \partial x^j} + \sum_{i=1}^2 a^i(\mathbf{x}) \frac{\partial v(\mathbf{x})}{\partial x^i} \quad (1.15)$$

with homogeneous Dirichlet boundary conditions. Obviously, the probability density function $p(\mathbf{x}, t | \mathbf{x}_0)$ can be approximated at each time t by the histogram of simulated trajectories of (1.8).

The survival probability $\Pr_{\text{surv}}(t)$ of $\mathbf{x}_\varepsilon(t)$ in Ω , averaged with respect to an initial density $p_0(\mathbf{x})$, is the probability

$$\Pr_{\text{surv}}(t) = \Pr\{t < \tau_\varepsilon\} = \int_{\Omega} \Pr\{t < \tau_\varepsilon | \mathbf{x}\} p_0(\mathbf{x}) d\mathbf{x} \quad (1.16)$$

that the trajectory is still inside the domain at time t . This probability can be obtained from the transition probability density function as

$$\Pr_{\text{surv}}(t) = \int_{\Omega} \int_{\Omega} p_\varepsilon(\mathbf{y}, t | \mathbf{x}) p_0(\mathbf{x}) d\mathbf{y} d\mathbf{x}. \quad (1.17)$$

The survival probability can be approximated at time t by counting the relative number of simulated trajectories that have not reached $\partial\Omega$ by time t .

The function

$$p_\varepsilon(\mathbf{y} | \mathbf{x}) = \int_0^\infty p_\varepsilon(\mathbf{y}, t | \mathbf{x}) dt, \quad (1.18)$$

which is the steady-state density of trajectories in Ω that started at \mathbf{x} , as described below, is the solution of the boundary value problem

$$\nabla_y \cdot \mathbf{J}(y | x) = \delta(x - y), \quad p_\varepsilon(y | x) = 0 \text{ for } y \in \partial\Omega \text{ and } x \in \Omega, \quad (1.19)$$

where the flux density vector is given by

$$J^i(y | x) = a^i(y) p_\varepsilon(y | x) - \varepsilon \sum_{j=1}^d \frac{\partial [\sigma^{i,j}(y) p_\varepsilon(y | x)]}{\partial y^j}. \quad (1.20)$$

Integrating (1.19) over the domain and using the divergence theorem, we obtain

$$F(x) = \oint_{\partial\Omega} \mathbf{J}(y | x) \cdot \mathbf{n}(y) dS_y = 1. \quad (1.21)$$

This means that the total flux out of the domain equals the total output of the source $\delta(x - y)$ in (1.19). This leads to the following interpretation of $p_\varepsilon(y | x)$. If a source is placed at x and all trajectories are absorbed at the boundary, then $p(y | x)$ is the steady-state density of trajectories in Ω that started at x .

This interpretation describes the situation where all absorbed trajectories are instantaneously re-injected at x . The total population of trajectories that started at x is then

$$N(x) = \int_{\Omega} p_\varepsilon(y | x) dy = \mathbb{E}[\tau_\varepsilon | x_\varepsilon(0) = x].$$

This equation can be written in the “population over flux” form

$$\begin{aligned} \mathbb{E}[\tau_\varepsilon | x(0) = x] &= \int_{\Omega} p_\varepsilon(y | x) dy = \frac{N(x)}{1} = \frac{N(x)}{\oint_{\partial\Omega} \mathbf{J}(y | x) \cdot \mathbf{n}(y) dS_y} \\ &= \frac{N(x)}{F(x)}. \end{aligned} \quad (1.22)$$

The identity (1.22) holds even if the normalization (1.21) is changed. The steady-state absorption rate in the boundary, of trajectories that start at x , is

$$\kappa(x) = \frac{F(x)}{N(x)}. \quad (1.23)$$

The conditional probability density function of the exit point $y \in \partial\Omega$, given $x_\varepsilon(0) = x \in \Omega$, is given by

$$\Pr\{x_\varepsilon(\tau_\varepsilon) = y | x_\varepsilon(0) = x\} = \frac{\mathbf{J}(y | x) \cdot \mathbf{n}(y)}{\oint_{\partial\Omega} \mathbf{J}(y | x) \cdot \mathbf{n}(y) dS_y}. \quad (1.24)$$

Note that due to the homogeneous Dirichlet boundary condition the undifferentiated terms drop from (1.20). The normalization condition in expression (1.24) guarantees that the density of exit points integrates to one over the boundary. The conditional mean first passage time $\bar{\tau}_\varepsilon(\mathbf{x}) = \mathbb{E}[\tau_\varepsilon | \mathbf{x}_\varepsilon(0) = \mathbf{x}]$, given $\mathbf{x}_\varepsilon(0) = \mathbf{x} \in \Omega$, is also the solution of the Pontryagin–Andronov–Vitt boundary value problem [Schuss (2010b)]

$$L_x^* \bar{\tau}_\varepsilon(\mathbf{x}) = -1 \quad \text{for } \mathbf{x} \in \Omega, \quad \bar{\tau}_\varepsilon(\mathbf{x}) = 0 \quad \text{for } \mathbf{x} \in \partial\Omega. \quad (1.25)$$

Also $\bar{\tau}_\varepsilon(\mathbf{x})$ can be approximated by running a simulation of (1.8) and averaging the times that trajectories that start at $\mathbf{x} \in \Omega$ survive in Ω .

1.3 The Survival Probability and the Eigenvalue Problem

The probability distribution function of the exit time can be expressed in terms of the probability density function $p_\varepsilon(\mathbf{y}, t | \mathbf{x})$ of the trajectories $\mathbf{x}_\varepsilon(t)$ from $\mathbf{x} \in \Omega$ to $\mathbf{y} \in \Omega$ in time t . Specifically, the non-self-adjoint operators L_y and L_x^* with homogeneous Dirichlet boundary conditions have the same eigenvalues λ_n , because the equations are real and the eigenfunctions $u_n(\mathbf{y})$ of L_y and $v_n(\mathbf{x})$ of L_x^* are bases that are bi-orthonormal in the sense that

$$\int_{\Omega} \bar{v}_n(\mathbf{y}) L_y u_m(\mathbf{y}) d\mathbf{y} = \int_{\Omega} \bar{u}_n(\mathbf{y}) L_y^* v_m(\mathbf{y}) d\mathbf{y} = \delta_{n,m}. \quad (1.26)$$

The solution of the Fokker–Planck equation can be expanded as

$$p_\varepsilon(\mathbf{y}, t | \mathbf{x}) = e^{-\lambda_0 t} u_0(\mathbf{y}) v_0(\mathbf{x}) + \sum_n e^{-\lambda_n t} u_n(\mathbf{y}) \bar{v}_n(\mathbf{x}), \quad (1.27)$$

where λ_0 is the real-valued principal eigenvalue and u_0, v_0 are the corresponding positive eigenfunctions, that is, solutions of $L_x(u_0) = -\lambda_0 u_0$ and $L_y^*(v_0) = -\lambda_0 v_0$, respectively. The joint probability density function of the exit point $\mathbf{y} \in \partial\Omega$ and the exit time τ_ε is given in (1.24), where the flux density vector is given by

$$\begin{aligned} J^i(\mathbf{y}, t | \mathbf{x}) &= a^i(\mathbf{y}) p_\varepsilon(\mathbf{y}, t | \mathbf{x}) - \varepsilon \sum_{j=1}^d \frac{\partial [\sigma^{i,j}(\mathbf{y}) p_\varepsilon(\mathbf{y}, t | \mathbf{x})]}{\partial y^j} \\ &= -\varepsilon \sum_{j=1}^d \sigma^{i,j}(\mathbf{y}) \left[e^{-\lambda_0 t} \frac{\partial u_0(\mathbf{y})}{\partial y^j} v_0(\mathbf{x}) + \sum_n e^{-\lambda_n t} \frac{\partial u_n(\mathbf{y})}{\partial y^j} \bar{v}_n(\mathbf{x}) \right]. \end{aligned}$$

The survival probability of $\mathbf{x}_\varepsilon(t)$ in Ω , averaged with respect to a uniform initial distribution, is given in terms of the probability density function $p_\varepsilon(\mathbf{y}, t | \mathbf{x})$ of the trajectories $\mathbf{x}_\varepsilon(t)$ as

$$\begin{aligned}\Pr_{\text{survival}}(t) &= \frac{1}{|\Omega|} \int_{\Omega} \Pr\{\tau_{\varepsilon} > t \mid \mathbf{x}\} d\mathbf{x} = \frac{1}{|\Omega|} \int_{\Omega} \int_{\Omega} p_{\varepsilon}(\mathbf{y}, t \mid \mathbf{x}) d\mathbf{y} d\mathbf{x} \\ &= e^{-\lambda_0 t} + \sum_n \frac{e^{-\lambda_n t}}{|\Omega|} \int_{\Omega} u_n(\mathbf{y}) d\mathbf{y} \int_{\Omega} \bar{v}_n(\mathbf{x}) d\mathbf{x}. \end{aligned}\quad (1.28)$$

The probability density function of the escape time is given by

$$\begin{aligned}\Pr\{\tau_{\varepsilon} = t\} &= -\frac{d}{dt} \Pr_{\text{survival}}(t*) \\ &= \lambda_0 e^{-\lambda_0 t} + \sum_n \frac{\lambda_n e^{-\lambda_n t}}{|\Omega|} \int_{\Omega} u_n(\mathbf{y}) d\mathbf{y} \int_{\Omega} \bar{v}_n(\mathbf{x}) d\mathbf{x} \end{aligned}\quad (1.29)$$

and can be approximated by the histogram of exit times in a simulation of (1.8).

1.4 Discussion

Problems of singular perturbations of elliptic boundary value problems come up as models of rare events in many disciplines, including classical statistical physics and astronomy [Chandrasekhar (1943)], [Gardiner (1985)], [Risken (1996)], [Schuss (2010b)], chemical kinetics [Kramers (1940)], [Berne and Pecora (1976)], communications [Viterbi (1967)], [Jazwinski (2007)], [Schuss (2012)] (see Sect. 2.8). The concepts and equations discussed in this chapter appear in all the mentioned disciplines, books and more. They are the departing point for the analysis presented in this book.

Chapter 2

A Primer of Asymptotics for ODEs

This chapter reviews elementary asymptotic methods for constructing asymptotic approximations to solutions of singularly perturbed first and second-order boundary-value problems for linear ordinary differential equations. References to textbooks on asymptotics in \mathbb{R}^1 are listed in Annotations 2.9. The first four sections discuss general theory and the remaining sections are devoted to examples and applications.

To gain some insight into the structure of the solution $u_\varepsilon(x)$ of (1.10), (1.11), consider first the one-dimensional case

$$\varepsilon u_\varepsilon'' + a(x) u_\varepsilon' = f(x) \quad \text{for } \alpha < x < \beta \quad (2.1)$$

$$u_\varepsilon(\alpha) = u_\alpha, \quad u_\varepsilon(\beta) = u_\beta. \quad (2.2)$$

In the limit $\varepsilon \rightarrow 0$ one or both conditions (2.2) are lost and the solution may develop singularities inside the interval or on its boundaries. The asymptotic approximation to the exact solution is described in this chapter and Sect. 2.1, where its explicit integral representation is used. Such representations are in general unavailable in higher dimensions, so that there is no obvious generalization of these methods for higher dimensions. Another approach, which is based on constructing an asymptotic solution to the boundary value problem by a singular perturbation method, is generalized to higher dimensions in Chap. 3.

The matched asymptotics method of constructing approximations to solutions of singular perturbations of linear second-order elliptic boundary value problems in \mathbb{R}^n is well-illustrated by the one-dimensional case. In this case explicit solutions can be constructed and expanded in the perturbation parameter by the Laplace method. The same expansion can be obtained without resorting to the exact solution, which is not available in higher dimensions. Probabilistic and physical interpretations of the results of this sections are given in [Schuss (2010b)].

2.1 The Laplace Expansion of Integrals

The Laplace method for evaluating integrals of the form

$$I(\varepsilon) = \int_{\alpha}^{\beta} f(x) \exp\left\{\frac{\Phi(x)}{\varepsilon}\right\} dx, \quad (2.3)$$

where ε is a small parameter, is based on the observation that the integrand peaks sharply at the maximum of $\Phi(x)$ when $\varepsilon \downarrow 0$, so that the main contribution to the integral comes from the absolute maxima of $\Phi(x)$ in the interval $[\alpha, \beta]$. We consider two cases, when $\Phi(x)$ achieves its maximum at the boundary and when $\Phi(x)$ achieves its maximum at an interior point. We assume that all functions in (2.3) are sufficiently regular.

We set $a(x) = -\Phi'(x)$, that is, $\Phi(x)$ can be viewed as the potential of the force field $a(x)$. If $\Phi(x)$ achieves its maximum at the boundary, at $x = \alpha$, say, then $\Phi'(\alpha) \leq 0$, that is, $a(\alpha) \geq 0$ and the main contribution to the integral comes from the point $x = \alpha$. If $a(\alpha) > 0$, the local structure of $\Phi(x)$ near $x = \alpha$ is

$$\Phi(x) = \Phi'(\alpha)(x - \alpha) + o(|x - \alpha|) = -a(\alpha)(x - \alpha) + o(|x - \alpha|) \quad (2.4)$$

and the integral is evaluated by changing the variable of integration to

$$z = a(\alpha)\left(\frac{s - \alpha}{\varepsilon}\right). \quad (2.5)$$

We obtain

$$\begin{aligned} \int_{\alpha}^{\beta} f(x) \exp\left\{\frac{\Phi(s)}{\varepsilon}\right\} ds &= \frac{\varepsilon}{a(\alpha)} \int_0^u f(\alpha)e^{-z} (1 + O(\varepsilon|z|)) dz \\ &= \frac{\varepsilon f(\alpha)}{a(\alpha)} (1 - e^{-u}) (1 + O(\varepsilon)), \end{aligned} \quad (2.6)$$

where

$$u = a(\alpha)\left(\frac{\beta - \alpha}{\varepsilon}\right).$$

It follows that

$$I(\varepsilon) = f(\alpha) \left[1 - \exp\left\{-\frac{a(\alpha)}{\varepsilon}(\beta - \alpha)\right\} \right] [1 + O(\varepsilon)] \quad (2.7)$$

(note that here $O(\varepsilon) < 0$).

Exercise 2.1 (Flatter extrema).

(i) Assume $a(\alpha) = a'(\alpha) = \dots = a^{(n-1)}(\alpha) = 0$, but $a^{(n)}(\alpha) > 0$. Replace the local expansion (2.4) with

$$\Phi(x) = -\frac{a^{(n)}(\alpha)}{(n+1)}(x-\alpha)^{n+1} + O(|x-\alpha|^{n+2})$$

to approximate the Laplace-type integral $\int_{\alpha}^x \exp\{\Phi(s)/\varepsilon\} ds$ by the incomplete Euler Gamma function $\Gamma(x, y) = \int_0^y t^{x-1} e^{-t} dt$.

(ii) Show that for $0 < y \ll 1$ and all $x > 0$ the asymptotic behavior of the incomplete Euler Gamma function is

$$\Gamma(x, y) = \frac{y^x}{x} (1 + o(1)), \quad (2.8)$$

whereas for $y \gg 1$ and $x > 0$, it is

$$\Gamma(x, y) = \Gamma(x) - \frac{y^x}{x} e^{-y} (1 + o(1)), \quad (2.9)$$

where $\Gamma(x)$ is Euler's Gamma function

$$\Gamma(x) = \Gamma(x, \infty).$$

(iii) Conclude that if $\Phi(x)$ attains its maximum at $x = \alpha$, then (2.7) is replaced with

$$I(\varepsilon) = f(\alpha) \frac{\Gamma\left(\frac{1}{n+1}, \frac{a^{(n)}(\alpha)}{\varepsilon(n+1)}(x-\alpha)^{n+1}\right)}{\Gamma\left(\frac{1}{n+1}\right)} \times (1 + O(\varepsilon^{1/(n+1)})). \quad (2.10)$$

(iv) If the maximum of $\Phi(x)$ is achieved at both endpoints, assume $a(\alpha) = a'(\alpha) = \dots = a^{(n-1)}(\alpha) = 0$, but $a^{(n)}(\alpha) > 0$, and $a(\beta) = a'(\beta) = \dots = a^{(m-1)}(\beta) = 0$, but $a^{(m)}(\beta) < 0$. Find the asymptotics of $I(\varepsilon)$.

(v) If $n > m$, then $\varepsilon^{1/(m+1)} \ll \varepsilon^{1/(n+1)}$ for $\varepsilon \ll 1$ and $\beta - \alpha \gg \varepsilon^{1/(n+1)}$. Conclude that

$$I(\varepsilon) = f(\alpha) [1 + O(\varepsilon^{(n-m)/(n+m+2)})].$$

For $0 < \beta - \alpha \ll \varepsilon^{1/(n+1)}$,

$$I(\varepsilon) = f(\alpha) O\left(\frac{(\beta - \alpha)^{n+1}}{\varepsilon}\right).$$

(vi) Consider the case $n = m$. □

2.2 The Asymptotics of a First-Order Initial Value Problem

Consider the initial value problem

$$\varepsilon u'_\varepsilon(x) + a(x) u_\varepsilon(x) = f(x) \quad \text{for } \alpha < x < \beta \quad (2.11)$$

$$u_\varepsilon(\alpha) = u_\alpha \quad (2.12)$$

and assume $a(x) > 0$ in the interval. The solution of the homogeneous problem (2.11) (with $f(x) = 0$) is given by

$$u_\varepsilon(x) = u_{\text{homog}}(x) = u_\alpha \exp \left\{ \frac{\Phi(x)}{\varepsilon} \right\},$$

where $\Phi(x) = - \int_\alpha^x a(z) dz$. The solution of the inhomogeneous problem with the homogeneous initial condition $u_\alpha = 0$, denoted $u_{\text{inhomog}}(x)$, is given by

$$u_\varepsilon(x) = u_{\text{inhomog}}(x) = \frac{1}{\varepsilon} \int_\alpha^x f(z) \exp \left\{ \frac{\Phi(z)}{\varepsilon} \right\} dz \quad (2.13)$$

so that the solution to (2.11) is given by

$$u_\varepsilon(x) = u_{\text{homog}}(x) + u_{\text{inhomog}}(x) \quad (2.14)$$

and can be expanded asymptotically for $\varepsilon \rightarrow 0$ by evaluating the integral by the Laplace method, as described in Sect. 2.1 above.

2.2.1 Matched Asymptotic Expansions

However, a direct and simpler method exists for the construction of a uniform asymptotic approximation for the solution, which can be generalized to higher dimensions, where explicit representations do not exist. Assume, for simplicity, that all functions and domains discussed here are sufficiently regular in x and that $a(x) > \delta > 0$, where δ is a constant. A naïve approximation is obtained by postulating that the solution has a regular asymptotic power series expansion of the form

$$u_{\text{outer}}(x) \sim u_0(x) + \varepsilon u_1(x) + \dots, \quad (2.15)$$

where $u_j(x)$ are regular functions of x , independent of ε . Substituting the asymptotic series (2.15) in (2.11) and comparing coefficients of like powers of ε on both sides of the equation, we obtain the hierarchy of equations

$$a(x)u_0(x) = f(x) \quad (2.16)$$

and

$$a(x)u_j(x) = -u'_{j-1}(x) \quad \text{for } j \geq 1. \quad (2.17)$$

Under the above regularity assumptions, the recurrence relation (2.17) defines all terms in the asymptotic series (2.15). The resulting series is not necessarily convergent; however, it can be shown (see Exercise 2.2 below) to be asymptotic to the solution $u_\varepsilon(x)$ for all $x \gg \varepsilon$. In general, the asymptotic series $u_{\text{outer}}(x)$ cannot satisfy the initial condition (2.12). This is due to the reduced order of (2.16) relative to that of (2.11). This fact indicates that the solution $u_\varepsilon(x)$ undergoes a sharp change near $x = \alpha$, which bridges the gap between the different values $u_0(\alpha) = f(\alpha)/a(\alpha)$ and $u_\varepsilon(\alpha) = u_\alpha$. To bridge this gap, both terms in (2.11) have to be of the same order of magnitude when ε is small, unlike the case in the asymptotic series (2.15). To resolve the behavior of the solution in the region of rapid change the scaled variables $\xi = x\varepsilon^{-\kappa}$ and $Y_\varepsilon(\xi) = u_\varepsilon(x)$ are introduced, with the positive constant κ chosen in such a way that all terms in (2.11) become of comparable magnitude. With the variable ξ , (2.11) becomes

$$\varepsilon^{1-\kappa} Y'_\varepsilon(\xi) + a(\varepsilon^\kappa \xi) Y_\varepsilon(\xi) = f(\varepsilon^\kappa \xi), \quad Y_\varepsilon(0) = u_0. \quad (2.18)$$

The small region $x = O(\varepsilon^\kappa)$ is stretched into the region $\xi = O(1)$. Clearly, the three terms in (2.18) become comparable if $\kappa = 1$. Expanding in asymptotic power series,

$$a(\varepsilon\xi) \sim a_0(\xi) + \varepsilon a_1(\xi) + \dots \quad (2.19)$$

$$f(\varepsilon\xi) \sim f_0(\xi) + \varepsilon f_1(\xi) + \dots \quad (2.20)$$

$$Y_\varepsilon(\xi) \sim Y_0(\xi) + \varepsilon Y_1(\xi) + \dots, \quad (2.21)$$

we obtain the hierarchy of equations

$$\frac{dY_0(\xi)}{d\xi} + a_0(\xi)Y_0(\xi) = f_0(\xi), \quad Y_0(0) = x_0 \quad (2.22)$$

$$\frac{dY_j(\xi)}{d\xi} + a_0(\xi)Y_j(\xi) = f_j(\xi) - \sum_{k=0}^{j-1} a_{j-k}(\xi)Y_k(\xi) \quad (2.23)$$

$$Y_j(0) = 0, \quad \text{for } j \geq 1.$$

Note that the series (2.19), (2.20) are regular Taylor expansions of regular functions and the sign \sim (asymptotic to) can actually be replaced with $=$ (equals). This is, however, not necessarily so for the series (2.21). The solution of (2.22) is

$$Y_0(\xi) = e^{-A(\xi)}u_\alpha + \int_{\alpha}^{\xi} e^{-[A(\xi)-A(\sigma)]} f_0(\sigma) d\sigma,$$

where $A(\xi) = \int_{\alpha}^{\xi} a_0(\eta) d\eta$. The Eq. (2.23) are readily solved in a similar manner. In terms of the original variable, we have $A(\xi) = a(\alpha)(x - \alpha)/\varepsilon$, so we obtain

$$\begin{aligned} Y_0\left(\frac{x}{\varepsilon}\right) &= e^{-a(\alpha)(x-\alpha)/\varepsilon} u_\alpha + \int_{\alpha}^{(x-\alpha)/\varepsilon} e^{-a(\alpha)[(x-\alpha)/\varepsilon-s]} f(\alpha) ds \\ &= e^{-a(\alpha)(x-\alpha)/\varepsilon} u_\alpha + f(\alpha) \frac{1 - e^{-a(\alpha)(x-\alpha)/\varepsilon}}{a(\alpha)}. \end{aligned}$$

Note that although $Y_0(\xi)$ is a regular function of ξ , it has an essential singularity as a function of ε at the point $\varepsilon = 0$ for all $x > 0$.

It is apparent that $\lim_{\xi \rightarrow 0} Y_0(\xi) = u_\alpha$ and $\lim_{\xi \rightarrow \infty} Y_0(\xi) = f(\alpha)/a(\alpha)$. We also observe that $\lim_{\xi \rightarrow \infty} Y_0(\xi) = f(\alpha)/a(\alpha) = u_\alpha(\alpha) = \lim_{\xi \rightarrow 0} u_{\text{outer}}(x)$. Thus the outer solution $u_{\text{outer}}(x)$ matches the boundary layer solution $Y_0(\xi)$ in the matching region between $x - \alpha = O(\varepsilon)$ and $x - \alpha = O(1)$. A uniform approximation is obtained by simply adding the two solutions and subtracting their common limit $f(\alpha)/a(\alpha)$; that is,

$$u_{\text{unif}}(x) \sim e^{-a(\alpha)(x-\alpha)/\varepsilon} u_\alpha - \frac{f(\alpha)}{a(\alpha)} e^{-a(\alpha)(x-\alpha)/\varepsilon} + \frac{f(x)}{a(x)} + \dots, \quad (2.24)$$

or $u_{\text{unif}}(x) \sim u_{\text{b.l.}}(x) + u_{\text{outer}}(x) - \ell$, where $u_{\text{b.l.}}(x) = Y_\varepsilon(x/\varepsilon)$ and ℓ is the common limit

$$\ell = \lim_{\xi \rightarrow \infty} u_{\text{b.l.}}(\xi) = \lim_{\xi \rightarrow 0} u_{\text{outer}}(\xi). \quad (2.25)$$

The first limit $\xi \rightarrow \infty$ in (2.25) means that x is kept fixed and $\varepsilon \rightarrow 0$ whereas the limit $\xi \rightarrow 0$ means that ε is kept fixed and $x \rightarrow \alpha$. Equation (2.25) is called the *matching condition*. It means that the boundary layer approximation $u_{\text{b.l.}}(x)$ and the outer solution $u_{\text{outer}}(x)$ match as functions of the scaled variable ξ in the matching region.

Example 2.1 (a uniform expansion). Consider the initial value problem

$$0.1u' + (x + 1)u = 1 \text{ for } x > 0, \quad u(0) = 1. \quad (2.26)$$

The first three terms of the outer expansion are

$$u_{\text{outer}}(x) = \frac{1}{x+1} + \frac{0.1}{(x+1)^3} + \frac{3 \times 0.1^2}{(x+1)^5} + \frac{15 \times 0.1^3}{(x+1)^7} + \dots$$

(dashed line in Fig. 2.1). The uniform expansion (2.24) that satisfies the matching condition (2.25) is given by

$$u_{\text{unif}}(x) = -1.145e^{-x/0.1} + \frac{1}{x+1} + \frac{0.1}{(x+1)^3} + \frac{3 \times 0.1^2}{(x+1)^5} + \frac{15 \times 0.1^3}{(x+1)^7}$$

(dotted line) and includes the leading term of the boundary layer, and the exact solution is

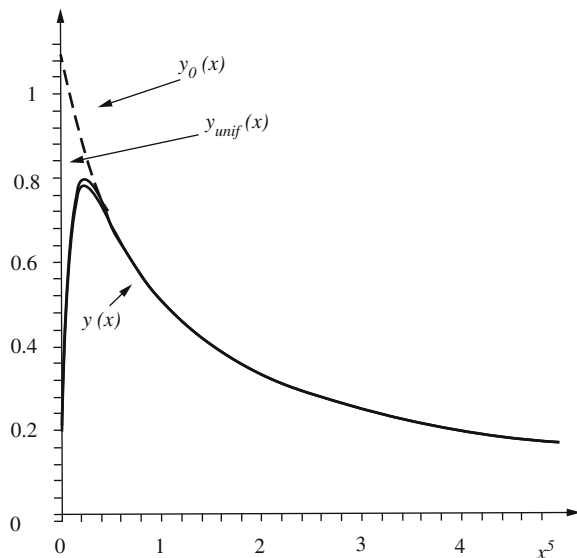
$$y(x) = 10 \int_0^x \exp \left\{ -\frac{(x+1)^2 + (s+1)^2}{0.2} \right\} ds$$

(solid line).

□

Exercise 2.2 (Convergence of the asymptotic expansion). Construct the full asymptotic series (2.21) and determine the nature of its convergence. □

Fig. 2.1 The three-term outer solution (dashed line), the uniform expansion (dotted line), and the exact solution (solid line)



2.2.2 An Application to Stochastic Differential Equations: The Exit Problem in \mathbb{R}^1

The exit problem (2.1), (2.2) is to calculate the mean first passage time of random trajectories of a stochastic differential equation to the boundary of a domain and the probability distribution of their exit points on the boundary. Calculations of the

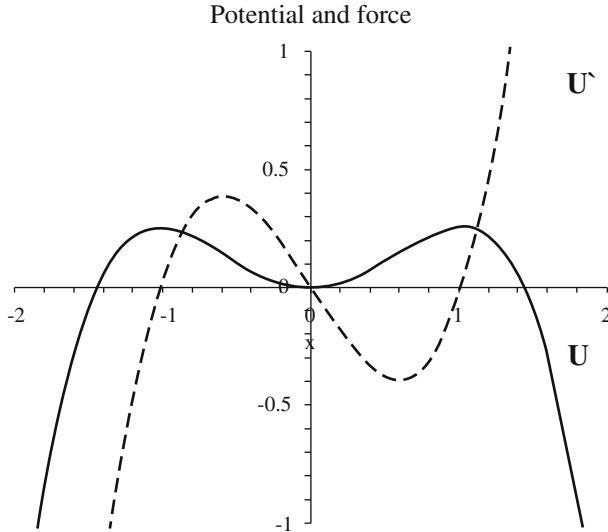


Fig. 2.2 The potential $U(x) = x^2/2 - x^4/4$ (solid line) and the force $F(x) = -U'(x)$ (dashed line). The domain of attraction of the stable equilibrium $x = 0$ is the interval $\Omega = (-1, 1)$

mean first passage time and of the exit probability in one dimension are considerably simplified if the diffusion coefficient is small. First, we note that small noise in a dynamical system is not a regular perturbation, in the sense that the behavior of the noiseless dynamics is close to that of the noisy system, but rather a singular perturbation, in the sense that it can cause large deviations from the noiseless behavior. For example, the origin is a locally stable attractor in the interval $-1 < x < 1$ for the one-dimensional dynamics

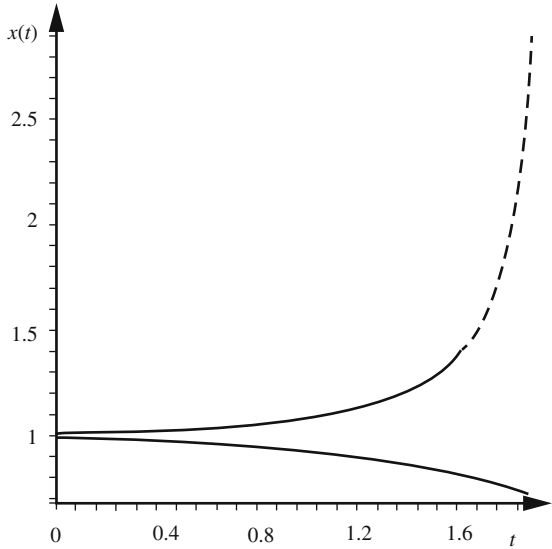
$$\dot{x} = -U'(x), \quad x(0) = x_0, \quad (2.27)$$

where the potential is $U(x) = x^2/2 - x^4/4$ (see Fig. 2.2). That is, if $-1 < x_0 < 1$, then $x(t) \rightarrow 0$ as $t \rightarrow \infty$ and if $|x_0| > 1$, then $|x(t)| \rightarrow \infty$ in finite time. Indeed, the explicit solution of (2.27) is given by

$$x(t) = \frac{x_0}{\sqrt{x_0^2(1 - e^{2t}) + e^{2t}}}. \quad (2.28)$$

If $|x_0| < 1$, the denominator is positive for all $t > 0$ and $x(t) \rightarrow 0$ as $t \rightarrow \infty$. On the other hand, if $|x_0| > 1$, then the denominator vanishes for $t = \log \sqrt{x_0^2/(x_0^2 - 1)}$, so the solution blows up in finite time. Therefore the solution that starts in the interval

Fig. 2.3 The solution (2.28) of the noiseless dynamics (2.27) with $x(0) = 0.99$ inside (bottom line) and $x(0) = 1.01$ outside (top line) the domain of attraction Ω



$\Omega = (-1, 1)$, which is the domain of attraction of the origin, never leaves it (see Fig. 2.3). In contrast, if small white noise is added to (2.27), it becomes the stochastic differential equation

$$dx = (-x + x^3) dt + \sqrt{2\varepsilon} dw, \quad x(0) = x_0, \quad (2.29)$$

where ε is a small parameter. The mean first passage time of $x(t)$ from $x = x_0 \in \Omega$ to the boundary of Ω is finite, because, according to (1.25), the mean first passage time $\bar{\tau}(x_0) = \mathbb{E}[\tau_\Omega | x(0) = x_0]$ is the solution of the boundary value problem

$$\varepsilon \bar{\tau}''(x) - U'(x) \bar{\tau}'(x) = -1 \quad \text{for } x \in \Omega, \quad \bar{\tau}(x) = 0 \quad \text{for } x \in \partial\Omega, \quad (2.30)$$

whose solution is given by

$$\bar{\tau}(x) = \frac{\int_{-1}^x \exp\left\{\frac{U(y)}{\varepsilon}\right\} \int_{-1}^y \exp\left\{\frac{U(y) - U(z)}{\varepsilon}\right\} dz dy}{\varepsilon \int_{-1}^1 \exp\left\{\frac{U(y)}{\varepsilon}\right\} dy}, \quad (2.31)$$

which is finite for all $x \in \Omega$. Thus almost all trajectories exit the domain of attraction Ω in finite time with probability one. In this section, we explore analytically large and small deviations caused by small noise in locally stable and unstable dynamical systems.

In many models the diffusion coefficient $\frac{1}{2}b^2(x)$ in the stochastic differential equation (2.1) is “small” in some sense so that it can be scaled with a small parameter ε and written as

$$dx = a(x) dt + \sqrt{2\varepsilon} b(x) dw, \quad x(0) = x. \quad (2.32)$$

The exit problem for the stochastic differential equation (2.32) is to find an asymptotic expression (for small ε) for the probabilities that the trajectories of (2.32) hit the boundaries of an interval (α, β) for the first time at α or at β , given that they start at $x \in (\alpha, \beta)$, as well as for the probability distribution function of the first passage time. The partial differential equations for these probability distributions are given in Sect. 1.2 (see, e.g., (1.24)). For small ε the boundary value problem (1.25) is now

$$L^\varepsilon p(x) = -f(x) \text{ for } \alpha < x < \beta, \quad p(\alpha) = 0, \quad p(\beta) = 0, \quad (2.33)$$

where the Fokker–Planck operator is defined by

$$L^\varepsilon p(x) = \varepsilon \frac{\partial^2 [\sigma(x)p(x)]}{\partial x^2} - \frac{\partial [a(x)p(x)]}{\partial x} \quad (2.34)$$

with $\sigma(x) = b^2(x)$. The boundary value problem (2.33) is a singular perturbation problem, because the reduced boundary value problem, corresponding to $\varepsilon = 0$,

$$L^0 p(x) = -f(x) \text{ for } \alpha < x < \beta, \quad p(\alpha) = 0, \quad p(\beta) = 0, \quad (2.35)$$

where $L^0 p(x) = -\partial a(x)p(x)/\partial x$, involves only a first-order differential equation. The boundary value problem (2.35) is in general overdetermined, because, in contrast to the solution of the second-order equation (2.33), the solution cannot satisfy, in general, both boundary conditions (2.35). The disappearance of a boundary condition in the limit $\varepsilon \rightarrow 0$ gives rise to a singular behavior of the solution to the boundary value problem (2.33). Boundary layers, which are regions of large gradients of the solution, appear near one or both boundary points. Other singularities of the solution appear as well.

2.3 Asymptotics of a Second-Order Boundary Value Problem

To understand intuitively the nature of the singularities of the boundary value problem (2.33), we consider the case $f(x) = -1$, which represents the Pontryagin–Andronov–Vitt equation for the mean first passage time of the trajectories of (2.32) from $x \in (\alpha, \beta)$ to the boundary of the interval. When ε is small, the trajectories of (2.32) can be expected to stay close to the trajectory of the reduced (noiseless)

dynamics

$$\dot{x} = a(x), \quad x(0) = x_0. \quad (2.36)$$

If the trajectory of (2.36) hits α , we may expect the exit probability to be concentrated about α , due to the small noise perturbation in the stochastic differential equation (2.32). Not all trajectories of (2.36), however, reach the boundary of the interval, as is the case in the example (2.27), whose trajectories in Ω stay there forever. The trajectories of the noisy dynamics (2.32), however, exit the interval in finite time with probability 1, as in the example (2.28). In this case it is not intuitively obvious what the probability of exit at α looks like.

The first passage time to the boundary is expected to be close to the first passage time of the noiseless system (2.32) when ε is small. The first passage time from a point x on a trajectory of (2.32) to the boundary, denoted $T_0(x)$, can be calculated directly from the reduced Eq. (2.36). Assuming that the trajectory of (2.36) that starts at x hits the boundary at α , we rewrite (2.36) as $dt = dx/a(x)$ and find by direct integration that $T_0(x) = \int_x^\alpha [a(s)]^{-1} ds$. Obviously, $T_0(x)$ is the solution of the first-order equation

$$a(x) T'_0(x) = -1, \quad T_0(\alpha) = 0. \quad (2.37)$$

The first passage time $T_0(x)$ is continuous in the interval up to the boundary point, where the trajectory of (2.36) that starts at x hits the boundary. For example, (2.27) in an interval (α, β) , such that $0 < \alpha < 1$ and $\beta > 1$, gives

$$T_0(x_0) = \frac{1}{2} \log \frac{x_0^2(1-\alpha^2)}{\alpha^2(1-x_0^2)} \text{ for } \alpha < x_0 < 1. \quad (2.38)$$

The time $T_0(x_0)$ to reach α from x_0 blows up as $x_0 \uparrow 1$. In the general case of (2.36), the time suffers a discontinuity as x approaches the boundary point, where trajectories of (2.36) enter the interval. At any point x in the interval such that the trajectory of (2.36) that starts at x never reaches the boundary, $T_0(x) = \infty$. In particular, if all trajectories of (2.36) stay forever in the interval, then $T_0(x) = \infty$ for all x . In this case, the solution to the inhomogeneous boundary value problem blows up in the limit $\varepsilon \rightarrow 0$ everywhere in the interval.

In contrast, the first passage time of the stochastic differential equation (2.32) is finite if the mean first passage time

$$\bar{\tau}_\varepsilon(x) = \mathbb{E} [\tau | x(0) = x]$$

is finite. This is the case, for example, if the Pontryagin–Andronov–Vitt boundary value problem (1.25), which is now

$$L^{*\varepsilon} \bar{\tau}_\varepsilon(x) = -1 \text{ for } \alpha < x < \beta, \quad \bar{\tau}_\varepsilon(\alpha) = 0, \quad \bar{\tau}_\varepsilon(\beta) = 0, \quad (2.39)$$

has a finite solution. Here $L^{*\varepsilon}$ is the backward Kolmogorov operator defined in (1.15), which for the stochastic differential equation (2.32) has the form

$$L^{*\varepsilon}\bar{\tau}_\varepsilon(x) = \varepsilon\sigma(x)\bar{\tau}_\varepsilon''(x) + a(x)\bar{\tau}_\varepsilon'(x). \quad (2.40)$$

Note that the differential equation (2.37) is obtained from the boundary value problem (2.39) by setting $\varepsilon = 0$ and dropping one of the boundary conditions.

If, for example, the diffusion coefficient $\sigma(x)$ is bounded below by a positive constant in the interval (i.e., if the backward Kolmogorov operator $L^{*\varepsilon}$ is not degenerate in the interval), the Pontryagin–Andronov–Vitt boundary value problem (2.39) has a unique finite solution for all $\varepsilon > 0$, regardless of the nature of the trajectories of the reduced dynamics (2.36). It follows that the first passage time to the boundary of almost all trajectories of the stochastic system (2.32) that start at any point in the interval, is finite. We conclude that, in the case where the noiseless dynamics (2.36) persists in the interval forever (and therefore $T_0(x) = \infty$ for all $\alpha < x < \beta$), the mean first passage time $\bar{\tau}_\varepsilon(x)$ becomes infinite in the limit $\varepsilon \rightarrow 0$. The exit problem in this case is to find an asymptotic expression for the mean first passage time and for the rate

$$\kappa_\varepsilon = \frac{1}{\bar{\tau}_\varepsilon} = \lambda_0, \quad (2.41)$$

where λ_0 is the principal eigenvalue and $\bar{\tau}_\varepsilon$ is the mean first passage time, averaged with respect to the principal eigenfunction of $L_x^{*\varepsilon}$ [Schuss (2010b)].

2.4 Asymptotics of a Homogeneous Second-Order Boundary Value Problem

In one dimension the homogeneous boundary value problem (1.10) becomes the ordinary differential equation

$$\begin{aligned} \varepsilon\sigma(x)u_\varepsilon''(x) + a(x)u_\varepsilon'(x) &= 0 \text{ for } \alpha < x < \beta \\ u_\varepsilon(\alpha) &= g_\alpha, \quad u_\varepsilon(\beta) = g_\beta, \end{aligned} \quad (2.42)$$

and g_α, g_β are given numbers. We assume that $a(x)$ and $\sigma(x)$ are uniformly Lipschitz continuous functions in $[\alpha, \beta]$ and that $\sigma(x)$ has a positive minimum in the interval.

As mentioned above, the exit distribution on the boundary of the interval; that is, at the points α, β , is Green's function for the boundary value problem (2.42), evaluated at these points. Under the given assumptions, the solution of (2.42) is given by

$$u_\varepsilon(x) = \frac{g_\alpha \int_x^\beta \exp\left\{\frac{\Phi(s)}{\varepsilon}\right\} ds + g_\beta \int_\alpha^x \exp\left\{\frac{\Phi(s)}{\varepsilon}\right\} ds}{\int_\alpha^\beta \exp\left\{\frac{\Phi(s)}{\varepsilon}\right\} ds},$$

where the potential is

$$\Phi(x) = - \int_\alpha^x \frac{a(y)}{\sigma(y)} dy. \quad (2.43)$$

According to (1.24), the exit distribution is

$$\begin{aligned} \Pr\{x(\tau) = \alpha \mid x(0) = x\} &= \lim_{\zeta \rightarrow 0} \int_{\alpha-\zeta}^{\alpha+\zeta} G(x, y) dy = \frac{\int_x^\beta \exp\left\{\frac{\Phi(s)}{\varepsilon}\right\} ds}{\int_\alpha^\beta \exp\left\{\frac{\Phi(s)}{\varepsilon}\right\} ds} \\ \Pr\{x(\tau) = \beta \mid x(0) = x\} &= \lim_{\zeta \rightarrow 0} \int_{\beta-\zeta}^{\beta+\zeta} G(x, y) dy = \frac{\int_\alpha^x \exp\left\{\frac{\Phi(s)}{\varepsilon}\right\} ds}{\int_\alpha^\beta \exp\left\{\frac{\Phi(s)}{\varepsilon}\right\} ds}. \end{aligned} \quad (2.44)$$

Denoting by τ_y the first passage time to y , we can write

$$\Pr\{x(\tau) = \alpha \mid x(0) = x\} = \Pr\{\tau_\alpha < \tau_\beta \mid x(0) = x\}.$$

An alternative derivation of (2.44) is obtained from (1.24), which shows that for trajectories that start at x , the probability of exit at β is the flux density at β , calculated from the Fokker–Planck equation with a source at x and absorbing boundaries at α and β . Specifically,

$$\Pr\{\tau_\beta < \tau_\alpha \mid x(0) = x\} = - \left. \frac{\partial \varepsilon \sigma(y) p_\varepsilon(y \mid x)}{\partial y} \right|_{y=\beta}, \quad (2.45)$$

where the function $p_\varepsilon(y \mid x)$ is the solution of the Fokker–Planck equation corresponding to the system (2.32),

$$\frac{\partial^2 \varepsilon \sigma(y) p_\varepsilon(y \mid x)}{\partial y^2} - \frac{\partial a(y) p_\varepsilon(y \mid x)}{\partial y} = -\delta(y - x) \text{ for } \alpha < x, y < \beta \quad (2.46)$$

$$p_\varepsilon(\alpha \mid x) = p_\varepsilon(\beta \mid x) = 0. \quad (2.47)$$

The solution of (2.46), (2.47) is given by

$$p_\varepsilon(y|x) = \frac{\exp\left\{-\frac{\Phi(y)}{\varepsilon}\right\}}{\varepsilon\sigma(y)} \times \left[\frac{\int_x^\beta \exp\left\{\frac{\Phi(s)}{\varepsilon}\right\} ds}{\int_\alpha^\beta \exp\left\{\frac{\Phi(s)}{\varepsilon}\right\} ds} \int_\alpha^y \exp\left\{\frac{\Phi(s)}{\varepsilon}\right\} ds - \int_\alpha^y H(s-x)\exp\left\{\frac{\Phi(s)}{\varepsilon}\right\} ds \right], \quad (2.48)$$

where $H(x)$ is the Heaviside step function. A detailed analysis of the asymptotic form of the function $p_\varepsilon(y|x)$ for small ε is given in Sect. 2.6.2. It is shown there that (2.45) implies (2.44).

2.5 Asymptotics of the Inhomogeneous Boundary Value Problem

The solution of the inhomogeneous boundary value problem is related to the mean first passage time, as shown in Sect. 1.3. Specifically, the complementary probability distribution function of the first passage time to the boundary,

$$v(x,t) = \Pr\{\tau > t | x(0) = x\} = \int_\alpha^\beta p_\varepsilon(y,t|x) dy,$$

where $p_\varepsilon(y,t|x)$ is the solution of the Fokker–Planck equation in (α, β) with homogeneous boundary conditions, is the solution of the backward Kolmogorov equation [Schuss (2010b)]

$$\frac{\partial v(x,t)}{\partial t} = L^{*\varepsilon} v(x,t) = \varepsilon\sigma(x) \frac{\partial^2 v(x,t)}{\partial x^2} - a(x) \frac{\partial v(x,t)}{\partial x} \quad (2.49)$$

with the boundary and initial conditions

$$v(\beta,t) = v(\beta,t) = 0 \text{ for } t > 0, \quad v(x,0) = 1 \text{ for } \alpha < x < b.$$

The solution is found by the method of separation of variables and is given by

$$v(x,t) = \sum_{n=0}^{\infty} v_n \Phi_n(x) e^{-\lambda_n t},$$

where λ_n and $\Phi_n(x)$ are the eigenvalues and eigenfunctions, respectively, of the self-adjoint boundary value problem

$$\left(e^{\Phi(x)/\varepsilon} \Phi'_n(x) \right)' + \frac{\lambda_n \sigma(x)}{\varepsilon} e^{\Phi(x)/\varepsilon} \Phi_n(x) = 0 \text{ for } \alpha < x < \beta$$

$$\Phi_n(\alpha) = \Phi_n(\beta) = 0.$$

The coefficients v_n in the expansion of the initial function $v(x, 0) = 1$ with respect to the eigenfunctions $\{\Phi_n(x)\}_{n=0}^\infty$, which are orthonormal with the weight $\sigma(x) e^{\Phi(x)/\varepsilon}$; that is,

$$v_n = \frac{\int_\alpha^\beta \sigma(x) e^{\Phi(x)/\varepsilon} \Phi_n(x) dx}{\int_\alpha^\beta \sigma(x) e^{\Phi(x)/\varepsilon} \Phi_n^2(x) dx}.$$

Thus, the probability distribution function of the first passage time from x to the boundary of the interval $[\alpha, \beta]$ is given by

$$\Pr\{\tau \leq t | x(0) = x\} = 1 - \sum_{n=0}^{\infty} v_n \Phi_n(x) e^{-\lambda_n t}. \quad (2.50)$$

The solution of the inhomogeneous boundary value problem; that is, the mean first passage time, is given by

$$\mathbb{E}[\tau | x(0) = x] = \int_0^\infty \Pr\{\tau > t | x(0) = x\} dt = \sum_{n=0}^{\infty} \frac{v_n \Phi_n(x)}{\lambda_n}. \quad (2.51)$$

If the initial point is distributed with density $\psi(x)$, the mean first passage time is

$$\mathbb{E}\tau = \sum_{n=0}^{\infty} \frac{v_n}{\lambda_n} \int_\alpha^\beta \Phi_n(x) \psi(x) dx.$$

In particular, if we begin to observe the dynamics a long time after it started, then, according to Sect. 1.3, the density of the surviving trajectories (the conditional probability density function, given $\tau > t$) at the moment observation begins, is approximately $\psi(x) = \psi_0(x)$, where $\psi_0(x)$ is the principal eigenfunction of the adjoint operator (the Fokker–Planck operator)

$$\varepsilon \frac{\partial^2 \sigma(x) \psi_n(x)}{\partial x^2} + \frac{\partial a(x) \psi_n(x)}{\partial x} = -\lambda_n \psi_n(x) \text{ for } \alpha < x < \beta$$

$$\psi_n(\alpha) = \psi_n(\beta) = 0,$$

normalized by $\int_\alpha^\beta \psi_0(x) dx = 1$. Then, due to the biorthogonality of the eigenfunctions $\{\Phi_n(x)\}$ and $\{\psi_n(x)\}$, the mean first passage time is

$$\begin{aligned}\mathbb{E}\tau_\varepsilon &= \int_{\alpha}^{\beta} \mathbb{E}[\tau_\varepsilon | x_\varepsilon(0) = x] \psi_0(x) dx = \sum_{n=0}^{\infty} \frac{v_n}{\lambda_n} \int_{\alpha}^{\beta} \psi_0(x) \Phi_n(x) dx \\ &= \frac{v_0}{\lambda_0} \int_{\alpha}^{\beta} \psi_0(x) \Phi_0(x) dx.\end{aligned}$$

An alternative calculation of the mean first passage time is based on the Pontryagin–Andronov–Vitt equation (2.39). The mean first passage time $\bar{\tau}_\varepsilon(x) = \mathbb{E}[\tau_\varepsilon | x_\varepsilon(0) = x]$ is the solution of the boundary value problem

$$L^{*\varepsilon} \bar{\tau}_\varepsilon(x) = -1 \text{ for } \alpha < x < \beta, \quad \bar{\tau}_\varepsilon(\alpha) = \bar{\tau}_\varepsilon(\beta) = 0,$$

where the backward Kolmogorov operator $L^{*\varepsilon}$ is defined by the left-hand side of (2.49). The solution is given by

$$\begin{aligned}\bar{\tau}_\varepsilon(x) &= \int_{\alpha}^x \exp\left\{-\frac{\Phi(s)}{\varepsilon}\right\} ds \frac{\int_{\alpha}^{\beta} \exp\left\{-\frac{\Phi(y)}{\varepsilon}\right\} \int_{\alpha}^y \exp\left\{\frac{\Phi(s)}{\varepsilon}\right\} ds dy}{\int_{\alpha}^{\beta} \exp\left\{-\frac{\Phi(s)}{\varepsilon}\right\} ds} \\ &\quad - \int_{\alpha}^x \exp\left\{-\frac{\Phi(y)}{\varepsilon}\right\} \int_{\alpha}^y \exp\left\{\frac{\Phi(s)}{\varepsilon}\right\} ds dy.\end{aligned}\tag{2.52}$$

Exercise 2.3 (The probability distribution function of the first passage time for the mathematical Brownian motion). Calculate the probability distribution function of the first passage time for the mathematical Brownian motion; that is, for $L_y = d^2/dy^2$. \square

Example 2.2 Mathematical Brownian motion with constant drift and the Ornstein–Uhlenbeck (OU) process. (a) Find the explicit expression for the probability density function $p_\varepsilon(y, t | x)$ of the trajectories $x(t)$ of Brownian motion with constant drift, defined by the stochastic differential equation

$$dx = -1 dt + \sqrt{2\varepsilon} dw$$

on the positive axis with absorption at the origin. Plot $p_\varepsilon(y, t | x)$ versus (y, t) for $x = 1$ and $\varepsilon = 0.01$ in the rectangle $0 < y < 2$, $0 < t < 2$.

(b) Use the expression

$$\Pr\{\tau_\varepsilon > t | x\} = \int_0^\infty p_\varepsilon(y, t | x) dy$$

to express $\Pr\{\tau_\varepsilon > t \mid x\}$ in terms of error functions and plot the probability density function of the first passage time from $x = 1$ to the origin for the values $\varepsilon = 0.01$ and $\varepsilon = 0.001$.

(c) Do the same for the OU process

$$dx = -x dt + \sqrt{2\varepsilon} dw.$$

Solution:

(a) The Fokker–Planck equation for $p_\varepsilon(y, t \mid x)$ is given by

$$p_t = p_x + \varepsilon p_{xx} \text{ for } t, x, y > 0, \quad (2.53)$$

with the initial and boundary conditions

$$p_\varepsilon(y, 0 \mid x) = \delta(y - x), \quad p_\varepsilon(0, t \mid x) = 0.$$

The substitution

$$p = q \exp\left\{-\frac{x + \frac{1}{2}t}{2\varepsilon}\right\} \quad (2.54)$$

converts the Fokker–Planck equation (2.53) to the diffusion equation $q_t = \varepsilon q_{xx}$ with the initial condition $q(y, 0 \mid x) = \delta(y - x) \exp\{x/2\varepsilon\}$ and the boundary condition $q(0, t \mid x) = 0$. The solution is found by solving the diffusion equation on the entire line with the initial condition $q(y, 0 \mid x) = \delta(y - x) \exp\{x/2\varepsilon\} - \delta(y + x) \exp\{x/2\varepsilon\}$. The solution is an odd function, due to the antisymmetric initial condition, and therefore vanishes at $y = 0$ (this is the method of images). Thus the solution of the initial boundary value problem (2.53), (2.54) is given by

$$\begin{aligned} p_\varepsilon(y, t \mid x) \\ = \frac{1}{2\sqrt{\pi\varepsilon t}} \exp\left\{-\frac{y - x + \frac{1}{2}t}{2\varepsilon}\right\} \left[\exp\left\{-\frac{(y - x)^2}{4\varepsilon t}\right\} - \exp\left\{-\frac{(y + x)^2}{4\varepsilon t}\right\} \right]. \end{aligned}$$

(b) We have

$$\begin{aligned} \Pr\{\tau_\varepsilon > t \mid x\} &= \int_0^\infty p_\varepsilon(y, t \mid x) dy \\ &= \frac{1}{2} \operatorname{erfc}\left(\frac{t - x}{2\sqrt{\varepsilon t}}\right) - \frac{1}{2} \left[\exp\left\{\frac{x}{\varepsilon}\right\} \operatorname{erfc}\left(\frac{t + x}{2\sqrt{\varepsilon t}}\right) \right]. \end{aligned}$$

It follows that the density of the first passage time is given by

$$\Pr \{ \tau_\varepsilon = t \mid x \} = \frac{x}{2\sqrt{\pi\varepsilon t^3}} \exp \left\{ -\frac{(t-x)^2}{4\varepsilon t} \right\}.$$

(c) Answer:

$$p_\varepsilon(y, t \mid x) = \frac{1}{\sqrt{2\pi\varepsilon(1-e^{-2t})}} \left[\exp \left\{ -\frac{1}{2} \frac{(-y+xe^{-t})^2}{\varepsilon(1-e^{-2t})} \right\} - \exp \left\{ -\frac{1}{2} \frac{(y+xe^{-t})^2}{\varepsilon(1-e^{-2t})} \right\} \right],$$

$$\Pr \{ \tau_\varepsilon > t \mid x \} = \operatorname{erf} \left(\frac{xe^{-t}}{\sqrt{2\varepsilon(1-e^{-2t})}} \right),$$

and

$$\Pr \{ \tau_\varepsilon = t \mid x \} = \frac{2xe^{-t} \exp \left\{ -\frac{1}{2} \frac{x^2 e^{-2t}}{\varepsilon(1-e^{-2t})} \right\}}{\sqrt{\pi(1-e^{-2t})^3}}.$$

Note that although τ_ε is finite with probability 1, and even has all moments, its probability density function peaks at time

$$t = -\frac{1}{2} \log \varepsilon (1 + O(\varepsilon)) \rightarrow \infty \text{ as } \varepsilon \rightarrow 0,$$

which reflects the fact that the first passage time of the noiseless system from x to the origin is infinite.

□

2.6 Examples and Applications to Stochastic Equations

2.6.1 Small Diffusion with the Flow: The Homogeneous Boundary Value Problem

Consider first a drift in the stochastic equation (2.32) that carries the trajectories across the interval, from left to right, say. That is, assume that $a(x) > \delta$ and $\sigma(x) > \delta$ for some $\delta > 0$. In this case the potential $\Phi(x)$ (see (2.43)) is a monotone decreasing function. The stochastic differential equation represents here a particle sliding down an incline with slightly fluctuating velocity. A discussion of this case is contained Sects. 2.2.2–2.5. Here the discussion is consolidated into two paragraphs.

To construct a boundary layer approximation near $x = \alpha$, we introduce the scaled variables $\xi = (x - \alpha)/\varepsilon$ and $U_\varepsilon(\xi) = u_\varepsilon(x)$, the interval $[\alpha, \beta]$ is mapped onto the interval $[0, (\beta - \alpha)/\varepsilon]$, which is approximated by the entire positive axis. Equation (2.42) becomes

$$\sigma(\alpha + \varepsilon\xi) U''_\varepsilon(\xi) + a(\alpha + \varepsilon\xi) U'_\varepsilon(\xi) = 0.$$

Expanding the coefficients in a Taylor's series and looking for a boundary layer approximation in the form $U_{\text{b.l.}}(\xi) \sim U_0(\xi) + \varepsilon U_1(\xi) + \dots$, we find that $U_0(\xi)$ satisfies the equation

$$\sigma(\alpha) U''_0(\xi) + a(\alpha) U'_0(\xi) = 0$$

with the boundary condition

$$\lim_{\xi \rightarrow 0} U_0(\xi) = g_\alpha$$

and the matching condition

$$\lim_{\xi \rightarrow \infty} U_0(\xi) = u_0.$$

The general solution is

$$U_0(\xi) = A \exp\{-a(\alpha)\xi/\sigma(\alpha)\} + B,$$

where A and B are constants to be determined by the boundary and matching conditions. The matching condition gives $B = u_0$ and the boundary condition gives $A = g_\alpha - u_0$, because $a(\alpha)/\sigma(\alpha) > 0$. Thus the boundary layer function is to leading order

$$U_{\text{bl}}(\xi) \sim (g_\alpha - u_0) \exp\left\{-\frac{a(\alpha)\xi}{\sigma(\alpha)}\right\} + u_0.$$

As yet, the constant u_0 is still undetermined.

A similar analysis at the other boundary involves the variables $\eta = (\beta - x)/\varepsilon$ and $V_\varepsilon(\eta) = u_\varepsilon(x)$ and gives $V_0(\eta) = C \exp\{a(\beta)\eta/\sigma(\beta)\} + D$, where C and D are constants. The boundary condition is $\lim_{\eta \rightarrow 0} V_0(\eta) = g_\beta$ and the matching condition is $\lim_{\eta \rightarrow \infty} V_0(\eta) = u_0$. Because $a(\beta)/\sigma(\beta) > 0$, the matching condition can be satisfied only if $C = 0$ and $D = u_0$. The boundary condition then implies that $u_0 = g_\beta$. Thus $V_0(\eta) = g_\beta$ and there is no boundary layer at the right endpoint.

A uniform approximation to $u_\varepsilon(x)$ is obtained by adding the boundary layer to the outer solution and subtracting their common limit in the matching region. This gives the uniform approximation

$$u_\varepsilon(x) \sim u_{\text{unif}}(x) = g_\beta + (g_\alpha - g_\beta) \exp\left\{-\frac{a(\alpha)(\alpha - x)}{\varepsilon\sigma(\alpha)}\right\} + O(\varepsilon), \quad (2.55)$$

where $O(\varepsilon)$ is uniform in the interval $[\alpha, \beta]$.

Returning to the exit problem, Green's function is approximated by

$$G(x, y) \sim \delta(y - \alpha) \exp\left\{-\frac{a(\alpha)(\alpha - x)}{\varepsilon\sigma(\alpha)}\right\} + \delta(y - \beta)\left(1 - \exp\left\{-\frac{a(\alpha)(\alpha - x)}{\varepsilon\sigma(\alpha)}\right\}\right) + O(\varepsilon)$$

and the exit probability is

$$\Pr\{\tau_\beta < \tau_\alpha | x(0) = x\} = \left(1 - \exp\left\{-\frac{a(\alpha)(\alpha - x)}{\varepsilon\sigma(\alpha)}\right\}\right) + O(\varepsilon)$$

$$\Pr\{\tau_\alpha < \tau_\beta | x(0) = x\} = \exp\left\{-\frac{a(\alpha)(\alpha - x)}{\varepsilon\sigma(\alpha)}\right\} + O(\varepsilon).$$

Exercise 2.4 (Full asymptotic expansion of the exit probability for positive drift). Obtain a full asymptotic expansion of the exit probability for the case $a(x) > \delta > 0$, $\sigma(x) > \delta > 0$. \square

Exercise 2.5 (Asymptotics for drift that vanishes on the boundary). Consider the exit probability for the case $a(x) > 0$ for $x > \alpha$, but $a(\alpha) = 0$ and $\sigma(x) > \delta > 0$. \square

A particular case of small diffusion with the flow is that of a flow directed toward the boundary with an unstable equilibrium point inside the interval, at a point ζ such that $\alpha < \zeta < \beta$, say. This is represented by a drift such that $(x - \zeta)a(x) > 0$ for $x \neq \zeta$. In this case, the potential $\Phi(x)$ has a maximum at ζ (like an inverted parabola) so that a particle placed anywhere in the interval slides down an incline toward the boundary, except at the point ζ , where it is at an unstable equilibrium. The outer solution may be discontinuous, because $a(x)$ changes sign at ζ and $a(\zeta) = 0$; that is, the solution to the reduced problem (2.42) may be one constant, u_α , say, for $\alpha \leq x < \zeta$, and another constant, u_β , say, for $\zeta < x \leq \beta$. In this case an *internal layer* at ζ has to be constructed to connect the two constants smoothly.

To do that, we assume that the local Taylor expansion of $a(x)$ near ζ is

$$a(x) = a'(\zeta)(x - \zeta) + O(|x - \zeta|^2) \quad (2.56)$$

with $a'(\zeta) > 0$ and introduce near ζ the scaled local variables $\xi = (x - \zeta)/\sqrt{\varepsilon}$ and $U_\varepsilon(\xi) = u_\varepsilon(x)$. Equation (2.42) becomes

$$\sigma(\zeta + \sqrt{\varepsilon}\xi) U''_\varepsilon(\xi) + \frac{1}{\sqrt{\varepsilon}} a(\zeta + \sqrt{\varepsilon}\xi) U'_\varepsilon(\xi) = 0.$$

Expanding $U_\varepsilon(\xi) \sim U_0(\xi) + \sqrt{\varepsilon}U_1(\xi) + \dots$ and using a Taylor expansion of the coefficients, we obtain the *internal layer equation*

$$\sigma(\zeta) U_0''(\xi) + \xi a'(\zeta) U_0'(\xi) = 0 \quad (2.57)$$

whose general solution is

$$U_0(\xi) = A \int_0^\xi \exp\left\{-\frac{s^2 a'(\zeta)}{2a(s)}\right\} ds + B,$$

where A and B are constants. The matching conditions for the internal layer function $U_\varepsilon(\xi)$ are $\lim_{\xi \rightarrow -\infty} U_\varepsilon(\xi) = u_\alpha$ and $\lim_{\xi \rightarrow \infty} U_\varepsilon(\xi) = u_\beta$. Because

$$\int_0^{+\infty} \exp\left\{-\frac{s^2 a'(\zeta)}{2\sigma(s)}\right\} ds = \pm \sqrt{\frac{\pi \sigma(\zeta)}{2a'(\zeta)}},$$

we find that

$$A = \frac{u_\beta - u_\alpha}{2} \sqrt{\frac{2a'(\zeta)}{\pi \sigma(\zeta)}}, \quad B = \frac{u_\beta + u_\alpha}{2}.$$

Under the given conditions, local boundary layer analysis indicates that there are no boundary layers so that the outer solution must satisfy the boundary conditions. This means that $u_\alpha = g_\alpha$, $u_\beta = g_\beta$ so that the leading term in the expansion of the internal layer function is

$$U_0(\xi) = \frac{g_\beta - g_\alpha}{2} \sqrt{\frac{2a'(\zeta)}{\pi \sigma(\zeta)}} \int_0^\xi \exp\left\{-\frac{s^2 a'(\zeta)}{2a(s)}\right\} ds + \frac{g_\beta + g_\alpha}{2}$$

and this is also the uniform approximation to the solution. Thus

$$u_\varepsilon(x) \sim \frac{g_\beta - g_\alpha}{2} \sqrt{\frac{2a'(\zeta)}{\pi \sigma(\zeta)}} \int_0^{(x-\zeta)/\sqrt{\varepsilon}} \exp\left\{-\frac{s^2 a'(\zeta)}{2a(s)}\right\} ds + \frac{g_\beta + g_\alpha}{2}.$$

It follows that in this case the exit probability is

$$\Pr\{\tau_\beta < \tau_\alpha | x(0) = x\} = \frac{1}{2} + \frac{1}{2} \sqrt{\frac{2a'(\zeta)}{\pi \sigma(\zeta)}} \int_0^{(x-\zeta)/\sqrt{\varepsilon}} \exp\left\{-\frac{s^2 a'(\zeta)}{2a(s)}\right\} ds + O(\varepsilon) \quad (2.58)$$

$$\Pr\{\tau_\alpha < \tau_\beta | x(0) = x\} = \frac{1}{2} - \frac{1}{2} \sqrt{\frac{2a'(\zeta)}{\pi \sigma(\zeta)}} \int_0^{(x-\zeta)/\sqrt{\varepsilon}} \exp\left\{-\frac{s^2 a'(\zeta)}{2a(s)}\right\} ds + O(\varepsilon).$$

It follows that a trajectory that starts on top of the potential barrier at $x = \zeta$ has about equal chances to reach either boundary, but if it starts at a point on the left of ζ its probability to reach α is nearly 1.

The mean first passage time from a point x in the interval to the boundary, denoted $\bar{\tau}_\varepsilon(x)$, can be evaluated directly from the Pontryagin–Andronov–Vitt equation

$$\varepsilon \sigma(x) \tau_\varepsilon''(x) + a(x) \tau_\varepsilon'(x) = -1, \quad \bar{\tau}_\varepsilon(\alpha) = \bar{\tau}_\varepsilon(\beta) = 0. \quad (2.59)$$

The equation can be integrated by quadratures and the integrals expanded for small ε . Alternatively, for $\alpha \ll x \leq \beta$, the solution can be expanded in a regular asymptotic power series

$$\bar{\tau}_\varepsilon(x) \sim T_0(x) + \varepsilon \bar{\tau}_1(x) + \dots, \quad (2.60)$$

where

$$T_0(x) = \int_x^\beta \frac{ds}{a(s)}, \quad \bar{\tau}_1(x) = \int_x^\beta \frac{\sigma(s)a'(s) ds}{a^3(s)},$$

and so on. A boundary layer is required near $x = \alpha$.

Exercise 2.6 (Construction of a boundary layer). Construct a boundary layer near $x = \alpha$ for the expansion (2.60). \square

Exercise 2.7 (Asymptotics inside the boundary layer). Consider now the case when the maximum of the function $\Phi(x) = - \int_\alpha^x [a(s)/\sigma(s)] ds$ is achieved at an internal point ζ and $\Phi(x)$ is monotonically increasing in the interval $[\alpha, \zeta]$ and monotonically decreasing in the interval $[\zeta, \beta]$. For any point outside an ε -neighborhood of ζ the analysis of the previous case applies. However, for trajectories that start in an ε -neighborhood of ζ the situation is different. Find the asymptotic expansion of the mean first passage time for this case. \square

2.6.2 Small Diffusion Against the Flow

This is the case when the matched asymptotics fails in the sense that matching and boundary conditions do not determine the full uniform asymptotic expansion of the exit probability and of the mean first passage time. Specifically, consider first the case of sharp boundaries; that is, assume that the drift points toward ζ at every point in the interval. Thus, for all x in the domain of attraction

$$(x - \zeta) a(x) < 0 \quad \text{for } x \neq \zeta. \quad (2.61)$$

This is the case, for example, for a particle in a double well potential as in Fig. 2.4. The attractor is $\zeta = x_A$ and the drift $a(x) = -U'(x)$ is positive for $x < x_A$ and negative for $x_A < x < x_C$ (see Fig. 2.5).

The exit problem in this case is that of small diffusion against the flow. In this case the potential $U(x)$ has a minimum at ζ and a maximum at one of the boundaries. Thus $U(x)$ in (2.43) forms a well with sharp boundaries. To escape the interval, a particle trapped in the well has to acquire from the noise sufficient energy to overcome the potential barrier. It is intuitively clear that it is more likely to escape the well at the side of the lowest barrier. A closer analysis is needed if both barriers are of equal height. To resolve this case, assume the expansion (2.56) with $a'(\zeta) < 0$ and obtain an outer solution of the boundary value problem (2.42) as above. In this case, however, the internal layer function diverges to infinity on either side of ζ so that there is no internal layer and the outer solution is a constant throughout the interval. In this case, there are boundary layers at both ends of the interval so that the uniform expansion has the form

$$\begin{aligned} u_{\text{unif}}(x) \sim & u_0 + (g_a - u_0) \exp \left\{ -\frac{a(\alpha)(x - \alpha)}{\varepsilon \sigma(\alpha)} \right\} \\ & + (g_\beta - u_0) \exp \left\{ \frac{a(\beta)(\beta - x)}{\varepsilon \sigma(\beta)} \right\}. \end{aligned} \quad (2.62)$$

Note that $a(\alpha) > 0 > a(\beta)$. Note, further, that although the boundary and matching conditions are satisfied by $u_{\text{unif}}(x)$, the constant u_0 is still undetermined. This is the failure mentioned at the beginning of this section.

Fig. 2.4 A potential $U(x)$ with two wells separated by a sharp barrier at x_C

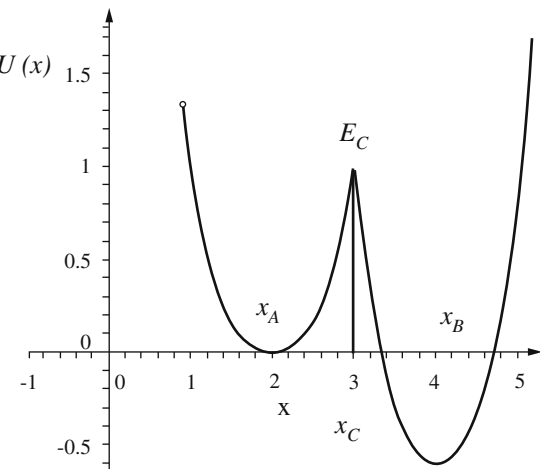
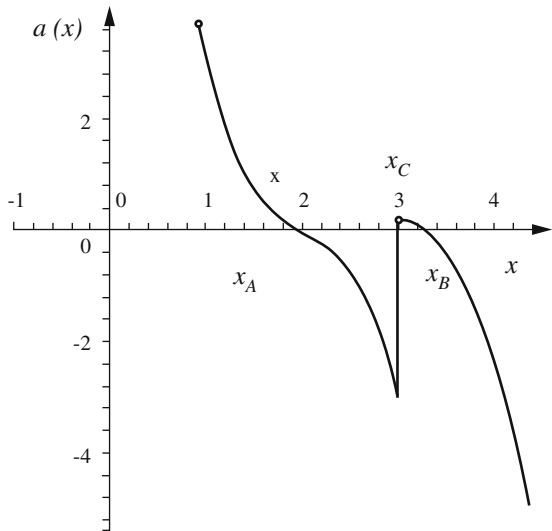


Fig. 2.5 At the barrier of the left well of the potential in Fig. 2.4 the (negative) drift $a(x_C^-) = -U'(x_C^-)$ points into the well (toward the attractor x_A)



To determine u_0 , we use the following identity.

Lemma 2.6.1 (The Lagrange identity). *For the operator $L^{*\varepsilon}$ defined in (2.42), if v_ε is a solution of $L^\varepsilon v_\varepsilon = 0$ and u_ε is the solution of the adjoint equation $L^{*\varepsilon} u_\varepsilon = 0$, then*

$$\int_{\alpha}^{\beta} v L^{*\varepsilon} u \, dx = \varepsilon \sigma(x) v_\varepsilon(x) u'_\varepsilon(x) \Big|_{\alpha}^{\beta} - \varepsilon [\sigma(x) v_\varepsilon(x)]' u_\varepsilon(x) \Big|_{\alpha}^{\beta} = 0. \quad (2.63)$$

This identity is obtained by straightforward integration by parts.

Choosing the solution $v_\varepsilon = e^{-U(x)/\varepsilon}$ and using the approximation (2.62) in (2.63), we obtain

$$u_0 \sim \frac{e^{-U(\alpha)/\varepsilon} a(\alpha) g_\alpha - e^{-U(\beta)/\varepsilon} a(\beta) g_\beta}{e^{-U(\alpha)/\varepsilon} a(\alpha) - e^{-U(\beta)/\varepsilon} a(\beta)},$$

having used the fact that

$$\exp \left\{ -\frac{U(\beta)}{\varepsilon} + a(\alpha) \frac{-\beta + \alpha}{\varepsilon \sigma(\alpha)} \right\} \ll e^{-U(\beta)/\varepsilon}.$$

The uniform solution is now given by

$$u_{\text{unif}}(x) = \frac{e^{-U(\alpha)/\varepsilon} a(\alpha) g_\alpha - e^{-U(\beta)/\varepsilon} a(\beta) g_\beta}{e^{-U(\alpha)/\varepsilon} a(\alpha) - e^{-U(\beta)/\varepsilon} a(\beta)} \quad (2.64)$$

$$\begin{aligned}
& + \frac{a(\beta)e^{-U(\beta)/\varepsilon}}{e^{-U(\alpha)/\varepsilon}a(\alpha) - e^{-U(\beta)/\varepsilon}a(\beta)} \exp\left\{-\frac{a(\alpha)(x-\alpha)}{\varepsilon\sigma(\alpha)}\right\} \\
& + \frac{a(\alpha)e^{-U(\alpha)/\varepsilon}}{e^{-U(\alpha)/\varepsilon}a(\alpha) - e^{-U(\beta)/\varepsilon}a(\beta)} \exp\left\{\frac{a(\beta)(\beta-x)}{\varepsilon\sigma(\beta)}\right\} + O(\varepsilon).
\end{aligned}$$

The probability of exit at β is the coefficient of g_β in (2.64), given by

$$\begin{aligned}
\Pr\{\tau_\beta < \tau_\alpha | x(0) = x\} = \\
\frac{-e^{-U(\beta)/\varepsilon}a(\beta)}{e^{-U(\alpha)/\varepsilon}a(\alpha) - e^{-U(\beta)/\varepsilon}a(\beta)} \left[1 - \exp\left\{-\frac{a(\alpha)(x-\alpha)}{\varepsilon\sigma(\alpha)}\right\}\right] \\
+ \frac{a(\alpha)e^{-U(\alpha)/\varepsilon}}{e^{-U(\alpha)/\varepsilon}a(\alpha) - e^{-U(\beta)/\varepsilon}a(\beta)} \exp\left\{\frac{a(\beta)(\beta-x)}{\varepsilon\sigma(\beta)}\right\} + O(\varepsilon).
\end{aligned}$$

If $U(\alpha) > U(\beta)$, the first term is exponentially close to 1, except for a boundary layer near α , and the second term is exponentially small throughout the interval. It follows that the exit probability at α is exponentially small in the interval, except for a boundary layer region near α , whereas the probability of exit at β is exponentially close to one, except for a boundary layer near α . This result agrees with (2.10) for the case $m = n = 0$.

If condition (2.61) is satisfied for $\alpha < x < \zeta < \beta$ and for $\alpha < \zeta < x < \beta$, but $a(\alpha) = 0$ or $a(\beta) = 0$, or both, the potential well is not cut off sharply at the edge but rather is cut off smoothly. This happens, for example, if the potential is defined in a larger interval containing $[\alpha, \beta]$ in its interior, it has a local minimum at ζ , and local maxima at α and β , say. This is the typical situation in modeling thermal activation (see [Schuss (2010b)]). The analysis of this case proceeds in a similar manner to that of the case of sharp boundaries in the sense that the outer solution is still an unknown constant u_0 , however, the boundary layer equations are different.

Exercise 2.8 (A flat barrier). Assume, as above, that $a(\alpha) = a'(\alpha) = \dots = a^{(n-1)}(\alpha) = 0$, but $a^{(n)}(\alpha) < 0$, and $a(\beta) = a'(\beta) = \dots = a^{(m-1)}(\beta) = 0$, but $a^{(m)}(\beta) > 0$, where m and n are positive integers. Construct the boundary layer near α by introducing the scaled variables $\xi = (x - \alpha)\varepsilon^{-\kappa}$, $U_\varepsilon(\xi) = u_\varepsilon(x)$ and write (2.42) as

$$\varepsilon^{1-2\kappa}\sigma(\alpha + \varepsilon^\kappa\xi) \frac{d^2U_\varepsilon(\xi)}{d\xi^2} + \varepsilon^{-\kappa}a(\alpha + \varepsilon^\kappa\xi) \frac{dU_\varepsilon(\xi)}{d\xi} = 0. \quad (2.65)$$

Expanding asymptotically all functions in powers of ε , obtain for $\varepsilon \ll 1$

$$\begin{aligned}
U_\varepsilon(\xi) &= U_0(\xi) + o(1), \quad a(\alpha + \varepsilon^\kappa\xi) = \frac{(\varepsilon^\kappa\xi)^n}{n!}a^{(n)}(\alpha) + O(\varepsilon^{\kappa+1}), \\
\sigma(\alpha + \varepsilon^\kappa\xi) &= \sigma(\alpha) + o(1).
\end{aligned}$$

(i) Show that the leading-order term, $U_0(\xi)$, satisfies the equation

$$\varepsilon^{1-2\kappa} \sigma(\alpha) \frac{d^2 U_0(\xi)}{d\xi^2} + \varepsilon^{(n-1)\kappa} \frac{\xi^n}{n!} a^{(n)}(\alpha) \frac{dU_0(\xi)}{d\xi} = 0.$$

(ii) Show that the two terms in the equation are comparable only if $1-2\kappa = (n-1)\kappa$; that is, only if $\kappa = 1/(n+1)$.

(iii) Choosing this value of κ , obtain

$$U_0(\xi) = A + B \int_0^\xi \exp \left\{ -\frac{a^{(n)}(\alpha) \eta^{n+1}}{(n+1)! \sigma(\alpha)} \right\} d\eta,$$

where A and B are constants.

(iv) Show that the boundary and matching conditions are $U_0(0) = g_\alpha$ and $U_0(\infty) = u_0$, respectively.

(v) Obtain a similar expression for a boundary layer function at β .

(vi) Construct the uniform approximation of $u_\varepsilon(x)$.

(vii) Note that the two terms in the Lagrange identity (2.63) are not of the same order of magnitude.

(viii) Use the asymptotic expansion in the Lagrange identity and find u_0 .

(ix) Find $\Pr\{\tau_\beta < \tau_\alpha \mid x(0) = x\}$ for x in (α, β) such that $(x-\alpha)^{n+1} \gg \varepsilon$ and $(\beta-x)^{m+1} \gg \varepsilon$; that is, for x outside the boundary layers (see Sect. 2.1).

(x) Find the boundary layer behavior from the asymptotics of the incomplete Gamma function (see (2.8) and (2.9)). \square

Exercise 2.9 (Equal and unequal barriers). Consider the different possible values of $m \geq 0$ and $n \geq 0$ in the boundary layers for equal and unequal potential barriers. \square

Exercise 2.10 (Matched asymptotics). Obtain the above results by constructing an asymptotic solution to the boundary value problem (2.46), (2.47) and then using (2.45). Use the method of matched asymptotics, as described above. \square

Exercise 2.11 (The first eigenfunction). Prove the following results:

(i) Let $u_\varepsilon(x)$ be the solution of the boundary value problem

$$\varepsilon u'' + a(x) u' = 0 \text{ for } \alpha < x < \beta, \quad u(\alpha) = g_\alpha, \quad u(\beta) = g_\beta,$$

where $a(x) = -U'(x)$. Let $\alpha = y_0 < y_1 < y_2 < \dots < y_n < y_{n+1} = \beta$ be the local maxima of $U(x)$ in the interval $[\alpha, \beta]$; denote by $s_1 < s_2 < \dots < s_\ell$ those points y_j where $U(s_j) = \max_i U(y_i)$ ($j = 1, \dots, \ell$), and by $x_1 < x_2 < \dots < x_m$ those points s_j where $a(x)$ vanishes to maximal order k (maximum with respect to j , $1 \leq j \leq m$). Assume that the local Taylor expansion of $a(x)$ about x_i is given by $a(x) = A_i(x - x_i)^k + \dots$, where $A_i > 0$, and let $B_i = (A_i)^{1/(k+1)}$. Then

$$u_\varepsilon(x) \sim \sum_{j=0}^{m-1} C_j \chi_{(x_j, x_{j+1})}(x) \text{ for } \varepsilon \ll 1 \text{ and fixed } x_j < x < x_{j+1},$$

where the indicator function is defined by

$$\chi_{(x_j, x_{j+1})}(x) = \begin{cases} 1 & \text{for } x_j < x < x_{j+1} \\ 0 & \text{otherwise,} \end{cases}$$

and

$$C_j = \frac{g_\alpha P_{m,j} + g_\beta Q_{m,j}}{P_m}, \quad P_{n,j} = \sum_{i=0}^j P_i, \quad Q_{n,j} = P_n - P_{n,j}$$

$$P_n = \sum_{j=0}^{n+1} \left[\left(\prod_{i=0}^{n+1} B_i \right) / B_{n-j+1} \right] = \sum_{j=0}^{n+1} P_j.$$

Construct boundary and internal layers to connect the constants C_j in adjacent intervals.

(ii) Show that

$$\Pr \{ \tau_\alpha < \tau_\beta \mid x(0) = x \} \sim \sum_{i=0}^{m-1} \frac{P_{m,j}}{P_m} \chi_{(x_j, x_{j+1})}(x)$$

(see Annotations 2.9). □

2.6.3 Small Diffusion Against the Flow: The Inhomogeneous Boundary Value Problem

To construct a uniform asymptotic approximation to the solution of the inhomogeneous boundary value problem (2.59) (here $\bar{\tau}_\varepsilon(x)$ represents the mean first passage time to the boundary of the interval), recall the boundary value problem (2.46), (2.47) and the expression (1.22) for the mean first passage time. Specifically, assume that the potential $U(y)$ in (2.43) forms a single well in the interval $[\alpha, \beta]$. Establish the asymptotic form of the solution to the boundary value problem (2.46), (2.47) by rewriting the explicit solution (2.48) in the form $p_\varepsilon(y \mid x) = [e^{-U(y)/\varepsilon} / \sigma(y)] q_\varepsilon(y \mid x)$ and obtain

$$q_\varepsilon(y | x) = \begin{cases} \frac{\int_x^\beta \exp\left\{\frac{U(s)}{\varepsilon}\right\} ds \int_\alpha^y \exp\left\{\frac{U(s)}{\varepsilon}\right\} ds}{\varepsilon \int_\alpha^\beta \exp\left\{\frac{U(s)}{\varepsilon}\right\} ds} & \text{for } \alpha < y < x < \beta \\ \frac{\int_\alpha^x \exp\left\{\frac{U(s)}{\varepsilon}\right\} ds \int_y^\beta \exp\left\{\frac{U(s)}{\varepsilon}\right\} ds}{\varepsilon \int_\alpha^\beta \exp\left\{\frac{U(s)}{\varepsilon}\right\} ds} & \text{for } \alpha < x < y < \beta. \end{cases}$$

2.6.4 The Boundary Value Problem with a Sharp Potential Barrier

If $U(y)$ forms a well and $U(\alpha) < U(\beta) = \max_{[\alpha, \beta]} U(y)$, and the boundaries are sharp; that is, $U'(\alpha) < 0$, and $U'(\beta) > 0$, the function $q_\varepsilon(y | x)$ can be approximated asymptotically for small ε as

$$\frac{\int_x^\beta \exp\left\{\frac{U(s)}{\varepsilon}\right\} ds}{\int_\alpha^\beta \exp\left\{\frac{U(s)}{\varepsilon}\right\} ds} \sim 1,$$

so that for $\alpha < y < x < \beta$ and y close to α (so that $U(y) < U(\alpha)$)

$$q_\varepsilon(y | x) = \frac{\int_x^\beta \exp\left\{\frac{U(s)}{\varepsilon}\right\} ds \int_\alpha^y \exp\left\{\frac{U(s)}{\varepsilon}\right\} ds}{\varepsilon \int_\alpha^\beta \exp\left\{\frac{U(s)}{\varepsilon}\right\} ds} \sim \frac{\exp\left\{\frac{U(\alpha)}{\varepsilon}\right\}}{-U'(\alpha)} \left(1 - e^{U'(\alpha)(y-\alpha)/\varepsilon}\right). \quad (2.66)$$

For $\alpha < x < y < \beta$ and y close to β

$$q_\varepsilon(y | x) = \frac{\int_\alpha^x \exp\left\{\frac{U(s)}{\varepsilon}\right\} ds \int_y^\beta \exp\left\{\frac{U(s)}{\varepsilon}\right\} ds}{\varepsilon \int_\alpha^\beta \exp\left\{\frac{U(s)}{\varepsilon}\right\} ds} \quad (2.67)$$

$$\begin{aligned} & \sim \frac{(1 - e^{U'(\beta)(y-\beta)/\varepsilon})}{\varepsilon} \int_{\alpha}^x \exp\left\{\frac{U(s)}{\varepsilon}\right\} ds \\ & = \left(1 - e^{U'(\beta)(y-\beta)/\varepsilon}\right) \begin{cases} \frac{\exp\left\{\frac{U(x)}{\varepsilon}\right\}}{-U'(x)} & \text{if } U(\alpha) < U(x) \\ \frac{\exp\left\{\frac{U(\alpha)}{\varepsilon}\right\}}{-U'(\alpha)} & \text{if } U(x) < U(\alpha). \end{cases} \end{aligned}$$

Thus, if $U(x) < U(\alpha)$, then for all $\alpha < y < \beta$

$$\lim_{\varepsilon \rightarrow 0} \exp\left\{-\frac{U(\alpha)}{\varepsilon}\right\} q_\varepsilon(y|x) = \frac{1}{-U'(\alpha)}.$$

That is, for y outside boundary layers and for x in the domain $U(x) < U(\alpha)$, this result means that

$$p_\varepsilon(y|x) \sim C_\varepsilon \frac{e^{-U(y)/\varepsilon}}{\sigma(y)} = p_{\text{outer}}(y), \quad (2.68)$$

where $C_\varepsilon = -e^{U(\alpha)/\varepsilon}/U'(\alpha)$. The result (2.68) means that for a potential $U(y)$ that forms a single well the outer solution to the boundary value problem (2.46), (2.47) is the solution to the asymptotic problem

$$\frac{\partial^2 \varepsilon \sigma(y) p_{\text{outer}}(y)}{\partial y^2} - \frac{\partial a(y) p_{\text{outer}}(y)}{\partial y} \sim 0 \text{ for } \alpha < x, y < \beta \quad (2.69)$$

given in (2.68). According to (2.66) and (2.67), the boundary layers for $q_\varepsilon(y|x)$ have the form

$$q_\varepsilon(y|x) \sim \frac{\exp\left\{\frac{U(\alpha)}{\varepsilon}\right\}}{-U'(\alpha)} \left(1 - e^{U'(\alpha)(y-\alpha)/\varepsilon}\right) \quad \text{for } y \text{ near } \alpha \quad (2.70)$$

$$q_\varepsilon(y|x) \sim \frac{\exp\left\{\frac{U(\alpha)}{\varepsilon}\right\}}{-U'(\alpha)} \left(1 - e^{U'(\beta)(y-\beta)/\varepsilon}\right) \quad \text{for } y \text{ near } \beta; \quad (2.71)$$

that is, the uniform asymptotic expansion of $p_\varepsilon(y|x)$ in the domains $\alpha < y < x < \beta$, and $\alpha < x < y < \beta$, $U(x) < U(\alpha)$, is given by

$$p_\varepsilon(y|x) \sim \frac{e^{-U(y)/\varepsilon}}{\sigma(y)} \frac{\exp\left\{\frac{U(\alpha)}{\varepsilon}\right\}}{-U'(\alpha)} \left(1 - e^{U'(\alpha)(y-\alpha)/\varepsilon}\right) \quad \text{for } \alpha < y < x < \beta$$

$$p_\varepsilon(y|x) \sim \frac{e^{-U(y)/\varepsilon}}{\sigma(y)} \frac{\exp\left\{\frac{U(\alpha)}{\varepsilon}\right\}}{-U'(\alpha)} \left(1 - e^{U'(\beta)(y-\beta)/\varepsilon}\right) \quad \text{for } \alpha < x < y < \beta.$$

It is argued below that this is the general asymptotic structure of the Green's function of the Fokker–Planck equation in a domain Ω , with homogeneous conditions on its boundary $\partial\Omega$, when the drift vector field has a single attractor in the domain. The construction of this expansion by direct asymptotic analysis of the differential equation is now straightforward. First, construct the outer solution, $p_{\text{outer}}(y)$, in the WKB (Wentzel–Kramers–Brillouin) form (2.68) and transform the Fokker–Planck equation (2.68) into the backward Kolmogorov equation by the substitution $p_\varepsilon(y|x) = p_{\text{outer}}(y) q_\varepsilon(y)$ to obtain

$$\varepsilon \sigma(y) q_\varepsilon''(y) + a(y) q_\varepsilon'(y) \sim 0 \quad \text{for } y \in \Omega, \varepsilon \ll 1 \quad (2.72)$$

with the matching and boundary conditions

$$q_\varepsilon(y) \sim C_\varepsilon \quad \text{for } y \in \Omega, \varepsilon \ll 1, \quad \text{and} \quad q_\varepsilon|_{\partial\Omega} = 0. \quad (2.73)$$

The boundary layers are constructed by introducing the stretched variable $\xi = \rho/\varepsilon$, defining $Q_\varepsilon(\xi) = q_\varepsilon(y)$, where $\rho = \text{dist}(y, \partial\Omega)$, and by expanding $Q_\varepsilon(\xi) = Q_0(\xi) + \varepsilon Q_1(\xi) + \dots$. Thus, $\rho = y - \alpha$ near α and the backward Kolmogorov equation (2.72) takes the form

$$\sigma(\alpha) Q_0''(\xi) + a(\alpha) Q_0'(\xi) \sim 0, \quad Q_0(0) = 0, \quad \lim_{\xi \rightarrow \infty} Q_0(\xi) = C_\varepsilon.$$

The solution is given by $Q_0(\xi) = C_\varepsilon(1 - e^{U'(\alpha)\xi})$, or equivalently, (2.70). The expression (2.71) is obtained in an analogous manner. We rewrite these expressions in the unified form

$$p_\varepsilon(y|x) \sim p_{\text{unif}}(y|x) = p_{\text{outer}}(y) q_\varepsilon(y)$$

$$= C_\varepsilon \frac{e^{-U(y)/\varepsilon}}{\sigma(y)} (1 - e^{U_n \rho / \varepsilon}), \quad (2.74)$$

where U_n is the outer normal derivative of $U(y)$ at the boundary point nearest y .

Finally, the mean first passage time is obtained from (1.22) with the asymptotic values (2.74). The normal component of the total flux is given by

$$\begin{aligned} F_\varepsilon(x) &\sim -\varepsilon\sigma(\beta)\frac{\partial p_{\text{unif}}(\beta|x)}{\partial y} + \varepsilon\sigma(\alpha)\frac{\partial p_{\text{unif}}(\alpha|x)}{\partial y} \\ &= C_\varepsilon [U'(\beta)e^{-U(\beta)/\varepsilon} - U'(\alpha)e^{-U(\alpha)/\varepsilon}] \sim -C_\varepsilon U'(\alpha)e^{-U(\alpha)/\varepsilon}, \end{aligned} \quad (2.75)$$

because $e^{-U(\beta)/\varepsilon} \ll e^{-U(\alpha)/\varepsilon}$ if $U(\alpha) < U(\beta)$. The total population is evaluated by the Laplace method as

$$N_\varepsilon(x) \sim C_\varepsilon \int_\alpha^\beta \frac{e^{-U(y)/\varepsilon}}{\sigma(y)} (1 - e^{U_n\rho/\varepsilon}) dy \sim C_\varepsilon \sqrt{\frac{2\pi\varepsilon}{U''(\zeta)}} \frac{e^{-U(\zeta)/\varepsilon}}{\sigma(\zeta)}, \quad (2.76)$$

where ζ is the point of minimum of $U(y)$ in the domain. Note that neither the total flux $F(x)$ nor the total population $N_\varepsilon(x)$ depends on x to leading order, as long as x is not in a boundary layer. Now, (1.22) gives

$$\tau_\varepsilon(x) = \frac{N_\varepsilon(x)}{F_\varepsilon(x)} \sim \sqrt{\frac{2\pi\varepsilon}{U''(\zeta)\sigma^2(\zeta)|U'(\alpha)|^2}} e^{[U(a)-U(\zeta)]/\varepsilon}. \quad (2.77)$$

The expression (2.77) is often written in the form

$$\bar{\tau}_\varepsilon = \omega^{-1} e^{\Delta E/\varepsilon}, \quad (2.78)$$

where $\Delta E = U(a) - U(\zeta)$ is the height of the lowest potential barrier, and

$$\omega = \sqrt{\frac{U''(\zeta)\sigma^2(\zeta)|U'(\alpha)|^2}{2\pi\varepsilon}}$$

is the so-called *attempt frequency*. Recalling the definition (1.23) of the escape rate, we obtain $\kappa_\varepsilon = \tau_\varepsilon^{-1} = \omega^{-1} e^{-\Delta E/\varepsilon}$.

Note that the value of the constant C_ε does not enter the expression (2.78) for the mean first passage time to the boundary. The value $C_\varepsilon = -e^{U(\alpha)/\varepsilon}/U'(\alpha)$ can be easily deduced from (2.75) by recalling that the total flux is 1,

$$1 = F(x) = C_\varepsilon [U'(\beta)e^{-U(\beta)/\varepsilon} - U'(\alpha)e^{-U(\alpha)/\varepsilon}] \sim -C_\varepsilon U'(\alpha)e^{-U(\alpha)/\varepsilon}.$$

2.6.5 The Problem for a Smooth Potential Barrier at the Boundary

At a smooth boundary $a(\alpha) = 0$, which usually happens when the potential $U(y)$ has a local maximum at the boundary of the well. In this case, we assume that $a'(\alpha) = a''(\alpha) = \dots = a^{(n-1)}(\alpha) = 0$, but $a^{(n)}(\alpha) > 0$. We assume that $U(y)$ has

a global maximum at $y = \alpha$. We proceed as in this chapter; that is, the local Taylor expansion of $a(y)$ about α is given by $a(y) = [a^{(n)}(\alpha)/n!](y - \alpha)^n + \dots$ and the scaled variable $\xi = (y - \alpha)/\varepsilon^\kappa$ transforms the asymptotic boundary value problem (2.72)–(2.73) into

$$\varepsilon^{1-2\kappa} \sigma(\alpha) Q_0''(\xi) + \varepsilon^{(n-1)\kappa} a^{(n)}(\alpha) \xi^n Q_0'(\xi) \sim 0 \quad (2.79)$$

$$Q_0(0) = 0, \quad \lim_{\xi \rightarrow \infty} Q_0(\xi) = C_\varepsilon, \quad (2.80)$$

where $q_\varepsilon(y) = Q_\varepsilon(\xi) = Q_0(\xi) + \varepsilon^\kappa Q_1(\xi) + \dots$. The two terms in (2.79) are comparable if $1 - 2\kappa = (n - 1)\kappa$; that is, if $\kappa = 1/(n + 1)$. Then (2.79) and (2.80) reduce to

$$\sigma(\alpha) Q_0''(\xi) + a^{(n)}(\alpha) \xi^n Q_0'(\xi) \sim 0, \quad Q_0(0) = 0, \quad \lim_{\xi \rightarrow \infty} Q_0(\xi) = C_\varepsilon,$$

whose solution is

$$Q_0(\xi) = \frac{C_\varepsilon A^{1/(n+1)}(n+1)}{\Gamma(\frac{1}{n+1})} \int_0^\xi e^{-Ax^{n+1}} dx,$$

where $A = a^{(n)}(\alpha)/\sigma(\alpha)(n + 1)$. Now,

$$\begin{aligned} Q_0'(0) &= \left(\frac{a^{(n)}(\alpha)}{\sigma(\alpha)} \right)^{1/(n+1)} \frac{(n+1)^{n/(n+1)}}{\Gamma(\frac{1}{n+1})} \\ &= [U^{(n+1)}(\alpha)]^{1/(n+1)} \frac{(n+1)^{n/(n+1)}}{\Gamma(\frac{1}{n+1})} \end{aligned}$$

and the total flux at the boundary in (2.75), $F_\varepsilon|_{\partial\Omega}$, is given by

$$\begin{aligned} F_\varepsilon|_{\partial\Omega} &= -\varepsilon\sigma(y)p_{\text{outer}}(y) \frac{\partial q_\varepsilon(y)}{\partial n_y} \Big|_{\partial\Omega} \\ &= C_\varepsilon \left[\varepsilon^{n/(n+1)} \exp\left\{-\frac{U(\alpha)}{\varepsilon}\right\} [U^{(n+1)}(\alpha)]^{1/(n+1)} \frac{(n+1)^{n/(n+1)}}{\Gamma(\frac{1}{n+1})} \right. \\ &\quad \left. + \varepsilon^{m/(m+1)} \exp\left\{-\frac{U(\beta)}{\varepsilon}\right\} [U^{(m+1)}(\beta)]^{1/(m+1)} \frac{(m+1)^{m/(m+1)}}{\Gamma(\frac{1}{m+1})} \right] \\ &\sim C_\varepsilon \varepsilon^{n/(n+1)} \exp\left\{-\frac{U(\alpha)}{\varepsilon}\right\} [U^{(n+1)}(\alpha)]^{1/(n+1)} \frac{(n+1)^{n/(n+1)}}{\Gamma(\frac{1}{n+1})}. \end{aligned}$$

To calculate the total population, $N_\varepsilon(\Omega)$, we assume that the local expansion of $U(y)$ near its point of minimum in the interval, ζ , is

$$U(y) = U(\zeta) + \frac{U^{(2\ell)}(\zeta)}{(2\ell)!} (y - \zeta)^{2\ell} + \dots,$$

where $U^{(2\ell)}(\zeta) > 0$ and ℓ is a positive integer. Then the integral in (2.76) gives for sufficiently small ε

$$\begin{aligned} N_\varepsilon(\Omega) &\sim \frac{C_\varepsilon e^{-U(\zeta)/\varepsilon}}{\sigma(\zeta)} \int_{\alpha}^{\beta} \exp\left\{-\frac{U^{(2\ell)}(\zeta)}{(2\ell)! \varepsilon} (y - \zeta)^{2\ell}\right\} dy \\ &\sim \frac{C_\varepsilon e^{-U(\zeta)/\varepsilon}}{\sigma(\zeta)} \left(\frac{(2\ell)! \varepsilon}{U^{(2\ell)}(\zeta)}\right)^{1/2\ell} \Gamma\left(\frac{1}{2\ell}\right). \end{aligned}$$

The resulting mean first passage time is given by

$$\begin{aligned} \tau_\varepsilon(\Omega) &= \frac{N_\varepsilon(\Omega)}{F_\varepsilon(\Omega)} \\ &\sim \frac{((2\ell)!)^{1/2\ell} \Gamma\left(\frac{1}{2\ell}\right) \Gamma\left(\frac{1}{n+1}\right)}{(n+1)^{\frac{n}{n+1}} \sigma(\zeta)} \frac{\varepsilon^{1/2\ell+1/(n+1)-1}}{\left[U^{(2\ell)}(\zeta)\right]^{1/2\ell} \left[U^{(n+1)}(\alpha)\right]^{1/(n+1)}} \\ &\quad \times \exp\left\{\frac{U(\alpha) - U(\zeta)}{\varepsilon}\right\}. \end{aligned}$$

In the typical case of $n = \ell = 1$ this reduces to

$$\tau_\varepsilon(\Omega) \sim \frac{\pi}{\omega_W \omega_B} e^{\Delta E/\varepsilon},$$

where the frequency at the bottom of the well and the imaginary frequency at the top of the potential barrier are given, respectively, by $\omega_W^2 = U''(\zeta)$ and $\omega_B^2 = -U''(\alpha)$. This gives the arrival rate from the domain Ω to the boundary, because

$$\kappa_\varepsilon(\Omega) = \tau_\varepsilon^{-1}(\Omega) = \frac{\omega_W \omega_B}{\pi} e^{-\Delta E/\varepsilon}. \quad (2.81)$$

Note that κ_ε is not the *escape rate* from the potential well, but rather the rate at which trajectories reach the top of the barrier. The top of the barrier (the transition state) is to leading order the stochastic separatrix; that is, only 50% of the trajectories that reach the transition state return to the well before escaping into the next well or into the continuum outside. Thus the *mean escape time*, denoted $\bar{\tau}_{\text{escape}}$, is twice the mean first passage time $\bar{\tau}_\varepsilon(\Omega)$; that is, the mean escape time is

$$\bar{\tau}_{\text{escape}} = 2\bar{\tau}_\varepsilon(\Omega) = \frac{2\pi}{\omega_W \omega_B} e^{\Delta E/\varepsilon}$$

and the escape rate, denoted κ_{escape} , is given by

$$\kappa_{\text{escape}} = \frac{1}{2} \kappa_\varepsilon(\Omega). \quad (2.82)$$

Note that all variables in the above analysis are dimensionless. In physical units the Arrhenius chemical reaction rate in the overdamped regime is given by

$$\kappa_{\text{Arrhenius}} = \frac{1}{2} \kappa_\varepsilon(\Omega) = \frac{\omega_W \omega_B}{2\pi\gamma} e^{-\Delta E/\varepsilon}, \quad (2.83)$$

where ω_W and ω_B have the dimension of frequency. The expression (2.83) was first derived by Kramers in 1940 [Kramers (1940)], [Chandrasekhar (1943)] for a model of a chemical reaction (e.g., dissociation) as overdamped diffusion over a potential barrier (the so-called *thermal activation*) [Schuss (2010b)].

2.6.6 The Second Eigenvalue of the Fokker–Planck Operator

If the potential $U(x)$ forms a single well in the interval $[\alpha, \beta]$, the exit time from the interval is exponentially large as a function of $1/\varepsilon$. It follows from (2.41) that the principal (the smallest) eigenvalue of the Fokker–Planck operator in the interval with absorbing boundary conditions is exponentially small. If the potential forms a sequence of wells in the interval, there may be several exponentially decaying eigenvalues for $\varepsilon \ll 1$. In particular, it can be shown [Schuss (1980b)] that the second eigenvalue has the form $\lambda_2 \sim D_2 e^{-\Delta E_2/\varepsilon}$, where ΔE_2 is the height of the highest barrier a trajectory has to cross in order to reach the bottom of the deepest well in the interval. The coefficient D_2 can be expressed in terms of the second derivatives of U at its points of local minimum and local maximum.

Exercise 2.12 (The second eigenfunction). Use the method of Exercise 2.11 to construct an asymptotic expansion of the first and second eigenfunctions of the Fokker–Planck operator with homogeneous (absorbing) boundary conditions when the potential forms multiple wells (see [Schuss (1980b)]). \square

2.7 A Diffusion Model of Random Signals

The phenomenology of loss of lock in tracking random signals is described here for the one-dimensional case (see Sect. 2.8 below). This section is developed further in Sect. 3.5 as an illustration of the asymptotic method in higher dimensions.

In filtering theory [Schuss (2012)] the signal statistics are often modeled as those of a diffusion process defined by a system of stochastic differential equations of the form

$$dx(t) = \mathbf{m}(x(t), t) dt + \sigma(x(t), t) dw(t). \quad (2.84)$$

The units of the components of $x(t)$ depend on the type of the signal. It can be volts, radians, hertz, meters (on the oscilloscope screen), and so on. Keeping in mind that the units of the Brownian motion $w(t)$ are $\sqrt{\text{sec}}$, Eq. (2.84) defines the units of the coefficients in terms of the units of the signal and of the Brownian motion. We assume therefore throughout this example that all variables are dimensionless. The statistics of the trajectories of (2.84) represent those of the physical signals that are transmitted in a given channel, for example, the statistics of all voltages that the antennas of all FM radio stations around the globe emit, classical music, jazz, rock, news, political gobbledegook, commercials, and so on. Not all components of the signal are necessarily transmitted.

Before transmission, the signal usually undergoes modulation by the transmitter and is converted into the amplitude of a carrier wave (AM transmission), or into the phase or frequency of a transmitted wave (phase modulation or FM transmissions, respectively), or any other form of modulation. The modulated signal is the voltage (or voltages) on the transmitter's antenna. The modulation is a memoryless transformation of the signal.

For example, in *amplitude modulated* (AM) transmission on carrier frequency ω_0 (usually measured in kHz) the modulated signal on the transmitter's antenna is the voltage

$$h(x(t), t) = \sqrt{2}x(t) \sin \omega_0 t. \quad (2.85)$$

Usually, the original random signal is filtered before it is modulated by (2.85). This means that it is first fed into a linear or nonlinear system of differential equations and the output is modulated by (2.85). This means that the filtered signal is a component of the output of a system of differential equations of the form (2.84).

In *phase modulated* transmission with carrier frequency ω_0 (usually measured in MHz) the modulated signal on the antenna is the voltage

$$h(x(t), t) = \sqrt{2} \sin[\omega_0 t + \beta x(t)]. \quad (2.86)$$

For a signal with $\text{Var } x(t) = 1$, we call β the *modulation index*. In *frequency modulated* (FM) transmission on carrier frequency ω_0 (usually in the range 88 MHz–105 MHz), the signal $x(t)$ is converted into a frequency by the transformation

$$h(x(t), t) = \sqrt{2} \sin \left(\omega_0 t + d_f \int_0^t x(s) ds \right), \quad (2.87)$$

where the parameter d_f is called the *frequency deviation*. The modulation in (2.87) is not a memoryless transformation of $x(t)$, because the integral contains all the past trajectory of the signal up to time t . The modulation (2.87) can, however, be viewed as a memoryless transformation of the output of a system of the form (2.84) if we define the two-dimensional signal $x(t) = (x_1(t), x_2(t))^T$ as the output of the

stochastic differential equations

$$dx_1(t) = m(x_1(t), t) dt + \sigma(x_1(t), t) dw, \quad dx_2(t) = d_f x_1(t) dt, \quad (2.88)$$

and then (2.87) can be written as the memoryless transformation of $x(t)$

$$h(x(t), t) = \sqrt{2} \sin(\omega_0 t + x_2(t)). \quad (2.89)$$

The modulated signal can also have several components, that is, $h(x(t), t)$ can be a vector. Components of the modulated signal (not necessarily all of them) are sent to the transmitter and are picked up by the receiver in a usually noisy transmission channel. There are many sources of noise in a transmission channel. These may include Johnson noise in the electronic components, atmospheric noise, jamming, interchannel interference, and so on.

The noisy output of the receiver's antenna, denoted $y(t)$, is usually modeled as the sum of the transmitted signal and the acquired noise; that is, the received signal can be written as the output of the stochastic differential equations

$$dy(t) = h(x(t), t) dt + \rho d\nu, \quad (2.90)$$

where $\nu(t)$ is a vector of independent standard Brownian motions, independent of $w(t)$, and ρ is the noise matrix. Usually ρ is assumed independent of $x(t)$, because otherwise the signal can be detected from the variance of the measurement noise $\rho \dot{\nu}$. Using white noise as a carrier is not an efficient method of modulation. However, ρ can be a function of t or even of $y(t)$ and t . We denote by y_0^t the trajectory of the measurements up to time t . All the information about the signal available at time t is contained in y_0^t .

Often, the measurement noise is assumed small, after appropriate scaling of the model. The assumption of small noise is often valid, because if the noise is not small, one may as well decide on the value of the signal by flipping a coin. When the measurement noise is small and the signal is linear, the system (2.84), (2.90), can be reduced to a standard form.

Thus, if $\|\rho\| \ll \|\sigma(x(t), t)\|$ and $\|\rho\sigma(x(t), t)\| \ll 1$ (e.g., in the maximum norm), and (2.84) is linear, the problem of estimating $x(t)$ with an observation process $y(t) \in \mathbb{R}^2$ that satisfies (2.90), can be reduced to the standard form

$$\dot{x} = Ax + \varepsilon B \dot{w}, \quad x(0) = x_0, \quad (2.91)$$

$$\dot{y} = h(x) + \varepsilon \dot{v}, \quad y(0) = 0, \quad (2.92)$$

where $\varepsilon \ll 1$.

The trackers of phase, frequency, angle, range, and other parameters are notorious for their tendency to lose their lock on the tracked signal. Phase is usually defined mod 2π , so a noise-induced jump of 2π in the tracked phase, a so-called cycle slip, causes only a short-lived disturbance (see Fig. 3.1). If cycle slips occur frequently, as

is the case in phase-locked loops for tracking FM signals, the signal is lost altogether and a sharp degradation in the tracking-loop performance ensues. In range or angle tracking (radar), once the tracking error exceeds a certain threshold, the lock detector indicates that the target is lost and has to be reacquired. In certain synchronization systems (e.g. cellular telephones) losses of lock are catastrophic and have to be made rare. Therefore the mean time between losses of lock is an important performance criterion for trackers. In this chapter the phenomenon of loss of lock is investigated in one- and two-dimensional trackers and an asymptotic method is developed for the calculation of the mean time to lose lock as a function of the tracking-loop parameters. This method can be generalized in a straightforward manner to higher-order phase trackers.

2.8 Loss of Lock in a First-Order Phase-Locked Loop in Phase-Modulated Radio Signals

The phase estimation error $e = x(t) - \tilde{x}_0(t)$ of the phase tracker (see [Schuss (2012)])

$$d\tilde{x}_0 = -m\tilde{x}_0 dt + \frac{\sigma}{\rho} [\cos \beta \tilde{x}_0 dy_1 - \sin \beta \tilde{x}_0 dy_2] \quad (2.93)$$

satisfies the stochastic differential equation

$$de = -(K\varepsilon e + \sin e) dt + \sqrt{2\varepsilon} dw_1, \quad (2.94)$$

which can be interpreted as the equation of motion of an overdamped Brownian particle in the potential field

$$U(e) = \frac{K\varepsilon e^2}{2} - \cos e. \quad (2.95)$$

Figure 2.6 shows the potential $U(e) = 0.01e^2 - \cos e$. The local minima at A, B, C are stable equilibria of the noiseless dynamics $\dot{e} = -U'(e)$, and the local maxima D, E are unstable equilibria.

Thus the error Eq. (2.94) can be written as

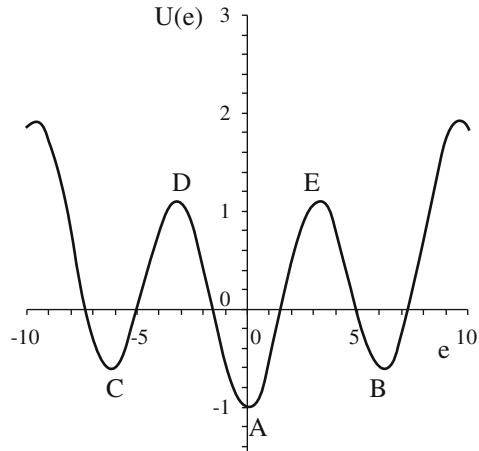
$$de = -U'(e) dt + \sqrt{2\varepsilon} dw_1. \quad (2.96)$$

When the noise is small, the error $e(t)$ stays for long periods of time near the stable equilibrium point A , where $e = 0$. The noise, however, regardless of how small, will eventually drive the error over the potential barrier at D or E , and $e(t)$ will end up near another locally stable equilibrium at B or C . It will then spend a long period of time in the potential well near B or C and will then be pushed by the noise over a potential barrier either back into the well near A or into the next potential well. The

tracker $x_0(t)$ is said to be locked on the true phase $x(t)$ as long as the tracking error stays near A . A noise-induced transition into a neighboring well is called *loss of lock* or *cycle slip*. The escape from a well, when it occurs, is quite rapid in the sense that the mean last passage time from A to B is about the same as the relaxation time of the noiseless system $\dot{e} = -U'(e)$, which is much shorter than the mean first exit time of $e(t)$ from the well at A .

The mean time between consecutive losses of lock is an important performance and design parameter of trackers. The mean time to lose lock of the tracker (2.93) is the mean time for $e(t)$ to go from A to B or C . This mean time is twice the mean time to reach either D or E , because only 50% of the trajectories that reach the top of the barrier, at E , say, reach B before they reach A . Thus the mean time to lose lock is twice the mean first passage time from A to D or to E . The mean time to lose lock is calculated by the method of matched asymptotics, as described above (see [Schuss (2012)]). Loss of lock in higher-order loops is studied in Sect. 3.5 below.

Fig. 2.6 The potential $U(e) = 0.01e^2 - \cos e$. The local minima at A, B, C are stable equilibria of the noiseless dynamics $\dot{e} = -U'(e)$, and the local maxima D, E are unstable equilibria



2.9 Annotations

Textbooks on asymptotic methods that can be consulted include [Olver (1974)], [O’Malley (1991)], [Kevorkian and Cole (1985)], [Bender (1978)], [O’Malley (1991)], [Holmes (2013)], and [Zauderer (1989)]. The examples and applications appear in [Schuss (1980b)], [Matkowsky and Schuss (1981)], [Schuss and Matkowsky (1979)], [Schuss (1980b)], [Matkowsky and Schuss (1981)], and [Schuss (2012)].

Chapter 3

Singular Perturbations in Higher Dimensions

3.1 Introduction

This chapter introduces the class of singular perturbation problems in elliptic and parabolic equations and their origin in stochastic differential equations. Concepts such as transition probability density function, first passage times of stochastic trajectories and their conditional moments, probability flux density, drift field, diffusion tensor, and so on, are defined and the boundary value problems they satisfy are described. Consider the boundary value problem (1.10), (1.11) of Chap. 1, which we write as

$$L_y u_\varepsilon(y) = 0 \text{ for } y \in \Omega, \quad u_\varepsilon(y) = g(y) \text{ for } y \in \partial\Omega, \quad (3.1)$$

and its adjoint problem

$$L_x^* u_\varepsilon(x) = 0 \text{ for } x \in \Omega, \quad u_\varepsilon(x) = g(x) \text{ for } y \in \partial\Omega, \quad (3.2)$$

which correspond to the Fokker–Planck equation and backward Kolmogorov equation for the stochastic system

$$dx = a(x) dt + \sqrt{2\varepsilon} B(x) dw(t), \quad x(0) = x, \quad (3.3)$$

in a domain Ω in \mathbf{R}^d , for flows $a(x)$ that cross the boundary $\partial\Omega$ of the domain.

As in the one-dimensional case, we consider an autonomous dynamical system driven by small noise and assume that the noiseless dynamics has a global attractor in a given domain. The boundary value problems (3.1) and (3.2) determine the mean first passage time and the exit distribution of the random trajectories on the boundary $\partial\Omega$ of the domain Ω . The small parameter ε makes this question into a singularly perturbed elliptic boundary value problems in Ω . Their solutions are based on the construction of a uniform asymptotic approximation to the solution of the stationary

Fokker–Planck equation (3.1) with a source in the domain and absorption on its boundary.

As mentioned above, we assume that the noiseless dynamics

$$\dot{\mathbf{x}} = \mathbf{a}(\mathbf{x}) \quad (3.4)$$

has a unique critical point \mathbf{x}_0 in Ω and that it is a global attractor. This means that $\mathbf{a}(\mathbf{x}_0) = \mathbf{0}$ and we assume that the eigenvalues of the matrix

$$\mathbf{A} = \left\{ \frac{\partial a^i(\mathbf{x}_0)}{\partial x^j} \right\}_{i,j=1}^d \quad (3.5)$$

of the linearized system $\dot{\mathbf{z}} = \mathbf{A}\mathbf{z}$ have negative real parts. Thus the trajectories of the system (3.4) that start in Ω cannot reach $\partial\Omega$. The case of other attractors, such as limit cycles, is considered separately. We distinguish between the case when the flow on $\partial\Omega$ points into Ω , and the case when its normal component vanishes on $\partial\Omega$. In the former case the boundary is called *noncharacteristic* and in the latter case it is *characteristic*. Denoting by $\mathbf{n}(\mathbf{x})$ the unit outer normal at the boundary, we distinguish between the two cases according to the inequalities

$$\mathbf{a}(\mathbf{x}) \cdot \mathbf{n}(\mathbf{x}) < 0 \text{ for } \mathbf{x} \in \partial\Omega, \quad (3.6)$$

if $\partial\Omega$ is noncharacteristic, and

$$\mathbf{a}(\mathbf{x}) \cdot \mathbf{n}(\mathbf{x}) = 0 \text{ for } \mathbf{x} \in \partial\Omega, \quad (3.7)$$

if $\partial\Omega$ is characteristic.

The Fokker–Planck equation (3.1) for the stationary probability density function $p_\varepsilon(\mathbf{y} | \mathbf{x})$ of the solution $\mathbf{x}(t, \varepsilon)$ of (3.3) with a source at \mathbf{x} , and absorption in $\partial\Omega$, is

$$\begin{aligned} & - \sum_{i=1}^d \frac{\partial [a^i(\mathbf{y}) p_\varepsilon(\mathbf{y} | \mathbf{x})]}{\partial y^i} + \sum_{i,j=1}^d \varepsilon \frac{\partial^2 [\sigma^{i,j}(\mathbf{y}) p_\varepsilon(\mathbf{y} | \mathbf{x})]}{\partial y^i \partial y^j} \\ & = - \delta(\mathbf{y} - \mathbf{x}), \end{aligned} \quad (3.8)$$

where $\boldsymbol{\sigma}(\mathbf{y}) = \mathbf{B}(\mathbf{y}) \mathbf{B}^T(\mathbf{y})$. The Fokker–Planck equation (3.8) can also be written as the conservation law

$$\begin{aligned} \nabla_{\mathbf{y}} \cdot \mathbf{J}(\mathbf{y} | \mathbf{x}) &= \delta(\mathbf{y} - \mathbf{x}) \\ J^i(\mathbf{y} | \mathbf{x}) &= a^i(\mathbf{y}) p_\varepsilon(\mathbf{y} | \mathbf{x}) - \varepsilon \sum_{j=1}^d \frac{\partial [\sigma^{i,j}(\mathbf{y}) p_\varepsilon(\mathbf{y} | \mathbf{x})]}{\partial y^j}. \end{aligned} \quad (3.9)$$

The function $p_\varepsilon(y | x)$ satisfies the absorbing boundary condition

$$p_\varepsilon(y | x) = 0 \text{ for } y \in \partial\Omega, x \in \Omega. \quad (3.10)$$

It was shown in Chap. 1 that the exit density at a point y on the boundary of the trajectories of (3.3) that start at a point $x \in \Omega$ is given by

$$\Pr \{x(\tau) \in y + dS_y | x(0) = x\} = \frac{\mathbf{J}(y | x) \cdot \mathbf{n}(y) dS_y}{\oint_{\partial\Omega} \mathbf{J}(y | x) \cdot \mathbf{n}(y) dS_y}, \quad (3.11)$$

and the mean first passage time to the boundary is given by

$$\bar{\tau}_\varepsilon(x) = \frac{\int_{\Omega} p_\varepsilon(y | x) dy}{\oint_{\partial\Omega} \mathbf{J}(y | x) \cdot \mathbf{n}(y) dS_y}. \quad (3.12)$$

Thus a uniform approximation to $p_\varepsilon(y | x)$ provides a full solution to the exit problem through Eqs. (1.24) and (3.12).

3.2 The WKB Method

As in the one-dimensional case, as $\varepsilon \rightarrow 0$ the function $p_\varepsilon(y | x)$ develops singularities in the domain and on its boundary. These singularities are resolved by constructing an approximate solution that contains all the singularities of $p_\varepsilon(y | x)$, as done in the one-dimensional case.

First, the Fokker–Planck equation (3.1) is transformed by assuming a solution in the WKB form [Naeh et al. (1990)]

$$p_\varepsilon(y | x) = K_\varepsilon(y | x) \exp \left\{ -\frac{\psi(y)}{\varepsilon} \right\} \quad (3.13)$$

with unknown functions $K_\varepsilon(y | x)$ and $\psi(y)$. The essential singularity of $p_\varepsilon(y | x)$ inside Ω is captured by the exponential term in (3.13) and that on $\partial\Omega$ by the pre-exponential factor $K_\varepsilon(y | x)$. Substituting (3.13) into (3.1) and collecting like powers of ε , we obtain at the leading order the first-order eikonal equation

$$\sum_{i,j=1}^d \sigma^{i,j}(y) \frac{\partial \psi(y)}{\partial y^i} \frac{\partial \psi(y)}{\partial y^j} + \sum_{i=1}^d a^i(y) \frac{\partial \psi(y)}{\partial y^i} = 0, \quad (3.14)$$

which has the form of a Hamilton–Jacobi equation and is solved by the method of characteristics [Courant and Hilbert (1989)], [Sneddon (1966)], or by optimizing

an appropriate action functional, as done in large deviations theory (see, e.g., [Freidlin and Wentzell (1984)], [Freidlin (1985)], [Ellis (1985)], [Deuschel and Stroock (1989)], [Dembo and Zeitouni (1993)]).

The function $K_\varepsilon(\mathbf{y} | \mathbf{x})$ is a regular function of ε for \mathbf{x} and \mathbf{y} in the domain and develops singularities at $\partial\Omega$ in the limit $\varepsilon \rightarrow 0$. The boundary condition (3.10) implies the boundary condition

$$K_\varepsilon(\mathbf{y} | \mathbf{x}) = 0 \quad \text{for } \mathbf{y} \in \partial\Omega, \mathbf{x} \in \Omega. \quad (3.15)$$

Next, to resolve these singularities, we decompose the function $K_\varepsilon(\mathbf{y} | \mathbf{x})$ further into the product

$$K_\varepsilon(\mathbf{y} | \mathbf{x}) = [K_0(\mathbf{y} | \mathbf{x}) + \varepsilon K_1(\mathbf{y} | \mathbf{x}) + \dots] q_\varepsilon(\mathbf{y} | \mathbf{x}), \quad (3.16)$$

where $K_0(\mathbf{y} | \mathbf{x})$, $K_1(\mathbf{y} | \mathbf{x})$, ... are regular functions in Ω and on its boundary and are independent of ε , and $q_\varepsilon(\mathbf{y} | \mathbf{x})$ is a boundary layer function. The functions $K_j(\mathbf{y} | \mathbf{x})$ ($j = 0, 1, \dots$) satisfy first-order partial differential equations and therefore cannot satisfy the boundary condition (3.15). The boundary layer function $q_\varepsilon(\mathbf{y} | \mathbf{x})$ satisfies the boundary condition

$$q_\varepsilon(\mathbf{y} | \mathbf{x}) = 0 \quad \text{for } \mathbf{y} \in \partial\Omega, \mathbf{x} \in \Omega, \quad (3.17)$$

the matching condition

$$\lim_{\varepsilon \rightarrow 0} q_\varepsilon(\mathbf{y} | \mathbf{x}) = 1 \quad \text{for all } \mathbf{x}, \mathbf{y} \in \Omega, \mathbf{x} \neq \mathbf{y}, \quad (3.18)$$

and the smoothness condition

$$\lim_{\varepsilon \rightarrow 0} \frac{\partial^i q_\varepsilon(\mathbf{y} | \mathbf{x})}{\partial(\mathbf{y}^j)^i} = 0, \quad \text{for all } \mathbf{x}, \mathbf{y} \in \Omega, \mathbf{x} \neq \mathbf{y}, i \geq 1, 1 \leq j \leq d. \quad (3.19)$$

The function $K_\varepsilon(\mathbf{y} | \mathbf{x})$ satisfies the *transport equation*

$$\begin{aligned} & \varepsilon \sum_{i,j=1}^d \frac{\partial^2 \sigma^{i,j}(\mathbf{y}) K_\varepsilon(\mathbf{y} | \mathbf{x})}{\partial \mathbf{y}^i \partial \mathbf{y}^j} \\ & - \sum_{i=1}^d \left(2 \sum_{j=1}^d \sigma^{i,j}(\mathbf{y}) \frac{\partial \psi(\mathbf{y})}{\partial \mathbf{y}^j} + a^i(\mathbf{y}) \right) \frac{\partial K_\varepsilon(\mathbf{y} | \mathbf{x})}{\partial \mathbf{y}^i} \\ & - \sum_{i=1}^d \left(\frac{\partial a^i(\mathbf{y})}{\partial \mathbf{y}^i} + \sum_{j=1}^d \left(\sigma^{i,j}(\mathbf{y}) \frac{\partial^2 \psi(\mathbf{y})}{\partial \mathbf{y}^i \partial \mathbf{y}^j} + 2 \frac{\partial \sigma^{i,j}(\mathbf{y})}{\partial \mathbf{y}^j} \frac{\partial \psi(\mathbf{y})}{\partial \mathbf{y}^j} \right) \right) K_\varepsilon(\mathbf{y} | \mathbf{x}) \\ & = -\delta(\mathbf{y} - \mathbf{x}). \end{aligned}$$

The equation for $q_\varepsilon(\mathbf{y} | \mathbf{x})$ is derived and studied in Sect. 3.2.2 below.

3.2.1 The Eikonal Equation

The eikonal function $\psi(\mathbf{y})$ in (3.13) can be constructed by solving the eikonal equation

$$\sum_{i,j=1}^d \sigma^{i,j}(\mathbf{y}) \frac{\partial \psi(\mathbf{y})}{\partial y^i} \frac{\partial \psi(\mathbf{y})}{\partial y^j} + \sum_{i=1}^d a^i(\mathbf{y}) \frac{\partial \psi(\mathbf{y})}{\partial y^i} = 0 \quad (3.20)$$

by the method of characteristics [Courant and Hilbert (1989)], [Sneddon (1966)]. In this method, a first-order partial differential equation of the form

$$F(\mathbf{x}, \psi, \mathbf{p}) = 0, \quad (3.21)$$

with $\mathbf{p} = \nabla \psi(\mathbf{x})$, is converted into a system of ordinary differential equations as follows,

$$\begin{aligned} \frac{d\mathbf{x}}{ds} &= \nabla_{\mathbf{p}} F \\ \frac{d\mathbf{p}}{ds} &= - \left(\frac{\partial F}{\partial \psi} \mathbf{p} + \nabla_{\mathbf{x}} F \right) \\ \frac{d\psi}{ds} &= \mathbf{p} \cdot \nabla_{\mathbf{p}} F. \end{aligned} \quad (3.22)$$

The function $\psi(\mathbf{x})$ is defined by the third equation at each point \mathbf{x} of the trajectory of the first equation. There is a neighborhood of the initial conditions (see below) that is covered by trajectories.

In the case at hand the function $F(\mathbf{x}, \psi, \mathbf{p})$ in the eikonal equation (3.20) has the form

$$F(\mathbf{x}, \psi, \mathbf{p}) = \sum_{i,j=1}^d \sigma^{i,j}(\mathbf{x}) p^i p^j + \sum_{i=1}^d a^i(\mathbf{x}) p^i,$$

so that the characteristic equations (3.22) are

$$\frac{d\mathbf{x}}{ds} = 2\sigma(\mathbf{x})\mathbf{p} + \mathbf{a}(\mathbf{x}) \quad (3.23)$$

$$\frac{d\mathbf{p}}{ds} = - \nabla_{\mathbf{x}} \mathbf{p}^T \sigma(\mathbf{x}) \mathbf{p} - \nabla_{\mathbf{x}} \mathbf{a}^T(\mathbf{x}) \mathbf{p} \quad (3.24)$$

$$\frac{d\psi}{ds} = \mathbf{p}^T \sigma(\mathbf{x}) \mathbf{p}. \quad (3.25)$$

The eikonal equation (3.20) is used in deriving the characteristic equation (3.25).

Note that the trajectories of the autonomous system (3.23), (3.24), which begin near the attractor $(\mathbf{x}_0, \mathbf{0})$, diverge. To see this, we linearize the system (3.23), (3.24)

around this point to obtain $z'(s) = 2\sigma(x_0)p(s) + Az(s)$ and $\pi'(s) = -a\pi(s)$, where A is defined in (3.5). It follows that $\pi(s) = e^{-As}\pi_0$, hence

$$z(s) = e^{As}z_0 + 2 \int_0^s e^{A(s-u)}\sigma(x_0)e^{-Au}\pi_0 du.$$

Both $z(s)$ and $\pi(s)$ diverge as $s \rightarrow \infty$, because the eigenvalues of $-A$ have positive real parts.

To integrate the characteristic equations (3.23) and (3.24), initial conditions can be imposed near the attractor $(x_0, \mathbf{0})$ by constructing $\psi(x)$ in the form of a power series. The truncation of the power series near the attractor provides an approximation to $\psi(x)$ and to $p = \nabla\psi(x)$, whose error can be made arbitrarily small. Expanding $\psi(x)$, $a(x)$, and $\sigma(x)$ in powers of $z = x - x_0$, we find from the eikonal equation (3.20) that $\nabla\psi(x_0) = 0$ so that the power series expansion of $\psi(x)$ begins as a quadratic form

$$\psi(x) = \frac{1}{2}x^T Q x + o(|x|^2), \quad (3.26)$$

and Q is the solution of the Riccati equation

$$2Q\sigma(x_0)Q + QA + A^T Q = \mathbf{0}. \quad (3.27)$$

Obviously, the first term in the power series expansion of $p = \nabla\psi(x)$ is given by

$$p = Qx + O(|x|^2). \quad (3.28)$$

In deriving (3.27) use is made of the facts that Q and σ are symmetric matrices and that a quadratic form vanishes identically if and only if it is defined by an anti-symmetric matrix [Schuss (1980b)]. The solution Q of (3.27) is a positive definite matrix [Schuss (1980b)], [Gantmacher (1998)].

Exercise 3.1 (Square root of a positive definite symmetric matrix). Show that a positive definite symmetric matrix has a positive definite symmetric square root. \square

Exercise 3.2 (The Riccati equation). Reduce the Riccati equation (3.27) to

$$AY + Y^T A^T = -I \quad (3.29)$$

by the substitutions $X = Q\sqrt{\sigma}$, where X is the solution of

$$2XX^T + XA + A^TX^T = \mathbf{0}$$

and $X = -\frac{1}{2}Y^{-1}$. Show that the solution of (3.29) is a symmetric matrix, given by $Y = \int_0^\infty e^{At}e^{A^Tt} dt$, and show that the integral converges. \square

Taking the contour

$$\frac{1}{2} \mathbf{x}^T \mathbf{Q} \mathbf{x} = \delta, \quad (3.30)$$

for some small positive δ , as the initial surface for the system (3.23)–(3.25) and using the approximate initial values $\psi(\mathbf{x}) = \delta$ and (3.28) at each point of the surface, we can integrate the system (3.23)–(3.25) analytically or numerically. Once the domain Ω is covered with characteristics, the approximate value of $\psi(\mathbf{x})$ can be determined at each point $\mathbf{x} \in \Omega$ as the value of the solution $\psi(s)$ of (3.25) at s such that the solution of (3.23) satisfies

$$\mathbf{x}(s) = \mathbf{x}. \quad (3.31)$$

The initial condition on the surface (3.30) determines the unique trajectory of the system (3.23)–(3.25) that satisfies (3.31) for some s . It can be found numerically by the method of shooting.

3.2.2 The Transport Equation

As mentioned in Sect. 3.2, the function $K_\varepsilon(\mathbf{y} | \mathbf{x})$ satisfies the transport equation

$$\begin{aligned} & \varepsilon \sum_{i,j=1}^d \frac{\partial^2 \sigma^{i,j}(\mathbf{y}) K_\varepsilon(\mathbf{y} | \mathbf{x})}{\partial y^i \partial y^j} - \sum_{i=1}^d \left(2 \sum_{j=1}^d \sigma^{i,j}(\mathbf{y}) \frac{\partial \psi(\mathbf{y})}{\partial y^j} + a^i(\mathbf{y}) \right) \frac{\partial K_\varepsilon(\mathbf{y} | \mathbf{x})}{\partial y^i} \\ & - \sum_{i=1}^d \left(\frac{\partial a^i(\mathbf{y})}{\partial y^i} + \sum_{j=1}^d \left(\sigma^{i,j}(\mathbf{y}) \frac{\partial^2 \psi(\mathbf{y})}{\partial y^i \partial y^j} + 2 \frac{\partial \sigma^{i,j}(\mathbf{y})}{\partial y^j} \frac{\partial \psi(\mathbf{y})}{\partial y^j} \right) \right) K_\varepsilon(\mathbf{y} | \mathbf{x}) \\ & = -\delta(\mathbf{y} - \mathbf{x}). \end{aligned} \quad (3.32)$$

The function $K_\varepsilon(\mathbf{y} | \mathbf{x})$ cannot have an internal layer at the global attractor point \mathbf{x}_0 in Ω . This is due to the fact that stretching $\mathbf{y} - \mathbf{x}_0 = \sqrt{\varepsilon} \boldsymbol{\xi}$ and taking the limit $\varepsilon \rightarrow 0$ converts the transport equation (3.32) to

$$\begin{aligned} & \sum_{i,j=1}^d \frac{\partial^2 \sigma^{i,j}(\mathbf{x}_0) K_0(\boldsymbol{\xi} | \mathbf{x})}{\partial \xi^i \partial \xi^j} - (2\mathbf{A}\mathbf{Q} + \mathbf{A}\boldsymbol{\xi} \cdot \nabla_{\boldsymbol{\xi}} K_0(\boldsymbol{\xi} | \mathbf{x})) \\ & - \text{tr}(\mathbf{A} + \boldsymbol{\sigma}(\mathbf{x}_0)\mathbf{Q}) K_0(\boldsymbol{\xi} | \mathbf{x}) = 0, \end{aligned}$$

whose bounded solution is $K_0(\boldsymbol{\xi} | \mathbf{x}) = \text{const.}$, because $\text{tr}(\mathbf{A} + \boldsymbol{\sigma}(\mathbf{x}_0)\mathbf{Q}) = 0$. The last equality follows from the Riccati equation (3.27) (left multiply by \mathbf{Q}^{-1} and take the trace).

In view of Eqs. (3.16)–(3.19), we obtain in the limit $\varepsilon \rightarrow 0$ the transport equation

$$\begin{aligned} & \sum_{i=1}^d \left(2 \sum_{j=1}^d \sigma^{i,j}(\mathbf{y}) \frac{\partial \psi(\mathbf{y})}{\partial y^j} + a^i(\mathbf{y}) \right) \frac{\partial K_0(\mathbf{y} | \mathbf{x})}{\partial y^i} \\ &= - \sum_{i=1}^d \left(\frac{a^i(\mathbf{y})}{\partial y^i} + \sum_{j=1}^d \left(\sigma^{i,j}(\mathbf{y}) \frac{\partial^2 \psi(\mathbf{y})}{\partial y^i \partial y^j} + 2 \frac{\partial \sigma^{i,j}(\mathbf{y})}{\partial y^j} \frac{\partial \psi(\mathbf{y})}{\partial y^j} \right) \right) K_0(\mathbf{y} | \mathbf{x}). \end{aligned} \quad (3.33)$$

Because the characteristics diverge, the initial value (at $s = 0$) on each characteristic is given at $\mathbf{y} = \mathbf{x}_0$ as $K_0(\mathbf{x}_0 | \mathbf{x}) = \text{const.}$ (e.g., $\text{const.} = 1$). With this choice of the constant the function $p_\varepsilon(\mathbf{y} | \mathbf{x})$ has to be renormalized.

Exercise 3.3 (The potential case). Show that if the diffusion matrix σ is constant and $\mathbf{a}(\mathbf{x}) = -\sigma \nabla \phi(\mathbf{x})$ for some function $\phi(\mathbf{x})$, then $\psi(\mathbf{x}) = \phi(\mathbf{x})$ and the WKB solution of the homogeneous Fokker–Planck equation (3.8) is given by $p_\varepsilon(\mathbf{y}) = e^{-\psi(\mathbf{y})/\varepsilon}$; that is, the solution of the transport equation (3.32) is $K_0 = \text{const.}$ \square

3.2.3 The Characteristic Equations

The transport equation has to be integrated numerically, together with the characteristic equations (3.23) and (3.24). To evaluate the partial derivatives $\partial^2 \psi(\mathbf{y}) / \partial y^i \partial y^j$ along the characteristics, we use Eqs. (3.26), (3.28), and $\partial^2 \psi(\mathbf{y}) / \partial y^i \partial y^j|_{\mathbf{y}=\mathbf{x}_0} = Q^{i,j}$ on the initial ellipsoid (3.30). The differential equations for $\partial^2 \psi(\mathbf{y}) / \partial y^i \partial y^j$ along the characteristics are derived by differentiating the characteristic equations (3.23) and (3.24) with respect to the initial values $\mathbf{x}(0) = \mathbf{x}_0$. Writing

$$\mathbf{x}_j(s) = \frac{\partial \mathbf{x}(s)}{\partial x_0^j}, \quad \mathbf{p}_j(s) = \frac{\partial \mathbf{p}(s)}{\partial x_0^j}, \quad Q^{i,j}(s) = \frac{\partial^2 \psi(\mathbf{x}(s))}{\partial y^i \partial y^j}, \quad (3.34)$$

we get the identity $\mathbf{p}_j(s) = \mathbf{Q}(s)\mathbf{x}_j(s)$. The initial conditions are

$$x_j^i(0) = \delta_{i,j} \quad (3.35)$$

$$p_j^i(0) = \left. \frac{\partial^2 \psi(\mathbf{y})}{\partial y^i \partial y^j} \right|_{\mathbf{y}=\mathbf{x}_0} = Q^{i,j}(0) = Q^{i,j} \quad (3.36)$$

and the dynamics is given by

$$\frac{d\mathbf{x}_j(s)}{ds} = \sum_{k=1}^d \left[2 \frac{\partial}{\partial x^k} \sigma(\mathbf{x}(s)) \mathbf{p}(s) + 2 \sigma(\mathbf{x}(s)) \mathbf{p}_k(s) + \frac{\partial}{\partial x^k} \mathbf{a}(\mathbf{x}(s)) \right] x_k^j(s) \quad (3.37)$$

$$\begin{aligned} \frac{d\mathbf{p}_j(s)}{ds} = & - \sum_{k=1}^d \left[\nabla_{\mathbf{x}} \mathbf{p}^T(s) \frac{\partial}{\partial x^k} \boldsymbol{\sigma}(\mathbf{x}(s)) \mathbf{p}(s) + 2 \nabla_{\mathbf{x}} \mathbf{p}_k^T(s) \boldsymbol{\sigma}(\mathbf{x}(s)) \mathbf{p}(s) \right. \\ & \left. + \nabla_{\mathbf{x}} \mathbf{a}^T(\mathbf{x}(s)) \mathbf{p}_k(s) + \frac{\partial}{\partial x^k} \nabla_{\mathbf{x}} \mathbf{a}^T(\mathbf{x}(s)) \mathbf{p}(s) \right] x_k^j(s). \end{aligned} \quad (3.38)$$

The transport equation (3.33) can be written on characteristics as

$$\begin{aligned} & \frac{dK_0(\mathbf{x}(s) | \mathbf{x})}{ds} \\ &= - \sum_{i=1}^d \left[\frac{a^i(\mathbf{x}(s))}{\partial y^i} + \sum_{j=1}^d \left(\sigma^{i,j}(\mathbf{x}(s)) Q^{i,j}(s) + 2 \frac{\partial \sigma^{i,j}(\mathbf{x}(s))}{\partial y^j} \mathbf{p}(s) \right) \right] \\ & \quad \times K_0(\mathbf{x}(s) | \mathbf{x}). \end{aligned} \quad (3.39)$$

In summary, the numerical integration of the eikonal and the transport equations consists in integrating numerically the differential equations (3.23)–(3.25), (3.37)–(3.39) with initial values of $\mathbf{x}_0 = \mathbf{x}(0)$ that cover the ellipsoid (3.30), with $\mathbf{p}(0)$ and $\psi(\mathbf{x}(0))$ given by $\mathbf{p}(0) = \mathbf{Q}\mathbf{x}(0)$ and $\psi(\mathbf{x}(0)) = \delta$, and the initial values (3.35), (3.36), and $K_0(\mathbf{x}(0) | \mathbf{x}) = 1$. Equations (3.34) have to be solved at each step of the integration to convert from $\mathbf{p}_j(s)$ to $\mathbf{Q}(s)$. Specific applications in communications theory are given in Sect. 3.5 below.

3.2.4 Boundary Layers at Non-characteristic Boundaries

Although the functions $K_j(\mathbf{x}(0) | \mathbf{x})$ in the expansion (3.16) are regular in the domain Ω and on its boundary, the boundary layer function $q_\varepsilon(\mathbf{y} | \mathbf{x})$ has an essential singularity at the boundary. Its normal derivatives at the boundary become infinite as $\varepsilon \rightarrow 0$ and its derivatives in the direction of the boundary vanish, because $q_\varepsilon(\mathbf{y} | \mathbf{x})$ vanishes there. Furthermore, the higher-order normal derivatives of $q_\varepsilon(\mathbf{y} | \mathbf{x})$ at the boundary are larger than the lower-order derivatives. More specifically, we postulate that for $\mathbf{y} \in \partial\Omega$, $\mathbf{x} \in \Omega$

$$\frac{\partial^k q_\varepsilon(\mathbf{y} | \mathbf{x})}{\partial \mathbf{n}_{\mathbf{y}}^k} = O(\varepsilon^{-k}) \quad \text{for } k = 0, 1, 2, \dots. \quad (3.40)$$

Keeping this in mind, we retain in (3.32) the second order partial derivatives of $q_\varepsilon(\mathbf{y} | \mathbf{x})$ and balance them with the first-order terms. The singularity of $q_\varepsilon(\mathbf{y} | \mathbf{x})$ is resolved by balancing near the boundary terms of similar orders of magnitude in (3.32).

To derive the boundary layer equation for $q_\varepsilon(\mathbf{y} | \mathbf{x})$, we introduced local coordinates near the boundary, $\rho(\mathbf{y}) = \text{dist}(\mathbf{y}, \partial\Omega)$ such that $\rho(\mathbf{y}) < 0$ for $\mathbf{y} \in \Omega$ and $d - 1$

coordinates in the boundary $s(\mathbf{y}) = (s_1, s_2, \dots, s_{d-1})$. In the transformation $\mathbf{y} \rightarrow (\rho(\mathbf{y}), s(\mathbf{y}))$, the point $\mathbf{y}' = (0, s(\mathbf{y}))$ is the orthogonal projection of \mathbf{y} on $\partial\Omega$. The boundary is mapped into the hyper-plane $\rho = 0$. Then $\nabla\rho(\mathbf{y})|_{\rho=0} = \mathbf{n}(\mathbf{y})$ for $\mathbf{y} \in \partial\Omega$, where $\mathbf{n}(\mathbf{y})$ is the unit outer normal to $\partial\Omega$ at \mathbf{y} .

Next, we introduce the stretched variable $\zeta = \rho/\varepsilon$, define $q_\varepsilon(\mathbf{y} | \mathbf{x}) = Q(\zeta, s, \varepsilon | \mathbf{x})$, and express the postulate (3.40) by assuming that the decomposition (3.16) becomes

$$K_\varepsilon(\mathbf{y} | \mathbf{x}) = [K_0(\rho, s | \mathbf{x}) + \varepsilon K_1(\rho, s | \mathbf{x}) + \dots] Q(\zeta, s, \varepsilon | \mathbf{x}).$$

Expanding all functions that appear in (3.13) in an asymptotic series in powers of ε and writing $Q(\zeta, s, \varepsilon | \mathbf{x}) \sim Q^0(\zeta, s | \mathbf{x}) + \varepsilon Q^1(\zeta, s | \mathbf{x}) + \dots$, we obtain for $Q^0(\zeta, s | \mathbf{x})$ the boundary layer equation

$$\left(\sum_{i,j=1}^d \sigma^{i,j}(\mathbf{y}') \nu^i(\mathbf{y}') \nu^j(\mathbf{y}') \right) \frac{\partial^2 Q^0}{\partial \zeta^2} - \left[\sum_{i=1}^d \left(2 \sum_{j=1}^d \sigma^{i,j}(\mathbf{y}') \frac{\partial \psi(\mathbf{y}')}{\partial y^j} + a^i(\mathbf{y}') \right) \nu^i(\mathbf{y}') \right] \frac{\partial Q^0}{\partial \zeta} = 0,$$

which we rewrite as $Q_{\zeta\zeta}^0 - A(s)Q_\zeta^0 = 0$, where

$$A(s) = \frac{\sum_{i=1}^d \left(2 \sum_{j=1}^d \sigma^{i,j}(\mathbf{y}') \frac{\partial \psi(\mathbf{y}')}{\partial y^j} + a^i(\mathbf{y}') \right) \nu^i(\mathbf{y}')}{\sum_{i,j=1}^d \sigma^{i,j}(\mathbf{y}') \nu^i(\mathbf{y}') \nu^j(\mathbf{y}')}. \quad (3.41)$$

The function $A(s)$ is positive on the boundary, because the denominator in (3.41) is a positive definite quadratic form and the numerator is the normal component of the direction of the characteristics at the boundary. Because the characteristics exit Ω , their direction at $\partial\Omega$ points away from Ω . This means that

$$\sum_{i=1}^d \left(2 \sum_{j=1}^d \sigma^{i,j}(\mathbf{y}') \frac{\partial \psi(\mathbf{y}')}{\partial y^j} + a^i(\mathbf{y}') \right) \nu^i(\mathbf{y}') > 0.$$

The boundary and matching conditions (3.17), (3.18) are expressed in the boundary layer function as $Q^0(0, s | \mathbf{x}) = 0$ and $\lim_{\zeta \rightarrow -\infty} Q^0(\zeta, s | \mathbf{x}) = 1$, so that the solution is

$$Q^0(\zeta, s | \mathbf{x}) = 1 - e^{A(s)\zeta}. \quad (3.42)$$

The uniform asymptotic expansion of the solution of the Fokker–Planck equation (3.8), valid up to the boundary $\partial\Omega$, is therefore given by

$$\begin{aligned} p_{\text{unif}}(\mathbf{y} | \mathbf{x}) &= [K_0(\mathbf{y} | \mathbf{x}) + O(\varepsilon)] \exp\left\{-\frac{\psi(\mathbf{y})}{\varepsilon}\right\} \\ &\times \left[1 - \exp\left\{\frac{A(\mathbf{s})\rho(\mathbf{y})}{\varepsilon}\right\}\right]. \end{aligned} \quad (3.43)$$

Equation (3.43) is a uniform approximation to $p(\mathbf{y} | \mathbf{x})$ for $\mathbf{x} \in \Omega$ outside the boundary layer, all $\mathbf{y} \in \Omega$, and $O(\varepsilon)$ is uniform for $\mathbf{x} \in \Omega$ outside the boundary layer and all $\mathbf{y} \in \Omega$.

To obtain a uniform approximation to $p(\mathbf{y} | \mathbf{x})$, valid for all $\mathbf{x}, \mathbf{y} \in \Omega$, we have to solve in Ω the equation

$$\varepsilon \sum_{i=1}^d \sum_{j=1}^d \sigma^{ij}(\mathbf{x}) \frac{\partial^2 p(\mathbf{y} | \mathbf{x})}{\partial x^i \partial x^j} + \sum_{i=1}^d a^i(\mathbf{x}) \frac{\partial p(\mathbf{y} | \mathbf{x})}{\partial x^i} = -\delta(\mathbf{y} - \mathbf{x}) \quad (3.44)$$

with the boundary condition

$$p(\mathbf{y} | \mathbf{x}) = 0 \text{ for } \mathbf{x} \in \partial\Omega, \mathbf{y} \in \Omega.$$

The analysis of this case is straightforward. The outer solution is a constant and the equation for the leading term $p^0(\zeta', s')$, in the boundary layer expansion in the variables (ζ', s') defined above, is

$$\sigma(s') \frac{\partial^2 p^0(\zeta', s')}{\partial \zeta'^2} + a_n(s') \frac{\partial p^0(\zeta', s')}{\partial \zeta'} = 0 \text{ for } \zeta' < 0, \quad (3.45)$$

where

$$\sigma(s') = \sum_{i,j=1}^d \sigma^{i,j}(0, s') \nu^i(s') \nu^j(s'), \quad a_n(s') = \sum_i a^i(0, s') \nu^i(s') < 0,$$

with the matching conditions

$$p^0(0, s') = 0, \quad \lim_{\zeta' \rightarrow -\infty} p^0(\zeta', s') = 1. \quad (3.46)$$

The solution is

$$p^0(\zeta', s') = 1 - e^{a_n(s')\zeta'/\sigma(s')}.$$

Now, the uniform approximation to $p(\mathbf{y} | \mathbf{x})$, valid for all $\mathbf{x}, \mathbf{y} \in \Omega$, can be written as

$$p_{\text{unif}}(\mathbf{y} | \mathbf{x}) = [K_0(\mathbf{y} | \mathbf{x}) + O(\varepsilon)] \exp\left\{-\frac{\psi(\mathbf{y})}{\varepsilon}\right\} \left[1 - \exp\left\{\frac{A(\mathbf{s})\rho(\mathbf{y})}{\varepsilon}\right\}\right] \\ \times \left[1 - \exp\left\{\frac{a_n(\mathbf{s}')\rho(\mathbf{x})}{\varepsilon\sigma(\mathbf{s}')}\right\}\right]. \quad (3.48)$$

3.2.5 Boundary Layers at Characteristic Boundaries in the Plane

We now assume that Ω is a bounded planar domain whose boundary $\partial\Omega$ consists of a finite number of piecewise smooth closed simple curves and write $x^1 = x$, $x^2 = y$ (i.e., $\mathbf{x} = (x, y)$). The boundary $\partial\Omega$ is characteristic if the drift vector $\mathbf{a}(x, y)$ is tangent to the boundary or vanishes there; that is, if (3.7) holds. In either case, the normal component of the drift vector $\mathbf{a}(\mathbf{x})$ vanishes at the boundary. At each point $(x, y) \in \Omega$, near the boundary, we denote by (x', y') its orthogonal projection on the boundary. We denote by $\mathbf{n}(x, y)$ and $\boldsymbol{\tau}(x, y)$ the unit outer normal and unit tangent at the boundary point $\mathbf{x}' = (x', y')$, respectively. The signed distance to the boundary is defined as

$$\begin{aligned} \rho(\mathbf{x}) &= -\text{dist}(\mathbf{x}, \partial\Omega) = -\sqrt{|\mathbf{x} - \mathbf{x}'|^2} \text{ for } \mathbf{x} \in \Omega \\ \rho(\mathbf{x}) &= \text{dist}(\mathbf{x}, \partial\Omega) = \sqrt{|\mathbf{x} - \mathbf{x}'|^2} \text{ for } \mathbf{x} \notin \Omega. \end{aligned}$$

The boundary corresponds to $\rho(\mathbf{x}) = 0$. We denote by $s(\mathbf{x})$ the arclength on a given component of the boundary, measured counterclockwise from a given boundary point to the point \mathbf{x}' . Thus the transformation $\mathbf{x} \rightarrow (\rho, s)$, where $\rho = \rho(\mathbf{x})$, $s = s(\mathbf{x})$ maps a strip near a connected component of the boundary onto the strip $|\rho| < \rho_0$, $0 \leq s \leq S$, where $\rho_0 > 0$ and S is the arclength of the given component of the boundary. The transformation is given by $\mathbf{x} = \mathbf{x}' + \rho\mathbf{n}(\mathbf{x})$, where \mathbf{x}' is a function of s . We write $\mathbf{n}(\mathbf{x}) = \mathbf{n}(s)$.

Assume, in addition to (3.7), the small ρ expansion in the strip $|\rho| < \rho_0$

$$\mathbf{a}(\mathbf{x}) = \{\rho^\alpha a^0(s)\mathbf{n}(s) + \rho^\beta B(s)\boldsymbol{\tau}(s)\} \{1 + o(1)\}, \quad (3.49)$$

for some $\alpha > 0$, $\beta \geq 0$. For the present analysis we assume that $\alpha = 1$, $\beta = 0$ (other cases are considered in [Matkowsky and Schuss (1977)]).

If the tangential component $B(s)$ of the drift vector vanishes at a point s , we say that s is a *critical point* in $\partial\Omega$. If there are no critical points on a given component of $\partial\Omega$, the speed $B(s)$ has a constant sign there, $B(s) > 0$, say, so that this component of $\partial\Omega$ is a limit cycle¹ for the noiseless dynamics

¹In the case of a center, all trajectories of the noiseless dynamics are closed.

$$\frac{d}{dt} \begin{pmatrix} x \\ y \end{pmatrix} = \mathbf{a}(x, y). \quad (3.50)$$

We write (3.49) in local coordinates as

$$\mathbf{a}(\rho, s) = [a^0(s)\rho\nabla\rho + B(s)\nabla s] [1 + o(1)]. \quad (3.51)$$

As mentioned above, the coefficient $B(s)$ is the speed of the deterministic motion on the boundary and we assume that $B(s) > 0$ for all $0 \leq s \leq S$, $a^0(s) \geq 0$, and that the efflux (exit density) has a limit as $\varepsilon \rightarrow 0$.

Before deriving the boundary layer equation, we turn to the analysis of the eikonal equation. First, we note that the solution of the eikonal equation is constant on the given component of the boundary. Indeed, with the obvious notation, the eikonal equation (3.20) can be written in local coordinates on $\partial\Omega$ as

$$\sum_{i,j=1}^2 \sigma^{i,j}(0, s) \frac{\partial\psi(0, s)}{\partial x^i} \frac{\partial\psi(0, s)}{\partial x^j} + B(s) \frac{\partial\psi(0, s)}{\partial s} = 0, \quad (3.52)$$

where $x^1 = x$, $x^2 = y$. To be well-defined on $\partial\Omega$, the function $\psi(0, s)$ must be a periodic function of s with period S . However, (3.52) implies that the derivative $\partial\psi(0, s)/\partial s$ does not change sign, because $B(s) > 0$ and the diffusion matrix $\sigma^{i,j}(0, s)$ is positive definite. Thus we must have

$$\psi(0, s) = \text{const.} = \hat{\psi}, \quad \nabla\psi(0, s) = 0 \text{ for all } 0 \leq s \leq S. \quad (3.53)$$

It follows that near $\partial\Omega$

$$\psi(\rho, s) = \hat{\psi} + \frac{1}{2}\rho^2 \frac{\partial^2\psi(0, s)}{\partial\rho^2} + o(\rho^2) \text{ as } \rho \rightarrow 0. \quad (3.54)$$

Setting $\phi(s) = \partial^2\psi(0, s)/\partial\rho^2$, and using (3.51), (3.54) in (3.20), we see that $\phi(s)$ must be the S -periodic solution of the Bernoulli equation

$$\sigma(s)\phi^2(s) + a^0(s)\phi(s) + \frac{1}{2}B(s)\phi'(s) = 0, \quad (3.55)$$

where $\sigma(s) = \sum_{i,j=1}^2 \sigma^{i,j}(0, s)\nu^i(s)\nu^j(s)$. Note that using (3.49) and (3.20), the drift vector in (3.32) can be written for our two-dimensional problem in local coordinates near the boundary, as

$$2 \sum_{j=1}^2 \sigma^{i,j}(\mathbf{y}) \frac{\partial\psi(\mathbf{y})}{\partial y^j} + a^i(\mathbf{y}) \quad (3.56)$$

$$\begin{aligned}
&= 2 \sum_{j=1}^2 \sigma^{i,j}(0, s) \frac{\partial \psi(0, s)}{\partial x^j} + a^i(0, s) + o(\rho) \\
&= \rho \left(2\phi(s) \sum_{j=1}^2 \sigma^{i,j}(0, s) \frac{\partial \rho}{\partial x^j} + a^0(s) \frac{\partial \rho}{\partial x^i} \right) + o(\rho).
\end{aligned}$$

To derive the boundary layer equation, we introduce the stretched variable $\zeta = \rho/\sqrt{\varepsilon}$ and define $q_\varepsilon(x, y | x_0, y_0) = Q(\zeta, s, \varepsilon | x_0, y_0)$. Expanding

$$Q(\zeta, s, \varepsilon | x_0, y_0) \sim Q^0(\zeta, s) + \sqrt{\varepsilon} Q^1(\zeta, s) + \dots, \quad (3.57)$$

and using (3.56), we obtain the boundary layer equation

$$\begin{aligned}
&\sigma(s) \frac{\partial^2 Q^0(\zeta, s)}{\partial \zeta^2} - \zeta (a^0(s) + 2\sigma(s)\phi(s)) \frac{\partial Q^0(\zeta, s)}{\partial \zeta} - B(s) \frac{\partial Q^0(\zeta, s)}{\partial s} \\
&= 0.
\end{aligned} \quad (3.58)$$

As in the previous section, the boundary and matching conditions (3.17) and (3.18) imply that

$$Q^0(0, s | x) = 0, \quad \lim_{\zeta \rightarrow -\infty} Q^0(\zeta, s | x) = 1. \quad (3.59)$$

The solution to the boundary value problem Eqs. (3.58), (3.59) is given by

$$Q^0(\zeta, s) = -\sqrt{\frac{2}{\pi}} \int_0^{\xi(s)\zeta} e^{-z^2/2} dz, \quad (3.60)$$

where $\xi(s)$ is the S -periodic solution of the Bernoulli equation

$$\sigma(s)\xi^3(s) + (a^0(s) + 2\sigma(s)\phi(s))\xi(s) + B(s)\xi'(s) = 0. \quad (3.61)$$

Setting $\xi_0(s) = \sqrt{-\phi(s)}$ in (3.55), we see that $\xi_0(s)$ is the S -periodic solution of the Bernoulli equation

$$B(s)\xi'_0(s) + a^0(s)\xi_0(s) - \sigma(s)\xi_0^3(s) = 0. \quad (3.62)$$

The solutions of the three Bernoulli equations (3.55), (3.61), and (3.62) are related to each other as follows: $\xi_0(s) = \sqrt{-\phi(s)} = \xi(s)$.

The uniform expansion of the solution of the Fokker–Planck equation (3.8), valid up to the boundary $\partial\Omega$, is given by

$$\begin{aligned} p_{\text{unif}}(\mathbf{x} | \mathbf{x}_0) &= [K_0(\mathbf{x} | \mathbf{x}_0) + O(\sqrt{\varepsilon})] \exp\left\{-\frac{\psi(\mathbf{x})}{\varepsilon}\right\} \\ &\times Q^0\left(\frac{\rho}{\sqrt{\varepsilon}}, s\right), \end{aligned} \quad (3.63)$$

where $O(\sqrt{\varepsilon})$ is uniform in $\mathbf{x} \in \bar{\Omega}$ for all fixed $\mathbf{x}_0 \in \Omega$.

3.3 The Boundary Value Problem With Non-characteristic Boundaries

The uniform expansion of $p_\varepsilon(\mathbf{y} | \mathbf{x})$ in the plane, (3.43) and (3.63), can be used for the asymptotic solution of the exit problem. First, we consider the normal component of the flux density vector (1.20) on the boundary (it is the exit density on $\partial\Omega$),

$$\begin{aligned} \mathbf{J}(\mathbf{y} | \mathbf{x}) \cdot \mathbf{n}(\mathbf{y}) &\Big|_{\mathbf{y} \in \partial\Omega} \\ &\sim -K_0(\mathbf{y}) \sum_{i,j=1}^d \varepsilon \sigma^{i,j}(\mathbf{y}) \exp\left\{-\frac{\psi(\mathbf{y})}{\varepsilon}\right\} \frac{\partial q_\varepsilon(\mathbf{y} | \mathbf{x})}{\partial y^i} n^j(\mathbf{y}), \end{aligned} \quad (3.64)$$

where $q_\varepsilon(\mathbf{y} | \mathbf{x})$ is the boundary layer function and in the local coordinates (ρ, s) . Recall that near the boundary, $\mathbf{y} = (0, s)$ on $\partial\Omega$.

If $\partial\Omega$ is a noncharacteristic boundary, we use the expansion (3.43) in (3.64) and obtain

$$\begin{aligned} \mathbf{J}(\mathbf{y} | \mathbf{x}) \cdot \mathbf{n}(\mathbf{y}) &\Big|_{\mathbf{y} \in \partial\Omega} \\ &\sim K_0(\mathbf{y}) \exp\left\{-\frac{\psi(\mathbf{y})}{\varepsilon}\right\} A(s) \sum_{i,j=1}^d \sigma^{i,j}(s) n^i(\mathbf{y}) n^j(\mathbf{y}), \end{aligned} \quad (3.65)$$

where $A(s)$ is given in (3.41). The latter simplifies (3.65) into

$$\begin{aligned} \mathbf{J}(\mathbf{y} | \mathbf{x}) \cdot \mathbf{n}(\mathbf{y}) &\Big|_{\mathbf{y} \in \partial\Omega} \\ &\sim K_0(\mathbf{y}) \exp\left\{-\frac{\psi(\mathbf{y})}{\varepsilon}\right\} \sum_{i=1}^d \left(2 \sum_{j=1}^d \sigma^{i,j}(\mathbf{y}) \frac{\partial \psi(\mathbf{y})}{\partial y^j} + a^i(\mathbf{y}) \right) n^i(\mathbf{y}). \end{aligned}$$

Thus, the small ε asymptotic expansion of the normal flux density (the exit density) on the boundary, of trajectories that start at a fixed point $\mathbf{x} \in \Omega$ (independent of ε) and exit at a point $\mathbf{y} \in \partial\Omega$, is given by

$$\Pr \{ \mathbf{x}_\varepsilon(\tau_\varepsilon) \in \mathbf{y} + dS_y \mid \mathbf{x}_\varepsilon(0) = \mathbf{x} \} \quad (3.66)$$

$$\sim \frac{K_0(\mathbf{y}) \exp \left\{ -\frac{\psi(\mathbf{y})}{\varepsilon} \right\} \sum_{i=1}^d \left(2 \sum_{j=1}^d \sigma^{i,j}(\mathbf{y}) \frac{\partial \psi(\mathbf{y})}{\partial y^j} + a^i(\mathbf{y}) \right) n^i(\mathbf{y}) dS_y}{\oint_{\partial\Omega} K_0(\mathbf{y}) \exp \left\{ -\frac{\psi(\mathbf{y})}{\varepsilon} \right\} \sum_{i=1}^d \left(2 \sum_{j=1}^d \sigma^{i,j}(\mathbf{y}) \frac{\partial \psi(\mathbf{y})}{\partial y^j} + a^i(\mathbf{y}) \right) n^i(\mathbf{y}) dS_y},$$

where τ_ε is the first passage time of the random trajectory $\mathbf{x}_\varepsilon(t)$ to the boundary.

The denominator in (3.66) can be evaluated asymptotically for small ε by the Laplace method. Thus, consider an isolated minimum point of $\psi(\mathbf{y})$ on $\partial\Omega$, say \mathbf{y}_k . At this point the gradient, $\nabla\psi(\mathbf{y}_k)$, is parallel to the outer normal $\mathbf{n}(\mathbf{y}_k)$; that is,

$$\mathbf{n}(\mathbf{y}_k) = \frac{\nabla\psi(\mathbf{y}_k)}{\|\nabla\psi(\mathbf{y}_k)\|}. \quad (3.67)$$

We can write the eikonal equation at \mathbf{y}_k as

$$\sum_{i,j=1}^d \sigma^{i,j}(\mathbf{y}_k) \frac{\partial \psi(\mathbf{y}_k)}{\partial y^j} n^i(\mathbf{y}_k) + \sum_{i=1}^d a^i(\mathbf{y}_k) n^i(\mathbf{y}_k) = 0. \quad (3.68)$$

This reduces the sums in both the numerator and denominator of (3.66) to

$$\sum_{i=1}^d \left(2 \sum_{j=1}^d \sigma^{i,j}(\mathbf{y}_k) \frac{\partial \psi(\mathbf{y}_k)}{\partial y^j} + a^i(\mathbf{y}_k) \right) n^i(\mathbf{y}_k) = -\mathbf{a}(\mathbf{y}_k) \cdot \mathbf{n}(\mathbf{y}_k). \quad (3.69)$$

To evaluate the integral in the denominator of (3.66) by the Laplace method, we define $\tilde{\psi} = \psi(\mathbf{y}_k)$ and assume that there are K distinct points of absolute minimum of $\psi(\mathbf{y})$ on $\partial\Omega$, denoted $\{\mathbf{y}_k\}_{k=1}^K$. Denoting by $H(\psi(\mathbf{y}_k))$ the $(d-1)$ -dimensional Hessian of ψ in $\partial\Omega$ at the point \mathbf{y}_k , and using (3.69), we obtain from the Laplace expansion that

$$\oint_{\partial\Omega} K_0(\mathbf{y}) \exp \left\{ -\frac{\psi(\mathbf{y})}{\varepsilon} \right\} \sum_{i=1}^d \left(2 \sum_{j=1}^d \sigma^{i,j}(\mathbf{y}) \frac{\partial \psi(\mathbf{y})}{\partial y^j} + a^i(\mathbf{y}) \right) n^i(\mathbf{y}) dS_y$$

$$\sim - (2\pi\varepsilon)^{(d-1)/2} e^{-\tilde{\psi}/\varepsilon} \sum_{k=1}^K \mathbf{a}(\mathbf{y}_k) \cdot \mathbf{n}(\mathbf{y}_k) K_0(\mathbf{y}_k) H^{-1/2}(\psi(\mathbf{y}_k)). \quad (3.70)$$

Now, Eq. (3.66) gives the efflux density as

$$\begin{aligned} & \lim_{\varepsilon \rightarrow 0} \Pr \left\{ \mathbf{x}_\varepsilon(\tau_\varepsilon) \in \mathbf{y} + dS_y \mid \mathbf{x}_\varepsilon(0) = \mathbf{x} \right\} \\ &= \frac{\sum_{k=1}^K \mathbf{a}(\mathbf{y}_k) \cdot \mathbf{n}(\mathbf{y}_k) K_0(\mathbf{y}_k) H^{-1/2} (\psi(\mathbf{y}_k)) \delta(\mathbf{y} - \mathbf{y}_k) dS_y}{\sum_{k=1}^K \mathbf{a}(\mathbf{y}_k) \cdot \mathbf{n}(\mathbf{y}_k) K_0(\mathbf{y}_k) H^{-1/2} (\psi(\mathbf{y}_k))}. \end{aligned} \quad (3.71)$$

The solution of the inhomogeneous backward Kolmogorov equation, $L^* \mathbf{x} u_\varepsilon(\mathbf{x}) = -1$ for $\mathbf{x} \in \Omega$ and $u_\varepsilon(\mathbf{x}) = 0$ for $\mathbf{x} \in \partial\Omega$ (the mean first passage time), is obtained from (1.22); that is, from

$$u_\varepsilon(\mathbf{x}) = \mathbb{E} [\tau_\varepsilon \mid \mathbf{x}_\varepsilon(0) = \mathbf{x}] = \frac{\int_{\Omega} p_\varepsilon(\mathbf{y} \mid \mathbf{x}) d\mathbf{y}}{\oint_{\partial\Omega} \mathbf{J}(\mathbf{y} \mid \mathbf{x}) \cdot \mathbf{n}(\mathbf{y}) dS_y} \quad (3.72)$$

by applying the Laplace expansion to both the volume integral in the numerator and the surface integral in the denominator. Denoting by $\mathcal{H}(\psi(\mathbf{x}_0))$ the d -dimensional Hessian of $\psi(\mathbf{x})$ at its absolute minimum in Ω , at the point \mathbf{x}_0 , say, we obtain from (3.70) the asymptotic approximation for small ε ,

$$\begin{aligned} \mathbb{E} [\tau_\varepsilon \mid \mathbf{x}_\varepsilon(0) = \mathbf{x}] &\sim \frac{\sqrt{2\pi\varepsilon} \mathcal{H}^{-1/2}(\psi(\mathbf{x}_0)) \exp \left\{ \frac{\tilde{\psi} - \psi(\mathbf{x}_0)}{\varepsilon} \right\}}{\sum_{k=1}^K \mathbf{a}(\mathbf{y}_k) \cdot \mathbf{n}(\mathbf{y}_k) K_0(\mathbf{y}_k) H^{-1/2} (\psi(\mathbf{y}_k))} \\ &\times \left[1 - \exp \left\{ \frac{a_n(s') \rho(\mathbf{x})}{\varepsilon \sigma(s')} \right\} \right]. \end{aligned} \quad (3.73)$$

Other cases of noncharacteristic boundaries are discussed in [Schuss (1980b)].

The WKB structure of the solution and Eqs. (3.72), (3.73), and (3.64), give the large-deviations theory result [Dembo and Zeitouni (1993)] that, for $\mathbf{x} \in \Omega$, outside the boundary layer,

$$\lim_{\varepsilon \rightarrow 0} \varepsilon \log \mathbb{E} \tau_\varepsilon = \lim_{\varepsilon \rightarrow 0} \varepsilon \left[\sup_{\mathbf{y} \in \partial\Omega} \log \mathbf{J}(\mathbf{y} \mid \mathbf{x}) \cdot \mathbf{n}(\mathbf{y}) - \sup_{\mathbf{y} \in \Omega} \log p_\varepsilon(\mathbf{y} \mid \mathbf{x}) \right].$$

This result is also valid for the case of a characteristic boundary.

Exercise 3.4 (Overdamped escape over a sharp potential barrier). The three-dimensional (or d -dimensional) overdamped motion of a Brownian particle diffusing in a field of force is described by the simplified Langevin–Smoluchowski equation (see [Schuss (2013)])

$$\gamma \frac{d\mathbf{x}}{dt} + \nabla U(\mathbf{x}) = \sqrt{\frac{2\gamma k_B T}{m}} \frac{d\mathbf{W}}{dt}, \quad (3.74)$$

where γ is the dynamical viscosity (friction) coefficient, k_B is Boltzmann's constant, T is absolute temperature, m is the mass of the particle, and $\mathbf{W}(t)$ is three-dimensional (or d -dimensional) standard Brownian motion. Assume the potential $U(\mathbf{x})$ forms a well; that is, it has a single minimum at a point \mathbf{x}_0 in a simply connected domain \mathcal{D} and $U(\mathbf{x})$ has no local maxima in Ω . Assume the boundary $\partial\Omega$ has a continuous outer normal $\mathbf{n}(\mathbf{x})$ and $\partial U(\mathbf{x})/\partial\nu > 0$ for all $\mathbf{x} \in \partial\Omega$.

- (i) What are the units of $\mathbf{W}(t)$?
- (ii) Introduce dimensionless displacement and time to reduce (3.74) to the form (3.3), where all parameters, variables, and functions are dimensionless. The domain Ω is mapped onto a domain, which we also denote by Ω . This corresponds to the case when the diffusion matrix is $\sigma(\mathbf{x}) = \mathbf{I}$ and the drift vector is $\mathbf{a}(\mathbf{x}) = -\nabla U(\mathbf{x})$. Choose ε and the unit of length such that $\Delta U = \max_{\partial\Omega} U(\mathbf{x}) - \min_{\Omega} U(\mathbf{x}) = 1$ and $\Omega = \mathcal{H}^{1/2}(U(\mathbf{x}_0)) = 1$. Show that $\varepsilon = k_B T / m \Delta U$, where $\Delta U = \max_{\partial\Omega} U(\mathbf{x}) - \min_{\Omega} U(\mathbf{x})$. Small ε means high potential barrier or low temperature.
- (iii) Show that $U(\mathbf{x})$ is the solution of the eikonal equation.
- (iv) Find the small ε expansion of the exit density on $\partial\Omega$ and of the mean first passage time in terms of the potential $U(\mathbf{x})$ and its derivatives.
- (v) Return to dimensional variables and express the Hessians in terms of vibration frequencies at the bottom of the potential well and at saddle points on the boundary.
- (vi) Derive the relation $\lambda = 1/\mathbb{E}\tau$ between the escape rate and the mean first passage time for this case of sharp boundaries (see Sect. 1.1).
- (vii) Express the pre-exponential term in the escape rate in terms of "attempt frequencies" at the bottom of the well and the frequencies of vibration in saddle points on the boundary.
- (viii) Express the exponential part in terms of "activation energy".
- (ix) Explain the effect of the normal derivative $\partial U(\mathbf{x})/\partial\mathbf{n}$ on the escape rate. \square

Exercise 3.5 (Escape at critical energy [Matkowsky et al. (1983)]). Consider the random motion of a one-dimensional Brownian particle diffusing in a field of force. It is described by the Langevin equation [Schuss (2010b)]

$$\ddot{x} + \gamma\dot{x} + \tilde{U}'(x) = \sqrt{\frac{2\gamma k_B T}{m}} \dot{w}, \quad (3.75)$$

where $\tilde{U}(x)$ is the potential of the force. Assume that the potential forms a well and $\tilde{U}(x)$ has a single local minimum at a point x_0 and a single maximum at the origin. Define the energy of a trajectory by $\mathcal{E}(t) = \dot{x}^2(t)/2 + U(x(t))$.

- (i) Introduce non-dimensional variables so that the Langevin equation (3.75) can be written in the form

$$\frac{d^2\xi}{d\tau^2} + \beta \frac{d\xi}{d\tau} + U'(\xi) = \sqrt{2\beta\varepsilon} \frac{dw}{d\tau},$$

where ξ is dimensionless displacement, τ is dimensionless time, β is a dimensionless friction coefficient, $U(\xi)$ is dimensionless potential, and $w(\tau)$ is dimensionless

Brownian motion. Assume that

$$\begin{aligned} \lim_{\xi \rightarrow \pm\infty} U(\xi) &= \mp\infty, \quad U'(\xi_0) = 0, \quad U''(\xi_0) = \omega_0^2 \\ U(0) &= U'(0) = 0, \quad U''(0) = -\omega_C^2, \end{aligned} \quad (3.76)$$

and that the dimensionless variables are chosen so that $\Delta U = U(0) - U(\xi_0) = 1$ and $\omega_0 = 1$. Define dimensionless energy $E(t) = \frac{1}{2}(d\xi/d\tau)^2 + U(\xi)$.

(ii) Define $\eta = d\xi/d\tau$ and write the dimensionless Langevin equation as the phase plane system

$$\frac{d\xi}{d\tau} = \eta, \quad \frac{d\eta}{d\tau} = -\beta\eta - U'(\xi) + \sqrt{2\beta\varepsilon} \frac{dw}{d\tau}. \quad (3.77)$$

(iii) Linearize the noiseless dynamics

$$\frac{d\xi}{d\tau} = \eta, \quad \frac{d\eta}{d\tau} = -\beta\eta - U'(\xi) \quad (3.78)$$

around the critical points $(\xi_0, 0)$ and $(0, 0)$ and show that the former is an attractor and the latter is a saddle point. Find the eigenvalues and eigenvectors of the matrices A_0 and A_C of the linearized system at both critical points, respectively.

(iv) Show that the boundary of the domain of attraction of the attractor $(\xi_0, 0)$ consists of the two unstable trajectories of (3.78) that emanate from the saddle point $(0, 0)$ in the direction of the eigenvector corresponding to the positive eigenvalue of A_C . The domain of attraction is denoted Ω and its boundary, denoted Γ , is called the *separatrix* of the system (3.78). Draw Γ and the flow lines of the plane flow (3.78) inside and outside Ω and interpret the flow portrait in terms of the motion of a particle. Determine the slope and the outer unit normal to Γ at the saddle point $(0, 0)$.

(v) Define the energy $E(\xi, \eta) = \frac{1}{2}\eta^2 + U(\xi)$ and the critical energy contour $\Gamma_C = \{E(\xi, \eta) = E_C\}$, where $E_C = 0$. Determine the slope of Γ_C at the saddle point and draw the separatrix and the contour Γ_C . Show that Γ_C forms a noncharacteristic boundary of the domain $\Omega_C = \{E(\xi, \eta) < E_C\}$, except for two critical points.

(vi) Construct a small ε asymptotic solution of the stationary Fokker–Planck equation (3.8) in Ω with absorbing boundary conditions on E_C , valid away from the saddle point at $(0, 0)$. Can this expansion be valid up to the saddle point? Use the expansion to determine the distribution of exit points on Γ_C of the trajectories of (3.77) that start out in Ω_C . Calculate the mean first passage time to Γ_C [Schuss (2010b)]. \square

3.4 The Boundary Value Problem in Planar Domains With Characteristic Boundaries

In the case of a two-dimensional system with a characteristic boundary, we use the expansions of Sect. 3.2.4 in Eqs. (3.64) and (3.72). Using (3.60) in (3.64) gives

$$\mathbf{J} \cdot \mathbf{n}|_{\partial\Omega}(s) \sim \sqrt{\frac{2\varepsilon}{\pi}} K_0(0, s) \xi(s) \sigma(s) e^{-\hat{\psi}/\varepsilon}, \quad (3.79)$$

hence the exit probability density is

$$\Pr [\mathbf{x}_\varepsilon(\tau_\varepsilon) \in \mathbf{x}(s) + d\mathbf{x}(s) | \mathbf{x}_0] \sim \frac{\int_0^s K_0(0, s) \xi(s) \sigma(s) ds}{\int_0^s K_0(0, s) \xi(s) \sigma(s) ds}, \quad (3.80)$$

where $ds = |\mathbf{d}\mathbf{x}|$.

The function $K_0(0, s)$ can be expressed in terms of the coefficients of the problem as follows. The function $K_0(0, s)$ is the solution of the transport equation (3.39). Using the assumption (3.51) and the eikonal equation (3.52), Eq. (3.39) on the boundary becomes

$$B(s) \frac{d}{ds} K_0(0, s) = -[a^0(s) + B'(s) + \sigma(s)d\phi(s)] K_0(0, s). \quad (3.81)$$

Using the fact that $\phi(s) = -\xi^2(s)$, we rewrite (3.81) in the separated form

$$\frac{dK_0}{K_0} = -\left(\frac{a^0}{B} + \frac{B'}{B} - \frac{\sigma\xi^2}{B}\right) ds. \quad (3.82)$$

Integrating (3.82) and simplifying it with the aid of (3.61), we obtain $K_0(0, s) = \hat{K}_0 \sqrt{-\phi(s)/B(s)}$, where $\hat{K}_0 = \text{const}$. Note that $\phi(s)$ cannot change sign, because if it vanishes at a point, it vanishes everywhere, as indicated by the Bernoulli equation (3.55). It has to be negative, because at a point s of local extremum, we have $\phi(s) = -a^0(s)/\sigma(s)$. The assumption that the boundary is an unstable limit cycle of the drift equation (3.4) implies that $a^0(s)/\sigma(s) \geq 0$.

Using these simplifications in (3.80) gives the more explicit expression for the exit density

$$\Pr \{\mathbf{x}_\varepsilon(\tau_\varepsilon) \in \mathbf{x} + d\mathbf{x} | \mathbf{x}_0\} \sim \frac{\int_0^s [\xi^2(s)\sigma(s)/B(s)] ds}{\int_0^s [\xi^2(s)\sigma(s)/B(s)] ds}. \quad (3.83)$$

The asymptotic expansion of the solution of the inhomogeneous backward Kolmogorov equation (the mean first passage time to the boundary from any fixed point $\mathbf{x} \in \Omega$) is calculated as above, but with the flux given by (3.79). We obtain

$$u_\varepsilon(\mathbf{x}) = \mathbb{E} [\tau_\varepsilon | \mathbf{x}_\varepsilon(0) = \mathbf{x}] \sim \frac{\pi^{3/2} \sqrt{2\varepsilon} \mathcal{H}^{-1/2}(\psi(\mathbf{0}))}{\int_0^S K_0(0, s) \xi(s) \sigma(s) ds} \exp\left\{ \frac{\hat{\psi}}{\varepsilon} \right\}, \quad (3.84)$$

where $\mathcal{H}(\psi(\mathbf{0}))$ is the Hessian at the stable equilibrium point $\mathbf{0}$.

Example 3.1 (Constant speed). If $a^0(s)/\sigma(s) = \text{const.} > 0$, then $\phi(s) = -a^0(s)/\sigma(s) = \text{const.}$ and $\xi(s) = \sqrt{-\phi(s)} = \sqrt{a^0(s)/\sigma(s)} = \text{const.}$, hence (3.80) gives

$$\Pr \{ \mathbf{x}_\varepsilon(\tau_\varepsilon) \in \mathbf{x} + d\mathbf{x} | \mathbf{x}_\varepsilon(0) = \mathbf{x}_0 \} \sim \frac{[\sigma(s)/B(s)] ds}{\int_0^S [\sigma(s)/B(s)] ds};$$

that is, the efflux density is inversely proportional to the local speed of motion of the drift on the boundary (see (3.4)).

If $B(s)$ changes sign on $\partial\Omega$, then $\psi(0, s)$ is not constant in general. If $\psi(0, s)$ has absolute minima at a finite number of points, the total efflux has to be evaluated by the Laplace method at these points. \square

Exercise 3.6 (Boundary with critical points [Matkowsky et al. (1983)]). If the speed $B(s)$ vanishes at isolated points or changes sign on a characteristic boundary $\partial\Omega$, the eikonal function on the boundary, $\psi(0, s)$, is not constant in general. Thus the following three classes of characteristic boundaries can be distinguished.

Type I: The speed doesn't vanish; $B(s) > 0$, as considered above.

Type II: The flow on the boundary is unidirectional with N unstable critical points;

$$B(s) \geq 0, \quad \begin{aligned} \frac{\partial^j B(s_i)}{\partial s^j} &= 0, \quad 0 \leq j < k_i, \quad i = 1, \dots, N \\ \frac{\partial^{k_i} B(s_i)}{\partial s^{k_i}} &\text{ are all } > 0 \text{ or all } < 0, \quad k_i \text{ even.} \end{aligned}$$

Type III: The flow on the boundary has N stable and N unstable critical points; $B(s)$ changes sign. At stable points s_i

$$\frac{\partial^j B(s_i)}{\partial s^j} = 0, \quad 0 \leq j < k_i, \quad \frac{\partial^{k_i} B(s_i)}{\partial s^{k_i}} < 0, \quad k_i \text{ odd, } i = 1, \dots, N.$$

At unstable points σ_i ,

$$\frac{\partial^j B(\sigma_i)}{\partial s^j} = 0, \quad 0 \leq j < l_i, \quad \frac{\partial^{l_i} B(\sigma_i)}{\partial s^{l_i}} > 0, \quad l_i \text{ odd, } i = 1, \dots, N.$$

- (i) Retain terms of order $\sqrt{\varepsilon}$ and ε in the boundary layer equation and use the transformation $\eta = \xi(s)\zeta$, as in Sect. 3.2.4.
- (ii) Introduce into the boundary layer equation the stretched variable $\phi = (s - s_i)\varepsilon^{-r}$, where r is chosen by balancing terms in the boundary layer equation, depending on the order of the zero of $B(s)$ at s_i . Choose the value of $\gamma(s_i)$ so that $\gamma'(s_i)$ remains bounded and S -periodic.
- (iii) Retain the second derivative with respect to ϕ in the stretched boundary layer equation. The resulting boundary layer equation is separated with respect to η and ϕ (or s). Solve it by separation of variables and obtain a singularly perturbed eigenvalue problem with periodic boundary conditions in the variable s .
- (iv) Use the matching condition to determine the η -dependence of the boundary layer function.
- (v) Find explicit expressions for the exit density and the mean first passage time for the exit problem [Schuss (2010b)]. \square

3.5 Loss of Lock in a Second-Order Phase-Locked Loop

This section illustrates the asymptotic method in higher dimensions in the context of filtering theory, as described in Sect. 2.7. The solution of the boundary value problem is given in explicit and numerical terms, as described above.

The case of a second-order phase-locked loop for FM transmission, which leads to a boundary value problem in the plane, is described in Sect. 2.7 as a two-dimensional problem. Specifically, in FM on carrier frequency ω_0 , the signal $x(t)$ is converted into a frequency by the transformation

$$h(x(t), t) = \sqrt{2} \sin \left(\omega_0 t + d_f \int_0^t x(s) ds \right). \quad (3.85)$$

The modulation in (3.85) can be viewed as a memoryless transformation of the output of a system of the form (2.84) if we define the two-dimensional signal $\mathbf{x}(t) = (x_1(t), x_2(t))^T$ as the output of the stochastic differential equations

$$dx_1(t) = m(x_1(t), t) dt + \sigma(x_1(t), t) dw, \quad dx_2(t) = d_f x_1(t) dt, \quad (3.86)$$

and then (3.85) can be written as the memoryless transformation of $\mathbf{x}(t)$

$$h(\mathbf{x}(t), t) = \sqrt{2} \sin (\omega_0 t + x_2(t)). \quad (3.87)$$

The scaled phase-locked loop equations for FM transmission of Brownian motion ($m = 0$ in (3.88)) are

$$dx = -mx dt + \sigma dw, \quad du = d_f x dt, \quad (3.88)$$

assuming that either one or both of

$$h^1(u(t), t) = \sqrt{A} \sin [\omega_0 t + u(t)], \quad h^2(u(t), t) = \sqrt{A} \cos [\omega_0 t + u(t)] \quad (3.89)$$

are measured in noisy channels with small independent noises. Here \tilde{x}_1 is the scaled u and \tilde{x}_2 is the scaled x . When both $h^1(u(t), t)$ and $h^2(u(t), t)$ are measured, they are given by the dimensionless equations: the signal model $(\tilde{x}^1, \tilde{x}^2)$ and its measurements $(\tilde{y}^1, \tilde{y}^2)$ in a noisy FM channel are the outputs of

$$\begin{aligned} d \begin{bmatrix} \tilde{x}_1 \\ \tilde{x}_2 \end{bmatrix} &= \begin{bmatrix} 0 & 1 \\ 0 & 0 \end{bmatrix} \begin{bmatrix} \tilde{x}_1 \\ \tilde{x}_2 \end{bmatrix} dt + \sqrt{\varepsilon} \begin{bmatrix} 0 \\ 1 \end{bmatrix} dw, \\ d \begin{bmatrix} \tilde{y}_1 \\ \tilde{y}_2 \end{bmatrix} &= \begin{bmatrix} \sin \tilde{x}_1 \\ \cos \tilde{x}_1 \end{bmatrix} dt + \sqrt{\varepsilon} d \begin{bmatrix} v_1 \\ v_2 \end{bmatrix}, \end{aligned} \quad (3.90)$$

where w , v_1 , and v_2 are standard Brownian motions. The phase and frequency estimation errors, e_1 and e_2 , respectively, have the dynamics

$$d \begin{bmatrix} e_1 \\ e_2 \end{bmatrix} = \begin{bmatrix} e_2 - \sin e_1 \\ -\sin e_1 \end{bmatrix} dt + \sqrt{\varepsilon} \begin{bmatrix} 1 & 0 \\ 1 & -1 \end{bmatrix} \begin{bmatrix} dv \\ dw \end{bmatrix}, \quad (3.91)$$

where $v(t)$ is a standard Brownian motion independent of $w(t)$.

To examine the loss of lock in the second-order phase-locked loop (3.90), we consider the case of small noise, $\varepsilon \ll 1$. As in the previous sections of this chapter, we examine the noiseless error dynamics (3.91). Linearizing the noiseless system (3.91) near its critical points $e_1 = 0$, $e_2 = n\pi$, where $n = 0, \pm 1, \pm 2, \dots$, we find that the critical points corresponding to even n are attractors, while the ones corresponding to odd n are saddle points. Thus the (e_1, e_2) plane is partitioned into domains of attraction of the stable equilibria at $(0, 2n\pi)$, which are separated by the trajectories that converge to the saddle points (the bounding trajectories in Fig. 3.2). This partition of the phase plane is analogous to the partition of the e -axis in Fig. 2.6 into domains of attraction of the stable equilibria of the potential $U(e)$.

Simulated noisy error trajectories of (3.91) of the phase tracker (3.90) are shown in Fig. 3.2. When a noisy error trajectory crosses a bounding separatrix it continues into another domain of attraction, so a typical phase-estimation-error trajectory looks like that in Fig. 3.1. The frequency estimation error, which looks like the derivative of the phase error, has sharp peaks, called *FM clicks*, which are distinctly audible in FM radio receivers. Figure 3.2 also shows trajectories that wander across many separatrices, forming bunches of phase slips, and last longer than a single phase slip.

Losses of lock are rare events if the noises are weak. As the noise increases, the frequency error spends longer and longer periods of time wandering in the tails of the separatrices, far from the locked state $e_1 = 0$, and the performance of the tracker deteriorates. This happens when the signal-to-noise ratio falls below a certain threshold (the dimensionless noise intensity ε crosses a certain threshold), beyond which the phase-locked loop becomes useless [Viterbi (1967)], [Snyder (1969)], [Bobrovsky and Schuss (1982)], [Schuss (1980b)], [Stensby (1997)].

Exercise 3.7 (Loss of lock in a second-order phase-locked loop).

1. Derive (3.90) and (3.91).
2. Plot the domains of attraction of (3.91), shown in Fig. 3.2.
3. Run simulations of (3.90) and (3.91) (see Figs. 3.1 and 3.2) and compare the error trajectories created by each system. \square

Exercise 3.8 (The threshold in the second-order phase-locked loop).

1. Use the simulations of Exercise 3.7 to calculate the mean time to lose lock. Show that up to the pre-exponential factor, the mean time to lose lock is $\tau \propto \exp\{0.78525/\varepsilon\}$ for frequency estimation and $\tau \propto \exp\{2/\varepsilon\}$ for phase estimation of a Brownian signal in the model of Exercise 2.8.
2. Plot the mean time to lose lock versus signal-to-noise ratio $= 1/\varepsilon$ to examine the threshold in the two phase-locked loops.

Fig. 3.1 A typical trajectory of the phase estimation error

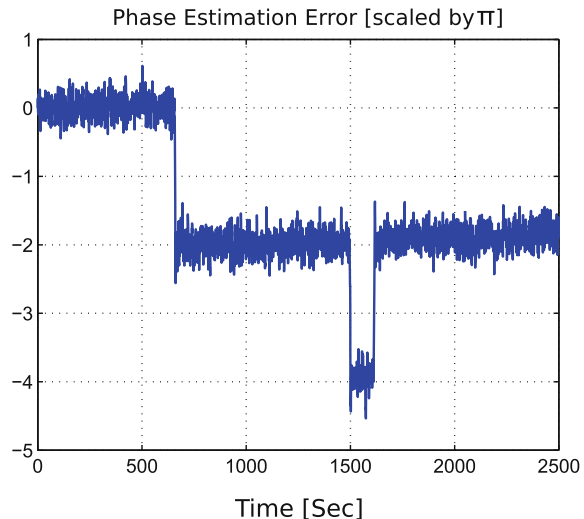
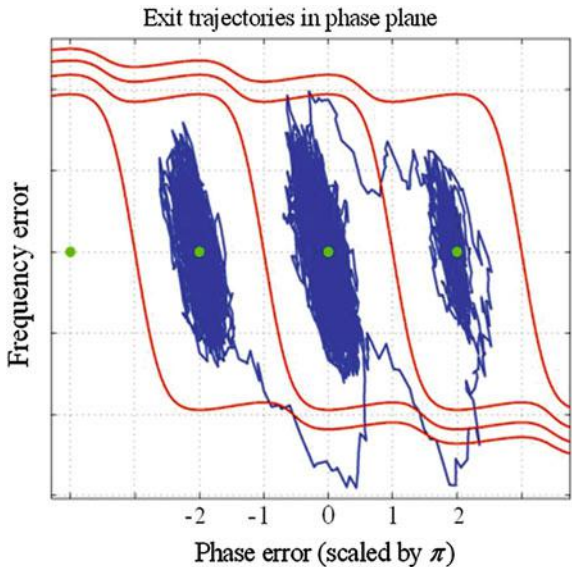


Fig. 3.2 The horizontal axis is the phase-estimation error e_1 and the vertical axis is the frequency estimation error e_2 . The dots are the local attractors at $e_1 = 0, \pm 2\pi, \dots, e_2 = 0$. The bounding curves are the separatrices that converge to the saddle points $e_1 = \pm\pi, \pm 3\pi, \dots, e_2 = 0$. Typical noisy error trajectories in the phase plane show escapes from the domains of attraction



3.5.1 The Phase Plane of the Reduced Problem

The reduced problem (3.91) is

$$\frac{d}{dt} \begin{bmatrix} e_1 \\ e_2 \end{bmatrix} = \begin{bmatrix} e_2 - \sin e_1 \\ -\sin e_1 \end{bmatrix}, \quad (3.92)$$

which we write as

$$\dot{\mathbf{x}} = \mathbf{a}(\mathbf{x}) = \begin{bmatrix} x_2 - \sin x_1 \\ -\sin x_1 \end{bmatrix}. \quad (3.93)$$

The system has a stable critical point at the origin, and its domain of attraction is denoted by Ω . The matrix \mathbf{A} of the linearized system about the origin,

$$\dot{\mathbf{x}} = \mathbf{A}\mathbf{x}, \quad (3.94)$$

is given by

$$\mathbf{A} = \left\{ \frac{\partial a^i(\mathbf{0})}{\partial x^j} \right\}_{i,j=1}^2 = \begin{bmatrix} -1 & -1 \\ 1 & 0 \end{bmatrix}, \quad (3.95)$$

and its eigenvalues, $\lambda_{\pm} = \frac{1}{2}(-1 \pm i\sqrt{3})$, have negative real parts. Thus the trajectories of the noiseless system (3.93) that start in Ω are attracted to the origin.

To identify the boundary $\partial\Omega$, we note that the noiseless dynamics (3.93) has saddle points at $x_1 = \pm\pi$, $x_2 = 0$, and the matrix \mathbf{a}_1 of the linearized system there,

$$\dot{\xi} = \mathbf{a}_1 \xi, \quad (3.96)$$

where $x_1 = 2(n+1)\pi + \xi_1$, $x_2 = \xi_2$, is given for $n = 0, \pm 1, \pm 2, \dots$ by

$$\mathbf{A}_1 = \left\{ \frac{\partial a^i(\pm\pi, 0)}{\partial x^j} \right\}_{i,j=1}^2 = \begin{bmatrix} 1 & 1 \\ 1 & 0 \end{bmatrix}. \quad (3.97)$$

Its eigenvalues are $\lambda_{+,-} = \frac{1}{2}(-1 \pm \sqrt{5})$, so the all trajectories of (3.93) are repelled from the saddle points, except the stable trajectories that enter the saddle point $(0, \pm\pi)$ in the direction of the eigenvector

$$\boldsymbol{\tau}_1 = \frac{-1}{\sqrt{1 + \lambda_-^2}} \begin{bmatrix} \lambda_- \\ 1 \end{bmatrix}. \quad (3.98)$$

Therefore, on the segment of the separatrix near the saddle point, where the solution of the linearized system (3.96) is asymptotically close to the solution of (3.93),

$$\begin{bmatrix} x_1(t) \\ x_2(t) \end{bmatrix} = \begin{bmatrix} 2(n+1)\pi \\ 0 \end{bmatrix} - \delta \boldsymbol{\tau}_1 e^{\lambda_-(t-t_1)} \text{ for } t > t_1, \quad (3.99)$$

where $[2(n+1)\pi, 0]^T - \delta \boldsymbol{\tau}_1$ is assumed to be a point on the separatrix, and the arc length from the saddle point $[2(n+1)\pi, 0]^T$ to $[x_1(t), x_2(t)]^T$ is $s = \delta e^{\lambda_-(t-t_1)}$.

To construct $\partial\Omega$ numerically, we can integrate the ordinary differential equation

$$\frac{dx_2}{dx_1} = \frac{-\sin x_1}{x_2 - \sin x_1} \quad (3.100)$$

with the initial point $x_2(x_1) = \lambda_-(x_1 \mp \pi)$ for sufficiently small $|x_2|$. The integration produces the separatrices shown in Fig. 3.2.

The local behavior of the noiseless error dynamics (3.93) near the separatrices (see Fig. 3.2) is determined by the drift vector $\mathbf{a}(\mathbf{x})$, which is tangent to the boundary, so its normal component vanishes there. We expand $\mathbf{a}(\mathbf{x})$ near the separatrix in a Taylor series in powers of the distance to the boundary. At each point $\mathbf{x} \in \Omega$ near the boundary, we denote its orthogonal projection on the boundary by \mathbf{x}' and the unit outer normal and unit tangent there by $\mathbf{n}(\mathbf{x}')$ and $\boldsymbol{\tau}(\mathbf{x}')$, respectively. We choose $\boldsymbol{\tau}(\mathbf{0}) = \boldsymbol{\tau}_1$. We define the signed distance to the boundary

$$\rho(\mathbf{x}) = -|\mathbf{x} - \mathbf{x}'| \text{ for } \mathbf{x} \in \Omega, \quad \rho(\mathbf{x}) = |\mathbf{x} - \mathbf{x}'| \text{ for } \mathbf{x} \notin \Omega. \quad (3.101)$$

The boundary corresponds to $\rho(\mathbf{x}) = 0$, and the unit outer normal at \mathbf{x}' is $\mathbf{n}(\mathbf{x}') = \nabla\rho|_{\rho=0}$. The unit outer normal at $\partial\Omega$ can also be expressed in terms of the drift, which is tangential to the boundary,

$$\mathbf{n}(\mathbf{x}') = \frac{-1}{|\mathbf{a}(\mathbf{x}')|} \begin{bmatrix} \sin x'_1 \\ x'_2 - \sin x'_1 \end{bmatrix}. \quad (3.102)$$

The signed arc length $s(\mathbf{x})$ is measured from the saddle point to \mathbf{x}' on the separatrix through the saddle point $(0, \pi)$. Choosing the eigenvector $\boldsymbol{\tau}_1$ as the positive direction on the separatrix, the tangent $\boldsymbol{\tau}(s)$ is defined as a continuous function of s for $-\infty < s < \infty$. The transformation $\mathbf{x} \rightarrow (\rho, s)$, where $\rho = \rho(\mathbf{x})$, $s = s(\mathbf{x})$, maps a finite strip near a connected component of the boundary onto the strip $|\rho| < \rho_0$, $-S < s < S$ for some $S, \rho_0 > 0$. The transformation is given by $\mathbf{x} = \mathbf{x}' + \rho\mathbf{n}(\mathbf{x})$, where the projection \mathbf{x}' is a function of s . We write $(\mathbf{n}(\mathbf{x}), \boldsymbol{\tau}(\mathbf{x})) = (\mathbf{n}(s), \boldsymbol{\tau}(s))$.

Because $\mathbf{a}(\mathbf{x}') \cdot \mathbf{n}(\mathbf{x}') = 0$, a Taylor expansion of the normal component of the drift in powers of ρ in the strip $|\rho| < \rho_0$ is

$$\begin{aligned} \mathbf{a}(\mathbf{x}) \cdot \mathbf{n}(\mathbf{x}') &= \sum_{i,j=1}^2 \frac{\partial a_i(\mathbf{x}')}{\partial x_j} n_i(\mathbf{x}') n_j(\mathbf{x}') \rho + O(\rho^2) \\ &= \frac{\sin x'_1 (x'_2(1 - \cos x'_1) - \sin x'_1)}{\sin^2 x'_1 + (x'_2 - \sin x'_1)^2} \rho + O(\rho^2). \end{aligned}$$

Setting

$$\frac{\sin x'_1 (x'_2(1 - \cos x'_1) - \sin x'_1)}{\sin^2 x'_1 + (x'_2 - \sin x'_1)^2} = a^0(s), \quad (3.103)$$

we find that

$$a^0(0) = \frac{-\lambda_-(2 + \lambda_-)}{\lambda_-^2 + (1 + \lambda_-)^2} > 0,$$

which implies that $a^0(s) > 0$ for all s , because the function is continuous and does not vanish. Therefore

$$\dot{\rho} = \nabla\rho \cdot \dot{\mathbf{x}} = a^0(s)\rho + O(\rho^2)$$

implies that $\rho(t) \approx \rho(0)e^{a^0(s)t}$, which decreases for every $\rho(0) < 0$ as t increases. This means that the trajectories of the noiseless dynamics inside Ω are repelled from the boundary.

The tangential component of the drift is the speed of motion on $\partial\Omega$ toward the saddle point, that is,

$$\begin{aligned} B(s) &= \mathbf{a}(\mathbf{x}') \cdot \boldsymbol{\tau}(\mathbf{x}') \\ &= -\operatorname{sgn}(x'_2)|\mathbf{a}(\mathbf{x}')| = -\operatorname{sgn}(x'_2)\sqrt{(x'_2 - \sin x'_1)^2 + \sin^2 x'_1}. \end{aligned} \quad (3.104)$$

Near the saddle point $(0, \pi)$ the speed is given by

$$B(s) \approx -x'_2 \sqrt{(1 + \lambda_-)^2 + \lambda_-^2}, \quad (3.105)$$

so it changes sign at the saddle point; it is thus a *stable critical point* of the noiseless error dynamics (3.93) on the boundary $\partial\Omega$. The local structure of the drift near $\partial\Omega$ is therefore

$$\mathbf{a}(\mathbf{x}) = \{\rho a^0(s)\mathbf{n}(s) + B(s)\boldsymbol{\tau}(s)\}\{1 + o(1)\}, \quad (3.106)$$

which in local coordinates is

$$\mathbf{a}(\rho, s) = a^0(s)\rho\nabla\rho + B(s)\nabla s + o(\rho). \quad (3.107)$$

3.5.2 The Mean Time to Lose Lock

The error dynamics (3.91) exhibit the general properties of higher-dimensional loss of lock problems. We have

$$\mathbf{b}(\mathbf{x}) = \begin{bmatrix} 1 & 0 \\ 1 & -1 \end{bmatrix}, \quad \boldsymbol{\sigma}(\mathbf{x}) = \frac{1}{2} \begin{bmatrix} 1 & 1 \\ 1 & 2 \end{bmatrix}, \quad (3.108)$$

so (3.91) has the autonomous form

$$d\mathbf{x} = \mathbf{a}(\mathbf{x})dt + \sqrt{\varepsilon} \mathbf{b}(\mathbf{x})d\mathbf{w}(t), \quad \mathbf{x}(0) = \mathbf{x}, \quad (3.109)$$

where the noiseless dynamics

$$d\mathbf{x} = \mathbf{a}(\mathbf{x})dt, \quad \mathbf{x}(0) = \mathbf{x} \quad (3.110)$$

has a stable attractor at the origin (see Fig. 3.2). The mean time to lose lock, which is the mean first passage time $u_\varepsilon(\mathbf{x}) = \mathbb{E}[\tau_\Omega | \mathbf{x}(0) = \mathbf{x}]$ from a point $\mathbf{x} \in \Omega$ (the domain of attraction of the origin) to the boundary $\partial\Omega$, is the solution of the boundary value problem for the Pontryagin-Andronov-Vitt equation

$$\mathcal{L}_\varepsilon^* u_\varepsilon(\mathbf{x}) = -1 \text{ for } \mathbf{x} \in \Omega, \quad u_\varepsilon(\mathbf{x}) = 0 \text{ for } \mathbf{x} \in \partial\Omega, \quad (3.111)$$

where the backward Kolmogorov operator for (3.109) is given by

$$\mathcal{L}_\varepsilon^* u_\varepsilon(\mathbf{x}) = \sum_{i,j=1}^2 \varepsilon \sigma^{i,j}(\mathbf{x}) \frac{\partial^2 u_\varepsilon(\mathbf{x})}{\partial x^i \partial x^j} + \sum_{i=1}^2 a^i(\mathbf{x}) \frac{\partial u_\varepsilon(\mathbf{x})}{\partial x^i}. \quad (3.112)$$

The escape of the two-dimensional estimation error ($e_1(t)$, $e_2(t)$) from the domain of attraction Ω of the stable equilibrium point at the origin (the dot in Fig. 3.2) to the separatrix $\partial\Omega$ is similar to that of the one-dimensional problem discussed in Sect. 2.7 above. In both cases the noiseless dynamics is stable, so the solution $u_\varepsilon(\mathbf{x})$ of the boundary value problem (3.112) (the mean first passage time to the boundary) becomes infinite in the limit $\varepsilon \rightarrow 0$. The outer solution fails to satisfy the boundary condition, which in the planar case is given not merely at two points, but rather on an entire curve (the separatrix in Fig. 3.2). The matched asymptotics method described in the previous sections has to be extended to a much more complicated geometry of the two-dimensional case.

The boundary layer analysis requires geometric considerations. Specifically, the stretched boundary layer variable has to be chosen in a manner that reflects the singularity of the solution, because due to the homogeneous boundary condition, the solution does not change along the boundary, so no boundary layer should be expected in the direction tangent to $\partial\Omega$. Therefore the boundary layer variable should be the stretched distance to the boundary, in the direction of the normal. The boundary layer function should satisfy a boundary layer equation with boundary and matching conditions as in the previous section. An important difference in the evaluation of the solution $u_\varepsilon(\mathbf{x})$ in the two-dimensional case is that the Pontryagin-Andronov-Vitt boundary value problem (3.112) cannot be written in an explicit form, unless it is self-adjoint in the sense that there exists a function $U(x_1, x_2)$ such that

$$\mathbf{a}(\mathbf{x}) = -\sigma \nabla U(\mathbf{x})$$

for some function $U(\mathbf{x})$, which in the original variables takes the form

$$\begin{bmatrix} e_2 - \sin e_1 \\ -\sin e_1 \end{bmatrix} = -\frac{1}{2} \begin{bmatrix} 1 & 1 \\ 1 & 2 \end{bmatrix} \begin{bmatrix} \partial U(e_1, e_2)/\partial e_1 \\ \partial U(e_1, e_2)/\partial e_2 \end{bmatrix}. \quad (3.113)$$

This is not the case here (see Exercise 3.9 below). Therefore a different criterion for the determination of the missing constant $u_\varepsilon(0, 0)$ in the matched asymptotic expansion has to be found. \square

Exercise 3.9 (The boundary value problem (3.111) is not self-adjoint). Why is (3.113) impossible? [Schuss (1980b)], [Schuss (2010b, Exercise 10.16)]. \square

The main result of this section, versed in the language stochastic differential equations and elliptic boundary value problems, is the following statement.

As in the previous section, the calculation of $u_\varepsilon(\mathbf{x})$ is given in the following theorem.

Theorem 3.5.1 (The asymptotics of the MFPT). *The asymptotic approximation to the mean first passage time $\bar{\tau}(\mathbf{x})$ for small ε is given by*

$$u_\varepsilon(\mathbf{x}) = \bar{\tau}(\mathbf{x}) = K(\varepsilon) \exp \left\{ \frac{\hat{\Psi}}{\varepsilon} \right\} (1 + o(1)), \quad (3.114)$$

where $K(\varepsilon)$ has an asymptotic series expansion in powers of ε , and $\hat{\Psi}$ is the minimum on the boundary $\partial\Omega$ of the domain of attraction Ω of the stable equilibrium point \mathbf{x}_0 of the nonzero solution of the eikonal equation for $\Psi(\mathbf{x})$,

$$\sum_{i,j=1}^d \sigma^{i,j}(\mathbf{x}) \frac{\partial \Psi(\mathbf{x})}{\partial x^i} \frac{\partial \Psi(\mathbf{x})}{\partial x^j} + \sum_{i=1}^d a^i(\mathbf{x}) \frac{\partial \Psi(\mathbf{x})}{\partial x^i} = 0, \quad (3.115)$$

$$\Psi(\mathbf{x}_0) = 0.$$

□

Note that (3.115) defines $\Psi(\mathbf{x})$ up to an additive constant, so if the condition at \mathbf{x}_0 is changed to any other value, then $\hat{\Psi}$ is redefined as $\hat{\Psi} = \min_{\mathbf{x} \in \partial\Omega} \Psi(\mathbf{x}) - \Psi(\mathbf{x}_0)$, so that (3.114) remains unchanged. The proof of Theorem 3.5.1 is divided into several steps. The results are described in Figs. 3.3, 3.4, 3.5, 3.6, 3.7 and 3.8.

3.5.3 The Boundary Layer Structure of $u_\varepsilon(\mathbf{x})$

First, we note that $u_\varepsilon(\mathbf{x}) \rightarrow \infty$ as $\varepsilon \rightarrow 0$ because, due to the stability of the attractor at the origin, all characteristics of the reduced parabolic partial differential equation (3.110) never leave Ω . Setting

$$C_\varepsilon = \sup_{\mathbf{x} \in \Omega} u_\varepsilon(\mathbf{x}), \quad U_\varepsilon(\mathbf{x}) = \frac{u_\varepsilon(\mathbf{x})}{C_\varepsilon}, \quad (3.116)$$

we obtain for all $\mathbf{x} \in \Omega$,

$$\sum_{i,j=1}^2 \varepsilon \sigma^{i,j}(\mathbf{x}) \frac{\partial^2 U_\varepsilon(\mathbf{x})}{\partial x^i \partial x^j} + \sum_{i=1}^2 a^i(\mathbf{x}) \frac{\partial U_\varepsilon(\mathbf{x})}{\partial x^i} = -\frac{1}{C_\varepsilon} = o(1) \text{ as } \varepsilon \rightarrow 0 \quad (3.117)$$

$$U_\varepsilon(\mathbf{x}) = 0 \text{ for } \mathbf{x} \in \partial\Omega.$$

The outer expansion of $U_\varepsilon(\mathbf{x})$,

$$U_\varepsilon(\mathbf{x}) \sim U^0(\mathbf{x}) + \varepsilon U^1(\mathbf{x}) + \dots,$$

gives

$$\sum_{i=1}^2 a^i(\mathbf{x}) \frac{\partial U^0(\mathbf{x})}{\partial x^i} = 0, \quad (3.118)$$

which can be written as

$$\frac{dU^0(\mathbf{x}(t))}{dt} = 0 \quad (3.119)$$

along the characteristics (3.110). This implies that $U^0(\mathbf{x}(t))$ is constant on the characteristics, which all converge to the origin. Thus $U^0(\mathbf{x})$ is constant throughout Ω . The normalization (3.116) implies that $U^0(\mathbf{x}) = 1$ for all $\mathbf{x} \in \Omega$. We note, however, that $U^0(\mathbf{x})$ fails to satisfy the boundary condition (3.117), and the higher-order corrections $U^i(\mathbf{x})$ cannot remedy this failure.

The reason for this failure is the expansion (3.118), which can be valid only under the assumption that the first term in (3.117) is smaller than the second one. Apparently, this assumption fails near the boundary, where both terms become of the same order of magnitude. To resolve the structure of the solution $U_\varepsilon(\mathbf{x})$ in this boundary layer zone, we change to local variables (ρ, s) (see Sect. 3.5.1, from (3.101)) and write

$$U_\varepsilon(\mathbf{x}) = v_\varepsilon(s, \rho). \quad (3.120)$$

Now we introduce the stretched variable $\xi = \rho/\sqrt{\varepsilon}$ and the boundary layer function $v_\varepsilon(s, \rho) = V_\varepsilon(\xi, s)$. Using the local structure (3.107) and expanding all functions in powers of $\varepsilon^{1/2}$, we transform the boundary value problem (3.117) to

$$\sigma^0(s) \frac{\partial^2 V_\varepsilon(\xi, s)}{\partial \xi^2} + a^0(s) \xi \frac{\partial V_\varepsilon(\xi, s)}{\partial \xi} + B(s) \frac{\partial V_\varepsilon(\xi, s)}{\partial s} = 0, \quad (3.121)$$

to leading-order in $\sqrt{\varepsilon}$, with the boundary and matching conditions

$$V_\varepsilon(0, s) = 0, \quad \lim_{\xi \rightarrow -\infty} V_\varepsilon(\xi, s) = \lim_{\rho \rightarrow 0} v^0(\rho, s) = 1, \quad (3.122)$$

where

$$\sigma^0(s) = \sum_{i,j=1}^2 \sigma^{i,j}(0, s) \rho_i \rho_j > 0, \quad v^0(\rho, s) = U^0(\mathbf{x}) = 1. \quad (3.123)$$

The solution of the boundary value problem (3.121), (3.122) is given by

$$V_\varepsilon(\xi, s) = -\sqrt{\frac{2}{\pi}} \int_0^{\gamma(s)\xi} e^{-z^2/2} dz, \quad (3.124)$$

where $\gamma(s)$ is the solution of Bernoulli's equation

$$B(s)\gamma'(s) + a^0(s)\gamma(s) - \sigma^0(s)\gamma^3(s) = 0, \quad \gamma(0) = \sqrt{\frac{a^0(0)}{\sigma^0(0)}}. \quad (3.125)$$

The substitution $\beta(s) = \gamma^{-2}(s)$ converts (3.125) into the linear equation

$$\beta'(s) - \frac{2a^0(s)}{B(s)}\beta(s) = -\frac{2\sigma^0(s)}{B(s)}, \quad \beta(0) = \frac{\sigma^0(0)}{a^0(0)}. \quad (3.126)$$

Because $B(0) = 0$, we construct the solution of (3.126) in the form $\beta(s) = \beta(0) + \beta_1(s)$, where $\beta_1(s)$ satisfies the linear equation

$$\beta'_1(s) - \frac{2a^0(s)}{B(s)}\beta_1(s) = f(s), \quad \beta_1(0) = 0, \quad (3.127)$$

where

$$f(s) = 2\frac{a^0(0)\sigma^0(s) - a^0(s)\sigma^0(0)}{a^0(s)B(s)}. \quad (3.128)$$

Because both numerator and denominator in (3.128) vanish linearly as $s \rightarrow 0$, the limit $f(0)$ is finite. The solution (3.127) is given by

$$\beta_1(s) = \int_0^s f(s') \exp \left\{ \int_{s'}^s \frac{2a^0(s'')}{B(s'')} ds'' \right\} ds'. \quad (3.129)$$

All integrals in (3.129) are finite, because $a^0(s) > 0$ and $B(s) < 0$ for $s > 0$. It follows that $\gamma(s)$ in (3.124) is a positive function.

Exercise 3.10 (Integration of the Bernoulli equation). Integrate the Bernoulli equation (3.125) numerically for the case of a second-order phase-locked loop and plot the graph of $\gamma(s)$ along the boundary. \square

In view of (3.124), the uniform leading-order approximation to $U_\varepsilon(\mathbf{x})$ is

$$U_\varepsilon(\mathbf{x}) = v_\varepsilon(s, \rho) \sim -\sqrt{\frac{2}{\pi}} \int_0^{\rho\gamma(s)/\sqrt{\varepsilon}} e^{-z^2/2} dz \quad (3.130)$$

(see (3.120)). Consequently, the uniform leading-order approximation to $u_\varepsilon(\mathbf{x})$ is $u_\varepsilon(\mathbf{x}) = C_\varepsilon v_\varepsilon(\rho, s)$, and C_ε is an as yet undetermined constant. To determine C_ε , we need to construct a normalized asymptotic approximation to the solution of the stationary Fokker–Planck equation

$$\begin{aligned} \mathcal{L}_\varepsilon p_\varepsilon(\mathbf{x}) &= \sum_{i,j=1}^2 \varepsilon \frac{\partial^2}{\partial x^i \partial x^j} [\sigma^{i,j}(\mathbf{x}) p_\varepsilon(\mathbf{x})] - \sum_{i=1}^2 \frac{\partial}{\partial x^i} [a^i(\mathbf{x}) p_\varepsilon(\mathbf{x})] \\ &= 0 \text{ for } \mathbf{x} \in \Omega, \end{aligned} \quad (3.131)$$

which we assume is normalized by

$$\int_{\Omega} p_\varepsilon(\mathbf{x}) d\mathbf{x} = 1. \quad (3.132)$$

Note that no boundary conditions are imposed on $p_\varepsilon(\mathbf{x})$. The normalization constant 1 is arbitrary.

The following lemma is proved by applying Green's identity.

Lemma 3.5.1 (The Lagrange identity). *If $p_\varepsilon(\mathbf{x})$ is a solution of the Fokker–Planck equation (3.131) and $u_\varepsilon(\mathbf{x})$ is a sufficiently regular function in Ω that satisfies the boundary condition (3.111), then*

$$\int_{\Omega} p_\varepsilon(\mathbf{x}) \mathcal{L}_\varepsilon^* u_\varepsilon(\mathbf{x}) d\mathbf{x} = \oint_{\partial\Omega} p_\varepsilon(\mathbf{x}) \varepsilon \sum_{i,j} \sigma^{ij}(\mathbf{x}) \frac{\partial u_\varepsilon(\mathbf{x})}{\partial x^j} n^i(\mathbf{x}) ds_x. \quad (3.133)$$

To proceed with the derivation of (3.114), we multiply both sides of (3.111) by the solution $p_\varepsilon(\mathbf{x})$ and use the Lagrange identity (3.133) for the boundary layer expansion (3.130), and (3.116). We obtain

$$-\int_{\Omega} p_\varepsilon(\mathbf{x}) dx \sim -C_\varepsilon \sqrt{\frac{2\varepsilon}{\pi}} \oint_{\partial\Omega} p_\varepsilon(\mathbf{x}) \sum_{i,j} \sigma^{ij}(\mathbf{x}) n^i(\mathbf{x}) \frac{\partial \rho(\mathbf{x})}{\partial x^j} \gamma(s) ds; \quad (3.134)$$

hence

$$C_\varepsilon \sim \frac{\int_{\Omega} p_\varepsilon(\mathbf{x}) dx}{\sqrt{\frac{2\varepsilon}{\pi}} \oint_{\partial\Omega} p_\varepsilon(\mathbf{x}) \sum_{i,j} \sigma^{ij}(\mathbf{x}) n^i(\mathbf{x}) n^j(\mathbf{x}) \gamma(s) ds}. \quad (3.135)$$

In view of (3.116) and (3.130), it suffices to show that (3.135) implies (3.114). Note that the normalization constant in (3.132) does not influence (3.135).

3.5.4 Asymptotic Solution of the Stationary Fokker–Planck Equation

We construct the asymptotic solution to (3.131), as above, by seeking a solution in the WKB form

$$p_\varepsilon(\mathbf{x}) = K_\varepsilon(\mathbf{x}) \exp\left\{-\frac{\Psi(\mathbf{x})}{\varepsilon}\right\}, \quad (3.136)$$

where $K_\varepsilon(\mathbf{x})$ has an asymptotic series expansion in powers of ε ,

$$K_\varepsilon(\mathbf{x}) = K_0(\mathbf{x}) + \varepsilon K_1(\mathbf{x}) + \dots, \quad (3.137)$$

with $K_0(\mathbf{x})$, $K_1(\mathbf{x})$, \dots regular functions in Ω and on its boundary and $\Psi(\mathbf{x})$ is a regular function. Substituting (3.136) into the Fokker–Planck equation (3.131) and comparing like powers of ε , we find at the leading-order $O(\varepsilon^{-1})$ that the eikonal function $\Psi(\mathbf{x})$ has to satisfy the eikonal equation (3.115) and $K_\varepsilon(\mathbf{x})$ has to satisfy the transport equation

$$\begin{aligned} & \varepsilon \sum_{i,j=1}^2 \frac{\partial^2 \sigma^{i,j}(\mathbf{x}) K_\varepsilon(\mathbf{x})}{\partial x^i \partial x^j} - \sum_{i=1}^2 \left[2 \sum_{j=1}^2 \sigma^{i,j}(\mathbf{x}) \frac{\partial \Psi(\mathbf{x})}{\partial x^j} + a^i(\mathbf{x}) \right] \frac{\partial K_\varepsilon(\mathbf{x})}{\partial x^i} \\ & - \sum_{i=1}^2 \left[\frac{\partial a^i(\mathbf{x})}{\partial x^i} + \sum_{j=1}^2 \left(\sigma^{i,j}(\mathbf{x}) \frac{\partial^2 \Psi(\mathbf{x})}{\partial x^i \partial x^j} + 2 \frac{\partial \sigma^{i,j}(\mathbf{x})}{\partial x^j} \frac{\partial \Psi(\mathbf{x})}{\partial x^j} \right) \right] K_\varepsilon(\mathbf{x}) = 0. \end{aligned} \quad (3.138)$$

The expansion (3.137) implies that the transport equation for $K_0(\mathbf{x})$ reduces to

$$\begin{aligned} & \sum_{i=1}^2 \left[2 \sum_{j=1}^2 \sigma^{i,j}(\mathbf{x}) \frac{\partial \Psi(\mathbf{x})}{\partial x^j} + a^i(\mathbf{x}) \right] \frac{\partial K_0(\mathbf{x})}{\partial x^i} \\ & = - \sum_{i=1}^2 \left[\frac{a^i(\mathbf{x})}{\partial x^i} + \sum_{j=1}^2 \left(\sigma^{i,j}(\mathbf{x}) \frac{\partial^2 \Psi(\mathbf{x})}{\partial x^i \partial x^j} + 2 \frac{\partial \sigma^{i,j}(\mathbf{x})}{\partial x^j} \frac{\partial \Psi(\mathbf{x})}{\partial x^j} \right) \right] K_0(\mathbf{x}). \end{aligned} \quad (3.139)$$

3.5.5 The Eikonal Equation for (3.136)

The method of characteristics described in Sect. 3.2.1 gives in the case at hand the function $F(\mathbf{x}, \Psi, \mathbf{p})$ in the eikonal equation (3.115) in the form

$$F(\mathbf{x}, \Psi, \mathbf{p}) = \sum_{i,j=1}^2 \sigma^{i,j}(\mathbf{x}) p^i p^j + \sum_{i=1}^2 a^i(\mathbf{x}) p^i \quad (3.140)$$

$$= \frac{1}{2} p_1^2 + p_1 p_2 + p_2^2 + (x_2 - \sin x_1) p_1 - \sin x_1 p_2, \quad (3.141)$$

so that the characteristic equations (3.22) are

$$\frac{dx}{dt} = 2\sigma(x)\mathbf{p} + \mathbf{a}(x) = \begin{bmatrix} 1 & 1 \\ 1 & 2 \end{bmatrix} \begin{bmatrix} p_1 \\ p_2 \end{bmatrix} + \begin{bmatrix} x_2 - \sin x_1 \\ -\sin x_1 \end{bmatrix}, \quad (3.142)$$

$$\frac{d\mathbf{p}}{dt} = -\nabla_x \mathbf{p}^T \sigma(x) \mathbf{p} - \nabla_x \mathbf{a}^T(x) \mathbf{p} = \begin{bmatrix} (p_1 + p_2) \cos x_1 \\ -p_1 \end{bmatrix}, \quad (3.143)$$

$$\frac{d\Psi}{dt} = \mathbf{p}^T \sigma(x) \mathbf{p} = \frac{1}{2} p_1^2 + p_1 p_2 + p_2^2. \quad (3.144)$$

First, we observe that the trajectories of the autonomous system (3.142), (3.143), which begin near the attractor $\mathbf{x} = \mathbf{p} = \mathbf{0}$ in the (\mathbf{x}, \mathbf{p}) space, diverge. To see this, we linearize the system (3.142), (3.143) around this point and obtain

$$\begin{aligned} \frac{d\mathbf{x}(t)}{dt} &= 2\sigma(\mathbf{0})\mathbf{p}(t) + \mathbf{a}\mathbf{x}(t), \\ \frac{d\mathbf{p}(t)}{dt} &= -\mathbf{a}\mathbf{p}(t), \end{aligned}$$

where \mathbf{a} is defined in (3.97). It follows that $\mathbf{p}(t) = e^{-at} \mathbf{p}(0)$, and hence

$$\mathbf{x}(t) = e^{At} \mathbf{x}_0 + 2 \int_0^t e^{A(t-u)} \sigma(\mathbf{0} e^{-Au} \mathbf{p}(0)) du.$$

For any $(\mathbf{x}(0), \mathbf{p}(0)) \neq (\mathbf{0}, \mathbf{0})$ both $\mathbf{x}(t)$ and $\mathbf{p}(t)$ diverge as $t \rightarrow \infty$, because the eigenvalues of $-A$ have positive real parts.

To integrate the characteristic equations (3.142) and (3.143), initial conditions can be imposed near the unstable critical point $(\mathbf{0}, \mathbf{0})$ by constructing $\Psi(\mathbf{x})$ in the form of a power series, as described in Sect. 3.2.1. The truncation of the power series near the attractor provides an approximation to $\Psi(\mathbf{x})$ and to $\mathbf{p} = \nabla \Psi(\mathbf{x})$, whose error can be made arbitrarily small. Expanding $\Psi(\mathbf{x})$, $\mathbf{a}(\mathbf{x})$, and $\sigma(\mathbf{x})$ in Taylor's series about the origin, we find from the eikonal equation (3.115) that $\nabla \Psi(\mathbf{0}) = \mathbf{0}$, so that the power series expansion of $\Psi(\mathbf{x})$ begins as a quadratic form

$$\Psi(\mathbf{x}) = \frac{1}{2} \mathbf{x}^T \mathbf{Q} \mathbf{x} + o(|\mathbf{x}|^2). \quad (3.145)$$

Substituting (3.145) into the eikonal equation (3.115) with the linearized drift $\mathbf{a}(\mathbf{x}) \approx a\mathbf{x}$ near the origin, we find (use Maple or Mathematica) that

$$\mathbf{Q} = \begin{pmatrix} 1.2 & -0.8 \\ -0.8 & 1.2 \end{pmatrix}, \quad \Psi(\mathbf{x}) \approx 0.6x_1^2 - 0.8x_1x_2 + 0.6x_2^2. \quad (3.146)$$

The matrix \mathbf{Q} is also the solution of the Riccati equation

$$2\mathbf{Q}\sigma(\mathbf{0})\mathbf{Q} + \mathbf{Q}\mathbf{A} + \mathbf{A}^T\mathbf{Q} = \mathbf{0}. \quad (3.147)$$

Note that \mathbf{Q} is the matrix of the second partial derivatives of $\Psi(\mathbf{x})$ at the critical point $\mathbf{x} = \mathbf{0}$ (the so-called *Hessian matrix*). Obviously, the first term in the power series expansion of $\mathbf{p} = \nabla\Psi(\mathbf{x})$ is given by

$$\mathbf{p} = \mathbf{Q}\mathbf{x} + O(|\mathbf{x}|^2) \approx \begin{bmatrix} 1.2x_1 - 0.8x_2 \\ -0.8x_1 + 1.2x_2 \end{bmatrix}. \quad (3.148)$$

In deriving (3.147), use is made of the facts that \mathbf{Q} and σ are symmetric matrices and that a quadratic form vanishes identically if and only if it is defined by an antisymmetric matrix. The solution of (3.147) is a positive definite matrix [Schuss (1980b, Exercise 7.5.2)], [Gantmacher (1998)].

Choosing for the initial surface for the system (3.142)–(3.144) the contour

$$\frac{1}{2}\mathbf{x}^T\mathbf{Q}\mathbf{x} = \delta, \quad (3.149)$$

for some small positive δ , and using the approximate initial values $\Psi(\mathbf{x}) = \delta$ and (3.148) at each point of the surface, we can integrate the system (3.142)–(3.144) analytically or numerically. Once the domain Ω is covered with characteristics, the approximate value of $\Psi(\mathbf{x})$ can be determined at each point $\mathbf{x} \in \Omega$ as the value of the solution $\Psi(t)$ of (3.144) at s such that the solution of (3.142) satisfies

$$\mathbf{x}(t) = \mathbf{x}. \quad (3.150)$$

The initial condition on the surface (3.149) determines the unique trajectory of the system (3.142)–(3.144) that satisfies (3.150) for some s . It can be found numerically by the method of shooting.

Figure 3.4 shows the lock domain Ω and characteristics that hit the separatrix. The lowest characteristic hits the saddle point $(\pi, 0)$. The initial conditions are given on the ellipse (3.149), $0.6x_1^2 - 0.8x_1x_2 + 0.6x_2^2 = 0.06$. The initial values are $x_1(0) = -0.08215$, $x_2(0) = -0.1344583556$, $p_1(0) = 0.0089866845$, $p_2(0) = -0.0956300267$. The characteristic above it hits at $(2.2500, 1.3384)$, the next ones at $(2.0000, 1.6239)$ and at $(1.7250, 1.9809)$, and the top one at $(1.6250, 2.0522)$.

Figure 3.4 shows the values of $\Psi(\cdot)$ along the characteristics of Fig. 3.3. The endpoints of the characteristic curves are on the separatrix, at arc lengths s and values $\Psi(0) = 0.78525$ (the bottom characteristic), $\Psi(1.66) = 0.85$ (the one above it), $\Psi(2.052) = 0.9205$ (the next one), $\Psi(2.45) = 1.1611$ (the one above it), and $\Psi(2.6) = 1.2814$ (the top characteristic). Figure 3.6 shows the graph of $\Psi(s) \approx P_{12}(s)$ vs arc length s on the separatrix. The points of Fig. 3.4 are marked with circles. Figure 3.6 shows an interpolation (with Maple) of the data points in Fig. 3.4

Fig. 3.3 The lock domain D in the (x_1, x_2) plane and characteristics that hit the separatrix

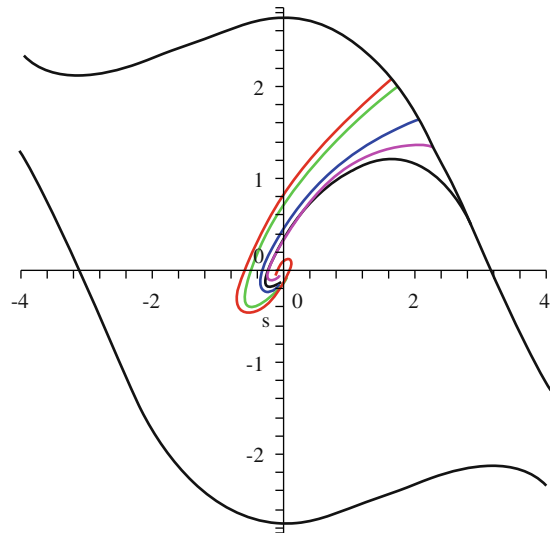
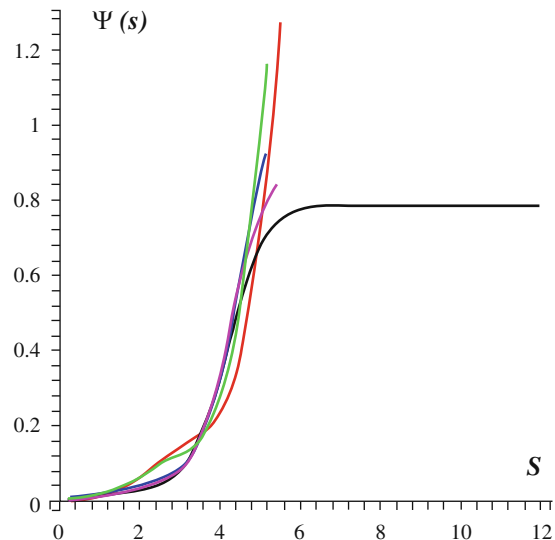


Fig. 3.4 The values of $\Psi(\cdot)$ along the characteristics of Fig. 3.3. The endpoints are on the separatrix



by the 12th-order polynomial

$$\begin{aligned} P_{12}(s) = & 0.78525 + 10^{-2} \times (0.33s - 0.36s^2 - 0.5s^3 - 0.3s^4 + 0.42s^6 + 0.6s^7 \\ & + 0.37s^8 - 0.23s^9 - 0.6s^{10} + 0.41s^{11} - 0.07s^{12}. \end{aligned} \quad (3.151)$$

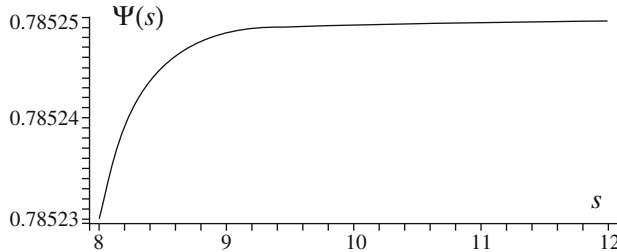
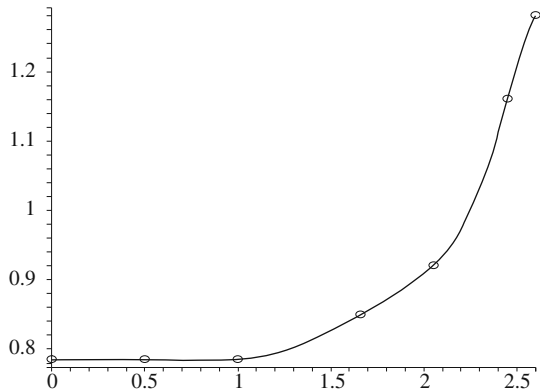


Fig. 3.5 Blow-up of the graph of $\Psi(t)$ near the saddle point $(\pi, 0)$. The value is $\Psi(\pi, 0) \approx 0.78525$

Fig. 3.6 Graph of $\Psi(s) \approx P_{12}(s)$ vs arc length s on the separatrix. The points of Fig. 3.4 are marked with circles



3.5.6 The Eikonal on the Separatrix

The eikonal equation (3.115), with $F(x, \Psi, p)$ given in (3.140), can be written in local coordinates (ρ, s) on $\partial\Omega$ as

$$\sum_{i,j=1}^2 \sigma^{i,j}(0, s) \frac{\partial \Psi(0, s)}{\partial x^i} \frac{\partial \Psi(0, s)}{\partial x^j} + B(s) \frac{\partial \Psi(0, s)}{\partial s} = 0 \quad (3.152)$$

with $B(s)$ given in (3.104). It follows that $\Psi(0, s)$ is minimal on $\partial\Omega$ at the saddle point $s = 0$. Changing the partial derivatives to local variables, we can write (3.152) as

$$\begin{aligned} & \sigma^0(s) \Psi_\rho^2(0, s) + 2 \sum_{i,j=1}^2 \sigma^{i,j}(0, s) \rho_i s_j \Psi_\rho(0, s) \Psi_s(0, s) \\ & + \sum_{i,j=1}^2 \sigma^{i,j}(0, s) s_i s_j \Psi_s^2(0, s) + B(s) \frac{\partial \Psi(0, s)}{\partial s} = 0, \end{aligned} \quad (3.153)$$

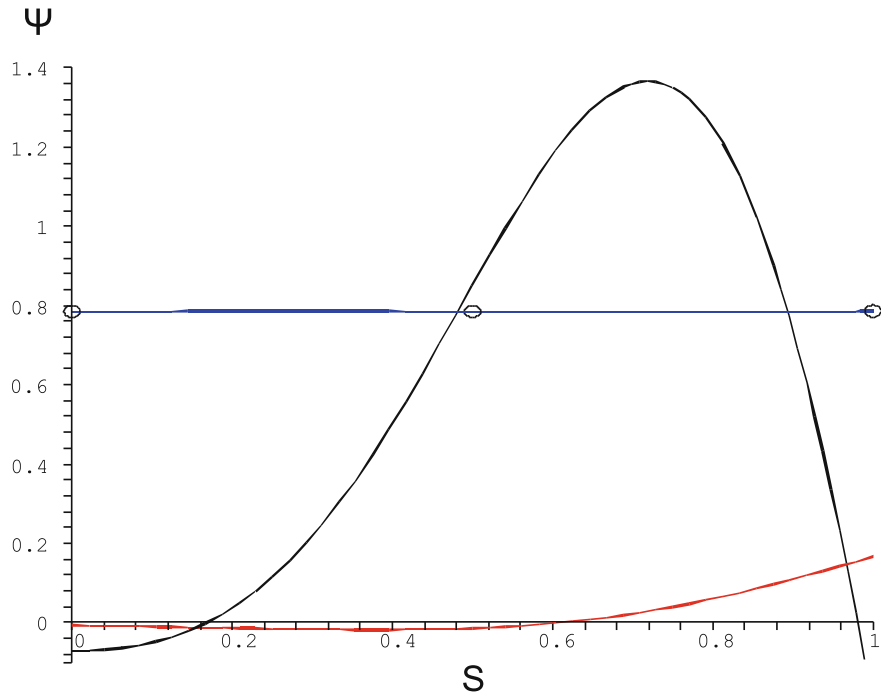
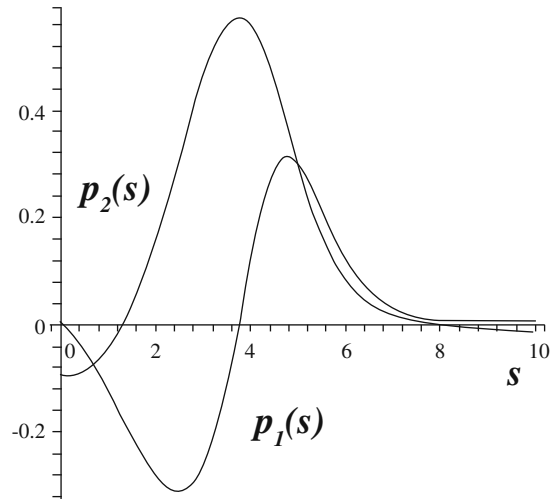


Fig. 3.7 The graphs of $\Psi(s)$ (flat line segment), $\Psi''(s)$ (flat curve near the axis), and $\Psi^{(iv)}(s)$ near the saddle point $s = 0$

Fig. 3.8 The partial derivatives $p_1(t) = \Psi_{x_1}(t)$ and $p_2(t) = \Psi_{x_2}(t)$ along the characteristic in Fig. 3.3



where $\sigma^0(s)$ is given in (3.123). If $\Psi(0, s)$ is constant on a segment of the separatrix near the saddle point (see Figs. 3.6 and 3.8), which show the partial derivatives $p_1(t) = \Psi_{x_1}(t)$ and $p_2(t) = \Psi_{x_2}(t)$ along the characteristic in Fig. 3.3, then the local expansion of $\Psi(\rho, s)$ about the separatrix in this segment is

$$\Psi(\rho, s) = \hat{\Psi} + \frac{\rho^2}{2} \Psi_{\rho\rho}(0, s) + O(\rho^3). \quad (3.154)$$

Setting $\phi(s) = \Psi_{\rho\rho}(0, s)$, the eikonal equation (3.153) on the segment of the separatrix can be written as

$$\rho^2 [\sigma^0(s)\phi^2(s) + B(s)\phi'(s)] + O(\rho^3) = 0.$$

It follows that

$$\sigma^0(s)\phi^2(s) + B(s)\phi'(s) = 0,$$

so

$$\phi(s) = \left[\phi^{-1}(s_0) + \int_{s_0}^s \frac{\sigma^0(u)}{B(u)} du \right]^{-1}, \quad (3.155)$$

where s_0 is the arc length to a point on the separatrix. Using the approximate values on the segment

$$\sigma^0(s) = \sigma^0(0), \quad B(s) \approx -\beta s, \quad (3.156)$$

where β is a positive constant (see Exercise 3.11 below), we obtain

$$\phi(s) \sim \frac{1}{\phi^{-1}(s_0) + \frac{\sigma^0(0)}{\beta} \log \frac{s}{s_0}} \text{ for } 0 < s < s_0. \quad (3.157)$$

Now, it follows from (3.154) and (3.157) that

$$\Psi(\rho, s) = \hat{\Psi} + \frac{1}{2} \frac{\rho^2}{\phi^{-1}(s_0) + \frac{\sigma^0(0)}{\beta} \log \frac{s}{s_0}} + O(\rho^3) \text{ for } 0 < s < s_0. \quad (3.158)$$

The value of $\phi(s_0)$ is negative near the saddle point, so that $\Psi_{\rho\rho}(0, s) < 0$ on the segment and $\Psi_{\rho\rho}(0, 0) = 0$.

Exercise 3.11 (The constants). Prove (3.156) with

$$\sigma^0(0) = \frac{\lambda_-^2 - \lambda_- + 2}{2(1 + \lambda_-^2)}, \quad \beta \approx \frac{-\lambda_- \sqrt{(1 + \lambda_-)^2 + \lambda_-^2}}{\sqrt{1 + \lambda_-^2}}. \quad (3.159)$$

□

3.5.7 The Transport Equation

Recall that $K_\varepsilon(\mathbf{x})$ satisfies the transport equation (3.138). Note that $K_\varepsilon(\mathbf{x})$ cannot have an internal layer at the global attractor point $\mathbf{0}$ in Ω . This is due to the fact that stretching $\mathbf{x} = \sqrt{\varepsilon} \boldsymbol{\xi}$ and taking the limit $\varepsilon \rightarrow 0$ (3.138) converts the transport equation into

$$\sum_{i,j=1}^2 \frac{\partial^2 \sigma^{i,j}(\mathbf{0}) K_0(\boldsymbol{\xi})}{\partial \xi^i \partial \xi^j} - (2A\mathbf{Q} + A\boldsymbol{\xi} \cdot \nabla_{\boldsymbol{\xi}} K_0(\boldsymbol{\xi}) - \text{tr}(A + \sigma(\mathbf{0})\mathbf{Q}) K_0(\boldsymbol{\xi})) = 0,$$

whose bounded solution is $K_0(\boldsymbol{\xi}) = \text{const}$, because $\text{tr}(A + \sigma(\mathbf{0})\mathbf{Q}) = 0$. The last equality follows from the Riccati equation (3.147) (left multiply by \mathbf{Q}^{-1} and take the trace). Because the characteristics diverge, the initial value (at $s = 0$) on each characteristic is given at $\mathbf{x} = \mathbf{0}$ as $K_0(\mathbf{0}) = \text{const}$, which we can choose as $\text{const} = 1$.

Exercise 3.12 (The potential case). Show that if the diffusion matrix σ is constant and $\mathbf{a}(\mathbf{x}) = -\sigma \nabla \phi(\mathbf{x})$ for some function $\phi(\mathbf{x})$, then $\Psi(\mathbf{x}) = \phi(\mathbf{x})$ and the WKB solution of the homogenous Fokker–Planck equation (3.131) is given by $p_\varepsilon(\mathbf{x}) = e^{-\Psi(\mathbf{x})/\varepsilon}$, that is, the solution of the transport equation (3.138) is $K_0 = \text{const}$. □

The transport equation has to be integrated numerically, together with the characteristic equations (3.142), (3.143). To evaluate the partial derivatives $\partial^2 \Psi(\mathbf{x}) / \partial x^i \partial x^j$ along the characteristics, we use (3.145), (3.148), and set

$$\left. \frac{\partial^2 \Psi(\mathbf{x})}{\partial x^i \partial x^j} \right|_{\mathbf{x}=\mathbf{0}} = Q^{i,j}$$

on the initial ellipsoid (3.149). The differential equations for $\partial^2 \Psi(\mathbf{x}) / \partial x^i \partial x^j$ along the characteristics are derived by differentiating the characteristic equations (3.142), (3.143) with respect to the initial values $\mathbf{x}(0)$ on the initial ellipse. Writing

$$\mathbf{x}_j(t) = \frac{\partial \mathbf{x}(t)}{\partial x_0^j}, \quad \mathbf{p}_j(t) = \frac{\partial \mathbf{p}(t)}{\partial x_0^j}, \quad Q^{i,j}(t) = \frac{\partial^2 \Psi(\mathbf{x}(t))}{\partial x^i \partial x^j}, \quad (3.160)$$

we get the identity $\mathbf{p}_j(t) = \mathbf{Q}(t)\mathbf{x}_j(t)$. Thus the matrix $\mathbf{P}(t)$, whose columns are the vectors $\mathbf{p}_j(t)$, and the matrix $\mathbf{X}(t)$, whose columns are the vectors $\mathbf{x}_j(t)$, are related by $\mathbf{P}(t) = \mathbf{Q}(t)\mathbf{X}(t)$, or

$$\mathbf{Q}(t) = \mathbf{P}(t)\mathbf{X}^{-1}(t). \quad (3.161)$$

The initial conditions are

$$x_j^i(0) = \delta_{i,j}, \quad (3.162)$$

$$p_j^i(0) = \left. \frac{\partial^2 \Psi(\mathbf{x})}{\partial x^i \partial x^j} \right|_{\mathbf{x}=\mathbf{0}} = Q^{i,j}(0) = Q^{i,j}, \quad (3.163)$$

and the dynamics are

$$\frac{d\mathbf{x}_j(t)}{dt} = \sum_{k=1}^2 \left\{ 2 \frac{\partial \sigma(\mathbf{x}(t))}{\partial x^k} \mathbf{p}(t) + 2 \sigma(\mathbf{x}(t)) \mathbf{p}_k(t) + \frac{\partial \mathbf{a}(\mathbf{x}(t))}{\partial x^k} \right\} x_k^j(t), \quad (3.164)$$

$$\begin{aligned} \frac{d\mathbf{p}_j(t)}{dt} = & - \sum_{k=1}^2 \left[\nabla_{\mathbf{x}} \mathbf{p}^T(t) \frac{\partial \sigma(\mathbf{x}(t))}{\partial x^k} \mathbf{p}(t) + 2 \nabla_{\mathbf{x}} \mathbf{p}_k^T(t) \sigma(\mathbf{x}(t)) \mathbf{p}(t) \right. \\ & \left. + \nabla_{\mathbf{x}} \mathbf{a}^T(\mathbf{x}(t)) \mathbf{p}_k(t) + \frac{\partial}{\partial x^k} \nabla_{\mathbf{x}} \mathbf{a}^T(\mathbf{x}(t)) \mathbf{p}(t) \right] x_k^j(t). \end{aligned} \quad (3.165)$$

Exercise 3.13 (The system (3.164), (3.165) for the second-order phase-locked loop).

1. Show that the system (3.164), (3.165) for the phase-locked loop model is

$$\frac{d}{dt} \frac{\partial x_1}{\partial x_1^0} = \frac{\partial p_1}{\partial x_1^0} + \frac{\partial p_2}{\partial x_1^0} + \frac{\partial x_2}{\partial x_1^0} - \cos x_1 \frac{\partial x_1}{\partial x_1^0}, \quad (3.166)$$

$$\frac{d}{dt} \frac{\partial x_1}{\partial x_2^0} = \frac{\partial p_1}{\partial x_2^0} + \frac{\partial p_2}{\partial x_2^0} + \frac{\partial x_2}{\partial x_2^0} - \cos x_1 \frac{\partial x_1}{\partial x_2^0},$$

$$\frac{d}{dt} \frac{\partial x_2}{\partial x_1^0} = \frac{\partial p_1}{\partial x_1^0} + 2 \frac{\partial p_2}{\partial x_1^0} - \cos x_1 \frac{\partial x_1}{\partial x_1^0},$$

$$\frac{d}{dt} \frac{\partial x_2}{\partial x_2^0} = \frac{\partial p_1}{\partial x_2^0} + 2 \frac{\partial p_2}{\partial x_2^0} - \cos x_1 \frac{\partial x_1}{\partial x_2^0},$$

$$\frac{d}{dt} \frac{\partial p_1}{\partial x_1^0} = \left(\frac{\partial p_1}{\partial x_1^0} + \frac{\partial p_2}{\partial x_1^0} \right) \cos x_1 - (p_1 + p_2) \sin x_1 \frac{\partial x_1}{\partial x_1^0}, \quad (3.167)$$

$$\frac{d}{dt} \frac{\partial p_1}{\partial x_2^0} = \left(\frac{\partial p_1}{\partial x_2^0} + \frac{\partial p_2}{\partial x_2^0} \right) \cos x_1 - (p_1 + p_2) \sin x_1 \frac{\partial x_1}{\partial x_2^0},$$

$$\frac{d}{dt} \frac{\partial p_2}{\partial x_1^0} = - \frac{\partial p_1}{\partial x_1^0}, \quad \frac{d}{dt} \frac{\partial p_2}{\partial x_2^0} = - \frac{\partial p_1}{\partial x_2^0}.$$

Then Eq. (3.160), $\partial x_i / \partial x_j^0 = x_{i,j}$, and $\partial p_i / \partial x_j^0 = p_{i,j}$ give

$$\dot{x}_{1,1} = p_{1,1} + p_{2,1} + x_{2,1} - \cos x_1 x_{1,1}, \quad (3.168)$$

$$\dot{x}_{1,2} = p_{1,2} + p_{2,2} + x_{2,2} - \cos x_1 x_{1,2},$$

$$\dot{x}_{2,1} = p_{1,1} + 2p_{2,1} - \cos x_1 x_{1,1},$$

$$\dot{x}_{2,2} = p_{1,1} + 2p_{2,2} - \cos x_1 x_{1,2},$$

$$\dot{p}_{1,1} = (p_{1,1} + p_{2,1}) \cos x_1 - (p_1 + p_2) \sin x_1 x_{1,1}, \quad (3.169)$$

$$\dot{p}_{1,2} = (p_{1,2} + p_{2,2}) \cos x_1 - (p_1 + p_2) \sin x_1 x_{1,2},$$

$$\dot{p}_{2,1} = -p_{1,1}, \quad \dot{p}_{2,2} = -p_{1,2}.$$

2. Show that the transport equation (3.139) can be written on the characteristics $\mathbf{x}(t)$ as

$$\begin{aligned} \frac{dK_0(\mathbf{x}(t))}{dt} &= -K_0(\mathbf{x}(t)) \quad (3.170) \\ &\times \sum_{i=1}^2 \left[\frac{\partial a^i(\mathbf{x}(t))}{\partial x^i} + \sum_{j=1}^2 \left(\sigma^{i,j}(\mathbf{x}(t)) Q^{i,j}(t) + 2 \frac{\partial \sigma^{i,j}(\mathbf{x}(t))}{\partial x^j} p_j(t) \right) \right]. \end{aligned}$$

3. Show that as $t \rightarrow \infty$, the characteristic that hits the saddle point coalesces with the separatrix on a segment near the saddle point.
4. Show that because $\sum_{i=1}^2 \partial a^i(\mathbf{x}(t))/\partial x^i = -\cos x_1$, along this segment

$$\sum_{i=1}^2 \frac{\partial a^i(\mathbf{x}(t))}{\partial x^i} \rightarrow 1, \quad \frac{\partial \sigma^{i,j}(\mathbf{x}(t))}{\partial x^j} p_j(t) y = 0, \quad \sum_{i=1}^2 \sum_{j=1}^2 \sigma^{i,j}(\mathbf{x}(t)) Q^{i,j}(t) \rightarrow 0$$

as $t \rightarrow \infty$, which implies that the transport equation near the saddle point can be written as

$$\frac{dK_0(\mathbf{x}(t))}{dt} = (-1 + o(1)) K_0(\mathbf{x}(t)) \text{ as } t \rightarrow \infty.$$

5. Conclude that $K_0(\mathbf{x}(t)) = K_0(\mathbf{x}(t_1)) e^{-(t-t_1)(1+o(1))} \rightarrow 0$ as $t \rightarrow \infty$, where $\mathbf{x}(t_1)$ is a point on the segment of the separatrix near the saddle point.
6. To express $K_0(\mathbf{x}(t))$ on the segment of the separatrix in terms of arc length s from the saddle point, recall that $s = \delta e^{\lambda_-(t-t_1)}$ (see (3.99)); now, because $\lambda_- < 0$,

$$K_0(s) = K_0(s_1) \left(\frac{s}{\delta} \right)^{-(1+o(1))/\lambda_-} \rightarrow 0 \text{ as } s \rightarrow 0. \quad (3.171)$$

Figure 3.3 shows that $\delta = 1$ can be assumed. \square

In summary, the numerical integration of the eikonal and the transport equations consists in integrating numerically the differential equations (3.142)–(3.144) and

(3.164)–(3.170) with initial values $\mathbf{x}(0)$ that cover the ellipse (3.149), with $\mathbf{p}(0)$ and $\Psi(\mathbf{x}(0))$ given by $\mathbf{p}(0) = \mathbf{Q}(0)\mathbf{x}(0)$ and $\Psi(\mathbf{x}(0)) = \delta$, and the initial values (3.162), (3.163), and $K_0(\mathbf{x}(0)) = 1$. The matrix $\mathbf{Q}(t)$ has to be evaluated from (3.161) at each step of the integration.

Exercise 3.14 (The characteristics for the second-order phase-locked loop).

1. Use the fact that $\sigma(\mathbf{x})$ in the case of the error dynamics (3.91) of the second-order phase-locked loop is a constant matrix, to simplify the characteristic equations (3.142), (3.143), (3.164), and (3.165).
2. Write the transport equation (3.170) in the form

$$\frac{dK_0(\mathbf{x}(t))}{dt} = -[\nabla \cdot \mathbf{a}(\mathbf{x}(t)) + \text{tr}(\sigma(\mathbf{x}(t))\mathbf{Q}(t))]K_0(\mathbf{x}(t)). \quad (3.172)$$

3. Integrate the characteristic equations (3.142)–(3.144) together with (3.164), (3.165) (that is, with (3.168) and (3.169)) and calculate $\mathbf{Q}(t)$ from (3.161).
4. Integrate the transport equation (3.170) and plot $K_0(t)$ on $\partial\Omega$. \square

3.5.8 Derivation of (3.114)

To complete the derivation of (3.114), we have to show that (3.135) implies (3.114). To do so, we use the WKB solution (3.136) in (3.135) and evaluate the integrals asymptotically for small ε by the Laplace method. The main contribution to the numerator comes from the minimum of $\Psi(\mathbf{x})$ in Ω at $\mathbf{x} = \mathbf{0}$. The value of the integral is given by

$$\int_{\Omega} p_{\varepsilon}(\mathbf{x}) d\mathbf{x} = \int_{\Omega} K_{\varepsilon}(\mathbf{x}) e^{-\Psi(\mathbf{x})/\varepsilon} d\mathbf{x} = \frac{2\pi\varepsilon K_0(\mathbf{0})e^{-\Psi(\mathbf{0})/\varepsilon}}{\mathcal{H}(\mathbf{0})} (1 + O(\varepsilon)), \quad (3.173)$$

where $\mathcal{H}(\mathbf{0})$ is the determinant of the Hessian matrix of $\Psi(\mathbf{0})$ and is equal to the determinant of \mathbf{Q} (see (3.146)). For the second-order phase-locked loop, we have $K_0(\mathbf{0}) = 1$, $\Psi(\mathbf{0}) = 0$, and $\det \mathbf{Q} = 0.8$. It follows that the value of the integral is $2.5\pi\varepsilon + O(\varepsilon^2)$.

Using the notation (3.123), the initial value $\gamma(0)$ (given in (3.125)), and the WKB solution (3.136), the integral in the denominator of (3.135) is evaluated by the Laplace method on $\partial\Omega$ as

$$\begin{aligned} & \sqrt{\frac{2\varepsilon}{\pi}} \oint_{\partial\Omega} p_{\varepsilon}(\mathbf{x}(s)) \sum_{i,j} \sigma^{ij}(\mathbf{x}(s)) n^i(s) n^j(s) \gamma(s) ds \\ &= \sqrt{\frac{2\varepsilon}{\pi}} \sqrt{2\pi\varepsilon} K_0(0) e^{-\Psi(0)/\varepsilon} \sigma^0(0) \sqrt{\frac{a^0(0)}{\sigma^0(0)}} (1 + O(\sqrt{\varepsilon})) \end{aligned}$$

$$= 2\varepsilon K_0(0) \sqrt{\frac{a^0(0)\sigma^0(0)}{\Psi''(0)}} e^{-\Psi(0)/\varepsilon} (1 + O(\sqrt{\varepsilon})). \quad (3.174)$$

The approximation (3.174) is valid if $K_0(0) \neq 0$ and $\Psi''(0) > 0$.

If $\Psi''(0) > 0$, but $K_0(s)$ on the boundary vanishes at the saddle point $s = 0$ as $K_0(s) = K_0 s^{2k}$, then the value of the integral is

$$\begin{aligned} & \sqrt{\frac{2\varepsilon}{\pi}} \oint_{\partial\Omega} p_\varepsilon(\mathbf{x}(s)) \sum_{i,j} \sigma^{ij}(\mathbf{x}(s)) n^i(s) n^j(s) \gamma(s) ds \\ &= K_0 \left(\frac{\varepsilon}{\Psi''(0)} \right)^{k+1/2} 2^{k+1} \Gamma(k+1) \sqrt{a^0(0)\sigma^0(0)} e^{-\Psi(0)/\varepsilon} (1 + o(1)), \end{aligned} \quad (3.175)$$

where $\Gamma(\cdot)$ is Euler's gamma function. Figure 3.7 shows the graphs of $\Psi(s)$ (flat line segment), $\Psi''(s)$ (flat curve near the axis), and $\Psi^{(iv)}(s)$ near the saddle point $s = 0$ for the characteristics of Fig. 3.3.

If $\Psi(s) = \Psi(0) = \hat{\Psi}$ on a finite interval $0 \leq s \leq s_0$ (see, e.g., Figs. 3.6 and 3.7), then

$$\begin{aligned} & \sqrt{\frac{2\varepsilon}{\pi}} \oint_{\partial\Omega} p_\varepsilon(\mathbf{x}(s)) \sum_{i,j} \sigma^{ij}(\mathbf{x}(s)) n^i(s) n^j(s) \gamma(s) ds \\ &= \sqrt{\frac{2\varepsilon}{\pi}} e^{-\hat{\Psi}/\varepsilon} \int_0^{s_0} K_0(s) \sigma^0(s) \gamma(s) (1 + o(1)) ds \end{aligned} \quad (3.176)$$

(see (3.171)).

In each of these cases, (3.114) follows by using (3.173) and (3.174) (or (3.175), or (3.176)) in (3.135). \square

3.5.9 Green's Function for the Boundary Value Problem is the Exit Density

The (normalized) absorption flux density of trajectories on the separatrix is calculated from the solution $p_\varepsilon(\mathbf{x} | \mathbf{y})$ of the boundary value problem

$$\sum_{i,j=1}^2 \varepsilon \frac{\partial^2 [\sigma^{i,j}(\mathbf{x}) p_\varepsilon(\mathbf{x} | \mathbf{y})]}{\partial x^i \partial x^j} - \sum_{i=1}^2 \frac{\partial [a^i(\mathbf{x}) p_\varepsilon(\mathbf{x} | \mathbf{y})]}{\partial x^i} = -\delta(\mathbf{x} - \mathbf{y}) \quad (3.177)$$

$$p_\varepsilon(\mathbf{x} \mid \mathbf{y})|_{\mathbf{x} \in \partial\Omega, \mathbf{y} \in \Omega} = 0, \quad (3.178)$$

where

$$\boldsymbol{\sigma}(\mathbf{x}) = \frac{1}{2}\mathbf{b}(\mathbf{x})\mathbf{b}^T(\mathbf{x}).$$

Note that $p_\varepsilon(\mathbf{x} \mid \mathbf{y})$ is Green's function for the inhomogeneous stationary Fokker–Planck equation (3.177) with the homogeneous boundary condition (3.178). In the case at hand, $\Psi(s) = \Psi(0) = \hat{\Psi}$ on a finite interval $0 \leq s \leq s_0$ (see, e.g., Figs. 3.6 and 3.7), so

$$\begin{aligned} p_\varepsilon(s) ds &= \Pr\{\mathbf{x}(\tau) \in \mathbf{x}(s) + ds \mid \mathbf{x}(0) = \mathbf{y}\} \\ &= \frac{\mathbf{J}(\mathbf{x}(s) \mid \mathbf{y}) \cdot \mathbf{n}(\mathbf{x}(s))}{F(\mathbf{y})} ds \\ &= \sqrt{\frac{2\varepsilon}{\pi}} \frac{p_\varepsilon(\mathbf{x}(s) \mid \mathbf{y})}{F(\mathbf{y})} \sum_{i,j} \sigma^{ij}(\mathbf{x}(s)) n^i(s) n^j(s) \tilde{\gamma}(s) ds \\ &= \frac{e^{-\Psi(s)/\varepsilon} K_0(s) \sigma^0(s) \tilde{\gamma}(s) (1 + o(1)) ds}{\int_{\partial\Omega} e^{-\Psi(s)/\varepsilon} K_0(s) \sigma^0(s) \tilde{\gamma}(s) (1 + o(1)) ds} \\ &\approx \frac{e^{-\Psi(s)/\varepsilon} (s)^{-1/\lambda_-} ds}{\int_{\partial\Omega} e^{-\Psi(s)/\varepsilon} K_0(s) \sigma^0(s) \tilde{\gamma}(s) ds} \end{aligned} \quad (3.179)$$

(see (3.171)), where $\sigma^0(s)$ and $\tilde{\gamma}(s)$ have been approximated by their values at $s = 0$. Figure 3.9 shows the exit density $p_\varepsilon(s)$ (3.179) on the upper branch of the separatrix for $\varepsilon = 0.005, 0.05, 0.1$, and 0.3 (from the top down at the origin). Figure 3.10 shows the point of maximal exit probability on the upper branch of the separatrix. The exit density (lower at $\varepsilon = 0$, upper at $\varepsilon = 0.3$) is maximal at $s_m \approx 0.8 + 1.3\sqrt{\varepsilon}$ (upper at $\varepsilon = 0$, lower at $\varepsilon = 0.3$) at arc length s_m from the saddle point [Schuss (1980b)], [Bobrovsky and Schuss (1982)].

3.6 Annotations

The exit problem in the theory of stochastic differential equations concerns the escape of the random trajectories of a dynamical system driven by noise from the domain of attraction of the underlying noiseless dynamics (see, e.g., [Kramers (1940)], [Ludwig (1975)], [Mangel and Ludwig (1977)], [Bobrovsky and Schuss (1982)], [Gardiner (1985)], [Freidlin and Wentzell (1984)], [Mel'nikov and Meshkov (1986)], [Hänggi et al. (1990)], [Risken (1996)] and references therein). Large deviations theory [Freidlin and Wentzell (1984)], [Ellis (1985)], [Deuschel and Stroock (1989)], [Dembo and Zeitouni (1993)] predicts that in the limit of vanishing noise escapes are concen-

Fig. 3.9 The exit density (3.179) on the upper branch of separatrix for $\varepsilon = 0.005, 0.05, 0.1, 0.3$ (from top down at the origin)

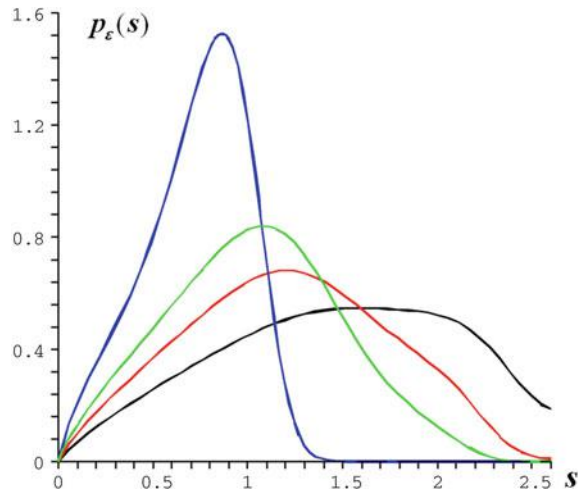
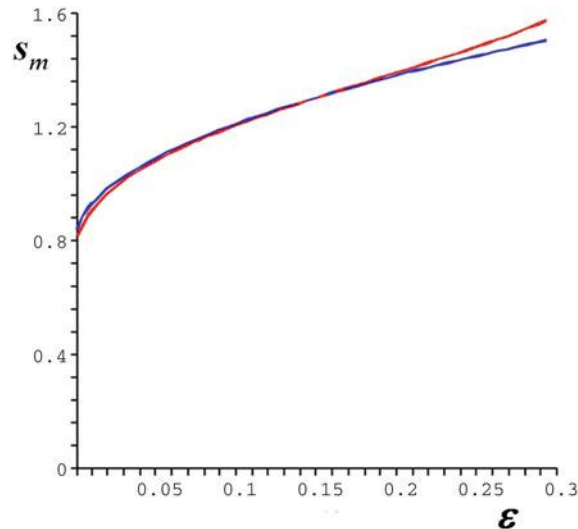


Fig. 3.10 The exit density (lower at $\varepsilon = 0$, upper at $\varepsilon = 0.3$) is maximal at $s_m \approx 0.8 + 1.3\sqrt{\varepsilon}$ (upper at $\varepsilon = 0$, lower at $\varepsilon = 0.3$)



trated at the absolute minima of an action functional on the separatrix (the boundary of the domain of attraction of an attractor of the noiseless dynamics). However, it has been observed in numerical simulations [Schuss (1980b)], [Bobrovsky and Schuss (1982)], [Katz (1985)], [Ryter and Meyr (1978)] that for finite noise strength this is not the case and actually, escaping trajectories avoid the absolute minimum so that the escape distribution is spread on the separatrix away from the points predicted by large deviations theory. Some analytical results concerning this saddle point avoidance phenomenon were given in [Schuss (1980b)], [Bobrovsky and Schuss (1982)], [Day Basel (1990)], [Day (1989)], [Day (1990a)], [Day (1992)], [Maier and Stein

PRE (1993b)], [Maier and Stein (1993a)], [Maier and Stein (1996a)], [Maier and Stein JST (1996b)], [Maier and Stein (1997)], [Maier et al. (1997)], and also in [Schuss and Spivak (1998)] and [Schuss and Spivak (2002)], where the analytical results are also compared with results of simulations.

Kramers' model of activated escape [Kramers (1940)] has become a cornerstone in statistical physics, with applications in many branches of science and mathematics. It has important applications in diverse areas such as communications theory [Bobrovsky and Schuss (1982)], [Viterbi (1967)], stochastic stability of structures [Katz (1985)], [Katz and Schuss (1985)], and even in the modern theory of finance [Wilmott et al. (1994)].

A vast literature on exit problems has been accumulated [Hänggi et al. (1990)] and the problem is still an active area of physical, chemical, biological, and mathematical research. The problem of distribution of the exit points is related to the distribution of energies of the escaping particles [Mel'nikov and Meshkov (1986)], [Büttiker et al. (1979)], to the phenomenon of saddle point avoidance elaborated by Berezhkovskii et al. (see the review [Nitzan and Schuss (1993)] and references therein), and to numerical simulations of escape problems (see, for example, also [Bobrovsky and Zeitouni (1992)]). The problem of determining the distribution of exit points has been studied in different contexts, under various assumptions, and by a variety of methods, analytical, numerical, and experimental in [Schuss (1980b)], [Maier and Stein PRE (1993b)], [Maier and Stein (1993a)], [Maier and Stein JST (1996b)], [Maier and Stein (1996a)], [Maier and Stein (1997)], [Maier et al. (1997)]. The well-known result

$$\bar{\tau}_1(A) \sim \frac{2\pi\varepsilon}{\gamma I_C \omega_A} e^{(E_C - E_A)/\varepsilon}$$

was derived by Kramers [Kramers (1940)] (see also [Chandrasekhar (1943)]) in the limit of small γ and in [Matkowsky et al. (1983)], for all γ . The Bernoulli equation

$$y_\Gamma(x)\beta'(x) + b_0(x)\beta(x) = \gamma\rho_y^2(x, y_\Gamma(x))\beta^3(x),$$

was derived in [Mangel and Ludwig (1977)].

The unexpected phenomenon of saddle point avoidance was first observed in a class of noise-driven dynamical systems lacking detailed balance [Bobrovsky and Schuss (1982)]. It was observed that the exit points on the boundary of the domain of attraction of the attractor of the noiseless dynamics is not necessarily peaked at the saddle point. This phenomenon, not being related to anisotropy in the noise or the dynamics [Nitzan and Schuss (1993)], is counterintuitive and requires explanation. It was studied under a variety of assumptions in [Day Basel (1990)], [Day (1989)], [Day (1990a)], [Day (1992)], [Maier and Stein PRE (1993b)], [Maier and Stein (1993a)], [Maier and Stein JST (1996b)], [Maier and Stein (1996a)], [Maier and Stein (1997)], [Maier et al. (1997)], [Nitzan and Schuss (1993)]. The significance of the problem in models of electronic signal tracking devices, such as RADAR, spread spectrum communications (as in cellular phones), and in various synchronization devices, is

that the determination of the exit distribution on the boundary of the domain of attraction indicates where to tune the lock detector that determines if the signal is lost and has to be acquired afresh.

The realization that the exit point on the separatrix in Kramers' activated escape problem is not at the saddle point, even for large values of the damping coefficient, came as a surprise. This phenomenon in the Kramers problem was first observed in numerical simulations of the Langevin dynamics [Katz (1985)], [Ryter and Meyr (1978)] and was initially interpreted as a numerical instability of the simulation scheme. The problem of the asymptotic convergence of the boundary layer expansion of the exit problem is discussed in [Kamienomostskaya (1952)], [Kamienomostskaya (1955)]. The convergence of the expansion (3.48) is discussed in [Kamin (1978)], [Devinatz and Friedman (1977)], [Devinatz and Friedman (1978)].

3.7 An Attractor Inside an Unstable Limit Cycle

The reduced equation in higher-dimensional boundary value problems, in contrast to the one-dimensional case, may have rich geometrical behavior, which influences the asymptotic structure of the solution of the boundary value problem. The rich behavior is illustrated by the example, where the reduced equation is that of the underdamped forced physical pendulum. This example represents several important physical systems, including the current-driven point Josephson junction, charged density waves, and more [Ben-Jacob et al. PRA (1982)]. It is an archetypical example of a multistable physical system that has many steady-states, some of which are equilibria and some are not. In the context of the Josephson junction, there are stable thermodynamical equilibrium states, in which no current flows through the junction, and a nonequilibrium steady-state, in which the junction carries a steady current. A measurable effect of the noise in the system is the switching of the current between its two steady values at random times, giving rise to an average current proportional to the probability of the conducting state. The random switching of the current on and off is analogous to gating in ionic channels of biological membranes [Hille (2001)].

The main difficulty in analyzing the thermal fluctuations and activated transitions between the steady-states is the fact that thermodynamics and the Boltzmann distribution of energies apply to this system only near the stable equilibria, whereas they do not apply near the nonequilibrium steady-state of the system. Thus the Maxwell–Boltzmann distribution in phase space has to be replaced with a probability distribution in the space of the trajectories of the system. This section shows how the Fokker–Planck equation and the Pontryagin–Andronov–Vitt equation can supplant the notions of energy and entropy in the nonequilibrium statistical mechanics of certain physical systems. Some of the predictions of this analysis were actually discovered in laboratory experiments [Christiano and Silvestrini (1988)].

3.7.1 The Reduced Equation: an Underdamped Forced Pendulum

The stochastic dynamics of the noisy underdamped forced physical pendulum is described by the Langevin equation (3.75),

$$\ddot{x} + \gamma\dot{x} + \tilde{U}'(x) = \sqrt{\frac{2\gamma k_B T}{m}} \dot{w}, \quad (3.180)$$

where $\tilde{U}(x)$ is the potential

$$U(x) = -\cos x - Ix. \quad (3.181)$$

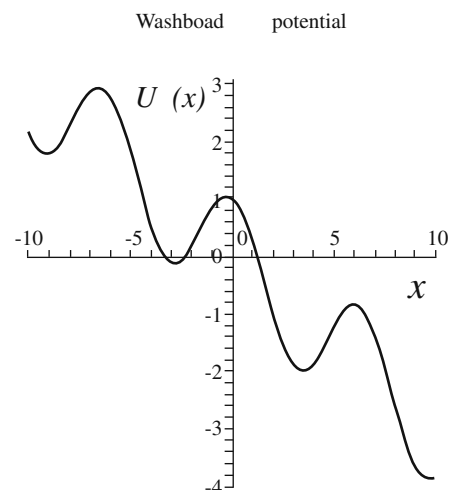
Here x represents the deflection angle and I represents an applied constant torque (see Fig. 3.11).

To understand the behavior of the noiseless system, we examine first the phase-plane dynamics of the forced pendulum. The dynamics of the pendulum depend on the values of γ and I . There is a range of values of these parameters, $I_{\min}(\gamma) < I < 1$ and $\gamma < \pi/4$, for which both stable equilibria and nonequilibrium stable steady-state solutions coexist. In the latter running state \dot{x} is a periodic function of x and $x(t) \rightarrow \infty$ as $t \rightarrow \infty$.

To explore this range of parameters, we represent the phase space trajectories by the ordinary differential equation

$$\frac{dy}{dx} = -\gamma + \frac{I - \sin x}{y}. \quad (3.182)$$

Fig. 3.11 The washboard potential $U(x) = \cos x - Ix$ for $I = 0.3$



Obviously, the system has stable equilibrium points on the x -axis, where $U'(x) = \sin x - I = 0$, at distances 2π apart, if $|I| < 1$. For $|I| > 1$ no such equilibria exist.

Exercise 3.15 (A stable periodic solution).

- (i) Show that a stable periodic solution of (3.182) can be constructed for small γ and $|I| < 1$ in the form

$$y \sim \frac{y_{-1}}{\gamma} + y_0 + \gamma y_1 + \dots \quad (3.183)$$

- (ii) Substitute (3.183) into (3.182), compare coefficients of like powers of γ and use the periodicity condition to find the coefficients y_{-1}, y_0, y_1, \dots . Obtain

$$y_S(x) = \frac{I}{\gamma} + \frac{\gamma}{I} \cos \left(x + \frac{\gamma^2}{I} \right) - \frac{1}{4} \left(\frac{\gamma}{I} \right)^3 \cos 2x + O \left(\frac{\gamma^5}{I^5} \right). \quad (3.184)$$

- (iii) Show that the domains of attraction Ω_S of the two types of stable states of the system are separated by separatrices.

- (iv) Draw the phase plane trajectories of the system (see Fig. 3.12).

- (v) Show that the running solution (3.184) disappears if γ is not sufficiently small.

- (vi) Scale $I = \gamma I_0$ and expand $y \sim y_0 + \gamma y_1 + \dots$ in (3.182) and then show that the first term, y_0 , satisfies the undamped and unforced pendulum equation, so that $y_0 = \sqrt{2 + 2 \cos x} = 2 |\cos x/2|$. Finally, obtain at the next order the periodicity condition $2\pi I_0 = \int_0^{2\pi} y_0 dx = 8$. \square

Fig. 3.12 The stable running solution (top) and separatrices, 2π apart in the phase space (x, \dot{x}) , for $\gamma = 0.1$ and $I = 0.3$. The thick curve is the critical trajectory $S = S_C$ that touches the x -axis. The energy of the system on the running solution slides to $-\infty$ down the washboard potential in Fig. 3.11

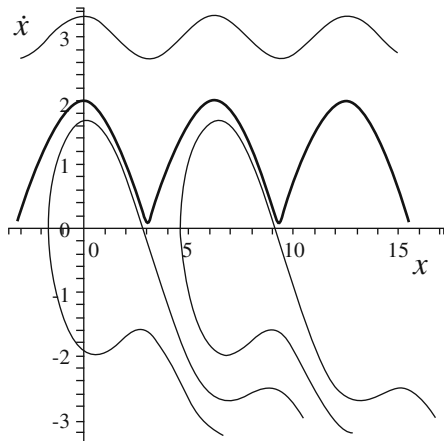
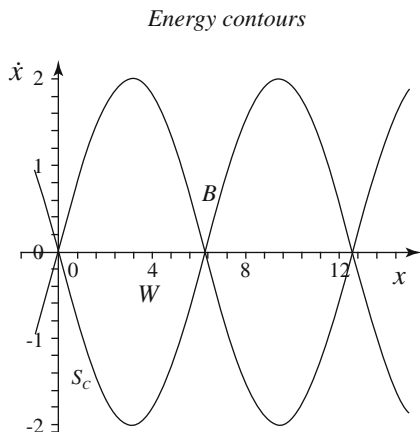


Fig. 3.13 In the limit $\gamma \rightarrow 0$ the stable running solution of Fig. 3.12 disappears to infinity and the critical energy contour $S = S_C$ and the separatrices coalesce



Exercise 3.16 (The critical trajectory).

- (i) Show that $I_0 = 4/\pi$ on the critical trajectory $S = S_C$ that touches the x -axis. Conclude that the maximal value of γ for which the running solution (3.184) exists, for given $|I| < 1$, is $\gamma_M(I) = \pi I/4$ and the minimal value of I for which the running solution exists, for a given value of γ , is $I_{\min}(\gamma) \approx 4\gamma/\pi$.
- (ii) Show that as $\gamma \uparrow \gamma_M$, the minimum of the periodic trajectory (3.184) approaches the x -axis. The critical trajectory S_C touches the separatrix at the unstable equilibrium point and has a cusp there. To this end, set $\gamma = \gamma_M$ in (3.182) and take the limit $x \rightarrow x_0$, where $I - \sin x_0 = 0$ (x_0 is the coordinate of the unstable equilibrium point). Obtain

$$y'(x_0) = -\gamma_M - \frac{\cos x_0}{y'(x_0)} = -\gamma_M - \frac{\sqrt{1 - I^2}}{y'(x_0)}.$$

- (iii) Show that the critical trajectory has two different slopes at the point x_0 where it touches the x -axis, by proving that

$$y'(x_0) = \frac{-\gamma_M \pm \sqrt{\gamma_M^2 + 4\sqrt{1 - I^2}}}{2}. \quad (3.185)$$

- (iv) Show that in the limit $\gamma \rightarrow 0$ Fig. 3.12 collapses to Fig. 3.13. □

Exercise 3.17 (Loss of bistability).

- (i) Show that if $|I| > 1$, then there is a stable running solution for all values of γ .
- (ii) Show that for $\gamma \gg 1$ and $|I| > 1$ an expansion in powers of $1/\gamma$ gives

$$y(x) = \frac{1 - \sin x}{\gamma} + \frac{I \cos x - \frac{1}{2} \sin 2x}{\gamma^3} + O\left(\frac{1}{\gamma^5}\right). \quad (3.186)$$

(iii) Obtain a uniform expansion of $y(x)$, valid for all γ and $|I| > 1$, by truncating the Fourier expansion of y as

$$y(x) = \frac{1}{\gamma} + \frac{I\gamma \cos x}{I^2 + \gamma^4} - \frac{\gamma^3 \sin x}{I^2 + \gamma^4} + \dots$$

Show that this expansion reduces to (3.184) and (3.186) in the appropriate limits.

(iv) Show that on this trajectory $x(t)$ increases in time and $y(t)$ is a periodic function. Show that the time average of $y(t) = \dot{x}(t)$ is not zero. \square

For $\gamma < \gamma_M$ and $I_{\min}(\gamma) < I < 1$, stable equilibrium solutions and the stable nonequilibrium solution (3.184) can coexist and the system can exhibit hysteresis. In this range of parameters, phase space is divided into a basin of attraction Ω_S of the stable nonequilibrium steady-state S and a basin of attraction of each of the stable equilibrium states E , denoted generically by Ω_E . The basins are separated from each other by separatrices, which correspond to solutions of (3.182) that converge asymptotically to the unstable equilibrium points at $y = 0$ and the local maxima of $U(x)$.

For given values of $\gamma < \gamma_M$, as I decreases toward $I_{\min}(\gamma)$, the separatrices and the nonequilibrium steady-state S approach each other. When $I = I_{\min}(\gamma)$, these curves coalesce, leading to the curve (3.187). Alternatively, for a given value of $|I| < 1$, when γ increases toward γ_M , the separatrices and S approach each other, as above. However, in this case, the unstable equilibrium points, which lie on the separatrices, do not move.

The phase space trajectory S can be characterized as the only periodic solution of the differential equation (3.182). For $I = I_{\min}(\gamma)$, a first approximation to the critical stable periodic trajectory S_C ; that is, the steady-state that has just coalesced with the separatrix, is given by

$$y(t) = \dot{x}(t) = 2 \left| \cos \frac{x(t) - \Delta}{2} \right|, \quad (3.187)$$

where $\Delta = -\arcsin I_{\min}(\gamma)$.

If the phase plane is wrapped on a cylinder; that is, the x -axis is reduced mod(2π), the stable nonequilibrium S becomes a stable limit cycle and the stable equilibria coalesce into a single stable equilibrium point. The domains of attraction of these stable states are separated by a separatrix. The noise-induced fluctuations about the limit cycle and rate of noise-induced transitions over the separatrix are the objects of interest in the next sections.

3.7.2 Asymptotics of the Fokker–Planck Equation Near the Limit Cycle

The noisy forced pendulum is described by the Langevin equation (3.75) with the potential (3.181), so the stable states of the reduced equation (noiseless dynamics) (3.182), now

$$\dot{x} = y, \quad \dot{y} = -\gamma y - \sin x + I, \quad (3.188)$$

as described above, become meta-stable due to noise-induced fluctuations and transitions between the domains of attraction of these states. Although the noisy system reaches steady-state, it is never in equilibrium, because it carries a steady current, proportional to \dot{y} . Therefore, as mentioned above, its fluctuations and noise-induced transitions cannot be described by thermodynamics, which is an equilibrium theory. The absence of a well-defined energy renders Kramers' formula (2.83) inapplicable for transitions from the running state (the limit cycle) to equilibrium, although it applies in the reverse direction.

Specifically, the Fokker–Planck equation (1.13) with the potential (3.181) has the stationary solution

$$p_\varepsilon = C e^{-E/\varepsilon}, \quad (3.189)$$

where the energy is

$$E = \frac{y^2}{2} + U(x).$$

This density actually represents the probability density function of fluctuations about an equilibrium state. It does not, however, represent the probability density function of fluctuations about nonequilibrium steady-states, because (3.189) is unbounded on S , and is not periodic in x . The phase space probability current density

$$\mathbf{J} = \begin{pmatrix} yp_\varepsilon \\ -U'(x)p_\varepsilon - \gamma y p_\varepsilon - \gamma \varepsilon \frac{\partial p_\varepsilon}{\partial y} \end{pmatrix}$$

vanishes for $p_\varepsilon = p_B$, whereas in the nonequilibrium steady-state, we expect a nonzero probability current flowing in the direction of decreasing $U(x)$. Therefore, instead of (3.189), we seek a solution of the Fokker–Planck equation that is bounded, periodic in x with the same period as $U(x)$, and produces a nonzero current in the appropriate direction. Thus the Maxwell–Boltzmann distribution of steady-state fluctuations, in which velocity and displacement are statistically independent, has to be replaced with a different steady-state distribution in phase space.

For small ε we seek the steady-state distribution in phase space as a periodic density of local fluctuations about the nonequilibrium steady-state in the WKB form

$$p_S = p_0 e^{-W/\varepsilon}, \quad (3.190)$$

where the functions $W(x, y)$ and $p_0(x, y, \varepsilon)$ remain to be determined. The periodic density of $p_S(x, y)$ is normalized over $[0, 2\pi] \times \mathbb{R}$. The eikonal function W replaces the notion of energy, which is not well defined for this damped non-isolated system; The function W plays a role similar to that of energy in (3.189). Both W and p_0 must be periodic on S , and p_0 is assumed to be a regular function of ε at $\varepsilon = 0$. Substituting (3.190) into the stationary Fokker–Planck equation (1.13) and expanding in powers of ε , we find that W satisfies the Hamilton–Jacobi (eikonal-type) equation

$$\gamma \left(\frac{\partial W}{\partial y} \right)^2 + y \frac{\partial W}{\partial x} - [\gamma y + U'(x)] \frac{\partial W}{\partial y} = 0. \quad (3.191)$$

At the same time, to leading order in ε , p_0 is the 2π -periodic (in x) solution of the transport equation

$$\left[2\gamma \frac{\partial W}{\partial y} - \gamma y - U'(x) \right] \frac{\partial p_0}{\partial y} + y \frac{\partial p_0}{\partial x} + \gamma \left[\frac{\partial^2 W}{\partial y^2} - 1 \right] p_0 = 0. \quad (3.192)$$

This approximation is valid throughout the domain of attraction of the running solution Ω_S , as long as $\varepsilon \ll 1$; that is, as long as the usual Boltzmann thermal energy $\varepsilon = k_B T$ is much less than the potential barrier.

We first show that the contours of constant W in phase space correspond to the deterministic nonequilibrium steady-state trajectories (see Exercise 3.15 for $0 \leq \gamma \leq \gamma_M(I)$). Using this property, we determine the function $W(x, y)$. To this end we consider the following equations in the phase space (x, y) : the equations of motion (3.188), the parametric equations for the constant- W contours

$$\dot{x} = y, \quad \dot{y} = -\gamma y - U'(x) + \gamma W_y, \quad (3.193)$$

and the parametric equations for the characteristic curves of the eikonal equation

$$\begin{aligned} \dot{x} &= y, & \dot{y} &= -\gamma y - U'(x) + \gamma W_y \\ \dot{W}_y &= -W_x + \gamma W_y, & \dot{W}_x &= U''(x)W_y, & \dot{W} &= \gamma W_y^2. \end{aligned} \quad (3.194)$$

Lemma 3.7.1 $W = \text{const. and } \nabla W = 0 \text{ on } S$.

Proof Indeed, calculating the total derivative \dot{W} on S from (3.188) and the eikonal equation (3.191), we find that $\dot{W} = -\gamma W_y^2 \leq 0$. Hence, to keep W periodic on S the right-hand side must vanish identically, rendering $W = \text{const.}$ on S . Now it follows from (3.191) that $W_x = 0$ on S as well, hence $\nabla W = 0$ on S .

Lemma 3.7.2 (W -contours). *The W -contours are the family of steady-state trajectories of*

$$\dot{x} = y, \quad \dot{y} = -\Gamma(W)y - U'(x), \quad (3.195)$$

where $\Gamma(W) = \gamma[1 - K(W)]$, where $K(W)$ is given in (3.197) for $0 \leq \Gamma(W) \leq \gamma_M(I)$, and they are given by the approximate expression (3.184)) with γ replaced by Γ .

Proof Indeed, first, we express W_y on the W -contours in terms of W . Consider the function

$$H(x, y) = \frac{y^2}{2} + U(x) + \gamma \int_{x_0}^x (y - W_y) dx,$$

where the integral is a line integral along the W -contour that passes through the point (x, y) . From (3.193), it is easy to see that $H = \text{const.}$ on any W -contour. The rate of change of $H(W)$ on a characteristic curve (3.194) is $\dot{H} = \gamma y W_y + \gamma^2 \int_{x_0}^x W_y (1 - W_{yy}) dx$. It follows that

$$H'(W) = \frac{dH}{dW} = \frac{\dot{H}}{\dot{W}} = \frac{y}{W_y} + \frac{\gamma}{W_y^2} \int_{x_0}^x W_y (1 - W_{yy}) dx. \quad (3.196)$$

It is shown below that $W_{yy} = 1 + O(\gamma)$ for small γ (see (3.204)), so (3.196) gives

$$H'(W) = \frac{y}{W_y} + O(\gamma^2) = \frac{1}{K(W)} + O(\gamma^2). \quad (3.197)$$

Using this result, we can rewrite (3.193) for small γ as (3.195), which has the same form as (3.188), except that γ has been replaced by Γ .

Note that (3.197) is actually valid only for values of K which are $O(1)$ for small γ , whereas for large values of K , for example, for K corresponding to the critical contour, the $O(\gamma^2)$ estimate of the integral in (3.196), which leads to (3.197), is no longer valid. However, the contribution of the integral to (3.195) is $O(1)$ only on short time intervals, because most of the time on the critical contour is spent near the stable equilibrium point. The influence of the integral on the solution of (3.195) is therefore negligible.

Theorem 3.7.1 (Nonequilibrium steady-state fluctuations). *The solution of the stationary Fokker–Planck equation (1.13) (the stationary probability density of fluctuations about S) is given by*

$$p_S(x, y) \approx \exp \left\{ -\frac{(\Delta A)^2}{2\varepsilon} \right\} \text{ for } \gamma \ll 1, \quad (3.198)$$

where the generalized action $A(\Gamma)$ of the steady-state trajectory through (x, y) (which corresponds to a different value of the friction constant Γ instead of γ) is given by

$$A(\Gamma) = \frac{1}{2\pi} \int_0^{2\pi} y \, dx \sim \frac{I}{\Gamma} \quad (3.199)$$

and $\Delta A = A(\Gamma) - A(\gamma)$.

Proof In view of (3.190), we need to evaluate $W(x, y)$. To determine its relation to Γ , we map the x, y plane to the W, x plane. Employing the relation $W_y = Ky + O(\gamma^2)$ and $\Gamma = \gamma(1 - K)$, we obtain to leading order in γ ,

$$W_\Gamma = \frac{\left(1 - \frac{\Gamma}{\gamma}\right)y}{\Gamma_y}. \quad (3.200)$$

Hence, to leading order in γ , we have

$$W(\Gamma) = \frac{1}{2} \int_0^\Gamma \left(1 - \frac{\Gamma}{\gamma}\right) (y^2)_\Gamma \, d\Gamma.$$

Integrating by parts, we obtain

$$W(\Gamma) = \frac{1}{2} \left[\left(1 - \frac{\Gamma}{\gamma}\right) y^2(\Gamma, x) + \frac{1}{\gamma} \int_0^\Gamma y^2(\Gamma, x) \, d\Gamma \right]. \quad (3.201)$$

The asymptotic expression (3.184) for $y(\gamma, x)$ gives in (3.201)

$$W(\Gamma) = \frac{1}{2} \left(\frac{I}{\Gamma} - \frac{I}{\gamma} \right)^2, \quad \gamma \leq \Gamma \leq \gamma_M, \quad (3.202)$$

because the right-hand side of (3.201) is independent of x on a W -contour. Thus (3.202) can be written in the form

$$W(\Gamma) \sim \frac{1}{2} [A(\Gamma) - A_0]^2, \quad (3.203)$$

where $A_0 = A|_{\Gamma=\gamma}$.

Next, we show that for small γ the solution p_0 of (3.192) is to leading order a constant. Choosing p_0 to have the average value 1 on S and employing (3.194) in the transport equation (3.192), we see that $\dot{p}_0 = -\gamma(W_{yy} - 1)p_0$ along the characteristic

curves. Differentiating (3.202) and employing (3.184) differentiated with respect to y , we find that

$$W_{yy} = 1 + O(\gamma), \quad (3.204)$$

so that $p_0 = 1 + O(\gamma^2)$.

Note that the quantity ΔA is the difference between the action associated with S and the action associated with the steady-state trajectory through (x, y) . A finer resolution of the local fluctuations about S can be achieved by considering the probability density function p_S in local coordinates near S .

Theorem 3.7.2 [The asymptotic structure of the solution] *The solution of the steady state Fokker–Planck equation is given by*

$$p_S(x, y) \sim \exp\left\{-\frac{\alpha(x)[y - y_S(x)]^2}{2\varepsilon}\right\} \text{ for } \frac{\gamma}{I} \ll 1, \quad (3.205)$$

where

$$\alpha(x) = 1 + \left(\frac{\gamma}{I}\right)^2 (I\pi + \cos x) + O\left(\frac{\gamma^4}{I^4}\right). \quad (3.206)$$

The variance of the local fluctuations is

$$\sigma_y^2 = \varepsilon \left[1 - 2\pi \frac{\gamma^2}{I} + O\left(\frac{\gamma^3}{I^3}\right) \right]. \quad (3.207)$$

Proof To derive (3.205), we introduce the variable $\delta = y_S(x) - y$, where $y_S(x)$ is given by (3.184). Recall that

$$W(x, y_S(x)) = W_x(x, y_S(x)) = W_y(x, y_S(x)) = 0. \quad (3.208)$$

It follows that the Taylor's expansion of W near S , given in powers of δ , is

$$W(x, y) = \frac{1}{2}\alpha(x)\delta^2 + \frac{1}{6}\beta(x)\delta^3 + \dots, \quad (3.209)$$

where $\alpha(x), \beta(x), \dots$, are as yet undetermined functions. It follows that the Taylor's expansions of $W_x(x, y)$ and $W_y(x, y)$ are given by

$$W_x(x, y) = -\frac{\nu_x(x, y)}{\nu_y(x, y)}\alpha(x)\delta + \frac{1}{2}\left[\alpha'(x) - \frac{\nu_x(x, y)}{\nu_y(x, y)}\beta(x)\right]\delta^2 + \dots \quad (3.210)$$

and

$$W_y(x, y) = \alpha(x)\delta + \frac{1}{2}\beta(x)\delta^2 + \dots \quad (3.211)$$

The functions $\nu_x(x, y)$ and $\nu_y(x, y)$ are the components of the unit normal vector $\mathbf{n}(x, y)$ to S at $(x, y_S(x))^T$. The vector $\mathbf{n}(x, y)$ is orthogonal to the vector $(y_S(x), -\gamma y_S(x) - U'(x))$, which defines the flow (3.188). Hence,

$$\begin{aligned}\nu_x(x, y) &= \frac{-[\gamma y_S(x) + U'(x)]}{\sqrt{y_S^2(x) + [\gamma y_S(x) + U'(x)]^2}} \\ \nu_y(x, y) &= \frac{-\gamma y_S(x)}{\sqrt{y_S^2(x) + [\gamma y_S(x) + U'(x)]^2}}.\end{aligned}\quad (3.212)$$

Substituting the expansions (3.210) and (3.211) of $W_x(x, y)$ and $W_y(x, y)$, respectively, into the eikonal equation (3.191), we obtain

$$\begin{aligned}\frac{\delta}{\nu_y(x, y)} &\left[\alpha(x) + \frac{1}{2}\beta(x)\delta \right] \{ \nu_y(x, y) [\gamma y_S(x) + U'(x)] - \nu_x(x, y)\gamma y_S(x) \} \\ &+ \delta^2 \left\{ \frac{1}{2}\alpha'(x)y_S(x) + \left[-\frac{\nu_x(x, y)}{\nu_y(x, y)} - \gamma \right] \alpha(x) + \gamma\alpha^2(x) \right\} = O(\delta^3).\end{aligned}$$

We have $\{ \nu_y(x, y) [\gamma y_S(x) + U'(x)] - \nu_x(x, y)\gamma y_S(x) \} = 0$, because this is the scalar product of the flow on S with its normal. Note that the function $\beta(x)$ is no longer needed for the calculation of $\alpha(x)$. It follows that $\alpha(x)$ satisfies the Bernoulli equation

$$\frac{1}{2}\alpha'(x)y_S(x) + \left[-\frac{\nu_x(x, y)}{\nu_y(x, y)} - \gamma \right] \alpha(x) + \gamma\alpha^2(x) = 0. \quad (3.213)$$

First, we convert (3.213) into a linear equation by the substitution $\alpha(x) = 1/\beta(x)$ to get

$$\beta'(x) - r(x)\beta(x) = t(x). \quad (3.214)$$

Here the coefficients are given by

$$r(x) = \frac{2}{y_S(x)} \left[\frac{\nu_x(x, y)}{\nu_y(x, y)} + \gamma \right] = \frac{2U''(x)}{y_S^2(x)}, \quad t(x) = \frac{2\gamma}{y_S(x)}. \quad (3.215)$$

The 2π -periodic solution of (3.214) is

$$\beta(x) = \frac{1}{R(x)} \left[\frac{R(0)}{1 - R(0)} \int_0^{2\pi} t(z)R(z) dz + \int_0^x t(z)R(z) dz \right], \quad (3.216)$$

where $R(z) = \exp \left\{ \int_z^{2\pi} r(u) du \right\}$.

The variance of the steady-state local fluctuations about S can be calculated from the above analysis. Noting that the function $\alpha(x)$ is the local frequency of the quasi-potential $W(x, y)$ in the y direction, we find that in the limit $\gamma/I \ll 1$, the variance of the local fluctuations of y , at fixed x , is given by

$$\sigma_y^2(x) = \frac{\int \delta^2 \exp\{-\alpha(x)\delta^2/2\varepsilon\} d\delta}{\int \exp\{-\alpha(x)\delta^2/2\varepsilon\} d\delta} = \frac{\varepsilon}{\alpha(x)}.$$

The average fluctuation of y is given by

$$\sigma_y^2 = \frac{\int dx \int \delta^2 \exp\{-\alpha(x)\delta^2/2\varepsilon\} d\delta}{\int dx \int \exp\{-\alpha(x)\delta^2/2\varepsilon\} d\delta} = \varepsilon \frac{\int \alpha^{-3/2}(x) dx}{\int \alpha^{-1/2}(x) dx}.$$

An expansion of $\alpha(x)$ in powers of γ/I yields (3.206), hence we obtain (3.207) for $\gamma/I \ll 1$ and the probability density function of the local fluctuations about S is given by (3.205).

3.7.3 The Boundary Value Problem for the Fokker–Planck Equation in Ω_S

We consider now the underdamped pendulum mod 2π in x ; that is, we wrap the phase space on a cylinder of radius 1 about the y -axis. The domain Ω_S becomes one period of Fig. 3.12 (and in the limit $\gamma \rightarrow 0-$ of Fig. 3.13). Note that the tails of the domains of attraction of the stable equilibria form a long ribbon wrapped around the cylinder. We retain the notation Ω_S for the domain of attraction on the cylinder. The periodic solution of the Fokker–Planck equation in the phase plane can be now normalized on the cylinder (on a single period). The nonequilibrium steady-state S becomes a stable limit cycle on the cylinder and the stable equilibria coalesce into a single one.

The *lifetime* of the nonequilibrium steady-state S is the mean first passage time from Ω_S to the separatrix and thus it is the solution of the homogeneous boundary value problem for the inhomogeneous stationary Fokker–Planck equation inside a single period. The mean lifetime is sufficiently long to establish a quasi-stationary probability density function in Ω_S . This probability density function, p_S , is (3.190) mod 2π in x and as seen above; it is essentially constant on W -contours. Thus the process can be considered as a one-dimensional stationary diffusion process in the space of W -contours. The range of attraction Ω_S of S corresponds to Γ in the range $0 \leq \Gamma \leq \gamma_M$.

Theorem 3.7.3 [The averaged Fokker–Planck equation in Ω_S] The leading term in the low-friction expansion of the stationary probability density function in Ω_S is the solution of the one-dimensional Fokker–Planck equation

$$\frac{\partial p}{\partial s} = \frac{\partial}{\partial A} \left\{ [A - A_0] p + \varepsilon \frac{\partial p}{\partial A} \right\} \text{ for } A > A(\gamma_M), \quad \frac{\gamma}{I} \ll 1, \quad (3.217)$$

where $A = A(\Gamma)$ is defined in (3.199) and $s = \gamma t$.

To derive (3.217), we note that the average of a function $F(x, y)$ over a W -contour is defined as

$$F(W) = \frac{1}{T_S} \int_0^{T_S} F(x(t), y(t)) dt, \quad (3.218)$$

where t is the parameter of (3.195), which represents time along the steady-state trajectory corresponding to $\Gamma(W)$, and $T_S = T_S(W)$ is the period of $y(t)$ on the trajectory (Fig. 3.14). We introduce W and x as coordinates in the Fokker–Planck equation

$$\begin{aligned} & \gamma \frac{\partial p(x, y, s)}{\partial s} \\ &= \gamma \varepsilon \frac{\partial^2 p(x, y, s)}{\partial y^2} - y \frac{\partial p(x, y, s)}{\partial x} + \frac{\partial [\gamma y + U'(x)] p(x, y, s)}{\partial y}, \end{aligned} \quad (3.219)$$

where the dimensionless time is $s = t\gamma$, and use the eikonal equation (3.191) to reduce it to

$$\gamma \frac{\partial p}{\partial s} = -y \frac{\partial p}{\partial x} + \gamma \varepsilon W_y^2 \frac{\partial^2 p}{\partial W^2} + \gamma (W_y^2 + \varepsilon W_{yy}) \frac{\partial p}{\partial W} + \gamma p. \quad (3.220)$$

An expansion in powers of γ leads to averaging (3.220) on W -contours, as defined in (3.218), as a solvability condition, because of the averages $\langle W_y^2 \rangle \sim 2W$ and $\langle W_{yy} \rangle \sim 1$. We obtain for an x -independent solution the averaged equation

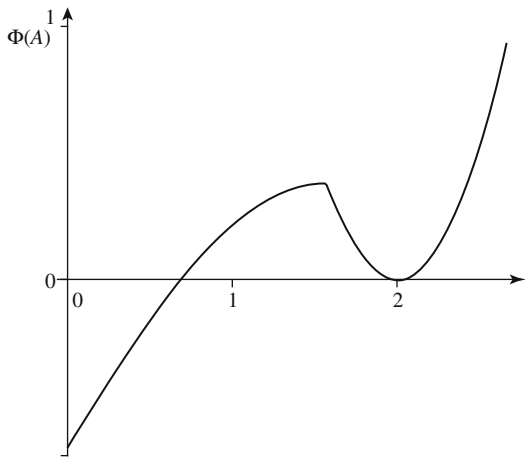
$$\frac{\partial p}{\partial s} = 2 \left\{ \varepsilon W \frac{\partial^2 p}{\partial W^2} + \left(W + \frac{1}{2} \varepsilon \right) \frac{\partial p}{\partial W} + \frac{p}{2} \right\}. \quad (3.221)$$

A considerable simplification of (3.221) is achieved if we choose the action $A = A(\Gamma)$ as the independent variable in (3.221), rather than W . Using the relation $W \sim \frac{1}{2} [A(\Gamma) - A_0]^2$ (see (3.203)) in (3.221), we obtain (3.217).

From the low friction expansion, we have the following

Corollary 3.7.1 In the limit $\gamma \rightarrow 0$ the global stationary probability density function in one period of the stationary underdamped dynamics is the stationary solution of the Fokker–Planck equation

Fig. 3.14 The effective global potential $\Phi(A)$ (3.223) in the steady-state Fokker–Planck equation (3.222)



$$\frac{\partial}{\partial A} \left\{ \Phi'(A)p + \varepsilon \frac{\partial p}{\partial A} \right\} = 0 \quad \text{for } A > 0, \quad (3.222)$$

where

$$\Phi(A) = \begin{cases} \frac{(A - A_0)^2}{2} & \text{for } A > A(\gamma_M) \\ \mathcal{E}(A) & \text{for } 0 < A < A(\gamma_M), \end{cases} \quad (3.223)$$

and where $A = I/4\pi$ for $0 < A < A(\gamma_M)$ (in the domain $E < E_B$), $\mathcal{E}(A) = E(I) - E_0$, $I = I(E)$ is the action on the closed E contour, and

$$E_0 = E_B - \frac{1}{2} \left(\frac{I(E_B)}{4\pi} - A_0 \right)^2.$$

The connection of two local stationary WKB solutions of the Fokker–Planck equation across the separatrix to form a global probability density function is in general not a trivial matter, because the separatrix can be a caustic for the eikonal equation and the eikonal function may be discontinuous there. An obvious necessary connection criterion is that the net total probability flux across the separatrix vanishes [Freidlin and Wentzell (1984)], [Graham and Tél (1985)]. In the case at hand the fluxes of the WKB solutions on both sides of the separatrix vanish, so choosing A on either side so that its unilateral limits there are the same connects $\Phi(A)$ continuously, although not smoothly.

Exercise 3.18 (The critical W -contour). Show that

- (i) The critical W -contour that first touches the separatrix does so at the unstable equilibrium point C of the noiseless dynamics (3.188). (HINT: C is a saddle point

for W because $W_y(x_0, 0) = 0$, see (3.200)), so $W_x \rightarrow 0$ as $(x, y) \rightarrow (x_0, 0)$. Thus W achieves its maximal value at (x_0, y) along any curve that reaches that point from the side of S_C that includes S , and W achieves its minimum value there along the separatrix.)

- (ii) Show that the critical W -contour has a cusp at C and that $\nabla W = 0$ there. (HINT: Recall that this contour has two different slopes at this point and the slope q of the separatrix at this point is different from either slope of the W -contour, because q is given by (3.185) with the negative square root, and with γ_M replaced by γ .)
- (iii) Show that W attains its minimum value along the separatrix at C , so that C is a saddle point of W . (HINT: Note that $\dot{W} = -\gamma W_y^2$ for motion on the separatrix, so the minimum of W on the separatrix is achieved at the unstable equilibrium point, toward which the separatrix converges.)
- (iv) Show the characteristic curve through C is the most probable path out of Ω_S [Freidlin and Wentzell (1984)]. \square

In addition to fluctuations about the nonequilibrium steady-state S , thermal noise can also cause transitions from the basin of attraction Ω_S of S , into one of the basins of attraction Ω_E of a stable equilibrium state.

Theorem 3.7.4 [*The solution of the inhomogeneous boundary value problem (the mean first passage time to S_C)*] For $\gamma < \gamma_M$ and $I_{min}(\gamma) < I < 1$ the mean first passage time from S to S_C is

$$\bar{\tau}_S \approx \frac{\sqrt{\pi}}{\gamma} \sqrt{\frac{\varepsilon}{\Delta W}} \exp\left\{\frac{\Delta W}{\varepsilon}\right\} \text{ for } \frac{\varepsilon}{\Delta W} \ll 1, \quad (3.224)$$

where

$$\Delta W = \frac{1}{2} \left(\frac{I}{\gamma} - \frac{I}{\gamma_M(I)} \right)^2 \approx \frac{1}{2} \left(\frac{I}{\gamma} - \frac{4}{\pi} \right)^2 \text{ for } \frac{\gamma}{I} \ll 1. \quad (3.225)$$

Proof To derive (3.224), we use the “population over flux” expression (1.22) to evaluate the mean first passage time. The solution of the boundary value problem

$$\frac{\partial}{\partial A} \left\{ \Phi'(A)p + \varepsilon \frac{\partial p}{\partial A} \right\} = -\delta(A - A_0) \text{ for } A > 0, \quad p(A(\gamma_M)) = 0, \quad (3.226)$$

is given by

$$p(A) = \frac{1}{\varepsilon} e^{-\Phi(A)/\varepsilon} \int_{A(\gamma_M)}^A H(A_0 - z) e^{\Phi(z)/\varepsilon} dz.$$

The boundary flux is $F = -\varepsilon p'(A(\gamma_M)) = 1$ and the population is

$$N = \int_{A(\gamma_M)}^{\infty} p(A) dA = \frac{\sqrt{2\pi\varepsilon}}{A(\gamma_M) - A_0} \exp\left\{\frac{(A(\gamma_M) - A_0)^2}{2\varepsilon}\right\} (1 + o(1)) \text{ as } \varepsilon \rightarrow 0,$$

hence, using (3.203), we obtain (3.224).

Exercise 3.19 (Numerical solution of the eikonal equation). By integrating numerically the characteristic equations (3.194), construct the solution of the eikonal equation (3.191), which is a 2π -periodic function of x .

- (i) Explain why initial conditions have to be given at a finite distance from S . (HINT: The initial conditions for (3.194) are given by (3.208) on S , however, S is a characteristic curve and a caustic; that is, an attractor of the characteristic curves.)
- (ii) Use the expansion (3.209)–(3.211) of W , W_x , and W_y as initial conditions for (3.194) near S . For a given x_0 , take the value of $y_S(x_0)$ as the approximation (3.184). Then use $y_S(x)$ in (3.184) and (3.212) to calculate $r(x)$ and $t(x)$ in (3.215) and calculate $\alpha(x)$ from (3.216) on a lattice $x_0 < x_1 < \dots < x_n = 2\pi + x_0$. Note that although the lattice $(x_i, y_S(x_i) - \delta)$, for $i = 0, 1, \dots, n$, which is parallel to the contour $W = 0$, can be used for assigning initial conditions, the vertical lattice $(x_0, y_S(x_0) - \delta(1 + i\Delta))$, for $i = 1, \dots, k$ with small δ and Δ , is more efficient for covering Ω_S with characteristics uniformly. Determine the initial values of W , W_x , and W_y on this lattice from (3.209)–(3.211).
- (iii) Evaluate the function W numerically to confirm the validity of the asymptotic approximations given above over a wide range of values of I and γ (see, e.g., [Kupferman et al. (1992)]). \square

3.8 Annotations

The theorem about pathwise convergence in the Smoluchowski overdamped limit was proved for finite time intervals in [Schuss (1980b)]. The GLE was derived from statistical mechanics in [Kubo (1957)], [Mori (1965)], [Berne and Pecora (1976)], [Mazur and Oppenheim (1970)], [Kim and Oppenheim (1972)], [Grote and Hynes (1980)], [Grote and Hynes (1981a)] and [Grote and Hynes JCP (1981b)]. The theorem about the overdamped limit of the generalized Langevin equation was proved in [Dygas et al. (1986)] and more recently in [Freidlin (2004)].

Continuum theories of diffusive systems describe the concentration field by the Nernst–Planck equation with fixed boundary concentrations [Hille (2001)], [Eisenberg (1999)], [Eisenberg (1998)], [Nonner and Eisenberg (1998)], [Nonner et al. (1999)], [Berry et al. (2000)], [Nonner et al. (2000)], [Nonner et al. (2001)], [Schuss et al. (2001)] and [Chen et al. (2014)]. In these theories there is no time-dependence of the macroscopic boundary concentrations. The force field does not fluctuate and is usually calculated from a Poisson equation coupled to the Nernst–Planck equations. The huge voltage fluctuations in the salt solution and in the channel are averaged out in these theories.

The question of the boundary behavior of the Langevin trajectories, corresponding to fixed boundary concentrations, arises both in the theory and in the practice of molecular simulations of diffusive motion [Berkowitz and McCammon (1982)], [Brooks and Karplus (1983)], [Belch and Berkowitz (1985)], [Naeh (2001)], [Nadler et al. (2002)], [Nadler et al. (2003)], [Roux (2000)]. The boundary behavior of diffusing particles in a finite domain has been studied in various cases, including absorbing, reflecting, sticky boundaries, and many other modes of boundary behavior [Mandl (1968)], [Karlin and Taylor (1981)]. In [Schumaker (2002)] a sequence of Markovian jump processes is constructed such that their transition probability densities converge to the solution of the Nernst–Planck equation with given boundary conditions, including fixed concentrations and sticky boundaries.

The Smoluchowski boundary layer was studied in [Marshall and Watson (1985)], [Yu et al. (1989)], [Hagan et al. SIAP (1989b)], [Hagan et al. (1987)], [Hagan et al. (1989a)], [Klosek and Hagan (1998)] and [Klosek (1995)]. The study of the relevant special functions, and especially of the Hurwitz zeta function, was done in [Singer (2006)].

The results about thermal activation of an underdamped Brownian particle over a potential barrier go back to [Kramers (1940)] and [Hänggi et al. (1990)]. The thermal activation of a steady-state system far from equilibrium, from a stable limit cycle across the separatrix, remained an open problem in Kramers’ 1940 paper [Kramers (1940)]. The need to find the expected time of the running state of the Josephson junction (the underdamped physical pendulum) arose with the advent of cryogenic devices based on the Josephson effect and related problems. The problem was solved in [Ben-Jacob et al. (1982)]–[Ben-Jacob et al. JAP (1983)], [Kupferman et al. (1992)], which are the basis for Sect. 3.7, and in the work of Risken and Vollmer [Risken (1996)], and [Coffey et al. (2004)].

Chapter 4

Eigenvalues of a Non-self-adjoint Elliptic Operator

4.1 Introduction

Precious little is known about the distribution of the eigenvalues of any second-order linear elliptic non-self-adjoint boundary value problem in any domain in \mathbb{R}^d for $d > 1$ (see Sect. 4.17). The singular perturbation asymptotics described in Chap. 3 are used here to construct an approximation to the entire spectrum of a non-self-adjoint Dirichlet problem for the Hopf vector field $\mathbf{a}(\mathbf{x})$, singularly perturbed by a small Laplacian. Consequently, we demonstrate the oscillatory decay of the survival probability of the stochastic dynamics

$$d\mathbf{x}_\varepsilon(t) = \mathbf{a}(\mathbf{x}_\varepsilon(t)) dt + \sqrt{2\varepsilon} \mathbf{b}(\mathbf{x}_\varepsilon(t)) d\mathbf{w}(t), \quad (4.1)$$

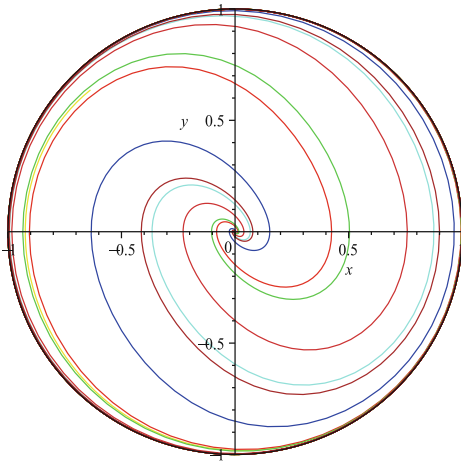
which is activated by small noise over the boundary of the domain of attraction Ω of the stable focus of the drift $\mathbf{a}(\mathbf{x})$, whose boundary $\partial\Omega$ is an unstable limit cycle of $\mathbf{a}(\mathbf{x})$ (Fig. 4.1 and Sect. 4.7). The oscillations are explained by the complex-valued higher-order eigenvalues of the Dirichlet problem for the non-self-adjoint Fokker–Planck operator in Ω with Dirichlet boundary conditions on $\partial\Omega$,

$$L_\varepsilon u(\mathbf{x}) = \varepsilon \sum_{i,j=1}^2 \frac{\partial^2 [\sigma^{i,j}(\mathbf{x}) u(\mathbf{x})]}{\partial x^i \partial x^j} - \sum_{i=1}^2 \frac{\partial [a^i(\mathbf{x}) u(\mathbf{x})]}{\partial x^i} = -\lambda_\varepsilon u(\mathbf{x}), \quad (4.2)$$

with $\sigma(\mathbf{x}) = \mathbf{b}(\mathbf{x})\mathbf{b}^T(\mathbf{x})$.

Experimental data and Brownian dynamics simulations of the model (4.1) (see (4.72) in Sect. 4.7 below) and (4.73) indicate oscillatory decay of the survival probability in Ω (see Fig. 4.10), which needs to be resolved. It is fairly obvious that while for a non-conservative drift $\mathbf{a}(\mathbf{x})$ the principal eigenvalue and eigenvector of the Fokker–Planck operator corresponding to (4.1) are real-valued, those of higher-order are complex-valued, which may give rise to oscillations in the probability density function of τ , the first passage time to the boundary. Although in the

Fig. 4.1 The field $\mathbf{a}(\mathbf{x}) = [y, -x - y(1 - x^2 - y^2)]^T$ has a stable focus at the origin and the boundary of the domain Ω is a limit cycle



small-noise limit the principal eigenvalue λ_0 and the mean first passage time $\bar{\tau}$ are related asymptotically by

$$\lambda_0 \sim \frac{1}{\bar{\tau}} \text{ for } \varepsilon \ll 1, \quad (4.3)$$

and the stationary (and quasi-stationary) exit point density on $\partial\Omega$ is the normalized flux of the principal eigenfunction $u_0(\mathbf{y})$ of the Fokker–Planck operator, higher-order eigenvalues and eigenfunctions can cause discernible oscillations in the survival probability of $\mathbf{x}_\varepsilon(t)$ in Ω . This, as well as other problems, raises the question of what the spectrum of the Fokker–Planck non-self-adjoint elliptic operator is and how it depends on the structure of the drift.

In this chapter it is shown that the oscillatory decay of the survival probability of the dynamics shown in Figs. 4.1 and 4.3, driven by small noise, is due to the complex eigenvalues of the non-self-adjoint Dirichlet problem (4.2) (see Fig. 4.2). The drift field $\mathbf{a}(\mathbf{x})$ is assumed to have a stable focus in Ω , whose boundary $\partial\Omega$ is an unstable limit cycle of $\mathbf{a}(\mathbf{x})$. The following notation is used to state the main results: s is arclength on $\partial\Omega = \{\mathbf{x}(s) : 0 \leq s < S\}$, measured clockwise, $\mathbf{n}(\mathbf{x})$ is the unit outer normal at $\mathbf{x} \in \partial\Omega$, $B(s) = |\mathbf{a}(\mathbf{x}(s))|$, and $\sigma(s) = \mathbf{n}(\mathbf{x}(s))^T \boldsymbol{\sigma}(\mathbf{x}(s)) \mathbf{n}(\mathbf{x}(s))$. The function $\xi(s)$ is defined in (3.62) above.

The WKB asymptotics show that the principal eigenvalue decays exponentially fast as $\varepsilon \rightarrow 0$. It is shown below that for small ε , the higher-order eigenvalues are given by

$$\lambda_{m,n} = 2n\omega_1 + m\omega_2 i + O(\varepsilon), \quad n = 1, \dots, \quad m = \pm 1, \pm 2, \dots, \quad (4.4)$$

where the frequencies ω_1 and ω_2 are expressed in terms of the coefficients of the Fokker–Planck operator L_ε as

$$\omega_1 = \frac{\omega_2}{2\pi} \int_0^S \frac{\sigma(s)\xi^2(s)}{B(s)} ds \quad \text{and} \quad \omega_2 = \frac{2\pi}{\int_0^S \frac{ds}{B(s)}}. \quad (4.5)$$

Also, the asymptotic structure of the eigenfunctions of L_ε and of its adjoint L_ε^* is constructed. The oscillatory decay of the survival probability is illustrated with a model of synaptic depression of a neuronal network in neurobiology (see Annotations 4.17).

The explicit expressions (4.4) and (4.5) are found by studying the boundary layer near the limit cycle, where the spectrum is hiding. The leading order asymptotic expansion of the principal eigenvalue λ_0 for small ε is related to the mean first passage time by (4.3), whose asymptotic structure was found in Chap. 3.

Section 4.2 below contains a refinement of the WKB analysis that is used in Sect. 4.7 below to demonstrate the oscillations in the survival probability and in the exit density. This result resolves the origin of the non-Poissonian nature of the time the voltage of neurons stays depolarized in population dynamics (see the discussion below).

4.2 Eigenvalues and the Survival Probability

The exit time distribution can be expressed in terms of the transition probability density function $p_\varepsilon(y, t | x)$ of the trajectories $x_\varepsilon(t)$ from $x \in \Omega$ to $y \in \Omega$ in time t . The probability density function is the solution of the Fokker–Planck equation (1.13). The non-self-adjoint operators L_y and L_x with homogeneous Dirichlet boundary conditions, defined in Sect. 1.2, have the same eigenvalues λ_n , because the equations are real and the eigenfunctions $u_n(y)$ of L_y and $v_n(x)$ of L_x^* form bi-orthonormal bases. The solution can be expanded as

$$p_\varepsilon(y, t | x) = e^{-\lambda_0 t} u_0(y) v_0(x) + \sum_n e^{-\lambda_n t} u_n(y) \bar{v}_n(x), \quad (4.6)$$

where λ_0 is the real-valued principal eigenvalue and u_0, v_0 are the corresponding positive eigenfunctions. The joint probability density function of the exit point $y \in \partial\Omega$ and the exit time τ is given in (1.24) with the time-dependent flux density vector given by

$$\begin{aligned} J^i(\mathbf{y}, t \mid \mathbf{x}) &= a^i(\mathbf{y}) p_\varepsilon(\mathbf{y}, t \mid \mathbf{x}) - \varepsilon \sum_{j=1}^d \frac{\partial [\sigma^{i,j}(\mathbf{y}) p_\varepsilon(\mathbf{y}, t \mid \mathbf{x})]}{\partial y^j} \\ &= -\varepsilon \sum_{j=1}^d \sigma^{i,j}(\mathbf{y}) \left[e^{-\lambda_0 t} \frac{\partial u_0(\mathbf{y})}{\partial y^j} v_0(\mathbf{x}) + \sum_n e^{-\lambda_n t} \frac{\partial u_n(\mathbf{y})}{\partial y^j} \bar{v}_n(\mathbf{x}) \right]. \end{aligned}$$

Note that due to the homogeneous Dirichlet boundary condition the undifferentiated terms drop from (1.20).

The survival probability of $\mathbf{x}_\varepsilon(t)$ in Ω , averaged with respect to a uniform initial distribution, is given in terms of the transition probability density function $p_\varepsilon(\mathbf{y}, t \mid \mathbf{x})$ of the trajectories $\mathbf{x}_\varepsilon(t)$ as

$$\begin{aligned} \text{Pr}_{\text{survival}}(t) &= \frac{1}{|\Omega|} \int_{\Omega} \text{Pr}\{t < \tau \mid \mathbf{x}\} d\mathbf{x} = \frac{1}{|\Omega|} \int_{\Omega} \int_{\Omega} p_\varepsilon(\mathbf{y}, t \mid \mathbf{x}) d\mathbf{y} d\mathbf{x} \\ &= e^{-\lambda_0 t} + \sum_n \frac{e^{-\lambda_n t}}{|\Omega|} \int_{\Omega} u_n(\mathbf{y}) d\mathbf{y} \int_{\Omega} \bar{v}_n(\mathbf{x}) d\mathbf{x}. \end{aligned} \quad (4.7)$$

The probability density function of the escape time is given by

$$\begin{aligned} \text{Pr}\{\tau = t\} &= -\frac{d}{dt} \text{Pr}_{\text{survival}}(t) \\ &= \lambda_0 e^{-\lambda_0 t} + \sum_n \frac{\lambda_n e^{-\lambda_n t}}{|\Omega|} \int_{\Omega} u_n(\mathbf{y}) d\mathbf{y} \int_{\Omega} \bar{v}_n(\mathbf{x}) d\mathbf{x}. \end{aligned} \quad (4.8)$$

4.3 The Principal Eigenvalue and the Structure of the Field $\mathbf{a}(\mathbf{x})$

The local geometry of Ω near $\partial\Omega$ is described in (3.107) and (3.51) in terms of the signed distance to the boundary, $\rho(\mathbf{x})$, and the arclength on the boundary $s(\mathbf{x})$, so the transformation $\mathbf{x} \rightarrow (\rho, s)$, where $\rho = \rho(\mathbf{x})$, $s = s(\mathbf{x})$, is a 1-1 smooth map of a strip near the boundary onto the strip $|\rho| < \rho_0$, $0 \leq s \leq S$, where $\rho_0 > 0$ and S is the arclength of the boundary. The transformation is given by $\mathbf{x} = \mathbf{x}' + \rho \nabla \rho(\mathbf{x}')$, where \mathbf{x}' is a function of s .

In the local representation (3.107) of the field $\mathbf{a}(\mathbf{x})$ in the boundary strip, the tangential component of the field at $\partial\Omega$ is $B(s) = \mathbf{a}(0, s) \cdot \nabla s = |\mathbf{a}(\mathbf{x}(s))| > 0$ and the normal derivative of the normal component is $a^0(s) \geq 0$ for all $0 \leq s \leq S$. The decomposition (3.107) for the field $\mathbf{a}(\rho, s)$ in Fig. 4.1 is given by $a^0(s) = 2 \sin^2 s$, $B(s) = 1$.

The principal eigenvalue λ_0 given in (4.3) is given more precisely by the asymptotic relation

$$\lambda_0 \sim \frac{1}{\bar{\tau}_\varepsilon(\mathbf{0})} \text{ for } \varepsilon \ll 1, \quad (4.9)$$

where $\bar{\tau}_\varepsilon(\mathbf{x})$ is the solution of the Pontryagin-Andronov-Vitt boundary value problem (1.25). The result of Sect. 3.4 gives the value $\bar{\tau}_\varepsilon(\mathbf{0})$ as

$$\bar{\tau}_\varepsilon(\mathbf{0}) \sim \frac{\pi^{3/2} \sqrt{2\varepsilon}}{\sqrt{\det Q} \int_0^S K_0(s) \xi(s) ds} \exp \left\{ \frac{\hat{\psi}}{\varepsilon} \right\}, \quad (4.10)$$

where $\psi(\mathbf{x})$ is the solution of the eikonal equation

$$\sigma(\mathbf{x}) \nabla \psi(\mathbf{x}) \cdot \nabla \psi(\mathbf{x}) + \mathbf{a}(\mathbf{x}) \cdot \nabla \psi(\mathbf{x}) = 0 \text{ for } \mathbf{x} \in \Omega \quad (4.11)$$

such that

$$\psi(\mathbf{x}) = \frac{1}{2} \mathbf{x}^T Q \mathbf{x} + O(|\mathbf{x}|^2) \text{ for } \mathbf{x} \rightarrow \mathbf{0} \quad (4.12)$$

with Q the solution of the Riccati equation

$$2Q\sigma(\mathbf{0})Q + QA + A^T Q = \mathbf{0}. \quad (4.13)$$

The eikonal function $\psi(\mathbf{x})$ is constant on $\partial\Omega$ with the local expansion

$$\psi(\rho, s) = \hat{\psi} + \frac{1}{2}\rho^2\phi(s) + o(\rho^2) \text{ for } \rho \rightarrow 0, \quad (4.14)$$

where $\phi(s)$ is the S -periodic solution of the Bernoulli equation

$$\sigma(s)\phi^2(s) + a^0(s)\phi(s) + \frac{1}{2}B(s)\phi'(s) = 0 \quad (4.15)$$

and where $\sigma(s) = \sigma(0, s)\nabla\rho(0, s) \cdot \nabla\rho(0, s)$. We may assume that $\sigma(s) = 1$ in the isotropic diffusion case. Thus, for the dynamics in Fig. 4.1, the value of the constant $\hat{\psi}$ is calculated by integrating the characteristic equations for the eikonal equation (4.11).

The function $K_0(s)$ is given by

$$K_0(s) = \frac{1}{B(s)} \exp \left\{ - \int_0^s \left[\frac{a_0(s') - \xi^2(s')}{B(s')} ds' \right] \right\}, \quad (4.16)$$

where $\xi(s)$ is the S -periodic solution of the Bernoulli equation

$$\sigma(s)\xi^3(s) + [a^0(s) + 2\sigma(s)\phi(s)]\xi(s) + B(s)\xi'(s) = 0, \quad (4.17)$$

which is defined up to a multiplicative constant that can be chosen to be 1. Equations (4.9) and (4.10) indicate that the first eigenvalue λ_0 decays exponentially fast as $\varepsilon \rightarrow 0$.

4.4 The Precise WKB Structure of the Principal Eigenfunction

4.4.1 The Eikonal Equation

In view of (4.9) and (4.10), the asymptotic structure of higher-order eigenfunctions is derived from that of the first one. The principal eigenfunction $u_0(\mathbf{y})$ has the WKB representation

$$u_0(\mathbf{y}) = K_\varepsilon(\mathbf{y}) \exp\left\{-\frac{\psi(\mathbf{y})}{\varepsilon}\right\}, \quad (4.18)$$

where the eikonal function $\psi(\mathbf{y})$ is solution of (4.11). First, we note that $\psi(\mathbf{y})$ is constant on the boundary, because in local coordinates on $\partial\Omega$ (4.11) can be written as

$$[\nabla\psi(0, s)]^T \boldsymbol{\sigma}(0, s) \nabla\psi(0, s) + B(s) \frac{\partial\psi(0, s)}{\partial s} = 0. \quad (4.19)$$

To be well-defined on the boundary, the function $\psi(0, s)$ must be periodic in s with period S . However, (4.19) implies that the derivative $\partial\psi(0, s)/\partial s$ does not change sign, because $B(s) > 0$ and the matrix $\boldsymbol{\sigma}(0, s)$ is positive definite. Thus we must have

$$\psi(0, s) = \text{const.} = \hat{\psi}, \quad \nabla\psi(0, s) = 0 \text{ for all } 0 \leq s \leq S. \quad (4.20)$$

It follows that near $\partial\Omega$ the following expansion holds,

$$\psi(\rho, s) = \hat{\psi} + \frac{1}{2}\rho^2 \frac{\partial^2\psi(0, s)}{\partial\rho^2} + o(\rho^2) \text{ as } \rho \rightarrow 0. \quad (4.21)$$

Setting $\phi(s) = \partial^2\psi(0, s)/\partial\rho^2$ and using (3.107) and (4.21) in (4.11), we see that $\phi(s)$ must be the S -periodic solution of the Bernoulli equation (3.61).

4.4.2 The Transport Equation

The function $K_\varepsilon(\mathbf{y})$ is a regular function of ε for $\mathbf{y} \in \Omega$, but has to develop a boundary layer to satisfy the homogenous Dirichlet boundary condition

$$K_\varepsilon(\mathbf{y}) = 0 \text{ for } \mathbf{y} \in \partial\Omega. \quad (4.22)$$

Therefore $K_\varepsilon(\mathbf{y})$ is further decomposed into the product

$$K_\varepsilon(\mathbf{y}) = [K_0(\mathbf{y}) + \varepsilon K_1(\mathbf{y}) + \dots] q_\varepsilon(\mathbf{y}), \quad (4.23)$$

where $K_0(\mathbf{y})$, $K_1(\mathbf{y})$, ... are regular functions in Ω and on its boundary and are independent of ε , and $q_\varepsilon(\mathbf{y})$ is a boundary layer function. The functions $K_j(\mathbf{y})$ ($j = 0, 1, \dots$) satisfy first-order partial differential equations and therefore cannot satisfy the boundary condition (4.22). Thus $K_0(\mathbf{y})$ has to be found by integrating the reduced transport equation along characteristics.

The boundary layer function $q_\varepsilon(\mathbf{y})$ satisfies the boundary condition

$$q_\varepsilon(\mathbf{y}) = 0 \text{ for } \mathbf{y} \in \partial\Omega, \quad (4.24)$$

the matching condition

$$\lim_{\varepsilon \rightarrow 0} q_\varepsilon(\mathbf{y}) = 1 \text{ for all } \mathbf{y} \in \Omega, \quad (4.25)$$

and the smoothness condition

$$\lim_{\varepsilon \rightarrow 0} \frac{\partial^i q_\varepsilon(\mathbf{y})}{\partial (\mathbf{y}^j)^i} = 0, \text{ for all } \mathbf{y} \in \Omega, i \geq 1, 1 \leq j \leq 2. \quad (4.26)$$

The function $K_\varepsilon(\mathbf{y})$ cannot have an internal layer at the global attractor point $\mathbf{0}$ in Ω , as discussed in Sect. 3.2.2.

In view of Eqs. (4.23)–(4.26), we obtain in the limit $\varepsilon \rightarrow 0$ the transport equation

$$\begin{aligned} & \sum_{i=1}^d \left[2 \sum_{j=1}^d \sigma^{i,j}(\mathbf{y}) \frac{\partial \psi(\mathbf{y})}{\partial \mathbf{y}^j} + a^i(\mathbf{y}) \right] \frac{\partial K_0(\mathbf{y} | \mathbf{x})}{\partial \mathbf{y}^i} \\ &= - \sum_{i=1}^d \left\{ \frac{a^i(\mathbf{y})}{\partial \mathbf{y}^i} + \sum_{j=1}^d \left[\sigma^{i,j}(\mathbf{y}) \frac{\partial^2 \psi(\mathbf{y})}{\partial \mathbf{y}^i \partial \mathbf{y}^j} + 2 \frac{\partial \sigma^{i,j}(\mathbf{y})}{\partial \mathbf{y}^j} \frac{\partial \psi(\mathbf{y})}{\partial \mathbf{y}^j} \right] \right\} K_0(\mathbf{y} | \mathbf{x}). \end{aligned} \quad (4.27)$$

Because the characteristics diverge, the initial value on each characteristic of the eikonal equation (4.11) is given at $\mathbf{y} = \mathbf{0}$ as $K_0(\mathbf{0}) = \text{const.}$ (e.g., $\text{const.} = 1$).

Note that using (3.51) and (4.11), the field in the transport equation (4.27) can be written in local coordinates near the boundary as

$$\begin{aligned} 2\sigma(\mathbf{y})\nabla\psi(\mathbf{y}) + \mathbf{a}(\mathbf{y}) &= 2\sigma(0, s)\nabla\psi(0, s) + \mathbf{a}(0, s) + o(\rho) \\ &= \rho [2\phi(s)\sigma(0, s)\nabla\rho(0, s) + a^0(s)\nabla\rho(0, s)] + o(\rho) \end{aligned} \quad (4.28)$$

and the transport equation for $K_0(\mathbf{y})$ can be written on $\partial\Omega$ as the linear equation

$$B(s)\frac{dK_0(0, s)}{ds} + [a^0(s) + \sigma(s)\phi(s) + B'(s)]K_0(0, s) = 0. \quad (4.29)$$

Using the relations (4.41) below, we obtain the solution

$$K_0(0, s) = K_0 \frac{\sqrt{-\phi(s)}}{B(s)}, \quad (4.30)$$

where $K_0 = \text{const.}$ (e.g., $K_0 = 1$).

4.4.3 The Boundary Layer Equation

To derive the boundary layer equation, we introduce the stretched variable $\zeta = \rho/\sqrt{\varepsilon}$ and define $q_\varepsilon(\mathbf{x}) = Q(\zeta, s, \varepsilon)$. Expanding all functions in (4.18) in powers of ε and

$$Q(\zeta, s, \varepsilon) \sim Q^0(\zeta, s) + \sqrt{\varepsilon}Q^1(\zeta, s) + \dots, \quad (4.31)$$

and using (4.28), we obtain the boundary layer equation

$$\sigma(s)\frac{\partial^2 Q^0(\zeta, s)}{\partial\zeta^2} - \zeta [a^0(s) + 2\sigma(s)\phi(s)]\frac{\partial Q^0(\zeta, s)}{\partial\zeta} - B(s)\frac{\partial Q^0(\zeta, s)}{\partial s} = 0. \quad (4.32)$$

The boundary and matching conditions (4.24), (4.25) imply that

$$Q^0(0, s) = 0, \quad \lim_{\zeta \rightarrow -\infty} Q^0(\zeta, s) = 1. \quad (4.33)$$

To solve (4.32), (4.33), we set $\eta = \xi(s)\zeta$, $Q^0(\zeta, s) = \tilde{Q}^0(\eta, s)$, and rewrite (4.32) as

$$\begin{aligned} \sigma(s)\xi^2(s)\frac{\partial^2 \tilde{Q}^0(\eta, s)}{\partial\eta^2} - \eta \left[a^0(s) + 2\sigma(s)\phi(s) + \frac{B(s)\xi'(s)}{\xi(s)} \right] \frac{\partial \tilde{Q}^0(\eta, s)}{\partial\eta} \\ - B(s)\frac{\partial \tilde{Q}^0(\eta, s)}{\partial s} = 0. \end{aligned} \quad (4.34)$$

Choosing $\xi(s)$ to be the S -periodic solution of the Bernoulli equation (3.61), the boundary value and matching problem (4.32), (4.33) becomes

$$\frac{\partial^2 \tilde{Q}^0(\eta, s)}{\partial \eta^2} + \eta \frac{\partial \tilde{Q}^0(\eta, s)}{\partial \eta} - \frac{B(s)}{\sigma(s) \xi^2(s)} \frac{\partial \tilde{Q}^0(\eta, s)}{\partial s} = 0, \quad (4.35)$$

$$\tilde{Q}^0(0, s) = 0, \quad \lim_{\eta \rightarrow -\infty} \tilde{Q}^0(\eta, s) = 1, \quad (4.36)$$

which has the s -independent solution

$$\tilde{Q}^0(\eta, s) = -\sqrt{\frac{2}{\pi}} \int_0^\eta e^{-z^2/2} dz, \quad (4.37)$$

that is,

$$Q^0(\zeta, s) = -\sqrt{\frac{2}{\pi}} \int_0^{\xi(s)\zeta} e^{-z^2/2} dz. \quad (4.38)$$

The uniform expansion of the first eigenfunction is given by

$$u_0(\mathbf{y}) = \exp \left\{ -\frac{\psi(\mathbf{y})}{\varepsilon} \right\} [K_0(\mathbf{y}) + O(\sqrt{\varepsilon})] \sqrt{\frac{2}{\pi}} \int_0^{\sqrt{\varepsilon}} e^{-z^2/2} dz, \quad (4.39)$$

where $O(\sqrt{\varepsilon})$ is uniform in $\mathbf{y} \in \bar{\Omega}$.

Setting $\xi_0(s) = \sqrt{-\phi(s)}$ in (3.61), we see that $\xi_0(s)$ is the S -periodic solution of the Bernoulli equation

$$B(s)\xi'_0(s) + a^0(s)\xi_0(s) - \sigma(s)\xi_0^3(s) = 0. \quad (4.40)$$

Thus the solutions of the three Bernoulli equations $\phi(s)$ of (3.61), $\xi(s)$ of (3.61), and $\xi_0(s)$ of (4.40) are related to each other as follows (see the reference in Sect. 4.17),

$$\xi_0(s) = \sqrt{-\phi(s)} = \xi(s). \quad (4.41)$$

Equations (4.21) and (4.41) indicate that near the boundary

$$\psi(\rho, s) = \hat{\psi} - \frac{\rho^2 \xi^2(s)}{2} + o(\rho^2), \quad (4.42)$$

so that (4.39) gives

$$u_0(\mathbf{y}) \sim \exp \left\{ -\frac{\eta^2}{2} \right\} [K_0(\mathbf{y}) + O(\sqrt{\varepsilon})] \sqrt{\frac{2}{\pi}} \int_0^\eta e^{-z^2/2} dz. \quad (4.43)$$

The eigenfunction expansion (4.6) and the uniform expansion of the first eigenfunction is given by

$$u_0(\mathbf{y}) = \exp \left\{ -\frac{\psi(\mathbf{y})}{\varepsilon} \right\} \left[K_0(\mathbf{y}) + O(\sqrt{\varepsilon}) \right] \sqrt{\frac{2}{\pi}} \int_0^{\sqrt{\varepsilon}} e^{-z^2/2} dz, \quad (4.44)$$

where $O(\sqrt{\varepsilon})$ is uniform in $\mathbf{y} \in \bar{\Omega}$. The normal flux density to leading order is therefore given by

$$\mathbf{J} \cdot \mathbf{n}|_{\partial\Omega}(s, t) \sim e^{-\lambda_0 t} \sqrt{\frac{2\varepsilon}{\pi}} K_0(0, s) \xi(s) \sigma(s) e^{-\hat{\psi}/\varepsilon} + \dots, \quad (4.45)$$

hence, for $\mathbf{y} \in \partial\Omega$ corresponding to $\rho = 0$ and arclength s , the exit-point density is given by

$$\begin{aligned} & \Pr\{\mathbf{x}(\tau) = \mathbf{y}, \tau = t \mid \mathbf{x}(0) = \mathbf{x}\} \\ &= \frac{K_0(0, s) \xi(s) \sigma(s) + e^{(\lambda_0 - \lambda_n)t} u_n(\mathbf{y}) v_n(\mathbf{x}) + \dots}{\int_0^s K_0(0, s) \xi(s) \sigma(s) ds + e^{(\lambda_0 - \lambda_n)t} u_n(\mathbf{y}) v_n(\mathbf{x}) + \dots}. \end{aligned} \quad (4.46)$$

Using (4.44), the principal eigenfunction can be written as

$$u_0(\mathbf{y}) \sim \exp \left\{ -\frac{\eta^2}{2} \right\} \left[K_0(\mathbf{y}) + O(\sqrt{\varepsilon}) \right] \sqrt{\frac{2}{\pi}} \int_0^\eta e^{-z^2/2} dz. \quad (4.47)$$

For $\eta = 0$, the first term in the expansion of $K_\varepsilon(\mathbf{x})$ is

$$K_0(0, s) = K_0 \frac{\sqrt{-\phi(s)}}{B(s)} \quad (4.48)$$

and we recover in the limit $t \rightarrow \infty$ the exit density at $\mathbf{y} = (0, s)$ as [Schuss (2010b)]

$$\Pr\{\mathbf{x}(\tau) = \mathbf{y} \mid \mathbf{x}\} \sim \frac{\frac{\xi^2(s) \sigma(s)}{B(s)}}{\int_0^s \frac{\xi^2(s) \sigma(s)}{B(s)} ds}. \quad (4.49)$$

4.4.4 The First Eigenfunction of the Adjoint Problem

The first eigenfunction $v_0(\mathbf{x})$ of the backward Kolmogorov operator L_x^* does not have the WKB structure (4.18), but rather converges to a constant as $\varepsilon \rightarrow 0$, at every $\mathbf{x} \in \Omega$ outside the boundary layer. Thus it consists of a boundary layer only. Expanding as in Sect. 4.4.3, we obtain the boundary value and matching problem

$$\sigma(s) \frac{\partial^2 Q^0(\zeta, s)}{\partial \zeta^2} + \zeta a^0(s) \frac{\partial Q^0(\zeta, s)}{\partial \zeta} + B(s) \frac{\partial Q^0(\zeta, s)}{\partial s} = 0 \quad (4.50)$$

$$Q^0(0, s) = 0, \quad \lim_{\zeta \rightarrow -\infty} Q^0(\zeta, s) = 1. \quad (4.51)$$

The scaling $\eta = \xi_0(s)$, with $\xi_0(s)$ the solution of (3.62), converts (4.50) and (4.51) into

$$\frac{\partial^2 \tilde{Q}^0(\eta, s)}{\partial \eta^2} + \eta \frac{\partial \tilde{Q}^0(\eta, s)}{\partial \eta} + \frac{B(s)}{\sigma(s)\xi^2(s)} \frac{\partial \tilde{Q}^0(\eta, s)}{\partial s} = 0, \quad (4.52)$$

$$\tilde{Q}^0(0, s) = 0, \quad \lim_{\eta \rightarrow -\infty} \tilde{Q}^0(\eta, s) = 1, \quad (4.53)$$

where $\tilde{Q}^0(\eta, s) = Q^0(\zeta, s)$. Now, (4.41) gives the s -independent solution (4.37) and hence (4.38), which is the uniform approximation to $v_0(\mathbf{y})$,

$$v_0(\mathbf{y}) = C_\varepsilon \operatorname{erf} \left(\frac{\rho(\mathbf{y})\xi(s(\mathbf{y}))}{\sqrt{\varepsilon}} \right), \quad (4.54)$$

where C_ε depends on the normalization. Thus

$$u_0(\mathbf{y}) \sim \exp \left\{ -\frac{\psi(\mathbf{y})}{\varepsilon} \right\} [K_0(\mathbf{y}) + O(\sqrt{\varepsilon})] v_0(\mathbf{y}), \quad (4.55)$$

which in the boundary layer coordinates has the form

$$u_0(\mathbf{y}) \sim \exp \left\{ -\frac{\eta^2}{2} \right\} [K_0(\mathbf{y}) + O(\sqrt{\varepsilon})] v_0(\mathbf{y}). \quad (4.56)$$

4.5 Higher-Order Eigenvalues

Higher-order eigenfunctions of the adjoint problem lead to the boundary layer equations

$$\frac{\partial^2 \tilde{Q}^0(\eta, s)}{\partial \eta^2} + \eta \frac{\partial \tilde{Q}^0(\eta, s)}{\partial \eta} + \frac{B(s)}{\sigma(s)\xi^2(s)} \frac{\partial \tilde{Q}^0(\eta, s)}{\partial s} = -\frac{\lambda}{\sigma(s)\xi^2(s)} \tilde{Q}^0(\eta, s), \quad (4.57)$$

$$\tilde{Q}^0(0, s) = 0, \quad \lim_{\eta \rightarrow -\infty} \tilde{Q}^0(\eta, s) = 0. \quad (4.58)$$

A separated solution, $\tilde{Q}^0(\eta, s) = R(\eta)T(s)$, leads to the eigenvalue problem

$$R''(\eta) + \eta R'(\eta) + \mu R(\eta) = 0, \quad R(0) = 0, \quad \lim_{\eta \rightarrow -\infty} R(\eta) = 0, \quad (4.59)$$

for the even function $R(\eta)$, where μ is the separation constant. The large η asymptotics of $R(\eta)$ is $R(\eta) \sim \exp\{-\eta^2/2\}$, so the substitution $R(\eta) = \exp\{-\eta^2/4\}W(\eta)$ converts (4.59) to the parabolic-cylinder eigenvalue problem

$$W''(\eta) + \left(\mu - \frac{1}{2} - \frac{\eta^2}{4}\right) W(\eta) = 0, \quad W(0) = 0, \quad \lim_{\eta \rightarrow -\infty} W(\eta) = 0. \quad (4.60)$$

The eigenvalues of (4.60) are $\mu_n = 2n$, ($n = 1, 2, \dots$), with the eigenfunctions

$$W_{2n+1}(\eta) = \exp\left\{-\frac{\eta^2}{4}\right\} H_{2n+1}\left(\frac{\eta}{\sqrt{2}}\right),$$

where $H_{2n+1}(x)$ are the Hermite polynomials of odd orders [Abramowitz and Stegun (1972)]. Thus the radial eigenfunctions are

$$R_n(\eta) = \exp\left\{-\frac{\eta^2}{4}\right\} W_{2n+1}(\eta) = \exp\left\{-\frac{\eta^2}{2}\right\} H_{2n+1}\left(\frac{\eta}{\sqrt{2}}\right). \quad (4.61)$$

The functions $T_{2n+1}(s)$ are given by

$$T_{2n+1}(s) = \exp\left\{-\lambda \int_0^s \frac{ds'}{B(s')} + (2n+1) \int_0^s \frac{\sigma(s')\xi^2(s')}{B(s')} ds'\right\}, \quad (4.62)$$

which has to be S -periodic. The period and angular frequency of rotation of the drift about the boundary are, respectively,

$$\mathcal{T} = \int_0^S \frac{ds'}{B(s')}, \quad \omega = \frac{2\pi}{\mathcal{T}}.$$

Therefore periodicity implies that

$$-\lambda \int_0^S \frac{ds}{B(s)} + 2n \int_0^S \frac{\sigma(s)\xi^2(s)}{B(s)} ds = 2\pi m i \quad (4.63)$$

for $m = \pm 1, \pm 2, \dots$. Thus, for $n = 1, \dots$, the eigenvalues are

$$\lambda_{m,n} = \left[\frac{n}{\pi} \int_0^S \frac{\sigma(s)\xi^2(s)}{B(s)} ds + mi \right] \omega \quad (4.64)$$

and the rotational eigenfunctions are

$$T_{m,n}(s) = \exp \left\{ -\lambda_{m,n} \int_0^s \frac{ds'}{B(s')} + 2n \int_0^s \frac{\sigma(s')\xi^2(s')}{B(s')} ds' \right\}. \quad (4.65)$$

The eigenfunctions $\tilde{Q}_{m,n}(\eta, s) = R_n(\eta)T_{m,n}(s)$ are given by

$$\begin{aligned} \tilde{Q}_{m,n}(\eta, s) &= \exp \left\{ -\frac{\eta^2}{2} \right\} H_{2n+1} \left(\frac{\eta}{\sqrt{2}} \right) \times \\ &\quad \exp \left\{ -mi\omega \int_0^s \frac{ds'}{B(s')} + 2n \int_0^s \frac{\sigma(s')\xi^2(s')}{B(s')} ds' \right\}. \end{aligned}$$

Thus the expressions (4.9), (4.10), and (4.64) define the spectrum of the non-self-adjoint operators L_y and L_x^* with homogeneous Dirichlet boundary conditions, defined in Sect. 1.2, as

$$Sp(L) = \left\{ \lambda_0(1 + O(\varepsilon)), \bigcup_{n \geq 0, m = \pm 1, \pm 2, \dots} \lambda_{m,n}(1 + O(\varepsilon)) \right\}. \quad (4.66)$$

As in (4.55), the forward eigenfunctions $u_n(\mathbf{y})$ are related to the backward eigenfunctions $v_n(\mathbf{y}) = \tilde{Q}_{m,n}(\eta, s)$ by

$$u_n(\mathbf{y}) \sim \exp \left\{ -\frac{\psi(\mathbf{y})}{\varepsilon} \right\} [K_0(\mathbf{y}) + O(\sqrt{\varepsilon})] \bar{v}_n(\mathbf{y}), \quad (4.67)$$

which in the boundary layer coordinates has the form

$$u_n(\mathbf{y}) \sim \exp \left\{ -\frac{\eta^2}{2} \right\} [K_0(\mathbf{y}) + O(\sqrt{\varepsilon})] \bar{v}_n(\mathbf{y}). \quad (4.68)$$

With the proper normalization the eigenfunctions $\{u_n(\mathbf{y})\}$ and $\{v_n(\mathbf{y})\}$ form a bi-orthonormal system.

4.6 Oscillatory Escape Time

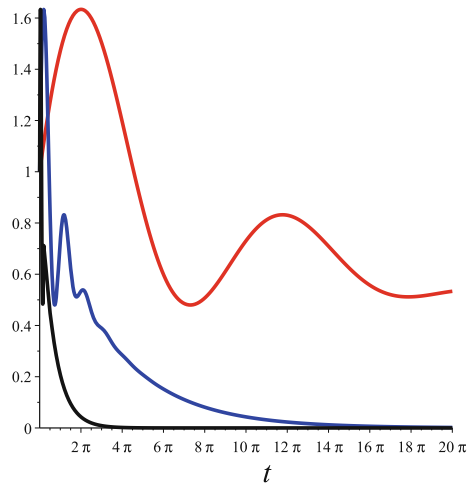
Figure 4.2 shows the oscillatory decay with parameters $\omega_1 = 1$ and $\omega_2 = 2$ in (4.4) and initial conditions chosen to give (1.29) as

$$\Pr\{\tau = t\} = e^{-0.001t} \sin 0.2t \quad (4.69)$$

$$\Pr\{\tau = t\} = e^{-0.1t} + e^{-0.5t} \sin 2t \quad (4.70)$$

$$\Pr\{\tau = t\} = e^{-0.5t} \sin 2.5t \quad (4.71)$$

Fig. 4.2 Oscillatory decay of the probability density function of the escape time according to (4.69) (red), (4.70) (blue), and (4.71) (black)



4.7 Spontaneous Activity in the Cerebral Cortex

The Hopf system described in Sect. 4.1 exhibits properties similar to those of the model (4.72) below, which describes the cerebral cortex that is continuously active in the absence of sensory stimuli (see Annotations in Sect. 4.17 for references). An example of this spontaneous activity is the phenomenon of voltage transitions between two distinct levels, called Up and Down states, observed simultaneously when recording from many neurons.

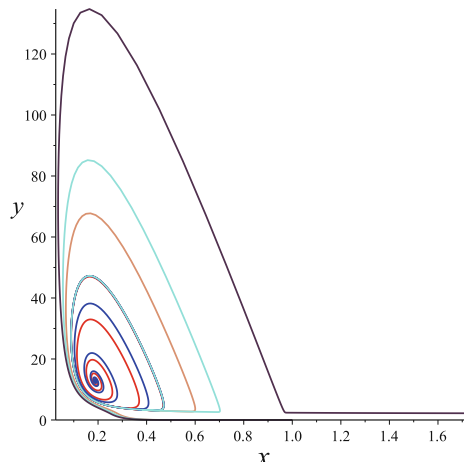
To model this phenomenon, we denote by x the (dimensionless) synaptic depression parameter, by y the synaptic membrane voltage, by U and t_r the utilization parameter and recovery time constant, respectively and by w_T the synaptic strength. We set τ to be the voltage time-scale, and σ to be the noise amplitude. The function $H(\cdot)$ is the Heaviside unit step, and \dot{w} is standard Gaussian white noise. The model

(see (4.73) below)

$$\begin{aligned}\dot{x} &= \frac{1-x}{t_r} - Ux(y-T)H(y-T), \\ \dot{y} &= -\frac{y}{\tau} + \frac{xUw_T}{\tau}(y-T)H(y-T) + \frac{\sigma}{\sqrt{\tau}} \dot{w},\end{aligned}\tag{4.72}$$

predicts that in a certain range of parameters, the noiseless ($\sigma = 0$) dynamics has two stable states, a focus, which corresponds to an Up state, and a stable equilibrium, which corresponds to a Down state. Their domains of attraction are separated by an unstable limit cycle (the blue curve in Fig. 4.3). The decay of the Up state was observed in experiments and simulations to be oscillatory. In view of the results of the previous section, the apparent synchronization is simply a manifestation of the complex eigenvalues of the non-self-adjoint Dirichlet boundary value problem for the corresponding Fokker–Planck operator inside the limit cycle. Thus the model (4.72) explains the oscillatory decay of the survival probability of the stochastic dynamics (4.1) that is activated over the boundary of the domain of attraction Ω of the stable focus of the drift $\mathbf{a}(\mathbf{x})$ by the small noise $\sqrt{2\varepsilon} \mathbf{b}(\mathbf{x}_\varepsilon(t)) \dot{\mathbf{w}}(t)$. As in the Hopf model (4.1), the boundary $\partial\Omega$ of the domain is an unstable limit cycle of the drift field $\mathbf{a}(\mathbf{x})$. The model shows that the oscillations are not due to mysterious synchronization, but rather to complex eigenvalues of the Dirichlet boundary value problem for the non-self-adjoint Fokker–Planck operator L_y in Ω . These are evaluated by a singular perturbation expansion of the spectrum of L_y .

Fig. 4.3 The phase-plane dynamics of the Holcman–Tsodyks model (4.72). The unstable limit cycle is marked blue. The parameters are $\tau = 0.05 \text{ sec}$, $t_r = 0.8 \text{ sec}$, $U = 0.5$, $w_T = 12.6 \text{ mV/Hz}$, $T = 2.0 \text{ mV}$



4.8 Numerical Study of Oscillatory Decay

The analysis in Sects. 4.1–4.7 is based on the assumption that the principal eigenfunction has the asymptotic WKB structure. There are cases, however, that this assumption does not hold (see Annotations 4.17 for further discussion). The case at hand differs from the case considered in the literature cited in the Annotations 4.17, in the dependence of the structure of the drift on the small noise intensity. Specifically, in the case at hand, we consider a distinguished limit, in which the (dimensionless) noise intensity and the distance of the focus to the boundary decay together. In this case, the phenomenon of cycling of the density of exit points around the limit cycle as the noise decreases disappears and the density concentrates around the boundary point closest to the focus.

It is necessary therefore to clarify the question of validity of the assumption in the sections studied above. In the absence of proof of asymptotic convergence a numerical solution and simulations of the stochastic dynamics can indicate the asymptotic convergence of the WKB construction. Thus we consider the Hopf-like case, where the focus is close to the limit cycle and ε is proportional to the distance of the focus from the boundary. Specifically, it is shown here that the dominant oscillation frequency, $1/\Im\{\lambda_2(\Omega)\}$, is independent of the relative noise strength in this distinguished limit. The density of exit points on $\partial\Omega$ is concentrated in a small arc of $\partial\Omega$ closest to the focus. The principal eigenvalue does not necessarily decay exponentially in the distinguished limit as $\varepsilon \rightarrow 0$. In the mathematical model of a neural network studied above (with synaptic depression), oscillation peaks are identified in the density of the time the network spends in a specific state. This observation explains the oscillations of stochastic trajectories around the focus prior to escape and also the non-Poissonian distribution of escape times. This phenomenon has been observed and reported in simulations of neural networks.

4.9 A Model of Up-State Dynamics in a Neuronal Network

Neuronal ensembles can exhibit spontaneous activities containing recurrent patterns. These patterns are characterized electro-physiologically by a transient depolarization, called an Up-state, in which the membrane potential decreases (in absolute value). This phenomenon is reproducible by a minimal mean-field model of a two-dimensional neuronal network with excitatory connections. The state variables in the model are the mean firing rate V , averaged over the population, and the synaptic depression μ . In a neuronal network, whose connections are mostly depressing synapses, the neural dynamics is modeled by the following stochastic equations,

$$\begin{aligned}\tau \dot{V} &= -V + J\mu R(V) + \sqrt{\tau}\sigma \dot{w} \\ \dot{\mu} &= \frac{1-\mu}{t_r} - UR(V),\end{aligned}\tag{4.73}$$

where V , the average voltage, is measured in mV with a base line at 0 mV , the average synaptic strength in the network is J (connectivity) and U and t_r are the utilization parameter and recovery time of the synaptic depression, and $\dot{\omega}$ is standard Gaussian white noise, respectively (see (4.72)). The first term on the right-hand side of the first equation of (4.73) accounts for the intrinsic biophysical decay to equilibrium. The second term represents the synaptic input, scaled by the synaptic depression parameter μ . The time τ measures the relaxation of the voltage V to equilibrium. The last term is a white-noise approximation to a train of Poissonian spikes and the sum of all uncorrelated sources of noise, with total amplitude $\sqrt{\tau}\sigma$, where σ is the amplitude for the voltage fluctuation. The average firing rate $R(V)$ (in Hz) is approximated by the threshold-linear voltage-dependence function

$$R(V) = \begin{cases} \alpha(V - T) & \text{if } V > T \\ 0 & \text{otherwise,} \end{cases} \quad (4.74)$$

where $T > 0$ is a threshold and $\alpha = 1\text{Hz}/mV$ is a conversion factor. The second equation in system (4.73) describes the activity-dependent synaptic depression according to the phenomenological model, where every incoming spike leads to an abrupt decrease in the instantaneous synaptic efficacy, measured by a utilization factor U , due to depletion of neurotransmitters. Between spikes, the synaptic efficacy returns to its original state $\mu = 1$ with a time constant t_r . When the network connectivity J exceeds a minimal value there are three critical points: two attractors, P_1 at $V = 0, \mu = 1$, a stable focus P_2 , and one saddle point P_S . The boundary of the basin of attraction Ω of P_2 is an unstable limit cycle and is defined as the Up-state (see Annotations 4.17).

For the sake of completeness, the dynamics of the noiseless system (4.73) are reproduced here. Note that the focus P_2 is close to the boundary $\partial\Omega$ (Fig. 4.4A). Simulated stochastic trajectories escape Ω in a small boundary neighborhood of P_2 (green). Specifically, at the intersection of the null isoclines (marked red in Fig. 4.4A). The simulated trajectories wind several times around P_2 before hitting $\partial\Omega$. The effect of the windings is expressed in the appearance of peaks in the probability density function of exit times (Fig. 4.4B). Indeed, the histogram of exit times contains several oscillatory peaks that coincide with the winding numbers of trajectories around the focus P_2 . The first peak is due mainly to trajectories that do not wind around the focus even once prior to escape, the second one is due to trajectories that wind once prior to escape, and so on. However, the dispersion of the exit times of trajectories that wind around the focus several times prior to escape is smoothed out in the tail of the density. It appears that the density of exit times in the Up-state is non-Poissonian, which leads to our study of the observed phenomenon in generic systems.⁴

Peak oscillations require the following two key ingredients: a stable focus inside an unstable limit cycle and a small distance between the focus and the cycle. The present framework allows explicit computation of the density of times in the Up-state, that is the density of the ISI, which is the density of the times the stochastic trajectories reach the threshold.

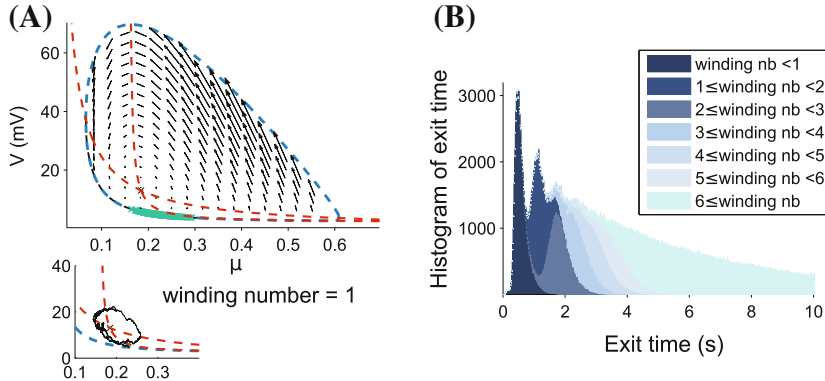


Fig. 4.4 Escape from the Up-state and distribution of time. (A): Phase portrait (V, μ) defined by (4.73). The phase space shows an unstable limit cycle (blue) and nullclines (red) that intersect at the focus near the limit cycle. The distribution of exit points (green) is concentrated on a small arc of the limit cycle. Lower panel: a winding trajectory of (4.73) (black). (B): Density of exit times, conditioned on the winding number; the peak oscillation corresponds to the winding number prior to escape. The histogram is obtained from 10^6 simulated trajectories of (4.73) that start at $(\mu_0, V_0) = (0.21, 20\text{ mV})$ with $\sigma = 0.0015$

4.10 The Phase Space of the Model

The mathematical description and analysis of the discussed phenomenon begins with the stochastic differential equation

$$d\mathbf{x}_\varepsilon(t) = \mathbf{b}(\mathbf{x}_\varepsilon(t)) dt + \sqrt{2\varepsilon} \mathbf{a}(\mathbf{x}_\varepsilon(t)) d\mathbf{w}(t), \quad (4.75)$$

with the drift field $\mathbf{b}(\mathbf{x})$,

$$\dot{\mathbf{x}}(t) = \mathbf{b}(\mathbf{x}(t)), \quad (4.76)$$

which has a single stable focus A , whose domain of attraction Ω is bounded by an unstable limit cycle. The focus A is close to the boundary $\partial\Omega$ in the following sense. Consider a transformation of the normal form of the Hopf system in the complex plane

$$\dot{z} = \mathbf{b}_0(z) = \lambda z(-1 + |z|^2 + i\omega) \quad (4.77)$$

by the Möbius transformation

$$\zeta = \Phi_\alpha(z) = \frac{z - \alpha}{1 - \alpha z}, \quad 0 < \alpha < 1. \quad (4.78)$$

The field $\mathbf{b}_0(z)$ has a stable focus at $A = 0$, whose domain of attraction is the circle $|z| = 1$, which is an unstable limit cycle of (4.77). We assume, as we may, that $\lambda = 1$ and ω is a real-valued parameter. The transformation (10.106) maps the disk $|z| \leq 1$ onto itself and sends the attractor $A = 0$ to the point $\zeta_0 = -\alpha$ on the real axis, which can be arbitrarily close to the boundary point $\zeta = -1$. Thus we obtain from $\mathbf{b}_0(z)$ a class of one-parameter vector fields $\mathbf{b}_\alpha(\zeta)$. The mapping (10.106) is represented in Fig. 4.5. The explicit expression for the field $\mathbf{b}_\alpha(\zeta)$ is

$$\begin{aligned}\dot{\zeta} &= \mathbf{b}_\alpha(\zeta) = \Phi_\alpha'(\Phi_\alpha^{-1}(\zeta)) \mathbf{b}_0(\Phi_\alpha^{-1}(\zeta)) \\ &= \frac{(1 - \alpha^2)\Phi_\alpha^{-1}(z)(-1 + |\Phi_\alpha^{-1}(z)|^2 + i)}{(1 - \alpha\Phi_\alpha^{-1}(\zeta))^2} \\ &= \lambda \frac{(\zeta + \alpha)(1 + \alpha\zeta)}{(1 - \alpha^2)} \left(-1 + \left| \frac{\zeta + \alpha}{1 + \alpha\zeta} \right|^2 + i\omega \right)\end{aligned}\quad (4.79)$$

and the specific system (4.75) that is considered here is

$$d\zeta = \mathbf{b}_\alpha(\zeta) dt + \sqrt{2\varepsilon} d\mathbf{w}(t). \quad (4.80)$$

The linearization of $\mathbf{b}_\alpha(\zeta)$ about $\zeta = -\alpha$ is given by

$$\mathbf{b}_\alpha(\zeta) = \lambda(-1 + i\omega)(\zeta - \zeta_0) + O(|\zeta - \zeta_0|^2) \quad (4.81)$$

so in real-valued coordinates the linearized system (4.79) can be written as

$$\frac{d}{dt} \begin{pmatrix} x + \alpha \\ y \end{pmatrix} = -\lambda \begin{pmatrix} 1 & \omega \\ -\omega & 1 \end{pmatrix} \begin{pmatrix} x + \alpha \\ y \end{pmatrix} \quad (4.82)$$

with eigenvalues $\mu = -\lambda(1 \pm i\omega)$.

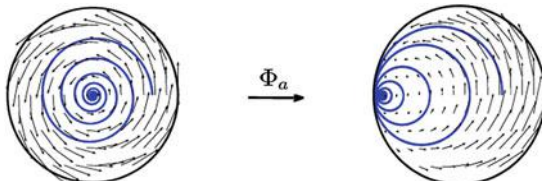


Fig. 4.5 Image of the Hopf vector field by a Möbius mapping. The mapped generic vector field has a focus arbitrarily close to the unstable limit cycle. The Hopf vector field (10.106) (Left) and its image (4.77) (Right)

4.11 Brownian Simulations of Oscillation Phenomena in (4.80)

Stochastic simulations of Eq. (4.80) (Fig. 4.6A) reveal that starting from any initial point in $\Omega = \{|\zeta| < 1\}$, except in a boundary layer near the limit cycle $|\zeta| = 1$, all stochastic trajectories first converge towards the focus ζ_0 . For a certain range of the noise intensities the noise contribution to the motion becomes dominant, because the field vanishes at a point in a region near the attractor ζ_0 , leading to exit in a relatively short time. The trajectories either exit or loop around the attractor before coming back close to a neighborhood R_α of the attractor ζ_0 . Figure 4.6B-E show various examples of trajectories making 0, 1, 2 and 3 loops prior to exit.

Unlike in the exit time problem (see [Schuss (2010b)] and the references therein), the simulated exit-time density shows periodic peaks (Fig. 4.6). As shown below, the analysis of the system (4.80) relates the peak frequency to the properties of the dynamics (4.79). In contrast to the exit problem, where the first eigenvalue of the Fokker-Planck operator is asymptotically the rate of the Poissonian escape process, in the case at hand higher-order complex-valued eigenvalues are needed to represent

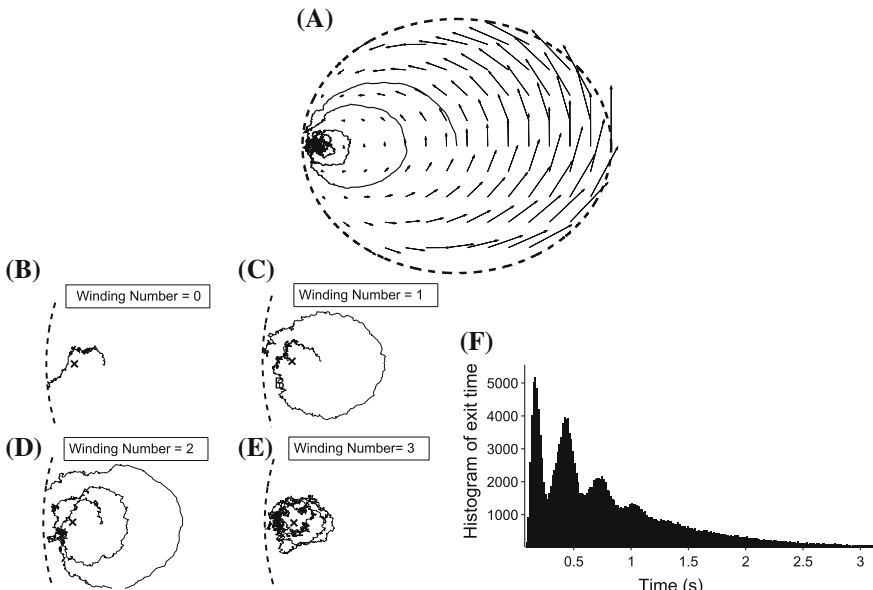


Fig. 4.6 Exit from an attractor near the characteristic boundary. The attractor has two imaginary eigenvalues leading to an oscillatory behavior of the stochastic trajectories before exit (parameters: $\alpha = 0.9$, $\varepsilon = 0.0025$, $\omega = 10$). (A) example of a trajectory. (B-E): trajectory making zero, one, two and three loops respectively around the attractor before exit. (F): Histogram of exit times of 200,000 trajectories starting at the initial point $(-0.8, 0)$

the density of escape times. In addition, simulations show that the density of exit points concentrates in a small boundary neighborhood $\partial\Omega \cap R_\alpha$ near ζ_0 , as the focus point moves closer to the boundary, whereas the exit density on a limit cycle without critical points is spread over the entire boundary, depending on the speed of the drift on the boundary.

The simulations give an estimate of the mean exit time $\bar{\tau}_\varepsilon$, which shows that it can become finite as ζ_0 moves toward the boundary to a distance that depends on ε and $\bar{\tau}_\varepsilon$ does not necessarily blow up exponentially for small noise as in the exit problem.

4.12 The Exit Density from a Focus Near a Limit Cycle

The local coordinates in the decomposition (3.51) can be chosen as (θ, ρ) , where θ is the argument of ζ in the complex plane and $\theta \in [-\pi, \pi]$. The vector field $\mathbf{b}_\alpha(\zeta)$ can be represented locally as

$$\mathbf{b}_\alpha(\rho, \theta) = -\rho[a_\alpha^0(\theta) + o(\rho)]\mathbf{n} + b_\alpha^*(\rho, \theta)\mathbf{t} \text{ for } \rho \ll 1, \quad (4.83)$$

where $\mathbf{t} = \mathbf{t}(\theta)$ and $\mathbf{n} = \mathbf{n}(\theta)$ are the unit tangent and unit outer normal to $\partial\Omega$, respectively. The two components $b_\alpha^0(\theta)$ and $b_\alpha^*(\rho, \theta)$ are given by (see Appendix 4.16.2)

$$a_\alpha^0(\theta) = \frac{2(1 - \alpha^2 - \omega\alpha \sin \theta)}{1 - \alpha^2} + O(\rho), \quad (4.84)$$

$$B_\alpha(\theta) = b_\alpha^*(0, \theta) = |\mathbf{b}(0, \theta)| = \frac{\omega}{1 - \alpha^2}(1 + 2\alpha \cos \theta + \alpha^2) + O(\rho). \quad (4.85)$$

Using these formulas in (4.49) for the isotropic case $\sigma(\theta) = 1$, explicit computations for α close to 1 give the leading order approximation to the exit density (see Appendix 4.16.1)

$$P_\alpha(\theta) \sim \frac{(1 + 2\alpha \cos \theta + \alpha^2)^{-3}}{\int_{-\pi}^{\pi} (1 + 2\alpha \cos s + \alpha^2)^{-3} ds}. \quad (4.86)$$

It is shown in Appendix 4.16.2 that for $1 - \alpha = O(\varepsilon)$ and $\varepsilon \ll 1$, the density of exit points does not depend on ε to leading order. In particular, the distribution of exit points does not cycle along the limit cycle as ε goes to zero. The reason is that when the focus is close to the limit cycle, the situation is almost equivalent to the one where the cycle contains critical points, for which there is no cycling.

To clarify the range of validity of the asymptotic formula (4.86), Brownian simulations of (4.75) are generated (see Fig. 4.7), and their statistics show that the numerical and analytical exit point densities are in agreement. Specifically, the exit point density is concentrated near the point $\theta = \pi$, which is the boundary point closest to the

attractor ζ_0 . The variance of $P_\alpha(\theta)$ is given by

$$\begin{aligned}\Lambda^2 &= \int_{-\pi}^{\pi} (\theta - \pi)^2 P_\alpha(\theta) d\theta \\ &= \frac{(32 \ln(2) - 11)\pi (\alpha - 1)^5 + O((\alpha - 1)^6)}{15 \times 16 (\alpha - 1)^5 + O((\alpha - 1)^6)} \mathcal{N}_\alpha,\end{aligned}$$

where

$$\mathcal{N}_\alpha = \frac{(1 - \alpha^2)^5}{2\pi (\alpha^4 + 4\alpha^2 + 1)} \quad (4.87)$$

and the standard deviation is

$$\Lambda \approx 0.06(1 - \alpha^2)^{5/2} \rightarrow 0 \text{ for } \alpha \rightarrow 1.$$

Note that the exit point density $P_\alpha(\theta)$ peaks at the point where the circulation $B_\alpha(\theta)$ is the slowest. Additional simulations for various ε are shown in Appendix 4.16.1.

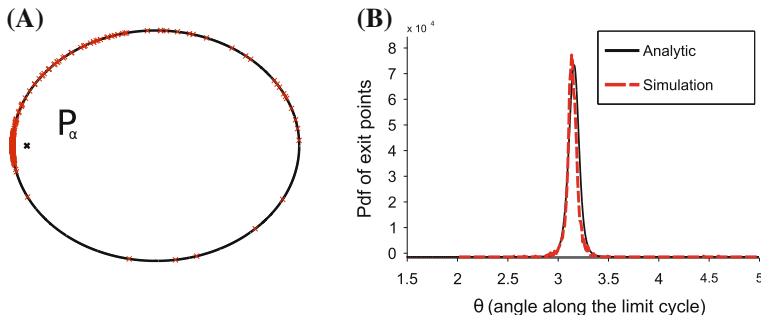


Fig. 4.7 Distribution of exit points. **A:** Exit points are concentrated in a small neighborhood of π at the boundary close the attractor P_α . **B:** The empirical exit point density of 50,000 simulated trajectories (red) and the expression (4.86) (black line). The parameters are $\alpha = -0.9$, $\omega = 10$, $\varepsilon = 0.005$

4.12.1 The Mean First Passage Time $\bar{\tau}_\varepsilon(x)$

The asymptotic approximation to $\bar{\tau}_\varepsilon(x)$, the solution of the Pontryagin–Andronov–Vitt boundary value problem, given in [Schuss (2010b, Sect. 10)], is independent of x outside the boundary layer and reduces in the case of (4.80) to

$$\bar{\tau}_\varepsilon(\mathbf{x}) \sim \frac{\pi^{3/2} \sqrt{2\varepsilon}}{\int_0^S K_0(s) \xi_\alpha(s) ds} \exp \left\{ \frac{\hat{\psi}_\alpha}{\varepsilon} \right\} \text{ for } \varepsilon \ll 1, \quad (4.88)$$

where $\xi_\alpha(s)$ is defined in (3.61),

$$K_0(s) = \frac{\xi_\alpha(s)}{B_\alpha(s)}, \quad (4.89)$$

and $\hat{\psi}_\alpha$ is the constant value of the eikonal function $\psi_\alpha(\mathbf{x})$ on $\partial\Omega$. The function $\psi_\alpha(\mathbf{x})$ is the solution of the eikonal equation

$$|\nabla \psi_\alpha(\mathbf{x})|^2 + \mathbf{b}_\alpha(\mathbf{x}) \cdot \nabla \psi_\alpha(\mathbf{x}) = 0 \text{ for } \mathbf{x} \in \Omega. \quad (4.90)$$

It is constructed, as in the previous chapter, by solving (4.90) near the focus $\mathbf{x}_0 = (-\alpha, 0)$ with the linearized drift (3.94),

$$\psi_x^2 + \psi_y^2 + \lambda[(x + \alpha + \omega y)\psi_x + (y - (x + \alpha)\omega)\psi_y] = 0,$$

as the quadratic form

$$\psi_\alpha(\mathbf{x}) = \frac{1}{2}(\mathbf{x} - \mathbf{x}_0)^T \mathbf{Q}_\alpha(\mathbf{x} - \mathbf{x}_0) + o(|\mathbf{x} - \mathbf{x}_0|^2) \text{ for } |\mathbf{x} - \mathbf{x}_0| \ll 1. \quad (4.91)$$

As mentioned above, $\psi_\alpha(\mathbf{x})$ is constant on $\partial\Omega$ and has the local expansion

$$\psi_\alpha(\rho, s) = \hat{\psi} + \frac{1}{2}\rho^2\phi(s) + o(\rho^2) \text{ for } \rho \rightarrow 0, \quad (4.92)$$

where $\phi(s)$ is the 2π -periodic solution of the Bernoulli equation

$$\sigma(s)\phi^2(s) + a^0(s)\phi(s) + \frac{1}{2}B_\alpha(s)\phi'(s) = 0 \quad (4.93)$$

and where $-\rho a^0(s)$ is the normal component of the drift $\mathbf{b}_\alpha(\mathbf{x})$ near $\partial\Omega$ and $B_\alpha(s)$ is its tangential component (local speed on the limit cycle). In the case at hand the component $a^0(s)$ is $a_\alpha^0(\theta)$, given in (4.83). For the transformed Hopf system (4.77) the mean first passage time can be evaluated asymptotically for $\text{dist}(\mathbf{x}_0, \partial\Omega) \ll 1$, that is, for $|\alpha - 1| \ll 1$.

As shown above, the solution $\phi(s)$ of (3.62) is related to the solution $\xi_\alpha(s)$ of (3.61) by

$$\sqrt{-\phi(s)} = \xi_\alpha(s). \quad (4.94)$$

The expression for the mean first passage time $\bar{\tau}_\varepsilon(\mathbf{x}_0)$ from the focus \mathbf{x}_0 to $\partial\Omega$ of the process defined in (4.80) is given by

$$\bar{\tau}(\mathbf{x}_0) \sim \frac{\pi^{3/2}\sqrt{2\varepsilon}}{\int_0^{2\pi} K_\alpha(s)\xi_\alpha(s) ds} \exp\left\{\frac{\hat{\psi}_\alpha}{\varepsilon}\right\} \text{ for } \varepsilon \ll 1, \quad (4.95)$$

where the local solution of the eikonal equation (4.90) near the attractor \mathbf{x}_0 is (4.91). To evaluate $\hat{\psi}_\alpha$ and ξ_α , we need an explicit expression for $\bar{\tau}(\mathbf{x}_0)$. We start by finding the matrix \mathbf{Q}_α of the quadratic form of (4.91), which is the solution of the Riccati equation

$$2\mathbf{Q}_\alpha \boldsymbol{\sigma}(P_\alpha) \mathbf{Q}_\alpha + \mathbf{Q}_\alpha \mathbf{A}_\alpha + \mathbf{A}_\alpha^T \mathbf{Q}_\alpha = \mathbf{0}, \quad (4.96)$$

where \mathbf{A}_α is the Jacobian matrix of \mathbf{b}_α at the attractor ζ_0 . Using (4.79), we obtain from Appendix 4.16.3 that

$$\mathbf{A}_\alpha = \begin{pmatrix} -1 & -\omega \\ \omega & -1 \end{pmatrix}. \quad (4.97)$$

The Riccati equation (4.96) reduces to

$$\mathbf{A}_\alpha \mathbf{X}_\alpha + \mathbf{X}_\alpha^T \mathbf{A}_\alpha^T = -\mathbf{I}, \quad (4.98)$$

and $\mathbf{X}_\alpha = \frac{1}{2} \mathbf{Q}_\alpha^{-1}$ is given by

$$\mathbf{X}_\alpha = \int_0^\infty e^{\mathbf{A}_\alpha t} e^{\mathbf{A}_\alpha^T t} dt. \quad (4.99)$$

Appendix 4.16.3 gives

$$\exp\{t\mathbf{A}_\alpha\} = e^{-t} \begin{pmatrix} \cos \omega t & -\sin \omega t \\ \sin \omega t & \cos \omega t \end{pmatrix}. \quad (4.100)$$

The integral (4.99) is

$$\mathbf{X}_\alpha = \frac{1}{2} \mathbf{I}, \quad \mathbf{Q}_\alpha = \mathbf{I}, \quad \text{and} \quad \det(\mathbf{Q}_\alpha) = 1. \quad (4.101)$$

To compute $\hat{\psi}_\alpha$, we note that

$$\sqrt{\det \mathbf{Q}} = \frac{1}{1 - \alpha^2} \quad (4.102)$$

$$\hat{\psi} = \frac{1}{2} \frac{(1-\alpha)^2}{1-\alpha^2}. \quad (4.103)$$

A better approximation of $\hat{\psi}_\alpha$ is obtained by solving the eikonal equation by the method of characteristics. The characteristics equations are defined by the function

$$F(x, \psi, p) = p_1^2 + p_2^2 + b_{\alpha 1}(x_1, x_2)p_1 + b_{\alpha 2}(x_1, x_2)p_2 \quad (4.104)$$

as

$$\begin{aligned} \dot{x} &= \nabla_p F(x, \psi, p) = 2p + b_\alpha \\ \dot{p} &= -\nabla_x b_\alpha^T p \\ \dot{\psi} &= p^T p = p_1^2 + p_2^2. \end{aligned} \quad (4.105)$$

Near the focus x_0 (see Fig. 4.7A) the eikonal has the local expansion

$$\psi_\alpha(x) = \frac{1}{2}(x - x_0)^T(x - x_0) + O(|x - x_0|^2) \text{ for } x \rightarrow \mathbf{0}. \quad (4.106)$$

When α is close to 1, the relation (4.91) for $x = (-1, 0)$ and $\lambda = 1$ gives

$$\hat{\psi}_\alpha = \psi_\alpha(-1) = \frac{1}{2}(1-\alpha)^2. \quad (4.107)$$

The denominator in (4.95) is given by (see Appendix 4.16.1)

$$\int_0^{2\pi} K_\alpha(s) \xi_\alpha(s) ds = \int_0^{2\pi} \frac{\xi_\alpha^2(s) ds}{Z_\alpha(s) B_\alpha(s)} = \frac{4\pi (\alpha^4 + 4\alpha^2 + 1)}{C(\omega)(1 + \alpha^2)}, \quad (4.108)$$

where

$$C(\omega) = \frac{3\omega}{8} - \frac{8/\omega}{1 + (4/\omega)^2} + \frac{4/\omega}{4 + (4/\omega)^2}.$$

Using these in (4.95) gives the mean first passage time from the focus to the limit cycle in the asymptotic form

$$\bar{\tau}_\varepsilon(x_0) \sim \frac{C(\omega)\sqrt{2\pi\varepsilon}(1+\alpha)^2}{4(1+4\alpha^2+\alpha^4)} \exp\left\{\frac{\hat{\psi}_\alpha}{\varepsilon}\right\} \text{ for } \varepsilon \ll 1. \quad (4.109)$$

When α is close to 1, (4.107) reduces (4.109) to the asymptotic formula

$$\bar{\tau}_\varepsilon(\zeta_0) \sim \frac{C(\omega)\sqrt{2\pi\varepsilon}}{6} \exp\left\{\frac{(1-\alpha)^2}{2\varepsilon}\right\}. \quad (4.110)$$

It is apparent from (4.110) that when the ratio $(1 - \alpha)^2/2\varepsilon$ is neither small nor large, the mean first passage time $\bar{\tau}_\varepsilon(\mathbf{x}_0)$ is of order $O(\sqrt{\varepsilon})$. Thus $\bar{\tau}_\varepsilon(\mathbf{x}_0)$ is not exponentially large for $\varepsilon \ll 1$, as is the case in Chap. 3. Indeed, when the attractor is near the boundary, the trajectory drifts away quickly and leaves the interior region of the domain Ω . When it returns sufficiently close to $\partial\Omega$, the small noise is sufficient to push it across the unstable cycle $\partial\Omega$. Figure 4.12 shows the decay of $\bar{\tau}_\varepsilon(\mathbf{x}_0)$ as \mathbf{x}_0 is moved toward the boundary. It also compares the logarithm of the analytical expression (4.110) with numerical Brownian dynamics simulations, ignoring possible small changes in the pre-exponential factor.

The phenomenon of oscillatory decay of the survival probability is demonstrated here in the distinguished limit $\varepsilon \ll 1$ and $\varepsilon/(1 - \alpha)^2 \sim 1$. Indeed, the parameter $\varepsilon/(1 - \alpha)^2$ is used in the WKB expansion in Sect. 4.14. The case $\alpha \rightarrow 1$ first and then $\varepsilon \rightarrow 0$ reduces to the exit problem from a characteristic boundary with a critical point (see the references in Annotations 4.17).

4.12.2 Numerical Study of the Eikonal Equation

The distinguished limit shown in formulas (4.109) and (4.110), $\bar{\tau}_\varepsilon(\mathbf{x}_0) = O(\sqrt{\varepsilon})$ as $\alpha \rightarrow 1$, leaves the question of asymptotic convergence of the expansion of $\tau_\varepsilon(\mathbf{x})$ unresolved. To resolve the transition from exponential growth to algebraic decay, we need to compute the constant value $\hat{\psi}_\alpha$ of the eikonal function $\psi_\alpha(\mathbf{x})$ as a function of α . In the previous section only the local behavior of $\psi_\alpha(\mathbf{x})$ for \mathbf{x} near $\partial\Omega$ was obtained in the limit $\alpha \rightarrow 1$. To evaluate $\psi_\alpha(\mathbf{x})$ over a larger range of values of α and \mathbf{x} , the characteristic equations have to be solved numerically.

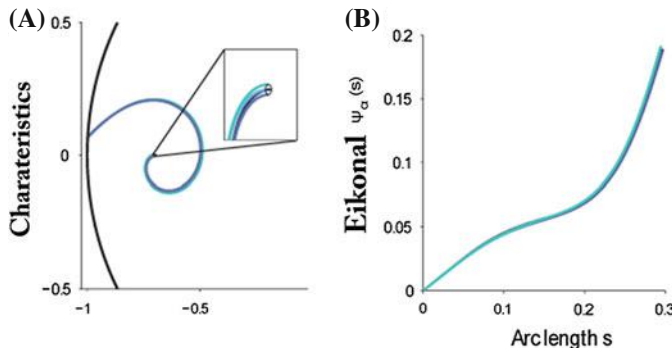


Fig. 4.8 The solution $\psi_\alpha(s)$ of the Eikonal equation. **A**: Characteristic trajectories $\mathbf{x}(t)$ obtained by solving numerically the characteristic equations (4.105). The initial points are chosen on the contour $|\mathbf{x} - \mathbf{x}_0| = \delta$. **B**: The Eikonal solution $\psi_\alpha(s)$, where s is the arclength along the characteristic $\mathbf{x}(t)$, is constant and its value does not depend on the initial conditions for the characteristics. The parameters are $\alpha = 0.7$, $\omega = 10$, $\delta = 0.001$.

To evaluate $\psi_\alpha(\mathbf{x}) = \hat{\psi}_\alpha$ for $\mathbf{x} \in \partial\Omega$, we note that near the focus $\mathbf{x}_0 = -\alpha$ the eikonal function is a quadratic form, which can be used to determine initial conditions for the characteristic equations. Thus the characteristic equations can be solved by assigning initial conditions on the circle $C_\alpha(\delta) = \{\mathbf{x} : \psi_\alpha(\mathbf{x}) = \delta^2/2\}$, defined in the complex \mathbf{x} -plane by $|\mathbf{x} + \alpha| = \delta$. The characteristic emanating from the point $\mathbf{x}(0) = -\alpha - \delta$ (on the real axis) has the initial components (up to an error of order δ^2)

$$\mathbf{x}(0) = -\alpha - \delta, \quad \mathbf{p}(0) = \begin{pmatrix} -\lambda\delta \\ 0 \end{pmatrix}, \quad \psi(0) = \frac{\lambda\delta^2}{2}. \quad (4.111)$$

The characteristic equations have an unstable focus at $(\mathbf{x}_0, \mathbf{0}, 0)$ in the 5-dimensional space $(\mathbf{x}, \mathbf{p}, \psi_\alpha)$. Thus 5-dimensional trajectories $(\mathbf{x}(t), \mathbf{p}(t), \psi_\alpha(t))$ that start on the initial surface $C_\alpha(\delta)$ diverge, and hit the boundary $\partial\Omega$ in finite time. The characteristics emanating from $C_\alpha(\delta)$ are plotted in Fig. 4.8A. They appear to oscillate before hitting $\partial\Omega$. The values of $\psi_\alpha(t)$ on each trajectory,

$$\psi_\alpha(t) = \frac{\delta^2}{2} + \int_0^t |\mathbf{p}(s)|^2 ds, \quad (4.112)$$

are shown in Fig. 4.8B. The hitting time t_α on the characteristic emanating from $\mathbf{x}(0) = -\alpha - \delta$, defined as

$$t_\alpha = \inf\{t > 0 : \mathbf{x}(t) \in \partial\Omega\}, \quad (4.113)$$

determines the value $\hat{\psi}_\alpha$ as

$$\hat{\psi}_\alpha = \psi_\alpha(t_\alpha) = \frac{\delta^2}{2} + \int_0^{t_\alpha} |\mathbf{p}(s)|^2 ds. \quad (4.114)$$

The times t_α are characterized by the winding number of the trajectory around the focus: when the focus is sufficiently close to the boundary, all characteristics emanating from $C_\alpha(\delta)$ escape without winding, but as the focus moves away from the boundary, the winding number increases (Fig. 4.9A), leading to a sudden increase in the time t_α for a characteristic to reach the boundary (Fig. 4.9B: note the small jumps), each time the winding number increases by one. The value $\hat{\psi}_\alpha$ decreases from the value $\hat{\psi}_\alpha = 0.5$ for $\alpha = 0$ to $(1 - \alpha)^2/2 = 0.005$ for $\alpha = \sqrt{0.99}$, so that $(1 - \alpha)^2/2\varepsilon$ can become of order 1 (Fig. 4.9C).

The numerical solution of the characteristic equations shows that the characteristics do not intersect inside the domain, so the eikonal equation with the conditions (4.111) has a unique twice differentiable solution. It follows that there is no cycling of the exit density on the boundary, [Dao Duc et al. (2016)], [Maier and Stein (1997)] and the results of Chap. 3 apply. Cycling here is defined as complete rotation of the

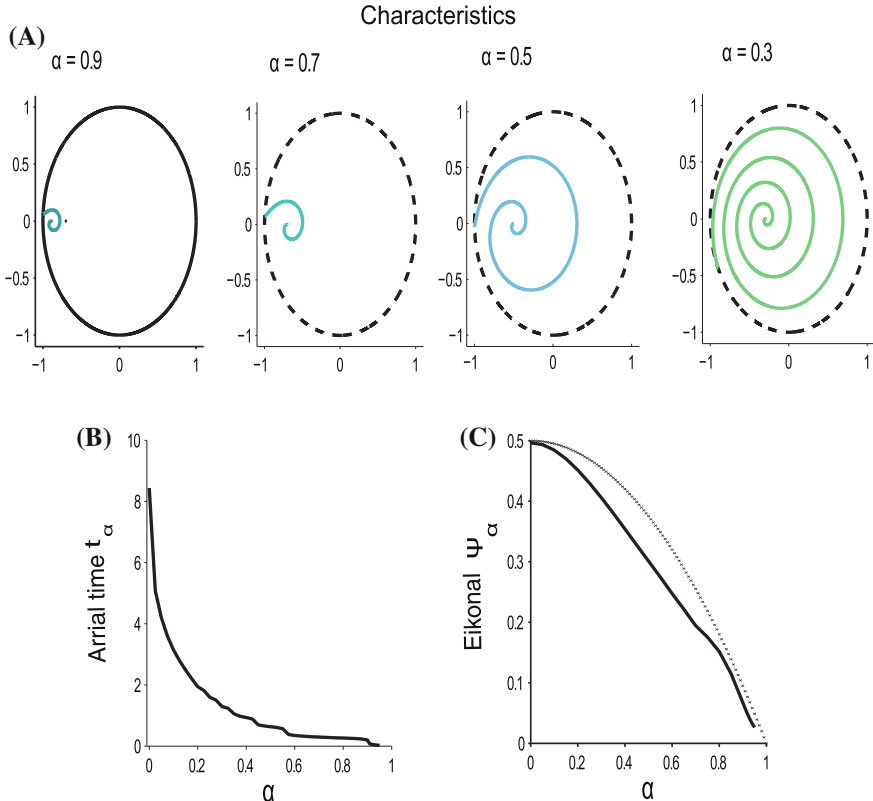


Fig. 4.9 The eikonal function $\hat{\psi}_\alpha$ on the boundary of the disk as a function of the focus position α . **A** : characteristic trajectories $x(t)$ for different values of α (0.3, 0.5, 0.7, 0.9). The associated winding numbers are 1, 2, 4, and 7. **B** : The arrival time t_α of the characteristic to the circle as a function of the parameter α . Note the small jump each time the winding number is increased by one. **C** : The eikonal function on the unit circle $\hat{\psi}_\alpha$ is a function of α , obtained by computing $\psi_\alpha(t_\alpha)$ (see (4.114) below, solid line) and the approximation is $\frac{1}{2}(1 - \alpha^2)$ (dashed line)

peak of the exit point density as the amplitude of the noise goes to zero (see Fig. 4.7B). Numerical simulations indicate that the peak is not exactly centered at $\theta = \pi$, but moves in a very small neighborhood of π as $\varepsilon \rightarrow 0$, confirming that there is no cycling here (see Appendix 4.16.2 and Annotations 4.17).

4.13 Normal Flux on $\partial\Omega$: the Exit Time Density

The exit time density $f_{\text{ETD}}(t)$ is the total normal flux on $\partial\Omega$ and is the time-derivative of the survival probability (9.4). It is given by (1.29) as

$$\begin{aligned} f_{\text{ETD}}(t) &= \Pr\{\tau = t\} = -\frac{d}{dt}\Pr_{\text{survival}}(t) \\ &= \int_{\Omega} \oint_{\partial\Omega} \mathbf{J}(\mathbf{y}, t | \mathbf{x}) \cdot \mathbf{n}(\mathbf{y}) p_0(\mathbf{x}) dS_y d\mathbf{x}, \end{aligned} \quad (4.115)$$

where $p_0(\mathbf{x})$ is the initial condition for the Fokker–Planck equation, which represents the density of initial points of the random trajectories. The exit time density $f_{\text{ETD}}(t)$ can be computed from the expansion (4.6). The forward and backward operators L_y and L_x^* have the same eigenvalues λ_n , and the eigenfunctions $\phi_n(\mathbf{y})$ of L_y and $\psi_n(\mathbf{x})$ of L_x^* form bi-orthonormal bases. A uniform initial distribution has the density $p_0(\mathbf{x}) = \mathbf{1}_{\Omega}|\Omega|^{-1}$, which gives

$$f_{\text{ETD}}(t) = C_0 e^{-\lambda_0 t} + \sum_n \Re(C_n e^{-\lambda_n t}).$$

The first eigenvalue λ_0 is real and positive. If $\lambda_0 \ll \Re(\lambda_{m,n})$ for all other eigenvalues, then it is the leading order approximation to the reciprocal of the mean first passage time. Indeed, the mean first passage time is the time integral of the survival probability and in view of (9.4) and (4.6), it is dominated by the reciprocal of the principal eigenvalue. If, however, there is no such spectral gap, higher-order eigenvalues contribute to the mean first passage time. In the former case, the expansion (4.10) is valid. In the latter case the other eigenvalues are not real-valued, as shown in Sect. 4.5. The general expression for the second (first non-real) eigenvalue is

$$\lambda_2 = \lambda_{1,0}(\varepsilon) = \omega_1 + i\omega_2 + O(\varepsilon), \quad (4.116)$$

where

$$\omega_2 = \frac{2\pi}{\int_0^S \frac{ds}{B_\alpha(s)}}, \quad \omega_1 = \frac{\omega_2}{\pi} \int_0^S \frac{\sigma(s)\xi_\alpha^2(s)}{B_\alpha(s)} ds. \quad (4.117)$$

These expressions are valid for any position of the attractor inside the domain Ω and which also apply when the attractor is in the boundary layer of the limit cycle, as shown in the next section by applying a conformal mapping to the second-order operator.

4.14 Computation of the Second Eigenvalue

The second eigenvalue is expressed in terms of ω_1 and ω_2 , which are computed next. First we use the conformal mapping $\mathbf{w} = \Psi_\alpha(z) = \Phi_\alpha^{-1}(z)$ to transform the eigenvalue problem

$$L_x^* \phi(\mathbf{x}) = \varepsilon \sum_{i,j=1}^2 \sigma^{i,j}(\mathbf{x}) \frac{\partial^2 \phi(\mathbf{x})}{\partial x^i \partial x^j} + \sum_{i=1}^2 b_\alpha^i(\mathbf{x}) \frac{\partial \phi(\mathbf{x})}{\partial x^i} = -\lambda \phi(\mathbf{x}) \quad (4.118)$$

for $\sigma^{i,j} = \delta^{i,j}$ with $\tilde{\phi}(\mathbf{w}) = \phi(z)$. We have

$$\Psi'_\alpha(z) = \frac{1 - \alpha^2}{(1 + \alpha z)^2} = \frac{(1 - \alpha \mathbf{w})^2}{1 - \alpha^2} \quad (4.119)$$

and

$$|\Psi'_\alpha(z)|^2 = \frac{1 - \alpha^2}{(1 + \alpha z)^2} = \frac{|1 - \alpha \mathbf{w}|^4}{(1 - \alpha^2)^2}. \quad (4.120)$$

The Laplace operator transforms into

$$\Delta \phi(z) = |\Psi'_\alpha(\Psi_\alpha^{-1}(\mathbf{w}))|^2 \Delta \tilde{\phi}(\mathbf{w}) \quad (4.121)$$

and the transport term – into

$$\sum_{i=1}^2 b_\alpha^i(z) \frac{\partial \phi(z)}{\partial x^i} = \sum_{i=1}^2 [\Phi'_\alpha(\Phi_\alpha^{-1}(\mathbf{w})) \mathbf{b}_0(\Phi_\alpha^{-1}(\mathbf{w}))]^i(z) \frac{\partial \phi(z)}{\partial x^i} \quad (4.122)$$

$$= \sum_{i=1}^2 [\mathbf{b}_0(\mathbf{w})]^i(z) \frac{\partial \tilde{\phi}(\mathbf{w})}{\partial \tilde{x}^i}, \quad (4.123)$$

where $\mathbf{w} = \tilde{x} + i \tilde{y} = R e^{i\tilde{\theta}}$. Thus,

$$\tilde{L}_x^*(\tilde{\phi}(\mathbf{w})) = \varepsilon \frac{|1 - \alpha \mathbf{w}|^4}{(1 - \alpha^2)^2} \Delta \tilde{\phi}(\mathbf{w}) + \sum_{i=1}^2 b_0^i(\mathbf{w}) \frac{\partial \tilde{\phi}(\mathbf{w})}{\partial x^i} = -\lambda \tilde{\phi}(\mathbf{w}) \quad (4.124)$$

$$\tilde{\phi}(\mathbf{w}) = 0 \text{ for } \mathbf{w} \in \partial\Omega, \quad (4.125)$$

where $\partial\Omega$ is the unit circle. This situation corresponds to the exit from a limit cycle, where the focus is at the center of the disk. The components of the field \mathbf{b}_0 near the limit cycle are given in (4.83) by

$$B_\alpha(\theta) = \omega, \quad a_0^0(\theta) = 2. \quad (4.126)$$

These expressions give the second eigenvalue as (4.116) with

$$\omega_2 = \frac{2\pi}{\int_0^{2\pi} \frac{ds}{B_\alpha(s)}} = \omega. \quad (4.127)$$

To compute the real part ω_1 , we find the 2π -periodic solution ξ_α of the Bernoulli equation (3.61), which takes the form

$$-\sigma_\alpha(\theta)\xi_\alpha^3(\theta) + 2\lambda\xi_\alpha(\theta) + \lambda\omega\xi'_\alpha(\theta) = 0, \quad (4.128)$$

with

$$\sigma_\alpha(s) = \varepsilon \frac{|1 - \alpha e^{is}|^4}{(1 - \alpha^2)^2} \quad (4.129)$$

and use it in the expression

$$\omega_1(\alpha) = \frac{\omega_2}{\pi} \int_0^{2\pi} \frac{\sigma_\alpha(s)\xi_\alpha^2(s)}{B(s)} ds = 4, \quad (4.130)$$

which is independent of α and ω (see Appendix 4.16.4).

4.15 Brownian Dynamics Simulations

To assess the accuracy of the theory developed above, the statistics of exits of trajectories of Brownian simulations of (4.80) are compared with the analytical expressions derived above. The density of exit points is found to be concentrated around a small arc of the boundary near the attractor x_0 (Fig. 4.7) and the density of exit times exhibits oscillation peaks in a specific range of values of α (Fig. 4.6). Note that no cycling of the exit point density as $\varepsilon \rightarrow 0$ is observed in (4.80) (see [Day (1994)] and [Dao Duc et al. (2016)]).

4.15.1 A Two-Term Approximation of the Exit-Time Density

The distribution of exit time can be well approximated by the first two exponentials. Indeed, starting with the expansion (4.115) and approximating the density of exit times obtained by Brownian simulations with the sum of the first two terms,

$$f_{\text{ETD}}(t) = C_0 e^{-\lambda_0 t} + C_1 e^{-\lambda_1 t} \cos(\omega_2 t + \phi), \quad (4.131)$$

where λ_0, λ_1 are the first and second eigenvalues, respectively, and C_0, C_1, ϕ are three constants. The peak oscillation is well approximated (Fig. 4.10) and the frequencies obtained by numerical simulations and analytically are in good agreement. Using the parameter $\omega_2 = \omega = 20$ (see (4.116)), it is apparent that it corresponds to the numerical parameter $k_5 = 20.944$. Approximating the first eigenvalue by the reciprocal of the mean first passage time and using formula (4.109) gives

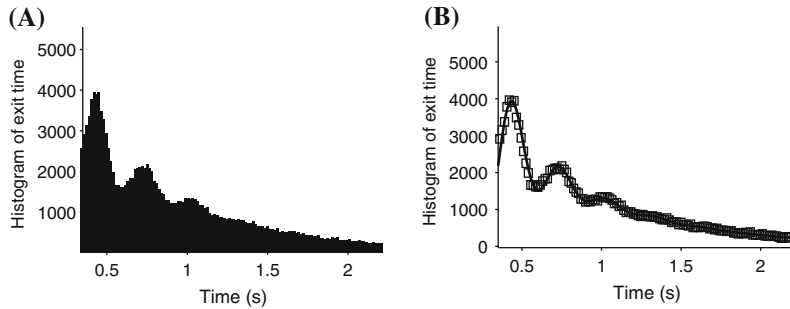


Fig. 4.10 Histogram of exit times (A) and its approximation (B). The histogram in Fig. 4.6 is fit with the function $y(t) = k_1 \exp(-k_2 t) + k_3 \exp(-k_4 t) \cos(k_5(t - k_6))$. The fit parameters are $k_1 = 5032$, $k_2 = 1.402$, $k_3 = 7407$, $k_4 = 4.042$, $k_5 = 20.944$, $k_6 = 0.45$

$$\lambda_0 \sim \tau_\alpha^{-1} = 1.57, \quad (4.132)$$

while the approximation (4.110) gives $\lambda_0 \sim \tau_\alpha^{-1} = 1.66$. To find the best fit approximation (4.131) to the exit time histogram shown in Fig. 4.6, we write

$$f_{\text{ETD}}(t) \approx k_1 \exp(-k_2 t) + k_3 \exp(-k_4 t) \cos(k_5(t - k_6)) \quad (4.133)$$

and obtain

$$\begin{aligned} C_0 &\approx k_1 = 5032, \quad \lambda_0 \approx k_2 = 1.402, \quad C_1 \approx k_3 = 7407, \\ \omega_1 &\approx k_4 = 4.042, \quad \omega_2 \approx k_5 = 20.944, \quad -\phi \approx k_6 = 0.45 \end{aligned} \quad (4.134)$$

(see Fig. 4.10). A good agreement with the real part of the second eigenvalue, which is $\omega_1 = 4$ (see Appendix 4.16.4), is found from (4.133) as $\omega_1 \approx k_4 = 4.042$. Thus the numerical simulations support the WKB approximation also for α close to 1. The values for the different parameters obtained analytically and numerically are given in Table 4.1 below.

Table 4.1 Comparison between theoretical eigenvalues and values estimated from the exit time histogram of the simulations (Fig. 4.10)

	Theoretical values	Fit from histogram
λ_0	1.57 (Eq. (4.132))	1.402
$\Re(\lambda_2)$	20 (chosen)	20.944
$\Im(\lambda_2)$	4 (Eq. (4.130))	4.042

4.15.2 Exit Time Densities in Three Ranges of Noise Amplitude

When the attractor is inside the domain, outside the boundary layer, the escape theory of Chap. 3 applies and the first eigenvalue characterizes the escape process. However,

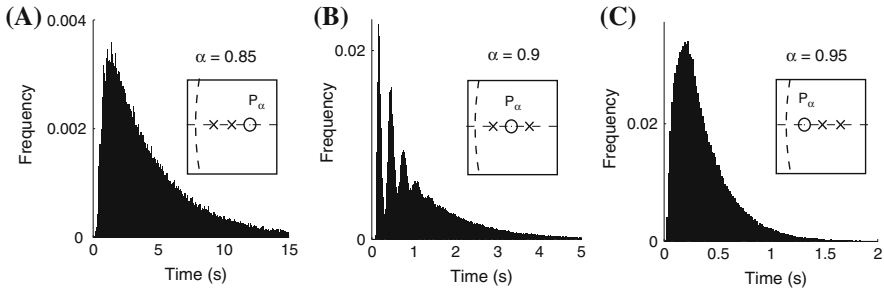


Fig. 4.11 The peak oscillations occur when the stable focus is at an optimal distance from the limit cycle. Histograms of exit time for different values of α . (A) $\alpha = 0.85$, peaks corresponding to the winding number of trajectories are not discernible. (B) $\alpha = 0.9$, peaks become discernible. (C) $\alpha = 0.95$, all exit times concentrate in the first peak. The number of simulated trajectories is 250,000, all starting at the point $(-0.8, 0)$

as the parameter $\eta = \varepsilon(1 - \alpha^2)^{-2}$ varies, three different regimes emerge:

1. For $\eta \ll 1$, the small noise dominates and the attractor is inside the domain outside the boundary layer. This regime is included in Chap. 3 for stochastic differential equations and the first eigenvalue is dominant. The density of exit times quickly becomes exponential, except for short events (Fig. 4.11A).
2. The second regime is obtained for $\eta \approx 1$. There are oscillatory peaks, as described above (see also Fig. 4.11B).
3. The case $\eta \gg 1$ corresponds to a large noise regime, characterized by short escape times. Most trajectories initially drift toward the attractor, which is close to the boundary, and then are pushed outside the domain Ω by the noise (Fig. 4.11C).

4.16 Appendices

4.16.1 *The Density of Exit Points*

Here an explicit expression of the exit points on $\partial\Omega$ is derived and shown to be concentrated in a small part of the boundary near the critical point, which is referred to as the effective escape region $\partial\Omega_e$. This result explains how the escape time is quantified: once a trajectory has missed its opportunity to escape, it has to go around the attractor, because it cannot escape anywhere else outside $\partial\Omega_e$. Thus the time to escape is exactly related to the time to loop, which is studied in the last appendix.

To approximate the probability density function of exit points $p_\alpha(\theta)$, we set

$$Z_\alpha^{-1}(\theta) = \xi_\alpha^2(\theta)\sigma(\theta)$$

to reduce the Bernoulli equation (3.62) to the first-order form

$$Z'_\alpha(\theta) - \frac{2b_\alpha^0(\theta)}{B_\alpha(\theta)} Z_\alpha(\theta) = -\frac{2}{B_\alpha(\theta)}. \quad (4.135)$$

A direct integration for $\sigma(s) = 1$ (isotropic case) gives

$$Z_\alpha(\theta) = \exp\{2(F_\alpha(\theta))\} \left[K_\alpha - \int_{-\pi}^{\theta} \frac{2}{B_\alpha(t)} \exp\{-2F_\alpha(t)\} dt \right], \quad (4.136)$$

where K_α is defined by the 2π -periodicity of the solution $Z_\alpha(-\pi) = Z_\alpha(\pi)$, and $F_\alpha(\theta)$ is given by

$$\begin{aligned} F_\alpha(\theta) &= \int_{-\pi}^{\theta} \frac{b_\alpha^0(s)}{B_\alpha(s)} ds = \int_{-\pi}^{\theta} \frac{2(1 - \alpha^2 - \omega\alpha \sin s)}{\omega(1 + 2\alpha \cos(s) + \alpha^2)} ds \\ &= \int_{-\pi}^{\theta} \frac{-2\alpha \sin s ds}{1 + 2\alpha \cos s + \alpha^2} + \int_{-\pi}^{\theta} \frac{2(1 - \alpha^2) ds}{\omega(1 + 2\alpha \cos s + \alpha^2)} \\ &= \ln \left[\frac{1 + 2\alpha \cos \theta + \alpha^2}{(1 - \alpha)^2} \right] + \int_{-\pi}^{\theta} \frac{2(1 - \alpha^2) ds}{\omega(1 + 2\alpha \cos s + \alpha^2)}. \end{aligned} \quad (4.137)$$

Changing the variable of integration in (4.137) to $u = \tan(s/2)$, we obtain that

$$F_\alpha(\theta) = \ln \left[\frac{1 + \beta^2 \tan^2(\theta/2)}{\beta^2(1 + \tan^2(\theta/2))} \right] + \frac{4}{\omega} \left[\arctan \left(\beta \tan \frac{\theta}{2} \right) + \frac{\pi}{2} \right] = \tilde{F}_\beta(\theta),$$

where $\beta = (1 - \alpha)/(1 + \alpha)$. Thus, we can write

$$\begin{aligned} Z_\alpha(\theta) &= \exp\{2(F_\alpha(\theta))\} \left[K_\alpha - \int_{-\pi}^{\theta} \frac{2}{B_\alpha(t)} \exp\{-2F_\alpha(t)\} dt \right] \\ &= \left[\frac{1 + \beta^2 \tan^2(\theta/2)}{1 + \tan^2(\theta/2)} \right]^2 \exp \left\{ \frac{8}{\omega} \arctan \left(\beta \tan \left(\frac{\theta}{2} \right) \right) \right\} (C_\beta - I_\beta(\theta)) \\ &= \tilde{Z}_\beta(\theta), \end{aligned} \quad (4.138)$$

where C_β is constant and $I_\beta(\theta)$ is given by

$$\begin{aligned} I_\beta(\theta) &= \frac{2e^{4\pi/\omega}}{\beta^4} \int_{-\pi}^{\theta} \frac{\exp\{-2F_\alpha(t)\}}{B_\alpha(t)} dt \\ &= \frac{2\beta}{\omega} \int_{-\pi}^{\theta} \frac{\exp\left\{\frac{-8}{\omega} \arctan\left(\beta \tan \frac{t}{2}\right)\right\} \left(1 + \tan^2 \frac{t}{2}\right)^3}{(1 + \beta^2 \tan^2 \frac{t}{2})^3} dt. \end{aligned} \quad (4.139)$$

The periodicity condition $\tilde{Z}_\beta(\pi) = \tilde{Z}_\beta(-\pi)$ gives

$$C_\beta = \frac{I_\beta(\pi)}{1 - e^{\frac{-8\pi}{\omega}}}. \quad (4.140)$$

To compute $I_\beta(\theta)$ from (4.139), we change the variable of integration to $\beta \tan(t/2) = \tan(u)$, so that

$$\begin{aligned} I_\beta(\theta) &= \frac{4}{\omega} \int_{-\frac{\pi}{2}}^{g_\beta(\theta)} \frac{e^{-8u/\omega} \left(1 + \frac{\tan^2 u}{\beta^2}\right)}{(1 + \tan^2 u)^2} du \\ &= \frac{4}{\omega \beta^4} \int_{-\frac{\pi}{2}}^{g_\beta(\theta)} e^{-8u/\omega} (\beta^2 \cos^2 u + \sin^2 u)^2 du, \end{aligned}$$

where $g_\beta(\theta) = \arctan(\beta \tan(\theta/2))$. We can use the approximation $\beta^2 \cos^2 u + \sin^2 u = \sin^2 u + O(\beta^2)$, because $0 < \beta = (1 - \alpha)/(1 + \alpha) \ll 1$, hence,

$$I_\beta(\theta) = \frac{4}{\omega \beta^4} \int_{-\frac{\pi}{2}}^{g_\beta(\theta)} e^{-8u/\omega} \sin^4 u du + O(\beta^2). \quad (4.141)$$

The identity

$$\int e^{ax} \cos bx dx = \frac{e^{ax}(a \cos bx + b \sin bx)}{a^2 + b^2}$$

gives

$$I_\beta(\theta) = \frac{1}{2\omega \beta^4} [e^{-8g_\beta(\theta)/\omega} J(2g_\beta(\theta)) - e^{-4\pi/\omega} J(-\pi) + O(\beta^2)], \quad (4.142)$$

where

$$J(x) = \frac{-3\omega}{8} + 2 \frac{-\frac{4}{\omega} \cos x + \sin x}{1 + (4/\omega)^2} + \frac{-\frac{4}{\omega} \cos 2x + 2 \sin 2x}{(4 + (4/\omega)^2)} > 0. \quad (4.143)$$

For $x = \pm\pi$, we obtain the approximation

$$J(-\pi) = J(\pi) = A, \quad (4.144)$$

where

$$\begin{aligned} A &= -\frac{3\omega}{8} - \frac{8/\omega}{1 + (4/\omega)^2} - \frac{4/\omega}{4 + (4/\omega)^2} \\ I_\beta(\pi) &= \frac{A(e^{-4\pi/\omega} - e^{4\pi/\omega})}{\omega}. \end{aligned}$$

Using (4.140), we get

$$\begin{aligned} C_\beta - I_\beta(\theta) &= \frac{1}{2\omega\beta^4} \left[\frac{A(e^{-4\pi/\omega} - e^{4\pi/\omega})}{\omega(1 - e^{-8\pi/\omega})} - J(2g_\beta(\theta)) + \frac{Ae^{4\pi/\omega}}{\omega} \right] \\ &= \frac{-e^{-8g_\beta(\theta)/\omega}}{2\omega\beta^4} J(2g_\beta(\theta)). \end{aligned} \quad (4.145)$$

Collecting the above results, we obtain an analytical expression for the density of exit time given $P_\alpha(\theta)$ in

$$K_0(0, s) = \frac{\xi(s)}{B(s)}, \quad P_\alpha(\theta) = \frac{\frac{\xi^2(\theta)\sigma(\theta)}{B(\theta)}}{\int_0^{2\pi} \frac{\xi^2(s)\sigma(s)}{B(s)} ds}. \quad (4.146)$$

Using (4.138) and (4.145), we obtain

$$\begin{aligned} p_\alpha(\theta) &= \mathcal{N}_\alpha \frac{\xi_\alpha^2(\theta)\sigma(\theta)}{B_\alpha(\theta)} = \mathcal{N}_\alpha \frac{1}{Z_\alpha(\theta)B_\alpha(\theta)} \\ &= 2\mathcal{N}_\alpha \left(\frac{1 + \beta^2 \tan^2(\theta/2)}{1 + \tan^2(\theta/2)} \right)^{-3} J(2g_\beta(\theta))^{-1} \beta^5, \end{aligned} \quad (4.147)$$

where

$$\mathcal{N}_\alpha^{-1} = \int_{-\pi}^{\pi} \frac{\xi_\alpha^2(\theta)\sigma(\theta)}{B_\alpha(\theta)} d\theta,$$

which gives the asymptotic behavior $p_\alpha(\theta) \sim \beta^{-6} \gg 1$ for $\theta \rightarrow \pm\pi$, while the density remains bounded outside a neighborhood of this point, because J is bounded independently of β . Neglecting the variation in J , we obtain that the leading order approximation of the exit density $p_\alpha(\theta)$ is

$$p_\alpha(\theta) = \frac{(1 + 2\alpha \cos \theta + \alpha^2)^{-3}}{\int_{-\pi}^{\pi} (1 + 2\alpha \cos s + \alpha^2)^{-3} ds}. \quad (4.148)$$

In Fig. 4.7, the analytical formula (4.148) is compared with Brownian simulations. It follows that the exit distribution is concentrated near the point $\theta = \pi$, which is the closest boundary point from the attractor x_0 . The width Λ of the distribution is the standard deviation of $p_\alpha(\theta)$, given by

$$\begin{aligned} \Lambda^2 &= \int_{\pi}^{\pi} (\theta - \pi)^2 p_\alpha(\theta) d\theta \\ &= \frac{(32 \ln(2) - 11)\pi (\alpha - 1)^5 + O((\alpha - 1)^6)}{15 \times 16 (\alpha - 1)^5 + O((\alpha - 1)^6)} \mathcal{N}_\alpha, \end{aligned} \quad (4.149)$$

where a computation gives

$$\mathcal{N}_\alpha = \frac{(1 - \alpha^2)^5}{2\pi (\alpha^4 + 4\alpha^2 + 1)}. \quad (4.150)$$

We conclude that the width is $\Lambda = C(1 - \alpha^2)^{5/2}$, where

$$C = \sqrt{\frac{32 \ln 2 - 11}{12 \times 15 \times 16}} \sim 0.06.$$

4.16.2 Expansion of the Field Near the Boundary and No Cycling

The expansion of the drift

$$\mathbf{b}_\alpha(z) = \frac{(z + \alpha)(1 + \alpha z)}{(1 - \alpha^2)} \left(-1 + \left| \frac{z + \alpha}{1 + \alpha z} \right|^2 + i\omega \right) \quad (4.151)$$

in the polar coordinates $(b_r, b_\theta) = (\Re e(\mathbf{b}_\alpha e^{-i\theta}, \Im m(\mathbf{b}_\alpha e^{-i\theta})))$, with $z = re^{i\theta}$, is given by

$$\begin{aligned}
b_\alpha(r, \theta) e^{-i\theta} &= \frac{(re^{i\theta} + \alpha)(1 + \alpha r e^{i\theta})re^{-i\theta}}{1 - \alpha^2} \left[-1 + \left| \frac{re^{i\theta} + \alpha}{1 + \alpha r e^{i\theta}} \right|^2 + i\omega \right] \\
&= \frac{r}{1 - \alpha^2} \left[r(1 + \alpha r \cos \theta + \alpha^2) + \alpha \cos \theta + i\alpha \sin \theta(r^2 - 1) \right] \times \\
&\quad \left[\frac{(\alpha^2 - 1)(r + 1)(r - 1)}{\alpha^2 r^2 + 2\alpha r \cos \theta + 1} + i\omega \right].
\end{aligned}$$

Hence

$$\begin{aligned}
b_r &= \frac{r(1 - r^2)}{1 - \alpha^2} \left[\frac{(1 - \alpha^2)(r(1 + \alpha^2) + \alpha \cos \theta(r^2 + 1))}{\alpha^2 r^2 + 2\alpha r \cos \theta + 1} + \omega \alpha \sin \theta \right] \\
b_\theta &= \frac{r}{1 - \alpha^2} \left[\frac{\alpha \sin \theta(r^2 - 1)^2(\alpha^2 - 1)}{\alpha^2 r^2 + 2\alpha r \cos \theta + 1} + \omega(r(1 + \alpha^2) + \alpha \cos \theta(r^2 + 1)) \right].
\end{aligned}$$

Near the limit cycle $r = 1$ the components are

$$\begin{aligned}
b_r &= 2(1 - r) \left(1 + \frac{\omega \alpha}{1 - \alpha^2} \sin \theta \right) + o(1 - r) \\
b_\theta &= \frac{\omega(1 + \alpha^2 + 2\alpha \cos \theta)}{1 - \alpha^2} - (1 - r) \frac{2\omega(1 + \alpha^2 + 2\alpha \cos \theta)}{1 - \alpha^2} + o(1 - r).
\end{aligned} \tag{4.152}$$

However, the normal form (1.3) of [Day Basel (1990)] can be written for the first equation of the system (4.152) as

$$dr_\varepsilon = B^{1/2}(1 - r_\varepsilon) (1 - \alpha^2 + \omega \alpha \sin \theta) dt + \sqrt{2\varepsilon} dw, \tag{4.153}$$

where $B = 4(1 - \alpha^2)^{-2}$. The period of cycling is given in Day Basel (1990, Sect. 3) as

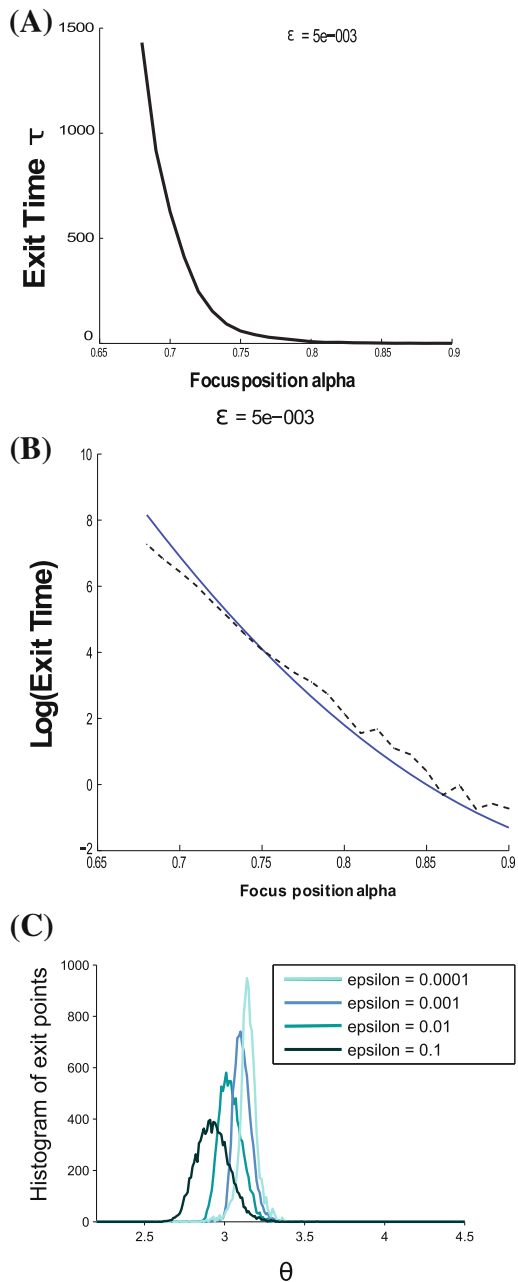
$$T_\varepsilon = B^{-1} \log \varepsilon^{-1/2} = \frac{(1 - \alpha^2)^2}{4} \log \varepsilon^{-1/2}. \tag{4.154}$$

In the distinguished limit $(1 - \alpha)^2 = O(\varepsilon)$, the period given in (4.154) becomes

$$T_\varepsilon = O(\varepsilon \log \varepsilon^{-1/2}) \rightarrow 0 \text{ as } \varepsilon \rightarrow 0,$$

which precludes cycling. It follows that the density function is that given in (4.146), which peaks around the boundary point $(r, \theta) = (1, \pi)$. Brownian simulations of (4.75) for the Hopf system with $\alpha = 0.95$ $0.001 \leq \varepsilon \leq 1$ show that the exit point density concentrates at $\theta = \pi$ (Figs. 4.7 and 4.12). The jitter around $\theta = \pi$ may reflect the phenomenon of skewing [Bobrovsky and Schuss (1982)].

Fig. 4.12 Mean first passage time for different focus positions and distribution of exit points for different noise amplitude ε . **A** and **B** mean first passage time decay with the distance to the boundary. The decays of $\tau(\eta)$ is shown in A. In B, we use for the comparison between the stochastic simulations (black) and the analytical expression Eq. 4.110 (blue). **C**, The distribution of exit points for different noise amplitude ε in the range 0.0001 to 0.1 are peaked close to $\theta = \pi$ (the convergence is logarithmic in ε)



4.16.3 The Jacobian of $\mathbf{b}(\zeta)$ at ζ_0

The Jacobian matrix of \mathbf{b}_α at the attractor $(-\alpha, 0)$ is denoted A_α . Its computation begins by first writing \mathbf{b}_α in Cartesian coordinates,

$$\mathbf{b}_\alpha(z) = \frac{(z + \alpha)(1 + \alpha z)}{(1 - \alpha^2)} \left(-1 + \left| \frac{z + \alpha}{1 + \alpha z} \right|^2 + i\omega \right). \quad (4.155)$$

Writing $R(x) = (x + \alpha)(1 + \alpha x)$, $S(x) = 1 + 2\alpha x + \alpha^2$ and $T(x, y) = (1 + \alpha x)^2 + \alpha^2 y^2$, we obtain

$$\begin{aligned} b_{\alpha 1}(x, y) &= \frac{(R(x) - y^2\alpha)(y^2 + x^2 - 1)}{T(x, y)} - \frac{yS(x)w}{(1 - \alpha^2)} \\ b_{\alpha 2}(x, y) &= \frac{yS(x)(x^2 + y^2 - 1)}{T(x, y)} + \frac{\omega(R(x) - \alpha y^2)}{1 - \alpha^2}. \end{aligned}$$

At the attractor $P_\alpha = -\alpha$, we have $R(-\alpha) = 0$ and $y = 0$. Thus the Jacobian matrix reduces to

$$\begin{aligned} A_\alpha &= \text{Jac}[\mathbf{b}_\alpha(-\alpha, 0)] \\ &= \begin{bmatrix} \frac{R'(-\alpha)(\alpha^2 - 1)}{T(-\alpha, 0)} & -\frac{\omega S(-\alpha)}{1 - \alpha^2} \\ \frac{\omega R'(-\alpha)}{1 - \alpha^2} & \frac{S(-\alpha)(\alpha^2 - 1)}{T(-\alpha, 0)} \end{bmatrix} \\ &= \begin{bmatrix} -1 & -\omega \\ \omega & -1 \end{bmatrix}. \end{aligned}$$

The Jacobian A_α is diagonalizable and its eigenvalues are

$$\lambda_1 = -1 + i\omega, \quad \lambda_2 = -1 - i\omega,$$

from which we get

$$\exp\{tA_\alpha\} = e^{-t} \begin{pmatrix} \cos \omega t & -\sin \omega t \\ \sin \omega t & \cos \omega t \end{pmatrix}. \quad (4.156)$$

4.16.4 The Real Part ω_1

To compute the real part ω_1 , we use the solution $\xi_\alpha(s)$ of the Bernoulli equation in

$$\omega_1 = \frac{\omega_2}{\pi} \int_0^{2\pi} \frac{\sigma_\alpha(s) \xi_\alpha^2(s)}{B(s)} ds, \quad (4.157)$$

where

$$\sigma_\alpha(s) = \frac{|1 - \alpha e^{is}|^4}{(1 - \alpha^2)^2} \quad (4.158)$$

and where ξ_α is the 2π -periodic solution of the Bernoulli equation (3.61), which is

$$-\sigma_\alpha(\theta) \xi_\alpha^3(\theta) + 2\lambda \xi_\alpha(\theta) + \lambda \omega \xi_\alpha'(\theta) = 0. \quad (4.159)$$

Setting

$$\sigma_\alpha(s) = \eta f_\alpha(s) \quad (4.160)$$

with $\eta = (1 - \alpha^2)^{-2}$, $f_\alpha(s) = |1 - \alpha e^{is}|^4$, and $Z(s) = \xi_\alpha^{-2}(s)$, we obtain the linear equation

$$Z'(s) - \frac{4}{\omega} Z(s) = -\frac{2}{\omega} \sigma_\alpha(s), \quad (4.161)$$

whose solution is

$$\xi_\alpha^{-2}(s) = Z_\alpha(s) = C_\alpha \exp \left\{ \frac{4}{\omega} s \right\} - \int_0^s \frac{2}{\omega} \sigma_\alpha(u) \exp \left\{ \frac{4}{\omega} (s-u) \right\} du. \quad (4.162)$$

The value of the constant C_α is found from the 2π -periodicity of the solution as

$$C_\alpha = \frac{2}{\omega} \frac{\exp \left\{ \frac{8}{\omega} \pi \right\}}{\exp \left\{ \frac{8}{\omega} \pi \right\} - 1} \int_0^{2\pi} \eta f_\alpha(u) \exp \left\{ -\frac{4}{\omega} u \right\} u.$$

It follows that

$$\begin{aligned} \omega_1 &= \frac{\omega_2}{2\pi} \int_0^{2\pi} \frac{\sigma_\alpha(s) \xi_\alpha^2(s)}{B(s)} ds \\ &= -\frac{\omega}{4\pi} \left[\log \left(\frac{\exp \left\{ \frac{8}{\omega} \pi \right\}}{\exp \left\{ \frac{8}{\omega} \pi \right\} - 1} \right) \int_0^{2\pi} f_\alpha(u) \exp \left\{ -\frac{4}{\omega} u \right\} du \right] \end{aligned}$$

$$\left. - \int_0^s f_\alpha(u) \exp \left\{ -\frac{4}{\omega} u \right\} du \right]^{2\pi}_0 = 4, \quad (4.163)$$

which is independent of α and ω .

4.17 Annotations

Definite information on eigenvalues of elliptic boundary value problems is available for non-self-adjoint operators that are small perturbations of self-adjoint operators [Faierman (1995)]. Otherwise, the available information mostly concerns the density of the eigenvalues in the complex plane [Sjöstrand (2009)]. The asymptotic expansion of eigenvalues for a non-self-adjoint operator in dimension 2 was shown in [Holcman and Schuss (2014b)].

The oscillatory decay of the survival probability is illustrated with a model of synaptic depression of a neuronal network in neurobiology (see, for example, [Tsodyks and Markram (1997)] and [Holcman and Tsodyks (2006)], [Tsodyks and Markram (1997)] and [Holcman and Tsodyks (2006)]).

The leading order asymptotic expansion of the principal eigenvalue λ_0 for small ε was found to be related to the mean first passage time by (4.3), whose asymptotic structure was found in [Matkowsky and Schuss (1982)] (see also [Dao Duc et al. (2016)]).

The Bernoulli equations (3.55), (3.61), and (4.161) were derived in [Mangel and Ludwig (1977)] [Matkowsky and Schuss (1982)] and [Dao Duc et al. (2016)] in the context of a boundary layer analysis of the Pontryagin–Andronov–Vitt boundary value problem (see [Schuss (2010b, Sects. 10.2.6, 10.2.8)]).

The Hopf system described in Sect. 4.1 [Dao Duc et al. (2014)] exhibits properties similar to the model (4.72) below, proposed in [Holcman and Tsodyks (2006)] to describe cerebral cortex activity. The cerebral cortex is continuously active in the absence of sensory stimuli. An example of this spontaneous activity is the phenomenon of voltage transitions between two distinct levels, called Up and Down states, observed simultaneously when recording from many neurons [Anderson et al. (2000)], [Cossart (2003)].

Neuronal ensembles exhibit recurrent activity, the origin of which remains unexplained: several computational studies have addressed successfully the role of noise in generating oscillations in recurrent networks [Nesse et al. (2008)]. Oscillatory decay is manifested experimentally in the appearance of Up and Down states in the spontaneous activity of the cerebral cortex and in the simulations of its mathematical models [Holcman and Tsodyks (2006)] and [Dao Duc et al. (2016)]. The oscillations are due to the competition between the driving noise and the underlying dynamical system [Dao Duc et al. (2015)].

The validity of the WKB assumption is discussed in Day Basel (1990, and references therein). More specifically, examples have been constructed in which the asymptotic WKB structure contains a boundary layer factor that is periodic along the boundary in $\log \varepsilon$ when the drift has certain structure near the boundary.

Neuronal ensembles can exhibit spontaneous activities containing recurrent patterns. These patterns are characterized electro-physiologically by a transient depolarization, called an Up-state, in which the membrane potential decreases (in absolute value). Particular attention has been given to the lifetime of the membrane voltage of neurons in these Up-states [Anderson et al. (2000)], [Hahn et al. (2007)]. This phenomenon is reproducible by a minimal mean-field model of a two-dimensional neuronal network with excitatory connections. The state variables in the model are the mean firing rate V , averaged over the population, and the synaptic depression μ [Tsodyks and Markram (1997)]. In a neuronal network, whose connections are mostly depressing synapses, the neural dynamics has been modeled in [Holcman and Tsodyks (2006)], [Tsodyks and Markram (1997)]. The state variables in the model (4.73), the mean firing rate V , averaged over the population, and the synaptic depression μ , were introduced in [Tsodyks and Markram (1997)].

The noiseless dynamics generated by (4.73) (with $\sigma = 0$) has been studied in the (V, μ) plane in [Holcman and Tsodyks (2006)]. When the network connectivity J exceeds a minimal value (see [Holcman and Tsodyks (2006)]) there are three critical points: two attractors, P_1 at $V = 0, \mu = 1$, a stable focus P_2 , and one saddle point P_S . The boundary of the basin of attraction Ω of P_2 is an unstable limit cycle and is defined as the Up-state [Holcman and Tsodyks (2006)] and [Dao Duc et al. (2015)].

The method of this chapter can also be applied to study subthreshold oscillations describing the resonant properties experimentally found in many types of neurons, such as stellate cells [Erchova et al. (2004)]. The model is a “resonate and fire” neuron, which consists of a second-order ordinary differential equation with additive white noise [Verechtchaguina et al. (2007)], [Verechtchaguina et al. (2006)]. Indeed, due to the stochastic opening and closing of ion channels, the membrane potential fluctuates around the holding potential. The model is reset once a given threshold is reached. Other possible models are the noisy FitzHugh–Nagumo or Morris–Lecar systems [Izhikevich (2005)]: these models exhibit subthreshold oscillations, appearing when the neuronal cell is depolarized below the action potential threshold. Driven by noise fluctuations, the simulated neural network [Verechtchaguina et al. (2007)] generates random spikes whose ISI shows resonant peaks in the underdamped regime. The generic mean-field model consists of two differential coupled equations [Verechtchaguina et al. (2007)]. The steady-state analysis in [Verechtchaguina et al. (2007)] reveals that there are generically two fixed points separated by a saddle point. One of the fixed points is a stable focus (with complex eigenvalues). This point is responsible for generating oscillations of the dynamics prior to exit through the saddle point. Spectral analysis of the simulated exits shows two peaks of the density of exit intervals and that the frequency of the second peak is double that of the first one. This distribution is approximated by the function $f(t) = A \exp(-at) + B \exp(-bt) \sin(wt + \phi)$ [Dao Duc et al. (2015)], where the parameters A, B, a, b, w, ϕ are fitted to the empirical distribution of in vivo electrophysiological time series to recover the network

mean synaptic connectivity. The analysis developed here clarifies the basis for the fit approximation used in [Verechtaguina et al. (2007)], [Verechtaguina et al. (2006)]. The normal form (4.77) of the Hopf system in the complex plane was proposed in [Kuznetsov (2004)].

The exit density on a limit cycle without critical points was shown to be spread over the entire boundary [Matkowsky and Schuss (1982)], [Matkowsky et al. (1983)], [Schuss (2010b)], depending on the speed of the drift on the boundary.

In Sect. 4.12.1, the case $\alpha \rightarrow 1$ first and then $\varepsilon \rightarrow 0$ reduces to the exit problem from a characteristic boundary with a critical point. An altogether different WKB expansion is developed for this case in [Matkowsky et al. (1983)] (see also the analysis in [Maier and Stein (1997)], [Day (1994)], [Day Basel (1990)] and [Bobrovsky and Schuss (1982)]).

The numerical solution of the characteristic equations in Sect. 4.12.2 shows that the characteristics do not intersect inside the domain, so the eikonal equation with the conditions (4.111) has a unique twice differentiable solution. It follows that there is no cycling of the exit density on the boundary [Maier and Stein (1997)] and the results of Chap. 3 apply (see [Day (1994)] and [Dao Duc et al. (2016)]). Cycling here is defined as complete rotation of the peak of the exit point density as the amplitude of the noise goes to zero (see Fig. 4.7B [Dao Duc et al. (2015)]). Numerical simulations indicate that the peak is not exactly centered at $\theta = \pi$, but moves in a very small neighborhood of π as $\varepsilon \rightarrow 0$, confirming that there is no cycling here (see Appendix 4.16.2).

The normal form of the drift field near the limit cycle, (4.152), can be used to examine the possibility of cycling of the exit density, as described in [Day Basel (1990)]. Cycling consists in the rotation of the exit point distribution around the boundary as $\varepsilon \rightarrow 0$ with period $O(\log \varepsilon^{-1/2})$ Day (1994, p. 242) and [Dao Duc et al. (2016)].

Chapter 5

Short-Time Asymptotics of the Heat Kernel

The problem of recovering geometric properties of a domain from the trace of the heat kernel for an initial-boundary value problem arises in NMR microscopy [Callaghan (1991)], in oil explorations, in non-invasive microscopy of cell structure, as well as in other applications. It is similar to the problem of “hearing the shape of a drum”, for which a Poisson-type summation formula relates geometric properties of the domain to the eigenvalues of the Dirichlet or Neumann problems for the Laplace equation. It is well known that the area, circumference, and the number of holes in a planar domain can be recovered from the short-time asymptotics of the solution of the initial-boundary value problem for the heat equation. It is also known that the length spectrum of closed billiard ball trajectories in the domain is contained in the spectral density of the Laplace operator with the given boundary conditions in the domain, from which the short-time hyper-asymptotics of the trace of the heat kernel can be obtained by the Laplace transform. However, the problem of recovering these lengths from measured values of the trace of the heat kernel (the “resurgence” problem) is unresolved. In this section, a simple algorithm is developed for extracting the lengths from the short-time hyper-asymptotic expansion of the trace. An alternative short-time expansion of the trace is given by constructing a ray approximation to Green’s function of the heat equation for a planar domain with Dirichlet or Neumann boundary conditions and by evaluating the trace by introducing the rays as global coordinates.

In these NMR measurements the trace of the Green’s function for the initial value problem for the heat equation with reflecting (Neumann) boundary conditions is measured directly. The problem is analogous to “hearing the shape of a drum”, where the solution of the wave equation in the domain is measured directly (it is “heard”). This problem consists in recovering geometrical properties of a domain from the eigenvalues of the Dirichlet or Neumann problems for the Laplace equation in a bounded domain.

Some history of the problem is cited below in Annotations 5.5.2. The mathematical statement of the problem is as follows. Green’s function for the heat equation in a smooth planar domain Ω , with homogeneous Dirichlet boundary conditions, satisfies

$$\frac{\partial G(\mathbf{y}, \mathbf{x}, t)}{\partial t} = D \Delta_{\mathbf{y}} G(\mathbf{y}, \mathbf{x}, t) \quad \text{for } \mathbf{y}, \mathbf{x} \in \Omega, t > 0 \quad (5.1)$$

$$G(\mathbf{y}, \mathbf{x}, 0) = \delta(\mathbf{y} - \mathbf{x}) \quad (5.2)$$

$$G(\mathbf{y}, \mathbf{x}, t) = 0 \text{ for } \mathbf{y} \in \partial\Omega, \mathbf{x} \in \Omega, t > 0. \quad (5.3)$$

Since D can be eliminated from (5.1) by scaling it into t , we assume henceforth that $D = 1$. The function $G(\mathbf{x}, \mathbf{x}, t) d\mathbf{x}$ is the probability of return to $\mathbf{x} d\mathbf{x}$ at time t of a free Brownian particle that starts at the point \mathbf{x} at time $t = 0$ and diffuses in Ω with diffusion coefficient 1, with absorption at the boundary $\partial\Omega$. If it is reflected at $\partial\Omega$, rather than absorbed, the Dirichlet boundary condition (5.3) is replaced with the Neumann condition

$$\frac{\partial G(\mathbf{y}, \mathbf{x}, t)}{\partial \mathbf{n}(\mathbf{y})} = 0 \text{ for } \mathbf{y} \in \partial\Omega, \mathbf{x} \in \Omega, t > 0, \quad (5.4)$$

where $\mathbf{n}(\mathbf{y})$ is the unit outer normal at the boundary point \mathbf{y} . The trace of the heat kernel is defined as

$$P(t) = \int_{\Omega} G(\mathbf{x}, \mathbf{x}, t) d\mathbf{x} \quad (5.5)$$

and can be represented by the Dirichlet series

$$P(t) = \sum_{n=1}^{\infty} e^{-\lambda_n t}, \quad (5.6)$$

where λ_n are the eigenvalues of Laplace equation with the Dirichlet or Neumann boundary conditions (5.3) or (5.4), respectively.

It has been shown in [Kac (1966)] that for a domain Ω with smooth boundary $\partial\Omega$, the leading terms in the expansion of $P(t)$ in powers of \sqrt{t} are

$$P_{\text{Kac}}(t) \sim \frac{|\Omega|}{4\pi t} - \frac{|\partial\Omega|}{8\sqrt{\pi t}} + \frac{1}{6}(1-r) + O(\sqrt{t}), \quad \text{for } t \rightarrow 0, \quad (5.7)$$

where $|\Omega|$ denotes the area of Ω , $|\partial\Omega|$ denotes the arc-length of $\partial\Omega$, and r is the number of holes in Ω . The full short time asymptotic power series expansion of $P(t)$ in the form

$$P(t) \sim \sum_{n=0}^{\infty} a_n t^{n/2-1} \quad (5.8)$$

can be deduced from the large s expansion of the Laplace transform

$$g(s) = \int_0^\infty \exp\{-s^2 t\} \left(P(t) - \frac{a_0}{t} \right) dt, \quad \left(a_0 = \frac{|\Omega|}{4\pi} \right) \quad (5.9)$$

in inverse powers of s . Such an expansion was given in [Stewartson and Waechter (1971)] in the form

$$\hat{g}(s) \sim \sum_{n=1}^{\infty} \frac{c_n}{s^n}, \quad (5.10)$$

where

$$c_n = a_n \Gamma\left(\frac{n}{2}\right). \quad (5.11)$$

The constants c_n are computable functionals of the curvature of the boundary. The full expansion is denoted

$$P_{\text{SW}}(t) \sim \frac{|\Omega|}{4\pi t} - \frac{|\partial\Omega|}{8\sqrt{\pi t}} + \frac{1}{6}(1-r) + \sum_{n=3}^{\infty} a_n t^{n/2-1} \text{ for } t \rightarrow 0. \quad (5.12)$$

If the boundary is not smooth, but has cusps and corners, the expansion contains a term of the order $t^{-\nu}$, where ν is a number between 0 and 1/2 (see Annotations 5.5.2 for further history of the recovery problem).

Here, we adopt a direct approach to the hyper-asymptotic short-time expansion of the trace, rather than expanding its Laplace transform. The results can be generalized to higher dimensions in a straightforward manner. We construct the expansion in the form

$$P(t) \sim P_{\text{SW}}(t) + \frac{1}{\sqrt{\pi t}} \sum_{n=1}^{\infty} P_n(\sqrt{t}) e^{-\delta_n^2/t}, \quad \text{for } t \rightarrow 0, \quad (5.13)$$

where δ_n , ordered by magnitude, are determined directly from the expansion to be related to l_n by (5.82), and $P_n(x)$ are power series in x . Transcendentally small terms may be, in fact, quite large and make a finite contribution to the expansion (5.13) [Meyer (1980)]. Indeed, given $P(t)$, e.g., from NMR measurements, we describe a simple numerical algorithm for recovering δ_n from $P(t)$.

The short-time expansion is based on the *ray asymptotic approximation* to the heat kernel and is used to evaluate its trace (see Annotations 5.5.2). Specifically, the rays are used as global coordinates to expand the double integral (5.5) asymptotically beyond all orders for short times. We show that the transcendentally small terms are due to rays reflected in the boundary, much like in the geometric theory of diffraction (see Annotations 5.5.2). In particular, the smallest exponent δ_1 is the width of the narrowest bottleneck in the domain. For the particular case of a circular domain, we

find that all diffractive closed trajectories contribute to the transcendentally small terms.

5.1 The One-Dimensional Case

The solution of the heat equation in an interval can be constructed by the method of images. Specifically, the Green function of the problem satisfies

$$\frac{\partial G(y, x, t)}{\partial t} = \frac{\partial^2 G(y, x, t)}{\partial y^2} \text{ for } 0 < x, y < a, t > 0 \quad (5.14)$$

$$G(y, x, 0) = \delta(y - x) \text{ for } 0 < x, y < a \quad (5.15)$$

$$\left(\frac{\partial}{\partial y}\right)^k G(0, x, t) = \left(\frac{\partial}{\partial y}\right)^k G(a, x, t) = 0 \text{ for } 0 < x < a, t > 0, k = 0, 1. \quad (5.16)$$

The method of images gives the representation

$$G(y, x, t) = \frac{1}{2\sqrt{\pi t}} \sum_{n=-\infty}^{\infty} \left[\exp\left\{-\frac{(y-x+2na)^2}{4t}\right\} - (-1)^k \exp\left\{-\frac{(y+x+2na)^2}{4t}\right\} \right], \quad (5.17)$$

for $k = 0, 1$. Note that if the infinite series is truncated after a finite number of terms, the boundary conditions are satisfied only in an asymptotic sense as $t \rightarrow 0$. That is, the boundary values of the truncated solution decay exponentially fast in t^{-1} as $t \rightarrow 0$ and the exponential rate increases together with the number of retained terms.

The trace is given by

$$\begin{aligned} & \int_0^a G(x, x, t) dx \\ &= \frac{1}{2\sqrt{\pi t}} \int_0^a \sum_{n=-\infty}^{\infty} \left[\exp\left\{-\frac{(na)^2}{t}\right\} + (-1)^k \exp\left\{-\frac{(x+na)^2}{t}\right\} \right] dx \\ &= \frac{1}{2\sqrt{\pi t}} \sum_{n=-\infty}^{\infty} \left[a \exp\left\{-\frac{(na)^2}{t}\right\} + (-1)^k \int_0^a \exp\left\{-\frac{(x+na)^2}{t}\right\} dx \right] \\ &= \frac{a}{2\sqrt{\pi t}} \sum_{n=-\infty}^{\infty} \exp\left\{-\frac{(na)^2}{t}\right\} + \frac{(-1)^k}{2} \\ &= \frac{a}{2\sqrt{\pi t}} + \frac{(-1)^k}{2} + \frac{a}{2\sqrt{\pi t}} \sum_{n \neq 0} \exp\left\{-\frac{(na)^2}{t}\right\}, \quad (k = 0, 1). \end{aligned} \quad (5.18)$$

On the other hand,

$$\int_0^a G(x, x, t) dx = \sum_{n=1}^{\infty} e^{-\lambda_n t}, \quad (5.19)$$

where $\{\lambda_n\}$ are the eigenvalues of the homogeneous Dirichlet or Neumann problem for the operator d^2/dx^2 in the interval $[0, a]$. Thus

$$\sum_{n=1}^{\infty} e^{-\lambda_n t} = \frac{a}{2\sqrt{\pi t}} + \frac{(-1)^k}{2} + \frac{a}{2\sqrt{\pi t}} \sum_{n \neq 0} \exp \left\{ -\frac{(na)^2}{t} \right\}, \quad (k = 0, 1). \quad (5.20)$$

If instead of a single interval of length a , we consider the heat equation in a set Ω consisting of K disjoint intervals of lengths l_j , ($j = 1, \dots, K$), respectively, the resulting expansion is

$$\sum_{n=1}^{\infty} e^{-\lambda_n t} = \frac{\sum_{j=1}^K l_j}{2\sqrt{\pi t}} + (-1)^k \frac{2K}{4} + \sum_{j=1}^K \frac{l_j}{2\sqrt{\pi t}} \sum_{n \neq 0} \exp \left\{ -\frac{(nl_j)^2}{t} \right\},$$

for $k = 0, 1.$ (5.21)

The numerator in the first term on the right-hand side of (5.21) can be interpreted as the “area” of Ω , so we denote it by $\sum_{j=1}^K l_j = |\Omega|$. The number $2K$ is the number of boundary points of Ω , which can be interpreted as the “circumference” of the boundary, so we denote it by $|\partial\Omega| = 2K$. The exponents in the sum on the right hand side of Eq. (5.21) can be interpreted as the “widths” of the components of Ω . Clearly, for small t , the term containing the smallest width, $r = \min_{1 \leq j \leq K} l_j$, will dominate the sum. Thus we can rewrite (5.21) as

$$\sum_{n=1}^{\infty} e^{-\lambda_n t} = \frac{|\Omega|}{2\sqrt{\pi t}} - \frac{|\partial\Omega|}{4} + \frac{mr}{\sqrt{\pi t}} \exp \left\{ -\frac{r^2}{t} \right\} + \sum_{l_j > r} \frac{l_j}{2\sqrt{\pi t}} \sum_{n \neq 0} \exp \left\{ -\frac{(nl_j)^2}{t} \right\},$$
(5.22)

where m is the number of the shortest intervals in Ω .

Equation (5.22) can be viewed as the short time asymptotic expansion of the sum on the left-hand side of the equation. The algebraic part of the expansion consists of the first two terms and all other terms are transcendentally small. The geometric information in the various terms of the expansion consists of the “area” of Ω and the “circumference” $|\partial\Omega|$ in the algebraic part of the expansion. The transcendental part of the expansion is dominated by the term containing the smallest “width” of the domain, r .

The geometric information about Ω contained in the algebraic part is the information given in the “Can one hear the shape of a drum” expansions [Kac (1966)],

[Stewartson and Waechter (1971)]. The geometric information contained in the transcendently small terms in (5.22) can be understood as follows. The terms nl_j in the exponents are the lengths of closed trajectories of billiard balls in Ω , or the lengths of closed rays reflected at the boundaries, as in [Balian and Bloch (1972)].

The representation (5.17) can be constructed as a short time approximation to the solution of the heat equation (5.14)–(5.16) by the ray method. In this method the solution is constructed in the form

$$G(y, x, t) = e^{-S^2(y, x)/4t} \sum_{n=0}^{\infty} Z_n(y, x) t^{n-1/2}. \quad (5.23)$$

Substituting the expansion (5.23) into the heat equation (5.14) and ordering terms by orders of magnitude for small t , we obtain at the leading order the *ray equation*, also called the eikonal equation (see (3.14)),

$$\left| \frac{\partial S(y, x)}{\partial y} \right|^2 = 1, \quad (5.24)$$

and at the next orders the transport equations (see Sect. 3.2.2)

$$\begin{aligned} 2 \frac{\partial S(y, x)}{\partial y} \frac{\partial Z_n(y, x)}{\partial y} + Z_n(y, x) \left(\frac{\partial^2 S(y, x)}{\partial y^2} + \frac{2n}{S(y, x)} \right) \\ = \frac{2}{S(y, x)} \frac{\partial^2 Z_{n-1}(y, x)}{\partial y^2}, \quad n = 0, 1, \dots. \end{aligned} \quad (5.25)$$

Setting

$$p(y, x) = \frac{\partial S(y, x)}{\partial y},$$

we write the equations (3.22) of the characteristics, or *rays* of the eikonal equation (5.24), as (see Sect. 3.2.1)

$$\frac{\partial y(\tau, x)}{\partial t} = 2p, \quad \frac{dp(\tau)}{dt} = 0, \quad \frac{dS(\tau)}{d\tau} = 2p^2(\tau) \quad (5.26)$$

with the initial conditions

$$y(0, x) = x, \quad p(0) = \pm 1, \quad S(0) = 0.$$

The condition $S(0) = 0$ is implied by the initial condition $G(x, y, 0) = \delta(x - y)$. The solutions are given by

$$y(\tau, x) = x + 2p\tau, \quad p(\tau) = \pm 1, \quad S(\tau) = 2\tau = \pm(y - x).$$

Thus $S(y, x)$ is the length of the ray from y to x . We denote this solution by $S_0(y, x)$. It is easy to see that the solution of the transport equations corresponding to $S_0(y, x)$ is given by $Z_0(y, x) = \text{const}$, and $Z_n(y, x) = 0$ for all $n \geq 1$. The initial condition (5.15) implies that

$$Z_0(y, x) = \frac{1}{2\sqrt{\pi}}.$$

Combined in (5.23), this solution gives Green's function for the heat equation on the entire line,

$$G_0(y, x, t) = \frac{1}{2\sqrt{\pi t}} \exp \left\{ -\frac{(y-x)^2}{4t} \right\},$$

which is the positive term corresponding to $n = 0$ in the expansion (5.17).

The ray from x to y is not the only one emanating from x . There are rays emanating from x that end at y after reflection in the boundary. Thus the ray from x that reaches y after it is reflected at the boundary 0 has length $y + x$. Therefore there is another solution of the eikonal equation, $S_1(y, x)$, which is the length of the reflected ray, given by $S_1(y, x) = y + x$. The ray from x that reaches y after it is reflected at the boundary a has length $2a - x - y$. The ray from x to 0, then to a , and then to y has length $2a + x - y$. Thus the lengths of all rays that reach y from x after any number of reflections in the boundary generate solutions of the eikonal equation, which are the lengths of the rays which in turn generate solutions of the heat equation. We denote them by $S_k(y, x)$ with some ordering. The corresponding solutions of the transport equation are

$$Z_{0,k}(y, x) = \frac{C_k}{2\sqrt{\pi}},$$

where C_k are constant. They are chosen so that the sum of all the ray solutions,

$$G_k(y, x, t) = \frac{Z_{0,k}(y, x)}{\sqrt{t}} e^{-S_k^2(y, x)/4t},$$

satisfies the boundary conditions (5.16). Note that for all $k \neq 0$

$$G_k(y, x, t) \rightarrow 0 \text{ as } t \rightarrow 0.$$

This construction recovers the solution (5.17).

5.2 The Ray Method for Short Time Asymptotics of Green's Function

The ray method is essentially the WKB method studied above. The small parameter ε is now the short time t . Thus the method consists in the construction of Green's function $G(\mathbf{y}, \mathbf{x}, t)$ (5.1)–(5.3) in the asymptotic form

$$G(\mathbf{y}, \mathbf{x}, t) \sim e^{-S^2(\mathbf{y}, \mathbf{x})/4t} \sum_{n=0}^{\infty} Z_n(\mathbf{y}, \mathbf{x}) t^{n-1}. \quad (5.27)$$

The function $S(\mathbf{y}, \mathbf{x})$ is the solution of the eikonal equation (see (3.14)), which takes the form

$$|\nabla_{\mathbf{y}} S(\mathbf{y}, \mathbf{x})|^2 = 1 \quad (5.28)$$

and the functions $Z_n(\mathbf{y}, \mathbf{x})$ solve the transport equations (see Sect. 3.2.2)

$$\begin{aligned} 2\nabla_{\mathbf{y}} S(\mathbf{y}, \mathbf{x}) \cdot \nabla_{\mathbf{y}} Z_n(\mathbf{y}, \mathbf{x}) + Z_n(\mathbf{y}, \mathbf{x}) \left[\Delta_{\mathbf{y}} S(\mathbf{y}, \mathbf{x}) + \frac{2n-1}{S(\mathbf{y}, \mathbf{x})} \right] = \\ \frac{2}{S(\mathbf{y}, \mathbf{x})} \Delta_{\mathbf{y}} Z_{n-1}(\mathbf{y}, \mathbf{x}), \text{ for } n = 0, 1, 2, \dots. \end{aligned} \quad (5.29)$$

The eikonal equation (5.28) is solved by the method of characteristics (see Sect. 3.2.1). Recall that the rays $\mathbf{y}(\tau, \mathbf{x})$ emanating from \mathbf{x} are the solutions of the system (3.22), which takes the form

$$\frac{d\mathbf{y}(\tau, \mathbf{x})}{d\tau} = 2\nabla_{\mathbf{y}} S(\mathbf{y}(\tau, \mathbf{x}), \mathbf{x}), \quad \frac{d\nabla_{\mathbf{y}} S(\mathbf{y}(\tau, \mathbf{x}), \mathbf{x})}{d\tau} = 0, \quad \frac{dS(\mathbf{y}(\tau, \mathbf{x}), \mathbf{x})}{d\tau} = 2. \quad (5.30)$$

The initial condition (5.2) implies that

$$\mathbf{y}(0, \mathbf{x}) = \mathbf{x}, \quad \nabla_{\mathbf{y}} S(\mathbf{y}(0, \mathbf{x}), \mathbf{x}) = \mathbf{n}, \quad S(\mathbf{y}(0, \mathbf{x}), \mathbf{x}) = 0, \quad (5.31)$$

where \mathbf{n} is a constant vector of unit length. The solution is given by

$$\mathbf{y}(\tau, \mathbf{x}) = \mathbf{x} + 2\mathbf{n}\tau, \quad S(\mathbf{y}, \mathbf{x}) = |\mathbf{y} - \mathbf{x}| = 2\tau, \quad \nabla_{\mathbf{y}} S(\mathbf{y}, \mathbf{x}) = \mathbf{n}. \quad (5.32)$$

The pair (τ, \mathbf{n}) uniquely determines the point $\mathbf{y} = \mathbf{y}(\tau, \mathbf{x})$ and the value of $S(\mathbf{y}, \mathbf{x})$ at the point. The parameter τ is half the distance from \mathbf{y} to \mathbf{x} or half the length of the ray from \mathbf{x} to \mathbf{y} . The vector \mathbf{n} is the unit vector in the direction from \mathbf{x} to \mathbf{y} .

The function $Z_0(\mathbf{y}, \mathbf{x})$ is easily seen to be a constant, $1/4\pi$, and $Z_n(\mathbf{y}, \mathbf{x}) = 0$ for all $n > 0$. This construction recovers the solution of the heat equation in the entire plane and disregards the boundary $\partial\Omega$, because in the plane every point can be seen

from every other point by a straight ray. Note that to calculate the function $P(t)$ in (5.5) only the values of $S(\mathbf{x}, \mathbf{x})$ and $Z_0(\mathbf{x}, \mathbf{x})$ are needed. Thus $S(\mathbf{x}, \mathbf{x}) = 0$ and the first approximation to $G(\mathbf{x}, \mathbf{x}, t)$ is

$$G(\mathbf{x}, \mathbf{x}, t) = \frac{1}{4\pi t},$$

hence the first approximation to $P(t)$ is

$$P_0(t) = \frac{|\Omega|}{4\pi t}.$$

There is another solution of the eikonal equation (5.28) constructed along rays that emanate from \mathbf{x} , but reach \mathbf{y} after they are reflected in $\partial\Omega$. The law of reflection is determined from the boundary conditions. Dirichlet and Neumann boundary conditions imply that the angle of incidence equals that of reflection. Similarly, there are solutions of the eikonal equation that are the lengths of rays that emanate from \mathbf{x} and reach \mathbf{y} after any number of reflections in $\partial\Omega$. We denote these solutions by $S_k(\mathbf{y}, \mathbf{x})$ with some ordering. Thus the full ray expansion of Green's function has the form

$$G(\mathbf{y}, \mathbf{x}, t) \sim \sum_{k=1}^{\infty} e^{-S_k^2(\mathbf{y}, \mathbf{x})/4t} Z_k(\mathbf{y}, \mathbf{x}, t), \quad (5.33)$$

where

$$Z_k(\mathbf{y}, \mathbf{x}, t) = \sum_{n=0}^{\infty} Z_{n,k}(\mathbf{y}, \mathbf{x}) t^{n-1}.$$

As above, each one of the series

$$e^{-S_k^2(\mathbf{y}, \mathbf{x})/4t} Z_k(\mathbf{y}, \mathbf{x}, t)$$

is called a *ray solution* of the diffusion equation. The boundary values of $Z_k(\mathbf{y}, \mathbf{x}, t)$ are chosen so that $G(\mathbf{y}, \mathbf{x}, t)$ in (5.33) satisfies the imposed boundary condition. In particular, the values of $S_k(\mathbf{x}, \mathbf{x})$ are the lengths of all rays that emanate from \mathbf{x} and are reflected from the boundary back to \mathbf{x} . Note that sums of ray solutions satisfy boundary conditions only at certain points.

To fix our ideas, we consider first simply connected domains. Setting

$$S_0(\mathbf{y}, \mathbf{x}) = |\mathbf{x} - \mathbf{y}|, \quad G_0(\mathbf{y}, \mathbf{x}, t) = \frac{1}{4\pi t} e^{-S_0^2(\mathbf{y}, \mathbf{x})/4t},$$

we consider first solutions corresponding to rays that are reflected only once at the boundary, and in particular, rays that are reflected back from the boundary to the

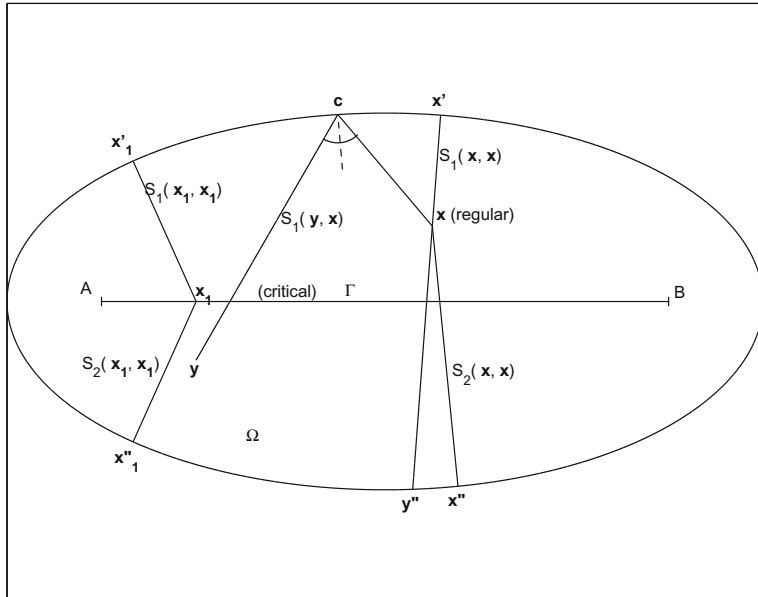


Fig. 5.1 The locus of critical points. Γ is the segment AB. The first eikonal is $S_1(\mathbf{x}, \mathbf{y}) = |\mathbf{x} - \mathbf{c}| + |\mathbf{c} - \mathbf{y}|$. It is the shortest reflected ray from \mathbf{x} to \mathbf{y} such that $\mathbf{x} - \mathbf{c}$ does not intersect Γ . For $\mathbf{x} = \mathbf{y}$ the diagonal values are $S_1(\mathbf{x}, \mathbf{x}) = |\mathbf{x} - \mathbf{x}'|$. The diagonal values of the second eikonal are $S_2(\mathbf{x}, \mathbf{x}) = 2|\mathbf{x} - \mathbf{x}''|$. The vectors $\mathbf{x} - \mathbf{x}'$ and $\mathbf{x} - \mathbf{x}''$ are orthogonal to the boundary. For $\mathbf{x}_1 \in \Gamma$ the two eikonals are equal

points of their origin. Such rays hit the boundary at right angles (see Fig. 5.1 and [Cohen and Lewis (1967)]). If there is only one minimal eikonal $S_1(\mathbf{x}, \mathbf{x}) > 0$, we say that \mathbf{x} is a *regular* point of Ω . If there is more than one minimal eikonal $S_1(\mathbf{x}, \mathbf{x})$, we say that \mathbf{x} is a *critical* point of Ω . We denote by Γ the locus of critical points in Ω . The eikonal $S_1(\mathbf{y}, \mathbf{x})$ is the length of the shortest ray from \mathbf{x} to \mathbf{y} with one reflection in the boundary such that the ray from \mathbf{x} to the boundary does not intersect Γ . For $\mathbf{x} = \mathbf{y}$ the eikonal $S_1(\mathbf{x}, \mathbf{x})$ is twice the distance of \mathbf{x} to the boundary. We denote by \mathbf{x}' the orthogonal projection of \mathbf{x} on the boundary along the shortest normal from \mathbf{x} to the boundary. When $\mathbf{y} = \mathbf{x}'$

$$S_1(\mathbf{x}', \mathbf{x}) = S_0(\mathbf{x}', \mathbf{x}) = |\mathbf{x} - \mathbf{x}'|. \quad (5.34)$$

The function

$$G_1(\mathbf{y}, \mathbf{x}, t) = e^{-S_1^2(\mathbf{y}, \mathbf{x})/4t} Z_1(\mathbf{y}, \mathbf{x}, t)$$

has to be chosen so that $G_0(\mathbf{x}', \mathbf{x}, t) - G_1(\mathbf{x}', \mathbf{x}, t) = 0$. In view of (5.34), we have to choose

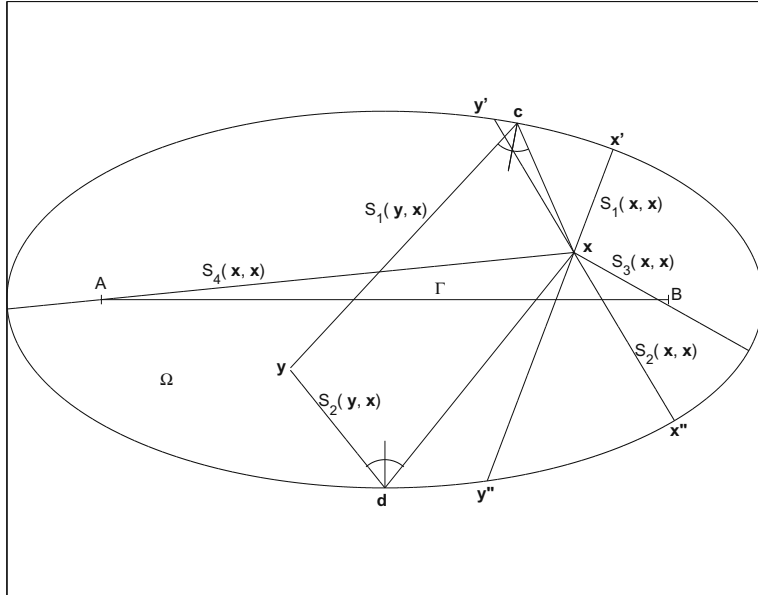


Fig. 5.2 The second and third eikonals. $S_2(x, y) = |x - d| + |d - y|$. It is the shortest reflected ray such that $x - d$ intersects Γ . The eikonals $S_3(x, x)$ and $S_4(x, x)$ are ordered according to magnitude

$$Z_1(x', x, t) = \frac{1}{4\pi t}.$$

When y'' is the other boundary point on the normal from x' to x , we have

$$\begin{aligned} G_0(y'', x, t) - G_1(y'', x, t) &= \frac{1}{4\pi t} e^{-|x-y''|^2/t} \\ &\quad - e^{-(|x'-x|+|y''-x'|)^2/t} Z_1(y'', x, t). \end{aligned} \quad (5.35)$$

Next, we consider in $\Omega - \Gamma$ the minimal among the remaining eikonals $S_k(x, x) > S_1(x, x)$ and denote it by $S_2(x, x)$. This eikonal is twice the length of a ray that emanates from x , intersects Γ once, and intersects the boundary $\partial\Omega$ at right angles at a point, denoted x'' . The eikonal $S_2(y, x)$ is the length of the ray from x to y with one reflection in the boundary such that the ray from x to the boundary intersects Γ once. When $y = x''$

$$S_2(x'', x) = S_0(x'', x) = |x - x''|. \quad (5.36)$$

When y' is the other boundary point on the normal that emanates from x'' (see Fig. 5.2), we have

$$S_2(y', x) = |x - x''| + |y' - x''|.$$

In general $\mathbf{x}' \neq \mathbf{y}'$ and $\mathbf{x}'' \neq \mathbf{y}''$. However, if the ray is a 2-periodic orbit (that hits the boundary at only 2 points), $\mathbf{x}' = \mathbf{y}'$ and $\mathbf{x}'' = \mathbf{y}''$ so that

$$S_2(\mathbf{y}'', \mathbf{x}) = S_0(\mathbf{y}'', \mathbf{x}) = |\mathbf{x} - \mathbf{y}''|$$

and

$$S_2(\mathbf{y}', \mathbf{x}) = |\mathbf{x} - \mathbf{x}''| + |\mathbf{y}'' - \mathbf{x}'|.$$

Because

$$|\mathbf{x} - \mathbf{y}''| < |\mathbf{x} - \mathbf{x}'| + |\mathbf{y}'' - \mathbf{x}'| < |\mathbf{x} - \mathbf{x}''| + |\mathbf{y}'' - \mathbf{x}'|$$

for all regular points \mathbf{x} , the order of magnitude of the boundary error (5.35) decreases if we use the approximation

$$G_0(\mathbf{y}, \mathbf{x}, t) \sim G_0(\mathbf{y}, \mathbf{x}, t) - G_1(\mathbf{y}, \mathbf{x}, t) - G_2(\mathbf{y}, \mathbf{x}, t) \quad (5.37)$$

with

$$Z_2(\mathbf{y}'', \mathbf{x}, t) = Z_1(\mathbf{y}'', \mathbf{x}, t) = Z_0(t).$$

5.3 The Trace

To find the short time asymptotics of the Dirichlet series (4.76), as given in (5.5),

$$P(t) = \int_{\Omega} G(\mathbf{x}, \mathbf{x}, t) d\mathbf{x}, \quad (5.38)$$

we use the ray expansion (5.33) for the evaluation of the integral. We retain in the resulting expansion only terms that are transcendentally small, since all algebraic terms are contained in the expansion (5.12).

5.3.1 Simply Connected Domains

We note that according to Sard's theorem, Γ is a set of measure zero and that all points in the domain $\Omega - \Gamma$ are regular. For any point $\mathbf{x} \in \Omega$, we denote by $r_1(\mathbf{x})$ its distance to the boundary and note that $S_1(\mathbf{x}, \mathbf{x}) = 2r_1(\mathbf{x})$. We also denote by $s_1(\mathbf{x})$ the arclength at the boundary point \mathbf{x}' (the orthogonal projection of \mathbf{x} on $\partial\Omega$ along the shortest normal from \mathbf{x} to $\partial\Omega$), measured from a boundary point where the arclength is set to 0 (see Fig. 5.2).

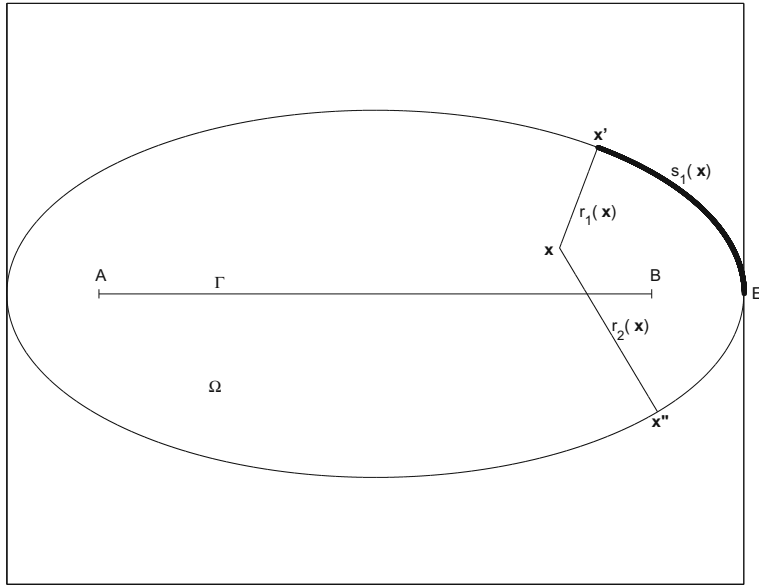


Fig. 5.3 The arclength $s_1(\mathbf{x})$ on the boundary is measured from the point E . Both transformations $\mathbf{x} \rightarrow (r_1(\mathbf{x}), s_1(\mathbf{x}))$ and $\mathbf{x} \rightarrow (r_2(\mathbf{x}), s_1(\mathbf{x}))$ are one-to-one mappings of $\Omega - \Gamma$. The images are given in Fig. 5.4 above

It follows that the change of variables in $\Omega - \Gamma$, given by

$$\mathbf{x} \rightarrow (r_1(\mathbf{x}), s_1(\mathbf{x})), \quad (5.39)$$

is a one-to-one mapping of $\Omega - \Gamma$ onto a strip $0 \leq r_1 \leq r_1(s_1)$, $0 \leq s_1 \leq L$, where $r_1(s_1)$ is the distance from the boundary point to Γ corresponding to arclength s_1 (Fig. 5.3).

We evaluate the integral over Ω separately for each summand k in the expansion (5.33). In this notation, we can write

$$\begin{aligned} \int_{\Omega} G_1(\mathbf{x}, \mathbf{x}, t) d\mathbf{x} &= \int_{\Omega} e^{-[S_1(\mathbf{x}, \mathbf{x})]^2/4t} \sum_{n=0}^{\infty} Z_{n,1}(\mathbf{x}, \mathbf{x}) t^{n-1} d\mathbf{x} \\ &= \int_0^L ds \int_0^{r_1(s_1)} e^{-r_1^2/t} J_1(r_1, s_1) Z_1(r_1, s_1, t) dr_1, \end{aligned} \quad (5.40)$$

where $J_1(r_1, s_1)$ is the Jacobian of the transformation and

$$Z_1(r_1, s_1, t) = \sum_{n=0}^{\infty} Z_{n,1}(\mathbf{x}, \mathbf{x}) t^{n-1}.$$

Note that the Jacobian vanishes neither inside $\Omega - \Gamma$ nor at $r_1 = 0$, because the transformation is one-to-one in $\Omega - \Gamma$; however, it does vanish on Γ .

We set $S_2(\mathbf{x}, \mathbf{x}) = 2r_2(\mathbf{x})$ and use it as a coordinate. We use $s_1(\mathbf{x})$ as the other coordinate of the point $\mathbf{x} \in \Omega - \Gamma$. Note that while $r_2(\mathbf{x})$ is the length of the longer normal from \mathbf{x} to $\partial\Omega$ (the one that intersects Γ), the other coordinate is the arclength corresponding to the shorter normal from \mathbf{x} to $\partial\Omega$ (the one that does not intersect Γ). The transformation

$$\mathbf{x} \rightarrow (r_2(\mathbf{x}), s_1(\mathbf{x})) \quad (5.41)$$

maps $\Omega - \Gamma$ onto the strip $r(s_1) \leq r_2 \leq l(s_1)$, $0 \leq s_1 \leq L$, where $l(s_1)$ is the length of the segment of the normal that starts at the boundary point $r_1 = 0$, s_1 and ends at its other intersection point with the boundary. This mapping is one-to-one as well. It follows that

$$\begin{aligned} \int_{\Omega} G_2(\mathbf{x}, \mathbf{x}, t) d\mathbf{x} &= \int_{\Omega} e^{-[S_2(\mathbf{x}, \mathbf{x})]^2/4t} \sum_{n=0}^{\infty} Z_{n,2}(\mathbf{x}, \mathbf{x}) t^{n-1} d\mathbf{x} \\ &= \int_0^L ds_1 \int_{r(s_1)}^{l(s_1)} e^{-r_2^2/t} J_2(r_2, s_1) Z_2(r_2, s_1, t) dr_2, \end{aligned} \quad (5.42)$$

where

$$Z_2(r_2, s_1, t) = \sum_{n=0}^{\infty} Z_{n,2}(\mathbf{x}, \mathbf{x}) t^{n-1}.$$

Note that for \mathbf{x} on Γ both transformations (5.39) and (5.41) are identical and

$$J_2(r_2, s_1) Z_2(r_2, s_1, t) = J_1(r_1, s_1) Z_1(r_1, s_1, t). \quad (5.43)$$

It follows that the two equations (5.40) and (5.42) combine together to give

$$\int_{\Omega} [G_1(\mathbf{x}, \mathbf{x}, t) + G_2(\mathbf{x}, \mathbf{x}, t)] d\mathbf{x} = \int_0^L \int_0^{l(s)} e^{-r^2/t} J(r, s) Z(r, s, t) dr ds, \quad (5.44)$$

where $s = s_1$, $r = r_1$, $J = J_1$, and $Z = Z_1$ for $0 < r < r_1(s_1)$, and $s = s_1$, $r = r_2$, $J = J_2$, and $Z = Z_2$ for $r_2(s_1) < r < l(s_1)$. Thus the domain of integration of the function $e^{-r^2/t} J(r, s) Z(r, s, t)$ in (5.44) is the domain enclosed by the s_1 -axis and the upper curve in Fig. 5.4. Now, for $t \ll 1$, we write the inner integral on the right-hand side of (5.44) as

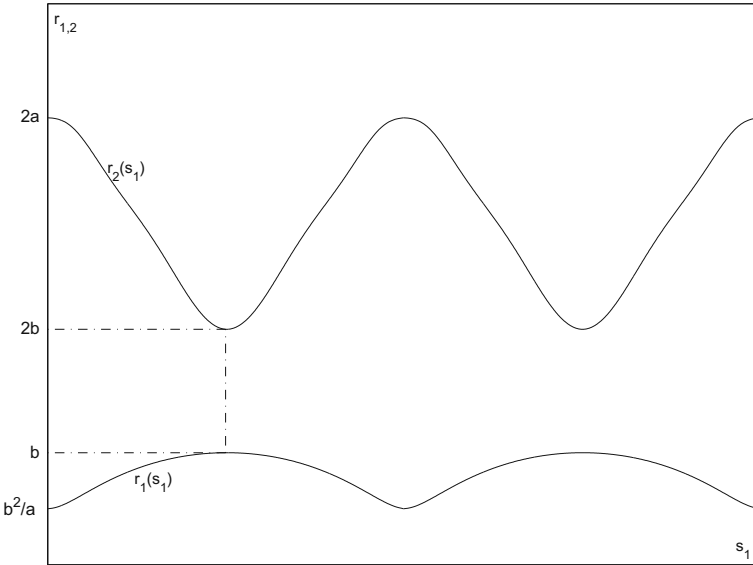


Fig. 5.4 The domain Ω is the ellipse $\frac{x^2}{a^2} + \frac{y^2}{b^2} \leq 1$. The domain enclosed between the s_1 -axis and the lower curve is the image of the ellipse under the transformation (5.39) and the domain enclosed between the upper and the lower curves is its image under (5.41)

$$\begin{aligned} \int_0^{l(s)} e^{-r^2/t} J(r, s) Z(r, s, t) dr &= \sqrt{\frac{\pi t}{2}} \operatorname{erf}\left(\frac{l(s)}{\sqrt{t}}\right) J(0, s) Z(0, s, t) \left(1 + O(\sqrt{t})\right) \\ &= \sqrt{\frac{\pi t}{2}} \left(1 - \frac{\exp\left\{-\frac{l^2(s)}{t}\right\} \sqrt{t}}{l(s)}\right) J(0, s) Z(0, s, t) \\ &\quad \times \left(1 + O(\sqrt{t})\right). \end{aligned}$$

Recall that $J(0, s)Z(0, s, t) \neq 0$. Only the exponentially small terms have to be considered, because the algebraic terms are included in the (5.10) expansion. Thus

$$\begin{aligned} &\int_0^L \int_0^{l(s)} e^{-r^2/t} J(r, s) Z(r, s, t) dr ds - \int_0^L \sqrt{\frac{\pi t}{2}} J(0, s) Z(0, s, t) \left(1 + O(\sqrt{t})\right) ds \\ &= - \int_0^L \exp\left\{-\frac{l^2(s)}{t}\right\} \frac{J(0, s) Z(0, s, t)}{l(s)} O(t) ds \quad \text{for } t \ll 1. \end{aligned}$$

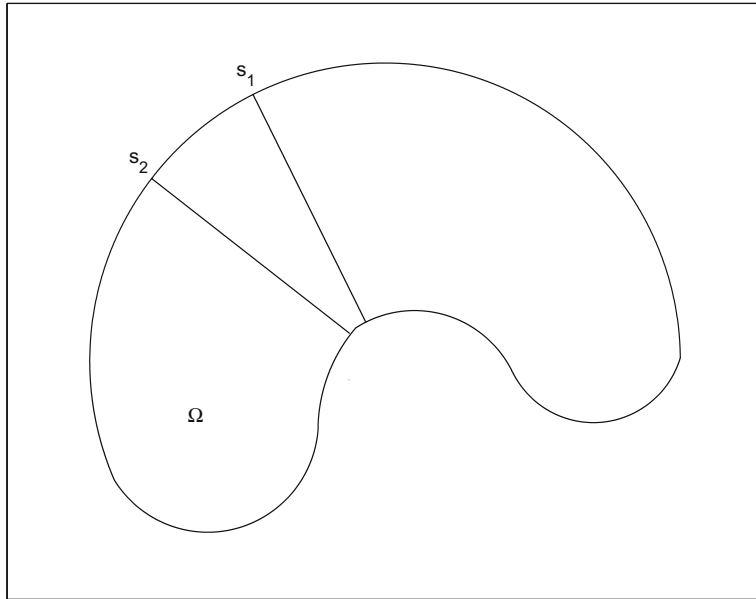


Fig. 5.5 The rays emanating from the boundary points s_1 and s_2 are orthogonal to the boundary at both ends. They are 2-periodic orbits

Evaluating the last integral by the Laplace method, we find that each point s_i , which is an extremum point of $l(s)$, contributes an exponential term of the form

$$\exp \left\{ -\frac{l^2(s_i)}{t} \right\} \frac{J(0, s_i) Z(0, s_i, t)}{l(s_i)} O(t^\nu), \quad (5.45)$$

where $\nu \geq 0$ and $O(t^\nu)$ depend on the type of the critical point s_i , and so also on the local behavior of $l^2(s)$ near s_i . The expression (5.45) means that some of the δ_n -s in the expansion (5.13) are the extremal values $l(s_i)$ and their multiples. These are half the lengths of the 2-periodic orbits of a billiard ball in Ω (see Fig. 5.5). In particular, the shortest neck is given by

$$\delta_1 = \frac{l}{2}. \quad (5.46)$$

The 2-periodic orbits of the ellipse are the major axes, which correspond to the lowest and highest points of the top curve in Fig. 5.4. There are other exponents as well, as discussed below. The pre-exponential terms in the expression (5.45) influence the factors $P_n(\sqrt{t})$ in (5.13). For example, if $l'(s_i) = 0$, $l''(s_i) \neq 0$, then $\nu = 3/2$. If the boundary is flatter, then $1 \leq \nu < 3/2$.

In addition to the 2-periodic orbits, there are ray solutions corresponding to rays from x to y that are reflected any number of times in the boundary. There are eikon-

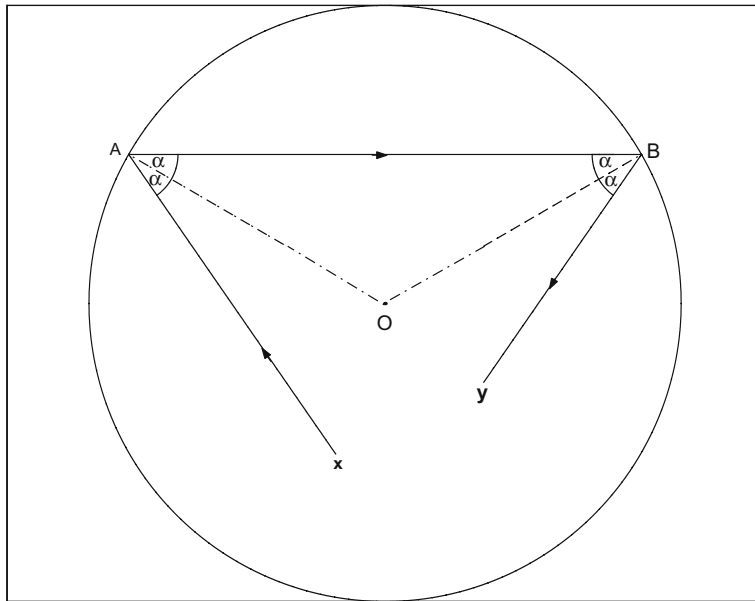


Fig. 5.6 The eikonal $S_3(y, x)$ with two reflections in the circle

als from x to y in Ω with $N - 1$ different vertices on the boundary, which have N vertices on $\partial\Omega$ if $x = y$ and $x \in \partial\Omega$ (this is a periodic orbit with $N - 1$ reflections). Among these periodic orbits there are eikonsals $S_N(x, x)$ with extremal length, denoted $S_{N,j}$, ($j = 1, \dots$). At points $x \in \Omega$ on a 2-periodic orbit the eikonal $S_N(x, x)$, which now has $N - 1$ vertices on the boundary, may reduce to the 2-periodic orbit with N reflections. Therefore the change of variables $x \rightarrow (S_N(x, x), s(x))$ will map the domain into a strip with extremal widths that are the differences between the lengths $S_{N,j}$ and the length of a 2-periodic orbit with N reflections. It follows that the evaluation of the trace by the Laplace method leads to exponents which are the extremal lengths of periodic orbits with any number of reflections (Fig. 5.6).

For example, there is an eikonal in a circle (centered at the origin) that is the ray from x to y with two reflections in the boundary (see Fig. 5.5). For $x = y$ it is the equilateral triangle (see Fig. 5.7) with

$$S(x, x) = R \left(2 \frac{\sqrt{2|x|^2 + 1 + \sqrt{8|x|^2 + 1}}}{\sqrt{4|x|^2 + 1 + \sqrt{8|x|^2 + 1}}} + \sqrt{4|x|^2 + 2 + 2\sqrt{8|x|^2 + 1}} \right).$$

The eikonal $S_3(x, y)$ reduces to a 2-periodic orbit with two reflections if $x = y = 0$ (the center of the circle). If x is on the circumference, the eikonal becomes the isosceles triangle with one vertex at x . To evaluate the contribution of the corresponding ray solution to the trace, we use this eikonal as a coordinate that varies

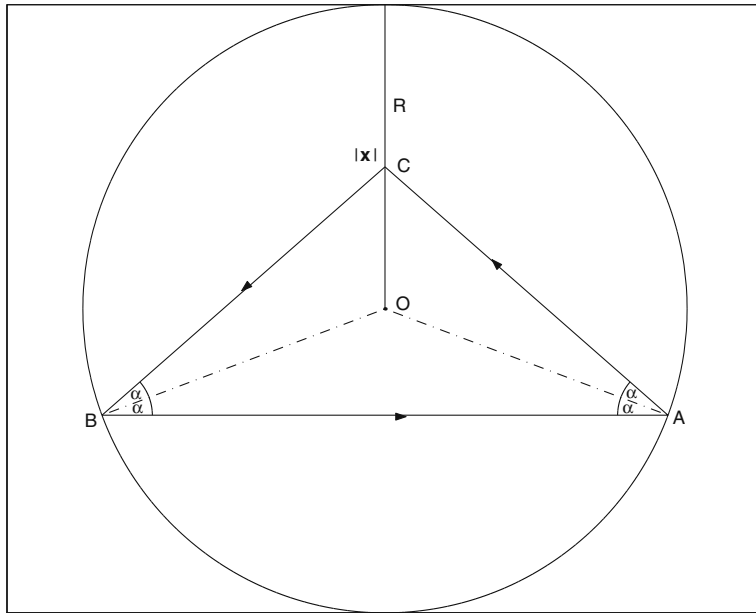


Fig. 5.7 The eikonal $S_3(x, x)$ with two reflections, where $|x| = OC$

between $4R$, the length of the 2-periodic orbit with two reflections, and $3\sqrt{3}R$, the circumference of the inscribed isosceles triangle. The contribution of this integral to the exponential sum in (5.13) contains exponents that are both lengths. Similarly, the 2-periodic orbit with 3 reflections has length $6R$ while the periodic orbit with 3 reflections at 3 different points has length $4\sqrt{2}R < 6R$. Obviously, if the pre-exponential factors vanish, these exponents do not appear in the expansion.

5.3.2 Multiply Connected Domains

Once again, we first consider rays from x to y that are reflected only once in the boundary. For every connected component of $\partial\Omega$, denoted $\partial\Omega_i$ ($i = 1, \dots, I$), a point x in Ω is regular with respect to $\partial\Omega_i$ if there is only one minimal eikonal $S_{i,1}(x, x) > 0$ with one reflection at $\partial\Omega_i$. We denote by Γ_i the locus of the irregular points of Ω with respect to $\partial\Omega_i$.

As above, we define in $\Omega - \Gamma_i$ the minimal eikonal with one reflection in $\partial\Omega_i$ such that $S_{i,2}(x, x) > S_{i,1}(x, x)$. We construct an approximation

$$G(y, x, t) \sim G_0(y, x, t) + \sum_{k=1}^2 \sum_{i=1}^I G_{i,k}(y, x, t),$$

where $G_{i,k}(\mathbf{y}, \mathbf{x}, t)$ are ray solutions with eikonals $S_{i,k}(\mathbf{y}, \mathbf{x})$ and $Z_{i,k}(\mathbf{y}, \mathbf{x})$ chosen so as to minimize the boundary values of the sum at the boundary points of rays orthogonal to the boundary, as above. The trace of the double sum is calculated by introducing the change of variables $2r_{i,k}(\mathbf{x}) = S_{i,k}(\mathbf{x}, \mathbf{x})$ and arclength $s_i(\mathbf{x})$ in $\partial\Omega_i$, as above. The Laplace evaluation of the integrals produces exponents that are the 2-periodic orbits in Ω .

Eikonal with two or more reflections contribute exponents that are lengths of extremal closed orbits with any number of reflections in the boundary, as in the case of simply connected domains. Thus the exponents δ_n in (5.13) consist of half the lengths of 2-periodic orbits in Ω and their multiples, and extremal lengths of closed periodic orbits with any number of reflections in the boundary and their multiples.

5.4 Recovering δ_1 from $P(t)$

The sum of $N \geq 3$ terms in (5.12),

$$Q_N(t) \sim \frac{|\Omega|}{4\pi t} - \frac{|\partial\Omega|}{8\sqrt{\pi t}} + \frac{1}{6}(1-r) + \sum_{n=3}^N a_n t^{n/2-1}, \quad \text{for } t \rightarrow 0. \quad (5.47)$$

is used to recover the geometrical information from the expansion (5.13), given the (measured) function $P(t)$. Note that

$$|\Omega| = \lim_{t \rightarrow 0} 4\pi t P(t), \quad |\partial\Omega| = -\lim_{t \rightarrow 0} 8\sqrt{\pi t} \left[P(t) - \frac{|\Omega|}{4\pi t} \right], \quad (5.48)$$

and so on. This way any number of terms in the expansion (5.12) can be determined.

Once $Q_n(t)$ has been determined, we can write

$$t[P(t) - Q_{2n-1}(t)] \sim \left[a_{2n} t^n + \frac{P_1(0)}{\sqrt{\pi}} \right] \left(1 + O(\sqrt{t}) \right) e^{-\delta_1^2/t}, \quad (5.49)$$

where the first $O(\sqrt{t})$ may depend on n . According to (5.78) and to Stirling's formula,

$$a_{2n} = \frac{\alpha}{l^{2n-2}} O\left(\frac{\Gamma(2n)}{\Gamma(n)}\right) = O(AB^n n^n) \quad \text{for } n \rightarrow \infty,$$

where

$$A = l^2 \alpha, \quad B = \frac{4}{el^2}.$$

There is some $\delta > 0$ such that

$$\max_{0 \leq t \leq \delta} \left\{ -t \log \left| a_{2n} t^n \left(1 + O(\sqrt{t}) \right) + \frac{P_1(0)}{\sqrt{\pi}} \left(1 + O(\sqrt{t}) \right) e^{-\delta_1^2/t} \right| \right\} \rightarrow \delta_1^2$$

as $n \rightarrow \infty$. Indeed, setting $b = \frac{P_1(0)}{\sqrt{\pi}}$, assuming $A, B, b > 0$, and defining

$$g(t) = -t \log \left(AB^n n^n t^n + be^{-\delta_1^2/t} \right), \quad (5.50)$$

we set $nt = u$ and rewrite (5.50) as

$$\begin{aligned} g(t) &= -u \log \sqrt[n]{A \left(\frac{4}{el^2} \right)^n u^n + be^{-n\delta_1^2/u}} \rightarrow -u \max \left\{ \log \frac{4}{el^2}, -\frac{\delta_1^2}{u} \right\} \\ &= \max \left\{ \delta_1^2, e \left(\frac{l}{2} \right)^2 (-y \log y) \right\} \text{ as } n \rightarrow \infty, \end{aligned} \quad (5.51)$$

where

$$y = \frac{u}{e} \left(\frac{2}{l} \right)^2.$$

Because

$$-y \log y \leq e^{-1},$$

we can write, according to (5.46),

$$\max_{0 < t < \delta} g(t) \rightarrow \max \left\{ \delta_1^2, \left(\frac{l}{2} \right)^2 \right\} = \delta_1^2 = \left(\frac{l}{2} \right)^2. \quad (5.52)$$

Note that the maximum is achieved at

$$t_{\max} = \frac{1}{en} \rightarrow 0 \text{ as } n \rightarrow \infty.$$

Equation (5.52) implies the following algorithm for determining δ_1 from the given values of $P(t)$. First, use the method of (5.48) to construct $Q_n(t)$ for a given n , and then find

$$\max_t \{-t \log |t[P(t) - Q_n(t)]|\} = \delta_1^2 + o(1) \text{ as } n \rightarrow \infty.$$

This algorithm works quite well with MAPLE.

5.5 Discussion

We illustrate our expansion for a disk, whose boundary has only one connected component and a single critical point. We consider points $\mathbf{x} = (x_1, y_1)$ and $\mathbf{y} = (x_2, y_2)$ inside a circle of radius R centered at the origin. The leading order eikonal is

$$S_0(\mathbf{y}, \mathbf{x}) = |\mathbf{x} - \mathbf{y}|.$$

When both \mathbf{x} and \mathbf{y} are on the x -axis, we have $y_1 = y_2 = 0$ and $S_0(\mathbf{y}, \mathbf{x}) = |x_1 - x_2|$. Defining $\mathbf{x}_1 = (x_1, 0)$ and $\mathbf{x}_2 = (x_2, 0)$, we see that the values of the eikonal on the x -axis are $S_0(\mathbf{x}_1, \mathbf{x}_2) = |x_1 - x_2|$. We assume that $x_1 > 0$. The boundary values of the eikonal are

$$S_0(\mathbf{x}_1, \mathbf{x}_2) = R - x_1 \quad \text{at } \mathbf{x}_2 = (R, 0)$$

and

$$S_0(\mathbf{x}_1, \mathbf{x}_2) = R + x_1 \quad \text{at } \mathbf{x}_2 = (-R, 0).$$

Thus the leading order ray approximation to Green's function $G(\mathbf{y}, \mathbf{x}, t)$,

$$G_0(\mathbf{y}, \mathbf{x}, t) = \frac{1}{4\pi t} e^{-S_0^2(\mathbf{y}, \mathbf{x})/4t},$$

misses the boundary conditions when \mathbf{x} and \mathbf{y} are on the x -axis, giving

$$G_0(\mathbf{x}_1, \mathbf{x}_2, t) = \frac{1}{4\pi t} e^{-(R-x_1)^2/4t} \quad \text{at } \mathbf{x}_2 = (R, 0)$$

and

$$G_0(\mathbf{x}_1, \mathbf{x}_2, t) = \frac{1}{4\pi t} e^{-(R+x_1)^2/4t} \quad \text{at } \mathbf{x}_2 = (-R, 0). \quad (5.53)$$

The next eikonal, denoted $S_1(\mathbf{y}, \mathbf{x})$, is given on the x -axis by $S_1(\mathbf{x}_1, \mathbf{x}_2) = 2R - x_1 - x_2$, and its boundary values are

$$S_1(\mathbf{x}_1, \mathbf{x}_2) = R - x_1 \quad \text{at } \mathbf{x}_2 = (R, 0)$$

and

$$S_1(\mathbf{x}_1, \mathbf{x}_2) = 3R - x_1 \quad \text{at } \mathbf{x}_2 = (-R, 0).$$

Thus the approximation of Green's function $G(\mathbf{y}, \mathbf{x}, t)$,

$$G(\mathbf{y}, \mathbf{x}, t) \sim G_0(\mathbf{y}, \mathbf{x}, t) - G_1(\mathbf{y}, \mathbf{x}, t),$$

corresponding to the ray solutions $G_0(\mathbf{y}, \mathbf{x}, t)$ and

$$G_1(\mathbf{x}, \mathbf{y}, t) = Z_1(\mathbf{x}, \mathbf{y}, t) e^{-S_1^2(\mathbf{y}, \mathbf{x})/4t},$$

will satisfy the boundary condition at (x_1, R) if $Z_1(\mathbf{y}, \mathbf{x}, t)$ is chosen so that

$$Z_1(\mathbf{x}_1, \mathbf{x}_2, t) = \frac{1}{4\pi t} \text{ at } \mathbf{x}_2 = (R, 0).$$

However, this approximation does not satisfy the boundary condition at $\mathbf{x}_2 = (-R, 0)$. The error in the boundary values at $\mathbf{x}_2 = (-R, 0)$ is

$$G_0(\mathbf{x}_1, \mathbf{x}_2, t) - G_1(\mathbf{x}_1, \mathbf{x}_2, t) = \frac{1}{4\pi t} e^{-(R+x_1)^2/4t} - Z_1(\mathbf{x}_1, \mathbf{x}_2, t) e^{-4(R-x_1)^2/4t}$$

and is of the same order of magnitude as that of the leading order approximation (5.53). To make up for the missed boundary condition the further approximation

$$G(\mathbf{y}, \mathbf{x}, t) \sim G_0(\mathbf{y}, \mathbf{x}, t) - G_1(\mathbf{y}, \mathbf{x}, t) - G_2(\mathbf{y}, \mathbf{x}, t) \quad (5.54)$$

can be used, with

$$G_2(\mathbf{y}, \mathbf{x}, t) = Z_2(\mathbf{y}, \mathbf{x}, t) e^{-s_1^2(\mathbf{y}, \mathbf{x})/4t},$$

where on the x -axis

$$s_1(\mathbf{x}_1, \mathbf{x}_2) = 2R + x_1 + x_2$$

and

$$Z_2(\mathbf{x}_1, \mathbf{x}_2, t) = \frac{1}{4\pi t} \text{ at } \mathbf{x}_2 = (-R, 0).$$

This eikonal corresponds to rays with two reflections in the boundary. The approximation (5.54) decreases the error in the boundary condition at $\mathbf{x}_2 = (-R, 0)$ to

$$-Z_1(\mathbf{x}_1, \mathbf{x}_2, t) e^{-4(R-x_1)^2/4t},$$

but misses the boundary condition at $\mathbf{x}_2 = (R, 0)$ with error

$$G_0(\mathbf{x}_1, \mathbf{x}_2, t) - G_1(\mathbf{x}_1, \mathbf{x}_2, t) - G_2(\mathbf{x}_1, \mathbf{x}_2, t) = -Z_2(\mathbf{x}_1, \mathbf{x}_2, t) e^{-(3R+x_1)^2/4t}$$

$\mathbf{x}_2 = (R, 0)$. This process gives successive approximations to Green's function with errors that decrease at transcendental rather than algebraic rates.

The approximation to the trace produced by $G_0(\mathbf{y}, \mathbf{x}, t)$ is the first algebraic term in the expansion (5.12). The contributions of the terms $-G_1(\mathbf{y}, \mathbf{x}, t)$ and $-G_2(\mathbf{y}, \mathbf{x}, t)$ in the approximation (5.54) of terms that are $O(\sqrt{t}e^{-R^2/t})$ are identical, but with opposite signs, and thus they cancel each other. The second term contributes a negative term that is $O(\sqrt{t}e^{-4R^2/t})$. The term $O(\sqrt{t}e^{-R^2/t})$ for small t corresponds to $O\left(\frac{1}{s}e^{-2R\sqrt{s}}\right)$ for large positive s in the Laplace plane. The number $2R$ is the length of the periodic orbit of a billiard ball bouncing inside a circle with the center removed, that is, inside the domain $\Omega - \Gamma$, where the set of critical points Γ consists of the center. Similarly, the term $O(\sqrt{t}e^{-4R^2/t})$ for small t corresponds to $O\left(\frac{1}{s}e^{-4R\sqrt{s}}\right)$ for large positive s in the Laplace plane. The number $4R$ is the length of the minimal periodic orbit of a billiard ball bouncing inside a disk. We conclude that the conjecture of [Berry et al. (1994)] should be supplemented with the orbit of length $2R$.

If Ω is an annulus between two concentric circles, of radii a and b , respectively, ($a > b$), the two connected components of the boundary are the two circles and there are no critical points in the domain relative to either one of them. In this case $\delta_1 = (a - b)$.

If Ω is the ellipse

$$\frac{x^2}{a^2} + \frac{y^2}{b^2} < 1$$

with $a > b$, the locus of critical points relative to the boundary is the segment

$$\Gamma = \left[-\frac{a^2 - b^2}{a}, \frac{a^2 - b^2}{a} \right]$$

on the x -axis. The segment Γ is the short diagonal of the evolute of the ellipse (the asteroid $(ax)^{2/3} + (by)^{2/3} = (a^2 - b^2)^{2/3}$). For the ellipse there are exponents in (5.13) which are $\delta_1 = 2b$ and its multiples and $\delta_2 = 2a$ and its multiples, as well as extremal periodic orbits with any number of reflections in the boundary.

Finally, we observe that if the boundary is reflecting (i.e., a homogeneous Neumann boundary condition), the exponential decay rate of the transcendental terms in the expansion of the trace is the same as in the case of absorbing boundary (homogeneous Dirichlet boundary condition). In this case the second term in the expansion (5.13) changes sign.

Obviously, rays that are reflected from the boundary more than once also give rise to ray solutions. The number of ray solutions needed in the expansion (5.33) is determined by the required degree of asymptotic approximation of the boundary

conditions. If only a finite sum of ray solutions satisfies the boundary conditions, the sum (5.33) is finite. Otherwise, additional ray solutions improve the degree of approximation of the boundary conditions, as described in the one-dimensional ray expansion in Sect. 5.1 above.

The derivation of the algorithm described in Sect. 5.4 suggests further conjectures of the type (5.78) [Berry et al. (1994)] concerning the coefficients of the power series $P_n(x)$ in the asymptotic series (5.13). They should relate the rate of growth of the coefficients of $P_1(x)$ to δ_2 , and so on. This will make the evaluation of δ_n possible for $n > 1$, as above.

Finally, the asymptotic convergence of the ray expansion follows from the maximum principle for the heat equation in a straightforward manner.

5.5.1 Construction of the Short-Time Asymptotic of the Fokker–Planck Equation with a Periodic Potential

We construct a formal short-time asymptotic expansion for the solution of the Fokker–Planck equation in dimension 1 associated to a stochastic process, where the drift is the gradient of a periodic potential. This method is used to recover the spatial structure from the displacement distribution of empirical data. We start with the stochastic process

$$\dot{X} = -\nabla U(X) + \sqrt{2D}\dot{w}, \quad (5.55)$$

where D is the diffusion coefficient, w is Brownian motion and the potential well is defined by

$$U(x) = -A \cos \omega x, \quad (5.56)$$

where the amplitude A and the frequency ω are parameters to be determined. The local minima of U are $x_k = \frac{2\pi k}{\omega}$, $k \in \mathbb{Z}$. The probability density function (pdf) $p(x, t)$ satisfies the Forward Fokker–Planck equation

$$\frac{\partial p}{\partial t} = D \frac{\partial^2 p}{\partial x^2} - \frac{\partial}{\partial x}[U(x)p] \quad (5.57)$$

$$p(x, t) \xrightarrow[t \rightarrow 0]{} \delta(x). \quad (5.58)$$

The general solution of Eq. 5.57 has a formal expansion on the eigenfunctions p_k of the operator

$$\mathcal{L}(p) = D \frac{\partial^2 p}{\partial x^2} - \frac{\partial}{\partial x}[U(x)p]. \quad (5.59)$$

So that

$$p(x, t) = \sum_{k=0}^{\infty} e^{-\lambda_k t} p_k(x) p_k^*(0), \quad (5.60)$$

where λ_k are the eigenvalues of the operator \mathcal{L} and p_k^* are eigenfunction of the adjoint operator \mathcal{L}^* . The formal expansion (5.60) provides long-time asymptotic behavior but is insufficient for short-time, because all terms might contribute and we thus need to use a lot of terms in the sum.

To construct a short-time asymptotic, we assume that the periodic wells W_k defined by the interval $I_k = [\frac{2\pi k}{\omega} - \frac{\pi}{2\omega}, \frac{2\pi k}{\omega} + \frac{\pi}{2\omega}]$ are deep, so that $A \gg 1$ and the escape time is exponentially long (Sect. 3.2), thus the probability distribution function will be concentrated at the bottom of the well at $x = 0$.

In this deep well limit, we approximate below the transition between neighboring wells as a Poissonian process, with equal escape rate 1/2. To construct the pdf, we truncated the process to an Ornstein–Uhlenbeck process with the same curvature of the potential U at the bottom of the wells. The Ornstein–Uhlenbeck process inside I_0 is

$$\begin{cases} \dot{Y} = -A\omega^2 Y + \sqrt{2D}\dot{w} \\ Y_0 = 0 \end{cases} \quad (5.61)$$

where the drift is the second-order approximation of the potential at 0 and indeed $\sin(\omega x) \approx \omega x$. Y is therefore a centered Gaussian variable of variance $\frac{D}{A\omega^2}(1 - e^{-2A\omega^2 t})$. The pdf of Y is

$$P_Y(x, t|0) = \frac{1}{\sqrt{\frac{2\pi D}{A\omega^2}(1 - e^{-2A\omega^2 t})}} \exp\left(-\frac{x^2}{\frac{2D}{A\omega^2}(1 - e^{-2A\omega^2 t})}\right), \quad (5.62)$$

which is an approximation of the pdf p of the initial process X , Eq. 5.55 conditioned so that the process does not leave the well I_0 . Using Bayes' law, as the wells cover the entire line \mathbb{R} , we have that

$$p(x, t) \approx \sum_k p(x, t|X(t)\text{located in well } I_k) p_k(t), \quad (5.63)$$

where the transition probability is

$$p_k(t) = Pr\{X(t) \text{ is located in well } I_k\} \quad (5.64)$$

from I_0 to well k at time t . The conditional probability $P_X(x, t|0, X(t) \text{ located in well } I_k)$ is the one for a process starting in I_k , approximated by

$$p(x, t | X(t) \text{ located in well } I_k) = P_Y(x, t | x_k) \quad (5.65)$$

$$= \frac{1}{\sqrt{\frac{2\pi D}{A\omega^2}(1 - e^{-2A\omega^2 t})}} \exp\left(-\frac{|x - x_k|^2}{\frac{2D}{A\omega^2}(1 - e^{-2A\omega^2 t})}\right).$$

The transition rate $p_k(t)$ satisfies the Markov chain equation

$$\dot{p}_k(t) = -2\lambda p_k(t) + \lambda p_{k-1}(t) + \lambda p_{k+1}(t), \quad (5.66)$$

$$p_0(t) = \delta_k \delta_t, \quad (5.67)$$

where $\lambda = \frac{1}{2\mathbb{E}[\tau_1]}$ and the mean time $\mathbb{E}[\tau_1]$ is the mean first passage time to the boundary of a well

$$\tau_1 = \inf \left\{ t \geq 0 : |X(t)| = \frac{2\pi}{\omega} \right\}. \quad (5.68)$$

The transition rate from one well to the neighboring ones can be computed from $\mathbb{E}[\tau_1]$ by multiplying by the factor 1/2. Kramer's escape rate formula is

$$\mathbb{E}[\tau_1] \approx \frac{\pi}{\sqrt{-U''(a)U''(s)}} \exp \frac{\Delta E}{\varepsilon} = \frac{\pi}{A\omega^2} \exp \left(\frac{2A}{D} \right), \quad (5.69)$$

where the energy barrier $\Delta E = 2A$, $\varepsilon = D$, the curvature at the saddle $U''(s) = -A\omega^2$ and the curvature at the minimum is $U''(a) = A\omega^2$. We have $p_k(t) = \Pr\{\tilde{Y}_t = k\}$, where the process

$$\tilde{Y}_t = \sum_{i=1}^{N_t} \xi_i \quad (5.70)$$

and ξ_i are i.i.d. random variables such that $\Pr\{\xi_1 = 1\} = \Pr\{\xi_1 = -1\} = \frac{1}{2}$ and N_t is a homogeneous Poisson process of parameter λ independent of ξ_i and for $k \in \mathbb{N}$,

$$\Pr\{\tilde{Y}_t = k\} = \Pr\{N_t^1 - N_t^2 = k\} \quad (5.71)$$

$$= \sum_{i=0}^{\infty} \Pr\{N_t^1 = i+k\} \Pr\{N_t^2 = i\} \quad (5.72)$$

$$= \sum_{i=0}^{\infty} \frac{(\frac{\lambda}{2}t)^{i+k}}{(i+k)!} e^{-\frac{\lambda}{2}t} \frac{(\frac{\lambda}{2}t)^i}{i!} e^{-\frac{\lambda}{2}t} \quad (5.73)$$

$$= e^{-\lambda t} \sum_{i=0}^{\infty} \frac{(\lambda t)^{2i+k}}{2^{2i+k} i!(i+k)!} = e^{-\lambda t} I_k(\lambda t). \quad (5.74)$$

Thus, we have

$$p_k(t) = e^{-\lambda t} I_{|k|}(\lambda t), \quad (5.75)$$

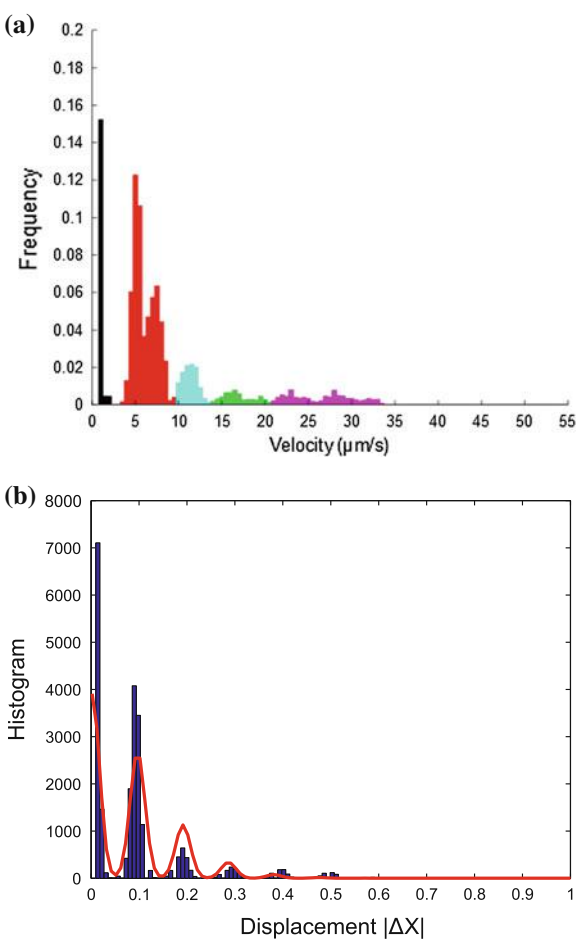
where I_k are the modified Bessel functions of the first kind [Abramowitz and Stegun (1972)].

In summary, the short-time asymptotic of the FPE is constructed by combining Bayes' law (5.76) with the Ornstein–Uhlenbeck approximation (5.65) and the exact solution of the Markov chain equation (5.71) and for $t \ll 1$,

$$p(x, t) \approx \sum_{k \in \mathbb{Z}} \frac{I_{|k|}(\lambda t) e^{-\lambda t}}{\sqrt{\frac{2\pi D}{A\omega^2}(1 - e^{-2A\omega^2 t})}} \exp\left(-\frac{|x - x_k|^2}{\frac{2D}{A\omega^2}(1 - e^{-2A\omega^2 t})}\right), \quad (5.76)$$

where $x_k = \frac{2\pi k}{\omega}$.

Fig. 5.8 Histogram of the increments $|\Delta X|$. (Upper) Histogram of the pdf of the increment $|\Delta X(t)|$ recorded at $\Delta t = 18$ ms. (Lower) A fit to the pdf computed in (5.76)



The above method can be applied to study the statistics of the random displacement $\Delta X(t) = X(t + \Delta t) - X(t)$. Indeed, under a stationarity assumption, it is equivalent to the statistics of

$$\langle |X(\Delta t) - X(0)| \rangle = \int_{\mathbb{R}} |y| p(y, \Delta t | 0) dy, \quad (5.77)$$

where $p(y, \Delta t | 0)$ is the transition probability in time Δt . Figure 5.8 shows the histogram of the increment $|\Delta X|$.

The above construction shows that peaks in the density of increments indicate periodic nanometer structures in live cell imaging.

5.5.2 Annotations

Much attention has been devoted in the literature to the recovery of the shape of a domain from the spectrum of the Dirichlet or Neumann boundary value problem for the Laplace equation (see [Kac (1966)], [Stewartson and Waechter (1971)], [Greiner (1971)], [Colin de Verdière (1973)], [Balian and Bloch (1972)], [Gutzwiller (1990)] and [Guillemin and Melrose (1979)] for some history and early results). For more recent work, see [Berry et al. (1994)], [Zelditch (2000)] and the references therein.

The expansion (5.10) was used in [Berry et al. (1994)] to deduce further geometric properties of Ω by extending $g(s)$ into the complex plane. Examples were given in [Berry et al. (1994)] of the resurgence of the length spectrum of closed billiard ball trajectories in the domain. It was conjectured in [Berry et al. (1994), Eq. (4)] that

$$a_n = \frac{\alpha \Gamma(n - \beta + 1)}{\Gamma\left(\frac{n}{2}\right) l^{n-2}}, \quad (5.78)$$

where α and β are constants of order unity and l is the shortest accessible geodesic (as defined in [Berry et al. (1994)]).

The full length spectrum of closed geodesics on a compact Riemannian manifold without boundary Ω appeared in the short time asymptotic expansion given in [Colin de Verdière (1973)],

$$P(t) \sim \frac{1}{\sqrt{\pi t}} \sum_{n=0}^{\infty} P_n(\sqrt{t}) e^{-\delta_n^2/t} \text{ for } t \rightarrow 0, \quad (5.79)$$

where δ_n are the lengths of closed geodesics on Ω and $P_n(x)$ are power series in x .

A different approach is based on the expansion of the spectral density [Balian and Bloch (1972)], [Gutzwiller (1990)], [Berry et al. (1994)]

$$d(s) = \sum_{n=1}^{\infty} \delta(s - \lambda_n) = \bar{d}(s) + d_{\text{osc}}(s), \quad (5.80)$$

where the non-oscillatory and oscillatory parts are, respectively,

$$\bar{d}(s) \sim \frac{|\Omega|}{\pi}, \quad d_{\text{osc}}(s) \sim \Re e \sum_j A_j(s) e^{-il_j \sqrt{s}} \text{ for } s \rightarrow \infty, \quad (5.81)$$

the second sum extends over the periodic orbits of billiard balls in Ω , and l_j are their lengths. The coefficients $A_j(s)$ depend on the stability of the orbits (see [Berry et al. (1994), Eqs. (11),(12)]).

Using the identity

$$\begin{aligned} \int_0^{\infty} \exp \left\{ -st - \frac{\delta_n^2}{t} \right\} dt &= \frac{2\delta_n K_1(2\delta_n \sqrt{s})}{\sqrt{s}} \\ &\sim \frac{\sqrt{\pi \delta_n}}{s} e^{-2\delta_n \sqrt{s}} \text{ for } s \rightarrow \infty, \end{aligned}$$

and formally extending the asymptotic relation (5.81) to the complex plane, we identify

$$\delta_n = \frac{l_n}{2}. \quad (5.82)$$

To construct the expansion the short-time *ray asymptotic approximation* to the heat kernel is followed, as in [Cohen and Lewis (1967)], [Cohen et al. (1972)], and [Tier and J.B. Keller (1978)].

The transcendentally small terms in the ray expansion are due to rays reflected in the boundary, much like in the geometric theory of diffraction [Seckler and Keller (1959)], [Keller (1962)], and [Lewis and J.B. Keller (1964)]. For the particular case of a circular domain, we find that all diffractive closed trajectories contribute to the transcendentally small terms [Berry et al. (1994), Sect. 3].

Part II

**Mixed Boundary Conditions for Elliptic
and Parabolic Equations**

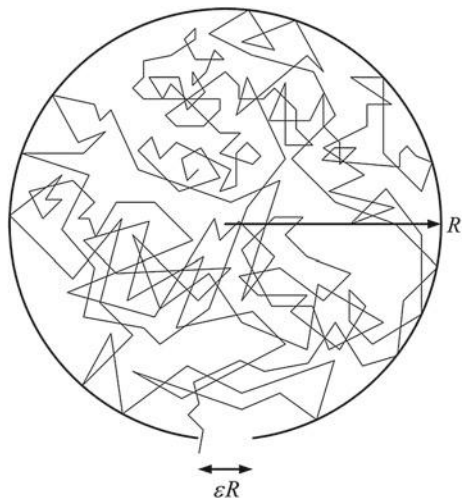
Chapter 6

The Mixed Boundary Value Problem

6.1 Introduction

The mixed Dirichlet–Neumann boundary value problem for the Poisson equation, which goes back to Lord Rayleigh (in the context of the theory of sound), has come up recently in neuroscience as the problem of calculating the mean first passage time of Brownian motion to a small absorbing window on the otherwise reflecting boundary of a bounded domain (see Fig. 6.1), as described below. The mean first passage time in this problem is also called the narrow escape time.

Fig. 6.1 Brownian trajectory escaping through a small absorbing window in a domain with otherwise reflecting boundary.



6.2 Formulation of the Mixed Boundary Value Problem

Consider a domain $\Omega \subset \mathbb{R}^d$, whose boundary $\partial\Omega$ is sufficiently smooth and consists of two parts, $\partial\Omega = \partial\Omega_a \cup \partial\Omega_r$, and the inhomogeneous mixed boundary value problem

$$\Delta v(\mathbf{x}) = -\frac{1}{D} \text{ for } \mathbf{x} \in \Omega \quad (6.1)$$

$$v(\mathbf{x}) = 0 \text{ for } \mathbf{x} \in \partial\Omega_a \quad (6.2)$$

$$\frac{\partial v(\mathbf{x})}{\partial n(\mathbf{x})} = 0 \text{ for } \mathbf{x} \in \partial\Omega_r, \quad (6.3)$$

where Ω is the diffusion coefficient and $n(\mathbf{x})$ is the unit outer normal vector to the boundary at $\mathbf{x} \in \partial\Omega$. Equation (6.1) is called the Pontryagin–Andronov–Vitt equation (see (1.25)). The asymptotic method for the mixed boundary value problem (6.1)–(6.3) can be generalized in a straightforward manner to the Poisson equation.

The Dirichlet part (6.2) in Figure 6.1 is the small arc of length εR and the Neumann part (6.3), $\partial\Omega_r$, is the large remaining arc of the circumference. If Ω is a subset of a two-dimensional Riemannian manifold, as in Figure 6.2, the Laplace operator (6.1) is replaced with the Laplace–Beltrami operator.

The Dirichlet boundary $\partial\Omega_a$ represents an absorbing part for Brownian trajectories while the Neumann boundary $\partial\Omega_r$ represents a reflecting part of $\partial\Omega$, as described below. As the size (e.g., the diameter) of the absorbing part decreases to zero, but that of the domain remains finite, the solution $v(\mathbf{x})$ increases indefinitely. A measure of smallness can be chosen as the ratio between the surface area of the absorbing boundary and that of the entire boundary, for example

$$\varepsilon = \left(\frac{|\partial\Omega_a|}{|\partial\Omega|} \right)^{1/(d-1)} \ll 1, \quad (6.4)$$

provided that the isoperimetric ratio remains bounded,

$$\frac{|\partial\Omega|^{1/(d-1)}}{|\Omega|^{1/d}} = O(1) \text{ for } \varepsilon \ll 1 \quad (6.5)$$

(see the pathological example below, in which (6.5) is violated). The compatibility condition

$$\int_{\partial\Omega_a} \frac{\partial v(\mathbf{x})}{\partial n} dS_x = -\frac{|\Omega|}{D} \quad (6.6)$$

is obtained by integrating (6.1) over Ω and using (6.2) and (6.3).

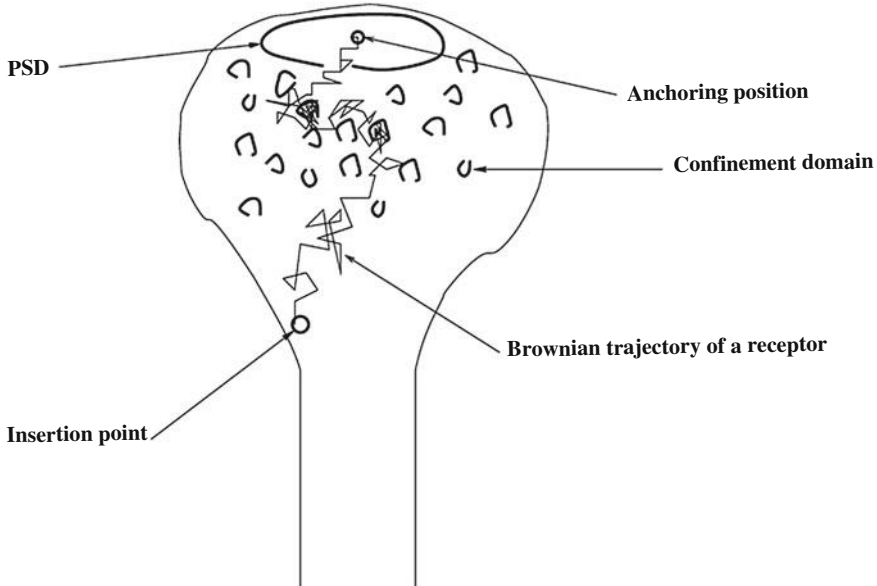


Fig. 6.2 Receptor movement on the neuronal membrane.

The solution $v(\mathbf{x})$ diverges to infinity as the absorbing hole $\partial\Omega_a$ shrinks to zero, e.g., as $\varepsilon \rightarrow 0$, except in a boundary layer near $\partial\Omega_a$, because the compatibility condition (6.6) fails in this limit. Our purpose here is to construct an asymptotic expansion of $v(\mathbf{x})$ for small ε .

6.2.1 The Narrow Escape Time Problem

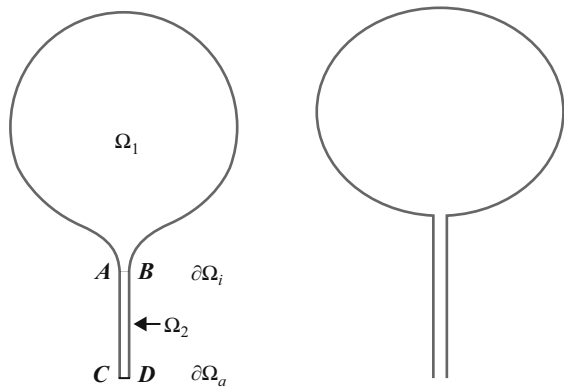
The solution $v(\mathbf{x})$ of the boundary value problem (6.1)-(6.3) represents the mean first passage time of free Brownian motion from a point $\mathbf{x} \in \Omega$ to the absorbing boundary $\partial\Omega_a$, that is, the expected escape time of a Brownian particle from confinement in Ω by the impermeable boundary $\partial\Omega_r = \partial\Omega - \partial\Omega_a$, as shown in Figures 6.1 and 6.3(left).

The lifetime in Ω of a Brownian trajectory that starts at a point $\mathbf{x} \in \Omega$ is the first passage time τ of the trajectory to the absorbing boundary $\partial\Omega_a$. The narrow escape time is defined as the conditional expectation

$$v(\mathbf{x}) = \mathbb{E}[\tau | \mathbf{x}(0) = \mathbf{x}]$$

and is finite under quite general conditions [Schuss (2010b)].

Fig. 6.3 Mathematical idealizations of the cross sections of neuronal spine morphologies as composite domains: **Left:** The bulky head Ω_1 is connected smoothly by an interface $\partial\Omega_i = AB$ to a narrow neck Ω_2 . The entire boundary is $\partial\Omega_r$ (reflecting), except for a small absorbing part $\partial\Omega_a = CD$. **Right:** The head, shown separately in Figure 6.1, is connected to the neck without a funnel.



6.2.2 A Pathological Example

The following pathological example shows that when (6.5) is violated the narrow escape time does not necessarily increase to infinity as the relative area of the hole decreases to zero. This is illustrated as follows. Consider a cylinder of length L and radius a . The boundary of the cylinder is reflecting, except for one of its bases (at $z = 0$, say), which is absorbing. The narrow escape problem becomes one-dimensional and its solution is

$$v(z) = Lz - \frac{z^2}{2}. \quad (6.7)$$

Here, there is neither a boundary layer nor a constant outer solution; the narrow escape time grows gradually with z . The narrow escape time, averaged with respect to a uniform initial distribution in the cylinder, is $\bar{\mathbb{E}}\tau = L^2/3$ and is independent of a , that is, the assumption that the narrow escape time becomes infinite is violated. It holds, however, if the domain is sufficiently thick, e.g., when a ball of radius independent of ε can be rolled on the reflecting boundary inside the domain.

6.2.3 The Matched Asymptotics Approach

In the matched asymptotics approach to the narrow escape problem from a domain Ω in \mathbb{R}^2 , a boundary layer solution is constructed near an absorbing window $\partial\Omega_a$ of size 2ε . First, the mixed boundary value problem (6.1)–(6.3) is converted to local coordinates (η, s) , where η is the distance of a point $x \in \Omega$ from the boundary $\partial\Omega$ and s is the arclength from the center of the window to the orthogonal projection of x on $\partial\Omega$. If $\partial\Omega$ is sufficiently smooth in a neighborhood of the window $\partial\Omega_a$, equation

(6.1) for the mean first passage time $v(\mathbf{x})$ is converted locally to

$$w_{\eta\eta} - \frac{\kappa}{1 - \kappa\eta} w_\eta + \frac{1}{1 - \kappa\eta} \left(\frac{1}{1 - \kappa\eta} w_s \right)_s = -\frac{1}{D}, \quad (6.8)$$

where $w(\eta, s) = v(\mathbf{x})$ and κ is the boundary curvature at the orthogonal projection of \mathbf{x} on $\partial\Omega$. If s is measured from the center of the arc $\partial\Omega_a$, the stretching $\eta = \varepsilon\hat{\eta}$, $s = \varepsilon\hat{s}$, $\hat{w}(\hat{\eta}, \hat{s}) = w(\eta, s)$ maps a boundary strip near $\partial\Omega_a$ into the upper half plane. Assuming, as we may, that the origin $\mathbf{x} = \mathbf{0}$ is at the center of $\partial\Omega_a$, we set $\mathbf{y} = \mathbf{x}/\varepsilon = (\hat{\eta}, \hat{s})$. An expansion in powers of ε gives the leading order boundary layer problem for (6.1)–(6.3) as

$$\hat{w}_{bl,\hat{\eta}\hat{\eta}} + \hat{w}_{bl,\hat{s}\hat{s}} = 0 \text{ for } 0 < \hat{\eta} < \infty, -\infty < \hat{s} < \infty \quad (6.9)$$

$$\hat{w}_{bl,\hat{\eta}}(0, \hat{s}) = 0 \text{ for } |\hat{s}| > 1, \quad \hat{w}_{bl}(0, \hat{s}) = 0 \text{ for } |\hat{s}| < 1. \quad (6.10)$$

We specify the growth condition $\hat{w}_{bl} \sim A \log |\mathbf{y}|$ as $|\mathbf{y}| \rightarrow \infty$, where A is an as yet undetermined constant. Setting $z = \hat{s} + i\hat{\eta}$, the transformation $\zeta = u + iv = \text{Arcsin } z = -i \text{Log}[iz + \sqrt{1 - z^2}]$ maps the upper half plane $\hat{\eta} > 0$ onto the semi-infinite strip $\hat{\Omega} = \{-\pi/2 < u < \pi/2, 0 < v < \infty\}$. The mixed boundary value problem (6.9), (6.10) is transformed into

$$\hat{W}_{uu}(u, v) + \hat{W}_{vv}(u, v) = 0 \text{ for } (u, v) \in \hat{\Omega}$$

$$\hat{W}_u \left(\pm \frac{\pi}{2}, v \right) = 0 \text{ for } 0 < v < \infty, \quad \hat{W}(u, 0) = 0 \text{ for } -\frac{\pi}{2} < u < \frac{\pi}{2},$$

where $\hat{W}(u, v) = \hat{w}_{bl}(\hat{\eta}, \hat{s})$. The solutions $\hat{W}(u, v) = Av$ for any A have the required logarithmic behavior for $|\mathbf{y}| \rightarrow \infty$, specifically,

$$\hat{w}_{bl} \sim A \log |\mathbf{y}| + \log 2 + o(1) \text{ as } |\mathbf{y}| \rightarrow \infty. \quad (6.11)$$

The constant A is related to the boundary flux by $A = 2\pi^{-1} \int_0^1 \hat{w}_{bl,\hat{\eta}}(0, \hat{s}) d\hat{s}$.

The leading term $w_{out}(\mathbf{x})$ in the outer expansion satisfies the original equation with the reduced boundary condition and the matching condition

$$\begin{aligned} \Delta_{\mathbf{x}} w_{out}(\mathbf{x}) &= -\frac{1}{D} \text{ for } \mathbf{x} \in \Omega \\ \frac{\partial w_{out}(\mathbf{x})}{\partial n} &= 0 \text{ for } \mathbf{x} \in \partial\Omega - \{\mathbf{0}\} \\ w_{out}(\mathbf{x}) &\sim A \left[\log \left(\frac{1}{\varepsilon} \right) + \log 2 + \log |\mathbf{x}| \right] \text{ for } \mathbf{x} \rightarrow \mathbf{0}. \end{aligned}$$

Now, the compatibility condition (6.6) gives

$$\mathbb{E}[\tau | \mathbf{x}(0) = \mathbf{x}] = v(\mathbf{x}) = \frac{|\Omega|}{\pi D} \left[\log \frac{1}{\varepsilon} + O(1) \right] \text{ for } \varepsilon \ll 1. \quad (6.12)$$

6.2.4 Higher-Order Asymptotics in the Unit Ball

If Neumann's function is defined as the solution of

$$\Delta G_s = \frac{1}{|\Omega|} \text{ for } \mathbf{x} \in \Omega, \quad \partial_r G_s = \delta(\cos \theta - \cos \theta_j) \delta(\phi - \phi_j) \text{ for } \mathbf{x} \in \partial\Omega, \\ (6.13)$$

$$\int_{\Omega} G_s d\mathbf{x} = 0,$$

then the following lemma holds.

Lemma 6.2.1 (Cheviakov, Ward, Straube). *Neumann's function on the unit ball in \mathbb{R}^3 , satisfying (6.13), is given by*

$$G_s(\mathbf{x}; \mathbf{x}_j) = \frac{1}{2\pi |\mathbf{x} - \mathbf{x}_j|} + \frac{1}{8\pi} (|\mathbf{x}|^2 + 1) \\ + \frac{1}{4\pi} \log \left(\frac{2}{1 - |\mathbf{x}| \cos \gamma + |\mathbf{x} - \mathbf{x}_j|} \right) - \frac{7}{10\pi}, \quad (6.14)$$

where γ is the angle between \mathbf{x} and \mathbf{x}_j , given by $\cos \gamma = \cos \theta \cos \theta_j + \sin \theta \sin \theta_j \cos(\phi - \phi_j)$.

6.2.5 The Narrow Escape Time Through Multiple Absorbing Windows

The matched asymptotic expansion of subsection 6.2.3 is generalized to the 3-dimensional unit ball with N small disjoint absorbing windows as follows. Assume $\partial\Omega_{\varepsilon_j}$ ($j = 1, \dots, N$) are absorbing windows, each of area $|\partial\Omega_{\varepsilon_j}| = O(\varepsilon^2)$ and assume $\varepsilon \rightarrow 0$. We need to construct a uniform asymptotic expansion of the solution to the mixed problem

$$\begin{aligned}\Delta v \equiv & v_{rr} + \frac{2}{r} v_r + \frac{1}{r^2 \sin^2 \theta} v_{\phi\phi} + \frac{\cot \theta}{r^2} v_\theta + \frac{1}{r^2} v_{\theta\theta} \\ = & -\frac{1}{D} \text{ for } r = |\mathbf{x}| \leq 1\end{aligned}\quad (6.15)$$

$$\begin{aligned}v = 0 \text{ for } \mathbf{x} \in \partial\Omega_a, & \bigcup_{j=1}^N \partial\Omega_{\varepsilon_j}, \quad j = 1, \dots, N, \\ v_r = 0 \text{ for } \mathbf{x} \in \partial\Omega \setminus \partial\Omega_a.\end{aligned}\quad (6.16)$$

The outer solution, valid away from $\partial\Omega_{\varepsilon_j}$, is given in the form of the expansion,

$$v(\mathbf{x}) \sim \varepsilon^{-1} v_0 + \log\left(\frac{\varepsilon}{2}\right) \chi_0 + v_1(\mathbf{x}) + \varepsilon \log\left(\frac{\varepsilon}{2}\right) v_2(\mathbf{x}) + \varepsilon v_3(\mathbf{x}) + \dots, \quad (6.17)$$

where the coefficients v_0, χ_0 are unknown constants, while $v_1(\mathbf{x}), v_2(\mathbf{x}), v_3(\mathbf{x})$, and higher-order coefficients are unknown functions, yet to be determined.

In the inner region, near the j th absorbing window, we introduce the local curvilinear coordinates (η, s_1, s_2) , where $\eta \equiv \varepsilon^{-1}(1 - r)$, $s_1 \equiv \varepsilon^{-1} \sin(\theta_j)(\phi - \phi_j)$, $s_2 \equiv \varepsilon^{-1}(\theta - \theta_j)$. The inner expansion is

$$v \sim \varepsilon^{-1} w_0 + \log\left(\frac{\varepsilon}{2}\right) w_1 + w_2 + \dots \quad (6.18)$$

Using (6.18) in (6.15) leads to

$$w_0 = v_0(1 - w_c), \quad (6.19)$$

where v_0 is a constant to be determined and w_c is the solution of the boundary layer equation

$$\mathcal{L}w_c \equiv w_{c\eta\eta} + w_{cs_1s_1} + w_{cs_2s_2} = 0 \text{ for } \eta \geq 0, \quad -\infty < s_1, s_2 < \infty \quad (6.20)$$

$$\partial_\eta w_c = 0 \text{ for } \eta = 0, \quad s_1^2 + s_2^2 \geq a_j^2, \quad w_c = 1 \text{ for } \eta = 0, \quad s_1^2 + s_2^2 \leq a_j^2 \quad (6.21)$$

$$w_c \rightarrow 0 \text{ for } \rho = \varepsilon^{-1}|\mathbf{x} - \mathbf{x}_j| \rightarrow \infty. \quad (6.22)$$

The boundary value problem (6.20), (6.21) with the matching condition (6.22) is the well-known electrified disk problem in electrostatics. Setting

$$L(\eta, \sigma) \equiv \frac{1}{2} \left([(\sigma + a_j)^2 + \eta^2]^{1/2} + [(\sigma - a_j)^2 + \eta^2]^{1/2} \right) \quad (6.23)$$

the solution of (6.20)–(6.22) can be written as

$$w_c = \frac{2}{\pi} \int_0^\infty \frac{\sin \mu}{\mu} e^{-\mu \eta/a_j} J_0\left(\frac{\mu \sigma}{a_j}\right) d\mu = \frac{2}{\pi} \sin^{-1}\left(\frac{a_j}{L}\right), \quad (6.24)$$

where $\sigma \equiv (s_1^2 + s_2^2)^{1/2}$ and the function $J_0(z)$ is the Bessel function of the first kind of order zero (see of order zero (see [Jac [Jackson (1998)]])�.

The far-field behavior of w_c in (6.24) is given by

$$w_c \sim \frac{2a_j}{\pi} \left[\frac{1}{\rho} + \frac{a_j^2}{6} \left(\frac{1}{\rho^3} - \frac{3\eta^2}{\rho^5} \right) + \dots \right] \text{ as } \rho \rightarrow \infty, \quad (6.25)$$

which is uniformly valid in η , s_1 , and s_2 . Thus (6.19) and (6.25) give the far-field expansion of w_0 as

$$w_0 \sim v_0 \left(1 - \frac{c_j}{\rho} + O(\rho^{-3}) \right) \text{ for } \rho \rightarrow \infty, \quad c_j \equiv \frac{2a_j}{\pi}, \quad (6.26)$$

where c_j is the electrostatic capacitance of the circular disk of radius a_j .

Writing the matching condition that the near-field behavior of the outer expansion (6.17) must agree with the far-field behavior of the inner expansion (6.18), we obtain the uniform expansion

$$\begin{aligned} v &\sim \frac{v_0}{\varepsilon} + v_1 + \varepsilon \log\left(\frac{\varepsilon}{2}\right) v_2 + \varepsilon v_3 + \dots \\ &\sim \frac{v_0}{\varepsilon} \left(1 - \frac{c_j}{\rho} \dots \right) + \log\left(\frac{\varepsilon}{2}\right) w_1 + w_2 + \dots. \end{aligned} \quad (6.27)$$

The definition $\rho \sim \varepsilon^{-1}|\mathbf{x} - \mathbf{x}_j|$ gives in (6.27) the expansion $v_1 \sim -v_0 c_j / |\mathbf{x} - \mathbf{x}_j|$ as $\mathbf{x} \rightarrow \mathbf{x}_j$ for $j = 1, \dots, N$, so that v_1 is the solution of the distributional equation

$$\begin{aligned} \Delta v_1 &= -\frac{1}{D} \text{ for } |\mathbf{x}| < 1, \\ \partial_r v_1 &= -2\pi v_0 \sum_{j=1}^N \frac{c_j}{\sin \theta_j} \delta(\theta - \theta_j) \delta(\phi - \phi_j) \text{ for } |\mathbf{x}| = 1. \end{aligned} \quad (6.28)$$

The solvability condition for (6.28) gives

$$v_0 = \frac{|\Omega|}{2\pi D N \bar{c}}, \quad \bar{c} \equiv \frac{1}{N} \sum_{j=1}^N c_j, \quad c_j = \frac{2a_j}{\pi}. \quad (6.29)$$

Thus, the solvability condition for the problem for v_1 determines the unknown leading-order constant v_0 in the outer expansion. The solution to (6.28), represented in terms of the Neumann functions (6.14), up to an unknown additive constant χ , is given by

$$v_1 = -2\pi v_0 \sum_{i=1}^N c_i G_s(x; x_i) + \chi, \quad \chi \equiv |\Omega|^{-1} \int_{\Omega} v_1 dx. \quad (6.30)$$

Iterating this procedure by expanding v_1 in the limit $x \rightarrow x_j$ and by using the near-field expansion of $G_s(x; x_j)$ gives

$$\chi = \log\left(\frac{\varepsilon}{2}\right) \chi_0 + \chi_1, \quad (6.31)$$

hence

$$w_1 = \left(\frac{v_0 c_j}{2} + \chi_0\right) (1 - w_c), \quad (6.32)$$

and

$$v_2 = -2\pi \sum_{i=1}^N c_i \left(\frac{v_0 c_i}{2} + \chi_0\right) G_s(x; x_i) + \chi_2. \quad (6.33)$$

Repeated iterations of this procedure determine all the functions v_k and w_k in the expansion (6.27).

6.3 Annotations

The matched asymptotics approach was developed in [Ward et al. (1993)] and [Ward et al. (2010)]. The expansion (6.17) was suggested in [Cheviakov et al. (2010); Cheviakov and Ward (2011)], where Lemma 6.2.1 in subsection 6.2.4 is proved and repeated iterations to determine all the functions v_k and w_k in the expansion (6.27) are used. The narrow escape problem in diffusion theory was considered first by Lord Rayleigh in [Rayleigh (1945)] and elaborated in [Fabrikant (1989)], [Fabrikant (1991)] and [Holcman and Schuss (2004)]; the terminology "narrow escape time" was introduced in [Singer et al. I (2006)]. A basic text on neuroscience is [Kandel et al. (2000)], where the terminology used in this chapter is explained. The neuronal cleft is discussed in [Alberts et al. (1994, Chapter 19)] and [Kandel et al. (2000)]. Recent computations are given in [Taflia and Holcman (2011)] and [Freche et al. (2011)]. The description of ionic channels, their selectivity, gating, and function is given in [Hille (2001)] (see also the Nobel lecture [MacKinnon (2003)]). The reconstruction of the spatial organization of protein and ions that define the channel pore from recordings of channel current-voltage characteristics is described in [Chen et al. (1997)], [Burger et al. (2007)]. The theoretical determination of ionic selectivity and channel conductance from the molecular structure were studied in [Chen et al. (1999)], [Boda et al. (2007)]. The Poisson–Nernst–Planck equations for channels were studied in [Eisenberg and Chen (1993)] and Brownian or molecular

dynamics simulations of the joint diffusive motion of protein and ions, as well as the computation of the time-dependent electric field, were studied, for example, in [Roux (2000)], [Aboud et al. (2003)]. The role of cell geometry in controlling the diffusion flux and in determining cell function is discussed at length in the following: [Harris and Stevens (1988)], [Korkotian et al. (2004)], [Bourne and Harris (2008)], [Newpher and Ehlers (2009)], and [Hotulainen and Hoogenraad (2010)]. Regulation of synaptic plasticity by geometry is discussed in [Svoboda et al. (1996)] , [Araya et al. (2007)] , [Korkotian et al. (2004)], [Biess et al. (2007)], and [Holcman and Kupka (2010)]. Regulation of the number and type of receptors that contribute to the shaping of the synaptic current is discussed in [Chen et al. (2000)] , [Triller and Choquet (2003)] , [Holcman and Triller (2006)], [Holcman et al. (2005)]. The case of proton binding sites on the viral envelope of the influenza virus is discussed in [Huang et al. (2002)] [Lagache et al. (2017)].

The time scale of the unraveling of a double strand DNA break is studied in [Lieber et al. (2009)] . It was shown in [Holcman and Schuss, JPA (2008a)] that splitting an absorbing window into two equal parts and moving them apart increases the absorption flux by nearly 50%. Note that the derivation of (7.54) requires a generalization of the method of [Holcman and Schuss (2004)] and [Singer et al. I (2006)], which consists in deriving and solving a Helmholtz integral equation on several windows. The solution depends on the separation between the windows in a strongly nonlinear way. The improved approximations (7.56)–(7.60) for the mean first passage time to two windows were obtained by the method of matched asymptotics in [Ward et al. (2010)].

Chapter 7

The Mixed Boundary Value Problem in \mathbb{R}^2

7.1 A Neumann–Dirichlet Boundary Value Problem

The method of matched asymptotics used in Sect. 6.2.3 fails in certain important cases that arise in neuroscience (see Figs. 6.3, 7.1, and 7.2). Consider, for example, free Brownian motion in a bounded domain $\Omega \subset \mathbb{R}^d$ ($d = 2, 3$), whose boundary $\partial\Omega$ is sufficiently smooth (the analysis in higher dimensions is similar to that for $d = 3$). The Brownian trajectory $x(t)$ is reflected at the boundary, except for a small hole $\partial\Omega_a$, where it is absorbed, as shown in Fig. 6.3. The lifetime in Ω of a Brownian trajectory that starts at a point $x \in \Omega$ is the first passage time τ of the trajectory to the absorbing boundary $\partial\Omega_a$. As the size (e.g., the diameter) of the absorbing hole decreases to zero, but that of the domain remains finite, as described in Sect. 6.2 and in particular, in Sect. 6.2.1. A measure of smallness can be chosen as the ratio between the surface area of the absorbing boundary and that of the entire boundary, for example (6.4) and (6.5). The narrow escape time $v(x)$ satisfies the mixed boundary value problem for the Pontryagin–Andronov–Vitt equation (6.1)–(6.3). If Ω is a subset of a two-dimensional Riemannian manifold, as in Fig. 6.2, the Laplace operator is replaced with the Laplace–Beltrami operator (see Sect. 7.3 below).

Example 7.1 (A pathological example). When (6.5) is violated the narrow escape time does not necessarily increase to infinity as the relative area of the hole decreases to zero. This is illustrated by the following example. Consider a cylinder of length L and radius a . The boundary of the cylinder is reflecting, except for one of its bases (at $z = 0$, say), which is absorbing. The narrow escape time problem becomes one-dimensional and its solution is

$$v(z) = Lz - \frac{z^2}{2}. \quad (7.1)$$

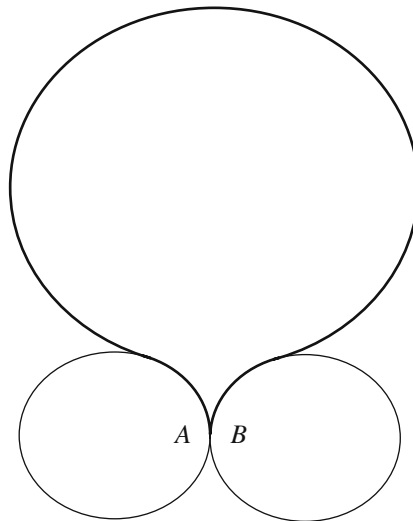


Fig. 7.1 **Left panel:** The planar (dimensional) domain Ω' is bounded by a large circular arc connected smoothly to a funnel formed by moving two tangent circular arcs of radius R_c apart a distance ε (i.e., $\overline{AB} = \varepsilon$). **Right panel:** Blowup of the cusp region. The solid, dashed, and dotted necks correspond to $\nu_{\pm} = 1, 0.4$, and 5 in (7.63), respectively

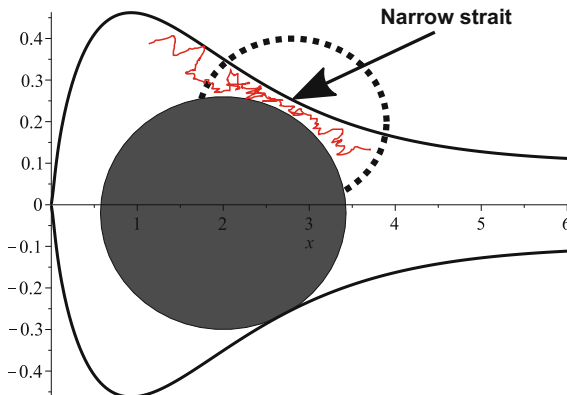


Fig. 7.2 Narrow straits formed by a partial block (solid disk) of the passage from the head to the neck of the domain enclosed by the black line. Inside the circle the narrow straits can be approximated by the gap between adjacent circles (a Brownian trajectory is moving inside the strait (red))

Here there is neither a boundary layer nor a constant outer solution; the narrow escape time grows gradually with z . The narrow escape time, averaged against a uniform initial distribution in the cylinder, is $\mathbb{E}\tau = L^2/3$ and is independent of a , that is, the assumption that the narrow escape time becomes infinite is violated. It holds, however, if the domain is sufficiently thick, e.g., if a ball of radius independent of ε can be rolled on the reflecting boundary inside the domain. \square

7.2 The Neumann Function

The Neumann function $N(\mathbf{x}, \xi)$ is a solution of the boundary value problem

$$\begin{aligned}\Delta_{\mathbf{x}} N(\mathbf{x}, \xi) &= -\delta(\mathbf{x} - \xi) \quad \text{for } \mathbf{x}, \xi \in \Omega, \\ \frac{\partial N(\mathbf{x}, \xi)}{\partial n(\mathbf{x})} &= -\frac{1}{|\partial\Omega|} \quad \text{for } \mathbf{x} \in \partial\Omega, \xi \in \Omega,\end{aligned}\tag{7.2}$$

and is defined up to an additive constant. Green's identity gives

$$\begin{aligned}&\int_{\Omega} [N(\mathbf{x}, \xi) \Delta v(\mathbf{x}) - v(\mathbf{x}) \Delta N(\mathbf{x}, \xi)] d\mathbf{x} \\&= \int_{\partial\Omega} \left[N(\mathbf{x}, \xi) \frac{\partial v(\mathbf{x})}{\partial n} - v(\mathbf{x}) \frac{\partial N(\mathbf{x}, \xi)}{\partial n} \right] dS_{\mathbf{x}} \\&= \int_{\partial\Omega} N(\mathbf{x}, \xi) \frac{\partial v(\mathbf{x})}{\partial n} dS_{\mathbf{x}} + \frac{1}{|\partial\Omega|} \int_{\partial\Omega} v(\mathbf{x}) dS_{\mathbf{x}}.\end{aligned}$$

On the other hand, equations (6.1) and (7.2) imply that

$$\int_{\Omega} [N(\mathbf{x}, \xi) \Delta v(\mathbf{x}) - v(\mathbf{x}) \Delta N(\mathbf{x}, \xi)] d\mathbf{x} = v(\xi) - \frac{1}{D} \int_{\Omega} N(\mathbf{x}, \xi) d\mathbf{x},$$

hence

$$\begin{aligned}v(\xi) - \frac{1}{D} \int_{\Omega} N(\mathbf{x}, \xi) d\mathbf{x} &= \int_{\partial\Omega} N(\mathbf{x}, \xi) \frac{\partial v(\mathbf{x})}{\partial n} dS_{\mathbf{x}} \\&\quad + \frac{1}{|\partial\Omega|} \int_{\partial\Omega} v(\mathbf{x}) dS_{\mathbf{x}}.\end{aligned}\tag{7.3}$$

Note that the second integral on the right-hand side of (7.3) is an additive constant. The integral

$$C_{\varepsilon} = \frac{1}{|\partial\Omega|} \int_{\partial\Omega} v(\mathbf{x}) dS_{\mathbf{x}}\tag{7.4}$$

is the average of $v(\mathbf{x})$ on the boundary. Now (7.3) takes the form

$$v(\xi) = \frac{1}{D} \int_{\Omega} N(\mathbf{x}, \xi) d\mathbf{x} + \int_{\partial\Omega_a} N(\mathbf{x}, \xi) \frac{\partial v(\mathbf{x})}{\partial n} dS_{\mathbf{x}} + C_{\varepsilon},\tag{7.5}$$

which is an integral representation of $v(\xi)$. Setting

$$g(x) = \frac{\partial v(x)}{\partial n} \text{ for } x \in \partial\Omega_a, \quad (7.6)$$

we use the boundary condition (6.2) and (7.6) to write (7.5) as

$$0 = \frac{1}{D} \int_{\Omega} N(x, \xi) dx + \int_{\Omega} N(x, \xi) g(x) dS_x + C_{\varepsilon}, \quad (7.7)$$

for all $\xi \in \partial\Omega_a$. Equation (7.7) is an integral equation for $g(x)$ and C_{ε} .

Theorem 7.2.1 [The Helmholtz equation] *Under the assumption that the solution $v(x)$ of (6.1)–(6.3) diverges to infinity for all $x \in \Omega$ as $\varepsilon \rightarrow \infty$, the leading order approximation to the boundary flux density $g(x)$ is the solution of the Helmholtz integral equation*

$$\int_{\partial\Omega_a} N(x, \xi) g(x) dS_x = -C_{\varepsilon} \text{ for } \xi \in \partial\Omega_a \quad (7.8)$$

for some constant C_{ε} .

Proof Indeed, to construct an asymptotic approximation to the solution, we note that the first integral in equation (7.7) is a regular function of ξ on the boundary. Indeed, due to the symmetry of the Neumann function, we have from (7.2)

$$\Delta_{\xi} \int_{\Omega} N(x, \xi) dx = -1 \text{ for } \xi \in \Omega \quad (7.9)$$

and

$$\frac{\partial}{\partial n(\xi)} \int_{\Omega} N(x, \xi) dx = -\frac{|\Omega|}{D} \text{ for } \xi \in \partial\Omega. \quad (7.10)$$

Equation (7.9) and the boundary condition (7.10) are independent of the hole $\partial\Omega_a$, so they define the first integral on the right-hand side of (7.7) as a regular function of ξ , up to an additive constant, also independent of $\partial\Omega_a$.

The assumption that for all $x \in \Omega$ the narrow escape time $v(x)$ diverges to infinity as $\varepsilon \rightarrow 0$ and (7.4) imply that $C_{\varepsilon} \rightarrow \infty$ in this limit. This means that for $\xi \in \partial\Omega_a$ the second integral in (7.7) must also become infinite in this limit, because the first integral is independent of $\partial\Omega_a$. Therefore, the leading order approximation to the solution $g(x)$ of the integral equation (7.7) is the solution of the Helmholtz equation (7.8). \square

7.3 The Mixed Boundary Value Problem on a Riemannian Manifold in \mathbb{R}^2

Again, the mixed boundary value problem arises in the context of a Brownian trajectory $\mathbf{x}(t)$ in a bounded domain Ω on a two-dimensional Riemannian manifold (Σ, g) (see the relevant references in Annotations 6.3). For a domain $\Omega \subset \Sigma$ with a smooth boundary $\partial\Omega$ (at least C^1), we denote by $|\Omega|_g$ the Riemannian surface area of Ω and by $|\partial\Omega|_g$ the arclength of its boundary, computed with respect to the metric g . The boundary $\partial\Omega$ is partitioned, as in the previous section, into an absorbing arc $\partial\Omega_a$ and the remaining part $\partial\Omega_r = \partial\Omega - \partial\Omega_a$ is reflecting for the Brownian trajectories. We assume that the absorbing part is small, that is, (6.4) holds in the form

$$\varepsilon = \frac{|\partial\Omega_a|_g}{|\partial\Omega|_g} \ll 1,$$

where Σ and Ω are independent of ε ; however, the partition of the boundary $\partial\Omega$ into absorbing and reflecting parts varies with ε . The first passage time τ of a Brownian trajectory from Ω to $\partial\Omega_a$ has finite expectation $u_\varepsilon(\mathbf{x}) = \mathbb{E}[\tau | \mathbf{x}(0) = \mathbf{x}]$ and the function $u_\varepsilon(\mathbf{x})$ satisfies the mixed Neumann–Dirichlet boundary value problem for the Poisson equation, (6.1)–(6.3), which in the context of Brownian motion is the Pontryagin–Andronov–Vitt equation, now written as

$$D\Delta_g u_\varepsilon(\mathbf{x}) = -1 \text{ for } \mathbf{x} \in \Omega \quad (7.11)$$

$$\frac{\partial u_\varepsilon(\mathbf{x})}{\partial n} = 0 \text{ for } \mathbf{x} \in \partial\Omega - \partial\Omega_a \quad (7.12)$$

$$u_\varepsilon(\mathbf{x}) = 0 \text{ for } \mathbf{x} \in \partial\Omega_a, \quad (7.13)$$

where D is the diffusion coefficient and Δ_g is the Laplace operator on Σ

$$\Delta_M f = \frac{1}{\sqrt{\det G}} \sum_{i,j} \frac{\partial}{\partial \xi_i} \left(g^{ij} \sqrt{\det G} \frac{\partial f}{\partial \xi_j} \right), \quad (7.14)$$

with

$$\mathbf{t}_i = \frac{\partial |\mathbf{x}|}{\partial \xi_i}, \quad g_{ij} = \langle \mathbf{t}_i, \mathbf{t}_j \rangle, \quad G = (g_{ij}), \quad g^{ij} = g_{ij}^{-1}. \quad (7.15)$$

Obviously, $u_\varepsilon(\mathbf{x}) \rightarrow \infty$ as $\varepsilon \rightarrow 0$, except for \mathbf{x} in a boundary layer near $\partial\Omega_a$.

Theorem 7.3.1 *Under the above assumptions $u_\varepsilon(\mathbf{x})$ is given by*

$$u_\varepsilon(\mathbf{x}) = \frac{|\Omega|_g}{\pi D} \left[\log \frac{1}{\varepsilon} + O(1) \right] \text{ for } \varepsilon \ll 1. \quad (7.16)$$

Proof Indeed, we fix the origin $\mathbf{0} \in \partial\Omega_a$ and represent the boundary curve $\partial\Omega$ in terms of the arclength s as $(x(s), y(s))$ and rescale s so that

$$\begin{aligned}\partial\Omega &= \left\{ (x(s), y(s)) : -\frac{1}{2} < s \leq \frac{1}{2} \right\} \\ \left(x\left(-\frac{1}{2}\right), y\left(-\frac{1}{2}\right) \right) &= \left(x\left(\frac{1}{2}\right), y\left(\frac{1}{2}\right) \right).\end{aligned}$$

We assume that the functions $x(s)$ and $y(s)$ are real analytic in the interval $2|s| < 1$ and that the absorbing part of the boundary $\partial\Omega_a$ is the arc

$$\partial\Omega_a = \{(x(s), y(s)) : |s| < \varepsilon\}.$$

The Neumann function can be written as

$$N(\mathbf{x}, \xi) = -\frac{1}{2\pi} \log d(\mathbf{x}, \xi) + v_N(\mathbf{x}; \xi) \text{ for } \mathbf{x} \in B_\delta(\xi), \quad (7.17)$$

where $B_\delta(\xi)$ is the geodesic ball of radius δ centered at ξ and $v_N(\mathbf{x}; \xi)$ is a regular function. Here $B_\delta(\xi) = \{\mathbf{x} \in \Sigma : d(\mathbf{x}, \xi) < \delta\}$; in the plane $d(\mathbf{x}, \xi) = |\mathbf{x} - \xi|$. We consider a normal geodesic coordinate system (x, y) at the origin, such that one of the coordinates coincides with the tangent coordinate to $\partial\Omega_a$. We choose unit vectors $\mathbf{e}_1, \mathbf{e}_2$ as an orthogonal basis in the tangent plane at 0 so that for any vector field $\mathbf{X} = x_1 \mathbf{e}_1 + x_2 \mathbf{e}_2$, the metric tensor g can be written as

$$g_{ij} = \delta_{ij} + \varepsilon^2 \sum_{kl} a_{ij}^{kl} x_k x_l + o(\varepsilon^2), \quad (7.18)$$

where $|x_k| \leq 1$, because ε is small. It follows that for \mathbf{x}, \mathbf{y} inside the geodesic ball of radius ε , centered at the origin, $d(\mathbf{x}, \mathbf{y}) = |\mathbf{x} - \mathbf{y}| + O(\varepsilon^2)$.

To construct an asymptotic expansion of the solution of (7.8) for small ε , we recall that when both \mathbf{x} and ξ are on the boundary, $v_N(\mathbf{x}, \xi)$ becomes singular (see [Garabedian (1964), p. 247, (7.46)] and the singular part gains a factor of 2, due to the singularity of the “image charge”. Denoting by \tilde{v}_N the new regular part, (7.8) becomes

$$\int_{|s'|<\varepsilon} \left[\tilde{v}_N(\mathbf{x}(s'); \xi(s)) - \frac{\log d(\mathbf{x}(s), \xi(s'))}{\pi} \right] f(s') S(ds') = C_\varepsilon, \quad (7.19)$$

where $S(ds')$ is the induced measure element on the boundary, $\mathbf{x} = (x(s), y(s))$, $\xi = (\xi(s), \eta(s))$, and $f(s') = g_0(\mathbf{x}(s'))$. Now, we expand

$$\log d(\mathbf{x}(s), \xi(s')) = \log \left(\sqrt{(x(s') - \xi(s))^2 + (y(s') - \eta(s))^2} \left(1 + O(\varepsilon^2) \right) \right)$$

and

$$S(ds)f(s) = \sum_{j=0}^{\infty} f_j s^j ds, \quad \tilde{v}_N(\mathbf{x}(s'); \boldsymbol{\xi}(s)) S(ds') = \sum_{j=0}^{\infty} v_j(s') s^j ds' \quad (7.20)$$

for $|s| < \varepsilon$, where $v_j(s')$ and f_j are unknown coefficients, to be determined from (7.19). To expand the logarithmic term in the last integral in (7.19), we recall that $x(s')$, $y(s')$, $\xi(s)$, and $\eta(s)$ are analytic functions of their arguments in the intervals $|s| < \varepsilon$ and $|s'| < \varepsilon$, respectively. Therefore

$$\begin{aligned} & \int_{-\varepsilon}^{\varepsilon} (s')^n \log d(\mathbf{x}(s), \boldsymbol{\xi}(s')) ds' \\ &= \int_{-\varepsilon}^{\varepsilon} (s')^n \log \sqrt{(x(s') - \xi(s))^2 + (y(s') - \eta(s))^2} (1 + O(\varepsilon^2)) ds' \\ &= \int_{-\varepsilon}^{\varepsilon} (s')^n \log \{|s' - s| (1 + O((s' - s)^2))\} (1 + O(\varepsilon^2)) ds'. \end{aligned} \quad (7.21)$$

We keep in the Taylor's expansion of $\log \{|s' - s| (1 + O((s' - s)^2))\}$ only the leading term, because higher-order terms contribute positive powers of ε to the series

$$\int_{-\varepsilon}^{\varepsilon} \log(s - s')^2 ds' = 4\varepsilon (\log \varepsilon - 1) + 2 \sum_{j=1}^{\infty} \frac{1}{(2j-1)j} \frac{s^{2j}}{\varepsilon^{2j-1}}. \quad (7.22)$$

For even $n \geq 0$ we have

$$\begin{aligned} & \int_{-\varepsilon}^{\varepsilon} (s')^n \log(s - s')^2 ds' \\ &= 4 \left(\frac{\varepsilon^{n+1}}{n+1} \log \varepsilon - \frac{\varepsilon^{n+1}}{(n+1)^2} \right) - 2 \sum_{j=1}^{\infty} s^{2j} \frac{\varepsilon^{n-2j+1}}{j(n-2j+1)}, \end{aligned} \quad (7.23)$$

whereas for odd n , we have

$$\int_{-\varepsilon}^{\varepsilon} (s')^n \log(s - s')^2 ds' = -4 \sum_{j=1}^{\infty} \frac{s^{2j+1}}{2j+1} \frac{\varepsilon^{n-2j}}{n-2j}.$$

Using the above expansion, we rewrite (7.19) as

$$0 = \int_{-\varepsilon}^{\varepsilon} \left\{ \frac{-1}{\pi} \log [|s' - s|^2 (1 + O((s' - s)^2)) (1 + O(\varepsilon^2))] + \sum_{j=0}^{\infty} v_j(s') s^j \right\} \\ \times \sum_{j=0}^{\infty} f_j s'^j ds' + C_{\varepsilon},$$

and expand in powers of s . At the leading order, we obtain

$$\begin{aligned} & \varepsilon (\log \varepsilon - 1) f_0 + \sum_p \left(\frac{\varepsilon^{2p+1}}{2p+1} \log \varepsilon - \frac{\varepsilon^{2p+1}}{(2p+1)^2} \right) f_{2p} \\ &= \frac{\pi}{2} \int_{-\varepsilon}^{\varepsilon} v_0(s') ds' + C_{\varepsilon}. \end{aligned} \quad (7.24)$$

Equation (7.24) and

$$\frac{1}{2} \int_{-\varepsilon}^{\varepsilon} f(s) S(ds) = \sum_p \frac{\varepsilon^{2p+1}}{(2p+1)} f_{2p}$$

determine the leading order term in the expansion of C_{ε} . Indeed, the compatibility condition (6.6) gives

$$\int_{-\varepsilon}^{\varepsilon} f(s) S(ds) = -|\Omega|_g, \quad (7.25)$$

so using the fact that $\int_{-\varepsilon}^{\varepsilon} v_0(s') S(ds') = O(\varepsilon)$, we find that the leading order expansion of C_{ε} in (7.24) is

$$C_{\varepsilon} = \frac{|\Omega|_g}{\pi} \left[\log \frac{1}{\varepsilon} + O(1) \right] \quad \text{for } \varepsilon \ll 1. \quad (7.26)$$

If the diffusion coefficient is D , (7.8) gives the narrow escape time from a point $\mathbf{x} \in \Omega$, outside the boundary layer, as

$$\mathbb{E}[\tau | \mathbf{x}] = u_{\varepsilon}(\mathbf{x}) = \frac{|\Omega|_g}{\pi D} \left[\log \frac{1}{\varepsilon} + O(1) \right] \quad \text{for } \varepsilon \ll 1. \quad (7.27)$$

See Annotations 7.10 for further elaboration on this problem.

Example 7.2 (Domains with corners). For a small hole at a corner of an opening angle α (see Fig. 7.3), the solution at $\mathbf{x} \in \Omega$, outside a boundary layer near the hole, is to leading order

$$u_\varepsilon(\mathbf{x}) = \frac{|\Omega|}{\Omega\alpha} \left(\log \frac{1}{\varepsilon} + O(1) \right). \quad (7.28)$$

Indeed, putting the origin at the apex of the angle and the real axis on one of the rays of the angle, the conformal mapping $z \mapsto z^{\pi/\alpha}$ of Ω flattens the corner and leaves $\partial\Omega_a$ small. The Neumann function for the upper half plane, $\pi^{-1} \log z$, is transformed into $\alpha^{-1} \log z$, so (7.27) gives (7.28).

To see that the area factor $|\Omega|$ remains unchanged under any conformal mapping $f : (x, y) \mapsto (u(x, y), v(x, y))$, we note that this factor is a consequence of the compatibility condition (6.6), that relates the area to the integral

$$\int_{\Omega} \Delta_{(x,y)} w \, dx \, dy = -\frac{|\Omega|}{D},$$

where $w(x, y) = \mathbb{E}[\tau | x(0) = x, y(0) = y]$ satisfies $\Delta_{(x,y)} w = -1/D$. According to the Cauchy–Riemann equations, the Laplacian transforms as

$$\Delta_{(x,y)} w = (u_x^2 + u_y^2) \Delta_{(u,v)} w$$

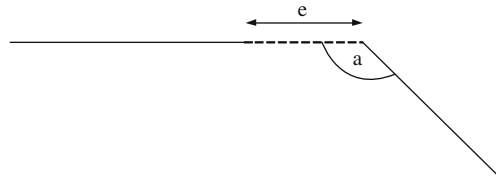


Fig. 7.3 A small opening near a corner of angle α

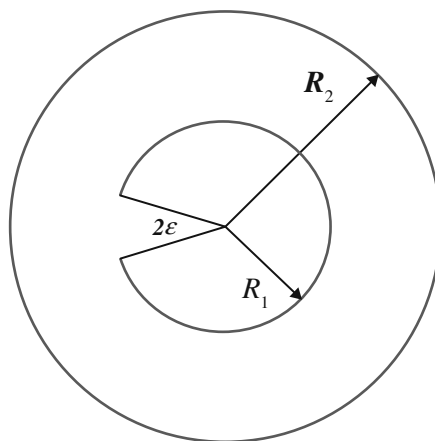


Fig. 7.4 An annulus $R_1 < r < R_2$. The particle is absorbed at an arc of length $2\varepsilon R_1$ (dashed line) at the inner circle. The solid lines indicate reflecting boundaries

and the Jacobian of the transformation is $J = u_x^2 + u_y^2$. Therefore,

$$\int_{\Omega} \Delta_{(x,y)} w \, dx \, dy = \int_{f(\Omega)} \Delta_{(u,v)} w \, du \, dv.$$

This means that the compatibility condition remains unchanged and gives the area of the original domain. Higher-order asymptotics are given in [Singer et al. III (2006a)]. \square

Exercise 7.1 (The solution in an annulus). Use a conformal mapping to find the leading asymptotic expansion of the solution with homogeneous Neumann conditions on the boundary of an annulus, with a small arc on one of the bounding circles, where homogeneous Dirichlet conditions are imposed (see Fig. 7.4). Higher order asymptotics are given in [Singer et al. III (2006a)]. \square

Example 7.3 (Domains with cusps). Consider the mixed boundary value problem for the Poisson (or Pontryagin–Andronov–Vitt) equation with a small Dirichlet boundary near a cusp. A cusp is a singular point of the boundary. As $\alpha = 0$ at the cusp, one expects to find a different asymptotic expansion than (7.28). As an example, consider the Pontryagin–Andronov–Vitt equation inside the domain Ω bounded between the circles $(x - 1/2)^2 + y^2 = 1/4$ and $(x - 1/4)^2 + y^2 = 1/16$ (see Fig. 7.5). *The conformal mapping $z \mapsto \exp\{\pi i(1/z - 1)\}$ maps Ω onto the upper half plane. Therefore, the solution outside a boundary layer near the cusp is to leading order*

$$u_\varepsilon(\mathbf{x}) = \frac{|\Omega|}{D} \left(\frac{1}{\varepsilon} + O(1) \right). \quad (7.29)$$

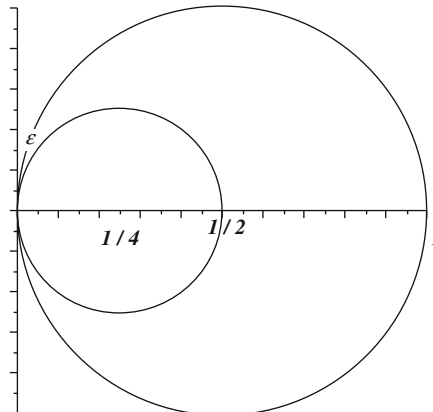


Fig. 7.5 The point $(0, 0)$ is a cusp point of the dotted domain bounded between the two circles. The small absorbing arc of length ε is located at the cusp point

This result can also be obtained by mapping the cusped domain to the unit circle. The absorbing boundary is then transformed to an exponentially small arc of length $\exp\{-\pi/\varepsilon\} + O(\exp\{-2\pi/\varepsilon\})$ and equation (7.29) is recovered.

If the ratio between the two radii, d , is less than 1, then Ω is mapped conformally onto the upper half plane by the function $\exp\{\pi i(1-z)/(d^{-1}-1)z\}$ (for $d = 1/2$ we arrive at the previous example), so the solution outside the boundary layer is to leading order

$$u_\varepsilon(\mathbf{x}) = \frac{|\Omega|}{(d^{-1}-1)D} \left(\frac{1}{\varepsilon} + O(1) \right). \quad (7.30)$$

The solution $u_\varepsilon(\mathbf{x})$ tends algebraically fast to infinity, much faster than the $O(\log \varepsilon^{-1})$ behavior near smooth or corner boundaries. The narrow escape time for a cusp is then much larger, because it is harder for the Brownian motion to enter a cusp than to enter a corner. The narrow escape time (7.29) can be written in terms of d instead of the area. Substituting $|\Omega| = \pi R^2(1-d^2)$, we find that

$$\mathbb{E}\tau = \frac{\pi R^2 d(1+d)}{D} \left(\frac{1}{\varepsilon} + O(1) \right), \quad (7.31)$$

where R is the radius of the outer circle. Note that although the area of Ω is a monotonically decreasing function of d , the narrow escape time is a monotonically increasing function of d and tends to a finite limit as $d \rightarrow 1$.

Similarly, one can consider different types of cusps and find that the leading order term in the asymptotic expansion of the solution is proportional to $1/\varepsilon^\lambda$, where λ is a parameter that describes the order of the cusp, and can be obtained by the same method of conformal mapping (see [Singer et al. III (2006a)]). \square

Example 7.4 (The mixed boundary value problem on the 3-sphere). Consider the Pontryagin–Andronov–Vitt equation on the surface of a 3-sphere of radius R , described by the spherical coordinates, (θ, ϕ) as

$$x = R \sin \theta \cos \phi, \quad y = R \sin \theta \sin \phi, \quad z = R \cos \theta.$$

In spherical coordinates, equations (7.14) and (7.15) give [John (1982)]

$$g_{\theta\theta} = R^2, \quad g_{\phi\phi} = R^2 \sin^2 \theta, \quad g_{\theta\phi} = g_{\phi\theta} = 0. \quad (7.32)$$

Therefore, for a function $f(\theta, \phi)$ on the 3-sphere, the Laplace–Beltrami operator Δ_M is given by

$$\Delta_M f = R^{-2} \left(\frac{\partial^2 f}{\partial \theta^2} + \cot \theta \frac{\partial f}{\partial \theta} + \frac{1}{\sin^2 \theta} \frac{\partial^2 f}{\partial \phi^2} \right).$$

(i) *Dirichlet conditions on a small absorbing cap.* This problem describes absorption of Brownian trajectories on the 3-sphere when they reach a short arc of a small

spherical cap, centered at the north pole $\theta = 0$, whose opening angle is $\delta \ll 1$ (see Fig. 7.6). Furthermore, due to rotational symmetry, the first passage time to the spherical cap is independent of the initial angle ϕ . Thus the solution $v(\theta)$ of the boundary value problem

$$\Delta_M v = R^{-2} (v'' + \cot \theta v') = -1 \quad (7.33)$$

$$v'(\pi) = 0, \quad v(\delta) = 0 \quad (7.34)$$

(the mean first passage time to the cap) is given by

$$v(\theta) = 2R^2 \log \frac{\sin \frac{\theta}{2}}{\sin \frac{\delta}{2}}. \quad (7.35)$$

(ii) *Mapping of the Riemann sphere.* A different approach to the construction of the solution to the mixed boundary value problem (i.e., of constructing the mean first passage time of Brownian motion on the 3-sphere) is based on the stereographic projection of the sphere onto the plane [Hille (1976)]. We may assume that the radius of the sphere is $1/2$ and project the point $Q = (\xi, \eta, \zeta)$ on the sphere (often called the Riemann sphere)

$$\xi^2 + \eta^2 + \left(\zeta - \frac{1}{2} \right)^2 = \left(\frac{1}{2} \right)^2$$

to the plane point $P = (x, y, 0)$ by the mapping

$$x = \frac{\xi}{1 - \zeta}, \quad y = \frac{\eta}{1 - \zeta}, \quad r^2 = x^2 + y^2 = \frac{\zeta}{1 - \zeta}.$$

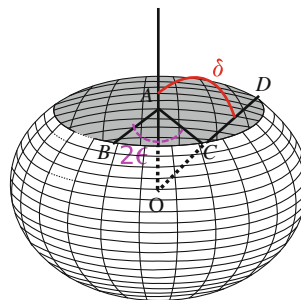


Fig. 7.6 A sphere of radius $R = 1/2$ without a spherical cap at the north pole with central angle $\angle AOD = \delta$ (red). In Example 7.4(i) the Brownian motion is absorbed at the boundary of the cap. In Example 7.4(ii) it is absorbed only at the arc of central angle $\angle BAC = 2\epsilon$ (purple) on the boundary of the cap

Conversely,

$$\xi = \frac{x}{1+r^2}, \quad \eta = \frac{y}{1+r^2}, \quad \zeta = \frac{r^2}{1+r^2}.$$

The stereographic projection is conformal and therefore transforms harmonic functions on the sphere to harmonic functions in the plane, and *vice versa*. However, the stereographic projection is not an isometry. The Laplace operator Δ_M on the sphere is mapped onto the operator $(1+r^2)^2 \Delta$ in the plane (Δ is the Cartesian Laplacian). The decapitated sphere is mapped onto the interior of a circle of radius

$$r_\delta = \cot \frac{\delta}{2}.$$

Therefore, the boundary value problem on the sphere is transformed into the planar Poisson radial problem

$$\Delta V = -\frac{1}{(1+r^2)^2} \text{ for } r < r_\delta,$$

subject to the absorbing boundary condition

$$V(r_\delta) = 0,$$

where

$$V(r) = v(\theta).$$

The solution of this problem is

$$V(r) = \frac{1}{4} \log \left(\frac{1+r_\delta^2}{1+r^2} \right). \quad (7.36)$$

Transforming back to the coordinates on the sphere, we get

$$v(\theta) = \frac{1}{2} \log \frac{\sin \frac{\theta}{2}}{\sin \frac{\delta}{2}}. \quad (7.37)$$

As the actual radius of the sphere is R rather than $1/2$, multiplying (7.37) by $(2R)^2$, we find that (7.37) is exactly (7.35).

(iii) The mixed boundary value problem for a short Dirichlet arc on a small cap. Consider again the mixed boundary value problem on a decapitated 3-sphere of radius $1/2$. Assume a Neumann boundary on the spherical cap but for a small Dirichlet arc (an absorbing window, see Fig. 7.6). The solution (the mean first passage time to the absorbing arc), is constructed by the stereographic projection of the preceding example, which gives

$$\begin{aligned}\Delta v &= -\frac{1}{(1+r^2)^2}, \text{ for } r < r_\delta, \quad 0 \leq \phi < 2\pi, \\ v(r, \phi) \Big|_{r=r_\delta} &= 0, \text{ for } |\phi - \pi| < \varepsilon, \\ \frac{\partial v(r, \phi)}{\partial r} \Big|_{r=r_\delta} &= 0, \text{ for } |\phi - \pi| > \varepsilon.\end{aligned}\tag{7.38}$$

The function

$$w(r) = \frac{1}{4} \log \left(\frac{1+r_\delta^2}{1+r^2} \right)$$

is the solution of the all-absorbing-boundary problem (7.36), so the function $u = v - w$ satisfies the mixed boundary value problem

$$\begin{aligned}\Delta u &= 0, \quad r < r_\delta, \text{ for } 0 \leq \phi < 2\pi, \\ u(r, \phi) \Big|_{r=r_\delta} &= 0, \text{ for } |\phi - \pi| < \varepsilon, \\ \frac{\partial u(r, \phi)}{\partial r} \Big|_{r=r_\delta} &= \frac{r_\delta}{2(1+r_\delta^2)}, \text{ for } |\phi - \pi| > \varepsilon.\end{aligned}\tag{7.39}$$

Scaling $\tilde{r} = r/r_\delta$, we find this mixed boundary value problem to be that of a planar disk, with the only difference that the constant $1/2$ is now replaced by $r_\delta^2/2(1+r_\delta^2)$. Therefore, the solution is given by

$$a_0 = -\frac{2r_\delta^2}{1+r_\delta^2} \left[\log \frac{\varepsilon}{2} + O(\varepsilon) \right].\tag{7.40}$$

Transforming back to the spherical coordinate system, we find the solution (the narrow escape time) as

$$\begin{aligned}v(\theta, \phi) &= \frac{1}{2} \log \frac{\sin \frac{\theta}{2}}{\sin \frac{\delta}{2}} \\ &\quad - \cos^2 \frac{\delta}{2} \left[\log \frac{\varepsilon}{2} + O(\varepsilon) \right] + \sum_{n=1}^{\infty} a_n \left(\frac{\cot \frac{\theta}{2}}{\cot \frac{\delta}{2}} \right)^n \cos n\phi.\end{aligned}\tag{7.41}$$

Averaging with respect to x with a uniform distribution (i.e., with respect to uniformly distributed initial conditions of the Brownian trajectory) on the decapitated sphere, we obtain the averaged narrow escape time

$$\mathbb{E}\tau = -\frac{1}{2} \left(\frac{\log \sin \frac{\delta}{2}}{\cos^2 \frac{\delta}{2}} + \frac{1}{2} \right) + \cos^2 \frac{\delta}{2} \left[\log \frac{2}{\varepsilon} + O(\varepsilon) \right].\tag{7.42}$$

Scaling the radius R of the sphere into (7.42), we find that for small ε and δ the averaged narrow escape time is

$$\mathbb{E}\tau = 2R^2 \left[\log \frac{1}{\delta} + 2 \log \frac{1}{\varepsilon} + 3 \log 2 - \frac{1}{2} + O(\varepsilon, \delta^2 \log \delta, \delta^2 \log \varepsilon) \right].$$

There are two different contributions to the solution. The ratio ε between the absorbing arc and the entire boundary brings in a logarithmic contribution, which is to leading order

$$\frac{|\Omega|_g}{\pi} \log \frac{1}{\varepsilon}.$$

However, the central angle δ gives an additional logarithmic contribution, of the form

$$\frac{|\Omega|_g}{2\pi} \log \frac{1}{\delta}.$$

The factor 2 difference in the asymptotic expansions is the same as encountered in the planar annulus problem. \square

Exercise 7.2 (i) Show that the maximum of the solution (of the narrow escape time) in Example 7.4(i) is attained at the point $\theta = \pi$ with the value

$$v_{\max} = v(\pi) = -2R^2 \log \sin \frac{\delta}{2} = 2R^2 \left[\log \frac{1}{\delta} + \log 2 + O(\delta^2) \right]. \quad (7.43)$$

(ii) Show that the narrow escape time, averaged with respect to a uniform initial distribution, is

$$\begin{aligned} \mathbb{E}\tau &= \frac{1}{2 \cos^2 \frac{\delta}{2}} \int_{-\delta}^{\pi} v(\theta) \sin \theta d\theta \\ &= -2R^2 \left[\frac{\log \sin \frac{\delta}{2}}{\cos^2 \frac{\delta}{2}} + \frac{1}{2} \right] \\ &= 2R^2 \left[\log \frac{1}{\delta} + \log 2 - \frac{1}{2} + O(\delta^2 \log \delta) \right]. \end{aligned}$$

(iii) Show that both the average narrow escape time and the maximum narrow escape time are

$$\mathbb{E}\tau = \frac{|\Omega|_g}{2\pi} \left(\log \frac{1}{\delta} + O(1) \right), \quad (7.44)$$

where $|\Omega|_g = 4\pi R^2$ is the surface area of the 3-sphere.

(iv) Show that this asymptotic expansion is the same as that for the planar problem of an absorbing circle in a disk. The result is two times smaller than the result (7.27)

that holds when the absorbing boundary is a small window in a reflecting boundary. Explain the difference in the factor 2 by the different aspect angle that the Brownian motion sees $\partial\Omega_a$. Show that the two problems also differ in that the narrow escape time is almost constant and has a boundary layer near the window, with singular fluxes near the edges, whereas in the problem of a puncture hole inside a domain the flux is regular and there is no boundary layer (the solution is simply obtained by solving the ordinary differential equation). \square

Exercise 7.3 (i) Show that if the Brownian trajectory in Example 7.4(iii) is initiated at the south pole $\theta = \pi$, then the narrow escape time is

$$\begin{aligned} v(\pi) &= -2R^2 \log \sin \frac{\delta}{2} - 4R^2 \cos^2 \frac{\delta}{2} \left[\log \frac{\varepsilon}{2} + O(\varepsilon) \right] \\ &= 2R^2 \left[\log \frac{1}{\delta} + 2 \log \frac{1}{\varepsilon} + 3 \log 2 + O(\varepsilon, \delta^2 \log \delta, \delta^2 \log \varepsilon) \right]. \end{aligned}$$

(ii) Show that $\phi = 0$ is the initial point (θ, ϕ) of the trajectory for which the narrow escape time is maximal in Exercise 7.4(i). Use the stationarity condition $\partial v / \partial \phi = 0$, which implies that $\phi = 0$, as expected (the opposite ϕ -direction to the center of the window).

(iii) Show that the infinite sum in equation (7.41) is $O(1)$. Conclude that for $\delta \ll 1$ the narrow escape time is maximal near the south pole $\theta = \pi$. However, for $\delta = O(1)$, the location of the maximal mean first passage time is more complex.

(iv) Show that the stereographic projection also leads to the determination of the narrow escape time for Brownian motion on a 3-sphere with a small hole, as discussed above, and an all reflecting spherical cap at the south pole. In this case, the image for the stereographic projection is the annulus. \square

7.3.1 Exit through Several Windows

The diffusion flux through a cluster of small absorbing windows in an otherwise reflecting boundary of a domain depends on the relative distance between the windows. For example, splitting an absorbing window into two equal parts and moving them apart increases the absorption flux by nearly 50% (see Annotations 6.3 for reference). Thus, the case of several targets is not a straightforward generalization of the single target case. In fact, the mean first passage time of a Brownian trajectory to any one of several targets $\partial\Omega_a$ contains information about their relative distances. In particular, when the small Dirichlet windows form a cluster, the mean first passage time to any one of them is influenced by the others, which is not the case for well separated windows.

First, we consider exit through two windows. For a regular domain in \mathbb{R}^2 with two Dirichlet arcs of lengths 2ε and 2δ (normalized by the perimeter $|\partial\Omega|$) and separated by the Euclidean distance $\Delta = \varepsilon + \Delta' + \delta$ between the centers, and in a regular domain in \mathbb{R}^3 with two Dirichlet circular windows of small radii a and b , separated by the Euclidean distance $\Delta = a + \Delta' + b$ between the centers (see Fig. 7.7), the narrow escape time $\bar{\tau}_\varepsilon$ is given by

$$\bar{\tau}_\varepsilon = \frac{|\Omega|}{\pi D \left(\log \frac{1}{\varepsilon} + \log \frac{1}{\delta} \right)} \frac{\log \frac{1}{\delta} \log \frac{1}{\varepsilon} - [\log |\varepsilon + \Delta' + \delta| + O(1)]^2}{1 + 2 \frac{\log |\varepsilon + \Delta' + \delta| + O(1)}{\log \frac{1}{\delta} + \log \frac{1}{\varepsilon}}} \quad (7.45)$$

as $a, b, \varepsilon, \delta, \Delta' \rightarrow 0$. As the windows drift apart the narrow escape time becomes the sum of the single window narrow escape times. A new result is obtained as the windows touch (for $d = 3$) or merge (for $d = 2$).

7.3.2 The Helmholtz Equation for Two Windows

To generalize (7.8) to the case of two windows, we note that the conditional narrow escape time $u(\mathbf{x}) = E[\tau | \mathbf{x}(0) = \mathbf{x}]$, of a Brownian trajectory $\mathbf{x}(t)$ that starts at $\mathbf{x} \in \Omega$ and escapes through a hole, is the solution of the mixed boundary value problem (6.1)–(6.3),

$$\Phi_A = - \int_A g(\mathbf{x}) dS_{\mathbf{x}}, \quad \Phi_B = - \int_B g(\mathbf{x}) dS_{\mathbf{x}},$$

where for $\mathbf{x} \in \partial\Omega_a$, the function $g(\mathbf{x}) = D\partial u(\mathbf{x})/\partial n$ is the absorption flux density. To compute the fluxes, we first integrate equation (6.1) over the domain and get

$$\Phi_A + \Phi_B = |\Omega|. \quad (7.46)$$

The solution of (6.1)–(6.3) is represented as

$$u(\xi) = \int_{\Omega} N(\mathbf{x}, \xi) d\mathbf{x} + \int_{\partial\Omega_a} N(\mathbf{x}, \xi) \frac{\partial u(\mathbf{x})}{\partial n} dS_{\mathbf{x}} + C,$$

where $C = |\partial\Omega|^{-1} \oint_{\partial\Omega} u(\mathbf{x}) dS_{\mathbf{x}}$ is a constant to be determined from the boundary condition (6.2) and $dS_{\mathbf{x}}$ is a surface area element on $\partial\Omega_a$. To determine C , we choose, respectively, $\xi \in A$ and $\xi \in B$, and using the boundary condition (6.2), we obtain the two equations

$$F(\xi) = \int_A N(\mathbf{x}, \xi) g_A(\mathbf{x}) dS_{\mathbf{x}} + \int_B N(\mathbf{x}, \xi) g_B(\mathbf{x}) dS_{\mathbf{x}} \text{ for } \xi \in A \cup B, \quad (7.47)$$

where

$$F(\xi) = - \left(\int_{\Omega} N(x, \xi) dx + C \right) \approx -C. \quad (7.48)$$

Equation (7.48), which is a generalization of (7.8), is also called the Helmholtz integral equation [Helmholtz (1860)]. We denote the centers of the absorbing disks (arcs) A and B by $\mathbf{0}_A$ and $\mathbf{0}_B$, respectively. The variables r and r' are the signed arclengths in A and B , measured from their centers. The equations for the fluxes g_A and g_B in the windows A and B form an approximate solution of (7.47) for well-separated windows A and B and constants \tilde{g}_A , \tilde{g}_B . They are only approximations, because the integral $\int_B N(x, \xi) g_B(x) dS_x$ is not constant for $\xi \in A$, though it is much smaller than $\int_A N(x, \xi) g_A(x) dS_x$ there. If, however, A and B are not well separated, the flux expressions are not even an approximate solution, because the integrals are of comparable orders of magnitude.

The solution of the two equations (7.48) when the windows are well separated is shown in the Helmholtz Lemma 8.1.1 below to be the flux densities through a single hole of size 2ε and is given by

$$g_A(x) \sim \frac{\tilde{g}_A f\left(\frac{r}{\varepsilon}\right)}{\sqrt{1 - \frac{r^2}{\varepsilon^2}}} \text{ for } x \in A, d = 2 \quad (7.49)$$

and a similar expression for $x \in B$, where $f(\alpha)$ is a positive smooth function for $|\alpha| \leq 1$ such that $f(0) = 1$.

7.3.3 Asymptotic Solution of the Helmholtz Equation

The expression (7.49) for the flux density, where $f(x)$ is a smooth positive even function for $-1 \leq x \leq 1$ and $f(0) = 1$, contains a constant \tilde{g}_A and, similarly, there is a constant \tilde{g}_B for window B . Thus the solution of (7.47) is

$$\begin{aligned} g_A(r) &= \frac{\tilde{g}_A f\left(\frac{r}{\varepsilon}\right)}{\sqrt{1 - \frac{r^2}{\varepsilon^2}}} \text{ for } -\varepsilon \leq r \leq \varepsilon, \\ g_B(r) &= \frac{\tilde{g}_B f\left(\frac{r}{\varepsilon}\right)}{\sqrt{1 - \frac{r^2}{\varepsilon^2}}} \text{ for } \varepsilon + \Delta' \leq r \leq 3\varepsilon + \Delta'. \end{aligned}$$

Because f is a positive smooth function for $-1 \leq x \leq 1$ and because for $1 + \Delta'/\varepsilon \leq x \leq 3 + \Delta'/\varepsilon$, such that $f(0) = f(2 + \Delta'/\varepsilon) = 1$, we have $f_\Delta(0) = f_\Delta(2 + \Delta'/\varepsilon) = 1$. For small ε and all $\xi \geq \varepsilon$, we approximate

$$\int_A N(\mathbf{x}, \xi) g_A(\mathbf{x}) dS_{\mathbf{x}} = \varepsilon \alpha \tilde{g}_A[N(\mathbf{0}_A, \mathbf{0}_B) + O(1)], \quad (7.50)$$

where

$$\alpha = \int_{-1}^1 \frac{f(x) dx}{\sqrt{1-x^2}} \quad (7.51)$$

and the Neumann function for the variables \mathbf{x} and ξ at the centers of the two windows, respectively, is given by

$$N(\mathbf{0}_A, \mathbf{0}_B) = -\frac{1}{\pi} \log(\varepsilon + \delta + \Delta') + O(1).$$

Using (7.50) and the Helmholtz Lemma 8.1.1 below, we get that

$$\begin{aligned} \int_A N(\mathbf{x}, \xi) g_A(\mathbf{x}) dS_{\mathbf{x}} &\approx \\ &\begin{cases} \frac{\alpha \varepsilon [-\log \varepsilon + \pi v_S(0, \varepsilon)] \tilde{g}_A}{D\pi} & \text{for } \xi \in A \\ -\varepsilon \alpha \tilde{g}_A N(\mathbf{0}_A, \mathbf{0}_B) + O(1) & \text{for } \xi \in B. \end{cases} \end{aligned} \quad (7.52)$$

An analogous expression is obtained for $\mathbf{x} \in B$ and $\xi \in A$ (with β instead of α). Using the boundary conditions (7.47) and the approximation (7.52), we obtain that

$$\begin{aligned} &\frac{\alpha \varepsilon (\log \varepsilon) \tilde{g}_A [1 + o(1)]}{\pi} + \frac{\beta \delta \tilde{g}_B [\log(\varepsilon + \delta + \Delta') + O(1)]}{\pi} \\ &= \frac{\varepsilon \alpha \tilde{g}_A [\log(\varepsilon + \delta + \Delta') + O(1)]}{\pi} + \frac{\beta \delta (\log \delta) \tilde{g}_B [1 + o(1)]}{\pi} = C. \end{aligned}$$

The flux condition (7.46) gives for small ε that

$$\int_A g_A(\mathbf{x}) dS_{\mathbf{x}} = \int_{-\varepsilon}^{\varepsilon} \frac{\tilde{g}_A f\left(\frac{r}{\varepsilon}\right)}{\sqrt{1 - \frac{r^2}{\varepsilon^2}}} dr (1 + o(1)) = \alpha \varepsilon \tilde{g}_A (1 + o(1)),$$

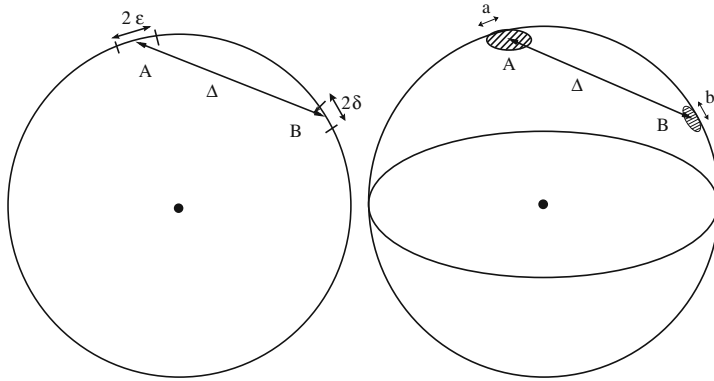


Fig. 7.7 Schematic representation of a disk and a sphere with two holes on the boundary. In the plane, the arclengths of the holes are 2δ and 2ε , respectively, at Euclidean distance Δ apart, while in \mathbb{R}^3 , the radii of the holes are, respectively, a and b

hence, for $d = 2$, (7.46) gives

$$\alpha\varepsilon\tilde{g}_A + \beta\delta\tilde{g}_B = -|\Omega|[1 + o(1)]. \quad (7.53)$$

Therefore, we get for the constant $C = \bar{\tau}_{A \cup B}$, which is the mean first passage time to any one of the two windows,

$$C = \frac{|\Omega|[1 + o(1)]}{\pi \left(\log \frac{1}{\varepsilon} + \log \frac{1}{\delta} \right)} \frac{\log \frac{1}{\delta} \log \frac{1}{\varepsilon} - [\log(\varepsilon + \Delta' + \delta) + O(1)]^2}{1 - 2 \frac{[\log(\varepsilon + \Delta' + \delta) + O(1)]}{\log \frac{1}{\delta} + \log \frac{1}{\varepsilon}}}. \quad (7.54)$$

Equation (7.54) reduces to the single window formula (7.27) in the limit $\delta \rightarrow 0$. The condition (7.46) gives

$$\alpha\varepsilon\tilde{g}_A + \beta\delta\tilde{g}_B = -|\Omega|(1 + o(1)). \quad (7.55)$$

The effect of varying the distance between the windows is shown in Fig. 7.8. The improved approximation

$$\bar{v} \sim \frac{|\Omega|}{D\pi} \left[-\frac{1}{2} \log \left(\frac{\varepsilon l}{4} \right) - \frac{\pi}{2} \log |x_2 - x_1| + \pi R_* \right] \quad (7.56)$$

for $O(\varepsilon) \ll |x_2 - x_1| \ll O(1)$,

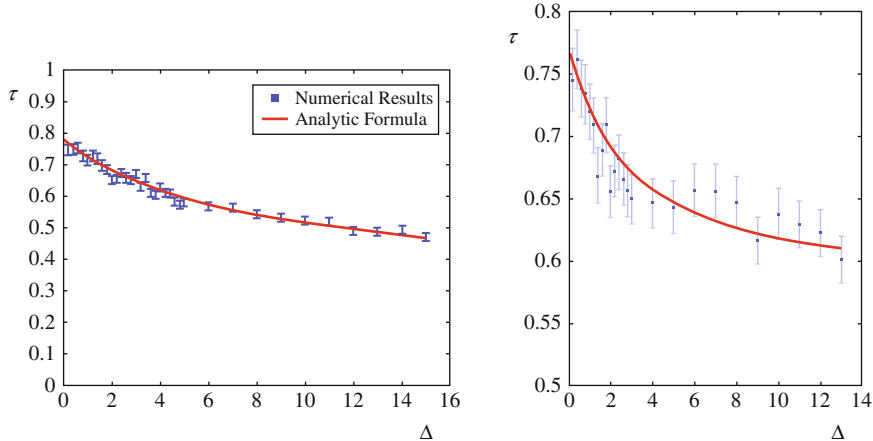


Fig. 7.8 The mean first passage time τ , normalized by τ_1 (the narrow escape time for a single window), as a function of the distance Δ between two holes, normalized by ε . **Top:** The mean first passage time for $d = 2, \varepsilon = \delta = 0.02, D = 1$. The cell radius is $R = 2$. The contribution of the regular part of the Green function is estimated as 1.3 by a numerical fit. **Bottom:** The values of the parameters are $d = 3, a = \varepsilon = \delta = 0.3, R = 2, D = 1$

where $R_* \equiv R(x_1^*, x_1^*)$ is the regular part of the Neumann function at $x_1^* \in \partial\Omega$, can be derived (see Annotations 6.3). In general,

$$\bar{v} \sim \begin{cases} \frac{|\Omega|}{D\pi} \left[-\log(\varepsilon d_1) + \pi R_* \right] & \text{for a two-window cluster} \\ \frac{|\Omega|}{D\pi} \left[-\frac{1}{2} \log \left(\frac{\varepsilon l}{4} \right) + \frac{\pi}{4} (R(x_1; x_1) + R(x_2; x_2) + 2G(x_1; x_2)) \right] & \text{for well-separated windows.} \end{cases}$$

Here $x_1^* \in \partial\Omega$ is the center of the two-window cluster, $R_* \equiv R(x_1^*, x_1^*)$ is the regular part of the Neumann function at x_1^* , and

$$d_1 = \frac{l}{2} \left[1 + \frac{2a}{l} \right]^{1/2}, \quad (7.57)$$

where $2a$ is the distance along the boundary between the two windows. For the special case of the unit disk $\Omega = \mathcal{D}(1)$, where the regular part R has the uniform value $R = 1/(8\pi)$, the Neumann function $G(x; \xi)$ with $\int_{\mathcal{D}(1)} G(x; \xi) dx = 0$ and $\xi \in \partial\mathcal{D}(1)$ is given by

$$G(x; \xi) = -\frac{1}{\pi} \log |x - \xi| + \frac{|x|^2}{4\pi} - \frac{1}{8\pi}, \quad R(\xi; \xi) = \frac{1}{8\pi}. \quad (7.58)$$

The solution to the boundary value problem with N equal Dirichlet arcs of length 2ε , centered at x_1, \dots, x_N on the boundary of the unit disk, averaged with respect to the initial position (the averaged mean first passage time), is

$$\bar{v} \sim \frac{1}{DN} \left[-\log\left(\frac{\varepsilon}{2}\right) + \frac{N}{8} - \frac{1}{N} \sum_{i=1}^N \sum_{j \neq i}^N \log |x_i - x_j| \right]. \quad (7.59)$$

The sum in (7.59) is minimized when $x_j = e^{2\pi ij/N}$ are the equally spaced N th roots of unity,

$$\begin{aligned} v(x) &\sim \frac{1}{DN} \left[-\log\left(\frac{\varepsilon N}{2}\right) + \frac{N}{8} - \pi \sum_{j=1}^N G(x; x_j) \right] \\ \bar{\tau} &\sim \frac{1}{DN} \left[-\log\left(\frac{\varepsilon N}{2}\right) + \frac{N}{8} \right] \end{aligned} \quad (7.60)$$

(see Annotations 6.3).

7.4 The Mixed Boundary Value Problem for Poisson's Equation in Dire Straits

Consider the mixed boundary value problem for Poisson's equation in a two-dimensional domain Ω with smooth boundary. Homogeneous Neumann conditions are imposed on the entire boundary $\partial\Omega$, except for a small absorbing window $\partial\Omega_a$ at the end of a cusp-shaped funnel, where homogeneous Dirichlet conditions are imposed, as shown in Fig. 7.1. The cusp can be formed, for example, by a partial block of a planar domain, as shown in Fig. 7.2. The solution $u(\mathbf{x}, a) = \bar{\tau}_{\mathbf{x} \rightarrow \partial\Omega_a}$ is the mean first passage time to $\partial\Omega_a$ of Brownian trajectories emanating from $\mathbf{x} \in \Omega$. Our purpose here is to construct an asymptotic approximation to the solution $u(\mathbf{x}, a)$ in the limit

$$\varepsilon = \frac{\pi |\partial\Omega_a|}{|\partial\Omega|} = \frac{\pi a}{|\partial\Omega|} \ll 1. \quad (7.61)$$

7.4.1 The Case of a Bottleneck

We assume that Ω is an asymmetric planar domain, as in Fig. 7.2 or an asymmetric version of the (dimensional) domain Ω' in Fig. 7.1. The (dimensional) representation of the boundary curves is given by

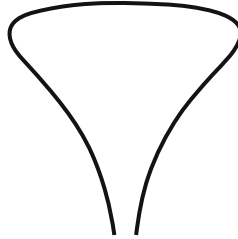


Fig. 7.9 A surface of revolution with a funnel. The z -axis points down

$y' = r_{\pm}(x')$, $\Lambda' < x' < 0$ for the upper and lower parts, respectively, (7.62)

where the x' -axis is horizontal with $x' = \Lambda'$ at AB . We assume that the parts of the curve that generate the funnel have the form

$$r_{\pm}(x') = O(\sqrt{|x'|}) \text{ near } x' = 0, \quad (7.63)$$

$$r_{\pm}(x') = \pm a' \pm \frac{(x' - \Lambda')^{1+\nu_{\pm}}}{\nu_{\pm}(1 + \nu_{\pm})\ell_{\pm}^{\nu_{\pm}}} (1 + o(1)) \text{ for } \nu_{\pm} > 0 \text{ near } x' = \Lambda',$$

where $a' = \frac{1}{2}\overline{AB} = \frac{1}{2}\varepsilon'$ is the radius of the gap, and the constants ℓ_{\pm} have dimension of length. For $\nu_{\pm} = 1$ the parameters ℓ_{\pm} are the radii of curvature R_c^{\pm} at $x' = \Lambda'$. To simplify the conformal mapping, we first rotate the domain by $\pi/2$ clockwise to assume the shape in Fig. 7.9. The rotated axes are renamed (x', y') as well.

Theorem 7.4.1 [*The mean first passage time to a bottleneck*] *The solution $u(\mathbf{x}, a)$ of the mixed boundary value problem in Ω' , for \mathbf{x} outside a boundary layer near $\partial\Omega'_a$ (the narrow escape time of Brownian motion to the end of the bottleneck) in the domain Ω' bounded by the curves (7.62) and (7.63), is given by*

$$\bar{\tau} = u(\mathbf{x}, a) \sim \frac{\pi|\Omega'|}{2D\sqrt{\tilde{\varepsilon}}}, \quad (7.64)$$

where $\tilde{\varepsilon} = 2r_c\varepsilon/(R_c + r_c)$. In dimensional units (7.64) is

$$\bar{\tau} = \sqrt{\frac{R_c(R_c + r_c)}{2r_c\varepsilon'}} \frac{\pi|\Omega'|}{2D} (1 + o(1)) \text{ for } \varepsilon' \ll |\partial\Omega'|, R_c, r_c. \quad (7.65)$$

In the symmetric case $R_c = r_c$ (7.65) reduces to

$$\bar{\tau} = \frac{\pi|\Omega'|}{2D\sqrt{\varepsilon'/R_c}} (1 + o(1)) \text{ for } \varepsilon' \ll |\partial\Omega'|, R_c. \quad (7.66)$$

The derivation of (7.64) begins with the mixed boundary value problem for the Pontryagin-Andronov-Vitt (or Poisson) equation (6.1)–(6.3), which we rewrite in dimensional variables as

$$\begin{aligned} D\Delta\bar{u}(\mathbf{x}') &= -1 \text{ for } \mathbf{x}' \in \Omega' \\ \frac{\partial\bar{u}(\mathbf{x}')}{\partial n} &= 0 \text{ for } \mathbf{x}' \in \partial\Omega' - \partial\Omega'_a \\ \bar{u}(\mathbf{x}') &= 0 \text{ for } \mathbf{x}' \in \partial\Omega'_a, \end{aligned} \quad (7.67)$$

is non-dimensionalized by introducing the variables $\mathbf{x}' = \ell_+\mathbf{x}$, $\Lambda' = \ell_+\Lambda$. The domain Ω' is mapped into Ω and

$$|\Omega'| = \ell_+^2 |\Omega|, \quad |\partial\Omega'| = \ell_+ |\partial\Omega|, \quad |\partial\Omega'_a| = \varepsilon' = \ell_+ |\partial\Omega_a| = \ell_+ \varepsilon. \quad (7.68)$$

Setting $\bar{u}(\mathbf{x}') = u(\mathbf{x}, a)$, (6.1)–(6.3) becomes

$$\begin{aligned} \frac{D}{\ell_+^2} \Delta u(\mathbf{x}, a) &= -1 \text{ for } \mathbf{x} \in \Omega \\ u(\mathbf{x}, a) &= 0 \text{ for } \mathbf{x} \in \partial\Omega_a \\ \frac{\partial u(\mathbf{x}, a)}{\partial n} &= 0 \text{ for } \mathbf{x} \in \partial\Omega_r = \partial\Omega - \partial\Omega_a. \end{aligned} \quad (7.69)$$

First, we consider the case $\nu_{\pm} = 1$, $\ell_+ = R_c$, and $l_- = r_c$, radius 1, and A has dimensionless radius r_c/R_c . This case can represent a partial block, as shown in Fig. 7.2. Under the scaling (7.68) the bounding circle B has dimensionless radius 1. We construct an asymptotic solution for small gap ε by first mapping the domain Ω in Fig. 7.1 (left) conformally into its image under the Möbius transformation of the two osculating circles A and B into concentric circles. To this end we move the origin of the complex plane to the center of the osculating circle B and set

$$w = w(z) = \frac{z - \alpha}{1 - \alpha z}, \quad (7.70)$$

where

$$\begin{aligned} \alpha &= -\frac{2\varepsilon R_c + 2R_c + \varepsilon^2 R_c + 2r_c \varepsilon + 2r_c}{2(\varepsilon R_c + r_c + R_c)} \\ &\pm \frac{\sqrt{\varepsilon(8R_c r_c + 4\varepsilon R_c^2 + 12\varepsilon R_c r_c + 4\varepsilon^2 R_c^2 + 8r_c^2 + 4\varepsilon^2 R_c r_c + \varepsilon^3 R_c^2 + 4\varepsilon r_c^2)}}{2(\varepsilon R_c + r_c + R_c)} \\ &= -1 \pm \sqrt{\frac{2r_c \varepsilon}{R_c + r_c}} + O(\varepsilon). \end{aligned} \quad (7.71)$$

The Möbius transformation (7.70) maps circle B into itself and Ω is mapped onto the domain $\Omega_w = w(\Omega)$ in Fig. 7.10. The straits in Fig. 7.1(left) are mapped onto the ring enclosed between the like-style arcs and the large disk is mapped onto the

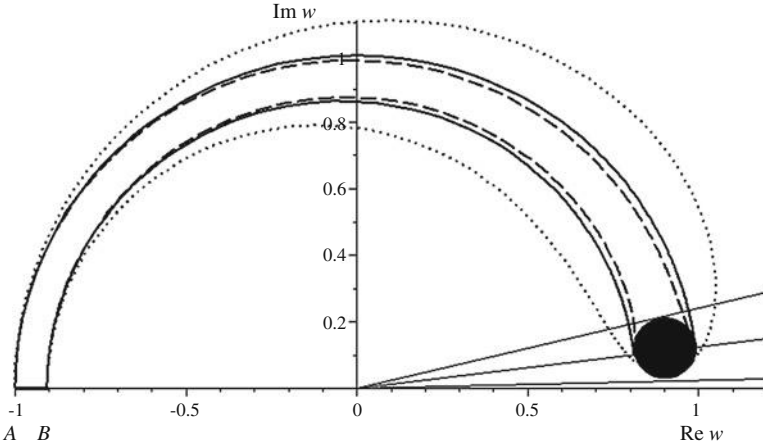


Fig. 7.10 The image $\Omega_w = w(\Omega)$ of the (dimensionless) domain Ω in Fig. 7.1 (left) under the conformal mapping (7.70). The different necks in Fig. 7.1 (right) are mapped onto the semi-annuli enclosed between the like-style arcs and the large disk in Ω is mapped onto the small black disk. The short black segment AB in Fig. 7.1 (right) (of length ε) is mapped onto the thick black segment AB (of length $2\sqrt{\tilde{\varepsilon}} + O(\varepsilon)$)

small black disk. The radius of the small black disk and the elevation of its center above the real axis are $O(\sqrt{\varepsilon})$. The short black segment of length ε in Fig. 7.1(right) is mapped onto a segment of length $2\sqrt{\varepsilon} + O(\varepsilon)$.

Setting $u(z, a) = v(w)$ and $\tilde{\varepsilon} = 2r_c\varepsilon/(R_c + r_c)$, the system (7.69) is converted into

$$\begin{aligned}\Delta_w v(w) &= -\frac{\ell_+^2}{\Omega|w'(z)|^2} = -\frac{(4\tilde{\varepsilon} + O(\tilde{\varepsilon}^{3/2}))\ell_+^2}{\Omega|w(1 - \sqrt{\tilde{\varepsilon}}) - 1 + O(\tilde{\varepsilon})|^4} \text{ for } w \in \Omega_w \quad (7.72) \\ \frac{\partial v(w)}{\partial n} &= 0 \text{ for } w \in \partial\Omega_w - \partial\Omega_{w,a} \\ v(w) &= 0 \text{ for } w \in \partial\Omega_{w,a}.\end{aligned}$$

The solution is bounded above and below by that from the inverse image of a circular ring cut by lines through the origin, tangent to the black disk at polar angles $\theta = c_1\sqrt{\tilde{\varepsilon}}$ (top) and $\theta = c_2\sqrt{\tilde{\varepsilon}}$ (bottom) for some positive constants c_1, c_2 , independent of $\tilde{\varepsilon}$. Therefore the solution (the mean first passage time from Ω to $\partial\Omega_a$) equals that from the inverse image of a ring cut by an intermediate angle $\theta = c\sqrt{\tilde{\varepsilon}}$ (middle).

The asymptotic analysis of (7.72) begins with the observation that the solution of the boundary value problem (7.72) is to leading order independent of the radial variable in polar coordinates $w = re^{i\theta}$. Fixing $r = 1$, we impose the homogeneous Neumann boundary condition (reflection) at $\theta = c\sqrt{\tilde{\varepsilon}}$, where $c = O(1)$ is a constant independent of $\tilde{\varepsilon}$ to leading order, and the homogeneous Dirichlet condition (absorption) at $\theta = \pi$. The outer solution, obtained by a regular expansion of $v(e^{i\theta})$, is given by

$$v_0(e^{i\theta}) = \tilde{A}(\theta - \pi), \quad (7.73)$$

where \tilde{A} is an as yet undetermined constant. It follows that

$$\frac{\partial v_0(e^{i\theta})}{\partial \theta} \Big|_{\theta=\pi} = -\tilde{A}. \quad (7.74)$$

To determine \tilde{A} , we integrate (7.72) over the domain to obtain at the leading order

$$2\sqrt{\tilde{\varepsilon}} \frac{\partial v_0(e^{i\theta})}{\partial \theta} \Big|_{\theta=\pi} = -2\sqrt{\tilde{\varepsilon}}\tilde{A} \sim -\frac{|\Omega'|}{D}, \quad (7.75)$$

hence

$$\tilde{A} \sim \frac{|\Omega'|}{2D\sqrt{\tilde{\varepsilon}}}. \quad (7.76)$$

Now (7.73) gives for $\theta = c\sqrt{\tilde{\varepsilon}}$ the leading order approximation (7.64). Returning to dimensional units, (7.64) becomes (7.65) and in the symmetric case $R_c = r_c$ (7.65) reduces to (7.66). \square

The following is a more explicit analysis of the symmetric case $\nu_{\pm} = 1$, $R_c = r_c$. The leading order approximation is obtained by an explicit integration of (7.72) with respect to θ ,

$$v(e^{i\theta}) = \frac{4\ell_+^2\tilde{\varepsilon}}{D} \int_{\theta}^{\pi} d\varphi \int_{c\sqrt{\tilde{\varepsilon}}}^{\varphi} \frac{d\eta}{|e^{i\eta} - 1 - e^{i\eta}\sqrt{\tilde{\varepsilon}}|^4}, \quad (7.77)$$

so that

$$\begin{aligned} v(e^{ic\sqrt{\tilde{\varepsilon}}}) &= \frac{4\ell_+^2\tilde{\varepsilon}}{D} \int_{c\sqrt{\tilde{\varepsilon}}}^{\pi} d\varphi \int_{\varphi}^{\pi} \frac{d\eta}{|e^{i\eta} - 1 - e^{i\eta}\sqrt{\tilde{\varepsilon}}|^4} \\ &= \frac{4\ell_+^2\tilde{\varepsilon}}{D} \int_{c\sqrt{\tilde{\varepsilon}}}^{\pi} \frac{(\pi - \eta) d\eta}{|e^{i\eta} - 1 - e^{i\eta}\sqrt{\tilde{\varepsilon}}|^4}. \end{aligned} \quad (7.78)$$

First, we evaluate asymptotically the integral

$$\frac{\ell_+^2\tilde{\varepsilon}}{D} \int_{c\sqrt{\tilde{\varepsilon}}}^{\pi} \frac{\eta d\eta}{|e^{i\eta} - 1 - e^{i\eta}\sqrt{\tilde{\varepsilon}}|^4} \quad (7.79)$$

by setting $\eta = \sqrt{\tilde{\varepsilon}}\zeta$ and noting that

$$\begin{aligned} \left| \frac{e^{i\zeta\sqrt{\tilde{\varepsilon}}} - 1}{i\zeta\sqrt{\tilde{\varepsilon}}} - 1 \right| &= \left| \frac{-2\sin^2 \frac{\zeta\sqrt{\tilde{\varepsilon}}}{2}}{i\zeta\sqrt{\tilde{\varepsilon}}} + \frac{\sin \zeta\sqrt{\tilde{\varepsilon}}}{\zeta\tilde{\varepsilon}} - 1 \right| \\ &= O(\zeta\sqrt{\tilde{\varepsilon}}) \text{ for all } \eta, \tilde{\varepsilon} > 0. \end{aligned} \quad (7.80)$$

It follows that

$$\begin{aligned} \frac{4\ell_+^2\tilde{\varepsilon}}{D} \int_{c\sqrt{\tilde{\varepsilon}}}^{\pi} \frac{\eta d\eta}{|e^{i\eta} - 1 - e^{i\eta}\sqrt{\tilde{\varepsilon}}|^4} &= \frac{4\ell_+^2}{D} \int_c^{\pi/\sqrt{\tilde{\varepsilon}}} \frac{\zeta d\zeta}{|1 + \zeta^2 + O(\tilde{\varepsilon}\zeta^2)|^2} \\ &= \frac{4}{D(c+1)} \left(1 + O(\sqrt{\tilde{\varepsilon}}) \right). \end{aligned} \quad (7.81)$$

Similarly, we obtain that

$$\begin{aligned} \frac{4\tilde{\varepsilon}}{D} \int_{c\sqrt{\tilde{\varepsilon}}}^{\pi} \frac{d\eta}{|e^{i\eta} - 1 - e^{i\eta}\sqrt{\tilde{\varepsilon}}|^4} &= \frac{4}{D\sqrt{\tilde{\varepsilon}}} \int_c^{\pi/\sqrt{\tilde{\varepsilon}}} \frac{d\zeta}{|1 + \zeta^2 + O(\tilde{\varepsilon}\zeta^2)|^2} \\ &= \frac{C}{D\sqrt{\tilde{\varepsilon}}} \left(1 + O(\sqrt{\tilde{\varepsilon}}) \right), \end{aligned} \quad (7.82)$$

where $C = O(1)$ is a constant, so that

$$v(e^{ic\sqrt{\tilde{\varepsilon}}}) = \frac{4\ell_+^2\pi C}{D\sqrt{\tilde{\varepsilon}}} \left(1 + O(\sqrt{\tilde{\varepsilon}}) \right). \quad (7.83)$$

To determine the value of the constant C , we note that (7.77) implies that

$$\begin{aligned} \frac{\partial v(e^{i\theta})}{\partial n} \Bigg|_{\partial\Omega_{w,a}} &= \frac{\partial v}{\partial\theta} \Big|_{\theta=\pi} = -\frac{4\ell_+^2\tilde{\varepsilon}}{D} \int_{c\sqrt{\tilde{\varepsilon}}}^{\pi} \frac{d\eta}{|e^{i\eta} - 1 - e^{i\eta}\sqrt{\tilde{\varepsilon}}|^4} \\ &= -\frac{4\ell_+^2 C}{D\sqrt{\tilde{\varepsilon}}} \left(1 + O(\sqrt{\tilde{\varepsilon}}) \right) \end{aligned} \quad (7.84)$$

and the integration of (7.72) over Ω_w gives

$$2\sqrt{\tilde{\varepsilon}} \frac{\partial v(e^{i\theta})}{\partial n} \Bigg|_{\partial\Omega_{w,a}} = -\frac{\ell_+^2|\Omega|}{D}. \quad (7.85)$$

Now, (6.3) and (7.85) imply that $4C = |\Omega|/2$, so that $u(\mathbf{x}, a)$ (the mean first passage time $\bar{\tau}$ to the straits $\partial\Omega_a$) is to leading order independent of \mathbf{x} outside a boundary layer near $\partial\Omega_a$ and

$$\bar{\tau} = u(\mathbf{x}, a) = \frac{\ell_+^2 \pi |\Omega|}{2D\sqrt{\tilde{\varepsilon}}} (1 + o(1)) = \frac{\pi |\Omega'|}{2D\sqrt{\tilde{\varepsilon}}} (1 + o(1)) \text{ for } \tilde{\varepsilon} \ll |\partial\Omega|, \ell_+, \quad (7.86)$$

which is (7.64).

Next, we consider for simplicity the symmetric case $\nu_+ = \nu_- > 1$, so $R_c = r_c = \infty$. After scaling (6.1)–(6.3) with (7.68), we can choose the bounding circles at A and B to have radius 1 and repeat the above analysis in the domain Ω_w enclosed by the dashed curves, shown in Fig. 7.10. The result (7.66) becomes

$$\bar{\tau} = \frac{\pi |\Omega'|}{2D\sqrt{\varepsilon'/\ell_+}} (1 + o(1)) \text{ for } \varepsilon' \ll |\partial\Omega'|, \ell_+. \quad (7.87)$$

7.4.2 The Case of Several Bottlenecks

In the case of a boundary value problem in a domain with a homogeneous Dirichlet condition imposed at the ends of several cusps (exit through any one of N well-separated necks) with dimensionless curvature parameters ℓ_j and widths $\tilde{\varepsilon}_j$, we construct the outer solution (7.73) at any one of the N absorbing windows so that (7.74) holds at each window. The integration of (7.72) over Ω_ω gives the following analog of (7.75),

$$\sum_{j=1}^N 2\sqrt{\tilde{\varepsilon}_j} \frac{\partial v_0(e^{i\theta})}{\partial\theta} \Big|_{\theta=\pi} = - \sum_{j=1}^N 2\sqrt{\tilde{\varepsilon}_j} A \sim - \frac{|\Omega'|}{D}, \quad (7.88)$$

hence

$$\tilde{A} \sim \frac{|\Omega'|}{2D \sum_{j=1}^N \sqrt{\tilde{\varepsilon}_j}}. \quad (7.89)$$

Equation (7.86) is then generalized to

$$\bar{\tau} = u(\mathbf{x}, a) = \frac{\pi |\Omega'|}{2D \sum_{j=1}^N \sqrt{\varepsilon'_j/\ell_j}} (1 + o(1)) \text{ for } \varepsilon'_j/\ell_j \ll |\partial\Omega'|. \quad (7.90)$$

Equations (7.66) and (7.65) are generalized in a similar manner.

To calculate the flux (exit probability density function) through any one of the N necks, we apply the transformation (7.70) separately for each bottleneck at the absorbing images $\partial\Omega_{w,a_1}, \dots, \partial\Omega_{w,a_N}$ to obtain images Ω_{w_j} for $j = 1, 2, \dots, N$. Then the probability of exiting through $\partial\Omega_{w,a_i}$ is the solution of the mixed boundary value problem

$$\begin{aligned} \Delta_w v(w) &= 0 \text{ for } w \in \Omega_{w_i} & (7.91) \\ \frac{\partial v(w)}{\partial n} &= 0 \text{ for } w \in \partial\Omega_{w_i} - \bigcup_{i=1}^N \partial\Omega_{w,a_i} \\ v(w) &= 1 \text{ for } w \in \partial\Omega_{w,a_i} \\ v(w) &= 0 \text{ for } w \in \partial\Omega_{w,a_j}, \quad j \neq i. \end{aligned}$$

The outer solution, which is the exit probability through window $\partial\Omega_{w,i}$, is an unknown constant p_i . We construct boundary layers at each absorbing boundary $\partial\Omega_{w,a_j}$ for $j \neq i$ by solving the boundary value problem in Ω_{w_j} , which is of the type shown in Fig. 7.10 with a neck of width ε_j . In each case the boundary layer is a linear function

$$v_j(\theta) = \delta_{i,j} - \tilde{A}_j(\theta - \pi) \text{ for all } j, \quad (7.92)$$

so that

$$v_j(0) \sim \delta_{i,j} + \tilde{A}_j\pi = p_i \text{ for all } j. \quad (7.93)$$

To determine the value of the constant p_i , we note that

$$\left. \frac{\partial v(e^{i\theta})}{\partial n} \right|_{\partial\Omega_{w,a}} = \left. \frac{\partial v_j(\theta)}{\partial \theta} \right|_{\theta=\pi} = -\tilde{A}_j, \quad (7.94)$$

so the integration of (7.91) over Ω_{w_i} gives to leading order

$$\sum_{j=1}^N \tilde{A}_j |\partial\Omega_{w,a_j}| = \sum_{j=1}^N 2\tilde{A}_j \sqrt{\varepsilon_j} = 0. \quad (7.95)$$

The $N + 1$ equations (7.93) and (7.95) for the unknowns $p_i, \tilde{A}_1, \dots, \tilde{A}_N$ give the exit probability from an interior point in the planar case as

$$p_i = \frac{\sqrt{\varepsilon'/\ell_i}}{\sum_{j=1}^N \sqrt{\varepsilon'_j/\ell_j}}. \quad (7.96)$$

7.4.3 The Mixed Boundary Value Problem on a Surface of Revolution

Consider the mixed boundary value problem on a surface of revolution generated by rotating the curve in Fig. 7.9 about its axis of symmetry and assume $\nu_+ = \nu_- = \nu$ and $\ell_+ = \ell_- = \ell$ (i.e., consider Brownian motion on the surface with absorption at the end of the funnel). The projection of the Brownian motion from the surface to the z -axis gives rise to a drift. The backward Kolmogorov operator (1.15) of the projected motion, scaled with (7.68), is given by

$$\mathcal{L}^* u(z) = \frac{D}{\ell^2} \left\{ \frac{1}{1 + r'^2(z)} u''(z) + \left[\frac{r'(z)}{r(z)(1 + r'^2)} - \frac{r'(z)r''(z)}{(1 + r'^2)^2} \right] u'(z) \right\}, \quad (7.97)$$

which corresponds to the stochastic differential equation

$$dz = a(z) dt + b(z) dw, \quad (7.98)$$

where the drift $a(z)$ and noise intensity $b(z)$ are given, respectively, by

$$a(z) = \frac{D}{\ell^2} \left\{ \frac{r'(z)}{r(z)(1 + r'^2)} - \frac{r'(z)r''(z)}{(1 + r'^2)^2} \right\}, \quad b(z) = \sqrt{\frac{2D}{\ell^2(1 + r'^2(z))}}, \quad (7.99)$$

and $w(t)$ is standard Brownian motion on the line. The potential of the drift is

$$A(z) = - \int_{\Lambda}^z a(t) dt. \quad (7.100)$$

To calculate the mean first passage time from $z = 0$ to the end of the funnel at $z = \Lambda$, we note that due to rotational symmetry, the solution of the mixed boundary value problem for the mean first passage time $u(z, \theta)$ on the surface is independent of θ . Therefore the problem reduces to the ordinary differential equation

$$\begin{aligned} \frac{1}{r(z)\sqrt{1 + r'^2(z)}} \frac{\partial}{\partial z} \left[\frac{r(z)}{\sqrt{1 + r'^2(z)}} \frac{\partial u(z)}{\partial z} \right] &= -\frac{\ell^2}{D} \\ u'(0) &= u(\Lambda) = 0. \end{aligned} \quad (7.101)$$

The solution is given by

$$u(0) = \frac{\ell^2}{2\pi D} \int_{\Lambda}^0 \frac{\sqrt{1 + r'^2(t)}}{r(t)} S(t) dt, \quad (7.102)$$

where $S(t)$ is the (scaled) area of the surface of revolution from $z = t$ to $z = 0$, given by

$$S(t) = 2\pi \int_t^0 r(s)\sqrt{1+r'^2(s)} ds. \quad (7.103)$$

The main contribution to (7.102) comes from $\Lambda < t < \Lambda + \delta$ for a sufficiently small δ such that $\delta \gg a$ (note that the singularity of $1/r(z)$ near $z = 0$ is integrable). Thus (7.102) and (7.103) give for $\nu > 0$

$$\begin{aligned} \bar{\tau} = u(0) &\sim \frac{\ell^2 S(\Lambda)}{2\pi D} \int_{\Lambda}^{\Lambda+\delta} \frac{\sqrt{1+r'^2(t)}}{r(t)} dt \\ &\sim \frac{S(\Lambda)}{2D} \frac{\left(\frac{\ell}{(1+\nu)a}\right)^{\nu/1+\nu}}{\sin \frac{\nu\pi}{1+\nu}} \nu^{1/1+\nu}, \end{aligned} \quad (7.104)$$

where $S = S(\Lambda)$ is the entire unscaled area of the surface. In particular, for $\nu = 1$, we get the mean first passage time

$$\bar{\tau} \sim \frac{S}{4D\sqrt{a/2\ell}}. \quad (7.105)$$

The case $\nu = 0$ corresponds to an absorbing circular cap of a small radius a on a closed surface. For a sphere the solution of (7.101) gives (7.35) again,

$$\bar{\tau}_{x \rightarrow \partial\Omega_i} = \frac{2R^2}{D} \log \frac{\sin \frac{\theta}{2}}{\sin \frac{\delta}{2}}, \quad (7.106)$$

where θ is the angle between x and the south-north axis of the sphere and $a = R \sin \delta/2$. If a right circular cylinder of a small radius a and length $L' = \ell L$ is attached to the surface at $z = \Lambda$, as in Fig. 6.3 (left), then the integration in (7.104) extends to $\Lambda - L$, giving

$$\begin{aligned} u(0) &\sim \frac{\ell^2 S(\Lambda)}{2\pi D} \int_{\Lambda}^0 \frac{\sqrt{1+r'^2(t)}}{r(t)} dt + \frac{\ell^2}{2\pi Da} \int_{\Lambda-L}^{\Lambda} [S(\Lambda) + 2\pi a(t - \Lambda)] dt \\ &= \frac{S(\Lambda)}{2\pi D} \int_{\Lambda}^0 \frac{\sqrt{1+r'^2(t)}}{r(t)} dt + \frac{S(\Lambda)L'}{2\pi Da} + \frac{L'^2}{2D}, \end{aligned} \quad (7.107)$$

where the integral is given by (7.104), (7.105), or (7.106) for the various values of ν . Note that while $\bar{\tau}$ on the surface depends on the fractional power $-\nu/(1+\nu)$ of the neck's radius a , the power of a in the three-dimensional case is $-3/2$, as indicated in (8.142) below.

The case $\nu = 0$ is not the limit of (7.104), because the line (7.63) blows up. This case corresponds to a conical funnel with an absorbing circle of small radius a and length H (see Fig. 7.12). We assume that the radius of the other base of the cone, b , is smaller than a , but that $b \ll S^{1/2}$. The generator of the cone is the line segment

$$r(x) = a + C(x - L) \text{ for } \Lambda - L < x < \Lambda, \quad (7.108)$$

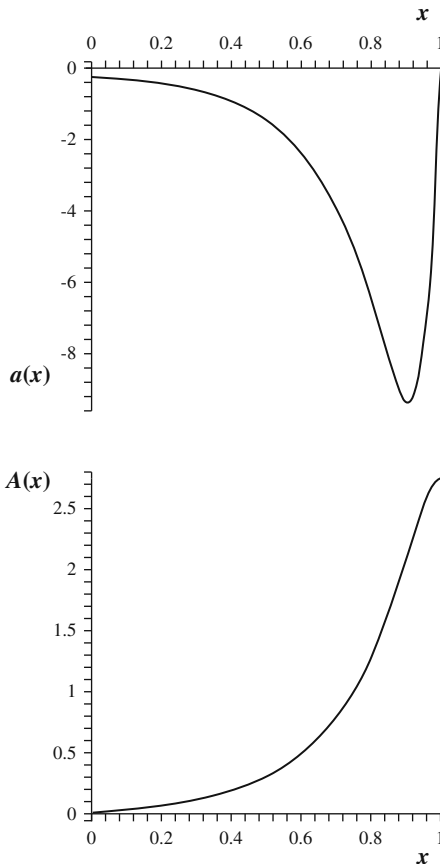


Fig. 7.11 The drift $a(z)$ in (7.99) (left panel) and its potential $A(z)$ (right panel) near the cusp. The projection of the Brownian motion on the axis of symmetry has an effective high barrier in the neck



Fig. 7.12 Narrow straits formed by a cone-shaped funnel

where C is the (positive) slope. In this case (7.107) is replaced by

$$u(0) = \frac{\mathcal{S}(\Lambda)}{2\pi D} \int_{\Lambda}^0 \frac{\sqrt{1+r'^2(t)}}{r(t)} dt + \frac{\mathcal{S}(\Lambda)\sqrt{1+C^2}}{2\pi DC} \log \left(1 + \frac{CL'}{a} \right) + \frac{(1+C^2)}{2DC^2} \left[(a+CL') \log \left(1 + \frac{CL'}{a} \right) + \frac{1}{2}[(a+CL')^2 - a^2] \right],$$

which reduces to (7.107) in the limit $CL' \ll a$ and for $a \ll CL'$ can be simplified to leading order to

$$u(0) = \frac{\mathcal{S}(\Lambda)}{2\pi D} \int_{\Lambda}^0 \frac{\sqrt{1+r'^2(t)}}{r(t)} dt + \frac{\mathcal{S}(\Lambda)\sqrt{1+C^2}}{2\pi DC} \log \frac{CL'}{a} + \frac{(1+C^2)L'^2}{2D} \log \frac{CL'}{a} + O(1). \quad (7.109)$$

Note that the last term in (7.109) blows up as $a \rightarrow 0$ while that in (7.107) does not. This is due to the degeneration of the narrow escape time problem in the cylinder.

7.5 A Composite Domain with a Bottleneck

A planar composite domain Ω with a bottleneck consists of a head Ω_1 connected through a small interface $\partial\Omega_i$ to a narrow cylindrical neck Ω_2 . Homogeneous Neumann boundary conditions are imposed on the boundary of Ω (i.e., it reflects

Brownian trajectories), except the far end of Ω_2 , denoted $\partial\Omega_a$, where homogeneous Dirichlet conditions are imposed (i.e., it absorbs Brownian trajectories). For example, in Fig. 6.3 (left) the interface $\partial\Omega_i$ is the black segment AB and the absorbing boundary $\partial\Omega_a$ is the segment CD at the bottom of the strip. The surface of revolution obtained by rotating the domain in the figure about its axis of symmetry has a similar structure. The interface $\partial\Omega_i$ in this case is a circle. Thus the length of the interface $|\partial\Omega_i|$ is given by

$$|\partial\Omega_i| = \begin{cases} a & \text{for a line segment} \\ 2\pi a & \text{for a circle.} \end{cases} \quad (7.110)$$

We denote by $u(\mathbf{x}, a) = \bar{\tau}_{\mathbf{x} \rightarrow \partial\Omega_a}$ the solution of the mixed boundary value problem for the Poisson equation in Ω , with homogeneous Neumann conditions on the entire boundary, except for $\partial\Omega_a$, where homogeneous Dirichlet conditions are imposed. Similarly, we denote by $u(\mathbf{x}, i) = \bar{\tau}_{\mathbf{x} \rightarrow \partial\Omega_i}$ the solution of the mixed boundary value problem for the Poisson equation in Ω_1 , with homogeneous Neumann conditions on the entire boundary $\partial\Omega_1$, except for $\partial\Omega_i$, where homogeneous Dirichlet conditions are imposed. These solutions represent the mean first passage time from $\mathbf{x} \in \Omega_1$ to the absorbing boundary $\partial\Omega_a$ at the end of the narrow neck and the mean first passage time $\mathbf{x} \in \Omega_1$ to the interface $\partial\Omega_i$, respectively.

To calculate $u(\mathbf{x}, a)$, we need the following lemma.

Green's identity. The solutions $u(\mathbf{x}, a)$ and $u(\mathbf{x}, i)$ satisfy the renewal equation

$$u(\mathbf{x}, a) = u(\mathbf{x}, i) + \int_{\partial\Omega_i} G(\mathbf{x} | \boldsymbol{\xi}) u(\boldsymbol{\xi}, a) d\boldsymbol{\xi}, \quad (7.111)$$

where $G(\mathbf{x} | \boldsymbol{\xi})$ is Green's function for the mixed boundary value problem

$$\begin{aligned} \Delta u(\mathbf{x}) &= 0 \quad \text{for } \mathbf{x} \in \Omega_1 \\ \frac{\partial u(\mathbf{x})}{\partial n} &= 0 \quad \text{for } \mathbf{x} \in \partial\Omega_1 - \partial\Omega_i \\ u(\mathbf{x}) &= \varphi(\mathbf{x}) \quad \text{for } \mathbf{x} \in \partial\Omega_i. \end{aligned} \quad (7.112)$$

Proof The identity follows from the fact that both sides of (7.111) satisfy (7.112) for $\mathbf{x} \in \Omega_1$ and coincide on $\partial\Omega_i$.

The identity (7.111) can be interpreted as the addition formula for mean first passage times

$$\bar{\tau}_{\mathbf{x} \rightarrow \partial\Omega_a} = \bar{\tau}_{\mathbf{x} \rightarrow \partial\Omega_i} + \bar{\tau}_{\partial\Omega_i \rightarrow \partial\Omega_a}, \quad (7.113)$$

where the mean first passage time $\bar{\tau}_{\partial\Omega_i \rightarrow \partial\Omega_a}$ is $\bar{\tau}_{\mathbf{x} \rightarrow \partial\Omega_a}$, averaged over $\partial\Omega_i$ with respect to the flux density of Brownian trajectories in Ω_1 into an absorbing boundary at $\partial\Omega_i$. The identity (7.113) is not as obvious as it may seem (see Schuss (2010b)] for further details).

Theorem 7.5.1 [The mixed boundary value problem in a composite domain] *The solution of the mixed boundary value problem for the Pontryagin–Andronov–Vitt equation in a composite domain Ω with homogeneous Neumann conditions on $\partial\Omega$, except for homogeneous Dirichlet conditions at the end of a narrow cylindrical neck of length L , is given by*

$$\bar{\tau}_{x \rightarrow \partial\Omega_a} = \bar{\tau}_{x \rightarrow \partial\Omega_i} + \frac{L^2}{2D} + \frac{|\Omega_1|L}{|\partial\Omega_a|D}. \quad (7.114)$$

Proof For the derivation of (7.114), we use Green's identity to connect the solutions in head and neck. First, we calculate $\bar{\tau}_{\partial\Omega_i \rightarrow \partial\Omega_a}$ and the absorption flux at the interface. In the narrow neck Ω_2 the boundary value problem (6.1)–(6.3) can be approximated by the one-dimensional boundary value problem

$$\begin{aligned} Du_{zz} &= -1 \\ u(0) &= 0, \quad u(L) = u_H, \end{aligned}$$

where the value at the interface $u(L) = u_H$ is yet unknown. The solution is given by

$$u(z) = -\frac{z^2}{2D} + Bz, \quad (7.115)$$

so that

$$u(L) = u_H = -\frac{L^2}{2D} + BL, \quad (7.116)$$

which relates the unknown constants B and u_H . The constant B is found by multiplying equation (6.1) by the Neumann function $N(\mathbf{x}, \mathbf{y})$, integrating over Ω_1 , applying Green's formula, and using the boundary conditions (6.2) and (6.3). Specifically, abbreviating $v(\mathbf{x}) = \bar{\tau}_{x \rightarrow \partial\Omega_a}$, we obtain for all $\mathbf{y} \in \partial\Omega_i$

$$v(\mathbf{y}) = -\frac{1}{D} \int_{\Omega_1} N(\mathbf{x}, \mathbf{y}) d\mathbf{x} - \int_{\partial\Omega_i} N(\mathbf{x}, \mathbf{y}) \frac{\partial v(\mathbf{x})}{\partial n} dS_{\mathbf{x}} + \frac{1}{|\Omega_1|} \int_{\Omega_1} v(\mathbf{x}) d\mathbf{x}. \quad (7.117)$$

Approximating, as we may, $v(\mathbf{y}) \approx u(L)$ and using (7.116), we obtain

$$\begin{aligned} -\frac{L^2}{2D} + BL &= -\frac{1}{D} \int_{\Omega_1} N(\mathbf{x}, \mathbf{y}) d\mathbf{x} - \int_{\partial\Omega_i} N(\mathbf{x}, \mathbf{y}) \frac{\partial v(\mathbf{x})}{\partial n} dS_{\mathbf{x}} \\ &\quad + \frac{1}{|\Omega_1|} \int_{\Omega_1} v(\mathbf{x}) d\mathbf{x}. \end{aligned} \quad (7.118)$$

Because $v(\mathbf{x})$ is the solution of the boundary value problem (6.1)–(6.3) in the entire domain $\Omega = \Omega_1 \cup \Omega_2$, the meaning of (7.118) is the connecting rule (7.113), where

$$\bar{\tau}_{\Omega_1 \rightarrow \partial\Omega_a} = \frac{1}{|\Omega_1|} \int_{\Omega_1} v(\mathbf{x}) d\mathbf{x} \quad (7.119)$$

$$\bar{\tau}_{\partial\Omega_i \rightarrow \partial\Omega_a} = u(L) \quad (7.120)$$

$$\bar{\tau}_{x \rightarrow \partial\Omega_i} = -\frac{1}{D} \int_{\Omega_1} N(\mathbf{x}, \mathbf{y}) d\mathbf{x} - \int_{\partial\Omega_i} N(\mathbf{x}, \mathbf{y}) \frac{\partial v(\mathbf{x})}{\partial n} dS_x. \quad (7.121)$$

Equation (7.119) gives the mean first passage time, averaged over Ω_1 . The averaging is a valid approximation, because the mean first passage time to $\partial\Omega_i$ is constant to begin with (except in a negligible boundary layer). Equation (7.120) is the mean first passage time from the interface to the absorbing end $\partial\Omega_a$ of the strip, and (7.121) follows from (7.7).

Matching the solutions in Ω_1 and Ω_2 continuously across $\partial\Omega_i$, we obtain the total flux on $\partial\Omega_i$ as

$$J = D \int_{\partial\Omega_i} \frac{\partial v(\mathbf{x})}{\partial \nu} dS_x = -(|\Omega_1| + |\Omega_2|). \quad (7.122)$$

Noting that $\partial v(\mathbf{x})/\partial n = -u'(0) = -B$, we get from (7.110) and (7.122) that

$$B = - \begin{cases} \frac{|\Omega_1|}{aD} + \frac{L}{D} & \text{for a line segment} \\ \frac{|\Omega_1|}{2\pi a D} a + \frac{L}{D} & \text{for a circle} \\ \frac{|\Omega_1|}{\pi a^2 D} + \frac{L}{D} & \text{for a circular disk.} \end{cases} \quad (7.123)$$

Finally, we put (7.113)–(7.123) together to obtain (7.114). The mean first passage time $\bar{\tau}_{x \rightarrow \partial\Omega_i}$ for the various domains is given in Sect. 7.4 above. \square

7.6 The Narrow Escape Time from Domains in \mathbb{R}^2 and \mathbb{R}^3 with Bottlenecks

The expression (7.114) for the narrow escape time from a domain with a bottleneck in the form of a one-dimensional neck, such as a dendritic spine (see Figs. 6.3 and 10.1 below), can be summarized as follows. Consider a domain Ω with head Ω_1 and a narrow cylindrical neck Ω_2 of length L and radius a , connected smoothly to the head. The radius of curvature at the connection is R_c . In the two-dimensional case

$$\bar{\tau}_{x \rightarrow \partial\Omega_a} = \begin{cases} \frac{|\Omega_1|}{\pi D} \log \frac{|\partial\Omega_1|}{a} + \frac{O(1)}{D} + \frac{L^2}{2D} + \frac{|\Omega_1|L}{aD} \\ \text{planar spine connected to the neck at a right angle} \\ \\ \frac{\pi|\Omega_1|}{D} \sqrt{\frac{R_c}{a}} (1 + o(1)) + \frac{L^2}{2D} + \frac{|\Omega_1|L}{2\pi a D} \\ \text{planar spine with a smooth connecting funnel} \\ \\ \frac{|\Omega_1|}{2\pi D} \log \frac{\sin \frac{\theta}{2}}{\sin \frac{\delta}{2}} + \frac{L^2}{2D} + \frac{|\Omega_1|L}{2\pi a D} \\ \text{spherical spine surface connected to the neck at a right angle} \\ \\ \frac{|\Omega_1|}{2D} \frac{\left(\frac{\ell}{(1+\nu)a}\right)^{\nu/1+\nu} \nu^{1/1+\nu}}{\sin \frac{\nu\pi}{1+\nu}} + \frac{L^2}{2D} + \frac{|\Omega_1|L}{2\pi a D} \\ \text{spherical spine surface with a smooth connecting funnel,} \end{cases} \quad (7.124)$$

where R is the radius of the sphere, $a = R \sin \delta/2$, and θ is the initial elevation angle on the sphere. If $|\Omega_1| \gg aL$ and $L \gg a$, the last term in (7.124) is dominant, which is the manifestation of the many returns of Brownian motion from the neck to the head prior to absorption at $\partial\Omega_a$. The last line of (7.124) agrees with the explicit calculation (7.107). Note that modulation of neck length changes the residence time significantly.

7.7 The Principal Eigenvalue and Bottlenecks

The narrow escape time is related to the leading eigenvalues of the Neumann or mixed Neumann–Dirichlet boundary value problem for the Laplace operator in domains that consist of compartments interconnected by narrow necks. In such domains the mean first passage time from one compartment to the other (see [Schuss (2013), Chapter 6]) is to leading order (in the limit of shrinking neck) independent of the initial point of the escaping trajectory and is twice the mean first passage time from the compartment to the narrowest passage in the bottleneck (e.g., the interval \mathbf{AB} in Fig. 7.13). Indeed, the reciprocal of this mean first passage time is to leading order the rate at which trajectories reach the bottleneck from the first compartment, so the reciprocal of the mean first passage time is the lowest eigenvalue of the mixed boundary value problem in the first compartment with Dirichlet conditions on the cross section of the neck.

There is a spectral gap of order 1 from the smallest eigenvalue to the next one. It follows that long transition times of Brownian trajectories between compartments connected by bottlenecks are exponentially distributed and therefore the leading eigenvalues of Neumann’s problem for the Laplace equation in a domain that consists

of compartments interconnected by narrow necks are to leading order the eigenvalues of a Markov chain with transition rates that are the reciprocals of the mean first passage times through the narrow necks, as is the case for diffusion in a potential landscape with several deep wells (high barriers) (see Annotations 7.10). The evaluation of the leading eigenvalues of the Neumann problem for the Laplace equation in domains with bottlenecks reduces to the computation of the leading order eigenvalue for the mixed Neumann–Dirichlet boundary value problem for the Laplace equation in a domain with reflecting (Neumann) boundary except for a small absorbing (Dirichlet) window at the end of a funnel.

7.7.1 Connecting Head and Neck

First, we consider the principal eigenvalue of the mixed Neumann–Dirichlet problem for the Laplace equation in a composite domain that consists of a head Ω_1 connected by a funnel to a narrow cylindrical neck Ω_2 . The boundary of the domain is reflecting (Neumann) and only the end of the cylinder $\partial\Omega_a$ is absorbing (Dirichlet), as in Fig. 6.3(left). The left half of the dumbbell-shaped domain shown in Fig. 7.13 is a composite domain if we consider the interval AB and absorbing boundary. In the three-dimensional case the Dirichlet boundary $\partial\Omega_a$ is a small absorbing disk at the end of the cylinder. The domain Ω_1 is the one shown in Fig. 7.1 and it is connected to the cylinder at an interface $\partial\Omega_i$, which in this case is the interval AB in Fig. 7.1. Using (7.114) and the fact that the principal eigenvalue of the mixed two- and three-dimensional Neumann–Dirichlet problems in domains with small Dirichlet and large Neumann parts of a smooth boundary is asymptotically the reciprocal of the mean first passage time, we find that the principal eigenvalue λ_1 in a domain with a single bottleneck is given by

$$\lambda_1 \sim \frac{1}{\bar{\tau}_{x \rightarrow \partial\Omega_i} + \frac{L^2}{2D} + \frac{|\Omega_1|L}{|\partial\Omega_a|D}}, \quad (7.125)$$

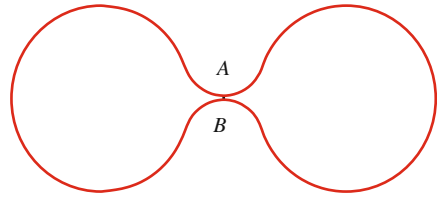
where $\bar{\tau}_{x \rightarrow \partial\Omega_i}$ is any one of the mean first passage times given in the previous sections, depending on the geometry of Ω_1 .

If a composite domain consists of a single head and N well-separated bottlenecks of different radii and neck lengths, the reciprocal of the mean first passage time is the sum of the reciprocals of the narrow escape times from a domain with a single bottleneck. That is, the principal eigenvalue λ_P is given by

$$\lambda_P \sim \sum_{j=1}^N \lambda_j. \quad (7.126)$$

This can be interpreted as the fact that the total efflux is the sum of N independent effluxes through the bottlenecks.

Fig. 7.13 A dumbbell-shaped domain is a composite domain that consists of two large compartments Ω_1 and Ω_3 connected by a narrow neck Ω_2 . The bottleneck is the interval AB .



7.7.2 The Principal Eigenvalue in Dumbbell-Shaped Domains

We consider now the principal eigenvalue of the Neumann problem in a two- or three-dimensional dumbbell-shaped domain that consists of two compartments Ω_1 and Ω_3 and a connecting neck Ω_2 that is effectively one-dimensional, such as shown in Fig. 7.13, or in a similar domain with a long neck.

Theorem 7.7.1 (The smallest eigenvalue in a dumbbell-shaped domain). *The smallest positive eigenvalue λ of the Neumann problem for the Laplace equation in the dumbbell is to leading order that of the two-state Markov process, which is $\lambda = -(\lambda_{I \rightarrow II} + \lambda_{II \rightarrow I})$, where the transition rates from I to II and from II to I are, respectively,*

$$\lambda_{I \rightarrow II} = \frac{1}{2\bar{\tau}_{\Omega_1 \rightarrow SS}}, \quad \lambda_{II \rightarrow I} = \frac{1}{2\bar{\tau}_{\Omega_3 \rightarrow SS}}. \quad (7.127)$$

Proof The stochastic separatrix for Brownian motion in a dumbbell domain is the locus of points from which a Brownian trajectory is equally likely to reach either compartment before the other (see [Schuss (2013), Chapter 6]. We assume, as we may, that the stochastic separatrix in the neck is the cross section at its center. In the planar case it is the segment AB in Fig. 7.13. Thus the mean time to traverse the neck from compartment Ω_1 to compartment Ω_3 is asymptotically twice the mean first passage time $\bar{\tau}_{x \rightarrow SS}$ from $x \in \Omega_1$ to the stochastic separatrix. This mean first passage time is to leading order independent of $x \in \Omega_1$ and can be denoted $\bar{\tau}_{\Omega_1 \rightarrow SS}$.

First, we note that when the neck is narrow, the mean residence time of a Brownian trajectory in Ω_1 or in Ω_3 is much larger than that in Ω_2 . Second, we note that the first passage time $\bar{\tau}_{x \rightarrow SS}$ for $x \in \Omega_1$ is exponentially distributed for long times and so is $\bar{\tau}_{x \rightarrow SS}$ for $x \in \Omega_3$. We can therefore coarse-grain the Brownian motion to a two-state Markov process (a telegraph process), which is in State I when the Brownian trajectory is in Ω_1 and is in State II when it is in Ω_3 . The state Ω_2 and the residence time there can be neglected relative to those in Ω_1 and Ω_3 . The transition rates from I to II and from II to I, given in (7.127), can be found from (7.125), with L half the length of the neck and $SS = \partial\Omega_a$. The radii of curvature $R_{c,1}$ and $R_{c,3}$ at the two funnels may be different, and the domain is either Ω_1 or Ω_3 , as the case may be.

The asymmetric Markovian random telegraph process jumps between two states, I and II, at independent exponentially distributed waiting times with rates $\lambda_{I \rightarrow II}$ and

$\lambda_{II \rightarrow I}$, respectively. The transition probability distribution function satisfies the linear differential equations (see http://en.wikipedia.org/wiki/Telegraph_process)

$$\begin{aligned}\frac{\partial P\{I, t | x, t_0\}}{\partial t} &= -\lambda_{I \rightarrow II} P\{I, t | x, t_0\} + \lambda_{II \rightarrow I} P\{II, t | x, t_0\}, \\ \frac{\partial P\{II, t | x, t_0\}}{\partial t} &= \lambda_{I \rightarrow II} P\{I, t | x, t_0\} - \lambda_{II \rightarrow I} P\{II, t | x, t_0\},\end{aligned}\quad (7.128)$$

which can be written in the obvious matrix notation as $\dot{\mathbf{p}} = \mathbf{A}\mathbf{p}$ with

$$\mathbf{A} = \begin{pmatrix} -\lambda_{I \rightarrow II} & \lambda_{II \rightarrow I} \\ \lambda_{I \rightarrow II} & -\lambda_{II \rightarrow I} \end{pmatrix}.$$

The eigenvalues of \mathbf{A} are 0 with the normalized eigenvector $(\frac{1}{2}, \frac{1}{2})^T$, and $-(\lambda_{I \rightarrow II} + \lambda_{II \rightarrow I})$ with the eigenvector $(1, -1)^T$. It follows that the nonzero eigenvalue of the system (7.128) is $\lambda = \lambda_{I \rightarrow II} + \lambda_{II \rightarrow I}$. Hence the Theorem follows. \square

For example, if the solid dumbbell consists of two general heads connected smoothly to the neck by funnels (see (8.171) below), the two rates are given by

$$\frac{1}{\lambda_{I \rightarrow II}} = \sqrt{2} \left[\left(\frac{R_{c,1}}{a} \right)^{3/2} \frac{|\Omega_1|}{R_{c,1} D} \right] (1 + o(1)) + \frac{L^2}{4D} + \frac{|\Omega_1| L}{\pi a^2 D} \quad (7.129)$$

$$\frac{1}{\lambda_{II \rightarrow I}} = \sqrt{2} \left[\left(\frac{R_{c,3}}{a} \right)^{3/2} \frac{|\Omega_3|}{R_{c,3} D} \right] (1 + o(1)) + \frac{L^2}{4D} + \frac{|\Omega_3| L}{\pi a^2 D}. \quad (7.130)$$

Next, we consider the Neumann problem for the Laplace equation in a domain that consists of any number of heads interconnected by narrow necks. The Brownian motion can be coarse-grained into a Markovian random walk that jumps between the connected domains at exponentially distributed times with rates determined by the first passage times and exit probabilities, as described in Sect. 7.7.1. This random walk can in turn be approximated by an effective coarse-grained anisotropic diffusion, as done, for example, for atomic migration in crystals (see Annotations 7.10 for references).

7.8 Diffusion of a Needle in Dire Straits

As an application of the methodology described above, we study the planar diffusion of a stiff thin rod (needle) of length l in an infinite horizontal strip of width $l_0 > l$. We assume that the rod is a long thin right circular cylinder with radius $a \ll l_0$ (Fig. 7.14). The planar motion of the rod is described by two coordinates of the centroid and the rotational angle θ between the axes of the strip and the rod. The y -coordinate of the center of the rod is measured from the axis of the strip. The motion of the

rod is confined to the dumbbell-shaped domain Ω shown in Fig. 7.14b. The rod turns around if the point (θ, y) crosses from the left domain L into the right domain R or in the reverse direction, as described in [Schuss (2013), Chapter 6]. If

$$\varepsilon = \frac{l_0 - l}{l_0} \ll 1, \quad (7.131)$$

the window AB becomes narrow and the mean first passage times $\bar{\tau}_{L \rightarrow AB}$ and $\bar{\tau}_{R \rightarrow AB}$, from the left or right domains to the segment AB , which is the stochastic separatrix SS , become much longer than those from AB to L or R . They also become independent of the starting position outside a boundary layer near the segment AB . Thus the definition of the time to turn around is independent of the choice of the domains L and R as long as they are well separated from the segment AB . The neck near the segment is the boundary layer region near $\theta = \pi/2$. We henceforth neglect the short times relative to the long ones.

To turn across the vertical position the rod has to reach the segment AB from the left domain L for the first time and then to reach the right domain R for the first time, having returned to L any number of times prior to reaching R . It is shown in [Schuss (2013), Chapter 6] that the mean time to turn, $\bar{\tau}_{L \rightarrow R}$, is asymptotically given by

$$\bar{\tau}_{L \rightarrow R} \sim 2\bar{\tau}_{L \rightarrow AB} \text{ for } \varepsilon \ll 1. \quad (7.132)$$

The time to turn around is invariant under translations along the strip (the x -axis), therefore it suffices to describe the rod movement by its angle θ and the y coordinate of its center. The position of the rod is defined for $\theta \bmod \pi$. Therefore the motion of the rod in the invariant strip can be mapped into that in the (θ, y) planar domain Ω (see Fig. 7.14b):

$$\Omega = \left\{ (\theta, y) : |y| < \frac{l_0 - l \sin \theta}{2}, \quad 0 < \theta < \pi \right\}. \quad (7.133)$$

Our purpose is to calculate the mean turnaround time $\bar{\tau}_{L \rightarrow R}$.

7.8.1 The Diffusion Law of a Needle in a Planar Strip

We begin with the derivation of the law of motion of a Brownian needle in a planar strip.

Theorem 7.8.1 (Equations of motion of a Brownian needle). *In a fixed system of Cartesian coordinates (x, y) , the translational and rotational motion of the centroid $(x(t), y(t))$ and the angle of rotation $\theta(t)$ of the rod is governed by the stochastic differential equations (in Itô's sense)*

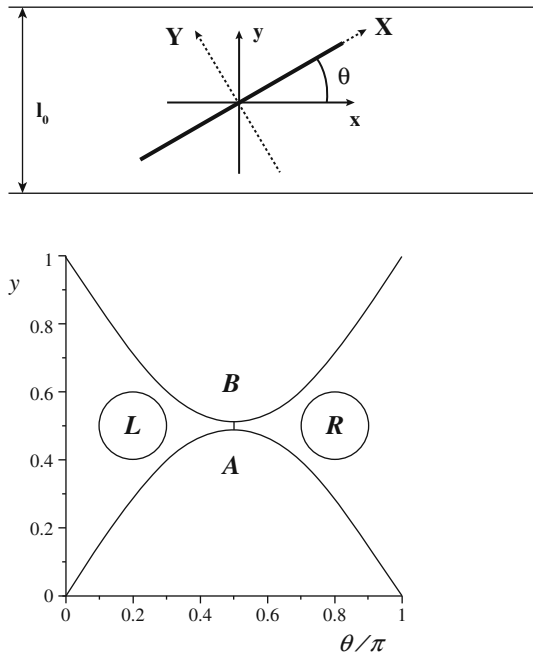


Fig. 7.14 Rod in a strip. **Top:** The strip width is l_0 and the rod length is $l < l_0$. The position of the rod is characterized by the angle θ and the fixed coordinates x and y and the rotating system of coordinates (X, Y, θ) . **Bottom:** The motion of the rod is confined to the domain Ω in the (θ, y) plane

$$\begin{aligned}\dot{x} &= \cos(\theta)\sqrt{2D_X} \dot{w}_1 - \sin(\theta)\sqrt{2D_Y} \dot{w}_2 \\ \dot{y} &= \sin(\theta)\sqrt{2D_X} \dot{w}_1 + \cos(\theta)\sqrt{2D_Y} \dot{w}_2 \\ \dot{\theta} &= \sqrt{2D_r} \dot{w}_3\end{aligned}\quad (7.134)$$

with co-normal reflection at the boundary of the domain in Fig. 7.14 (bottom panel).

Proof In a rotating system of coordinates (X, Y, θ) , where the instantaneous X -axis is parallel to the long axis of the rod and the Y -axis is perpendicular to it, the diffusive motion of the rod is an anisotropic Brownian motion, and can be described by the stochastic equations

$$\dot{X} = \sqrt{2D_X} \dot{w}_1, \quad \dot{Y} = \sqrt{2D_Y} \dot{w}_2, \quad \dot{\theta} = \sqrt{2D_r} \dot{w}_3,$$

where D_X is the longitudinal diffusion coefficient along the axis, D_Y the transversal diffusion constant, and D_r the rotational diffusion coefficient. Due to the anisotropy, in general the rod makes larger excursions in the X -direction than in the Y -direction and this is usually characterized by the ratio D_Y/D_X . Transforming into a fixed system

of Cartesian coordinates (x, y) , the motion of the centroid $(x(t), y(t))$ and the angle of rotation $\theta(t)$ of the rod is governed by the Itô equations (7.134). \square

Theorem 7.8.2 (The probability density function, mean first passage time, and boundary conditions). *The probability density function of the rod in the product space $\Omega \times \mathbb{R}$,*

$$p(t, x, y, \theta) dx = \Pr\{(x(t), y(t), \theta(t)) \in x + dx\}, \quad (7.135)$$

satisfies the Fokker–Planck equation

$$\frac{\partial p(t, x)}{\partial t} = -\nabla \cdot \mathbf{J}(t, x),$$

where the flux is given by

$$\mathbf{J}(t, x) = - \begin{pmatrix} \left[D_X \cos^2 \theta + D_Y \sin^2 \theta \right] \frac{\partial p}{\partial x} + \frac{1}{2} [(D_X - D_Y) \sin 2\theta] \frac{\partial p}{\partial y} \\ \left[D_X \sin^2 \theta + D_Y \cos^2 \theta \right] \frac{\partial p}{\partial y} + \frac{1}{2} [(D_X - D_Y) \sin 2\theta] \frac{\partial p}{\partial x} \\ D_r \frac{\partial p}{\partial \theta} \end{pmatrix}. \quad (7.136)$$

The boundary conditions are π -periodic in θ , and the normal flux $-D_r \partial p(t, x, y, \theta)/\partial \theta$ is π -antiperiodic in θ .

The mean first passage time $\bar{\tau}_{L \rightarrow AB}$ is the solution $u(\theta, y)$ of the mixed Pontryagin–Andronov–Vitt boundary value problem

$$D_r \frac{\partial^2 u(\theta, y)}{\partial \theta^2} + D_y(\theta) \frac{\partial^2 u(\theta, y)}{\partial y^2} = -1 \text{ for } (\theta, y) \in \Omega_1, \quad (7.137)$$

where $D_y(\theta) = D_X \sin^2 \theta + D_Y \cos^2 \theta$ and $\Omega_1 = \Omega \cap \left\{ \theta < \frac{\pi}{2} \right\}$, with the mixed boundary conditions

$$\frac{\partial u}{\partial \tilde{n}} = 0 \text{ for } (\theta, y) \text{ on the curved boundary and at } \theta = 0 \quad (7.138)$$

$$u\left(\frac{\pi}{2}, y\right) = 0 \text{ for } |y| < l_0 - l, \quad (7.139)$$

where the co-normal derivative of $u(\theta, y)$ on the curved boundary boundary is given by

$$\frac{\partial u}{\partial \tilde{n}} = \nabla u(\theta, y) \cdot \tilde{\mathbf{n}}(\theta) \text{ for } (\theta, y) \text{ on the curved boundary} \quad (7.140)$$

and the co-normal vector $\tilde{\mathbf{n}}(\theta)$ is given by

$$\tilde{\mathbf{n}}(\theta) = \begin{pmatrix} D_r & 0 \\ 0 & D_y(\theta) \end{pmatrix} \mathbf{n}(\theta) \quad (7.141)$$

with $\mathbf{n}(\theta)$ the unit outer normal vector at the curved boundary.

Proof Putting (7.134) in the matrix form

$$\dot{\mathbf{x}}(t) = \mathbf{B}(\theta) \dot{\mathbf{w}}, \quad (7.142)$$

where

$$\mathbf{x} = \begin{pmatrix} x \\ y \\ \theta \end{pmatrix}, \quad \mathbf{w} = \begin{pmatrix} w_1 \\ w_2 \\ w_3 \end{pmatrix}$$

and

$$\mathbf{B}(\theta) = \sqrt{2} \begin{pmatrix} \cos \theta & -\sin \theta & 0 \\ \sin \theta & \cos \theta & 0 \\ 0 & 0 & 1 \end{pmatrix} \begin{pmatrix} \sqrt{D_X} & 0 & 0 \\ 0 & \sqrt{D_Y} & 0 \\ 0 & 0 & \sqrt{D_r} \end{pmatrix},$$

defines the Fokker–Planck equation. Because $\mathbf{J}(t, \mathbf{x})$ is π -periodic in θ and the position of the rod is defined modulo π the boundary conditions are π -periodic in θ and the normal flux $-D_r \partial p(t, x, y, \theta)/\partial \theta$ is π -antiperiodic in θ .

The mean first passage time is the solution of the mixed boundary value problem (1.25) with the backward Kolmogorov operator (1.15), defined by the stochastic system (7.142). Because the BKO is translation-invariant with respect to x it reduces to (7.137). The boundary conditions follow from [Schuss (2013), Theorem 2.7.1] (with $\kappa(\mathbf{x}, t) = 0$ for state-dependent diffusion matrix and curved boundaries). \square

7.8.2 The Turnaround Time $\bar{\tau}_{L \rightarrow R}$

Equation (7.132) shows that it suffices to calculate the mean first passage time $\bar{\tau}_{L \rightarrow AB}$ in order to calculate the turn around time $\bar{\tau}_{L \rightarrow R}$. The latter is the solution of the Pontryagin–Andronov–Vitt mixed boundary value problem in Ω (the domain on the left in Fig. 7.14b) with Dirichlet conditions on the short segment AB .

Theorem 7.8.3 (The turnaround time). *The mean turnaround time of a Brownian needle of length l in a narrow strip of width l_0 , such that $\varepsilon = (l_0 - l)/l_0 \ll 1$, is given by*

$$\bar{\tau}_{L \rightarrow R} = \frac{\pi(\pi - 2)}{D_r \sqrt{l_0(l_0 - l)}} \sqrt{\frac{D_X}{D_r}} \left(1 + O\left(\sqrt{\frac{l_0 - l}{l_0}}\right) \right). \quad (7.143)$$

Proof Introducing the dimensionless variables

$$X' = \frac{X}{l_0}, \quad Y' = \frac{Y}{l_0}, \quad \xi(t) = \frac{x(t)}{l_0}, \quad \eta(t) = \frac{y(t)}{l_0}$$

and the normalized diffusion coefficients

$$D'_X = \frac{D_X}{l_0^2}, \quad D'_Y = \frac{D_Y}{l_0^2}, \quad D_\eta(\theta) = \frac{D_y(\theta)}{l_0^2},$$

we find that the domain Ω in (7.133) is mapped into

$$\Omega' = \left\{ (\theta, \eta) : |\eta| < \frac{1 - (1 - \varepsilon) \sin \theta}{2}, \quad 0 < \theta < \pi \right\}. \quad (7.144)$$

To convert (7.137) to canonical form, we introduce the variable

$$\varphi(\theta) = \int_0^\theta \sqrt{\frac{D_\eta(\theta')}{D_r}} d\theta', \quad (7.145)$$

which defines the inverse function $\theta = \theta(\varphi)$, and set $u(\theta, y) = U(\varphi, \eta)$ to obtain

$$U_{\varphi\varphi}(\varphi, \eta) + U_{\eta\eta}(\varphi, \eta) = U_\varphi(\varphi, \eta) \sqrt{D_r} \frac{dD_\eta^{-1/2}(\theta)}{d\theta} - \frac{1}{D_\eta(\theta)}. \quad (7.146)$$

The domain Ω' , defined in (7.144), is mapped into the similar domain

$$\Omega'' = \left\{ (\varphi, \eta) : |\eta| < \frac{1 - (1 - \varepsilon) \sin \theta(\varphi)}{2}, \quad 0 < \varphi < \varphi(\pi) \right\} \quad (7.147)$$

in the (φ, η) plane. Because the co-normal direction at the boundary becomes normal, so does the co-normal derivative. The curved boundary in the scaled Fig. 7.14b is denoted $\partial\Omega''$. It follows that the no-flux boundary condition (7.138) and the absorbing condition (7.139) become

$$\begin{aligned} \frac{\partial U(\varphi, \eta)}{\partial n} &= 0 \text{ for } (\theta(\varphi), \eta) \text{ on } \partial\Omega'' \\ \frac{\partial U(0, \eta)}{\partial \varphi} &= 0 \text{ for } |\eta| < \frac{1}{2} \\ U\left(\varphi\left(\frac{\pi}{2}\right), \eta\right) &= 0 \text{ for } |\eta| < \frac{\varepsilon}{2}, \end{aligned} \quad (7.148)$$

respectively. The gap at $\theta = \pi/2$ is preserved and the (dimensionless) radius of curvature of the boundary at the gap is

$$R' = \frac{2D_\eta \left(\frac{\pi}{2}\right)}{(1-\varepsilon)D_r} = \frac{2D_X}{(1-\varepsilon)l_0^2 D_r}. \quad (7.149)$$

First, we simplify (7.146) by setting

$$g(\varphi) = \sqrt{D_r} \frac{dD_\eta^{-1/2}(\theta)}{d\theta}, \quad U(\varphi, \eta) = f(\varphi)V(\varphi, \eta) \quad (7.150)$$

and choosing $f(\varphi)$ such that $f'(\varphi) = \frac{1}{2}f(\varphi)g(\varphi)$. Note that

$$\left. \frac{dD_\eta^{-1/2}(\theta)}{d\theta} \right|_{\theta=0, \pi/2, \pi} = 0. \quad (7.151)$$

Equation (7.146) becomes

$$V_{\varphi\varphi} + V_{\eta\eta} = \frac{1}{f(\varphi)} \left\{ [g(\varphi)f'(\varphi) - f''(\varphi)]V - \frac{1}{D_\eta(\theta(\varphi))} \right\}. \quad (7.152)$$

Next, we move the origin to the center of curvature of the lower boundary by setting

$$\zeta = -\left(\eta - R' - \frac{\varepsilon}{2}\right) + i\left[\varphi - \varphi\left(\frac{\pi}{2}\right)\right]$$

and use the conformal mapping

$$w = w(z) = \frac{z - \alpha}{1 - \alpha z}, \quad (7.153)$$

where

$$\begin{aligned} \alpha &= -\frac{2\varepsilon R_c + 2R_c + \varepsilon^2 R_c + 2r_c \varepsilon + 2r_c}{2(\varepsilon R_c + r_c + R_c)} \\ &\pm \frac{\sqrt{\varepsilon(8R_c r_c + 4\varepsilon R_c^2 + 12\varepsilon R_c r_c + 4\varepsilon^2 R_c^2 + 8r_c^2 + 4\varepsilon^2 R_c r_c + \varepsilon^3 R_c^2 + 4\varepsilon r_c^2)}}{2(\varepsilon R_c + r_c + R_c)} \\ &= -1 \pm \sqrt{\frac{2r_c \varepsilon}{R_c + r_c}} + O(\varepsilon), \end{aligned} \quad (7.154)$$

to write

$$\omega = \frac{\zeta - R'\alpha}{R' - \alpha\zeta}, \quad (7.155)$$

with $\omega = \rho e^{i\psi}$. We also have

$$w'(\zeta) = \frac{1}{R'} \frac{(1 + \alpha w)^2}{1 - \alpha^2} \quad (7.156)$$

$$|w'(\zeta)|^2 = \frac{1}{R'^2} \left| \frac{(1 + w\alpha)^2}{1 - \alpha^2} \right|^2 = \frac{|1 - w + \sqrt{\varepsilon} w|^4}{4\varepsilon R'^2} (1 + O(\sqrt{\varepsilon})). \quad (7.157)$$

The image Ω_ω of the domain Ω is given in Fig. 7.15 and is similar to Ω_w in Fig. 7.10, except for a small distortion near $\psi = c\sqrt{\varepsilon}$, which we neglect, as we may. Setting $V(\varphi, \eta) = W(\rho, \psi)$, fixing $\rho = 1$ in Ω_ω , as in Sect. 7.4, and abbreviating $W = W(\psi, 1)$, equation (7.152) becomes to leading order

$$W_{\psi\psi} + \frac{h(\psi)}{|\omega'(\zeta)|^2} W = -\frac{1}{|\omega'(\zeta)|^2 k(\psi)}, \quad (7.158)$$

where

$$h(\psi) = \frac{f''(\varphi) - g(\varphi)f'(\varphi)}{f(\varphi)} \Big|_{\rho=1}, \quad k(\psi) = f(\varphi)D_\eta(\theta(\varphi))|_{\rho=1}. \quad (7.159)$$

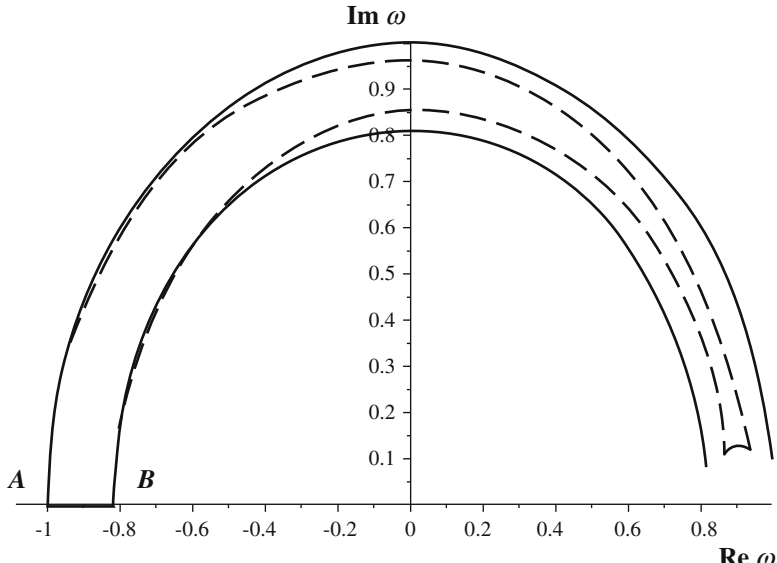


Fig. 7.15 The image Ω_ω of the domain Ω under the mapping (7.155). The values of the parameters are $\varepsilon = 0.01$ with the approximation $D_Y \ll D_X$. The domain is enclosed by the real segment AB , the dashed arcs, and the small closing cap. The solid circular arcs are the conformal images of arcs of the osculating circles at the narrow neck, as in Fig. 7.10

Using (7.72) and neglecting terms of order $O(\varepsilon)$, we rewrite (7.158) as

$$W_{\psi\psi} + \frac{4\varepsilon R'^2 h(\psi)}{|e^{i\psi}(1 - \sqrt{\varepsilon}) - 1|^4} W = -\frac{4\varepsilon R'^2}{|e^{i\psi}(1 - \sqrt{\varepsilon}) - 1|^4 k(\psi)}. \quad (7.160)$$

In view of (7.151), the boundary conditions (7.148) become

$$W_\psi(c\sqrt{\varepsilon}) = 0, \quad W(\pi) = 0. \quad (7.161)$$

The outer solution of (7.160) is a linear function $W_{\text{outer}}(\psi) = a\psi + b$, where a and b are yet undetermined constants. The uniform approximation is constructed as $W_{\text{uniform}}(\psi) = W_{\text{outer}}(\psi) + W_{\text{bl}}(\psi)$, where the boundary layer $W_{\text{bl}}(\psi)$ is a function $Y(\xi)$ of the boundary layer variable $\xi = \psi/\sqrt{\varepsilon}$. The boundary layer equation is

$$Y''(\xi) + \frac{4R'^2 h(0)}{(1 + \xi^2)^2} Y(\xi) = -\frac{4R'^2}{(1 + \xi^2)^2 k(0)}, \quad (7.162)$$

which is simplified by the substitution $Y(\xi) = \tilde{Y}(\xi) + 1/h(0)k(0)$ to

$$\tilde{Y}''(\xi) + \frac{4R'^2 h(0)}{(1 + \xi^2)^2} \tilde{Y}(\xi) = 0. \quad (7.163)$$

The boundary conditions (7.161) become $\tilde{Y}'(c) = 0$ and $\tilde{Y}(\infty) = 1/h(0)k(0)$.

The boundary layer equation (7.163) has two linearly independent solutions, $\tilde{Y}_1(\xi)$ and $\tilde{Y}_2(\xi)$, which are linear for sufficiently large ξ . Initial conditions for $\tilde{Y}_1(\xi)$ and $\tilde{Y}_2(\xi)$ can be chosen so that $\tilde{Y}_2(\xi) \rightarrow \text{const}$ as $\xi \rightarrow \infty$ (e.g., $\tilde{Y}_2(0) = -4.7$, $\tilde{Y}'_2(0) = -1$, see Fig. 7.16). Thus the boundary layer function is given by

$$W_{\text{bl}}(\psi) = A\tilde{Y}_1\left(\frac{\psi}{\sqrt{\varepsilon}}\right) + B\tilde{Y}_2\left(\frac{\psi}{\sqrt{\varepsilon}}\right) + C, \quad (7.164)$$

where A and B are constants to be determined and C is related to the constant $1/h(0)k(0)$ and is also determined below from the boundary and matching conditions.

The matching condition is that $W_{\text{bl}}(\psi) = A\tilde{Y}_1(\psi/\sqrt{\varepsilon}) + B\tilde{Y}_2(\psi/\sqrt{\varepsilon}) + C$ remains bounded as $\xi \rightarrow \infty$, which implies $A = 0$. It follows that at the absorbing boundary $\psi = \pi$ we have

$$\begin{aligned} W_{\text{unif}}(\pi) &= a\pi + b' = 0 \\ W'_{\text{unif}}(\pi) &= a, \end{aligned} \quad (7.165)$$

where the constant b' incorporates all remaining constants. At the reflecting boundary we have to leading order

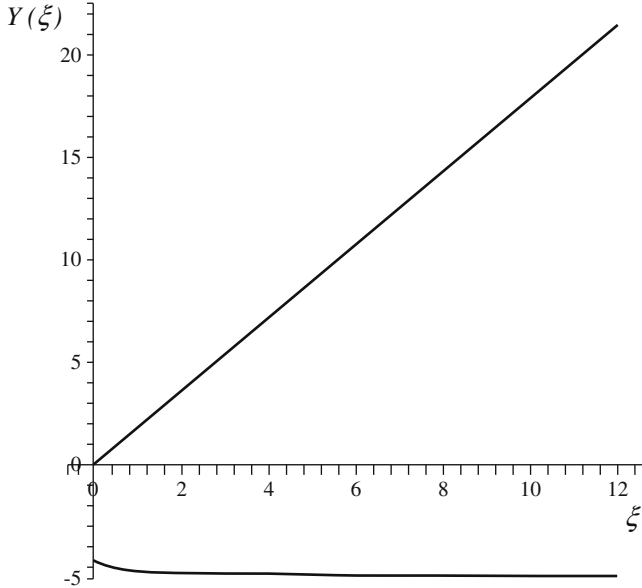


Fig. 7.16 Two linearly independent solutions of (7.163). The linearly growing solution $Y_1(\xi)$ (red) satisfies the initial conditions $Y_1(0) = 0$, $Y'_1(0) = 2$. The asymptotically constant solution $Y_2(\xi)$ (blue) satisfies the initial conditions $Y_2(0) = -4.7$, $Y'_2(0) = -1$. The asymptotic value is $Y_2(\infty) \approx -5$

$$W'_{\text{unif}}(c\sqrt{\varepsilon}) = W'_{\text{outer}}(c\sqrt{\varepsilon}) + W'_{\text{bl}}(c\sqrt{\varepsilon}) = a + B \frac{\tilde{Y}'_2(c)}{\sqrt{\varepsilon}} = 0, \quad (7.166)$$

which gives

$$B = -\frac{a\sqrt{\varepsilon}}{\tilde{Y}'_2(c)}, \quad b' = -a\pi. \quad (7.167)$$

The uniform approximation to $W(\omega)$ is given by

$$W_{\text{unif}}(\rho e^{i\psi}) = a \left(\psi - \pi - \frac{\sqrt{\varepsilon}}{\tilde{Y}'_2(c)} \right), \quad (7.168)$$

so that using (7.150), (7.151), and (7.156), we obtain from (7.168)

$$\begin{aligned} \left. \frac{\partial u}{\partial n} \right|_{\zeta \in \partial \Omega_a} &= f\left(\varphi\left(\frac{\pi}{2}\right)\right) \left. \frac{\partial W(\rho e^{i\psi})}{\partial \psi} \right|_{\psi=\pi} \left. \omega'(\zeta) \right|_{\zeta=-1} \left. \frac{\partial \varphi}{\partial \theta} \right|_{\theta=\pi/2} \\ &= a \sqrt{\frac{2}{\varepsilon R'}} (1 + O(\sqrt{\varepsilon})). \end{aligned} \quad (7.169)$$

Because $W(\omega)$ scales with $1/f(\varphi)$ relative to $V(\varphi, \eta)$, we may choose at the outset $f(\varphi(\pi/2)) = 1$.

Finally, to determine the value of a , we integrate (7.137) over Ω , use (7.169), and the fact that

$$\int_{\partial\Omega_a} dy = l_0 \varepsilon,$$

to obtain $a = -|\Omega| \sqrt{R'}/l_0 D_r \sqrt{2\varepsilon}$. Now (7.168) gives the mean first passage time at any point x in the head as

$$\bar{\tau}_{L \rightarrow AB} = u(x) \sim W\left(\rho e^{ic\sqrt{\varepsilon}}\right) \sim -a\pi = \frac{\pi |\Omega| \sqrt{R'}}{l_0 D_r \sqrt{2\varepsilon}} (1 + O(\sqrt{\varepsilon})) \text{ for } \varepsilon \ll 1. \quad (7.170)$$

Reverting to the original dimensional variables, we get

$$\bar{\tau}_{L \rightarrow AB} = \frac{\pi \left(\frac{\pi}{2} - 1\right)}{D_r \sqrt{l_0(l_0 - l)}} \sqrt{\frac{D_X}{D_r}} \left(1 + O\left(\sqrt{\frac{l_0 - l}{l_0}}\right)\right), \quad (7.171)$$

which together with (7.132) is (7.143). \square

7.9 Applications of the Narrow Escape Time

Example 7.5 (Effective diffusion on a membrane with obstacles). The random motion of receptors on the surface of a neuron is usually restricted by many impenetrable obstacles. These often consist of noninteracting molecules, or fences that are assemblies of several molecules, or corrals that are collections of fences with small holes; microtubules and the cytoskeleton network can also form obstacles. The explicit expression for the narrow escape time determines asymptotically the relation between the variation in the obstacle density and in the effective diffusion constant in the high crowding limit and is also used to examine the asymptotic approximation by Brownian dynamics simulations. A simplified model of diffusion with obstacles is free Brownian motion in a domain whose boundary consists of identical reflecting circles enveloped by a reflecting closed curve.

The narrow escape time from a square of side L with reflecting circles of radius a centered at the corners (Fig. 7.17a) over the entire range of possible straits is given by (7.27), (7.66), and (7.90), depending on the crowding. In particular, the narrow escape time is given by (7.90) to leading order and can be approximated by

$$\bar{\tau}_n = \frac{\bar{\tau}}{n}, \quad (7.172)$$

where $\bar{\tau}$ is the mean first passage time to a single escape window in a neck with the other windows closed (reflecting instead of absorbing).

For small $a \ll L$, the narrow escape time is independent of a , though dependent on (x, y) , so the circles can be ignored to leading order, but it increases with a . When the width of the straits $L - 2a$ is about $2a$, that is, when $a \approx L/4$, the opening between the circles can be considered small, so according to (7.27) and (7.172) it can be approximated by

$$\bar{\tau} = \frac{|\Omega|}{4D\pi} \left[\log \frac{1}{\varepsilon} + O(1) \right] \text{ with } \varepsilon = (L - 2a)/L \approx 0.5, \quad (7.173)$$

because there are four well separated straits for escape. For $L - 2a \ll a/2$ (i.e., for $\varepsilon \ll 1$), thus a uniform approximation to the narrow escape time from the center can be obtained by patching the three regimes numerically, which gives

$$\bar{\tau} \approx \begin{cases} c_1 & \text{for } 0.8 < \varepsilon < 1 \\ c_2 |\Omega| \log \frac{1}{\varepsilon} + d_1 & \text{for } 0.55 < \varepsilon < 0.8 \\ c_3 \frac{|\Omega|}{\sqrt{\varepsilon}} + d_2 & \text{for } \varepsilon < 0.55 \end{cases} \quad (7.174)$$

with $d_1, d_2 = O(1)$.

□

Exercise 7.4 (The mean first passage time to the boundary of a square).

(i) Solve the Pontryagin–Andronov–Vitt boundary value problem by separation of variables to find the mean first passage time c_1 from the center to the boundary of an unrestricted square of side L .

(ii) Show that it is given approximately by

$$c_1 = u(L/2, L/2) \approx \frac{4L^2}{\pi^3 D} \frac{\cosh \frac{\pi}{2} - 1}{\cosh \pi}. \quad (7.175)$$

(iii) Show that for $L = 1$ and $D = 1$ the value is $c_1 \approx 0.076$ in agreement with Brownian dynamics simulations (see Fig. 7.17b and [Holcman et al. (2011)]). □

The coefficient c_2 is obtained from (7.173) as $c_2 = 1/2\pi D \approx 0.16$. Similarly, the coefficient c_3 is obtained from (7.66) and (7.172) as $c_3 \approx \pi/4\sqrt{2} D \approx 0.56$. The coefficients d_i are chosen by patching $\bar{\tau}$ continuously between the different regimes. We get

$$d_1 = c_1 + c_2 |D(r_1)| \log(1 - 2r_1), \quad (7.176)$$

and

$$d_2 = c_1 + c_2 [|D(r_1)| \log(1 - 2r_1) - |D(r_2)| \log(1 - 2r_2)] \\ - c_3 |D(r_2)| (1 - 2r_2)^{-1/2}.$$

Simulations with $D = 1$ in a square of side $L = 1$ with 4 reflecting circles of radius r , centered at the corners, show that the uniform approximation by the patched formula (7.174) is in good agreement with Brownian results (Fig. 7.17b), where the statistics were collected from 1,000 escape times of Brownian trajectories per graph point. The trajectories start at the square center.

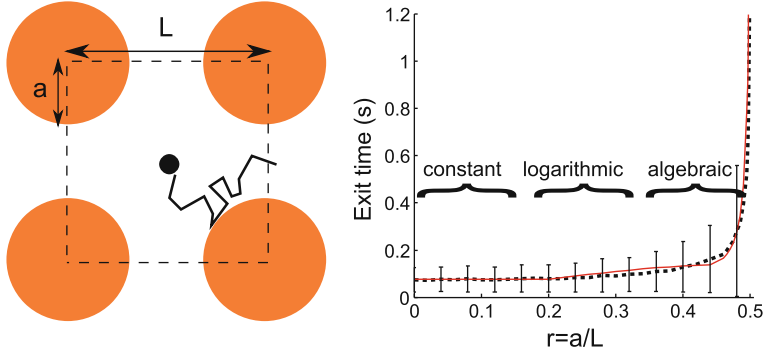


Fig. 7.17 **Left panel:** Narrow escape time from a domain with $D = 1$, $L = 1$. Statistics were obtained from 1000 exit times/point of simulated Brownian trajectories (dashed line). **Right panel:** narrow escape time vs obstacle scaled radius $r = a/L = \frac{1}{2}(1 - \varepsilon)$. The analytical approximation is (7.174) (continuous curve) with $0 < r = r_1 = 0.2$, $r_1 < r < r_2 = 0.45$, and $0.45 < r < 0.5$

To calculate the effective diffusion coefficient of the Brownian motion on an isotropic square lattice with crowded obstacles in a domain Ω with a reflecting boundary, we first coarse-grain it into a random walk between the centers of adjacent squares. Then we approximate the master equation for the transition probability density function of the random walk by the two-dimensional diffusion equation [Schuss (2010b)]. Because the mean exit time from a single lattice square is long, the first eigenvalue of the mixed Neumann–Dirichlet problem in a single cell is well separated from the higher ones. It follows that the waiting time in the cell is exponentially distributed with rate

$$\lambda = \frac{2}{\bar{\tau}}, \quad (7.177)$$

where $\bar{\tau}$ is given in (7.174). This is due to the fact that a Brownian trajectory at the center of the straits is equally likely to return or move to the next lattice square.

The first coarse-graining of the diffusion in a plane with a lattice of obstacles is to a Markovian jump process, as in Theorem 7.7.1. The coarse-grained process jumps between neighboring centers of the lattice squares that are L apart at exponential waiting times with rate λ , given in (7.177). The next coarse-graining is a diffusion

approximation to the master equation for the transition probability density function of the Markovian jump process. The diffusion approximation is given by

$$\frac{\partial p}{\partial t} = \bar{D} \left(\frac{\partial^2 p}{\partial x^2} + \frac{\partial^2 p}{\partial y^2} \right), \quad \bar{D} = \frac{\lambda L^2}{4} \quad (7.178)$$

(see Annotations 7.10 for references).

In the above simplified model of crowding, the circular obstacles are arranged in a quadratic lattice, as shown in Fig. 7.18a. Simulations of Brownian trajectories with recording of the escape times from one cell to the other give the statistics in (Fig. 7.18a) with fixed L and variable a . According to (7.174), (7.177), (7.178), as a increases the effective diffusion constant \bar{D} decreases. Fig. 7.18c shows the diffusion coefficient ratio Ω_a / Ω_0 , where Ω_a is computed from the Brownian simulations on the square lattice described above with obstacles of radius a . For $a = 0.3$, the simulation shows that $\Omega_a / \Omega_0 \approx 0.7$ whereas a direct computation using the mean first passage time (7.174) gives

$$\frac{\bar{\tau}_0}{\bar{\tau}_a} = \frac{c_1}{c_2 |\Omega| \log \varepsilon^{-1} + d_1} \approx 0.69, \quad (7.179)$$

where $\varepsilon = (L - 2a)/L = 0.4$. Thus the simulations show that the effective observed diffusion is as in classical diffuson theory and the effective diffusion coefficient $\Omega_a / \Omega_0 = \bar{\tau}_0 / \bar{\tau}_a$ decreases nonlinearly as a function of the radius a , as given by the uniform formula (7.174).

The three regimes of eq. (7.174) (Fig. 7.18c) are recovered: a non-crowded regime for $a < 0.2L$, where the effective diffusion coefficient does not show any apparent decrease, a region $0.2L < a < 0.4L$, where the leading order term of the effective diffusion coefficient is logarithmic, and for $a > 0.4L$ the effective diffusion coefficient decays as $\sqrt{(L - 2a)/L}$, in agreement with (7.174).

7.10 Annotation to the Narrow Escape Time Problem

The narrow escape time was calculated for small absorbing windows in a smooth reflecting boundary in [Gandolfi et al. (1985)], in the series of papers [Ward and Van De Velde (1992)]–[Ward et al. (1993)], and numerically later in [Grigoriev et al. (2002)], using Green's function and matched asymptotics in [Holcman and Schuss (2004)], [Kolokolnikov et al. (2005)]. A new method was introduced in [Singer et al. I (2006)]–[Singer and Schuss (2006)], [Schuss et al. (2007)], more recent confirmatory results were given in [Bénichou and Voituriez (2008)], [Coombs et al. (2009)] and higher-order expansions are in [Cheviakov et al. (2010)]. Several more complex cases, such as the narrow escape time through a window at a corner or at a cusp in the boundary and the narrow escape time on Riemannian manifolds, were solved in [Singer et al. I (2006)]–[Singer et al. III (2006a)].

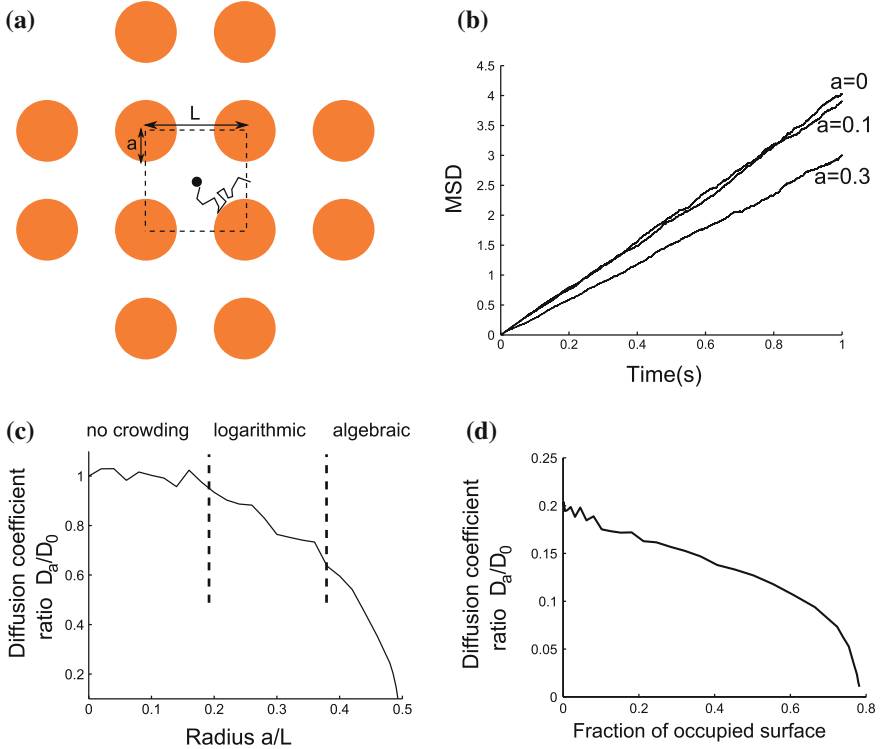


Fig. 7.18 Organization of the neuronal membrane. (a) Schematic representation of a Brownian particle diffusing in a crowded microdomain. (b) Mean Square Displacement of the particle in a domain paved with microdomains. The mean square displacement is linear showing that crowding does not affect the nature of diffusion. The effective diffusion coefficient is computed from $\langle \text{MSD}(t)/4t \rangle$. (c) Effective diffusion coefficient computed from the mean square displacement for different radiiuses of the obstacles. Brownian simulations (continuous curve): there are three regions (separated by the dashed lines). While there is no crowding for $a < 0.2$, the decreasing of the effective diffusion coefficient for $0.2 < a < 0.4$ is logarithmic, and like square root for $a > 0.4$. (d) Effective diffusion coefficient of a particle diffusing in a domain as a function of the fraction of the occupied surface. An AMPAR has a diffusion coefficient of $0.2 \mu\text{m}^2/\text{sec}$ in a free membrane [Renner et al. (2009)]

Further elaboration of Theorem 7.3.1 is given in [Singer et al. I (2006a)]. The calculation of the narrow escape time in composite domains with long necks started in [Biess et al. (2007)], [Schuss et al. (2007)] and [BerezBarzykin et al. (2009)] and ultimately accomplished in [Holcman and Schuss (2011)]. The narrow escape time problem in a planar domain with an absorbing window at the end of a funnel was considered in [Holeman et al. (2011)]. The case of planar domains that consist of large compartments interconnected by funnel-shaped bottlenecks was solved in [Holcman et al. (2011)]. In dimension 3, obstacles alter diffusion, studied numerically in [Biess et al. (2011)]. The result (7.66) was found in [Holcman et al. (2011)]. The coarse-

graining of diffusion into a Markov chain is discussed in [Hänggi et al. (1990)] (see also [Holcman et al. (2011)]). Section 7.4 is based on [Holcman et al. (2011)]. Section 7.4.2 is based on [Holcman and Schuss, PLA (2008)], [Holcman and Schuss, JPA (2008a)], and [Holcman and Schuss (2012a)]. Section 7.5 is based on [Holcman and Schuss (2011)].

This chapter develops a boundary layer theory for the solution of the mixed Neumann–Dirichlet problem for the Poisson equation in geometries in which the methodologies of the above mentioned references failed. These methodologies were used for the narrow escape problem. In the geometries considered here the small Dirichlet part is located at the end of narrow straits connected smoothly to the Neumann boundary of the domain. Additional problems related to Brownian motion in composite domains that contain a cylindrical narrow neck connected smoothly or sharply to the head are considered in [Holcman and Schuss (2011)]. These include the asymptotic evaluation of the narrow escape time, of the leading eigenvalue in dumbbell-shaped domains and domains with many heads interconnected by narrow necks, the escape probability through any one of several narrow necks, and more. The case of diffusion in a potential landscape with several deep wells (high barriers) is considered in [Schuss SIREV (1980a)], [Schuss (1980b)] and [Matkowsky and Schuss (1981)].

The random walk approximation in a dumbbell domain can in turn be approximated by an effective coarse-grained anisotropic diffusion, as done, for example, for atomic migration in crystals [Schuss (1980b), Ch.8, Sect. 2] for effective diffusion on a surface with obstacles [Holcman et al. (2011)], and for a general diffusion on a potential landscape with deep wells [Hänggi et al. (1990)]. The derivations are given in, [Schuss (1980b), page 205] and also in Chap. 5 Sect. 5.5.1.

The effect of obstacles on the diffusion constant has been studied in the biological context for the last two decades [Eisinger et al. (1986)], [Edidin et al. (1991)], [Sheetz (1993)], [Kusumi et al. (1993)], [Saxton (1995)], [Saxton and Jacobson (1997)], [Suzuki and Sheetz (2001)], [Kusumi et al. (2005)], and more recently it was demonstrated, using single-particle imaging [Borgdorff and Choquet (2002)], [Tardin et al. (2003)], [Triller and Choquet (2003)], [Choquet (2010)], that the effective diffusion constant can span a large spectrum of values, from 0.001 to $0.2 \mu\text{m}^2/\text{sec}$ [Choquet (2010)].

Formula (7.178) can be used to estimate the density of obstacles on the membrane of a neuronal dendrite. Using the experimentally measured single receptor trajectory on the surface of a neuron by single particle tracking methods, see for example [Borgdorff and Choquet (2002)], [Triller and Choquet (2003)], [Choquet (2010)], we use the fact that the receptor effective diffusion coefficient varies from 0.01 to $0.2 \mu\text{m}^2/\text{sec}$. To estimate the density of obstacles from (7.174), (7.177), (7.178), a reference density has to be chosen. Choosing the reference diffusion coefficient to be that of receptors moving on a free membrane (with removed cholesterol), estimated to be $0.17 \leq D \leq 0.2 \mu\text{m}^2/\text{sec}$ [Renner et al. (2009)], while with removed actin, the resulting effective diffusion coefficient is $0.19 \mu\text{m}^2/\text{sec}$. Using $D = 0.2 \mu\text{m}^2/\text{sec}$ to estimate the crowding effect based on the measured diffusion coefficient (Fig. 7.18d), it can be seen that a reduction of the diffusion coefficient from $D = 0.2 \mu\text{m}^2/\text{sec}$

to $D = 0.04 \mu\text{m}^2/\text{sec}$ is achieved when 70% of the membrane surface is occupied by obstacles. This implies that obstacles impair the diffusion of receptors and are thus responsible for the large decrease of the measured diffusion coefficient (up to 5 times).

In a biochemical context, the narrow escape times (7.27), (7.66), and (7.90) account for the local geometry near an active binding site occluded by the molecular structure of the protein. This is the case for proton binding sites located on spike proteins, located on the viral envelope and involved in membrane fusion [Huang et al. (2002)]. The NET is used to coarse-grained acidification by Markovian jump processes and influenza escape from endosome [Lagache et al. (2017)].

Another application is that of the turn around time of Brownian needle. The result of Sect. 7.8 provides the precise time scale of the unraveling of a double stranded DNA break confined between two-dimensional membranes [Lieber et al. (2009)]. In higher dimensions, the NET asymptotic methodology was used to compute the search for small target by a monomer of a polymer [Amitai et al. (2017a)] and the mean looping time of a Rouse, Random Cross-Linked [Shukron et al. (2017)] and β -polymer model. The computation uses the expansion of the first eigenvalue of the Laplacian when a small tubular neighborhood of size ε of a submanifold of codimension three is removed [Amitai et al. (2017b)].

Applications of the narrow escape time in neuroscience are discussed in Sect. 8.6 below.

Chapter 8

Narrow Escape in \mathbb{R}^3

The mixed boundary value problem for the Poisson (or Pontryagin–Andronov–Vitt) equation in three dimensions is more complicated than that in two dimensions, primarily because the singularity of Neumann’s function for a regular domain is more complicated than (6.4).

8.1 The Neumann Function in Regular Domains in \mathbb{R}^3

The Neumann function for a bounded domain $\Omega \subset \mathbb{R}^3$ with a sufficiently smooth boundary $\partial\Omega$ has the form [Garabedian (1964)]

$$N(\mathbf{x}, \xi) = \frac{1}{4\pi|\mathbf{x} - \xi|} + v_S(\mathbf{x}, \xi), \quad (8.1)$$

where $v_S(\mathbf{x}, \xi)$ has a weaker singularity at $\mathbf{x} = \xi$ when $\mathbf{x} \in \partial\Omega$ and $\xi \in \Omega \cup \partial\Omega$ (see Theorem 8.1.1 below). It follows that only the singular part of the Neumann function contributes to the leading order approximation to the solution of the integral equation (7.8). Thus, we obtain for the leading order approximation to the absorption flux density $g_0(\mathbf{x})$ on $\partial\Omega_a$ and to the leading order approximation C_0 of the constant solution C (the mean first passage time) the Helmholtz integral equation [Helmholtz (1860)]

$$\frac{1}{2\pi} \int_{\partial\Omega_a} \frac{g_0(\mathbf{x}')}{|\mathbf{x}' - \xi|} dS_{\mathbf{x}'} = -C_0. \quad (8.2)$$

The constant C_0 is also the electrostatic capacity of the window [Jackson (1998)].

The structure of Neumann’s function for a regular domain in \mathbb{R}^3 is described in the following theorem [Popov (1992)].

Theorem 8.1.1 (Popov). Assume $\Omega \subset \mathbb{R}^3$ is a bounded domain whose boundary $\partial\Omega$ has continuous partial derivatives up to order three. Then for $z \in \partial\Omega$, $y \in \Omega \cup \partial\Omega$, the structure of the Neumann function (in dimensionless variables) is

$$N(y, z) = \frac{1}{2\pi|y - z|} - \frac{1}{8\pi} [L(z) + N(z)] \log |y - z| + v_S(y, z), \quad (8.3)$$

where $L(z)$ and $N(z)$ are the principal curvatures of $\partial\Omega$ at z and $v_S(y, z)$ is a bounded function of x, y in Ω .

Proof We can assume that the domain is given by $\Omega = \{x \in \mathbb{R}^3 : F(x) < 0\}$, where $F \in C^3(\mathbb{R}^3)$. The Neumann function $N(x, y)$ for this domain is the solution of the boundary value problem

$$\Delta_x N(x, y) = -\delta(x - y) + \frac{1}{|\Omega|} \text{ for } x, y \in D \quad (8.4)$$

$$\frac{\partial N(x, y)}{\partial \nu_x} = 0 \text{ for } x \in \partial\Omega, y \in \Omega, \quad (8.5)$$

where $\mathbf{n}(x)$ is the outer unit normal to the boundary $\partial\Omega$. If x or y (or both) are in $\partial\Omega$, then only half of any sufficiently small ball about a boundary point is contained in Ω , which means that the singularity of Neumann's function is $(2\pi|x - y|)^{-1}$. Therefore Neumann's function for $y \in \partial\Omega$ can be written as

$$N(x, y) = \frac{1}{2\pi|x - y|} + v(x, y), \quad (8.6)$$

where $v(x, y)$ satisfies

$$\Delta_x v(x, y) = \frac{1}{|\Omega|} \text{ for } x \in \Omega, y \in \partial\Omega \quad (8.7)$$

and the boundary condition

$$\frac{\partial v(x, y)}{\partial \nu_x} = \frac{1}{2\pi} \frac{\mathbf{n}(x) \cdot (x - y)}{|x - y|^3} \text{ for } x, y \in \partial\Omega. \quad (8.8)$$

Green's identity requires the evaluation of two integrals. The first is the volume integral, which by (8.4) is

$$\begin{aligned} \int_{\Omega} [N(x, y) \Delta_x v(x, z) - v(x, z) \Delta_x N(x, y)] dx &= \int_{\Omega} N(x, y) \frac{1}{|\Omega|} dx + v(y, z) \\ &\quad - \frac{1}{|\Omega|} \int_{\Omega} v(x, z) dx, \end{aligned}$$

and the second is the surface integral, which by (8.5) is

$$\oint_{\partial\Omega} \left[N(\mathbf{x}, \mathbf{y}) \frac{\partial v(\mathbf{x}, \mathbf{z})}{\partial \nu_x} - v(\mathbf{x}, \mathbf{z}) \frac{\partial N(\mathbf{x}, \mathbf{y})}{\partial \nu_x} \right] dS_x \\ = \oint_{\partial\Omega} \left[\frac{1}{2\pi|\mathbf{x} - \mathbf{y}|} + v(\mathbf{x}, \mathbf{y}) \right] \frac{\mathbf{n}(\mathbf{x}) \cdot (\mathbf{x} - \mathbf{z})}{2\pi|\mathbf{x} - \mathbf{z}|^3} dS_x.$$

Thus, for $\mathbf{z} \in \partial\Omega$, Green's identity gives

$$v(\mathbf{y}, \mathbf{z}) = -\frac{1}{|\Omega|} \int_{\Omega} [N(\mathbf{x}, \mathbf{y}) - v(\mathbf{x}, \mathbf{z})] d\mathbf{x} \\ + \oint_{\partial\Omega} \left[\frac{1}{2\pi|\mathbf{x} - \mathbf{y}|} + v(\mathbf{x}, \mathbf{y}) \right] \frac{\mathbf{n}(\mathbf{x}) \cdot (\mathbf{x} - \mathbf{z})}{2\pi|\mathbf{x} - \mathbf{z}|^3} dS_x. \quad (8.9)$$

To determine the singularity of this integral when \mathbf{y} approaches \mathbf{z} , we use the method of successive approximations to expand $v(\mathbf{x}, \mathbf{y})$ as

$$v(\mathbf{x}, \mathbf{y}) \sim v_0(\mathbf{x}, \mathbf{y}) + v_1(\mathbf{x}, \mathbf{y}) + v_2(\mathbf{x}, \mathbf{y}) + \dots, \quad (8.10)$$

where $v_{i+1}(\mathbf{x}, \mathbf{y})$ is more regular than $v_i(\mathbf{x}, \mathbf{y})$. For \mathbf{y} or \mathbf{z} (or both) in $\partial\Omega$, the first term is the most singular part

$$v_0(\mathbf{y}, \mathbf{z}) = \frac{1}{4\pi^2} \oint_{\partial\Omega} \frac{\mathbf{n}(\mathbf{x}) \cdot (\mathbf{x} - \mathbf{z})}{|\mathbf{x} - \mathbf{y}||\mathbf{x} - \mathbf{z}|^3} dS_x.$$

To extract its dominant part, we consider $\mathbf{z} \in \partial\Omega$ and move the origin to \mathbf{z} , setting $\mathbf{z} = \mathbf{0}$. Taking a sufficiently small patch of the boundary $\partial\Omega_z$ about \mathbf{z} , we assume that it can be projected orthogonally onto a circular disk Ω_a of radius a in the tangent plane to $\partial\Omega$ at \mathbf{z} . We can assume, therefore, that $\partial\Omega_z$ can be represented as

$$x_3 = f_z(x_1, x_2) \\ = \frac{1}{2} L(z)x_1^2 + \frac{1}{2} N(z)x_2^2 + o(x_1^2 + x_2^2) \text{ for } (x_1, x_2) \in \Omega_a, \quad (8.11)$$

where $L(z)$ and $N(z)$ are the principal curvatures of $\partial\Omega$ at \mathbf{z} . If a is sufficiently small, then $o(x_1^2 + x_2^2) \ll L(z)x_1^2 + N(z)x_2^2$. The canonical representation (8.11) assumes that $\partial\Omega_z$ has at least one non-zero curvature and that the quadratic part in the Taylor's expansion of $f_z(x_1, x_2)$ about the origin is represented in principal axes.

The asymptotically dominant part as $\mathbf{y} \rightarrow \mathbf{z}$ is determined by the integral over the patch $\partial\Omega_z$, which we write as

$$v_0(\mathbf{y}, \mathbf{0}) \sim \frac{1}{4\pi^2} \int_{\partial\Omega_z} \frac{\mathbf{n}(\mathbf{x}) \cdot \mathbf{x} \, dS_x}{\sqrt{(x_1 - y_1)^2 + (x_2 - y_2)^2 + (x_3 - y_3)^2} [x_1^2 + x_2^2 + x_3^2]^{3/2}}.$$

In the representation (8.11)

$$\begin{aligned}\mathbf{n}(\mathbf{x}) &= \frac{(L(z)x_1, N(z)x_2, -1) + o(\sqrt{x_1^2 + x_2^2})}{\sqrt{1 + L^2(z)x_1^2 + N^2(z)x_2^2}} \\ \mathbf{n}(\mathbf{x}) \cdot \mathbf{x} &= \frac{L(z)x_1^2 + N(z)x_2^2 - x_3}{\sqrt{1 + L^2(z)x_1^2 + N^2(z)x_2^2}} \\ dS_x &= \sqrt{1 + |\nabla f_z|^2} \, dx_1 \, dx_2 \sim \sqrt{1 + L^2(z)x_1^2 + N^2(z)x_2^2} \, dx_1 \, dx_2,\end{aligned}$$

so that

$$v_0(\mathbf{y}, \mathbf{0}) \sim \frac{1}{4\pi^2} \int_{\Omega_a} \frac{(L(z)x_1^2 + N(z)x_2^2 - x_3) \, dx_1 \, dx_2}{\sqrt{(x_1 - y_1)^2 + (x_2 - y_2)^2 + (x_3 - y_3)^2} [x_1^2 + x_2^2 + x_3^2]^{3/2}}. \quad (8.12)$$

The patch $\partial\Omega_z$ is represented in polar coordinates in Ω_a as

$$\begin{pmatrix} x_1 \\ x_2 \\ x_3 \end{pmatrix} = \begin{pmatrix} r \cos \phi \\ r \sin \phi \\ r^2 \left(\frac{L(z)}{2} \cos^2 \phi + \frac{N(z)}{2} \sin^2 \phi + o(1) \right) \end{pmatrix},$$

so transforming \mathbf{y} into spherical coordinates

$$\begin{pmatrix} y_1 \\ y_2 \\ y_3 \end{pmatrix} = |\mathbf{y}| \begin{pmatrix} \sin \theta \cos \phi_0 \\ \sin \theta \sin \phi_0 \\ \cos \theta \end{pmatrix},$$

we can write (8.12) as

$$v_0(\mathbf{y}, \mathbf{0}) \sim \frac{1}{4\pi^2} \int_0^{2\pi} I(|\mathbf{y}|, \phi, \theta) \, d\phi, \quad (8.13)$$

where

$$\begin{aligned}I(|\mathbf{y}|, \phi, \theta) &= \int_0^a \frac{\left[\frac{1}{2} Lr^2 \cos^2 \phi + \frac{1}{2} Nr^2 \sin^2 \phi + o(r^2) \right] r \, dr}{\left[r^2 + |\mathbf{y}|^2 - 2r|\mathbf{y}| \sin \theta \cos(\phi - \phi_0) + O(r^2|\mathbf{y}| + r^4) \right]^{1/2} \left[r^2 + O(r^4) \right]^{3/2}}\end{aligned}$$

$$\sim \frac{1}{2} [L \cos^2 \phi + N \sin^2 \phi] \int_0^a \frac{dr}{[r^2 + |\mathbf{y}|^2 - 2r|\mathbf{y}| \sin \theta \cos(\phi - \phi_0)]^{1/2}}. \quad (8.14)$$

Integration with respect to r gives

$$\begin{aligned} & \int_0^a \frac{dr}{[r^2 + |\mathbf{y}|^2 - 2r|\mathbf{y}| \sin \theta \cos(\phi - \phi_0)]^{1/2}} \\ &= \log \frac{a - |\mathbf{y}| \sin \theta \cos(\phi - \phi_0) + \sqrt{a^2 + |\mathbf{y}|^2 - 2a|\mathbf{y}| \sin \theta \cos(\phi - \phi_0)}}{|\mathbf{y}| (1 - \sin \theta \cos(\phi - \phi_0))} \\ &= \log \frac{1}{|\mathbf{y}|} + O(1), \end{aligned}$$

for $\mathbf{y} \neq \mathbf{0}$. It follows from (8.13) that for $\mathbf{y} \neq z$ the leading order singularity is

$$v_0(\mathbf{y}, z) \sim \frac{1}{8\pi} [L(z) + N(z)] \log \frac{1}{|\mathbf{y} - z|} + O(1). \quad (8.15)$$

□

Example 8.1 (Neumann's function for a ball in \mathbb{R}^3). The canonical representation (8.11) of a hemisphere of (dimensionless) radius R at the south pole is $x_3 = R - \sqrt{R^2 - (x_1^2 + x_2^2)}$, so $L(z) = N(z) = \frac{1}{R}$. Therefore, for $|z| = R$,

$$N(\mathbf{y}, z) = \frac{1}{2\pi|\mathbf{y} - z|} + \frac{1}{4\pi R} \log \frac{1}{|\mathbf{y} - z|} + O(1), \quad (8.16)$$

in agreement with [*Kellogg (1954, p. 247, Exercise 4)*].

□

8.1.1 Elliptic Absorbing Window

The solution of the mixed boundary value problem in a large domain of volume $|\Omega|$ with a small elliptic Dirichlet window on an otherwise Neumann boundary $\partial\Omega$ can be calculated explicitly to leading order (see Annotations 8.7 below).

Theorem 8.1.2 *Assume the boundary $\partial\Omega$ of a bounded domain $\Omega \subset \mathbb{R}^3$ is sufficiently regular and the absorbing boundary $\partial\Omega_a$ is the ellipse*

$$\frac{x^2}{a^2} + \frac{y^2}{b^2} \leq 1, \quad z = 0, \quad (b \leq a). \quad (8.17)$$

If

$$\varepsilon = \left(\frac{|\partial\Omega_a|}{|\partial\Omega|} \right)^{1/2} \ll 1,$$

and

$$\frac{|\Omega|^{2/3}}{|\partial\Omega|}, \frac{|\partial\Omega|}{|\Omega|^{2/3}} = O(1) \text{ for } \varepsilon \ll 1,$$

then the solution of the mixed boundary value problem (the mean first passage time from a point \mathbf{x} in Ω to $\partial\Omega_a$)

$$\Delta v(\mathbf{x}) = -\frac{1}{D} \text{ for } \mathbf{x} \in \Omega \quad (8.18)$$

$$v(\mathbf{x}) = 0 \text{ for } \mathbf{x} \in \partial\Omega_a \quad (8.19)$$

$$\frac{\partial v(\mathbf{x})}{\partial n(\mathbf{x})} = 0 \text{ for } \mathbf{x} \in \partial\Omega_r, \quad (8.20)$$

is to leading order

$$v(\mathbf{x}) = \mathbb{E}\tau(a, b) \sim \frac{|\Omega|}{2\pi Da} K(e), \quad (8.21)$$

where $K(\cdot)$ is the complete elliptic integral of the first kind and e is the eccentricity of the ellipse.

For example, in the case of a circular hole, we have $e = 0$ and $K(0) = \pi/2$, so that

$$\mathbb{E}\tau(a, a) \sim v(\mathbf{x}) = \frac{|\Omega|}{4Da} = O\left(\frac{1}{\varepsilon}\right). \quad (8.22)$$

We begin with the following lemma of Helmholtz [Helmholtz (1860)].

Lemma 8.1.1 (Helmholtz). Assume $\partial\Omega_a$ is the ellipse

$$\frac{x^2}{a^2} + \frac{y^2}{a^2} \leq 1, \quad z = 0, \quad (b \leq a).$$

Then the solution of the Helmholtz equation (8.2)) is

$$g_0(\mathbf{x}) = \frac{\tilde{g}_0}{\sqrt{1 - \frac{x^2}{a^2} - \frac{y^2}{a^2}}}, \quad (8.23)$$

where \tilde{g}_0 is a constant.

Proof Indeed, we define for $\mathbf{y} = (x, y)^T$

$$M(\mathbf{y}) = 1 - \frac{x^2}{a^2} - \frac{y^2}{a^2} \quad (b \leq a)$$

and introduce polar coordinates in the ellipse $\partial\Omega_a$

$$\mathbf{x} = \mathbf{y} + (\rho \cos \theta, \rho \sin \theta)^T,$$

with origin at the point \mathbf{y} . The integral in (8.2) takes the form

$$\int_{\partial\Omega_a} \frac{g_0(\mathbf{x})}{|\mathbf{x} - \mathbf{y}|} dS_x = \int_0^{2\pi} d\theta \int_0^{\rho_0(\theta)} \frac{\tilde{g}_0 d\rho}{\sqrt{M(\mathbf{x})}}, \quad (8.24)$$

where $\rho_0(\theta)$ denotes the distance between \mathbf{y} and the boundary of the ellipse in the direction θ . Expanding $M(\mathbf{x})$ in powers of ρ , we find that

$$M(\mathbf{x}) = 1 - \frac{(x + \rho \cos \theta)^2}{a^2} - \frac{(y + \rho \sin \theta)^2}{a^2} = M(\mathbf{y}) - 2\phi_1\rho - \phi_2\rho^2, \quad (8.25)$$

where

$$\phi_1 = \frac{x \cos \theta}{a^2} + \frac{y \sin \theta}{a^2}, \quad \phi_2 = \frac{\cos^2 \theta}{a^2} + \frac{\sin^2 \theta}{a^2}.$$

Solving the quadratic equation (8.25) for ρ and taking the positive root, we obtain

$$\rho(\mathbf{x}) = \frac{1}{\phi_2} \left\{ -\phi_1 + [\phi_1^2 + \phi_2(M(\mathbf{y}) - M(\mathbf{x}))]^{1/2} \right\}.$$

Therefore, for fixed \mathbf{y} and θ ,

$$d\rho(\mathbf{x}) = -\frac{1}{2} \frac{dM(\mathbf{x})}{[\phi_1^2 + \phi_2(M(\mathbf{y}) - M(\mathbf{x}))]^{1/2}},$$

and the integral (8.24) takes the form

$$\begin{aligned} \int_{\partial\Omega_a} \frac{g_0(\mathbf{x})}{|\mathbf{x} - \mathbf{y}|} dS_x &= \frac{1}{2} \int_0^{2\pi} d\theta \int_0^{M(\mathbf{y})} \frac{dM(\mathbf{x})}{[\phi_1^2 + \phi_2(M(\mathbf{y}) - M(\mathbf{x}))]^{1/2}} \frac{\tilde{g}_0}{\sqrt{M(\mathbf{x})}} \\ &= \frac{1}{2} \int_0^{2\pi} d\theta \int_0^{M(\mathbf{y})} \frac{\tilde{g}_0 dz}{\sqrt{\phi_1^2 + \phi_2 z \sqrt{M(\mathbf{y}) - z}}}. \end{aligned}$$

Substituting

$$s = \frac{z}{M(\mathbf{y})}, \quad \psi = \frac{\phi_1^2}{\phi_2 M(\mathbf{y})},$$

we find that

$$\begin{aligned}
\int_{\partial\Omega_a} \frac{g_0(\mathbf{x})}{|\mathbf{x} - \mathbf{y}|} dS_x &= \int_0^{2\pi} d\theta \frac{\tilde{g}_0}{2\sqrt{\phi_2}} \int_0^1 \frac{ds}{\sqrt{\psi + s\sqrt{1-s}}} \\
&= \int_0^{2\pi} d\theta \frac{\tilde{g}_0}{2\sqrt{\phi_2}} 2 \arctan \sqrt{\frac{\psi + s}{1-s}} \Big|_0^1 \\
&= \int_0^{2\pi} \frac{\tilde{g}_0}{2\sqrt{\phi_2}} (\pi - 2 \arctan \sqrt{\psi}) d\theta \\
&= \int_0^{2\pi} \frac{\tilde{g}_0 d\theta}{2\sqrt{\frac{\cos^2 \theta}{a^2} + \frac{\sin^2 \theta}{a^2}}} \left(\pi - 2 \arctan \frac{\frac{x \cos \theta}{a^2} + \frac{y \sin \theta}{a^2}}{\sqrt{\frac{\cos^2 \theta}{a^2} + \frac{\sin^2 \theta}{a^2}} M(\mathbf{y})} \right).
\end{aligned}$$

The arctan term changes sign when θ is replaced by $\theta + \pi$, therefore its integral vanishes, and we are left with

$$\begin{aligned}
\int_{\partial\Omega_a} \frac{g_0(\mathbf{x})}{|\mathbf{x} - \mathbf{y}|} dS_x &= \frac{\pi \tilde{g}_0}{2} \int_0^{2\pi} \frac{d\theta}{\sqrt{\frac{\cos^2 \theta}{a^2} + \frac{\sin^2 \theta}{a^2}}} \\
&= 2\pi b \tilde{g}_0 \int_0^{\frac{\pi}{2}} \frac{d\theta}{\sqrt{1 - \frac{a^2 - a^2}{a^2} \sin^2 \theta}} \\
&= 2\pi b \tilde{g}_0 K(e),
\end{aligned} \tag{8.26}$$

where $K(\cdot)$ is the complete elliptic integral of the first kind [Abramowitz and Stegun (1972)] and e is the eccentricity of the ellipse

$$e = \sqrt{1 - \frac{a^2}{b^2}}, \quad (a > b).$$

We note that the integral (8.26) is independent of \mathbf{y} , so we conclude that (8.23) is the solution of the integral equation (8.2). \square

Proof To prove Theorem 8.1.2, we note that the solution $v(\mathbf{x})$ outside a boundary layer near $\partial\Omega_a$ (the mean first passage time) is to leading order the constant C_0 in (8.2), therefore we need to determine the value of the constant \tilde{g}_0 in the theorem. To this end, we use the value

$$\int_{\partial\Omega_a} g_0(\mathbf{x}) dS_x = \int_{-a}^a dx \int_{-b\sqrt{1-\frac{x^2}{a^2}}}^{b\sqrt{1-\frac{x^2}{a^2}}} \frac{\tilde{g}_0 dy}{\sqrt{1 - \frac{x^2}{a^2} - \frac{y^2}{a^2}}} = 2\pi ab\tilde{g}_0$$

and apply the compatibility condition (6.6) to obtain

$$\tilde{g}_0 = -\frac{|\Omega|}{2\pi Da b}.$$

Hence, by Eq. (8.26),

$$C_0 = -\frac{1}{2\pi} \int_{\partial\Omega_a} \frac{g_0(\mathbf{x})}{|\mathbf{x} - \mathbf{y}|} dS_x = \frac{|\Omega|}{2\pi Da} K(e). \quad (8.27)$$

It follows that

$$\mathbb{E}[\tau | \mathbf{x}(0) = \mathbf{x}] = v(\mathbf{x}) \sim \frac{|\Omega|}{2\pi Da} K(e). \quad \square$$

8.1.2 Second-Order Asymptotics for a Circular Window

To obtain higher-order asymptotics of the solution, we use Popov's theorem 8.1.1 and the Helmholtz Lemma 8.1.1 in (7.8). We get the following theorem

Theorem 8.1.3 *Under the assumptions of Popov's theorem 8.1.1 and Theorem 8.1.2 for a circular window of radius $a \ll |\partial\Omega|^{1/2}$, the solution of the mixed boundary value problem (8.18)–(8.20) is*

$$v(\mathbf{x}) = \frac{|\Omega|}{4aD \left[1 + \frac{L(\mathbf{0}) + N(\mathbf{0})}{2\pi} a \log a + o(a \log a) \right]}. \quad (8.28)$$

Proof To obtain higher-order asymptotics of the solution, we use Popov's theorem 8.1.1 and the Helmholtz Lemma 8.1.1 in (7.8), which, in view of (8.3), now becomes the generalized Helmholtz equation

$$\int_{\partial\Omega_a} g(\mathbf{x}) \left[\frac{1}{2\pi|\mathbf{x} - \mathbf{y}|} + H(\mathbf{x}, \mathbf{y}) \log |\mathbf{x} - \mathbf{y}| + O(1) \right] dS_x = -C \text{ for } \mathbf{y} \in \partial\Omega_a \quad (8.29)$$

$$H(\mathbf{x}, \mathbf{y}) = -\frac{1}{8\pi} [L(\mathbf{y}) + N(\mathbf{y})] \sim -\frac{1}{8\pi} [L(\mathbf{0} + N(\mathbf{0})) \text{ for } \mathbf{x}, \mathbf{y} \in \partial\Omega_a, \varepsilon \ll 1,$$

where $L(\mathbf{0})$ and $N(\mathbf{0})$ are the principal curvatures at the center $\mathbf{0}$ of $\partial\Omega_a$. To solve (8.29), we expand $g(\mathbf{x}) = g_0(\mathbf{x}) + g_1(\mathbf{x}) + g_2(\mathbf{x}) + \dots$, where $g_{i+1}(\mathbf{x}) \ll g_i(\mathbf{x})$ for $\varepsilon \ll 1$ and choose

$$g_0(\mathbf{x}) = -\frac{-2C}{a\pi\sqrt{1 - \frac{|\mathbf{x}|^2}{a^2}}}. \quad (8.30)$$

According to Lemma 8.1.1, if $\partial\Omega_a$ is a circular disk of radius a , then

$$\frac{1}{2\pi} \int_{\partial\Omega_a} \frac{g_0(\mathbf{x})}{|\mathbf{x} - \mathbf{y}|} dS_{\mathbf{x}} = C \quad \text{forall } \mathbf{y} \in \partial\Omega_a. \quad (8.31)$$

It follows that $g_1(\mathbf{x})$ satisfies the integral equation

$$\frac{1}{2\pi} \int_{\partial\Omega_a} \frac{g_1(\mathbf{x})}{|\mathbf{x} - \mathbf{y}|} dS_{\mathbf{x}} = \frac{2C}{a\pi} \int_{\partial\Omega_a} \frac{H(\mathbf{x}, \mathbf{y}) \log |\mathbf{x} - \mathbf{y}|}{\sqrt{1 - \frac{|\mathbf{x}|^2}{a^2}}} dS_{\mathbf{x}}. \quad (8.32)$$

Setting $y = a\eta$, $\mathbf{x} = a\xi$, and changing to polar coordinates in the integral on the right hand side of (8.32), we obtain

$$\frac{1}{2\pi} \int_{\partial\Omega_a} \frac{g_1(\mathbf{x})}{|\mathbf{x} - \mathbf{y}|} dS_{\mathbf{x}} = \frac{2Ca^2}{a\pi} \int_0^{2\pi} d\theta \int_0^1 \frac{H(a\xi, a\eta) [\log a + \log |\xi - \eta|]}{\sqrt{1 - r^2}} r dr, \quad (8.33)$$

which gives in the limit $\varepsilon \rightarrow 0$ (e.g., keeping $|\Omega|$ fixed and $a \rightarrow 0$) that

$$\frac{1}{2\pi} \int_{\partial\Omega_a} \frac{g_1(\mathbf{x})}{|\mathbf{x} - \mathbf{y}|} dS_{\mathbf{x}} = -\frac{C[L(\mathbf{0}) + N(\mathbf{0})]}{2\pi} a \log a + o(a \log a). \quad (8.34)$$

As in the pair (8.30), (8.31), we obtain that

$$g_1(\mathbf{x}) = \frac{-C[L(\mathbf{0}) + N(\mathbf{0})]}{\pi^2 \sqrt{1 - \frac{|\mathbf{x}|^2}{a^2}}} \log a + o(\log a). \quad (8.35)$$

To determine the asymptotic value of the constant C , we recall that $g(\mathbf{x}) = \partial u(\mathbf{x})/\partial\nu$ and use in (6.6) the approximation

$$g(\mathbf{x}) \sim g_0(\mathbf{x}) + g_1(\mathbf{x}) \sim \frac{-2C}{a\pi\sqrt{1 - \frac{|\mathbf{x}|^2}{a^2}}} \left[1 + \frac{L(\mathbf{0}) + N(\mathbf{0})}{2\pi} a \log a \right].$$

We obtain the solution (the narrow escape time) in dimensionless variables as

$$v(\mathbf{x}) = \frac{|\Omega|}{4aD \left[1 + \frac{L(\mathbf{0}) + N(\mathbf{0})}{2\pi} a \log a + o(a \log a) \right]},$$

which is (8.28). \square

Exercise 8.1 (Higher-order asymptotics for an elliptical window). Use Popov's theorem 8.1.1 to construct higher-order asymptotics for an elliptical window. \square

Higher-order asymptotics of the principal eigenvalue of the Laplace equation in Ω with the mixed Neumann–Dirichlet boundary conditions (8.19), (8.20) are derived from the asymptotic representation $\lambda_1(a) \sim (\mathbb{E}\tau)^{-1}$ for $a \ll |\partial\Omega|^{1/2}$, which gives

$$\lambda_1(a) = \frac{4aD}{|\Omega|} \left[1 + \frac{L(\mathbf{0}) + N(\mathbf{0})}{2\pi} a \log a + o(a \log a) \right]. \quad (8.36)$$

If Ω is a ball of radius R , then $L(\mathbf{0}) + N(\mathbf{0}) = \frac{2}{R}$ and the solution $v(\mathbf{x}) = C$ is given (in dimensional variables) by

$$\begin{aligned} v(\mathbf{x}) &= \frac{|\Omega|}{4aD \left[1 - \frac{a}{\pi R} \log \frac{R}{a} + o\left(\frac{a}{R} \log \frac{R}{a}\right) \right]} \\ &= \frac{|\Omega|}{4aD} \left[1 + \frac{a}{\pi R} \log \frac{R}{a} + o\left(\frac{a}{R} \log \frac{R}{a}\right) \right]. \end{aligned} \quad (8.37)$$

Exercise 8.2 (Full asymptotic expansion). Construct the full asymptotic expansion for a circular window (see the references in Annotations 8.7). \square

8.2 The First Eigenvalue for Two Small Dirichlet Windows

Recall that the leading eigenvalue λ_0 of the mixed boundary value problem in a domain with small Dirichlet boundary is asymptotically the reciprocal of the narrow escape time $\bar{\tau}_{A \cup B}$. The latter is given in the following theorem.

Theorem 8.2.1 (Narrow escape time from two windows). *The leading order expansion of the solution of the mixed boundary value problem (8.18)–(8.20) (the narrow escape time) in a bounded domain $\Omega \subset \mathbb{R}^3$ with a smooth Neumann (reflecting) boundary, with two circular Dirichlet (absorbing) windows A and B of dimensionless radii a and b , respectively, whose centers are $\Delta = a + \Delta' + b$ apart on the boundary $\partial\Omega$, is given in the limit $a, b, \Delta' \rightarrow 0$ by*

$$\tilde{\tau}_{A \cup B} = \frac{|\Omega|}{4(a+b)D\tilde{r}} \frac{1 - 16ab\tilde{r}^2 \left(\frac{1}{2\pi|a+\Delta'+b|} + O(1) \right)^2}{1 - \frac{8ab\tilde{r}}{a+b} \left(\frac{1}{2\pi|a+\Delta'+b|} + O(1) \right)}. \quad (8.38)$$

Here $\tilde{r} = \tilde{r}(\Delta', a, b)$ is a function of Δ', a, b that varies monotonically between $\tilde{r}(0, 0, 0) \approx 0.6$ and $\tilde{r}(\Delta', 0, 0) \rightarrow 1$ as $\Delta' \rightarrow \infty$.

Proof The analysis of the 3-dimensional case differs from that in Sect. 7.3.1 in the explicit computation of the solution of the Helmholtz integral equation (7.52),

$$\int_A N(\mathbf{x}, \boldsymbol{\xi}) g_A(\mathbf{x}) dS_{\mathbf{x}} \approx \begin{cases} \frac{1}{2\pi} \tilde{\alpha} a \tilde{g}_A & \text{for } \boldsymbol{\xi} \in A \\ a^2 \tilde{g}_A \alpha [N(\mathbf{0}_A, \mathbf{0}_B) + O(1)], & \text{for } \boldsymbol{\xi} \in B, \end{cases} \quad (8.39)$$

$$\int_B N(\mathbf{x}, \mathbf{x}') g_B(\mathbf{x}) dS_{\mathbf{x}} \approx \begin{cases} \frac{\tilde{\beta} b \tilde{g}_B (1 + o(1))}{2D\pi} & \text{for } \mathbf{x}' \in B, \quad b < 1 \\ a^2 \tilde{g}_B \beta [N(\mathbf{0}_A, \mathbf{0}_B) + O(1)] & \text{for } \mathbf{x}' \in A, \quad b < 1, \end{cases} \quad (8.40)$$

where b is the radius of B and

$$\tilde{\alpha} = \beta = \tilde{\beta} = \int_0^{2\pi} d\theta \int_0^1 \frac{f(r, \theta) r dr}{\sqrt{1-r^2}}, \quad (8.41)$$

where $f(r, \theta)$ is a positive smooth function in the windows and equals 1 in their centers, as described in Sect. 7.3.3.

Now, we approximate equations (7.47)–(7.48) by

$$-C = \frac{1}{2\pi} \tilde{\alpha} a \tilde{g}_A (1 + o(1)) + a^2 \tilde{g}_B \beta [N(\mathbf{0}_A, \mathbf{0}_B) + O(1)]$$

$$-C = \frac{1}{2\pi} \tilde{\beta} b \tilde{g}_B (1 + o(1)) + a^2 \tilde{g}_A \alpha [N(\mathbf{0}_A, \mathbf{0}_B) + O(1)]$$

and find that the flux integral in a window is

$$\int_A g_A(\mathbf{x}) dS_{\mathbf{x}} = a^2 \alpha \tilde{g}_A (1 + o(1)). \quad (8.42)$$

The condition (7.46) for two windows of radii a and b , respectively, is

$$a^2\alpha\tilde{g}_A + a^2\beta\tilde{g}_B = -|\Omega|(1 + o(1)).$$

It follows that the solution (the narrow escape time) is

$$v(\mathbf{x}) = \bar{\tau}_{A \cup B} = \frac{|\Omega|[1 + o(1)]}{4(a+b)r} \frac{1 - 16r^2ab \left[\frac{1}{2\pi|a+\Delta'+b|} [1 + O(\rho)] \right]^2}{1 - \frac{8abr}{a+b} \left[\frac{1}{2\pi|a+\Delta'+b|} [1 + O(\rho)] \right]}, \quad (8.43)$$

where

$$\rho = \min \left(1, |a + \Delta' + b| \log \frac{1}{|a + \Delta' + b|} \right).$$

Here $r = \pi\alpha/2\tilde{\alpha}$ and α is defined by (7.51). The expression (8.6) was used for the Neumann function. For a fixed Ω , the parameter r depends on Δ' , a , and b so we write $r = r(\Delta', a, b)$. If Δ' is large, then $f(x, \theta) = \text{const}$, so $\lim_{\Delta' \rightarrow \infty} r(\Delta', a, b) = 1$. For $a, b, \Delta' \rightarrow 0$, we determine the value of $r(0, a, b)$ by fitting to numerical simulations of Brownian motion in a sphere with two tangent circular holes (see below). Equation (8.43) is (8.38). \square

Brownian simulations and comparison of (8.43) to the mean first passage time (Fig. 7.8) give a good agreement with the approximation

$$r(\Delta', a, a) = \frac{0.6 + \Delta'}{1 + \Delta'}. \quad (8.44)$$

A striking consequence of (8.43) is that moving the two windows apart from $\Delta' = 0$ to $\Delta' = \infty$ changes r from 0.6 to 1 and changes the mean first passage time by the factor 0.6. This means that clustering decreases the first eigenvalue (the flux) by about 40%.

8.2.1 Multiple Absorbing Windows

We consider Brownian motion with diffusion coefficient D in a bounded domain $\Omega \subset \mathbb{R}^3$, whose smooth boundary $\partial\Omega$ reflects Brownian trajectories, except for M circular absorbing windows $A_i \subset \partial\Omega$, ($i = 1, 2, \dots, M$) of small dimensionless radii ε_i , clustered in the sense that every window A_i has within a distance comparable to ε_i a neighboring window A_j .

Theorem 8.2.2 (The mixed boundary value problem with multiple Dirichlet windows). *The leading order asymptotics of the solution to the mixed boundary*

value problem (of the narrow escape time) with homogeneous Dirichlet conditions on $\bigcup_1^M A_i$ for $\sum_1^M \varepsilon_i \ll 1$ are given by

$$v(\mathbf{x}) = \bar{\tau}_{\bigcup A_i} \approx \frac{|\Omega|}{4D} \frac{1}{\sum_{i=1}^M \varepsilon_i \left(1 - 2 \sum_{i \neq j} \varepsilon_j N(i, j) \right)}, \quad (8.45)$$

where $N(i, j)$ is the Neumann function for Ω at the centers of A_i and A_j , respectively.

Proof The solution (narrow escape time) $v(\mathbf{x})$ has the representation (7.5)

$$v(\xi) = \int_{\Omega} N(\mathbf{x}, \xi) d\mathbf{x} + D \int_{\partial\Omega_a} N(\mathbf{x}, \xi) \frac{\partial v(\mathbf{x})}{\partial n} dS_{\mathbf{x}} + C, \quad (8.46)$$

where C is a constant to be determined from the absorbing boundary condition. The condition that $v(\mathbf{x})$ vanishes on $\bigcup_1^M A_i$ is

$$F(\xi) = \sum_{i=1}^M \int_{A_i} N(\mathbf{x}, \xi) g_i(\mathbf{x}) dS_{\mathbf{x}} \text{ for } \xi \in \bigcup_{i=1}^M A_i, \quad (8.47)$$

where

$$F(\xi) = - \left(\int_{\Omega} N(\mathbf{x}, \xi) d\mathbf{x} + C \right). \quad (8.48)$$

The probability flux density in window A_i is denoted $g_i(\mathbf{x})$. Integration of the Poisson equation (6.1) over Ω gives the total flux in $\bigcup_{i=1}^M A_i$ as

$$\sum_{i=1}^M \int_{A_i} g_i(\mathbf{x}) dS_{\mathbf{x}} = - \frac{|\Omega|}{D}. \quad (8.49)$$

We denote by $\mathbf{0}_i$ the center of A_i . Proceeding as in the derivation of (8.39) and (8.40) in the proof of Theorem 8.2.1, we obtain for $\xi = \xi_j \in A_j$ a system of $M + 1$ linear equations for the unknown constants \tilde{g}_i and C ,

$$\frac{\pi}{2} \varepsilon_j \tilde{g}_j + \sum_{i \neq j}^M 2\pi \varepsilon_i^2 \tilde{g}_i N(i, j) = F(\xi_j) \approx -C, \quad j = 1, \dots, M, \quad (8.50)$$

$$2\pi \sum_{i=1}^M \varepsilon_i^2 \tilde{g}_i = - \frac{|\Omega|}{D}, \quad (8.51)$$

where $N(i, j) = N(\mathbf{0}_i, \mathbf{0}_j)$. Equation (8.51) is the solvability condition (8.49). If all radii ε_i can be scaled by $\varepsilon_i = \varepsilon \tilde{\varepsilon}_i$, where $\varepsilon = \min_{1 \leq i \leq M} \varepsilon_i \ll 1$ and $\tilde{\varepsilon}_i = O(1)$ as $\varepsilon \rightarrow 0$, then for windows separated by distances $\Delta_{i,j}$,

$$\max_{i,j} [2\varepsilon N(i, j)] = \max_{i,j} \frac{1}{\pi \left(\tilde{\varepsilon}_i + \tilde{\varepsilon}_j + \frac{\Delta_{i,j}}{\varepsilon} \right)} [1 + o(1)] < 1. \quad (8.52)$$

Scaling $G_j = \pi \varepsilon_j \tilde{g}_j / C$, we write the symmetric matrix of the system (8.50) (with 1/2 on the diagonal) as

$$\mathbf{M} = \begin{pmatrix} 1/2 & 2\tilde{\varepsilon}_2 N(1, 2) & \dots & 2\tilde{\varepsilon}_M N(1, M) \\ 2\tilde{\varepsilon}_2 N(1, 2) & . & . & . \\ . & . & . & . \\ 2\tilde{\varepsilon}_M N(1, M) & \dots & . & 1/2 \end{pmatrix}. \quad (8.53)$$

We decompose \mathbf{M} as

$$\mathbf{M} = \frac{1}{2} \mathbf{I}_M + \varepsilon \mathbf{A},$$

where \mathbf{I}_M is the identity matrix and \mathbf{A} contains off-diagonal terms. Writing $\mathbf{1}_M$ (respectively $\tilde{\mathbf{G}}_M$) for a vector with all components equal to one (respectively, components G_j), (8.50) becomes

$$\left(\frac{1}{2} \mathbf{I}_M + \varepsilon \mathbf{A} \right) \tilde{\mathbf{G}}_M = -\mathbf{1}_M \quad (8.54)$$

and can be inverted as the convergent series

$$\tilde{\mathbf{G}}_M = -2 \sum_{k=0}^{\infty} (-2\varepsilon \mathbf{A})^k \mathbf{1}_M. \quad (8.55)$$

All terms can contribute to the sum, because $\varepsilon N(i, j)$ can be of order 1. The interaction of the cluster with window j is given by

$$G_j = -2 - 2 \sum_{k=0}^{\infty} (-2\varepsilon)^k \sum_{i_1, \dots, i_k} N(j, i_1) N(i_1, i_2) \dots N(i_{k-1}, i_k), \quad (8.56)$$

where the sum is over all non-diagonal pairs (not all i_k are different). The nonlinearity depends on the number of windows. In the first approximation,

$$\tilde{\mathbf{G}}_M \approx -2(\mathbf{I}_M - 2\varepsilon\mathbf{A})\mathbf{1}_M \quad (8.57)$$

and

$$\pi \frac{\varepsilon_j \tilde{g}_j}{C} = G_j = -2 \left(1 - 2\varepsilon \sum_{i \neq j} \tilde{\varepsilon}_i N(i, j) \right). \quad (8.58)$$

Using the condition (8.51), we obtain for the constant C the equation

$$-4C \sum_{i=1}^M \varepsilon_i \left(1 - 2 \sum_{i \neq j} \varepsilon_i N(i, j) \right) = -\frac{|\Omega|}{D},$$

thus the solution $v(\mathbf{x})$ outside the boundary layer near the Dirichlet boundary (narrow escape time through $\bigcup A_i$) is (8.45). \square

In the case of maximal packing, around a disk of radius ε surrounded by touching windows of the same radius, the maximum number of touching disk is $M = 6$ in dimension 2. Thus at order 1, using formula (8.45), we can estimate the MTA in the cluster of disks (see Fig. 8.1). Using the symmetries of order 3 in Fig. 8.1, formula (8.45) for this specific cluster is

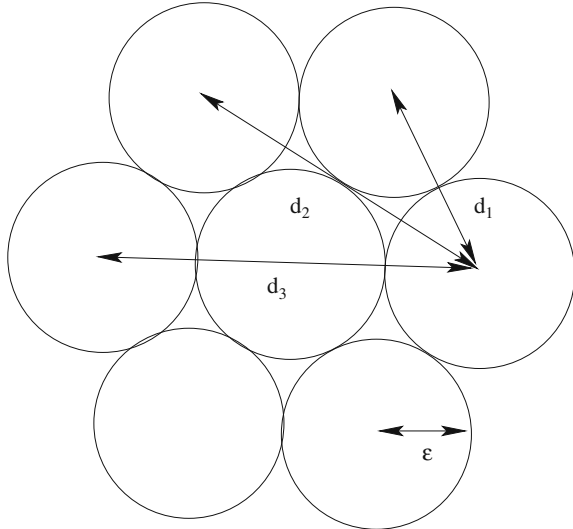
$$\bar{\tau}_{fl} \approx \frac{|\Omega|}{4DM\varepsilon} \left(1 + 2\varepsilon \frac{\sum_{i \neq j} N(i, j)}{M} + o(\varepsilon) \right). \quad (8.59)$$

We label 0 the centered window and the other windows are labeled clockwise from 1 to 6. The contribution to the sum of the central window is $MN(0, 1)$ while that of the non centered windows is to leading order $M(3N(0, 1) + 2N(1, 3) + N(1, 4))$, where $N(0, 1) = \frac{1}{2\pi Dd_1}$, $N(1, 3) = \frac{1}{2D\pi d_2}$, $N(1, 4) = \frac{1}{2\pi Dd_3}$, and $d_1 = 2\varepsilon$, $d_1 = 2\sqrt{3}\varepsilon$, $d_3 = 4\varepsilon$. Thus

$$\begin{aligned} \bar{\tau}_{fl} &\approx \frac{|\Omega|}{4DM\varepsilon} \{1 + 2\varepsilon[4N(0, 1) + 2N(1, 3) + N(1, 4) + O(1)]\} \\ &= \frac{|\Omega|}{4DM\varepsilon} \left[1 + \frac{2}{\pi} \left(1 + \frac{1}{2\sqrt{3}} + \frac{1}{8} \right) \right] + O(1). \end{aligned}$$

Fig. 8.1 Cluster of 6

Dirichlet windows packed at the density limit. Each disk has a radius ε and using the three distances d_1, d_2, d_3 , we can use formula (8.45) to estimate the mean first passage time to the cluster.



8.2.2 Higher-Order Expansion of the NET Through Many Small Windows on a Sphere

A large number of windows $n \gg 1$ are distributed on the surface of a domain Ω with surface S_a . The windows cover a fraction of the surface defined by the ratio $\sigma = \frac{n\pi\varepsilon^2}{|S_a|}$. We recall that the leading order term in the NET $\langle\tau\rangle_{ES}$ expansion for a Brownian particle to arrive at one of the small windows is given by [Reingruber et al. (2009)]

$$\langle\tau\rangle_{ES} = \frac{|\Omega|}{D} \left(\frac{1}{C_{S_a}} + \frac{f(\sigma)}{4n\varepsilon} \right), \quad (8.60)$$

where $|\Omega|$ is the volume, C_{S_a} the capacitance of the surface ∂S_a containing the absorbing windows and the function $f(\sigma)$ is in general difficult to compute, because it depends on the local geometry. To leading order, $f(\sigma) = 1$ as σ tends to 0 [Berg and Purcell (1977)]. When the surface S_a is a sphere of radius a , the capacitance $C_{S_a} = 4\pi a$ and the MFPT is given by

$$\langle\tau\rangle_{ES} = \frac{|\Omega|}{D} \left(\frac{1}{4\pi a} + \frac{f(\sigma)}{4n\varepsilon} \right). \quad (8.61)$$

The function f is found from the Neumann function, the solution of

$$\begin{aligned} \Delta\tilde{\mathcal{N}}(\mathbf{x}, \mathbf{x}_0) &= -\delta(\mathbf{x} - \mathbf{x}_0) \text{ for } \mathbf{x} \in \mathbb{R}^3 \\ \frac{\partial\tilde{\mathcal{N}}}{\partial n}(\mathbf{x}, \mathbf{x}_0) &= 0 \text{ for } \mathbf{x} \in S_a. \end{aligned}$$

For the case of a ball B_a , it depends on the inner ball of radius a :

$$\tilde{\mathcal{N}}(\mathbf{x}, \mathbf{x}_0) = \frac{1}{4\pi|\mathbf{x} - \mathbf{x}_0|} + \frac{a}{4\pi D|\mathbf{x}_0||\mathbf{x} - \frac{a^2\mathbf{x}_0}{|\mathbf{x}_0|^2}|} + \frac{1}{4\pi a} \times \log \left(\frac{\frac{|\mathbf{x}_0||\mathbf{x}|}{a^2} (1 - \cos(\theta))}{1 - \frac{|\mathbf{x}_0||\mathbf{x}|}{a^2} \cos(\theta) + \left(1 + \left(\frac{|\mathbf{x}_0||\mathbf{x}|}{a^2}\right)^2 - 2\frac{|\mathbf{x}_0||\mathbf{x}|}{a^2} \cos(\theta)\right)^{\frac{1}{2}}} \right).$$

When \mathbf{x} and \mathbf{x}_0 are on the sphere $S_a = \partial B_a$, $|\mathbf{x}_0| = |\mathbf{x}| = a$, the Neumann function reduces to [Lagache et al. (2016)]

$$\tilde{\mathcal{N}}(\mathbf{x}, \mathbf{x}_0) = \frac{1}{2\pi|\mathbf{x} - \mathbf{x}_0|} + \frac{1}{4\pi a} \log \left(\frac{|\mathbf{x} - \mathbf{x}_0|}{2a + |\mathbf{x} - \mathbf{x}_0|} \right).$$

Following the steps described in Sect. 8.2.1 or ([Lagache et al. (2016)] and [Lindsay et al. (2016)]), we get when the non-overlapping absorbing holes are randomly distributed

$$f(\sigma) = 1 - 8\frac{\sigma}{\pi} + \frac{\varepsilon}{a\pi} (1 - 4\sigma) \log \left(\frac{\varepsilon}{a} \right) + o \left(\frac{\varepsilon}{a} \right), \quad (8.62)$$

and when they are regularly distributed (equally spaced)

$$f(\sigma) = 1 - 4\frac{\sqrt{\sigma}}{\pi} + \frac{\varepsilon}{a\pi} \log \left(\sqrt{\sigma} \right) + o \left(\frac{\varepsilon}{a} \right). \quad (8.63)$$

For a small coverage $\sigma \ll 1$ and $8\frac{\sigma}{\pi} < 4\frac{\sqrt{\sigma}}{\pi}$, the MFPT of a Brownian particle to an absorbing hole is larger for randomly distributed holes as compared to regularly distributed holes. The result for a regular distribution is similar to the arrangement of the Fekete points on a sphere that minimizes the MFPT [Cheviakov et al. (2013)].

Formulas (8.62) and (8.63) predict that the MFPT formula is different than previously reported based on an effective approximation where $f(\sigma) = 1 - \sigma$ [Zwanzig (1990)] or on an interpolation procedure using Brownian simulations for which it was suggested that $f(\sigma) = \frac{1 - \sigma}{1 + 3.8\sigma^{1.25}}$ [Berezkovskii et al. (2004)]. This difference may also be explained from the differences in the arrangement of windows.

8.2.3 Application to Leakage in a Conductor of Brownian Particles

A conductor of Brownian particles is a bounded domain Ω , with a source of particles on the boundary or in the interior (of strength $\phi(\mathbf{x})$). The boundary $\partial\Omega$ reflects

Brownian trajectories (at a Neumann boundary $\partial\Omega_r$) and contains a target, which is the absorbing (Dirichlet) part $\partial\Omega_a$ of $\partial\Omega$. That is, Ω conducts trajectories from the source to the target $\partial\Omega_a$, where they are absorbed. Some of the Brownian trajectories may leak out of Ω , if $\partial\Omega_r$ contains one or more small absorbing holes (see Fig. 8.4). The calculation of the leakage flux is not the same as that in the narrow escape problem, because the total flux on the boundary remains bounded as the small holes shrink. Our purpose is to find the portion of the total flux that leaks out through the small holes. We assume for simplicity that there is only one leakage hole in $\partial\Omega_r$, denoted $S(\varepsilon)$.

The (dimensionless) stationary density $u(\mathbf{x})$ of the Brownian particles is the solution of the mixed boundary value problem

$$\begin{aligned} D\Delta u(\mathbf{x}) &= 0 \text{ for } \mathbf{x} \in \Omega \\ \frac{\partial u(\mathbf{x})}{\partial \nu} &= 0 \text{ for } \mathbf{x} \in \partial\Omega_r \\ -D \frac{\partial u(\mathbf{x})}{\partial \nu} &= \phi(\mathbf{x}) \text{ for } \mathbf{x} \in \partial\Omega_s \\ u(\mathbf{x}) &= 0 \text{ for } \mathbf{x} \in \partial\Omega_a \cup S(\varepsilon). \end{aligned} \quad (8.64)$$

Our aim is to derive an asymptotic expression for the flux through the leaking hole $S(\varepsilon)$,

$$J_\varepsilon = D \int_{S(\varepsilon)} \frac{\partial u(\mathbf{x})}{\partial \nu} dS_x, \quad (8.65)$$

in terms of the solution $u_0(\mathbf{x})$ of the reduced problem (without $S(\varepsilon)$). First, we find the flux of each eigenfunction and then, using eigenfunction expansion, we calculate J_ε . Every eigenfunction $u_\varepsilon(\mathbf{x})$ of the homogeneous problem (8.64) satisfies

$$-D\Delta u_\varepsilon(\mathbf{x}) = \lambda(\varepsilon)u_\varepsilon(\mathbf{x}) \text{ for } \mathbf{x} \in D \quad (8.66)$$

$$\frac{\partial u_\varepsilon(\mathbf{x})}{\partial \nu} = 0 \text{ for } \mathbf{x} \in \partial\Omega_s \cup \partial\Omega_r \quad (8.67)$$

$$u_\varepsilon(\mathbf{x}) = 0 \text{ for } \mathbf{x} \in S(\varepsilon) \cup \partial\Omega_a. \quad (8.68)$$

The eigenvalues have a regular expansion (see Annotations 8.7)

$$\lambda(\varepsilon) = \lambda(0) + \lambda_1\varepsilon + o(\varepsilon), \quad (8.69)$$

where $\lambda(0)$ is the eigenvalue of the reduced problem (for Ω without the small hole $S(\varepsilon)$).

The reduced Green function (without the small hole) is the solution of the mixed boundary value problem with $D = 1$,

$$-\Delta G(\mathbf{x}, \mathbf{y}) = \delta(\mathbf{x} - \mathbf{y}) \text{ for } \mathbf{x}, \mathbf{y} \in \Omega \quad (8.70)$$

$$\frac{\partial G(\mathbf{x}, \mathbf{y})}{\partial \nu} = 0 \text{ for } \mathbf{x} \in \partial\Omega_s \cup \partial\Omega_r, \mathbf{y} \in \Omega \quad (8.71)$$

$$G(\mathbf{x}, \mathbf{y}) = 0, \text{ for } \mathbf{x} \in \partial\Omega_a, \mathbf{y} \in \Omega. \quad (8.72)$$

Multiplying (8.70) by $u_\varepsilon(\mathbf{x})$ and integrating over Ω , we get

$$u_\varepsilon(\mathbf{x}) = -\lambda(\varepsilon) \int_{\Omega} G(\mathbf{x}, \mathbf{y}) u_\varepsilon(\mathbf{y}) d\mathbf{y} + \int_{S(\varepsilon)} G(\mathbf{x}, \mathbf{y}) \frac{\partial u_\varepsilon(\mathbf{y})}{\partial \nu} dS_y. \quad (8.73)$$

In view of the boundary condition (8.68), we get from (8.73) for all $\mathbf{x} \in S(\varepsilon)$

$$\lambda(\varepsilon) \int_{\Omega} G(\mathbf{x}, \mathbf{y}) u_\varepsilon(\mathbf{y}) d\mathbf{y} = \int_{S(\varepsilon)} G(\mathbf{x}, \mathbf{y}) \frac{\partial u_\varepsilon(\mathbf{y})}{\partial \nu} dS_y. \quad (8.74)$$

The integral on the left-hand side of (8.74) can be expanded about the center of $S(\varepsilon)$ in the form

$$\int_{\Omega} \lambda(\varepsilon) G(\mathbf{x}, \mathbf{y}) u_\varepsilon(\mathbf{y}) d\mathbf{y} = G_0(\varepsilon) + O(|\mathbf{x}|) \text{ for } \mathbf{x} \in S(\varepsilon), \quad (8.75)$$

where the origin is assumed to be in the center of $S(\varepsilon)$ and the (x_1, x_2) -plane is that of $S(\varepsilon)$.

As in Sect. 8.1.2, Green's function for the mixed boundary value problem has the form

$$G(\mathbf{x}, \mathbf{y}) = \frac{1}{2\pi|\mathbf{x} - \mathbf{y}|} + H(\mathbf{x}, \mathbf{y}) \log |\mathbf{x} - \mathbf{y}| + v_S(\mathbf{x}, \mathbf{y}), \quad (8.76)$$

for $\mathbf{x} \in \partial\Omega$, $\mathbf{y} \in \Omega \cup \partial\Omega$, where $H(\mathbf{x}, \mathbf{y})$ depends locally on the principal curvatures [Aubin (1998)] of the boundary and $v_S(\mathbf{x}, \mathbf{y})$ is a continuous function of $\mathbf{x}, \mathbf{y} \in \Omega$ and on $\partial\Omega$. We assume that $H(\mathbf{x}, \mathbf{y})$ is bounded. Using (8.76) and the expansion (8.75) in (8.74) and writing

$$\frac{\partial u_\varepsilon(\mathbf{y})}{\partial \nu} = \frac{C_0(\varepsilon)}{\sqrt{1 - \frac{|\mathbf{y}|^2}{\varepsilon^2}}} + O(|\mathbf{y}|) \text{ for } \mathbf{y} \in S(\varepsilon), \quad (8.77)$$

where $C_0(\varepsilon)$ is an as yet undetermined coefficient, we obtain

$$G_0(\varepsilon) + O(|\mathbf{x}|) = \int_{S(\varepsilon)} \left[\frac{1}{2\pi|\mathbf{x} - \mathbf{y}|} + H(\mathbf{x}, \mathbf{y}) \log |\mathbf{x} - \mathbf{y}| + v_S(\mathbf{x}, \mathbf{y}) \right] \times \\ \left[\frac{C_0(\varepsilon)}{\sqrt{1 - \frac{|\mathbf{y}|^2}{\varepsilon^2}}} + O(|\mathbf{y}|) \right] dS_y. \quad (8.78)$$

At $\mathbf{x} = \mathbf{0}$, we get

$$G_0(\varepsilon) = \frac{C_0(\varepsilon)\pi\varepsilon}{2} + \int_{S(\varepsilon)} O(|\mathbf{y}|) \left[\frac{1}{2\pi|\mathbf{y}|} + H(0, \mathbf{y}) \log |\mathbf{y}| \right] dS_y \\ + \int_{S(\varepsilon)} \frac{C_0(\varepsilon) [H(\mathbf{0}, \mathbf{y}) \log |\mathbf{y}| + v_S(\mathbf{0}, \mathbf{y})]}{\sqrt{1 - \frac{|\mathbf{y}|^2}{\varepsilon^2}}} dS_y + \int_{S(\varepsilon)} O(|\mathbf{y}|) dS_y.$$

It follows that

$$G_0(\varepsilon) = \left(\frac{\pi\varepsilon}{2} + O(\varepsilon^2 \log \varepsilon) \right) C_0(\varepsilon) + O(\varepsilon^2 \log \varepsilon),$$

so that

$$C_0(\varepsilon) = \frac{G_0(\varepsilon) + O(\varepsilon^2 \log \varepsilon)}{\frac{\pi\varepsilon}{2} + O(\varepsilon^2 \log \varepsilon)}. \quad (8.79)$$

Now, (8.77) gives

$$D \int_{S(\varepsilon)} \frac{\partial u_\varepsilon(\mathbf{y})}{\partial \nu} dS_y = D \frac{G_0(\varepsilon) + O(\varepsilon^2 \log \varepsilon)}{\frac{\pi\varepsilon}{2} + O(\varepsilon^2 \log \varepsilon)} \int_{S(\varepsilon)} \frac{dS_y}{\sqrt{1 - \frac{|\mathbf{y}|^2}{\varepsilon^2}}} \\ + D \int_{S(\varepsilon)} O(|\mathbf{y}|) dS_y = 4\varepsilon D \frac{G_0(\varepsilon) + O(\varepsilon^2 \log \varepsilon)}{1 + O(\varepsilon \log \varepsilon)} + O(\varepsilon^2 \log \varepsilon). \quad (8.80)$$

To determine $G_0(\varepsilon)$, we integrate (8.66) and get the total flux condition

$$\lambda(\varepsilon) \int_{\Omega} u_\varepsilon(\mathbf{x}) d\mathbf{x} = D \int_{S(\varepsilon)} \frac{\partial u_\varepsilon(\mathbf{y})}{\partial \nu} dS_y + D \int_{\partial\Omega_a} \frac{\partial u_\varepsilon(\mathbf{y})}{\partial \nu} dS_y. \quad (8.81)$$

We also recall that (8.72) implies that

$$\int_{\partial\Omega_a} G(\mathbf{x}, \mathbf{y}) \frac{\partial u_\varepsilon(\mathbf{y})}{\partial \nu} dS_y = 0 \text{ for } \mathbf{x} \in \partial\Omega_a,$$

hence, using equations (8.74) and (8.81), we get the two equations

$$\begin{aligned}\lambda(\varepsilon) \int_{\Omega} u_{\varepsilon}(\mathbf{x}) d\mathbf{x} &= 4\varepsilon D \frac{G_0(\varepsilon) + O(\varepsilon^2 \log \varepsilon)}{1 + O(\varepsilon \log \varepsilon)} + O(\varepsilon^2 \log \varepsilon) + D \int_{\partial\Omega_a} \frac{\partial u_{\varepsilon}(\mathbf{y})}{\partial \nu} dS_y \\ G_0(\varepsilon) &= \lambda(\varepsilon) \int_{\Omega} G(\mathbf{0}, \mathbf{y}) u_{\varepsilon}(\mathbf{y}) d\mathbf{y}. \end{aligned}\quad (8.82)$$

This gives

$$\begin{aligned}\lambda(\varepsilon) \int_{\Omega} u_{\varepsilon}(\mathbf{x}) d\mathbf{x} &= 4\varepsilon D \frac{\lambda(\varepsilon) \int_{\Omega} G(\mathbf{0}, \mathbf{y}) u_{\varepsilon}(\mathbf{y}) d\mathbf{y} + O(\varepsilon^2 \log \varepsilon)}{1 + O(\varepsilon \log \varepsilon)} \\ &\quad + O(\varepsilon^2 \log \varepsilon) + D \int_{\partial\Omega_a} \frac{\partial u_{\varepsilon}(\mathbf{y})}{\partial \nu} dS_y. \end{aligned}$$

Solving for $\lambda(\varepsilon)$, we find that

$$\begin{aligned}\lambda(\varepsilon) &= \frac{D \int_{\partial\Omega_a} \frac{\partial u_{\varepsilon}(\mathbf{y})}{\partial \nu} dS_y + O(\varepsilon^2 \log \varepsilon)}{\int_{\Omega} u_{\varepsilon}(\mathbf{x}) d\mathbf{x} - \frac{4\varepsilon D}{1 + O(\varepsilon \log \varepsilon)} \int_{\Omega} G(\mathbf{0}, \mathbf{y}) u_{\varepsilon}(\mathbf{y}) d\mathbf{y} + O(\varepsilon^2 \log \varepsilon)} \\ &= \frac{D \int_{\partial\Omega_a} \frac{\partial u_{\varepsilon}(\mathbf{y})}{\partial \nu} dS_y}{\int_{\Omega} u_{\varepsilon}(\mathbf{x}) d\mathbf{x}} \left(1 + \frac{4\varepsilon \int_{\Omega} G(\mathbf{0}, \mathbf{y}) u_{\varepsilon}(\mathbf{y}) d\mathbf{y}}{\int_{\Omega} u_{\varepsilon}(\mathbf{x}) d\mathbf{x}} \right) + O(\varepsilon^2 \log \varepsilon). \end{aligned}\quad (8.83)$$

Note that due to (8.69),

$$\frac{D \int_{\partial\Omega_a} \frac{\partial u_{\varepsilon}(\mathbf{y})}{\partial \nu} dS_y}{\int_{\Omega} u_{\varepsilon}(\mathbf{x}) d\mathbf{x}} = \lambda(0) + O(\varepsilon). \quad (8.84)$$

Obviously, $u_{\varepsilon} \rightarrow u_0$ as $\varepsilon \rightarrow 0$, where u_0 is the corresponding eigenfunction of the reduced problem (in the absence of the small hole, see Annotations 8.7), so

$$\begin{aligned} \lim_{\varepsilon \rightarrow 0} \int_{\Omega} G(\mathbf{x}, \mathbf{y}) u_{\varepsilon}(\mathbf{y}) d\mathbf{y} &= \int_{\Omega} G(\mathbf{x}, \mathbf{y}) u_0(\mathbf{y}) d\mathbf{y} \\ \lim_{\varepsilon \rightarrow 0} \int_{\partial\Omega_a} \frac{\partial u_{\varepsilon}(\mathbf{y})}{\partial \nu} dS_y &= \int_{\partial\Omega_a} \frac{\partial u_0(\mathbf{y})}{\partial \nu} dS_y. \end{aligned}$$

Therefore, using (8.82)–(8.84) in (8.80), we find that the flux of $u_{\varepsilon}(\mathbf{x})$ through the small hole is

$$\begin{aligned} J(\varepsilon) &= D \int_{S(\varepsilon)} \frac{\partial u_{\varepsilon}(\mathbf{y})}{\partial \nu} dS_y = 4\varepsilon \lambda(0) D \int_{\Omega} G(\mathbf{0}, \mathbf{y}) u_0(\mathbf{y}) d\mathbf{y} + O(\varepsilon^2 \log \varepsilon) \\ &= 4\varepsilon D u_0(\mathbf{0}) + O(\varepsilon^2 \log \varepsilon). \end{aligned} \quad (8.85)$$

The function $DG(\mathbf{x}, \mathbf{y})$ is Green's function for the mixed boundary value problem (8.70)–(8.72) with diffusion coefficient D , rather than 1. Finally, expanding the solution $u(\mathbf{x})$ of (8.64) in eigenfunctions, we obtain from (8.85)

$$J_{\varepsilon} = 4\varepsilon D u_0(\mathbf{0}) (1 + O(\varepsilon \log \varepsilon)), \quad (8.86)$$

where $u_0(\mathbf{x})$ is the solution of the reduced problem (8.64). In dimensional variables, we obtain

$$J_{\varepsilon} = 4a D p_0(\mathbf{0}) + O\left(\frac{a^2}{|\Omega|^{2/3}} \log \frac{a}{|\Omega|^{1/3}}\right), \quad (8.87)$$

where $p_0(\mathbf{0})$ is the value of the reduced stationary density (without the perforation) at the hole.

Remark 8.2.1 Note that the asymptotic formula (8.86) holds if $\varepsilon \ll L/R$, so the source is outside the boundary layer near the hole.

8.3 Activation Through a Narrow Opening

Both the singular perturbation problem of Part I and the narrow escape problem of Part II are combined in the problem of escape of particles diffusing in a field of force and escaping through a narrow absorbing window in an otherwise reflecting boundary. In the presence of a deep potential well, there are two long time scales, the mean escape time from the well and the mean time to reach the absorbing window. The two time scales are expressed in an Arrhenius-like formula for the activation rate through narrow openings. The activation rates for the different geometries are summarized in equations (8.120)–(8.127) below.

As in traditional theories, our point of departure is the Smoluchowski equation

$$\dot{\mathbf{x}} + \frac{1}{\gamma} \nabla \phi(\mathbf{x}) = \sqrt{\frac{2k_B T}{m\gamma}} \dot{\mathbf{w}}, \quad (8.88)$$

where m is the mass, $\gamma = \eta/m$ is the dynamical viscosity, while η is the friction coefficient, $\phi = \Phi/m$ is the potential per unit mass and $\Phi(x)$ is the potential, T is temperature, k_B is Boltzmann's constant, and $\dot{\mathbf{w}}$ is a vector of n independent δ -correlated Gaussian white noises.

The motion (8.88) is confined to a bounded domain Ω , whose boundary $\partial\Omega$ is reflecting, but for a small absorbing window $\partial\Omega_a$ ($\partial\Omega = \partial\Omega_a \cup \Omega_r$). As above, the assumption that the window is small means that

$$\delta = \left(\frac{|\partial\Omega_a|}{|\partial\Omega|} \right)^{1/(d-1)} \ll 1 \quad (8.89)$$

(δ is a small parameter).

The probability density function $p_\delta(\mathbf{x}, t)$ of $\mathbf{x}(t)$ is the solution of the Fokker–Planck equation

$$\gamma \frac{\partial p_\delta}{\partial t} = \varepsilon \Delta p_\delta + \nabla \cdot (p_\delta \nabla \phi) \equiv \mathcal{L}_\delta p_\delta, \quad (8.90)$$

with the initial condition

$$p_\delta(\mathbf{x}, 0) = p_0(\mathbf{x}), \quad (8.91)$$

and mixed boundary value problem for $t > 0$

$$p_\delta = 0, \text{ for } \mathbf{x} \in \partial\Omega_a \quad (8.92)$$

$$\varepsilon \frac{\partial p_\delta}{\partial n} + p_\delta \frac{\partial \phi}{\partial n} = 0, \text{ for } \mathbf{x} \in \partial\Omega_r, \quad (8.93)$$

where $\varepsilon = k_B T/m$ and $p_0(\mathbf{x})$ is the initial probability density function (e.g., $p_0(\mathbf{x}) = |\Omega|^{-1}$ for a uniform distribution). The function

$$u_\delta(\mathbf{x}) = \int_0^\infty p_\delta(\mathbf{x}, t) dt, \quad (8.94)$$

which is the mean time the particle spends at \mathbf{x} before it escapes through the narrow window, is the solution of the mixed boundary value problem

$$\mathcal{L}_\delta u_\delta = -\gamma p_0, \text{ for } \mathbf{x} \in \Omega \quad (8.95)$$

$$u_\delta = 0, \text{ for } \mathbf{x} \in \partial\Omega_a \quad (8.96)$$

$$\varepsilon \frac{\partial u_\delta}{\partial n} + u_\delta \frac{\partial \phi}{\partial n} = 0, \text{ for } \mathbf{x} \in \partial\Omega_r. \quad (8.97)$$

The function $g_\delta = u_\delta e^{\phi/\varepsilon}$ is the solution of the adjoint mixed boundary value problem

$$\mathcal{L}_\delta^* g_\delta = -\gamma p_0 e^{\phi/\varepsilon}, \quad \text{for } \mathbf{x} \in \Omega \quad (8.98)$$

$$\frac{\partial g_\delta(\mathbf{x})}{\partial n} = 0, \quad \text{for } \mathbf{x} \in \partial\Omega_r \quad (8.99)$$

$$g_\delta(\mathbf{x}) = 0, \quad \text{for } \mathbf{x} \in \partial\Omega_a.$$

Equation (8.98) can be written in the divergence form

$$\nabla \left(e^{-\phi/\varepsilon} \nabla g_\delta \right) = -\frac{\gamma p_0}{\varepsilon}. \quad (8.100)$$

The adjoint operators \mathcal{L}_δ and \mathcal{L}_δ^* , defined by (8.90), (8.95)–(8.97) and (8.98), (8.99), respectively, have bi-orthogonal systems of normalized eigenfunctions, $\{\psi_i(\mathbf{x}, \delta)\}$ and $\{\varphi_i(\mathbf{x}, \delta)\}$ ($i = 0, 1, \dots$) and we can expand

$$p_\delta(\mathbf{x}, t) = \sum_{i=0}^{\infty} a_i(\delta) \psi_i(\mathbf{x}, \delta) e^{-\lambda_i(\delta)t/\gamma}, \quad (8.101)$$

where $\lambda_i(\delta)$ are the eigenvalues of \mathcal{L}_δ . The $a_i(\delta)$ are the Fourier coefficients of the initial function $p_0(\mathbf{x})$. In the limit $\delta \rightarrow 0$ the Dirichlet part of the boundary conditions, (8.92), is dropped, so that $\lambda_0(\delta) \rightarrow 0$ (the first eigenvalue of the problem (8.90), (8.93) with $\partial\Omega_r = \partial\Omega$), with the normalized eigenfunction

$$\psi_0(\mathbf{x}, 0) = \frac{\exp\{-\phi(\mathbf{x})/\varepsilon\}}{\int_{\Omega} \exp\{-\phi(\mathbf{x})/\varepsilon\} d\mathbf{x}}, \quad (8.102)$$

and $a_0(\delta) \rightarrow 1$. It follows from (8.94) and (8.101) that for all $\mathbf{x} \in \Omega$

$$u_\delta(\mathbf{x}) = \gamma \sum_{i=0}^{\infty} \frac{a_i(\delta) \psi_i(\mathbf{x}, \delta)}{\lambda_i(\delta)} \rightarrow \infty, \quad \text{as } \delta \rightarrow 0. \quad (8.103)$$

In particular, the first passage time $\tau_\delta = \inf\{t > 0 \mid \mathbf{x}(t) \in \partial\Omega_a\}$ diverges. That is, $\lim_{\delta \rightarrow 0} \tau_\delta = \infty$ on almost every trajectory $\mathbf{x}(t)$. Obviously, the mean first passage time,

$$\bar{\tau}_\delta = \int_{\Omega} u_\delta(\mathbf{x}) d\mathbf{x} = \gamma \sum_{i=0}^{\infty} \frac{a_i(\delta)}{\lambda_i(\delta)}, \quad (8.104)$$

also diverges as $\delta \rightarrow 0$. It is the purpose of this chapter to find the orders of magnitude of $u_\delta(\mathbf{x})$ and $\bar{\tau}_\delta$ for small δ .

8.3.1 The Neumann Function

As in Sect. 7.2, the Neumann function for Ω is the solution of the boundary value problem

$$\begin{aligned}\Delta_y N(\mathbf{x}, \mathbf{y}) &= -\delta(\mathbf{x} - \mathbf{y}), \quad \text{for } \mathbf{x}, \mathbf{y} \in \Omega, \\ \frac{\partial N(\mathbf{x}, \mathbf{y})}{\partial n_y} &= -\frac{1}{|\partial\Omega|}, \quad \text{for } \mathbf{x} \in \Omega, \mathbf{y} \in \partial\Omega.\end{aligned}\tag{8.105}$$

Using Green's identity and the boundary conditions (8.96)–(8.97) and (8.105) gives

$$\begin{aligned}&\int_{\Omega} N(\mathbf{x}, \mathbf{y}) \Delta_y u_{\delta}(\mathbf{y}) d\mathbf{y} \\ &= \int_{\Omega} u_{\delta}(\mathbf{y}) \Delta_y N(\mathbf{x}, \mathbf{y}) d\mathbf{y} + \int_{\partial\Omega} \left(N(\mathbf{x}, \mathbf{y}) \frac{\partial u_{\delta}(\mathbf{y})}{\partial n_y} - u_{\delta}(\mathbf{y}) \frac{\partial N(\mathbf{x}, \mathbf{y})}{\partial n_y} \right) dS_y \\ &= -u_{\delta}(\mathbf{x}) + \int_{\partial\Omega_a} N(\mathbf{x}, \mathbf{y}) \frac{\partial u_{\delta}(\mathbf{y})}{\partial n_y} dS_y - \frac{1}{\varepsilon} \int_{\partial\Omega_r} N(\mathbf{x}, \mathbf{y}) u_{\delta}(\mathbf{y}) \frac{\partial \phi(\mathbf{y})}{\partial n_y} dS_y \\ &\quad + \frac{1}{|\partial\Omega|} \int_{\partial\Omega_r} u_{\delta}(\mathbf{y}) dS_y.\end{aligned}\tag{8.106}$$

On the other hand, (8.95) gives

$$\begin{aligned}&\int_{\Omega} N(\mathbf{x}, \mathbf{y}) \Delta_y u_{\delta}(\mathbf{y}) d\mathbf{y} = \int_{\Omega} N(\mathbf{x}, \mathbf{y}) \left[-\frac{\gamma p_0}{\varepsilon} - \frac{1}{\varepsilon} \nabla \cdot (u_{\delta} \nabla \phi) \right] d\mathbf{y} \\ &= -\frac{\gamma}{\varepsilon} \int_{\Omega} N(\mathbf{x}, \mathbf{y}) p_0(\mathbf{y}) d\mathbf{y} - \frac{1}{\varepsilon} \int_{\Omega} \nabla_y \cdot [N(\mathbf{x}, \mathbf{y}) u_{\delta}(\mathbf{y}) \nabla_y \phi(\mathbf{y})] d\mathbf{y} \\ &\quad + \frac{1}{\varepsilon} \int_{\Omega} u_{\delta}(\mathbf{y}) \nabla_y \phi(\mathbf{y}) \cdot \nabla_y N(\mathbf{x}, \mathbf{y}) d\mathbf{y} \\ &= -\frac{\gamma}{\varepsilon} \int_{\Omega} N(\mathbf{x}, \mathbf{y}) p_0(\mathbf{y}) d\mathbf{y} - \frac{1}{\varepsilon} \int_{\partial\Omega_r} N(\mathbf{x}, \mathbf{y}) u_{\delta}(\mathbf{y}) \frac{\partial \phi(\mathbf{y})}{\partial n} dS_y \\ &\quad + \frac{1}{\varepsilon} \int_{\Omega} u_{\delta}(\mathbf{y}) \nabla_y \phi(\mathbf{y}) \cdot \nabla_y N(\mathbf{x}, \mathbf{y}) d\mathbf{y}.\end{aligned}\tag{8.107}$$

Combining (8.106) and (8.107) yields

$$\begin{aligned} & -u_\delta(\mathbf{x}) + \frac{1}{|\partial\Omega|} \int_{\partial\Omega_r} u_\delta(\mathbf{y}) dS_y + \int_{\partial\Omega_a} N(\mathbf{x}, \mathbf{y}) \frac{\partial u_\delta(\mathbf{y})}{\partial n_y} dS_y \\ &= -\frac{\gamma}{\varepsilon} \int_{\Omega} N(\mathbf{x}, \mathbf{y}) p_0(\mathbf{y}) d\mathbf{y} + \frac{1}{\varepsilon} \int_{\Omega} u_\delta(\mathbf{y}) \nabla_y \phi(\mathbf{y}) \cdot \nabla_y N(\mathbf{x}, \mathbf{y}) d\mathbf{y}. \end{aligned} \quad (8.108)$$

In view of (8.103), the integral $\int_{\Omega} N(\mathbf{x}, \mathbf{y}) p_0(\mathbf{y}) d\mathbf{y}$ can be neglected to leading order, because it is uniformly bounded for smooth initial distributions¹ p_0 as $\delta \rightarrow 0$, while all other terms in (8.108) are unbounded. For $\mathbf{x} \in \Omega$, at a distance $O(1)$ away from the window, the Neumann function is uniformly bounded.

Note that integrating (8.100) and using the boundary conditions (8.99), we obtain the compatibility condition

$$\int_{\partial\Omega_a} \frac{\partial u_\delta}{\partial n} dS = -\frac{\gamma}{\varepsilon}. \quad (8.109)$$

From the fact that the normal derivative $\partial u_\delta(\mathbf{y})/\partial n_y$ is negative on $\partial\Omega_a$, (8.109) this implies that $\int_{\partial\Omega_a} N(\mathbf{x}, \mathbf{y}) \partial u_\delta(\mathbf{y})/\partial n_y dS_y$ is uniformly bounded. It follows that for $\mathbf{x} \in \Omega$, at a distance $O(1)$ (with respect to δ) away from the window, the integral equation (8.108) is to leading order

$$u_\delta(\mathbf{x}) \sim \frac{1}{|\partial\Omega|} \int_{\partial\Omega} u_\delta(\mathbf{y}) dS_y - \frac{1}{\varepsilon} \int_{\Omega} u_\delta(\mathbf{y}) \nabla_y \phi(\mathbf{y}) \cdot \nabla_y N(\mathbf{x}, \mathbf{y}) d\mathbf{y}, \quad (8.110)$$

which is the integral representation of the boundary value problem $\mathcal{L}_\delta u_\delta = 0$ with the no flux boundary condition (8.97) on the entire boundary (i.e., with $\partial\Omega_r = \partial\Omega$), whose solution is the Boltzmann distribution

$$u_\delta(\mathbf{x}) \sim C_\delta e^{-\phi(\mathbf{x})/\varepsilon}. \quad (8.111)$$

Equation (8.111) represents the average time the particle spent prior to absorption at a point \mathbf{x} at a distance $O(1)$ away from the absorbing window.

Due to the absorbing boundary condition (8.96), equation (8.108) reduces to

$$\begin{aligned} & \int_{\partial\Omega_a} N(\mathbf{x}, \mathbf{y}) \frac{\partial u_\delta(\mathbf{y})}{\partial n_y} dS_y \\ &= \left\{ \frac{-1}{|\partial\Omega|} \int_{\partial\Omega_r} u_\delta(\mathbf{y}) dS_y + \frac{1}{\varepsilon} \int_{\Omega} u_\delta(\mathbf{y}) \nabla_y \phi(\mathbf{y}) \cdot \nabla_y N(\mathbf{x}, \mathbf{y}) d\mathbf{y} \right\} (1 + o(1)) \end{aligned} \quad (8.112)$$

¹For non-smooth p_0 the integral is not uniformly bounded. For example, for $p_0 = \delta(\mathbf{x} - \mathbf{x}_0)$ we have $\int_{\Omega} N(\mathbf{x}, \mathbf{y}) p_0(\mathbf{y}) d\mathbf{y} = N(\mathbf{x}, \mathbf{x}_0)$, which becomes singular as $\mathbf{x} \rightarrow \mathbf{x}_0$. However, this is an integrable singularity, and as such it does not affect the leading order asymptotics in δ .

for all $\mathbf{x} \in \partial\Omega_a$. Substituting (8.111) in (8.112) yields an integral equation for the flux $\partial u_\delta / \partial n$ into the absorbing window,

$$\int_{\partial\Omega_a} N(\mathbf{x}, \mathbf{y}) \frac{\partial u_\delta(\mathbf{y})}{\partial n_y} dS_y = -C_\delta e^{-\phi(\mathbf{x})/\varepsilon} (1 + o(1)) \text{ for } \delta \ll 1. \quad (8.113)$$

If $\phi(\mathbf{x})$ does not change much in the window, we can use the constant approximation $\phi(\mathbf{x}) \approx \phi(\text{window}) = \phi_0$.

In three dimensions

$$N(\mathbf{x}, \mathbf{y}) = \frac{1}{4\pi|\mathbf{x} - \mathbf{y}|} + v_S(\mathbf{x}, \mathbf{y}), \quad (8.114)$$

where by Popov's theorem 8.1.1 v_S has a logarithmic singularity, so the leading order contribution to (8.113) is due to the leading order singular part of the Neumann function. Thus the leading order approximation $\partial u_0 / \partial n$ to the absorption flux is the solution of

$$\frac{1}{2\pi} \int_{\partial\Omega_a} \frac{\partial u_0(\mathbf{y})}{\partial n_y} \frac{dS_y}{|\mathbf{x} - \mathbf{y}|} = -C_\delta e^{-\phi_0/\varepsilon}. \quad (8.115)$$

Note that the singularity of the Neumann function at the boundary is twice as large as it is inside the domain, due to the contribution of the regular part (the “image charge”). For that reason the factor $\frac{1}{4\pi}$ in Eq. (8.114) is replaced by $\frac{1}{2\pi}$.

8.3.2 Solution of the Mixed Boundary Value Problem

The integral equation (8.115) was considered in Sect. 8.1, where an analytical solution for the case of an elliptical absorbing window $\partial\Omega_a$ was given in the form

$$\frac{\partial u_0(y_1, y_2)}{\partial n} = -\frac{C_\delta e^{-\phi_0/\varepsilon}}{\sqrt{1 - \frac{y_1^2}{a^2} - \frac{y_2^2}{b^2}}}, \quad (8.116)$$

where a and b are the ellipse semi-axes, and $\mathbf{y} = (y_1, y_2)$ are local cartesian coordinates in the ellipse. The value of the constant C_δ is calculated, using the compatibility condition (8.109), to be

$$C_\delta = \frac{\gamma K(e)}{2\pi\varepsilon a} e^{\phi_0/\varepsilon}, \quad (8.117)$$

where e is the eccentricity of the ellipse and $K(\cdot)$ is the complete elliptic integral of the first kind. In a three-dimensional domain, the density of the time spent at point

\mathbf{x} before escape through an elliptical absorbing window is given by (see (8.111))

$$u_\delta(\mathbf{x}) \approx \frac{\gamma K(e)}{2\pi\varepsilon a} \exp\left\{\frac{\phi_0 - \phi(\mathbf{x})}{\varepsilon}\right\}. \quad (8.118)$$

Equations (8.104) and (8.118) now give the mean first passage time as

$$\bar{\tau}_\delta = \frac{\gamma K(e) e^{\phi_0/\varepsilon}}{2\pi\varepsilon a} \int_{\Omega} \exp\left\{-\frac{\phi(\mathbf{x})}{\varepsilon}\right\} d\mathbf{x}. \quad (8.119)$$

If the barrier is sufficiently high, we evaluate the integral in (8.119) by the Laplace method, assuming that ϕ has a single global minimum ϕ_m at \mathbf{x}_m ,

$$\int_{\Omega} \exp\left\{-\frac{\phi(\mathbf{x})}{\varepsilon}\right\} d\mathbf{x} \approx \frac{(2\pi\varepsilon)^{n/2}}{\prod_{i=1}^n \omega_i} \exp\left\{-\frac{\phi_m}{\varepsilon}\right\},$$

where ω_i are the frequencies (the eigenvalues of the Hessian of the potential) at the minimum \mathbf{x}_m . For reactions that consist in passing through a small elliptical window (assuming no returns are possible) the reaction rate is the modified Kramers formula (2.81)

$$\kappa_\delta = \frac{1}{\bar{\tau}_\delta} \sim \frac{a\omega_1\omega_2\omega_3}{\sqrt{2\pi\varepsilon}\gamma K(e)} e^{-\Delta E/\varepsilon}, \quad (8.120)$$

where $\Delta E = \phi_0 - \phi_m$. In the special case of a circular window, we obtain

$$\kappa_\delta \sim \frac{4a\omega_1\omega_2\omega_3}{(2\pi)^{3/2}\gamma\sqrt{\varepsilon}} e^{-\Delta E/\varepsilon}, \quad (8.121)$$

where a is the radius of the window. Note that ΔE is not the barrier height. We conclude that the activation rate is of Arrhenius form and has two contributions. The first is due to the potential, while the second is due to the geometry of the absorbing window alone. Unlike the free diffusion case considered in Part I, geometrical properties of the domain, such as its volume, are not included in the leading order asymptotics of the reaction rate.

Secondly, in the limit of large ε , the power series approximation

$$e^{-(\phi(\mathbf{x})-\phi_0)/\varepsilon} = 1 - \frac{\phi(\mathbf{x}) - \phi_0}{\varepsilon} + \frac{(\phi(\mathbf{x}) - \phi_0)^2}{2\varepsilon^2} \dots$$

in (8.119) gives

$$k \sim \frac{2\pi\varepsilon a}{\gamma K(e)|\Omega|} \left(1 - \frac{\langle\phi\rangle - \phi_0}{\varepsilon} + O(\varepsilon^{-2})\right)^{-1}, \quad (8.122)$$

where $\langle \phi \rangle = |\Omega|^{-1} \int_{\Omega} \phi(\mathbf{x}) d\mathbf{x}$ is the spatial average of the potential. The rate can also be rewritten in an Arrhenius form as

$$k \sim \frac{2\pi\varepsilon a}{\gamma K(e)|\Omega|} e^{-\langle \Delta E \rangle/\varepsilon}, \quad (8.123)$$

where $\langle \Delta E \rangle = \phi_0 - \langle \phi \rangle$. In the case of large ε the reaction rate depends not merely on the geometry of the window, but also on the geometry of the domain itself through its volume. Large ε means that the motion is diffusion limited, therefore, fine details of the potential are less important and the spatial averaged potential has only an $O(\varepsilon^{-1})$ effect.

Finally, we give rate functions for small and large ε for several geometries. For the case of diffusion in a ball of radius R , the results of Sect. 8.1 show that

$$\begin{aligned} k &\sim \frac{4\varepsilon a}{\gamma|\Omega|} \left[1 + \frac{a}{R} \log \frac{R}{a} + O\left(\frac{a}{R}\right) \right]^{-1} e^{-\langle \Delta E \rangle/\varepsilon} \text{ for } \varepsilon \gg \Delta E \\ k &\sim \frac{4\varepsilon a \omega_1 \omega_2 \omega_3}{\gamma(2\pi)^{3/2}} \left[1 + \frac{a}{R} \log \frac{R}{a} + O\left(\frac{a}{R}\right) \right]^{-1} e^{-\Delta E/\varepsilon} \text{ for } \varepsilon \ll \Delta E. \end{aligned} \quad (8.124)$$

In two dimensions the singularity of the Neumann function is logarithmic, so the leading order approximation to the activation rate is

$$\begin{aligned} k &\sim \frac{\pi\varepsilon}{\gamma|\Omega|} \frac{e^{-\langle \Delta E \rangle/\varepsilon}}{\left[\log \delta^{-1} + O(1)\right]} \text{ for } \varepsilon \gg \Delta E \\ k &\sim \frac{\varepsilon \sqrt{\omega_1 \omega_2}}{2\gamma} \frac{e^{-\Delta E/\varepsilon}}{\left[\log \delta^{-1} + O(1)\right]} \text{ for } \varepsilon \ll \Delta E. \end{aligned} \quad (8.125)$$

The remainder $O(1)$ is important, because in real life applications even if δ is small, $\log \delta^{-1}$ is not necessarily large.

If the boundary of the absorbing window contains a singular point of $\partial\Omega$, such as a corner or a cusp, the order of magnitude of the activation rate may change. Thus, if the window is at a corner of angle α then the rate is

$$\begin{aligned} k &\sim \frac{\alpha\varepsilon}{\gamma|\Omega|} \frac{e^{-\langle \Delta E \rangle/\varepsilon}}{\left[\log \delta^{-1} + O(1)\right]} \text{ for } \varepsilon \gg \Delta E \\ k &\sim \frac{\alpha\varepsilon \sqrt{\omega_1 \omega_2}}{2\pi\gamma} \frac{e^{-\Delta E/\varepsilon}}{\left[\log \delta^{-1} + O(1)\right]} \text{ for } \varepsilon \ll \Delta E. \end{aligned} \quad (8.126)$$

If the absorbing window is near a cusp, then $\bar{\tau}_\delta$ grows algebraically, rather than logarithmically. For example, in the domain bounded between two tangent circles, the activation rate is

$$\begin{aligned} k &\sim \frac{(d^{-1} - 1)\varepsilon}{\gamma|\Omega|} [\delta + O(\delta^2)] e^{-\langle \Delta E \rangle / \varepsilon} \text{ for } \varepsilon \gg \Delta E \\ k &\sim \frac{(d^{-1} - 1)\varepsilon\sqrt{\omega_1\omega_2}}{2\pi\gamma} [\delta + O(\delta^2)] e^{-\Delta E / \varepsilon} \text{ for } \varepsilon \ll \Delta E, \end{aligned} \quad (8.127)$$

where $d < 1$ is the ratio of the radii.

8.3.3 Deep Well – A Markov Chain Model

The principal eigenvalue λ_0 of the mixed boundary value problem in a domain $\Omega \subset \mathbb{R}^d$ that contains a deep potential well and the boundary conditions are Neumann on a part $\partial\Omega_r$ of the boundary $\partial\Omega$, except for a small Dirichlet window $\partial\Omega_a$ of dimensionless diameter $\delta = (|\partial\Omega_a|/|\partial\Omega_r|)^{d-1} \ll 1$. The relation between λ_0 and the narrow escape time $\bar{\tau}_\delta$ is the key to the asymptotic expansion of the eigenvalue.

The modified Kramers formulas (8.120) or (8.125) can be explained by coarse-graining the diffusive motion into a simplified 3-state Markov model when the domain contains a deep well $\Omega_W \subset \Omega$. The three states of the Markov process are (i) state W – the trajectory is trapped in the deep well; (ii) state D – the trajectory diffuses in the domain $\Omega_D = \Omega - \Omega_W$, outside the well; (iii) state A – the trajectory is absorbed in the small hole. Once the trajectory is absorbed in the small hole, its motion is terminated, so A is a terminal state of the Markov chain. For simplicity, we assume $\Omega \subset \mathbb{R}^2$.

Not all transition times between the different states are finite with probability 1, so not all expected transition times are necessarily finite. The particle, however, leaves the well W to the outer region Ω in finite expected time; that is,

$$\Pr\{\tau_{W \rightarrow D} < \infty\} = 1, \quad \mathbb{E}\tau_{W \rightarrow D} < \infty. \quad (8.128)$$

For small ε , the mean time spent in the well, $\mathbb{E}\tau_{W \rightarrow D}$, is exponentially large and is given by (see Part I)

$$\mathbb{E}\tau_{W \rightarrow D} \sim \frac{2\pi\sqrt{\frac{\partial^2\phi(\mathbf{x}_S)}{\partial s^2}}}{\sqrt{-\frac{\partial^2\phi(\mathbf{x}_S)}{\partial \rho^2}\sqrt{H(\mathbf{x}_W)}}} \exp\left\{\frac{\phi(\mathbf{x}_S) - \phi(\mathbf{x}_W)}{\varepsilon}\right\}, \quad (8.129)$$

where ρ and s are the distance to and arclength on $\partial\Omega_W$, respectively, \mathbf{x}_W is the deepest point of the well, \mathbf{x}_S is the point on $\partial\Omega_W$ where ϕ achieves its minimum, and $H(\mathbf{x}_W)$ is the Hessian of ϕ at the minimum.

The time $\tau_{D \rightarrow W}$, however, is not finite with probability 1, because there is a finite probability $\Pr\{\tau_{D \rightarrow A} < \tau_{D \rightarrow W}\}$ of termination at A without returning to W , and there is no return from A to W . Consequently, $\mathbb{E}\tau_{D \rightarrow W} = \infty$. However, $\mathbb{E}\tau_{D \rightarrow A}$ and $\mathbb{E}[\tau_{D \rightarrow W} | \tau_{D \rightarrow W} < \tau_{D \rightarrow A}]$ are finite. For small ε, δ , the conditional mean time $\mathbb{E}[\tau_{D \rightarrow W} | \tau_{D \rightarrow W} < \tau_{D \rightarrow A}]$ is asymptotically the same as $\mathbb{E}\tau_{D \rightarrow W}$ for a problem without the small absorbing window, because the conditioning (see [Schuss (2010b, Sect. 6.5)]) changes the drift only near A , to repel the trajectory from the window, so the effect on the conditional mean time is small, regardless of whether this mean time is long or short. The transition probabilities from the outer domain to the absorbing window and to the well are

$$\begin{aligned} & \Pr\{\tau_{D \rightarrow A} < \tau_{D \rightarrow W}\} \\ & \sim \frac{\mathbb{E}[\tau_{D \rightarrow W} | \tau_{D \rightarrow W} < \tau_{D \rightarrow A}]}{\mathbb{E}[\tau_{D \rightarrow W} | \tau_{D \rightarrow W} < \tau_{D \rightarrow A}] + \mathbb{E}[\tau_{D \rightarrow A} | \tau_{D \rightarrow A} < \tau_{D \rightarrow W}]} \end{aligned} \quad (8.130)$$

$$\begin{aligned} & \Pr\{\tau_{D \rightarrow W} < \tau_{D \rightarrow A}\} \\ & \sim \frac{\mathbb{E}[\tau_{D \rightarrow A} | \tau_{D \rightarrow A} < \tau_{D \rightarrow W}]}{\mathbb{E}[\tau_{D \rightarrow W} | \tau_{D \rightarrow W} < \tau_{D \rightarrow A}] + \mathbb{E}[\tau_{D \rightarrow A} | \tau_{D \rightarrow A} < \tau_{D \rightarrow W}]} \end{aligned}$$

respectively. The conditional mean transition time $\mathbb{E}[\tau_{D \rightarrow W} | \tau_{D \rightarrow W} < \tau_{D \rightarrow A}]$ from Ω_D to Ω_W is similar to (8.129),

$$\begin{aligned} & \mathbb{E}[\tau_{D \rightarrow W} | \tau_{D \rightarrow W} < \tau_{D \rightarrow A}] \quad (8.131) \\ & \sim \frac{2\pi\sqrt{\frac{\partial^2\phi(\mathbf{x}_S)}{\partial s^2}}}{\sqrt{-\frac{\partial^2\phi(\mathbf{x}_S)}{\partial\rho^2}\sqrt{H(\mathbf{x}_D)}}} \exp\left\{\frac{\phi(\mathbf{x}_S) - \phi(\mathbf{x}_D)}{\varepsilon}\right\}, \end{aligned}$$

where \mathbf{x}_D is the deepest point of the potential in the outer domain, $\phi(\mathbf{x}_W) < \phi(\mathbf{x}_D) < \phi(\mathbf{x}_S)$. The mean transition time $\mathbb{E}[\tau_{D \rightarrow A} | \tau_{D \rightarrow A} < \tau_{D \rightarrow W}]$ from Ω_D to the absorbing window is given by (8.125)

$$\mathbb{E}[\tau_{D \rightarrow A} | \tau_{D \rightarrow A} < \tau_{D \rightarrow W}] \sim \frac{2\gamma\log\delta^{-1}}{\varepsilon\sqrt{H(\mathbf{x}_D)}} \exp\left\{\frac{\phi_0 - \phi(\mathbf{x}_D)}{\varepsilon}\right\}. \quad (8.132)$$

If we assume that the effect of the small window on the mean escape time, $\log\delta^{-1}$ (or $1/\delta$ in three dimensions), is larger than that of the energy barrier, $\exp\{[\phi_0 - \phi(\mathbf{x}_S)]/\varepsilon\}$, then, according to our assumption that the potential is relatively flat outside the deep well, $\mathbb{E}[\tau_{D \rightarrow W} | \tau_{D \rightarrow W} < \tau_{D \rightarrow A}] \ll \mathbb{E}[\tau_{D \rightarrow A} | \tau_{D \rightarrow A} < \tau_{D \rightarrow W}]$, so

(8.130) implies

$$\Pr\{\tau_{D \rightarrow A} < \tau_{D \rightarrow W}\} \sim \frac{\mathbb{E}[\tau_{D \rightarrow W} | \tau_{D \rightarrow W} < \tau_{D \rightarrow A}]}{\mathbb{E}[\tau_{D \rightarrow A} | \tau_{D \rightarrow A} < \tau_{D \rightarrow W}]}.$$
 (8.133)

The mean absorption times $\mathbb{E}\tau_{i \rightarrow A}$ are finite for $i = D, W$. They satisfy the renewal equations (see [Schuss (2010b, Sect. 9.2)])

$$\begin{aligned} \mathbb{E}\tau_{D \rightarrow A} &= \Pr\{\tau_{D \rightarrow A} < \tau_{D \rightarrow W}\} \mathbb{E}[\tau_{D \rightarrow A} | \tau_{D \rightarrow A} < \tau_{D \rightarrow W}] \\ &\quad + \Pr\{\tau_{D \rightarrow W} < \tau_{D \rightarrow A}\} \mathbb{E}\tau_{W \rightarrow A}, \end{aligned}$$
 (8.134)

$$\mathbb{E}\tau_{W \rightarrow A} = \mathbb{E}\tau_{W \rightarrow D} + \mathbb{E}\tau_{D \rightarrow A}.$$
 (8.135)

Adding equations (8.134) and (8.135), and dividing by $\Pr\{\tau_{D \rightarrow A} < \tau_{D \rightarrow W}\} = 1 - \Pr\{\tau_{D \rightarrow W} < \tau_{D \rightarrow A}\}$, we obtain

$$\mathbb{E}\tau_{W \rightarrow A} = \mathbb{E}[\tau_{D \rightarrow A} | \tau_{D \rightarrow A} < \tau_{D \rightarrow W}] + \frac{\mathbb{E}\tau_{W \rightarrow D}}{\Pr\{\tau_{D \rightarrow A} < \tau_{D \rightarrow W}\}}.$$
 (8.136)

Both $\mathbb{E}[\tau_{D \rightarrow A} | \tau_{D \rightarrow A} < \tau_{D \rightarrow W}]$ and $1 / \Pr\{\tau_{D \rightarrow A} < \tau_{D \rightarrow W}\}$ have the same order of magnitude as functions of δ , however $\mathbb{E}\tau_{W \rightarrow D}$ is exponentially large in $1/\varepsilon$. Therefore,

$$\mathbb{E}\tau_{W \rightarrow A} \sim \frac{\mathbb{E}\tau_{W \rightarrow D}}{\Pr\{\tau_{D \rightarrow A} < \tau_{D \rightarrow W}\}}.$$
 (8.137)

Now, by Eq. (8.135), we have

$$\begin{aligned} \mathbb{E}\tau_{D \rightarrow A} &\sim \mathbb{E}\tau_{W \rightarrow D} \left(\frac{1}{\Pr\{\tau_{D \rightarrow A} < \tau_{D \rightarrow W}\}} - 1 \right) \\ &\sim \frac{\mathbb{E}\tau_{W \rightarrow D}}{\Pr\{\tau_{D \rightarrow A} < \tau_{D \rightarrow W}\}}, \end{aligned}$$
 (8.138)

because $\Pr\{\tau_{D \rightarrow A} < \tau_{D \rightarrow W}\} \rightarrow 0$ as $\delta \rightarrow 0$. The meaning of Eqs. (8.137) and (8.138) is that for each realization of the Markov chain, for example, the sequence $DWDWDWDWDWDWDWA$, the number of visits in state D is larger by 1, or equal to the number of visits at state W . The mean time that the trajectory spends at state W is exponentially larger than the mean time spent at state D . Therefore, the mean time to absorption is approximately the average number of visits at state D times the average time of a single visit in the deep well. The average number of visits in state D prior to absorption is $1 / \Pr\{\tau_{D \rightarrow A} < \tau_{D \rightarrow W}\}$, as in a geometric distribution, and (8.137) follows. We conclude that

$$\mathbb{E}\tau_{D \rightarrow A} \sim \mathbb{E}\tau_{W \rightarrow A},$$
 (8.139)

that is, the initial state (or coordinate) of the trajectory has no (leading order) significance for the mean first passage time $\bar{\tau}_\delta$, which by equations (8.133) and (8.137) is

$$\bar{\tau}_\delta \sim \mathbb{E}\tau_{W \rightarrow A} \sim \frac{\mathbb{E}\tau_{W \rightarrow D}}{\Pr\{\tau_{D \rightarrow W} < \tau_{D \rightarrow A}\}}. \quad (8.140)$$

Substituting (8.129), (8.131)-(8.133) in (8.140) yields

$$\bar{\tau}_\delta = \frac{2\gamma \log \delta^{-1}}{\varepsilon \sqrt{H(\mathbf{x}_W)}} \exp \left\{ \frac{\phi_0 - \phi(\mathbf{x}_W)}{\varepsilon} \right\}, \quad (8.141)$$

in agreement with Eq. (8.125). Thus (8.141) determines the asymptotics of the principal eigenvalue λ_0 through the relation $\lambda_0 = 1/\bar{\tau}_\delta$.

Exercise 8.3 (Generalization of a rod). Refine the model in Sect. 7.8 by replacing the stiff rod segment of the DNA with a pair of balls connected by a spring. Assume that $l > l_0$, so that the segment has to shrink in order to turn.

- (i) Find the mean time to turn.
- (ii) Solve the problem in a three-dimensional cylinder. □

Finally, we refer to [Tsaneva et al. (2009)] and [Cartailler et al. (2016a)] for the case of an activation through a narrow opening when the field is a repulser instead of an attractor. In that case, the escape occurs through trajectories confined to the boundary.

8.4 The Mixed Boundary Value Problem in a Solid Funnel-Shaped Domain

Consider the mixed boundary value problem in the solid of revolution obtained by rotating the symmetric domain Ω' in Fig. 7.1(left) about its axis of symmetry. The absorbing end of the neck becomes a circular disk of radius $a' = \varepsilon'/2$.

Theorem 8.4.1 *The solution to the mixed boundary value problem (the mean first passage time to the absorbing boundary at the end of the funnel) in the solid of revolution, obtained by rotating the symmetric planar domain (7.63) of Sect. 7.4.1, is given by*

$$\bar{\tau} = \frac{1}{\sqrt{2}} \left(\frac{\ell_+}{a'} \right)^{3/2} \frac{V}{\ell_+ D} (1 + o(1)) \text{ for } a' \ll \ell_+, \quad (8.142)$$

where $V = |\Omega'|$ is the volume of the domain.

Proof. Due to cylindrical symmetry of the boundary value problem (7.69) the mean first passage time in cylindrical coordinates centered on the axis of symmetry is independent of the angle. It follows that with the scaling (7.68) the boundary value problem (7.69) in the scaled spatial domain Ω can be written in cylindrical coordinates as

$$\Delta u = \frac{\partial^2 u}{\partial r^2} + \frac{1}{r} \frac{\partial u}{\partial r} + \frac{\partial^2 u}{\partial z^2} = -\frac{\ell_+^2}{D}. \quad (8.143)$$

Equation (8.143) can be considered as a two-dimensional problem in the planar cross section by a plane through the axis of symmetry of Ω in the (r, z) plane. Here r is the distance to the axis of symmetry of Ω , the z axis is perpendicular to that axis and the origin is inside the cross section of Ω , at the intersection of the axis with the tangent to the osculating circle to the cross section at the gap. Setting $u_1 = ur^{1/2}$, Eq. (8.143) takes the form

$$\frac{\partial^2 u_1(r, z)}{\partial r^2} + \frac{\partial^2 u_1(r, z)}{\partial z^2} = -\frac{\ell_+^2}{D} \left[r^{1/2} + \frac{u_1(r, z)}{4r^2} \right] \quad (8.144)$$

in the cross section, with mixed boundary conditions, as in the planar case. We assume that in dimensionless variables $\overline{AB} = \varepsilon \ll 1 < |\Omega|^{1/3}$, so the funnel is a narrow passage. The transformation to the rotated and translated coordinates is given by $\tilde{r} = r - 1 - \varepsilon/2$, $\tilde{z} = -z + 1$. Setting $u_1(r, z) = \tilde{u}(\tilde{r}, \tilde{z})$, Eq. (8.144) becomes

$$\frac{\partial^2 \tilde{u}(\tilde{r}, \tilde{z})}{\partial \tilde{r}^2} + \frac{\partial^2 \tilde{u}(\tilde{r}, \tilde{z})}{\partial \tilde{z}^2} = -\frac{\ell_+^2}{D} \left[\left(\tilde{r} + 1 + \frac{\varepsilon}{2} \right)^{1/2} - \frac{\tilde{u}(\tilde{r}, \tilde{z})}{4 \left(\tilde{r} + 1 + \frac{\varepsilon}{2} \right)^2} \right]. \quad (8.145)$$

The construction of the asymptotic expansion of the solution of the boundary layer equation (7.160) is similar to that in Sect. 7.8.2. We construct an asymptotic solution for small gap ε by first mapping the cross section in the (r, z) -plane conformally into its image under the Möbius transformation (7.153),

$$w(\zeta) = \rho e^{i\eta} = \frac{\zeta - \alpha}{1 - \alpha\zeta}, \quad (8.146)$$

where α is given in (7.71) for the symmetric case $R_c = r_c = 1$. Setting $\tilde{u}(\zeta) = v(w)$, Eq. (8.145) becomes

$$\Delta_w v(w) = \frac{-\ell_+^2}{D|w'(\zeta)|^2} \left[\left| \operatorname{Re} \left| \frac{w + \alpha}{1 + \alpha w} \right| + 1 + \frac{\varepsilon}{2} \right|^{1/2} + \frac{v}{4 \left| \operatorname{Re} \left| \frac{w + \alpha}{1 + \alpha w} \right| + 1 + \frac{\varepsilon}{2} \right|^2} \right]. \quad (8.147)$$

Because the normalized head of Fig. 7.1(left) is mapped into the narrow hot dog-shaped region in Fig. 7.10, whose width is $\sqrt{\varepsilon}$ at $\rho = 1$, we approximate

$$w = e^{i\eta} + O(\sqrt{\varepsilon}), \quad \left| \frac{w + \alpha}{1 + \alpha w} \right| = 1 + O(\sqrt{\varepsilon}). \quad (8.148)$$

We also have

$$w'(\zeta) = \frac{(1 + \alpha w)^2}{\alpha^2 - 1} \quad (8.149)$$

$$|w'(\zeta)|^2 = \left| \frac{(1 + w\alpha)^2}{1 - \alpha^2} \right|^2 = \frac{|1 - w + \sqrt{\varepsilon} w|^4}{4\varepsilon} (1 + O(\sqrt{\varepsilon})), \quad (8.150)$$

so that (8.144) reduces to

$$\Delta_w v = - \frac{\ell_+^2}{D} \frac{4\varepsilon(1 + O(\sqrt{\varepsilon}))}{|1 - w + \sqrt{\varepsilon} w|^4} \left(\sqrt{2} + \frac{1}{16} v \right), \quad (8.151)$$

or equivalently,

$$v'' + \frac{\varepsilon}{4|e^{i\eta} - 1 - e^{i\eta}\sqrt{\varepsilon}|^4} v = \frac{\ell_+^2}{D} \frac{4\sqrt{2}\varepsilon}{|e^{i\eta} - 1 - e^{i\eta}\sqrt{\varepsilon}|^4} (1 + O(\sqrt{\varepsilon})). \quad (8.152)$$

Setting $v = \ell_+^2(y - 16\sqrt{2})/D$, we obtain the leading order equation

$$y''(\eta) + \frac{\varepsilon}{4|e^{i\eta} - 1 - e^{i\eta}\sqrt{\varepsilon}|^4} y(\eta) = 0. \quad (8.153)$$

The boundary conditions are

$$y'(c\sqrt{\varepsilon}) = 0, \quad y(\pi) = 16\sqrt{2}. \quad (8.154)$$

The outer solution is the linear function

$$y_{\text{outer}}(\eta) = M\eta + N, \quad (8.155)$$

where M and N are yet undetermined constants. The absorbing boundary condition in (8.154) gives

$$y_{\text{outer}}(\pi) = M\pi + N = 16\sqrt{2}. \quad (8.156)$$

A boundary layer correction is needed to satisfy the boundary conditions at the reflecting boundary at $\eta = c\sqrt{\varepsilon}$. To resolve the boundary layer at $\eta = c\sqrt{\varepsilon}$, we set $\eta = \sqrt{\varepsilon}\xi$ and expand

$$\frac{\varepsilon^2}{|e^{i\eta} - 1 - e^{i\eta}\sqrt{\varepsilon}|^4} = \frac{1}{(1 + \xi^2)^2} + O(\sqrt{\varepsilon}).$$

Writing $y_{\text{bl}}(\eta) = Y(\xi)$, we obtain to leading order the boundary layer equation

$$Y''(\xi) + \frac{1}{4(1 + \xi^2)^2} Y(\xi) = 0, \quad (8.157)$$

which has two linearly independent solutions, $Y_1(\xi)$ and $Y_2(\xi)$ that are linear functions for sufficiently large ξ . Initial conditions for $Y_1(\xi)$ and $Y_2(\xi)$ can be chosen so that $Y_2(\xi) \rightarrow \text{const}$ as $\xi \rightarrow \infty$ (e.g., $Y_2(0) = -4.7$, $Y'_2(0) = -1$, see Fig. 7.15). Setting

$$y_{\text{bl}}(\eta) = AY_1\left(\frac{\eta}{\sqrt{\varepsilon}}\right) + BY_2\left(\frac{\eta}{\sqrt{\varepsilon}}\right), \quad (8.158)$$

where A and B are constants to be determined, we seek a uniform approximation to $y(\eta)$ in the form $y_{\text{unif}}(\eta) = y_{\text{outer}}(\eta) + y_{\text{bl}}(\eta)$. The matching condition is that $AY_1\left(\eta/\sqrt{\varepsilon}\right) + BY_2\left(\eta/\sqrt{\varepsilon}\right)$ remains bounded as $\xi \rightarrow \infty$, which implies $A = 0$. It follows that at the absorbing boundary $\eta = \pi$ we have

$$y_{\text{unif}}(\pi) = M\pi + \beta - 5B = 16\sqrt{2}, \quad y'_{\text{unif}}(\pi) = M. \quad (8.159)$$

At the reflecting boundary, we have to leading order

$$y'_{\text{unif}}(c\sqrt{\varepsilon}) = y'_{\text{outer}}(c\sqrt{\varepsilon}) + y'_{\text{bl}}(c\sqrt{\varepsilon}) = M + B \frac{Y'_2(c)}{\sqrt{\varepsilon}} = 0, \quad (8.160)$$

which gives

$$B = -\frac{M\sqrt{\varepsilon}}{Y'_2(c)}, \quad N = 16\sqrt{2} - \frac{5M\sqrt{\varepsilon}}{Y'_2(c)} - M\pi. \quad (8.161)$$

The uniform approximation to $v(w)$ is given by

$$v_{\text{unif}}(\rho e^{i\eta}) = M \left(\eta - \pi - \frac{5\sqrt{\varepsilon}}{Y'_2(c)} \right), \quad (8.162)$$

so that using (8.149), we obtain from (8.162)

$$\frac{\partial u}{\partial n} \Big|_{\zeta \in \partial \Omega_a} = \frac{\partial v(\rho e^{i\eta})}{\partial \eta} \Big|_{\eta=\pi} w'(\zeta) \Big|_{\zeta=-1} = \frac{2M}{\sqrt{\varepsilon}} [1 + O(\sqrt{\varepsilon})]. \quad (8.163)$$

To determine the value of M , we integrate (7.69) over Ω , use (8.163), and the fact that

$$\int_{\partial\Omega_a} dS = \frac{\pi\varepsilon^2}{4}, \quad (8.164)$$

to obtain $M = -2\ell_+^2|\Omega|/D\pi\varepsilon^{3/2}$. Now (8.162) gives the mean first passage time at any point x in the head as

$$\bar{\tau} = u(x) \sim v \left(\rho e^{c\sqrt{\varepsilon}} \right) \sim 2\varepsilon^{-3/2} \frac{\ell_+^2 |\Omega|}{D} = 2\varepsilon^{-3/2} \frac{|\Omega'|}{\ell_+ D} \text{ for } \varepsilon \ll 1. \quad (8.165)$$

The dimensional radius of the absorbing end of the funnel is $a' = \ell_+\varepsilon/2$ (see (7.68)), so (8.165) can be written in physical units as (8.142). This completes the proof.

The generalization of (8.142) to exit through N well-separated necks is found by noting that (8.164) becomes

$$\int_{\partial\Omega_a} dS = \sum_{j=1}^N \frac{\pi\varepsilon_j^2}{4}, \quad (8.166)$$

and the integration of (7.67) over Ω' gives the compatibility condition (dimensional)

$$\int_{\partial\Omega'} \frac{\partial u(x')}{\partial n'} dS' = M \sum_{j=1}^N \frac{\ell_j \pi \varepsilon_j^2}{4\sqrt{\varepsilon_j}} = -\frac{|\Omega'|}{D}, \quad (8.167)$$

which determines

$$M = -\frac{4|\Omega'|}{D \sum_{j=1}^N \ell_j \pi \varepsilon_j^{3/2}}. \quad (8.168)$$

Hence, using the dimensional $a'_j = \ell_j \varepsilon_j/2$, we obtain

$$\bar{\tau} = -M\pi = \frac{1}{\sqrt{2}} \frac{|\Omega'|}{D \sum_{j=1}^N \ell_j \left(\frac{a'_j}{\ell_j} \right)^{3/2}}. \quad (8.169)$$

To calculate the total flux of Green's function through any neck (the exit probability from any one of the N necks), we note that the boundary layer function is to leading order linear, as in Sect. 7.4.2. Therefore in the three-dimensional case the exit probability is given by

$$p_i = \frac{\varepsilon_i^{3/2} \ell_i}{\sum_{j=1}^N \varepsilon_j^{3/2} \ell_j} = \frac{a_i'^{3/2} \ell_i^{-1/2}}{\sum_{j=1}^N a_j'^{3/2} \ell_j^{-1/2}}. \quad (8.170)$$

Finally, the analogous expression for the narrow escape time (7.124) in three dimensions is as follows.

Theorem 8.4.2 (The solution of the mixed boundary value problem in a composite domain in \mathbb{R}^3). *The solution of the mixed boundary value problem in a composite domain $\Omega \subset \mathbb{R}^3$ with a bottleneck in the form of a narrow circular cylinder of cross section area πa^2 is given by*

$$\bar{\tau}_{x \rightarrow \partial\Omega_a} = \begin{cases} \frac{|\Omega_1|}{4aD} \left[1 + \frac{a}{\pi R} \log \frac{R}{a} \right] + \frac{O(1)}{D} + \frac{L^2}{2D} + \frac{|\Omega_1|L}{\pi a^2 D} \\ \text{solid spherical head of radius } R \text{ connected to the neck at a right angle} \\ \\ \frac{|\Omega_1|}{4aD} \left(1 + \frac{(L_x + R_x)}{2\pi} \left| \frac{\partial\Omega_a}{\pi} \right|^{1/2} \log \sqrt{\frac{|\partial\Omega_1|}{|\partial\Omega_a|}} \right) \\ + \frac{L^2}{2D} + \frac{|\Omega_1|L}{\pi a^2 D} + \frac{O(1)}{D} \\ \text{a general head connected to the neck at a right angle} \\ \\ \frac{1}{\sqrt{2}} \left(\frac{R_c}{a} \right)^{3/2} \frac{|\Omega_1|}{R_c D} (1 + o(1)) + \frac{L^2}{2D} + \frac{|\Omega_1|L}{\pi a^2 D} \\ \text{a general head connected smoothly to the neck by a funnel}, \end{cases} \quad (8.171)$$

where R_c is the curvature at the cusp

Discussion of the $O(1)$ term in (8.171) is given in a reference in Annotations 8.7. Note, in addition, that modulation of neck length changes the residence time significantly. Comparing (7.124) with (8.171), we note that the geometry of the connection affects the residence time stronger in two than in three dimensions.

8.5 The Mixed Boundary Value Problem with a Dirichlet Ribbon

A ribbon is a two-dimensional manifold with nontrivial topology on a sphere and is thus not a small window in the sense of the theory developed above. Therefore the mixed boundary value problem with a Dirichlet ribbon requires an adjustment of the theory to this geometry. The mixed boundary value problem in this case can represent the search by a calcium ion in a pre-synaptic terminal for a small target hidden between a membrane and a vesicle (see Fig. 8.3). The ionic motion can be modelled locally as diffusion in the domain Ω enclosed between two tangent spheres

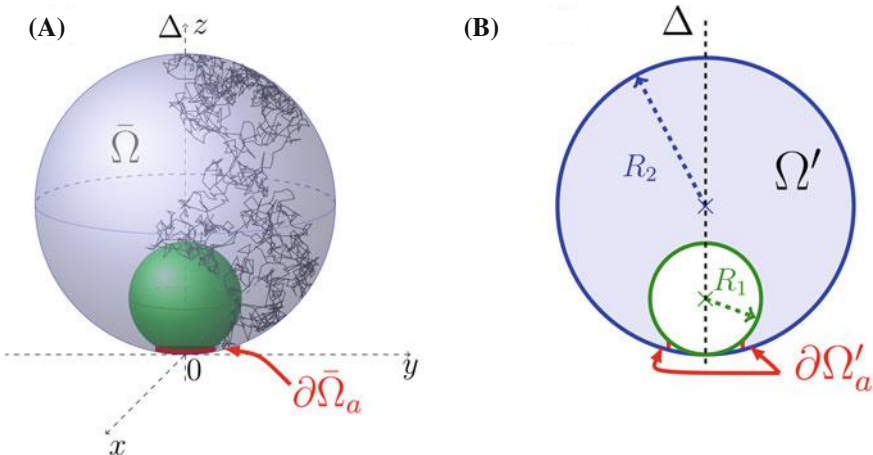


Fig. 8.2 A Brownian search for a narrow ribbon (red) in the domain $\bar{\Omega}$ enclosed between tangent reflecting spheres (blue and green). **B:** The projection of $\bar{\Omega}$ on its plane of symmetry is the planar domain Ω' enclosed by two circles. The projection of the ribbon target consists of two short arcs (red)

of different radii, R_1 and R_2 ($R_1 < R_2$). The smaller sphere may represent a small vesicle containing neurotransmitter molecule that are released into the synaptic cleft when the ion reaches the ribbon and triggers a reaction (see Fig. 8.4).

There are two natural scales here, the size of the vesicle relative to that of the pre-synaptic terminal and the size of the calcium ion that squeezes between them, relative to that of the vesicle. The smaller scale is that of the ion, so on this scale the radii R_1 and R_2 are much bigger than the ion, which can be considered a Brownian particle if electrical interactions are neglected. Under these conditions an asymptotic expansion in the limit $R_1 \ll R_2$ can be applied to the final result (see (8.195) below). If the ionic scale is commensurate with the radii, an altogether different expansion has to be constructed. The search target is a narrow ribbon of (dimensional) width ε (dimensionless width $\varepsilon' \ll 1$) with $\varepsilon = \varepsilon'R$, where R is a typical length in the problem. The radius of the ribbon is

$$r_a = \sqrt{\alpha\varepsilon}(1 + O(\varepsilon)) = \sqrt{\varepsilon'} \sqrt{\frac{2RR_2R_1}{\sqrt{R_1^2 + R_2^2}}}(1 + O(\varepsilon')), \quad (8.172)$$

where

$$\alpha = \frac{2R_2R_1}{\sqrt{R_1^2 + R_2^2}}. \quad (8.173)$$

Scaling the cylindrical coordinates $(r, z) = R_2(r', z')$ by setting

$$R'_1 = \frac{R_1}{R_2}, \quad R' = \frac{R}{R_2}, \quad r'_a = \frac{r_a}{R_2} = \sqrt{\varepsilon'} \sqrt{\frac{2R'R'_1}{\sqrt{1+R'^2}}} (1 + O(\varepsilon')), \quad (8.174)$$

maps the domain Ω into the dimensionless domain Ω' , enclosed between spheres of dimensionless radii R'_1 and 1, respectively. Projecting the cylindrically symmetric domain Ω' enclosed between the two spheres into a plane of symmetry (through the common axis of the two spheres), maps Ω' into a planar domain enclosed between the circles $r'^2 + z'^2 - 2z'R'_1 = 0$ and $r'^2 + z'^2 - 2z' = 0$ in the (r', z') plane, shown as the cusp in the middle frame of Fig. 8.2 (denoted $\tilde{\Omega}'$). The absorbing band in Ω' is mapped into the short circular arc $\partial\tilde{\Omega}'_a$ joining the two circles (marked red). The radius r'_a of the ribbon and the radius of the arc are to leading order the same for $\varepsilon' \ll 1$ (see (8.174)).

Due to the cylindrical symmetry of the three-dimensional boundary value problem (6.1)–(6.3) for the mean first passage time from $\mathbf{x} \in \Omega$ to the ribbon, $v(\mathbf{x})$, in cylindrical coordinates (r', z', θ) , we set $v(\mathbf{x}) = V(r', z', \theta)$, which is independent of θ , and thus we are left with the two-dimensional mixed boundary value problem in $\tilde{\Omega}'$

$$\begin{aligned} \frac{\partial^2 V(r', z')}{\partial r'^2} + \frac{1}{r'} \frac{\partial V(r', z')}{\partial r'} + \frac{\partial^2 V(r', z')}{\partial z'^2} &= -\frac{1}{\Omega'} \text{ for } (r', z') \in \tilde{\Omega}' \\ \frac{\partial V(r', z')}{\partial n'} &= 0 \text{ for } (r', z') \in \tilde{\Omega}' \setminus \partial\tilde{\Omega}'_a \\ V(r', z') &= 0 \text{ for } (r', z') \in \tilde{\Omega}', \end{aligned} \quad (8.175)$$

where $\Omega' = \Omega/R_2^2$. Note that the dimension of (8.175) is time.

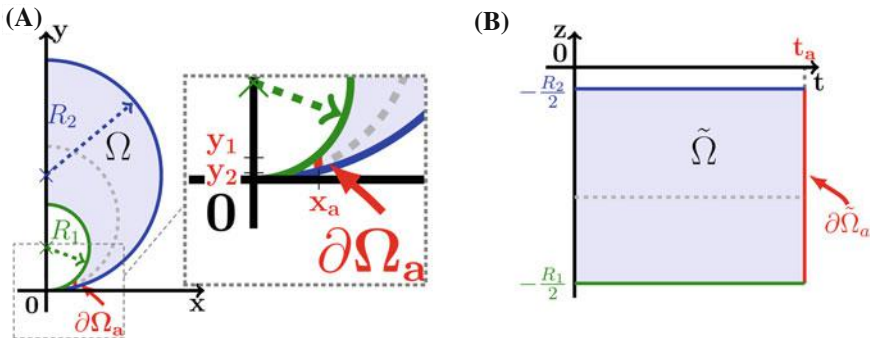


Fig. 8.3 Conformal mapping. The domain $\tilde{\Omega}$ in frame (B) is the conformal image of the domain $\tilde{\Omega}'$ in frame (A) under the inversion $\omega = f(\xi) = 1/\xi$. Circles of radius r' centered at $(0, r')$ are mapped into the lines $\operatorname{Re}(\xi) = 1/2r'$: the gray dashed circle in frame (A) is mapped into the dashed horizontal line in frame (B)

To construct a uniform asymptotic expansion of the solution of (8.175) for $\varepsilon' \ll 1$, we introduce the complex variable $\xi = r' + iz'$ and apply the inversion $\omega = x + iy = f(\xi) = 1/\xi$, which maps the right half of $\bar{\Omega}'$ into the rectangle

$$\tilde{\Omega} = \left\{ 0 < t < \frac{1}{r'_a}, -\frac{1}{2R'_1} < z < -\frac{1}{2} \right\}, \quad (8.176)$$

shown in Fig. 8.3B (see the reference in Annotations 8.7). Setting $V(\xi) = u(\omega)$, Eq.(8.175) becomes

$$(t^2 + z^2)^2 \Delta u + \frac{t^2 + z^2}{t} \left(\frac{\partial t}{\partial r'} \frac{\partial u}{\partial t} + \frac{\partial z}{\partial r'} \frac{\partial u}{\partial z} \right) = -\frac{1}{\Omega'} \text{ for } (t, z) \in \tilde{\Omega} \quad (8.177)$$

$$u_t(0, z) = 0, \quad u\left(\frac{1}{r'_a}, z\right) = 0 \text{ for } -\frac{1}{2R'_1} < z < -\frac{1}{2} \quad (8.178)$$

$$u_z\left(t, -\frac{1}{2}\right) = 0, \quad u_z\left(t, -\frac{1}{2R'_1}\right) = 0 \text{ for } 0 < t < \frac{1}{r'_a}. \quad (8.179)$$

Note that

$$\frac{\partial t}{\partial r'} = -t^2 + z^2, \quad \frac{\partial z}{\partial r'} = -2tz.$$

Scaling

$$t = \frac{X}{r'_a}, \quad u(x, z) = U(X, z),$$

equation (8.177) becomes

$$\begin{aligned} r'^{-4} X^4 U_{zz} + r'^{-2} (X^2 z^2 U_{zz} - 2X^2 z U_z + X^4 U_{XX} - X^3 U_X) \\ + 2X^2 z^2 U_{XX} + z^4 U_{zz} - 2z^3 U_z + \frac{1}{\Omega'} = O(r'_a) \end{aligned}$$

for $0 < X < 1$ and $-1/2 < z < -1/2R'_1$. The boundary conditions (8.178), (8.179) become

$$U_X(0, z) = 0 = U(1, z) = 0 \text{ for } -\frac{1}{2R'_1} < z < -\frac{1}{2} \quad (8.180)$$

$$U_z\left(X, -\frac{1}{2}\right) = U_z\left(X, -\frac{1}{2R'_1}\right) = 0 \text{ for } 0 < X < 1. \quad (8.181)$$

A regular expansion in powers of r'_a ,

$$U(X, z) = U^0(X, z) + r'_a U^1(X, z) + r'^2_a U^2(X, z) + \dots, \quad (8.182)$$

gives at the leading-order $O(r_a'^{-2})$ the equation $X^4 U_{zz}^0(X, z) = 0$, hence $U^0(X, z) = U^0(X)$ (independent of z). At order $O(r_a'^{-1})$, we obtain the equation

$$X^4 U_{zz}^1 + X^4 U_{XX}^0 - X^3 U_X^0 = 0. \quad (8.183)$$

The solvability condition for (8.183) is

$$\int_{-1/2}^{-1/2 R'_1} [X^4 U_{XX}^0 - X^3 U_X^0] dz = 0,$$

so that

$$X^4 U_{XX}^0 - X^3 U_X^0 = 0. \quad (8.184)$$

It follows that $U^0(X) = A(1 - X^2)$, where A is an unknown constant. The next term in the expansion (8.182), $U^1(X, y)$, is determined from the equation of order $O(1)$,

$$X^4 U_{YY}^2 + X^4 U_{XX}^1 + 2X^2 y^2 U_{yy}^1 - X^3 U_X^1 - 2Xy U_y^1 + 2X^2 y^2 U_{XX}^0 + \frac{1}{\Omega'} = 0, \quad (8.185)$$

whose solvability condition, in view of $U^0(X, y) = A(1 - X^2)$, is

$$\frac{1 - R'_1}{2} \left[X^4 U_{XX}^1 - X^3 U_X^1 + \frac{1}{\Omega'} \right] + 2X^2 \int_{-1/2}^{-R'_1/2} [y^2 U_{yy}^1 - 2Xy U_y^1] dy = 0. \quad (8.186)$$

Equation (8.184) implies that $U^1(X, y)$ is independent of y , because (8.185) is not separated. Thus (8.186) reduces to

$$\begin{aligned} X^4 U_{XX}^1 - X^3 U_X^1 + \frac{1}{\Omega'} &= 0 \text{ for } 0 < X < 1 \\ U^1(1) &= 0. \end{aligned} \quad (8.187)$$

It follows that the outer solution is $U_{\text{out}} = A$ and that (8.187) is a boundary layer equation that has to match to the outer solution for $0 < X < 1$ as $\varepsilon' \rightarrow 0$.

Near the absorbing boundary $X = 1$, we set $1 - X = \zeta$ and $U^1(X) = Y(\zeta)$. Thus

$$\begin{aligned} Y''(\zeta) + \frac{1}{1 - \zeta} Y'(\zeta) &= -\frac{1}{\Omega'(1 - \zeta)^4} \\ Y(0) &= 0. \end{aligned} \quad (8.188)$$

A local power series expansion near $\zeta = 0$ gives

$$Y(\zeta) = Y'(0)\zeta - \frac{(Y'(0)\Omega' + 1)\zeta^2}{2\Omega'} + O(\zeta^3).$$

Thus local expansion in the original variable x near the boundary $x = 1/r'_a$ can be written as

$$u_{\text{in}}(x) = A + r'_a \left[Y'(0)(1 - r'_a x) - \frac{(Y'(0)\Omega' + 1)(1 - r'_a x)^2}{2D} + O(\zeta^3) \right]. \quad (8.189)$$

Note that $Y'(0)$ can be of order $O(r'_a^{-1/2})$. The boundary condition (8.188) gives

$$u_{\text{in}}(x) = B(1 - r'_a x) + O(r'^2_a), \quad (8.190)$$

where B is an unknown constant. The boundary layer $u_{\text{in}}(x)$ satisfies the boundary condition $u_{\text{in}}(1/r'_a) = 0$ and matches to the constant outer solution as $r'_a x \rightarrow 0$. Therefore $u_{\text{in}}(x)$ is, indeed, a uniform expansion.

To compute the unknown constant A , we use the leading term $U^0(X) = A(1 - X^2) = A[1 - (r'_a x)^2]$ to evaluate

$$\frac{\partial u}{\partial n} \Big|_{\partial \tilde{\Omega}_a} \approx \frac{dA[1 - (r'_a x)^2]}{dx} \Big|_{x=1/r'_a} = -2Ar'_a. \quad (8.191)$$

The compatibility condition (6.6), obtained by integrating (8.175) over the planar domain $\bar{\Omega}'$, is

$$-\frac{|\bar{\Omega}'|}{\Omega'} = \int_{\partial \Omega'_a} \frac{\partial V(r', z')}{\partial n'} ds, \quad (8.192)$$

which under the change of variables given by the inversion $t + iz = 1/(r' + iz')$ becomes

$$\frac{|\bar{\Omega}'|}{\Omega'} = \int_{-1/2}^{1/2R'_1} \frac{\partial u(x, y)}{\partial x} \frac{y^2 - r'^{-2}}{(y^2 + r'^{-2})^{3/2}} dy \approx \frac{1}{2} \left(\frac{1}{R'_1} - 1 \right) Ar'^2_a. \quad (8.193)$$

Hence

$$A = \frac{2|\bar{\Omega}'|}{\Omega' \left(\frac{1}{R'_1} - 1 \right) r'^2_a} = \frac{|\bar{\Omega}| \sqrt{R_1^2 + R_2^2}}{D\varepsilon' R R_1 (R_2 - R_1)},$$

so the solution of the mixed boundary value problem (the mean first passage time from $\mathbf{x} \in \Omega$ to the ribbon) is to leading order in ε'

$$v(\mathbf{x}) = \mathbb{E}[\tau | r, z, \theta] = \frac{2|\bar{\Omega}'|}{\Omega' \left(\frac{1}{R'_1} - 1 \right) r'^2} = \frac{|\bar{\Omega}| \sqrt{R_1^2 + R_2^2}}{D\varepsilon' R R_1 (R_2 - R_1)} \times \quad (8.194)$$

$$\left[1 - \varepsilon' \frac{2RR_1R_2}{\sqrt{R_1^2 + R_2^2}} \left(\frac{r}{r^2 + z^2} \right)^2 \right] [1 + o(\varepsilon')].$$

Note that $|\bar{\Omega}| = \pi(R_2^2 - R_1^2)$ in (8.194) is the area of the cross section, not the volume of the domain Ω . In the limit $R_1 \ll R_2$ and with $R = R_2$, (8.194) reduces in dimensional variables to

$$v(\mathbf{x}) = \mathbb{E}[\tau | r, z, \theta] = \frac{|\Omega|}{4D\varepsilon} \left[1 - 2\varepsilon R_1 \left(\frac{r}{r^2 + z^2} \right)^2 \right] \left[1 + o\left(\frac{\varepsilon}{R_2}\right) \right]. \quad (8.195)$$

As mentioned above, the diffusion to a ribbon can describe calcium ions near a vesicle in the pre-synaptic terminal. The rare event of hitting the ribbon determines the rate of vesicular release, which likely depends on the distance of the hitting spot to the calcium channels on the membrane. It is as yet unclear how the rate of vesicular release can vary over 6 orders of magnitude for the same synapse [Kochubey et al. (2011)]. The cusp geometry and rare events may hold the key to the resolution of this drastic modulation of the vesicular release rate (see, for example, the discussion in [Guerrier and Holcman (2015)]).

8.6 Selected Applications in Molecular Biophysics

8.6.1 Leakage from a Cylinder

The theory of Sect. 8.2.3 has an application in the neurophysiology of a neuronal synapse (shown schematically in Fig. 8.4). The synapse contains three cylinder-shaped structures: the neck (outer membrane), the cleft and the membrane of the endoplasmic reticulum, schematically modeled in Fig. 8.5 (see Annotations 8.7). The endoplasmic reticulum, which is a large store of calcium ions, lines the entire spine membrane. Calcium ions, on their way from the spine-head to the dendritic shaft, can be pumped out of the spine neck by pump proteins embedded in the spine outer membrane, which can be modeled as small absorbing windows in the impermeable surface of the membrane (see Fig. 8.6). Similarly, calcium ions can be transported in and out of the endoplasmic reticulum. As mentioned at the beginning

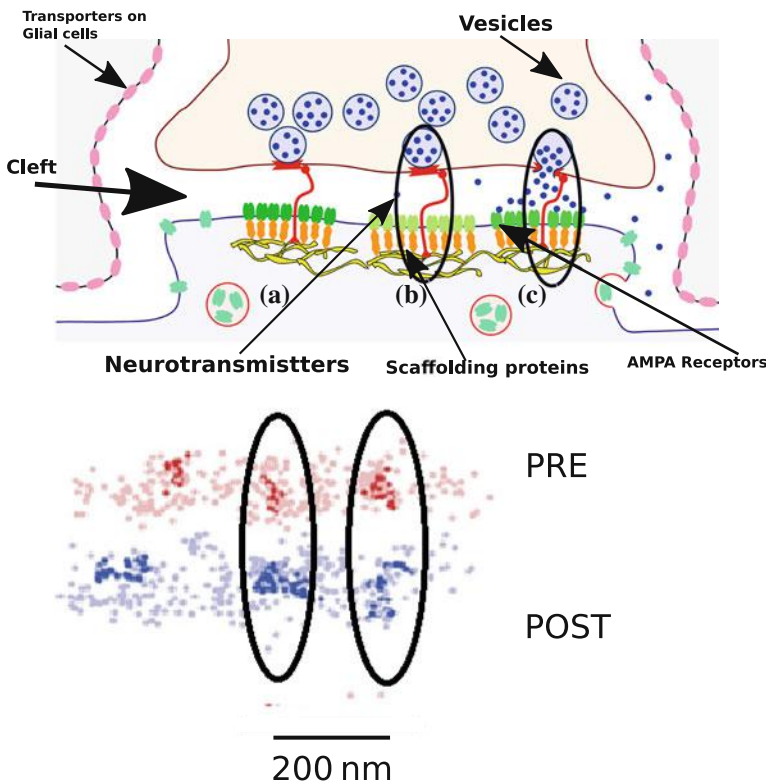


Fig. 8.4 Schematic representation of a synapse. (Upper) The diagram shows the pre- (upper part) and post-synaptic (lower) terminals membranes. Neurotransmitter molecules (blue dots) are released in the cleft, surrounded by glial cells G and the AMPA receptors (green) form the absorbing boundary for the neurotransmitters. Clusters of AMPARs (a,b,c) are co-localized in nano-columns with release sites of vesicle fusion, mediated by adhesion molecules (red) [Freche et al. (2011)], [Freche et al. (2013)]. (Lower) Experimental confirmation of the predicted column organization of the synapse (in [Freche et al. (2011)]), using super-resolution of markers: RIM (red) for the pre-synaptic terminal and PSD95 (blue) for the post-synaptic [Tang et al. (2016)]

of the chapter, the synaptic cleft function can be modeled as the leakage through the post-synaptic density .

To determine the regulatory role of the geometry in the functioning of these biological structures , we consider a circular cylinder of length L and radius R , whose bases, S_0 and S_L , are centered at the z -axis, at $z = 0$ and $z = L$, respectively, and are parallel to the (x, y) plane (see Fig. 8.6). Assume that the lateral surface S_r is impermeable to ions (i.e., reflects Brownian trajectories), a constant net flux is injected at S_0 , and that S_L is absorbing. Our purpose is to find the flux through a small absorbing circular hole $S(a)$ of (dimensional) radius a on the lateral surface of the cylinder. We consider two problems, (i) a given flux at S_0 , absorption at S_L , and reflection at $r = R$, and (ii) a given flux at (e.g., a point source at distance r

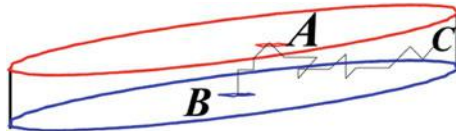
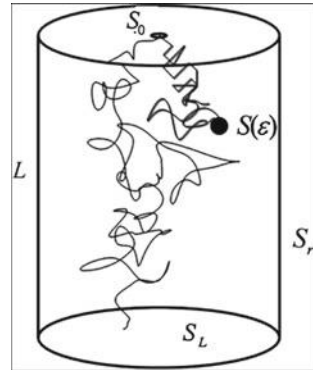


Fig. 8.5 An idealized model of the synaptic cleft. Neurotransmitters are injected at **A** and can find a receptor on the post-synaptic density **B** or be absorbed by the surrounding glial cells **C**

Fig. 8.6 A Brownian trajectory that starts at the top of the neck (S_0) can leak out through a pump or exchanger on the neck ($S(\varepsilon)$) or be absorbed at the base of the neck on the dendrite (S_L)



from the center of S_0), reflection at S_L , and absorption at $r = R$. Problem (i) can describe the diffusion flux of calcium ions through pumps in the neck of a neuronal spine, by applying (8.87), while (ii) can describe the flux of neurotransmitters from a vesicle, released at distance r from the center of the presynaptic membrane S_0 , into the NMDA or AMPA channels in the postsynaptic membrane in the synaptic cleft (see Fig. 8.5): if the point of injection **A** is moved r away from the center of S_0 , the decay of the flux through the receptor at the center of the post-synaptic density **B** is given by (8.87). Here the point **0** is the center of the hole in S_L .

We scale variables with L , so the dimensionless polar coordinates in the cylinder are

$$0 < \zeta < 1, \quad 0 < \rho < \frac{R}{L}, \quad 0 \leq \theta < 2\pi.$$

The solution of the reduced problem (i) for the dimensionless system (8.64) with influx density $\phi(\rho, \theta)$ at $\zeta = 0$ is constructed by the method of separation of variables as

$$u_0(\rho, \zeta, \theta) \tag{8.196}$$

$$= - \sum_{n=0}^{\infty} \sum_{m=1}^{\infty} \frac{\sinh \frac{\lambda_n(1-\zeta)}{R}}{L \lambda_n \cosh \frac{\lambda_n L}{R}} J_n \left(\frac{\lambda_n L \rho}{R} \right) (A_n \cos n\theta + B_n \sin n\theta),$$

where $J_n(\cdot)$ ($n = 0, 1, \dots$) are Bessel functions, λ_n are the roots of $J'_n(\cdot)$, for $n = 0$,

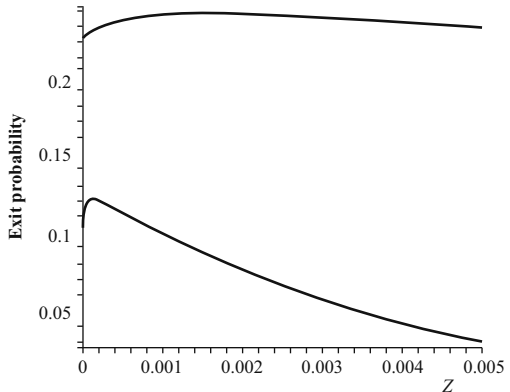
$$A_{0,m} = \frac{L}{\pi R J_0^2(\lambda_{0,m})} \int_0^{R/L} \int_0^{2\pi} \phi(\sigma, \theta) J_0\left(\frac{\lambda_{0,m} L \sigma}{R}\right) d\theta \sigma d\sigma$$

and for $n > 0$

$$A_n + i B_n = \frac{2L\lambda_n^2}{\pi R (\lambda_n^2 - n^2) J_n^2(\lambda_n)} \int_0^{R/L} \int_0^{2\pi} \phi(\sigma, \theta) e^{in\theta} J_n\left(\frac{\lambda_n L \sigma}{R}\right) d\theta \sigma d\sigma.$$

For a point source at the center of S_0 the exit probability through a small hole at $r = R$ and z is shown in Fig. 8.7. If the source is uniformly distributed in S_0 , the dimensionless solution of the reduced problem (i) is $u_0\left(\frac{R}{L}, \zeta, \theta\right) = C(1 - \zeta)$, where C is a constant.

Fig. 8.7 The probability $\Pr\{\tau_{\text{hole}} < \tau_{S_0}\}$ to exit through a single pump of radius $\varepsilon = 1\text{nm}$ on the neck membrane at distance z from the source, according to (8.196). Upper curve $L/R = 5$, lower curve $L/R = 100$



The dimensionless solution of the reduced problem (ii) with influx density $\phi(\rho, \theta)$ at $\zeta = 0$ is given by

$$\begin{aligned} u_0(\rho, \zeta, \theta) \\ = \sum_{n=0}^{\infty} \sum_{m=1}^{\infty} \frac{\cosh \frac{\gamma_n(1-\zeta)}{R}}{L \gamma_n \sinh \frac{\gamma_n L}{R}} J_n\left(\frac{\gamma_n L \rho}{R}\right) (A_n \cos n\theta + B_n \sin n\theta), \end{aligned}$$

where γ_n are the roots of $J_n(\cdot)$,

$$A_{0,m} = \frac{L}{\tilde{D}\pi R J_0'^2(\gamma_{0,m})} \int_0^{R/L} \int_0^{2\pi} \phi(\sigma, \theta) J_0\left(\frac{\gamma_{0,m} L \sigma}{R}\right) d\theta \sigma d\sigma,$$

and for $n > 0$

$$A_n + iB_n = \frac{2L}{\tilde{D}\pi R J_n'^2(\gamma_n)} \int_0^{R/L} \int_0^{2\pi} \phi(\sigma, \theta) e^{in\theta} J_n\left(\frac{\gamma_n L \sigma}{R}\right) d\theta \sigma d\sigma.$$

For a point source at $(\zeta, \rho, \theta) = (0, 0, 0)$, the density at the other end $\zeta = 1$ is

$$u_0(\rho, 1, 0) = \sum_{m=1}^{\infty} \frac{L J_0\left(\frac{\gamma_{0,m} L \rho}{R}\right)}{\tilde{D}\pi R \gamma_{0,m} J_0'^2(\gamma_{0,m}) \sinh \frac{\gamma_{0,m} L}{R}}. \quad (8.197)$$

Because the efflux through the lateral equals the influx through S_0 , the probability that a Brownian particle injected at the source will reach a hole centered at $(r, L, 0)$ (in dimensional variables) is, according to (7.61), (8.86) or (8.87),

$$\Pr\{\tau_{\text{hole}} < \tau_{S_r}\} = \frac{4aL}{\pi R^2} \sum_{m=1}^{\infty} \frac{J_0\left(\frac{\gamma_{0,m} r}{R}\right)}{\gamma_{0,m} J_0'^2(\gamma_{0,m}) \sinh \frac{\gamma_{0,m} L}{R}} + O\left(\frac{a^2}{R^2} \log \frac{a}{R}\right). \quad (8.198)$$

If $r = 0$, then

$$\Pr\{\tau_{\text{hole}} < \tau_{S_r}\} = \frac{4aL}{\pi R^2} \sum_{m=1}^{\infty} \frac{1}{\gamma_{0,m} J_0'^2(\gamma_{0,m}) \sinh \frac{\gamma_{0,m} L}{R}} + O\left(\frac{a^2}{R^2} \log \frac{a}{R}\right).$$

The sensitivity of the flux to the location of the post-synaptic density in the synaptic cleft is shown in Fig. 8.8. The flux, averaged over a uniform distribution of the post-synaptic density is shown in Fig. 8.9. The sensitivity to the height of the cleft is also shown in the figures. These sensitivities may hint at a possible way of coding memory in the cleft of a neuronal synapse by changing the location of the post-synaptic density or its size (e.g., anchoring more NMDA or AMPA channels there).

8.6.2 Applications of the Mixed Boundary Value Problem

Computer simulations of ions diffusing in solution tend to be inefficient, mainly because hitting a target much smaller than the vessel in which the ions are diffusing

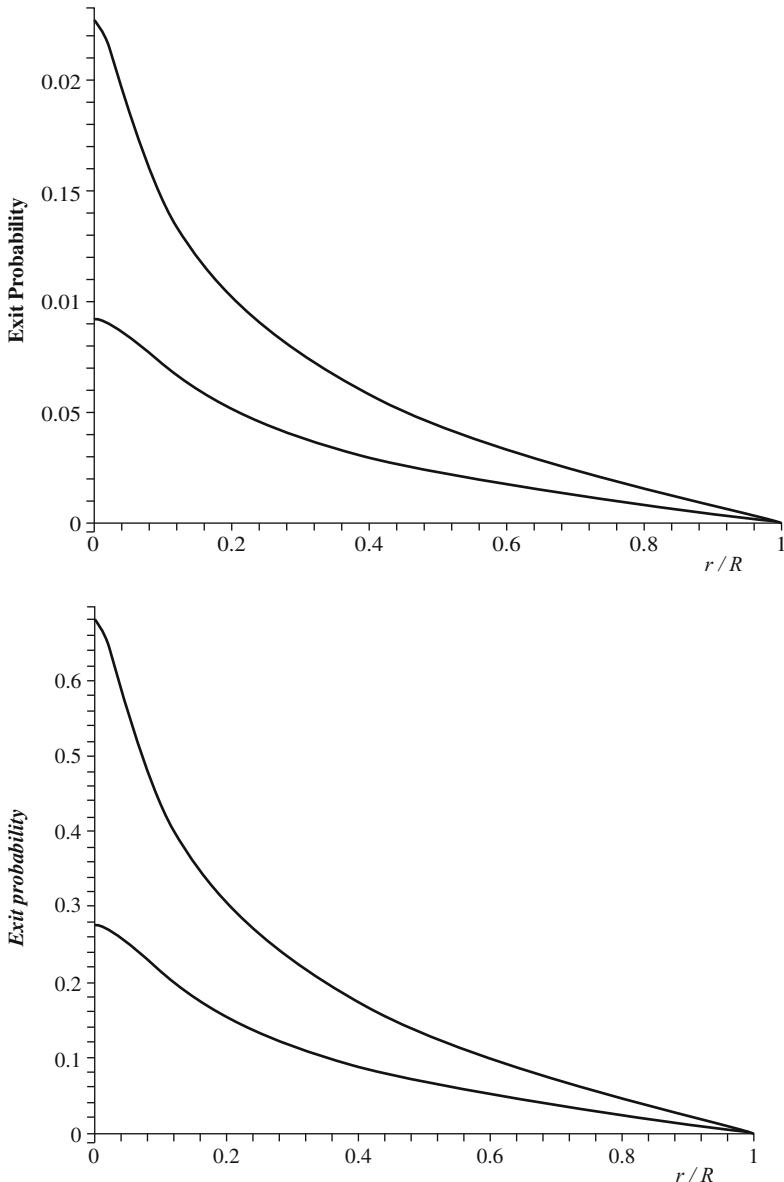
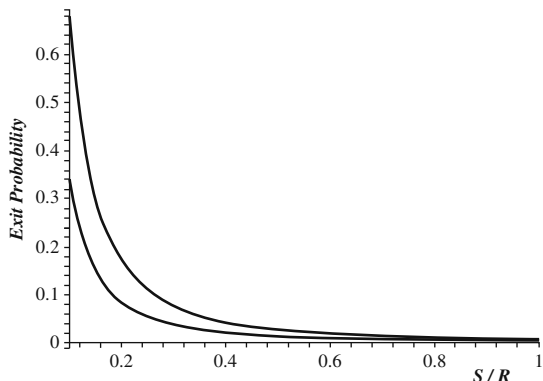


Fig. 8.8 **Left panel:** The exit probability $\Pr\{\tau_{\text{hole}} < \tau_{S_r}\}$ vs relative distance r/R from center for a single AMPAR channel of radius $\varepsilon = 1\text{nm}$ in the post-synaptic density, according to (8.198). Upper curve $L/R = 0.05$, lower curve $L/R = 0.1$. **Right panel:** the same for a cluster of 7 channels in the post-synaptic density

Fig. 8.9 The exit probability where 20 AMPAR channels are located in the post-synaptic density $\Pr\{\tau_{\text{hole}} < \tau_{S_i}\}$ vs S/R for 20 AMPAR channels scattered uniformly within radius $S < R$, according to the integrated (8.198) with respect to a uniform density. Top curve $S/R = 0.05$, lower curve $S/R = 0.1$



is a rare event on the time scale of the simulation time steps. The criteria for convergence of a simulated Brownian trajectory depend on the quantity of interest in the simulation. Thus, a criterion for convergence of a simulated trajectory as the time step of the simulation decreases is the convergence of the first passage time out of the domain of attraction of a stable equilibrium, as described in Part I, or the first passage time to a small target, as described in Part II. For example, the time for a Brownian trajectory moving in a volume of 1mm^3 to enter a protein channel embedded in a cell membrane is practically impossible to simulate, due to the exceedingly large number of simulation steps.

It becomes clear, from the present analysis, why ions take so long to enter the channel. According to (8.21), the mean time between arrivals of ions at the channel is

$$\bar{\tau} = \frac{\mathbb{E}\tau}{N} = \frac{1}{4DaC}, \quad (8.199)$$

where N is the number of ions in the simulation and C is their concentration. A coarse estimate of $\bar{\tau}$ at the biological concentration of 0.1 Molar, channel radius $a = 20\text{\AA}$, diffusion coefficient $D = 1.5 \times 10^{-9}\text{m}^2/\text{sec}$ is $\bar{\tau} \approx 1\text{nsec}$. In a Brownian dynamics simulation of ions in solution with a time step which is 10 times the relaxation time of the Langevin equation to the Smoluchowski (diffusion) equation, at least 1000 simulation steps are needed on average for the *first* ion to arrive at the channel. It should be taken into account that most of the ions that arrive at the channel do not cross it.

The mixed narrow escape problem comes up in problems of escape from a domain composed of a big subdomain with a small hole, connected to a thin cylinder (or cylinders) of length L . If ions that enter the cylinder do not return to the big subdomain, the mean first passage time to the far end of the cylinder is given by (8.171). The generalization to a domain composed of many big subdomains with small holes connected by narrow cylinders is straightforward. Thus the results of Sect. 7.7.2 carry over to the three-dimensional case.

The case of a sphere of volume $|\Omega| = 4\pi R^3/3$ with a small opening of size ε connected to a thin cylinder of length L is relevant in biological micro-structures, such as dendritic spines in neurobiology. Indeed, the mean time for a calcium ion to diffuse from the spine-head to the parent dendrite through the neck controls the spine-dendrite coupling. This coupling is involved in the induction of processes such as synaptic plasticity. Formula (7.114) is useful for the interpretation of experiments and for the confirmation of the diffusive motion of ions from the spine-head to the dendrite.

Another significant application of the narrow escape formula is to provide a new definition of the forward binding rate constant in micro-domains. Indeed, the forward chemical constant is really the flux of particles to a given portion of the boundary, depending on the substrate location. To model chemical reactions in micro-structures, where a bounded domain contains only a few particles that bind to a given number of binding sites, the forward binding rate,

$$k_{\text{forward}} = \frac{1}{\bar{\tau}},$$

has to be computed with $\bar{\tau}$ given in (8.199) (see the references in Annotations 8.7 below).

8.7 Annotations

The expansion (8.10) was proposed in [Silbergleit et al. (2003)]. For further analysis of the $O(1)$ term in (8.15), see *loc. cit.* An explicit solution to the Helmholtz equation (8.2) can be found when the hole $\partial\Omega_a$ is an ellipse [Rayleigh (1945)], [Lurie (1964)]. Third-order asymptotics for many windows is solved in [Cheviakov et al. (2010)].

The asymptotics of two and multiple small absorbing windows in Theorem 8.2.2 were resolved in [Holcman and Schuss, JPA (2008a)] and [Holcman and Schuss, PLA (2008)]. If in Theorem 8.2.2 the number of absorbing windows on a surface increases while their combined surface area remains constant, the narrow escape time through the holes increases [Holcman and Schuss, JPA (2008a)], [Reingruber et al. (2009)] and [Cheviakov et al. (2010)]. However, the asymptotics for a large number of windows, N with surface fraction $N\varepsilon^2 = o(1)$ has not yet been elucidated. Such analysis requires the computation of three terms in the expansion (8.45). The narrow escape time does not necessarily tend to zero as N goes to infinity, depending on the organization of windows and the initial distribution of the Brownian trajectories. This is the case, for example, in an annular domain with holes only on the inner circle (sphere), while Brownian trajectories start on the outer circle (sphere). Some analysis was initiated in [Berg and Purcell (1977)], however this problem calls for further analysis to treat the double asymptotics of large N and small ε , see also [Lagache et al. (2016)] and [Lindsay et al. (2016)].

The derivation of (8.84), $u_\varepsilon \rightarrow u_0$ as $\varepsilon \rightarrow 0$, where u_0 is the corresponding eigenfunction of the reduced problem (in the absence of the small hole) is elaborated in [Ward and Keller (1993)].

The $O(1)$ term in (8.171) can be computed for the sphere using the explicit expression of the Neumann–Green function [Cheviakov et al. (2010)]. The mapping and Fig. 8.3B were given in [Guerrier and Holcman (2015)]. A new definition of the forward binding rate constant in micro-domains is discussed in [Holcman and Schuss (2005b)].

Leakage is described in Sect. 8.6 and in [Toresson and Grant (2005)], and the synaptic cleft is described in [Alberts et al. (1994, Chap. 19)].

Chapter 9

Short-Time Asymptotics of the Heat Kernel and Extreme Statistics of the NET

9.1 Introduction

The first of N i.i.d. Brownian trajectories that arrive at a small target sets a time scale which is much shorter than that of the arrival of a typical trajectory. The shortest arrival time is computed here analytically in an asymptotic approximation for large N . The asymptotic expression is computed here based on the short-time asymptotics of the pdf of the first time to a small target in 1, 2 and 3 dimensions. These are referred to in the statistical physics literature as extreme statistics.

The analysis begins with the time-dependent solution of the Fokker–Planck equation and the short-time asymptotics of the survival probability of a single Brownian trajectory. Previous studies of the short-time asymptotics of the diffusion equation concern the asymptotics of the trace of the heat kernel [Colin de Verdière (1973)] and [Schuss and Spivak (2005)]. Here, an estimate of the survival probability is derived by resorting to a new method, which is based on the construction of the asymptotics of Green’s function of the Helmholtz equation. First, a general framework is set for the computation of the pdf of the FAT and of the conditional pdf of the second arrival, given that the first one has already occurred. Here a population of N Brownian trajectories in one dimension (a ray or an interval) is considered. Then the Poissonian approximation to diffusion escape is presented: we consider the case of a bulk domain with a window connected to a narrow cylinder (dendritic spine shape). Finally, the pdf of the extreme escape time through small windows is constructed in dimensions 2 and 3.

9.1.1 *The pdf of the First Escape Time*

The narrow escape problem (NEP) for the shortest arrival time of N non-interacting i.i.d. Brownian trajectories (ions) in a bounded domain Ω to a binding site is defined as follows. Denote by t_i the arrival times and by τ^1 the shortest one,

$$\tau^1 = \min(t_1, \dots, t_N), \quad (9.1)$$

where t_i are the i.i.d. arrival times of the N ions in the medium. The NEP is to find the PDF and the MFPT of τ^1 . The complementary PDF of τ^1 is given by

$$\Pr\{\tau^1 > t\} = \Pr^N\{t_1 > t\}, \quad (9.2)$$

where $\Pr\{t_1 > t\}$ is the survival probability of a single particle prior to binding at the target. This probability can be computed from the following boundary value problem. Assuming that the boundary $\partial\Omega$ contains N_R binding sites $\partial\Omega_i \subset \partial\Omega$ ($\partial\Omega_a = \bigcup_{i=1}^{N_R} \partial\Omega_i$, $\partial\Omega_r = \partial\Omega - \partial\Omega_a$), the pdf of a Brownian trajectory is the solution of the initial boundary value problem (IBVP)

$$\begin{aligned} \frac{\partial p(\mathbf{x}, t)}{\partial t} &= D\Delta p(\mathbf{x}, t) \quad \text{for } \mathbf{x} \in \Omega, t > 0 \\ p(\mathbf{x}, 0) &= p_0(\mathbf{x}) \quad \text{for } \mathbf{x} \in \Omega \\ \frac{\partial p(\mathbf{x}, t)}{\partial \mathbf{n}} &= 0 \quad \text{for } \mathbf{x} \in \partial\Omega_r \\ p(\mathbf{x}, t) &= 0 \quad \text{for } \mathbf{x} \in \partial\Omega_a. \end{aligned} \quad (9.3)$$

The survival probability is

$$\Pr\{t_1 > t\} = \int_{\Omega} p(\mathbf{x}, t) d\mathbf{x}, \quad (9.4)$$

so that

$$\Pr\{\tau^1 = t\} = \frac{d}{dt} \Pr\{\tau^1 < t\} = N(\Pr\{t_1 > t\})^{N-1} \Pr\{t_1 = t\}, \quad (9.5)$$

where

$$\Pr\{t_1 = t\} = \oint_{\partial\Omega_a} \frac{\partial p(\mathbf{x}, t)}{\partial \mathbf{n}} dS_x, \quad (9.6)$$

$$\Pr\{t_1 = t\} = N_R \oint_{\partial\Omega_1} \frac{\partial p(\mathbf{x}, t)}{\partial \mathbf{n}} dS_x. \quad (9.7)$$

Putting all the above together results in the pdf

$$\Pr\{\tau^1 = t\} = NN_R \left[\int_{\Omega} p(\mathbf{x}, t) d\mathbf{x} \right]^{N-1} \oint_{\partial\Omega_1} \frac{\partial p(\mathbf{x}, t)}{\partial \mathbf{n}} dS_{\mathbf{x}}. \quad (9.8)$$

The first arrival time is computed from the survival probability of a particle and the flux through the target. Obtaining an explicit or asymptotic expression is not possible in general.

9.1.2 The pdf of the First Arrival Time in an Interval

To obtain an analytic expression for the pdf of the first arrival time (9.8) of a particle inside a narrow neck, we model it as a segment of length L , with a reflecting boundary at $x = 0$ and absorbing boundary at $x = L$. Then the diffusion boundary value problem (9.3) becomes

$$\frac{\partial p}{\partial t} = D \frac{\partial^2 p}{\partial x^2} \quad \text{for } 0 < x < L, t > 0 \quad (9.9)$$

$$p(x, 0) = \delta(x) \quad \text{for } 0 < x < L \quad (9.10)$$

$$p(L, t) = \frac{\partial p(0, t)}{\partial x} = 0 \quad \text{for } t > 0, \quad (9.11)$$

where the initial condition corresponds to a particle initially at the origin. The general solution is given by the eigenfunction expansion

$$p(x, t) = 2 \sum_{n=0}^{\infty} e^{-D\lambda_n^2 t} \cos \lambda_n x, \quad (9.12)$$

where the eigenvalues are

$$\lambda_n = \frac{\pi}{L} \left(n + \frac{1}{2} \right). \quad (9.13)$$

The survival probability (9.4) of a particle is thus given by

$$\Pr\{t_1 > t\} = \int_0^L p(x, t) dx = 2 \sum_{n=0}^{\infty} \frac{(-1)^n}{\lambda_n} e^{-D\lambda_n^2 t}. \quad (9.14)$$

The pdf of the arrival time to L of a single Brownian trajectory is the probability efflux at the absorbing boundary $\partial\Omega_a$, given by

$$-\oint_{\Omega_a} \frac{\partial p(\mathbf{x}, t)}{\partial \mathbf{n}} dS_{\mathbf{x}} = -\frac{\partial p(L, t)}{\partial x} = 2 \sum_{n=0}^{\infty} (-1)^n \lambda_n e^{-D\lambda_n^2 t}. \quad (9.15)$$

Therefore, the pdf of the first arrival time in an ensemble of N particles to one of N_R independent absorbers is given by

$$\Pr\{\tau^{(1)} = t\} = 2NN_R \left(2 \sum_{n=0}^{\infty} \frac{(-1)^n}{\lambda_n} e^{-D\lambda_n^2 t} \right)^{N-1} \sum_{n=0}^{\infty} (-1)^n \lambda_n e^{-D\lambda_n^2 t}. \quad (9.16)$$

For numerical purposes, we approximate (9.16) by the sum of n_0 terms,

$$\Pr\{\tau^{(1)} = t\} \approx f_{n_0}(t) = NN_R \left(\sum_{n=0}^{n_0} \frac{(-1)^n}{\lambda_n} e^{-D\lambda_n^2 t} \right)^{N-1} \sum_{n=0}^{n_0} (-1)^n \lambda_n e^{-D\lambda_n^2 t}. \quad (9.17)$$

Figure 9.1a, b show the pdf of the first arrival time for $N = 5$ and $N = 500$ Brownian particles with diffusion coefficient $D = 1$, which start at $x = 0$ at time 0 and exit the interval at $x = 1$. These figures confirm the validity of the analytical approximation (9.16) with only $n_0 = 100$ terms in the slowly converging alternating series.

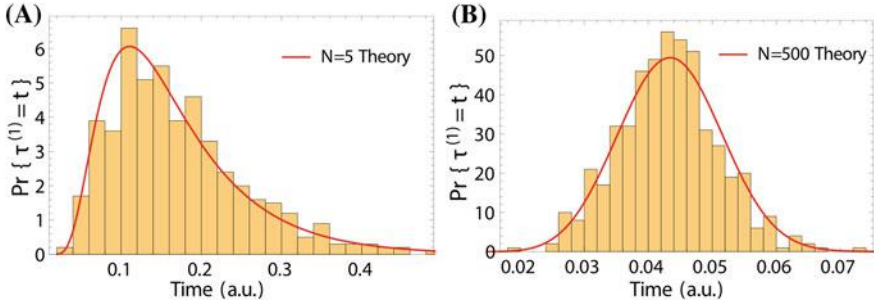


Fig. 9.1 Histograms of the arrival times to the boundary of the fastest particle, obtained from Brownian simulations with Euler's scheme. The number of Brownian particles is $N = 5$ in A and $N = 500$ in B. The analytical solution (red curves) is obtained by setting $n_0 = 100$ in (9.17)

9.1.3 Asymptotics of the Expected Shortest Time $\bar{\tau}^1$

The MFPT of the first among N i.i.d. Brownian paths is given by

$$\bar{\tau}^1 = \int_0^\infty \Pr\{\tau^1 > t\} dt = \int_0^\infty [\Pr\{t_1 > t\}]^N dt, \quad (9.18)$$

where t_1 is the arrival time of a single Brownian path. Writing the last integral in (9.18) as

$$\bar{\tau}^1 = \int_0^\infty e^{N \ln g(t)} dt, \quad (9.19)$$

it can be expanded for $N \gg 1$ by Laplace's method. Here

$$g(t) = \sum_{n=0}^{\infty} \frac{(-1)^n}{\lambda_n} e^{-D\lambda_n^2 t} \quad (9.20)$$

(see (9.14)).

9.1.4 Escape from a Ray

Consider the case $L = \infty$ and the IBVP

$$\begin{aligned} \frac{\partial p(x, t)}{\partial t} &= D \frac{\partial^2 p(x, t)}{\partial x^2} \quad \text{for } x > 0, t > 0 \\ p(x, 0) &= \delta(x - a) \quad \text{for } x > 0, \quad p(0, t) = 0 \quad \text{for } t > 0, \end{aligned} \quad (9.21)$$

whose solution is

$$p(x, t) = \frac{1}{\sqrt{4Dt}} \left[\exp \left\{ -\frac{(x-a)^2}{4Dt} \right\} - \exp \left\{ -\frac{(x+a)^2}{4Dt} \right\} \right]. \quad (9.22)$$

The survival probability with $D = 1$ is

$$\Pr\{t_1 > t\} = \int_0^\infty p(x, t) dx = 1 - \frac{2}{\sqrt{\pi}} \int_{a/\sqrt{4t}}^\infty e^{-u^2} du. \quad (9.23)$$

To compute the MFPT in (9.18), we use the expansion of the complementary error function

$$\frac{2}{\sqrt{\pi}} \int_x^\infty e^{-u^2} du = \frac{e^{-x^2}}{x\sqrt{\pi}} \left(1 - \frac{1}{2x^2} + O(x^{-4}) \right) \quad \text{for } x \gg 1, \quad (9.24)$$

which gives

$$I_N \equiv \int_0^\infty [\Pr\{t_1 > t\}]^N dt \approx \int_0^\infty \exp \left\{ N \ln \left(1 - \frac{e^{-(a/\sqrt{4t})^2}}{(a/\sqrt{4t})\sqrt{\pi}} \right) \right\} dt, \quad (9.25)$$

and with the approximation

$$I_N \approx \int_0^\infty \exp \left\{ -N \frac{\sqrt{4t} e^{-\frac{a^2}{4t}}}{a\sqrt{\pi}} \right\} dt = \frac{a^2}{4} \int_0^\infty \exp \left\{ -N \frac{\sqrt{u} e^{-\frac{1}{u}}}{\sqrt{\pi}} \right\} du. \quad (9.26)$$

To evaluate the integral (9.26), we make the monotone change of variable

$$w = w(t) = \sqrt{t} e^{-1/t}, \quad w'(t) = \sqrt{t} e^{-\frac{1}{t}} \left(\frac{1}{2t} + \frac{1}{t^2} \right). \quad (9.27)$$

Note that for small t ,

$$w'(t) \approx w \frac{1}{t^2} \quad (9.28)$$

and $\ln w \approx -1/t$. Thus,

$$w'(t) \approx w(\ln w)^2. \quad (9.29)$$

Breaking with $N' = \frac{N}{\sqrt{\pi}}$

$$\begin{aligned} I_N &\approx \frac{a^2}{4} \int_0^\infty \exp\{-N'w\} \frac{1}{\frac{dw}{dt}} dw \\ &\approx \frac{a^2}{4} \left(\int_0^\delta \exp\{-N'w\} \frac{a^2}{w(\ln(w))^2} dw + \int_\delta^\infty \exp\{-N'w\} \frac{1}{\frac{dw}{dt}} dw \right) \end{aligned}$$

for some $0 < \delta < 1$, the second integral turns out to be exponentially small in N and is thus negligible relative to the first one. Integrating by parts,

$$\begin{aligned} I_N &\approx \frac{a^2}{4} \int_0^\delta \exp\{-N'w\} \frac{1}{w(\ln(w))^2} dw \\ &\approx O(\exp(-aN)) + \frac{a^2}{4} N' \int_0^\delta \exp\{-N'w\} \frac{1}{\ln|w|} dw \end{aligned}$$

and changing the variable to $u = N'w$, we obtain

$$N' \int_0^\delta \exp\{-N'w\} \frac{a^2}{4 \ln |w|} dw = \int_0^{N'\delta} \frac{a^2 \exp\{-u\}}{4 |\ln u/N'|} du.$$

Expanding

$$\frac{1}{|\ln u/N'|} = \frac{1}{\ln N'} \left(1 + \frac{|\ln u|}{\ln N'} + O\left(\frac{|\ln u|}{\ln N'}\right)^2 \right)$$

for $u > \varepsilon > 0$, we obtain,

$$N' \int_0^\delta \exp\{-N'w\} \frac{a^2}{4 \ln w} dw \approx \int_0^{N'\delta} \exp\{-u\} \frac{a^2}{4 |\ln N'|} \left(1 + \frac{|\ln u|}{\ln N'} \right) du.$$

Thus, breaking the integral into two parts, from $[0, \varepsilon]$ (which is negligible) and $[\varepsilon, \infty[$, we get

$$\bar{\tau}^1 \approx \frac{a^2}{4D \ln \frac{N}{\sqrt{\pi}}} \quad \text{for } N \gg 1. \quad (9.30)$$

9.2 Escape from an Interval $[0, a]$

We follow the steps of the previous section, where Green's function for the homogeneous IBVP is now given by the infinite sum

$$p(x, t | y) = \frac{1}{\sqrt{4D\pi t}} \sum_{n=-\infty}^{\infty} \left[\exp \left\{ -\frac{(x-y+2na)^2}{4t} \right\} - \exp \left\{ -\frac{(x+y+2na)^2}{4t} \right\} \right]. \quad (9.31)$$

The conditional survival probability is

$$\begin{aligned} \Pr\{t_1 > t | y\} &= \int_0^a p(x, t | y) dx \\ &= \frac{1}{\sqrt{4D\pi t}} \sum_{n=-\infty}^{\infty} \int_0^a \left[\exp \left\{ -\frac{(x-y+2na)^2}{4t} \right\} - \exp \left\{ -\frac{(x+y+2na)^2}{4t} \right\} \right] dx \\ &= \int_0^a \frac{1}{\sqrt{4D\pi t}} \left[\exp \left\{ -\frac{(x-y)^2}{4t} \right\} - \exp \left\{ -\frac{(x+y)^2}{4t} \right\} \right] dx + S_1(y, t) - S_2(y, t), \end{aligned} \quad (9.32)$$

where

$$\begin{aligned} S_1 &= \frac{1}{\sqrt{4D\pi t}} \sum_{n=1}^{\infty} \int_0^a \left[\exp \left\{ -\frac{(x+y+2na)^2}{4t} \right\} - \exp \left\{ -\frac{(x-y+2na)^2}{4t} \right\} \right] dx \\ S_2 &= \frac{1}{\sqrt{4D\pi t}} \sum_{n=1}^{\infty} \int_0^a \left[\exp \left\{ -\frac{(x+y-2na)^2}{4t} \right\} - \exp \left\{ -\frac{(x-y-2na)^2}{4t} \right\} \right] dx. \end{aligned}$$

Note that the integrand in the third line of (29), denoted $p_1(x, t | y)$, satisfies the initial condition $p_1(x, 0 | y) = \delta(x - y)$ and the boundary condition $p_1(0, t | y) = p_1(x, t | 0) = 0$, but $p_1(a, t | y) \neq 0$ and $p_1(x, t | a) \neq 0$. However, with the first correction,

$$\begin{aligned} p_2(x, t | y) &= \frac{1}{\sqrt{4D\pi t}} \left[\exp \left\{ -\frac{(x-y)^2}{4t} \right\} - \exp \left\{ -\frac{(x+y)^2}{4t} \right\} \right. \\ &\quad + \exp \left\{ -\frac{(x-y-2a)^2}{4t} \right\} - \exp \left\{ -\frac{(x+y-2a)^2}{4t} \right\} \\ &\quad \left. + \exp \left\{ -\frac{(x-y+2a)^2}{4t} \right\} - \exp \left\{ -\frac{(x+y+2a)^2}{4t} \right\} \right] \end{aligned} \quad (9.33)$$

it satisfies the same initial condition for x and y in the interval, and the boundary conditions

$$\begin{aligned} p_2(x, t | 0) &= \frac{1}{\sqrt{4D\pi t}} \left[\exp \left\{ -\frac{(x+2a)^2}{4t} \right\} - \exp \left\{ -\frac{(x-2a)^2}{4t} \right\} \right] \\ p_2(x, t | a) &= 0. \end{aligned}$$

Higher-order approximations correct the one boundary condition and corrupt the other, though the error decreases at higher exponential rates. The first line of (9.33) gives the approximation

$$\begin{aligned} \int_0^a \frac{1}{\sqrt{4\pi t}} \left[\exp \left\{ -\frac{(x+y)^2}{4t} \right\} - \exp \left\{ -\frac{(x-y)^2}{4t} \right\} \right] dx &= \frac{1}{\sqrt{\pi}} \int_{(y-a)/2\sqrt{t}}^{y/2\sqrt{t}} e^{-u^2} du \\ &\sim 1 - \max \frac{2\sqrt{t}}{\sqrt{\pi}} \left[\frac{e^{-y^2/4t}}{y}, \frac{e^{-(a-y)^2/4t}}{a-y} \right] \quad \text{as } t \rightarrow 0, \end{aligned} \quad (9.34)$$

where the maximum occurs at $\min[y, a - y]$ for $0 < y < a$ (the shortest ray from y to the boundary). Starting at $x = a/2$, this gives

$$\Pr\{t_1 > t\} = \int_0^a \frac{1}{\sqrt{4\pi t}} \left[\exp\left\{-\frac{(x-a/2)^2}{4t}\right\} - \exp\left\{-\frac{(x+a/2)^2}{4t}\right\} \right] dx \quad \text{as } t \rightarrow 0,$$

so changing $x + a/2 = z\sqrt{4t}$ in the first integral and $x - a/2 = z\sqrt{4t}$ in the second, we get

$$\begin{aligned} \frac{1}{\sqrt{\pi}} \int_{-a/4\sqrt{t}}^{a/4\sqrt{t}} e^{-z^2} dz - \frac{1}{\sqrt{\pi}} \int_{a/4\sqrt{t}}^{3a/4\sqrt{t}} e^{-z^2} dz &\approx 1 - \frac{4\sqrt{t}e^{-a^2/16t}}{a\sqrt{\pi}} - \frac{2\sqrt{t}e^{-a^2/16t}}{a\sqrt{\pi}} - \frac{4\sqrt{t}e^{-9a^2/16t}}{6a\sqrt{\pi}} \\ &= 1 - \frac{6\sqrt{t}e^{-a^2/16t}}{a\sqrt{\pi}} - \frac{2\sqrt{t}e^{-9a^2/16t}}{3a\sqrt{\pi}}. \end{aligned} \quad (9.35)$$

The second integral in the second line of (9.33) is

$$I_{3/2} = - \int_0^a \frac{1}{\sqrt{4\pi t}} \left[\exp\left\{-\frac{(x-3a/2)^2}{4t}\right\} \right] dx. \quad (9.36)$$

Set $x - 3a/2 = -z\sqrt{4t}$, then (9.36) becomes

$$I_{3/2} = -\frac{1}{\sqrt{\pi}} \int_{a/4\sqrt{t}}^{3a/4\sqrt{t}} \exp\{-z^2\} dz = -\frac{1}{\sqrt{\pi}} \int_{a/4\sqrt{t}}^{\infty} \exp\{-z^2\} dz + \frac{1}{\sqrt{\pi}} \int_{3a/4\sqrt{t}}^{\infty} \exp\{-z^2\} dz. \quad (9.37)$$

Thus the second line of (9.33) is

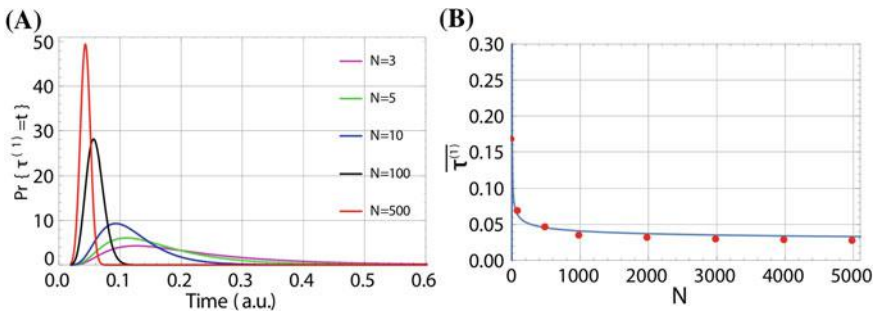


Fig. 9.2 A Plot of $\Pr\{\tau^{(1)} = t\}$ (escape from an interval) for $N = 3, 5, 10, 100$, and 500 with $n_0 = 100$ terms in the series of (9.17). B Decay of the expected arrival time of the fastest particle vs N (red points). The plot of the asymptotic formula (9.41) is (blue) with parameter $\frac{0.282}{\log N}$

$$\begin{aligned}
& - \int_0^a \frac{1}{\sqrt{4\pi t}} \left[\exp \left\{ -\frac{(x - 3a/2)^2}{4t} \right\} - \exp \left\{ -\frac{(x - 5a/2)^2}{4t} \right\} \right] dx \\
& \approx - \frac{2\sqrt{t}}{a\sqrt{\pi}} e^{-a^2/16t} + \frac{2\sqrt{t}}{5a\sqrt{\pi}} e^{-25a^2/16t}, \tag{9.38}
\end{aligned}$$

and in the third line of (9.33), we get

$$\begin{aligned}
& \int_0^a \frac{1}{\sqrt{4\pi t}} \left[\exp \left\{ -\frac{(x + 3a/2)^2}{4t} \right\} - \exp \left\{ -\frac{(x + 5a/2)^2}{4t} \right\} \right] dx \\
& \approx \frac{2\sqrt{t}}{3a\sqrt{\pi}} e^{-9a^2/16t} - \frac{2\sqrt{t}}{5a\sqrt{\pi}} e^{-49a^2/16t}, \tag{9.39}
\end{aligned}$$

hence

$$\int_0^\infty [\Pr\{t_1 > t\}]^N dt \approx \int_0^\infty \exp \left\{ N \ln \left(1 - \frac{8\sqrt{t}}{a\sqrt{\pi}} e^{-a^2/16t} \right) \right\} dt \tag{9.40}$$

and the expected time of the fastest particle that starts at the center of the interval is (9.30) with a replaced by $a/2$ and N replaced by $2N$. That is,

$$\bar{\tau}^1 \approx \frac{a^2}{16D \ln \frac{2N}{\sqrt{\pi}}} \quad \text{for } N \gg 1. \tag{9.41}$$

Figure 9.2a shows a plot of the pdf analytical approximation of shortest arrival time (9.17) with $n_0 = 100$ terms, $D = 1$ and $L = 1$ for $N = 4, 6$, and 10 . As the number of particles increases, the mean first arrival time decreases (Fig. 9.2b) and according to Eq. (9.41), the asymptotic behavior is given by $C/\log N$, where C is a constant. We show below the pdf of the fastest Brownian particle.

9.3 The FAT in a Bounded Domain in $\mathbb{R}^{2,3}$

To generalize the previous result to the case of N i.i.d. Brownian particles in a bounded domain $\Omega \subset \mathbb{R}^{2,3}$, we assume that the particles are initially injected at a point $y \in \Omega$ and they can escape through a single small absorbing window $\partial\Omega_a$ in the boundary $\partial\Omega$ of the domain. The pdf of the first passage time to $\partial\Omega_a$ is given by (9.8).

9.3.1 Asymptotics in \mathbb{R}^3

To determine the short-time asymptotics of the pdf, we use the Laplace transform of the IBVP (9.3) and solve the resulting elliptic mixed Neumann–Dirichlet BVP. The Dirichlet part of the boundary consists of N well-separated small absorbing windows, $\partial\Omega_a = \bigcup_{j=1}^N \partial\Omega_j$, and the reflecting (Neumann) part is $\partial\Omega_r = \partial\Omega - \partial\Omega_a$, so that the IBVP (9.3) has the form

$$\begin{aligned}\frac{\partial p(\mathbf{x}, t | \mathbf{y})}{\partial t} &= D \Delta p(\mathbf{x}, t | \mathbf{y}) & (9.42) \\ p(\mathbf{x}, 0 | \mathbf{y}) &= \delta(\mathbf{x} - \mathbf{y}) \quad \text{for } \mathbf{x}, \mathbf{y} \in \Omega \\ \frac{\partial p(\mathbf{x}, t | \mathbf{y})}{\partial \mathbf{n}} &= 0 \quad \text{for } \mathbf{x} \in \partial\Omega_r \\ p(\mathbf{x}, t | \mathbf{y}) &= 0 \quad \text{for } t > 0, \mathbf{x} \in \partial\Omega_a.\end{aligned}$$

We consider first the case $N = 1$. The Laplace transform of (9.3),

$$\hat{p}(\mathbf{x}, q | \mathbf{y}) = \int_0^\infty p(\mathbf{x}, t | \mathbf{y}) e^{-pt} dt, \quad (9.43)$$

gives the BVP

$$\begin{aligned}-\delta(\mathbf{x} - \mathbf{y}) + q \hat{p}(\mathbf{x}, q | \mathbf{y}) &= D \Delta \hat{p}(\mathbf{x}, q | \mathbf{y}) \quad \text{for } \mathbf{x}, \mathbf{y} \in \Omega \\ \frac{\partial \hat{p}(\mathbf{x}, q | \mathbf{y})}{\partial \mathbf{n}} &= 0 \quad \text{for } \mathbf{x} \in \partial\Omega_r \\ \hat{p}(\mathbf{x}, q | \mathbf{y}) &= 0 \quad \text{for } \mathbf{x} \in \partial\Omega_a.\end{aligned}$$

Green's function for the Neumann problem in Ω is the solution of

$$\begin{aligned}-\Delta_x \hat{G}(\mathbf{x}, q | \mathbf{y}) + q \hat{G}(\mathbf{x}, q | \mathbf{y}) &= \delta(\mathbf{x} - \mathbf{y}) \quad \text{for } \mathbf{x}, \mathbf{y} \in \Omega, & (9.44) \\ \frac{\partial \hat{G}_q(\mathbf{x}, q | \mathbf{y})}{\partial n_x} &= 0 \quad \text{for } \mathbf{x}, \mathbf{y} \in \partial\Omega.\end{aligned}$$

The asymptotic solution of (9.44) in \mathbb{R}^3 is given by

$$\hat{G}(\mathbf{x}, q | \mathbf{y}) = \frac{e^{-\sqrt{q}|\mathbf{x} - \mathbf{y}|}}{4\pi||\mathbf{x} - \mathbf{y}||} + R_q(\mathbf{x}, \mathbf{y}), \quad (9.45)$$

where $R_q(\mathbf{x}, \mathbf{y})$ is more regular than the first term. When \mathbf{x} (or \mathbf{y}) is on the boundary,

$$\hat{G}(\mathbf{x}, q | \mathbf{y}) = e^{-\sqrt{q}|\mathbf{x}-\mathbf{y}|} \left(\frac{1}{2\pi||\mathbf{x}-\mathbf{y}||} + \frac{H(\mathbf{x})}{2\pi} \log |\mathbf{x}-\mathbf{y}| + R(\mathbf{x}, \mathbf{y}) \right), \quad (9.46)$$

where $R(\mathbf{x}, \mathbf{y})$ is more regular than the logarithmic term and $H(\mathbf{x})$ is a geometric factor [Singer et al. I (2006), Singer et al. III (2006a)]. Using Green's identity, we obtain that

$$\begin{aligned} & \int_{\Omega} \left[\hat{p}(\mathbf{x}, q | \mathbf{y}) \Delta_{\mathbf{x}} \hat{G}(\mathbf{x}, q | \mathbf{y}) - \Delta_{\mathbf{x}} \hat{p}(\mathbf{x}, q | \mathbf{y}) \hat{G}(\mathbf{x}, q | \mathbf{y}) \right] d\mathbf{y} \\ &= \int_{\partial\Omega} \left[\hat{p}(\mathbf{x}, q | \mathbf{y}) \frac{\partial \hat{G}(\mathbf{x}, q | \mathbf{y})}{\partial n_{\mathbf{x}}} - \frac{\partial \hat{p}(\mathbf{x}, q | \mathbf{y})}{\partial n_{\mathbf{x}}} \hat{G}(\mathbf{x}, q | \mathbf{y}) \right] dS_y, \end{aligned}$$

hence

$$\hat{p}(\mathbf{x}, q | \mathbf{y}) = \hat{G}(\mathbf{x}, q | \mathbf{y}) - \int_{\partial\Omega_a} \frac{\partial \hat{p}(\mathbf{x}, q | \mathbf{y}')}{\partial n_{\mathbf{x}}} \hat{G}(\mathbf{x}, q | \mathbf{y}') dS_{y'}. \quad (9.47)$$

If the absorbing window $\partial\Omega_a$ is centered at $\mathbf{x} = \mathbf{a}$, then, for $\mathbf{x} \in \partial\Omega_a$,

$$0 = \hat{G}(\mathbf{a}, q | \mathbf{y}) - \int_{\partial\Omega_a} \frac{\partial \hat{p}(\mathbf{a}, q | \mathbf{y}')}{\partial n_{\mathbf{x}}} \hat{G}(\mathbf{a}, q | \mathbf{y}') dS_{y'}. \quad (9.48)$$

This is a Helmholtz equation and the solution is given by [Singer et al. I (2006), Singer et al. III (2006a)]

$$\hat{p}(\mathbf{a}, q | \mathbf{y}) = \frac{C}{\sqrt{a^2 - r^2}}, \quad (9.49)$$

where $r = |\mathbf{a} - \mathbf{y}|$. Thus, C is computed from

$$0 = G_q(\mathbf{a}, \mathbf{y}) - \int_{\partial\Omega_a} \frac{\partial \hat{p}(\mathbf{a}, q, \mathbf{y} | \mathbf{y}')}{\partial n_{\mathbf{x}}} G_q(\mathbf{a}, \mathbf{y}') dS_y \quad (9.50)$$

and to leading order,

$$G_q(\mathbf{a}, \mathbf{y}) = \int_{\partial\Omega_a} \frac{Ce^{-\sqrt{q}|\mathbf{y}-\mathbf{a}|}}{\sqrt{a^2 - r^2}} \left(\frac{1}{2\pi||\mathbf{y}-\mathbf{a}||} + \frac{H(\mathbf{x})}{2\pi} \log |\mathbf{y}-\mathbf{a}| + R(\mathbf{y}, \mathbf{a}) \right) dS_y.$$

If $\partial\Omega_a$ is a disk of radius a , then

$$G_q(\mathbf{a}, \mathbf{y}) \approx C \int_{\partial\Omega_a} \frac{e^{-\sqrt{q}r}}{\sqrt{a^2 - r^2}} \frac{1}{2\pi r} 2\pi r dr = \frac{\pi}{2} [I_0(\sqrt{q}a) - L_0(\sqrt{q}a)] C, \quad (9.51)$$

where I_0 is the modified Bessel function of the first kind and L_0 is the Struve function. Thus,

$$\hat{p}(\mathbf{x}, q | \mathbf{y}) = G_q(\mathbf{x}, \mathbf{y}) - G_q(\mathbf{a}, \mathbf{y}) \frac{2}{\pi [I_0(\sqrt{q}a) - L_0(\sqrt{q}a)]} \int_{\partial\Omega_a} \frac{G_q(\mathbf{x}, \mathbf{y}) dS_y}{\sqrt{a^2 - r^2}}.$$

For $|\mathbf{a} - \mathbf{x}| \gg a$ and $q \gg 1$, we have $I_0(\sqrt{q}a) - L_0(\sqrt{q}a) \approx \frac{2}{\pi\sqrt{q}a}$

$$\hat{p}(\mathbf{x}, q | \mathbf{y}) \approx G_q(\mathbf{x}, \mathbf{y}) - G_q(\mathbf{a}, \mathbf{y}) G_q(\mathbf{a}, \mathbf{x}) \frac{2}{\pi [I_0(\sqrt{q}a) - L_0(\sqrt{q}a)]} \int_{\partial\Omega_a} \frac{dS_y}{\sqrt{a^2 - r^2}},$$

hence, for a small circular window of radius a

$$\hat{p}(\mathbf{x}, q | \mathbf{y}) \approx G_q(\mathbf{x}, \mathbf{y}) - 2\pi\sqrt{q}a^2 G_q(\mathbf{a}, \mathbf{y}) G_q(\mathbf{a}, \mathbf{x}) + o(a^2) \quad \text{for } a \ll 1. \quad (9.52)$$

For small t and $\mathbf{x}, \mathbf{y} \in \Omega$, we obtain the leading order approximation in Eq. 9.45,

$$\mathcal{L}^{-1}[G_q(\mathbf{x}, \mathbf{y})] \approx \frac{1}{(4\pi t)^{3/2}} e^{-\frac{|\mathbf{x} - \mathbf{y}|^2}{4t}}. \quad (9.53)$$

The inverse Laplace transform [Abramowitz and Stegun (1972), p. 1026; 29.3.87] gives

$$\mathcal{L}^{-1}\left(\sqrt{q} \frac{e^{-\sqrt{q}|\mathbf{x}-\mathbf{y}|}}{|\mathbf{x}-\mathbf{y}|}\right) = \frac{1}{4\sqrt{\pi t^3}} e^{-\frac{|\mathbf{x}-\mathbf{y}|^2}{4t}} H_2\left(\frac{|\mathbf{x}-\mathbf{y}|}{2\sqrt{t}}\right), \quad (9.54)$$

where $H_2(x) = 4x^2 - 2$ is the Hermite polynomial of degree 2. For the Dirichlet boundary and $\mathbf{a} \in \partial\Omega$, the image charge adds a factor of 1/2 to yield

$$G_q(\mathbf{a}, \mathbf{y}) G_q(\mathbf{a}, \mathbf{x}) 2\pi\sqrt{q}a^2 = \sqrt{q}a^2 \frac{e^{-\sqrt{q}(|\mathbf{a}-\mathbf{y}| + |\mathbf{a}-\mathbf{x}|)}}{2\pi|\mathbf{a}-\mathbf{y}||\mathbf{a}-\mathbf{x}|} \quad (9.55)$$

and

$$\mathcal{L}^{-1} [G_q(\mathbf{a}, \mathbf{y}) G_q(\mathbf{a}, \mathbf{x}) \sqrt{q} a^2] = \frac{a^2}{(4\pi t)^3} e^{-\frac{(|\mathbf{a}-\mathbf{y}|+|\mathbf{a}-\mathbf{x}|)^2}{4t}} \frac{1}{|\mathbf{a}-\mathbf{y}||\mathbf{a}-\mathbf{x}|} \times H_2\left(\frac{|\mathbf{a}-\mathbf{y}|+|\mathbf{a}-\mathbf{x}|}{2\sqrt{t}}\right).$$

Finally,

$$\mathcal{L}^{-1}(\hat{p}(\mathbf{x}, q | \mathbf{y})) = \frac{1}{\sqrt{(4\pi t)^3}} \left[e^{-\frac{|\mathbf{x}-\mathbf{y}|^2}{4t}} - \frac{a^2}{|\mathbf{a}-\mathbf{y}||\mathbf{a}-\mathbf{x}|} \right. \\ \left. \times e^{-\frac{(|\mathbf{a}-\mathbf{y}|+|\mathbf{a}-\mathbf{x}|)^2}{4t}} H_2\left(\frac{|\mathbf{a}-\mathbf{y}|+|\mathbf{a}-\mathbf{x}|}{2\sqrt{t}}\right) \right].$$

Setting $\delta = |\mathbf{a} - \mathbf{y}|$, we write the short-time asymptotics of the survival probability as

$$S(t) \approx \int_{\Omega} p_t(\mathbf{x}, \mathbf{y}) d\mathbf{x} \\ = \frac{1}{\sqrt{(4\pi t)^3}} \int_{\Omega} \left[e^{-\frac{|\mathbf{x}-\mathbf{y}|^2}{4t}} - \frac{a^2}{|\mathbf{a}-\mathbf{y}||\mathbf{a}-\mathbf{x}|} \right. \\ \left. \times e^{-\frac{(|\mathbf{a}-\mathbf{y}|+|\mathbf{a}-\mathbf{x}|)^2}{4t}} H_2\left(\frac{|\mathbf{a}-\mathbf{y}|+|\mathbf{a}-\mathbf{x}|}{2\sqrt{t}}\right) \right] d\mathbf{x} \\ = I_1(t) - I_2(t) - I_3(t) - I_4(t),$$

where for

$$H_2\left(\frac{|\mathbf{a}-\mathbf{y}|+|\mathbf{a}-\mathbf{x}|}{2\sqrt{t}}\right) \approx \frac{(|\mathbf{a}-\mathbf{y}|+|\mathbf{a}-\mathbf{x}|)^2}{t} \quad \text{for small } t, \quad (9.56)$$

and

$$I_1(t) = \frac{1}{\sqrt{(4\pi t)^3}} \int_{\Omega} e^{-\frac{|\mathbf{x}-\mathbf{y}|^2}{4t}} d\mathbf{x} \quad (9.57)$$

$$I_2(t) = \frac{1}{\sqrt{(4\pi t)^3}} \frac{a^2 \delta}{t} \int_{\Omega} \frac{1}{|\mathbf{a} - \mathbf{x}|} e^{-\frac{(\delta + |\mathbf{a} - \mathbf{x}|)^2}{4t}} d\mathbf{x} \quad (9.58)$$

$$I_3(t) = \frac{1}{\sqrt{(4\pi t)^3}} \frac{2a^2}{t} \int_{\Omega} e^{-\frac{(\delta + |\mathbf{a} - \mathbf{x}|)^2}{4t}} d\mathbf{x} \quad (9.59)$$

$$I_4(t) = \frac{1}{\sqrt{(4\pi t)^3}} \frac{a^2}{\delta t} \int_{\Omega} |\mathbf{a} - \mathbf{x}| e^{-\frac{(\delta + |\mathbf{a} - \mathbf{x}|)^2}{4t}} d\mathbf{x}. \quad (9.60)$$

Each integral is evaluated in the short-time approximation.

$$\begin{aligned} I_1(t) &= \frac{1}{\sqrt{(4\pi t)^3}} \int_{\Omega} e^{-\frac{|\mathbf{x} - \mathbf{y}|^2}{4t}} d\mathbf{x} \approx 1 - \frac{2}{\sqrt{\pi}} \int_{R_a/\sqrt{4t}}^{\infty} e^{-u^2} du \\ &\approx 1 - \sqrt{4t} \frac{e^{-(R_a/\sqrt{4t})^2}}{R_a \sqrt{\pi}} \left[1 + O\left(\left(\frac{R_a}{\sqrt{4t}}\right)^2\right) \right], \end{aligned} \quad (9.61)$$

where R_a is the radius of the maximal ball inscribed in Ω . The integral I_2 is evaluated by the change of variables $\mathbf{z} = \mathbf{x} - \mathbf{a}$ and then $\eta = (\delta + r)/\sqrt{4t}$, where $r = |\mathbf{z}|$ (recall that $\mathbf{a} \in \Omega_a$),

$$\begin{aligned} I_2(t) &= \frac{1}{\sqrt{(4\pi t)^3}} \frac{a^2 \delta}{t} \int_{\Omega} \frac{1}{|\mathbf{a} - \mathbf{x}|} e^{-\frac{(\delta + |\mathbf{a} - \mathbf{x}|)^2}{4t}} d\mathbf{x} \\ &= \frac{1}{\sqrt{(4\pi t)^3}} \frac{a^2 \delta}{t} \int_{\Omega + \mathbf{a}} \frac{1}{|\mathbf{z}|} e^{-\frac{(\delta + |\mathbf{z}|)^2}{4t}} 2\pi |\mathbf{z}|^2 d|\mathbf{z}| \\ &\approx \frac{2\pi}{\sqrt{(4\pi t)^3}} \frac{a^2 \delta}{t} \int_{\frac{\delta}{\sqrt{4t}}}^{\frac{\delta+R}{\sqrt{4t}}} e^{-\eta^2} (\sqrt{4t}\eta - \delta) \sqrt{4t} d\eta, \end{aligned}$$

where R is the radius of the largest half-ball centered at $\mathbf{a} \in \Omega_a$ and inscribed in Ω . For short time,

$$\int_{\frac{\delta}{\sqrt{4t}}}^{\frac{\delta+R}{\sqrt{4t}}} e^{-\eta^2} d\eta \approx \frac{1}{2} \left\{ \frac{\sqrt{4t}}{\delta} e^{-\left(\frac{\delta}{\sqrt{4t}}\right)^2} \right\} \left(1 - \frac{4t}{2\delta^2} + 12 \frac{t^2}{\delta^4} \right) \quad (9.62)$$

$$\int_{\frac{\delta}{\sqrt{4t}}}^{\frac{\delta+R}{\sqrt{4t}}} \eta e^{-\eta^2} d\eta = \frac{1}{2} \left\{ e^{-\left(\frac{\delta}{\sqrt{4t}}\right)^2} - e^{-\left(\frac{\delta+R}{\sqrt{4t}}\right)^2} \right\} \approx \frac{1}{2} e^{-\left(\frac{\delta}{\sqrt{4t}}\right)^2}.$$

Therefore,

$$\begin{aligned} I_2(t) &\approx \frac{1}{\sqrt{(4\pi t)^3}} \frac{2\pi a^2 \delta}{t} \left\{ 2te^{-\left(\frac{\delta}{\sqrt{4t}}\right)^2} \right. \\ &\quad \left. - \delta\sqrt{4t} \frac{1}{2} \left[\frac{\sqrt{4t}}{\delta} e^{-\left(\frac{\delta}{\sqrt{4t}}\right)^2} \right] \left(1 - \frac{4t}{2\delta^2} + 12\frac{t^2}{\delta^4} \right) \right\} \\ &\approx \frac{4a^2}{\delta\sqrt{\pi}} \frac{1}{\sqrt{t}} \left(1 - \frac{6t}{\delta^2} \right) e^{-\left(\frac{\delta}{\sqrt{4t}}\right)^2}. \end{aligned} \tag{9.63}$$

Now,

$$\begin{aligned} I_3(t) &= \frac{1}{\sqrt{(4\pi t)^3}} \frac{2a^2}{t} \int_{\Omega} e^{-\frac{(\delta + |\mathbf{a} - \mathbf{x}|)^2}{4t}} d\mathbf{x} \\ &= \frac{2\pi}{\sqrt{(4\pi t)^3}} \frac{2a^2}{t} \int_{\frac{\delta}{\sqrt{4t}}}^{\frac{\delta+R}{\sqrt{4t}}} e^{-\eta^2} (\sqrt{4t}\eta - \delta)^2 \sqrt{4t} d\eta \\ &= \frac{2\pi}{\sqrt{(4\pi t)^3}} \frac{2a^2}{t} \int_{\frac{\delta}{\sqrt{4t}}}^{\frac{\delta+R}{\sqrt{4t}}} e^{-\eta^2} (4t\eta^2 - 2\sqrt{4t}\eta\delta + \delta^2) \sqrt{4t} d\eta, \end{aligned}$$

that we write as $I_3(t) = I_3^{(1)}(t) + I_3^{(2)}(t) + I_3^{(3)}(t)$. The approximation

$$\int_{\frac{\delta}{\sqrt{4t}}}^{\frac{\delta+R}{\sqrt{4t}}} e^{-\eta^2} \eta^2 d\eta \approx \frac{\delta}{2\sqrt{4t}} e^{-\left(\frac{\delta}{\sqrt{4t}}\right)^2} + \frac{1}{4} \frac{\sqrt{4t}}{\delta} e^{-\left(\frac{\delta}{\sqrt{4t}}\right)^2} \left(1 - \frac{4t}{2\delta^2} + o(t) \right),$$

gives

$$\begin{aligned}
I_3^{(1)}(t) &= \frac{2\pi\delta}{\pi^{3/2}} \frac{a^2}{t\sqrt{4t}} e^{-\left(\frac{\delta}{\sqrt{4t}}\right)^2} + \frac{2a^2}{2t\pi^{3/2}} \frac{1}{\delta^2} \sqrt{4t} e^{-\left(\frac{\delta}{\sqrt{4t}}\right)^2} \left(1 - \frac{4t}{2\delta^2}\right) \\
I_3^{(2)}(t) &= -\frac{4\pi a^2 \delta}{t\sqrt{4t}\pi^{3/2}} e^{-\left(\frac{\delta}{\sqrt{4t}}\right)^2} \\
I_3^{(3)}(t) &= \frac{2\pi a^2 \delta}{t\sqrt{4t}\pi^{3/2}} e^{-\left(\frac{\delta}{\sqrt{4t}}\right)^2} \left(1 - \frac{4t}{2\delta^2} + o(t)\right).
\end{aligned}$$

Summing the three contributions, the leading order terms cancel and we end up with

$$I_3(t) = \frac{4a^2\sqrt{t}}{\pi^{1/2}\delta^3} e^{-\left(\frac{\delta}{\sqrt{4t}}\right)^2}. \quad (9.64)$$

To compute I_4 , we decompose it into

$$\begin{aligned}
I_4(t) &= \frac{1}{\sqrt{(4\pi t)^3}} \frac{a^2}{\delta t} \int_{\Omega} |\mathbf{a} - \mathbf{x}| e^{-\frac{(\delta + |\mathbf{a} - \mathbf{x}|)^2}{4t}} d\mathbf{x} \\
&= \frac{2\pi}{\sqrt{(4\pi t)^3}} \frac{a^2}{\delta t} \int_{\frac{\delta}{\sqrt{4t}}}^{\frac{\delta+R}{\sqrt{4t}}} e^{-\eta^2} (\sqrt{4t}\eta - \delta)^3 \sqrt{4t} d\eta \\
&= J_1(t) + J_2(t) + J_3(t) + J_4(t).
\end{aligned} \quad (9.65)$$

Direct computations give

$$J_1(t) = \frac{2\pi(4t)^2}{\sqrt{(4\pi t)^3}} \frac{a^2}{\delta t} \int_{\frac{\delta}{\sqrt{4t}}}^{\frac{\delta+R}{\sqrt{4t}}} e^{-\eta^2} \eta^3 d\eta = \frac{4a^2\delta}{\sqrt{\pi}(4t)^{3/2}} \left(1 + \frac{4t}{\delta^2}\right) e^{-\left(\frac{\delta}{\sqrt{4t}}\right)^2}, \quad (9.66)$$

where the approximation

$$\int_{\frac{\delta}{\sqrt{4t}}}^{\frac{\delta+R}{\sqrt{4t}}} \eta^3 e^{-\eta^2} d\eta \approx \left(1 + \frac{\delta^2}{4t}\right) e^{-\left(\frac{\delta}{\sqrt{4t}}\right)^2} \quad (9.67)$$

was used. Next,

$$\begin{aligned} J_2(t) &= -\frac{2\pi}{\sqrt{(\pi)^3}} \frac{a^2}{\delta t} \int_{\frac{\delta}{\sqrt{4t}}}^{\frac{\delta+R}{\sqrt{4t}}} e^{-\eta^2} 3\eta^2 \delta d\eta \\ &= -\frac{12a^2\delta}{\sqrt{\pi}(4t)^{3/2}} \left(1 + \frac{2t}{\delta^2} \left(1 - \frac{2t}{\delta^2} + \frac{12t^2}{\delta^4} + o(t^2) \right) \right) e^{-\left(\frac{\delta}{\sqrt{4t}}\right)^2}, \end{aligned}$$

where we have used

$$\int_{\frac{\delta}{\sqrt{4t}}}^{\frac{\delta+R}{\sqrt{4t}}} \eta^2 e^{-\eta^2} d\eta \approx \left[\frac{\delta}{2\sqrt{4t}} + \frac{\sqrt{4t}}{4\delta} \left(1 - \frac{4t}{2\delta^2} + 12\frac{t^2}{\delta^4} + o(t^2) \right) \right] e^{-\left(\frac{\delta}{\sqrt{4t}}\right)^2}.$$

Using (9.62), we get

$$J_3(t) = \frac{2\pi}{\sqrt{(4t\pi^3)}} \frac{a^2}{\delta t} \int_{\frac{\delta}{\sqrt{4t}}}^{\frac{\delta+R}{\sqrt{4t}}} e^{-\eta^2} 3\eta \delta^2 d\eta = \frac{12a^2\delta}{\sqrt{\pi}(4t)^{3/2}} e^{-\frac{\delta^2}{4t}}. \quad (9.68)$$

Finally,

$$\begin{aligned} J_4(t) &= -\frac{2\pi}{4t\sqrt{(\pi)^3}} \frac{a^2}{\delta t} \int_{\frac{\delta}{\sqrt{4t}}}^{\frac{\delta+R}{\sqrt{4t}}} e^{-\eta^2} \delta^3 d\eta \\ &= -\frac{4a^2\delta}{(4t)^{3/2}\sqrt{\pi}} e^{-\frac{\delta^2}{4t}} \left[1 - \frac{2t}{\delta^2} + \frac{12t^2}{\delta^4} + o(t^2) \right]. \end{aligned}$$

Direct computations show that the terms $O(t^{-3/2})$ and $O(t^{-1/2})$ cancel out in the computation of I_4 and there remains only the term of order $O(t^{1/2})$,

$$I_4(t) = -\frac{9a^2}{\sqrt{\pi}\delta^3} t^{1/2} e^{\{-\delta^2/4t\}}. \quad (9.69)$$

Summing (9.61), (9.64), and (9.65), we get

$$S(t) = \int_{\Omega} p_t(\mathbf{x}, \mathbf{y}) d\mathbf{x}$$

$$\begin{aligned}
&= 1 - \sqrt{4t} \frac{e^{-(R_a/\sqrt{4t})^2}}{R_a \sqrt{\pi}} - \frac{a^2}{\delta \pi^{1/2} \sqrt{t}} e^{-\delta^2/4t} + o\left(t^{1/2} e^{-\left(\frac{\delta}{\sqrt{4t}}\right)^2}\right) \\
&\approx 1 - \frac{a^2}{\delta \pi^{1/2} \sqrt{t}} e^{-\delta^2/4t}.
\end{aligned}$$

It follows that in three dimensions, the expected FAT to a small circular window of radius a , $\bar{\tau}^3$, is given by

$$\begin{aligned}
\bar{\tau}^3 &= \int_0^\infty [\Pr\{t_1 > t\}]^N dt \approx \int_0^\infty \exp N \log \left(1 - \frac{a^2}{\delta \pi^{1/2} \sqrt{t}} e^{-\delta^2/4t}\right) dt \\
&\approx \int_0^\infty \exp \left(-N \frac{4(a/\delta)}{\delta \pi^{3/2} \sqrt{t}} e^{-\delta^2/4t}\right) dt \\
&\approx \delta^2 \int_0^\infty \exp \left(-N' \frac{1}{\sqrt{u}} e^{-1/4u}\right) du,
\end{aligned}$$

where $N' = N \frac{4a^2}{\pi^{1/2} \delta^2}$.

Using the method developed in Sect. 9.1.4 with the change of variable,

$$w = w(t) = \frac{1}{\sqrt{t}} e^{-1/t}, \quad w'(t) = \frac{1}{\sqrt{t}} e^{-\frac{1}{t}} \left(-\frac{1}{2t} + \frac{1}{4t^{3/2}}\right), \quad (9.70)$$

we have, with $w' \approx 4w(\log(w))^{3/2}$,

$$\bar{\tau}^3 \approx \delta^2 \int_0^\infty \frac{\exp(-N'w)}{4w(\log(w))^{3/2}} dw.$$

When the diffusion coefficient is D , the formula can be further integrated and becomes

$$\bar{\tau}^3 \approx \frac{\delta^2}{2D \sqrt{\log \left(N \frac{4a^2}{\pi^{1/2} \delta^2}\right)}}. \quad (9.71)$$

The next term in the expansion can be obtained by accounting for the logarithmic singularity in the expansion of Green's function. When there are p windows, whose distances from the initial position of the Brownian particle are $d_k = \text{dist}(P_0, P_k)$, formula (9.71) changes to

$$\bar{\tau}^3 \approx \frac{\delta_m^2}{2D \sqrt{\log \left(N \frac{4a^2}{\pi^{1/2} \delta_m^2} \right)}}, \quad (9.72)$$

where $\delta_m^2 = \min(d_1^2, \dots, d_p^2)$. The asymptotic formula (9.71) is compared in Fig. 9.3 with results of Brownian simulations and shows very good agreement. When the absorbing windows are ellipses, the Green's function approach, based on the narrow escape methodology, can be applied as well [Holcman and Schuss (2015)].

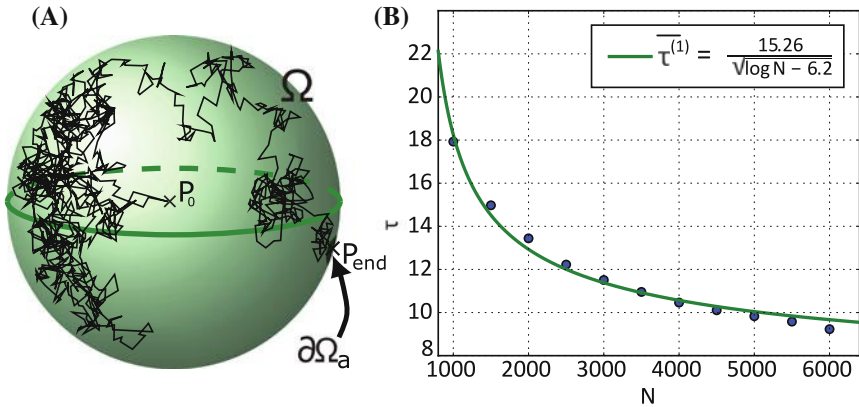


Fig. 9.3 Extreme statistics of the narrow escape time through a small window in \mathbb{R}^3 . **A** The geometry of the expected FAT. In the simulation, the sphere has radius $5 \mu\text{m}$, the absorbing window $\partial\mathcal{S}_a$ has radius $\varepsilon = 0.1 \mu\text{m}$, and the diffusion coefficient is $D = 0.2 \mu\text{m}^2\text{s}^{-1}$. The trajectory starts at P_0 (cross) and ends at P_{end} . **B** Plot of the expected FAT vs N with 2000 simulated runs. The asymptotic solution (red curve) is $A / \log(N + B)$

9.3.2 Asymptotics in \mathbb{R}^2

Consider the diffusion of N Brownian i.i.d. particles in a domain $\Omega \subset \mathbb{R}^2$ with a small absorbing arc $\partial\Omega_a$ of length 2ε on the otherwise reflecting boundary $\partial\Omega$. To compute the pdf of the FAT to $\partial\Omega_a$, we follow the steps of the analysis of Sect. 9.3.1 in \mathbb{R}^3 .

The Neumann–Green function (9.44) in \mathbb{R}^2 , the solution of the BVP

$$-\Delta_x \hat{G}(x, q | y) + q \hat{G}(x, q | y) = \delta(x - y) \quad \text{for } x, y \in \Omega, \quad (9.73)$$

$$\frac{\partial \hat{G}_q(x, q | y)}{\partial n_x} = 0 \quad \text{for } x, y \in \partial\Omega, \quad (9.74)$$

is given for $\mathbf{x}, \mathbf{y} \in \partial\Omega$ by [Chen and Ward (2011)[p. 51]]

$$\hat{G}(\mathbf{x}, q | \mathbf{y}) = \frac{1}{\pi} K_0(\sqrt{q}|\mathbf{x} - \mathbf{y}|) + R(\mathbf{x}, \mathbf{y}), \quad (9.75)$$

where $R(\mathbf{x}, \mathbf{y})$ is its regular part. For a disk, the analytical expression is given by the series

$$R(\mathbf{x}, \mathbf{y}) = \frac{1}{\pi} \sum_0^{\infty} \sigma_n \cos(n(\psi - \psi_0)) \frac{K'_n(\sqrt{q})}{I'_n(\sqrt{q})} I_n(r\sqrt{q}) I_n(r_0\sqrt{q}), \quad (9.76)$$

where $\sigma_0 = 1$, $\sigma_n = 2$ for $n \geq 2$ and $\mathbf{x} = r e^{i\psi}$, $\mathbf{y} = r_0 e^{i\psi_0}$. The integral representation (9.47) of the solution is

$$\hat{p}(\mathbf{x}, q | \mathbf{y}) = \hat{G}(\mathbf{x}, q | \mathbf{y}) - \int_{\partial\Omega_a} \frac{\partial \hat{p}(\mathbf{x}, q | \mathbf{y}')}{\partial n_x} \hat{G}(\mathbf{x}, q | \mathbf{y}') dS_y, \quad (9.77)$$

so choosing $\mathbf{x} \in \partial\Omega_a$,

$$0 = \hat{G}(\mathbf{x}, q | \mathbf{y}) - \int_{\partial\Omega_a} \frac{\partial \hat{p}(\mathbf{x}, q | \mathbf{y}')}{\partial n_x} \hat{G}(\mathbf{x}, q | \mathbf{y}') dS_y. \quad (9.78)$$

This Helmholtz equation has the constant solution [Holcman and Schuss (2015)]

$$\frac{\partial \hat{p}(\mathbf{x}, q | \mathbf{y}')}{\partial n_x} = C \text{ for all } \mathbf{x} = \mathbf{a} \in \partial\Omega_a. \quad (9.79)$$

To leading order, we get

$$\hat{G}(\mathbf{a}, q | \mathbf{y}) = \frac{C}{\pi} \int_{\partial\Omega_a} K_0(\sqrt{q}|\mathbf{a} - \mathbf{y}|) ds_y, \quad (9.80)$$

where ds_y is arclength element in $\partial\Omega_a$. When $|\mathbf{x} - \mathbf{y}| \leq 4\varepsilon$ and $\sqrt{q}\varepsilon \ll 1$ in the large q expansion of Green's function,

$$K_0(\sqrt{q}|\mathbf{x} - \mathbf{y}|) = -\log(\sqrt{q}|\mathbf{x} - \mathbf{y}|) + \log 2 - \gamma_0 + o(1), \quad (9.81)$$

we obtain

$$\hat{G}(\mathbf{a}, q | \mathbf{y}) = \frac{C}{\pi} \int_{\partial\Omega_a} [-\log(\sqrt{q}|\mathbf{a} - \mathbf{y}|) + \log 2 - \gamma_0 + o(1)] ds_y; \quad (9.82)$$

that is,

$$\hat{G}(\mathbf{a}, q | \mathbf{y}) = \frac{2C}{\pi} \int_0^\varepsilon [-\log(\sqrt{q}r) + \log 2 - \gamma_0 + o(1)] dr. \quad (9.83)$$

Therefore the leading order approximation of C is

$$C = \frac{\pi \hat{G}(\mathbf{a}, q | \mathbf{y})}{2\varepsilon [-\log(\sqrt{q}\varepsilon) + O(\varepsilon)]}. \quad (9.84)$$

Finally, (9.77) gives for $|\mathbf{a} - \mathbf{x}| \gg \varepsilon$

$$\hat{p}(\mathbf{x}, q | \mathbf{y}) \approx \hat{G}(\mathbf{x}, q | \mathbf{y}) + \frac{\pi \hat{G}(\mathbf{a}, q | \mathbf{y}) \hat{G}(\mathbf{a}, q | \mathbf{x})}{\log(\sqrt{q}\varepsilon) + O(\varepsilon)}. \quad (9.85)$$

The inversion formula [Abramowitz and Stegun (1972), p. 1028] for $k > 0$,

$$\mathcal{L}^{-1}(K_0(k\sqrt{q})) = \frac{1}{2t} e^{-\frac{k^2}{4t}}, \quad (9.86)$$

gives

$$\mathcal{L}^{-1}\hat{G}(\mathbf{x}, q | \mathbf{y}) = \frac{1}{4\pi t} e^{-\frac{|\mathbf{x} - \mathbf{y}|^2}{4t}}. \quad (9.87)$$

For an initial point far from the boundary layer near the window, the expansion [Abramowitz and Stegun (1972), p. 378]

$$K_0(z) = \sqrt{\frac{\pi}{2z}} e^{-z} \left(1 + O\left(\frac{1}{z}\right)\right) \quad \text{for } z \gg 1, \quad (9.88)$$

gives in (9.75)

$$\hat{G}(\mathbf{a}, q | \mathbf{y}) \hat{G}(\mathbf{a}, q | \mathbf{x}) = \frac{1}{2\pi} \sqrt{\frac{1}{qs_1 s_2}} e^{-\sqrt{q}(s_1 + s_2)} (1 + O(q^{-1/2})), \quad (9.89)$$

where $s_1 = |\mathbf{a} - \mathbf{y}|$ and $s_2 = |\mathbf{a} - \mathbf{x}|$,

$$\begin{aligned} \frac{\pi \hat{G}(\mathbf{a}, q | \mathbf{y}) \hat{G}(\mathbf{a}, q | \mathbf{x})}{-\log(\sqrt{q}\varepsilon) + O(\varepsilon)} &= \frac{e^{-\sqrt{q}(s_1 + s_2)}}{-2 \log(\sqrt{q}\varepsilon)} \sqrt{\frac{1}{qs_1 s_2}} (1 + O(q^{-1/2})), \\ &\approx \frac{e^{-\sqrt{q}(s_1 + s_2)}}{-2 \log(\varepsilon) + O(1)} \sqrt{\frac{1}{qs_1 s_2}} (1 + O(q^{-1/2})). \end{aligned}$$

The inversion formula

$$\mathcal{L}^{-1} \left(\frac{1}{\sqrt{q}} e^{-k\sqrt{q}} \right) = \frac{1}{\sqrt{\pi t}} e^{-\frac{k^2}{4t}} \quad (9.90)$$

gives

$$\frac{\pi \mathcal{L}^{-1}(\hat{G}(\mathbf{a}, q | \mathbf{y}) \hat{G}(\mathbf{a}, q | \mathbf{x}))}{-\log(\sqrt{q}\varepsilon) + O(\varepsilon)} = \frac{1}{-2\log(\varepsilon) + O(1)} \frac{1}{\sqrt{\pi t s_1 s_2}} e^{-\frac{(s_1 + s_2)^2}{4t}}. \quad (9.91)$$

Hence, we obtain the short-time asymptotics of the survival probability

$$\begin{aligned} S(t) &\approx \int_{\Omega} p_t(\mathbf{x}, \mathbf{y}) d\mathbf{x} \\ &= \frac{1}{4\pi t} \int_{\Omega} e^{-\frac{|\mathbf{x} - \mathbf{y}|^2}{4t}} d\mathbf{x} \\ &\quad - \frac{1}{-2\log(\varepsilon)\sqrt{s_2} + O(1)} \frac{1}{\sqrt{\pi t}} \int_{\Omega} \sqrt{\frac{1}{|\mathbf{a} - \mathbf{x}|}} e^{-\frac{(|\mathbf{a} - \mathbf{x}| + s_2)^2}{4t}} d\mathbf{x} \\ &= R_1(t) + R_2(t), \end{aligned} \quad (9.92)$$

where

$$R_1(t) = \frac{1}{4\pi t} \int_{\Omega} e^{-\frac{|\mathbf{x} - \mathbf{y}|^2}{4t}} d\mathbf{x} \approx 1 - e^{-(R_a/\sqrt{4t})^2}, \quad (9.93)$$

and R_a is the radius of the maximal disk inscribed in Ω . The second term is

$$\begin{aligned} R_2(t) &= - \frac{1}{-2\log(\varepsilon)\sqrt{s_2} + O(1)} \frac{1}{\sqrt{\pi t}} \int_{\Omega} \sqrt{\frac{1}{|\mathbf{a} - \mathbf{x}|}} e^{-\frac{(|\mathbf{a} - \mathbf{x}| + s_2)^2}{4t}} d\mathbf{x} \\ &\approx - \frac{1}{-2\log(\varepsilon)\sqrt{s_2} + O(1)} \sqrt{\frac{\pi}{t}} \int_0^{R_a} e^{-\frac{(r + s_2)^2}{4t}} \sqrt{r} dr. \end{aligned} \quad (9.94)$$

The small t Laplace expansion and the two successive changes of variable, $u = s_2 r / 2t$ and $v = u^{3/2}$, give

$$\int_0^{R_a} e^{-\frac{(r+s_2)^2}{4t}} \sqrt{r} dr \approx \frac{2}{3} \left(\frac{2t}{s_2} \right)^{3/2} e^{-\frac{s_2^2}{4t}} \int_0^\infty e^{-v^{3/2}} dv. \quad (9.95)$$

Thus, with

$$I = \int_0^\infty e^{-v^{2/3}} dv = \frac{3\sqrt{\pi}}{4}, \quad (9.96)$$

the value $\int_0^\infty e^{-v^{2/3}} dv = \frac{3\sqrt{\pi}}{4}$ gives

$$R_2(t) - \frac{1}{-2 \log(\varepsilon) + O(1)} \frac{\sqrt{2}\pi t}{s_2^2} e^{-\frac{s_2^2}{4t}}. \quad (9.97)$$

We conclude therefore that the survival probability (9.92) is approximately

$$S(t) \approx 1 - \frac{1}{2 \log(\frac{1}{\varepsilon})} \frac{\sqrt{2}\pi t}{s_2^2} e^{-\frac{s_2^2}{4t}}, \quad (9.98)$$

where the contribution of (9.93) is negligible. Thus the expected FAT is given by

$$\begin{aligned} \bar{\tau}^2 &= \int_0^\infty [\Pr\{t_1 > t\}]^N dt \approx \int_0^\infty \exp \left\{ N \log \left(1 - \frac{1}{2 \log(\frac{1}{\varepsilon})} \frac{\sqrt{2}\pi t}{s_2^2} e^{-\frac{s_2^2}{4t}} \right) \right\} dt \\ &\approx \int_0^\infty \exp \left\{ -N \frac{1}{2 \log(\frac{1}{\varepsilon})} \frac{\sqrt{2}\pi t}{s_2^2} e^{-\frac{s_2^2}{4t}} \right\} dt. \end{aligned}$$

The computation of the last integral follows the steps described in Sect. 9.2. The change of variable $w = t \exp\{-s_2^2/4t\}$ leads to the asymptotic formula with diffusion coefficient D

$$\bar{\tau}^2 \approx \frac{s_2^2}{4D \log \left(\frac{\pi \sqrt{2}N}{8 \log(\frac{1}{\varepsilon})} \right)}.$$

This formula is compared with Brownian simulations in Fig. 9.4. The dependence on the window size here is $\log(\frac{1}{\varepsilon})$.

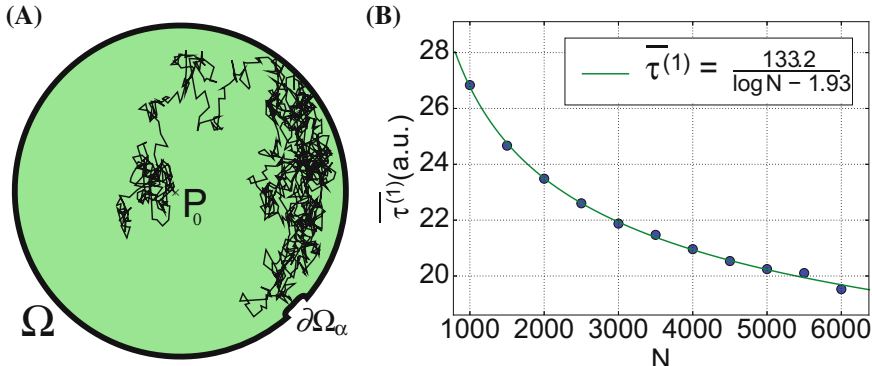


Fig. 9.4 Escape through a narrow opening in a planar disk. **A** The geometry of the expected FAT. **B** Plot of the expected FAT vs N . The asymptotic solution (red curve) is of the form $\frac{\alpha}{\log N + \beta}$

9.4 Statistics of the Arrival Time of the Second Particle

We turn to the computation of the conditional pdf of the arrival time $\tau^{(2)}$ of the second particle, which is that of the minimum of the shortest arrival time in the ensemble of $N - 1$ trajectories after the first one has arrived, conditioned on their locations at time $\tau^{(1)}$. The time $\tau^{(1)} + \tau^{(2)}$ is that of arrival of the first two particles to reach the target. The conditional distribution of the arrival time $\tau^{(2)}$ of the second particle, given the positions of the $N - 1$ particles at time $\tau^{(1)}$, can be computed from their joint probability distribution at positions (x_1, \dots, x_{N-1}) and the first particle has already arrived at time $\tau^{(1)} = s$,

$$\begin{aligned} & \Pr\{\tau^{(2)} = t\} \\ &= \int_0^t \int_{\Omega} \cdots \int_{\Omega} \Pr\{\tau^{(2)} = t, \tau^1 = s, \mathbf{x}_1(s) = x_1, \dots, \mathbf{x}_{N-1}(s) = x_{N-1}\} dx_1 \cdots dx_N ds \end{aligned} \quad (9.99)$$

and

$$\begin{aligned} & \Pr\{\tau^{(2)} = t, \tau^1 = s, x_1(s) = x_1, \dots, x_{N-1}(s) = x_{N-1}\} \\ &= \Pr\{\tau^{(2)} = t | \tau^1 = s, x_1(s) = x_1, \dots, x_{N-1}(s) = x_{N-1}\} \\ &\quad \times \Pr\{\tau^1 = s\} \Pr\{x_1(s) = x_1, \dots, x_{N-1}(s) = x_{N-1}\}. \end{aligned}$$

Because all particles are independent,

$$\Pr\{\mathbf{x}_1(s) = x_1, \dots, \mathbf{x}_{N-1}(s) = x_{N-1}\} = \prod_{i=1}^{N-1} \Pr\{\mathbf{x}_i(s) = x_i\}$$

so that

$$\Pr\{\tau^{(2)} = t\} = \int_0^t \Pr\{\tau^{(2)} = t | \tau^1 = s\} \left(\int_0^L \Pr\{\mathbf{x}_1(s) = x_1\} dx_1 \right)^N \Pr\{\tau^1 = s\} ds. \quad (9.100)$$

9.4.1 Poissonian-Like Approximation

The pdf (9.100) can be evaluated under some additional assumptions. For example, if the Brownian trajectories escape from a deep potential well, the escape process is well approximated by a Poisson process with rate equal the reciprocal of the mean escape time from the well [Schuss (2010b)]. Also, when Brownian particles escape a domain $\Omega = B \cup C$, which consists of a bulk B and a narrow cylindrical neck C , the escape process from Ω can be approximated by a Poisson process, according to the narrow escape theory [Holcman and Schuss (2015)]. Here the motion in the narrow cylinder C is approximated by one-dimensional Brownian motion in an interval of length L .

Consequently, under the Poisson approximation, the arrival of the first particle is much faster than the escape of the second one from the bulk compartment B , thus we can use the approximation that all particles are still in the bulk B after the arrival of the first one. The bulk is represented by the position $x = 0$ in an approximate one-dimensional model. This assumption simplifies (9.100) to

$$\left(\int_0^L \Pr\{\mathbf{x}_1(s) = x_1\} dx_1 \right)^N \approx 1, \quad (9.101)$$

so that

$$\Pr\{\tau^{(2)} = t\} = \int_0^t \Pr\{\tau^{(2)} = t | \tau^1 = s\} \Pr\{\tau^1 = s\} ds. \quad (9.102)$$

The Markovian property of the Poisson process gives

$$\Pr\{\tau^{(2)} = t | \tau^1 = s\} = \Pr\{\tau^{(2)} = t - s\} \quad (9.103)$$

so that $\tau^{(2)}$ has the same pdf as τ^1 with $N - 1$ particles, which we approximate to be the same for large N , that is,

$$\Pr\{\tau^{(2)} = t\} = \int_0^t f(t-s) f(s) ds, \quad (9.104)$$

where (recall (9.16))

$$f(s) = \Pr\{\tau^1 = s\} = NN_R g(t)^N h(t). \quad (9.105)$$

In one dimension, $g(t) = \sum_{n=0}^{N_t} \frac{(-1)^n}{\lambda_n} e^{-D\lambda_n^2 t}$ and $h(t) = \sum_{n=0}^{N_t} (-1)^n \lambda_n e^{-D\lambda_n^2 t}$. It follows that

$$\Pr\{\tau^{(2)} = t\} \approx N^2 N_R^2 \int_0^t g(s)^{N-1} h(s) g(t-s)^{N-1} h(t-s) ds. \quad (9.106)$$

9.4.2 $\Pr\{\tau^{(2)}\}$ of N Brownian i.i.d. Trajectories in a Segment

As in the first paragraph of Sect. 9.4, Eqs. (9.99) and (9.100) are valid with Ω replaced by the segment $[0, L]$. That is,

$$\begin{aligned} & \Pr\{\tau^{(2)} = t\} \\ &= \int_0^t \int_0^L \cdots \int_0^L \Pr\{\tau^{(2)} = t, \tau^1 = s, x_2(s) = x_2, \dots, x_N(s) = x_N\} dx_2 \cdots dx_N ds \end{aligned}$$

and

$$\begin{aligned} & \Pr\{\tau^{(2)} = t, \tau^1 = s, x_2(s) = x_1, \dots, x_{N-1}(s) = x_N\} \\ &= \Pr\{\tau^{(2)} = t | \tau^1 = s, x_2(s) = x_1, \dots, x_{N-1}(s) = x_N\} \\ & \quad \times \Pr\{\tau^1 = s\} \Pr\{x_2(s) = x_1, \dots, x_{N-1}(s) = x_N\}. \end{aligned}$$

Because all particles are independent,

$$\Pr\{x_2(s) = x_1, \dots, x_N(s) = x_{N-1}\} = \prod_{i=1}^{N-1} \Pr\{x_{i+1}(s) = x_i\}, \quad (9.107)$$

hence,

$$\Pr\{\tau^{(2)} = t\} = \int_0^t \Pr\{\tau^{(2)} = t | \tau^1 = s\} \times \quad (9.108)$$

$$\left(\int_0^L \Pr\{x_1(s) = x_1\} dx_1 \right)^{N-1} \Pr\{\tau^1 = s\} ds. \quad (9.109)$$

To compute the survival probability

$$S(s) = \int_0^L \Pr\{x_1(s) = x_1\} dx_1, \quad (9.110)$$

we use the short-time asymptotics of the one-dimensional diffusion equation. Modifying equation (9.9) for short-time diffusion of a particle starting at 0, we get

$$\begin{aligned} \frac{\partial p(x, t)}{\partial t} &= D \frac{\partial^2 p(x, t)}{\partial x^2} \quad \text{for } x > 0, t > 0 \\ p(x, 0) &= \delta(x) \quad \text{for } x > 0, \quad p(L, t) = 0 \quad \text{for } t > 0. \end{aligned} \quad (9.111)$$

The short-time diffusion is well approximated by the fundamental solution (except at the boundary, where the error is exponentially small in $1/t$)

$$p(x, t) = \frac{1 + o(t)}{\sqrt{4Dt}} \exp\left\{-\frac{x^2}{4Dt}\right\}. \quad (9.112)$$

Thus the survival probability at short time t is

$$S(t) = \int_0^L \frac{1 + o(t)}{\sqrt{4Dt}} \exp\left\{-\frac{x^2}{4Dt}\right\} dx. \quad (9.113)$$

The short-time asymptotic expansion (9.24) (see below) and the change of variable $x = u\sqrt{4Dt}$ in the integral (9.113) give

$$S(t) = 1 - \frac{1}{\sqrt{\pi}} \int_{L/\sqrt{4Dt}}^{\infty} [\exp\{-u^2\}] du \quad (9.114)$$

$$\approx 1 - \sqrt{4Dt} \frac{\exp\{-(L/\sqrt{4Dt})^2\}}{\sqrt{\pi} L} \left(1 - 2 \frac{Dt}{L^2} + O\left(\frac{t^2}{L^4}\right) \right). \quad (9.115)$$

It follows from (9.108) that the pdf of the second arrival time is

$$\Pr\{\tau^{(2)} = t\} = [1 + o(1)] \int_0^t \Pr\{\tau^1 = s\} \Pr\{\tau^1 = t - s\} \times \quad (9.116)$$

$$\left(1 - \sqrt{4Ds} \frac{\exp\left\{-\left(\frac{L}{\sqrt{4Ds}}\right)^2\right\}}{\sqrt{\pi}L} \right)^{N-1} ds.$$

Figure 9.5 compares results of the stochastic simulations with the analytical formula (9.106) for the second fastest arrival time $\tau^{(2)}$ to the boundary 1 of the interval $[0, 1]$ among 20 particles. We use the analytical formula (9.106) (no correction) and (9.116), which contains the shift correction due to the distribution of the particles in the interval at time $\tau^{(1)}$, when the first particle has arrived at $x = L$.

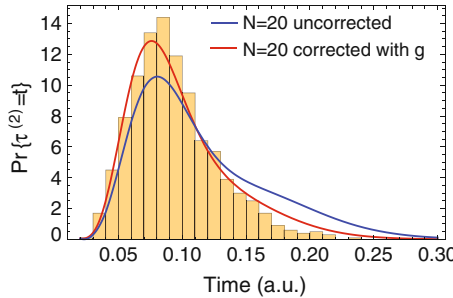


Fig. 9.5 Histogram of the arrival time of the second fastest particle, obtained from Brownian simulations with Euler's scheme. The fastest is computed for $N = 20$ in **B**. The analytical solution with no correction is given by (9.103) (blue) and compared to (9.116) with the correction (red). There are $n_0 = 6$ terms in the series (9.17)

This figure shows how the corrected formula gives a better agreement with the Brownian simulations, thus proving that the distribution of the Brownian particles inside the interval contributes to the decrease of the arrival time of the second particle. The fit to simulation data is based on the eigenfunction expansion

$$\Pr\{\tau^{(2)} = t\} = [1 + o(1)] \int_0^t \Pr\{\tau^1 = s\} \Pr\{\tau^1 = t - s\} \times \left(2 \sum_{n=0}^{\infty} \frac{(-1)^n}{\lambda_n} e^{-D\lambda_n^2 t} \right)^{N-1} ds, \quad (9.117)$$

which is equivalent to (9.116). Formula (9.105) is used for $\Pr\{\tau^1 = s\}$. Note that the alternating series contains an even number of terms.

To conclude, the internal distribution of the particles is given by

$$\left(1 - \sqrt{4Ds} \frac{\exp\left\{-\left(\frac{L}{\sqrt{4Ds}}\right)^2\right\}}{\sqrt{\pi}L} \right)^{N-1}$$

and causes the faster arrival of the second particle relative to the first one. This example shows the deviation from the purely Poissonian approximation.

9.4.3 Applications of the FAT in Biophysics

The extreme statistics of the first particle to a small target in confined geometry is used to compute this time scale analytically and clarify the role of key parameters such as the initial number of particles, the size of the target and the distance of the release location with respect to the position of the target.

The present asymptotics have several key applications: activation of molecular processes are often triggered by the arrival of the first particles (ions or molecules) to target-binding sites. The simplest model of the motion of calcium ions in cell biology, such as neurons or a dendritic spine (neglecting electrostatic interactions) is that of independent Brownian particles in a bounded domain. The first two calcium ions that arrive at channels (such as TRP) can trigger the first step of biochemical amplification leading to the photoreponse in a fly photoreceptor. Another example is the activation of a Ryanodine receptor (RyaR), mediated by the arrival of two calcium ions to the receptor binding sites, which form small targets. Ryanodin receptors are located at the base of the dendritic spine. Computing the distribution of arrival times of Brownian particles at the base, when they are released at the center of the spine head, is a model for calcium release during synaptic activation. Computing the distribution of arrival time reveals that the fastest ions can generate a fast calcium response following synaptic activity. Thus the fastest two calcium ions can cross a sub-cellular structure, thus setting the time scale of activation, which can be much shorter than the time defined by the classical forward rate, usually computed as the steady-state Brownian flux into the target, or by the narrow escape time [Holcman and Schuss (2015)].

9.4.4 Annotations

Fast activation of biochemical pathways in cell biology is often initiated by the first arrival of a particle to a small target. This is the case of calcium activation in synapses of neuronal cells [Guerrier et al. (2014), Volfovsky et al. (1967), Holcman et al. (2005)], fast photoreponse in rods [Reingruber et al. PNAS (2013)], cones and fly photoreceptors, and many more. However, the time scale underlying these fast activations is not very well understood.

Chapter 10

The Poisson–Nernst–Planck Equations in a Ball

The diffusion of ions (charged particles) is often described by the Poisson–Nernst–Planck equations, which couple nonlinearly the charge concentration and the electric potential [Rubinstein (1990)]. The Poisson–Nernst–Planck model of electro-diffusion is used, among other applications, to describe the motion of ions in neuronal micro-compartments [Holcman and Yuste (2015)]. It remains at this time an open question how to determine the relaxation and the steady state distribution of voltage when an initial charge of ions is injected into a domain bounded by an impermeable dielectric membrane [Bezanilla (2008)].

The purpose of this chapter is to extend the narrow escape time method to the construction of an asymptotic solution to the stationary Poisson–Nernst–Planck equations in a ball. In this geometry the Poisson–Nernst–Planck system reduces to the Liouville–Gelfand–Bratú (LGB) equation [Frank-Kamenetskii (1955)], with the difference that the boundary condition is Neumann, not Dirichlet, and there is a minus sign in the exponent of the exponential term. The entire boundary is impermeable to particles (ions) and the electric field satisfies the compatibility condition of Poisson’s equation. These differences replace attraction by repulsion, thus changing completely the solution of the Liouville–Gelfand–Bratú equation, as described below. The role of the NET methodology is to resolve the connection of the ball to the narrow neck, as discussed in the linear case above.

10.1 Introduction

In this chapter, the Poisson–Nernst–Planck model is used for the computation of the distribution in a ball of a single species of unscreened positive charges in different regimes, including the limit of large total charge. The stationary Poisson–Nernst–Planck equations with Neumann and no-flux conditions, respectively, on the bound-

ary of a bounded domain Ω reduce to Poisson's equation, which models the electrical potential, with an exponential term, which models the density of charges in Ω .

10.2 Synopsis of Results

The solution of the stationary Poisson–Nernst–Planck equation in spherical symmetry in 1, 2, and 3 dimensions is expressed in terms of the (dimensionless) total charge λ and the asymptotic approximations of solutions are computed for small and large λ . The one-dimensional case is solved explicitly and it is characterized by a logarithmic singularity, which develops at the boundary in the limit of large λ .

The explicit solution in the two-dimensional case has a singularity on the boundary as well. A similar asymptotic behavior is observed in three dimensions, although the solution cannot be computed explicitly and an asymptotic and numerical argument for large λ is provided, exhibiting, again, logarithmic singularity at the boundary. Note that the logarithmic singularity in three dimensions cannot be derived from the analysis of the phase portrait, as done in the Liouville–Gelfand–Bratú equation, because it occurs at the initial point of the dynamics.

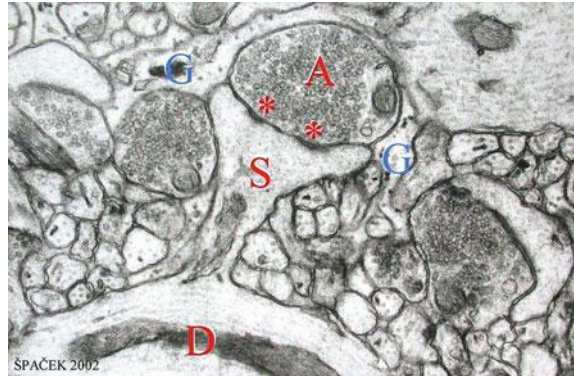
The modeling and analysis in this chapter is motivated by the need to compute voltage changes in bounded domains and to see how it develops a boundary layer for large λ . It is found that the drop of the solution from the center to the boundary converges to a finite value as λ increases to infinity. The analytical results are used to predict the voltage change (solution of the Poisson–Nernst–Planck equation) for idealized neuronal microdomains, such as dendritic spines. These structures (see Fig. 10.1) are idealized as spherical domains filled with ionic solution and enclosed by a dielectric membrane connected to the dendrite by a cylindrical narrow neck.

No local electro-neutrality is assumed in the Poisson–Nernst–Planck equations here. To derive a relation between the outward current and the voltage, the steady-state escape-rate of moving charges (ions) from a ball to a narrow absorbing neck is calculated. The ball with a narrow neck is an idealization of the spherical spine structure. It is found here that the current of absorbed charges is controlled by the small absorbing window in the sphere, as predicted by the narrow escape time theory of the previous chapters (see also [Schuss et al. (2007)] and [Holcman and Schuss (2014c)]), while the voltage is independently regulated by the coupled Poisson–Nernst–Planck equations.

10.3 Poisson–Nernst–Planck Equations in a Ball

The Poisson–Nernst–Planck equations represent the electric potential and the diffusing charge concentration in a given domain. Here, it is in a ball Ω of radius R , whose dielectric boundary $\partial\Omega$ is represented as the compatibility condition for Poisson's equation and its impermeability to the passage of charges is represented as a no-flux

Fig. 10.1 Geometrical representations of dendritic spines (Electron-Microscopy image) (courtesy of J. Spacek). Abbreviations G: glial cells, S: spine, D: dendrite, A: axon



boundary condition for the Nernst–Planck equation. Assume that there are N positive ions of valence z in Ω and that there is an initial charge density $q(\mathbf{x})$ in Ω such that

$$\int_{\Omega} q(\mathbf{x}) d\mathbf{x} = N. \quad (10.1)$$

The charge in Ω is

$$Q = zeN,$$

where e is the electronic charge. The charge density $\rho(\mathbf{x}, t)$ of ions diffusing with diffusion coefficient D is the solution of the Nernst–Planck equation

$$D \left[\Delta \rho(\mathbf{x}, t) + \frac{ze}{kT} \nabla (\rho(\mathbf{x}, t) \nabla \phi(\mathbf{x}, t)) \right] = \frac{\partial \rho(\mathbf{x}, t)}{\partial t} \quad \text{for } \mathbf{x} \in \Omega \quad (10.2)$$

$$D \left[\frac{\partial \rho(\mathbf{x}, t)}{\partial n} + \frac{ze}{kT} \rho(\mathbf{x}, t) \frac{\partial \phi(\mathbf{x}, t)}{\partial n} \right] = 0 \quad \text{for } \mathbf{x} \in \partial\Omega \quad (10.3)$$

$$\rho(\mathbf{x}, 0) = q(\mathbf{x}) \quad \text{for } \mathbf{x} \in \Omega, \quad (10.4)$$

where the electric potential $\phi(\mathbf{x}, t)$ is the solution in Ω of Maxwell's equation (Gauss' law)

$$\Delta \phi(\mathbf{x}, t) = -\frac{ze\rho(\mathbf{x}, t)}{\varepsilon\varepsilon_0} \quad \text{for } \mathbf{x} \in \Omega \quad (10.5)$$

with the boundary condition

$$\frac{\partial \phi(\mathbf{x}, t)}{\partial n} = -\sigma(\mathbf{x}, t) \quad \text{for } \mathbf{x} \in \partial\Omega, \quad (10.6)$$

where $\sigma(\mathbf{x}, t)$ is the surface charge density on the boundary $\partial\Omega$. In the steady state and in spherical symmetry

$$\sigma(\mathbf{x}, t) = \frac{Q}{4\epsilon\epsilon_0\pi R^2}. \quad (10.7)$$

10.3.1 The Steady-State Solution

The steady density in (10.2) is (Fig. 10.2)

$$\rho(\mathbf{x}) = N \frac{\exp\left\{-\frac{ze\phi(\mathbf{x})}{kT}\right\}}{\int_{\Omega} \exp\left\{-\frac{ze\phi(\mathbf{x})}{kT}\right\} d\mathbf{x}}, \quad (10.8)$$

hence (10.5) gives

$$\Delta\phi(\mathbf{x}) = -\frac{zeN \exp\left\{-\frac{ze\phi(\mathbf{x})}{kT}\right\}}{\epsilon\epsilon_0 \int_{\Omega} \exp\left\{-\frac{ze\phi(\mathbf{x})}{kT}\right\} d\mathbf{x}}. \quad (10.9)$$

In spherical symmetry in \mathbb{R}^d (10.9) can be written in spherical coordinates as

$$\phi''(r) + \frac{d-1}{r}\phi'(r) = -\frac{zeN \exp\left\{-\frac{ze\phi(r)}{kT}\right\}}{S_d \epsilon\epsilon_0 \int_0^R \exp\left\{-\frac{ze\phi(r)}{kT}\right\} r^{d-1} dr} < 0, \quad (10.10)$$

where S_d is the surface area of the unit sphere in \mathbb{R}^d . The boundary conditions are

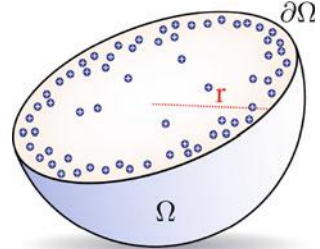
$$\frac{\partial\phi(0)}{\partial r} = 0, \quad \frac{\partial\phi(R)}{\partial r} = -\frac{Q}{\epsilon\epsilon_0 S_d R^{d-1}}. \quad (10.11)$$

The inequality in (10.10) means that $\phi(r)$ has a maximum at the origin and decreases toward the boundary (see Fig. 10.3A). The radius is normalized by setting $r = Rx$ for $0 < x < 1$ and

$$u(x) = \frac{ze\phi(r)}{kT}, \quad \lambda = \frac{(ze)^2 N}{\epsilon\epsilon_0 k T}, \quad (10.12)$$

to write (10.10) as

Fig. 10.2 Schematic representation of the distribution of a single unscreened ionic specie in a dielectric ball



$$u''(x) + \frac{d-1}{x} u'(x) = - \frac{\lambda \exp\{-u(x)\}}{S_d R^{d-2} \int_0^1 \exp\{-u(x)\} x^{d-1} dx} \quad (10.13)$$

$$u(0) = 0, \quad u'(0) = 0.$$

Note that we have dropped here the compatibility condition on the boundary at $x = 1$, which is automatically satisfied by the solution. Incorporating the denominator of the right-hand side of (10.13) into the parameter λ by defining the parameter μ and setting

$$\lambda = \mu S_d R^{d-2} \int_0^1 \exp\{-u(x)\} x^{d-1} dx \quad (10.14)$$

converts the initial value problem (10.13) to

$$u''(x) + \frac{d-1}{x} u'(x) = -\mu \exp\{-u(x)\} \quad (10.15)$$

$$u(0) = u'(0) = 0.$$

10.3.2 Existence of Solutions

First, we show that solutions of (10.15) exist in dimensions $1 \leq d \leq 3$ only for μ in the range $0 \leq \mu < \mu^*$ for some positive μ^* .

The Solution in One Dimension

Solving (10.15) explicitly in dimension $d = 1$, we obtain (see Appendix 10.3.1 and Eq. (10.46))

$$u_\lambda^{1d}(x) = \log \cos^2 \left(\sqrt{\frac{\lambda}{2I_\lambda}} x \right), \quad (10.16)$$

where I_λ is the solution of the implicit equation

$$I_\lambda = \frac{2}{\lambda} \tan^2 \sqrt{\frac{\lambda}{2I_\lambda}}. \quad (10.17)$$

The graph of $u_\lambda^{1d}(x)$ is shown in Fig. 10.4A, while that of λ/I_λ versus λ is shown in Fig. 10.4B. We have $0 < \mu(\lambda) = \lambda/I_\lambda \leq \pi^2/2$ and $\lim_{\lambda \rightarrow \infty} \mu(\lambda) = \pi^2/2$. The solution u_λ^{1d} exists for all $\lambda > 0$ and a logarithmic singularity develops at the boundary $x = 1$ when $\lambda \rightarrow \infty$.

The Solution in Two Dimensions

The solution in the two-dimensional case is constructed in Appendix 10.7 as

$$u_\lambda^{2d}(x) = \log \left(1 - \frac{\lambda}{8I_\lambda} x^2 \right)^2, \quad (10.18)$$

where

$$I_\lambda = \pi + \frac{\lambda}{8}, \quad \mu(\lambda) = \frac{\lambda}{I_\lambda}, \quad \lim_{\lambda \rightarrow \infty} \mu(\lambda) = 8.$$

The graph of $u_\lambda^{2d}(x)$ is shown in Fig. 10.4C, while that of λ/I_λ is in Fig. 10.4D. Obviously, the solution (10.18) develops a logarithmic singularity as $\lambda \rightarrow \infty$.

The Solution in Three Dimensions

Because the solution of the initial value problem (10.15) in dimension $d = 3$ cannot be expressed explicitly, we note first that it exists for all λ , while there is a critical value μ^* , above which there is no regular solution. Unlike in dimensions one and two, the value of μ^* can only be estimated numerically. Indeed, phase-plane analysis shows that the solution of (10.15) is unique whenever it exists. However, it is not possible to use the phase-plane to study the singularity of the equation, because it occurs at the initial point. To study the asymptotic explosion of the solution, we use an asymptotic argument. The solution is also constructed numerically (see Appendix 10.6.1).

First, we show that the problem (10.13) has a unique regular solution for all $\lambda \geq 0$ when the solution is finite. The proof of uniqueness of the solution follows the phase-plane analysis of (10.15). Indeed, the change of variables

$$\begin{aligned} s = -\log r, \quad u(r) = U(s), \quad v(s) = \frac{dU(s)}{ds}, \quad w = \mu e^{-2s} e^{-U(s)} \\ w'(s) = -2w(s) - U'(s)w(s) = w(s)[-2 - v(s)], \end{aligned} \quad (10.19)$$

converts (10.15) to the system

$$v'(s) = v(s) - w(s), \quad w'(s) = -w(s)[2 + v(s)] \quad (10.20)$$

and be reduced to the first-order ordinary differential equation

$$\frac{dw}{dv} = \frac{-w(2 + v)}{v - w}. \quad (10.21)$$

The phase space of (10.20) contains exactly two critical points, the origin $\mathbf{0}$ is a saddle point and its stable manifold has the tangent line $w = 3v$, denoted \mathbf{T} , while the point $P_a = (-2, -2)$ is an unstable node. The initial conditions $u(0) = u'(0) = 0$ for the solution of (10.15) impose $\lim_{s \rightarrow \infty} U(s) = u(0) = 0$ and $\lim_{s \rightarrow \infty} U'(s) = -\lim_{r \rightarrow 0} ru'(r) = v(0) = 0$, hence the constraints

$$\lim_{s \rightarrow \infty} v(s) = 0, \quad \lim_{s \rightarrow \infty} w(s) = \lim_{s \rightarrow \infty} \mu e^{-2s} e^{-U(s)} = 0. \quad (10.22)$$

Thus the trajectory of the solution of (10.15) in the first quadrant, which satisfies the constraints (10.22), has to be on the separatrix that converges to the saddle point. Any value $U(0)$ implies that $\mu e^{-U(0)}$ gives the value $v(0) = U'(0)$ that has to be chosen on the separatrix. Therefore, starting in the first quadrant, a trajectory of (10.20) converges to the saddle point if and only if it starts on the separatrix with the tangent \mathbf{T} . The stable branch at the saddle point tends to infinity as s decreases toward 0. Indeed, the local expansion of (10.21) near the saddle point is

$$w(v) = 3v + \frac{3}{5}v^2 - \frac{3}{175}v^3 + \dots, \quad (10.23)$$

which gives the phase portrait shown in Fig. 10.5. Along the separatrix we have $w'(v) > 0$, except at the origin, which implies that for an initial $v(0)$, there is a unique solution. However, phase-plane analysis of the singular solution is inapplicable. Indeed, as shown below, the singularity occurs precisely at the initial value and thus the Cauchy problem cannot be defined. It follows that the problem (10.13) has a finite solution and the phase diagram plotted in Fig. 10.5 ensures that for any finite initial condition $(v(0), w(0))$ on the separatrix in the first quadrant, there is a unique solution to (10.20) that satisfies (10.22).

A numerical solution of (10.13) gives the graph shown in Fig. 10.3E, which is the solution $u(x)$ of (10.3) for $\mu \leq \mu^* = 11.2$. The dashed line ($\mu^* = 14$) blows up before reaching $x = 1$, while the dotted graph is finite throughout the interval. To estimate an upper bound for μ^* , we note that whenever the solution exists for some μ near μ^* , its asymptotic behavior for x close to 1 shows that $u''(1) \gg u'(1)$ (see the blue graph in Fig. 10.3). Indeed, to show that under the assumption $u''(1) \gg u'(1)$ the latter inequality is self-consistent, we note that near $x = 1$ the solution of (10.15) can be approximated by the solution of the simpler problem

$$\tilde{u}''(x) = -\mu \exp \{-\tilde{u}(x)\}, \quad (10.24)$$

given by

$$\tilde{u}(x) \sim \log \cos^2 \left(\sqrt{\frac{\mu}{2}} x \right). \quad (10.25)$$

Thus $\tilde{u}(x)$ is finite in the interval as long as

$$\mu < \frac{\pi^2}{2} = 4.934802202 = \mu^* \quad (10.26)$$

and

$$\frac{\tilde{u}'(x)}{\tilde{u}''(x)} \leq \frac{|\sqrt{\mu} - \sqrt{\mu^*}|}{\sqrt{\mu^*}} \ll 1. \quad (10.27)$$

We conclude at this stage that for fixed values of $\mu > \mu^*$, the solution blow-ups inside the interval $0 < x < 1$ (frames A, C, E of Fig. 10.4). When $\mu < \mu^*$ varies with λ according to (10.14), the solutions exist for all values of λ (frames B, D, F of Fig. 10.4). Figure 10.4A-C-E shows the potential drop between the center and the surface of the sphere as a function of λ for $1 \leq d \leq 3$. Figure 10.3 shows the numerical solution of the three-dimensional case, compared with the asymptotic expansions in two regimes. It is shown in Appendix 10.6.2 that for $\lambda \ll 1$, the expansion of the solution is $u(x) = -\lambda x^2/8\pi + O(\lambda^2)$ (see (10.57)).

As mentioned above, for $\lambda \gg 1$ the approximation $u(x) \approx 2 \log(1 - x^2)$, relevant near $x = 1$, can be used in the entire domain $x \in [0, 1]$. The analytical approximations (red) are compared with the numerical solutions (see Appendix 10.6.1)

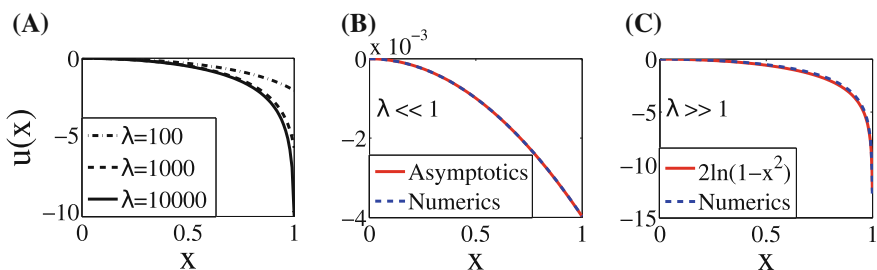


Fig. 10.3 Asymptotic behavior of the potential $u(x)$ in a ball. (A) change in the profile $u(x)$ for 3 values of the parameter $\lambda = 10^2, 10^3, 10^4$. (B, C) We present two regimes: for $\lambda = 0.1 \ll 1$, we have $u(x) = -\lambda x^2/8\pi + O(\lambda^2)$ (see (10.57)) and $\lambda \gg 1$, where $u(x) \approx 2 \log(1 - x^2)$. The analytical approximations (red) are compared with the numerical solutions (see Appendix)

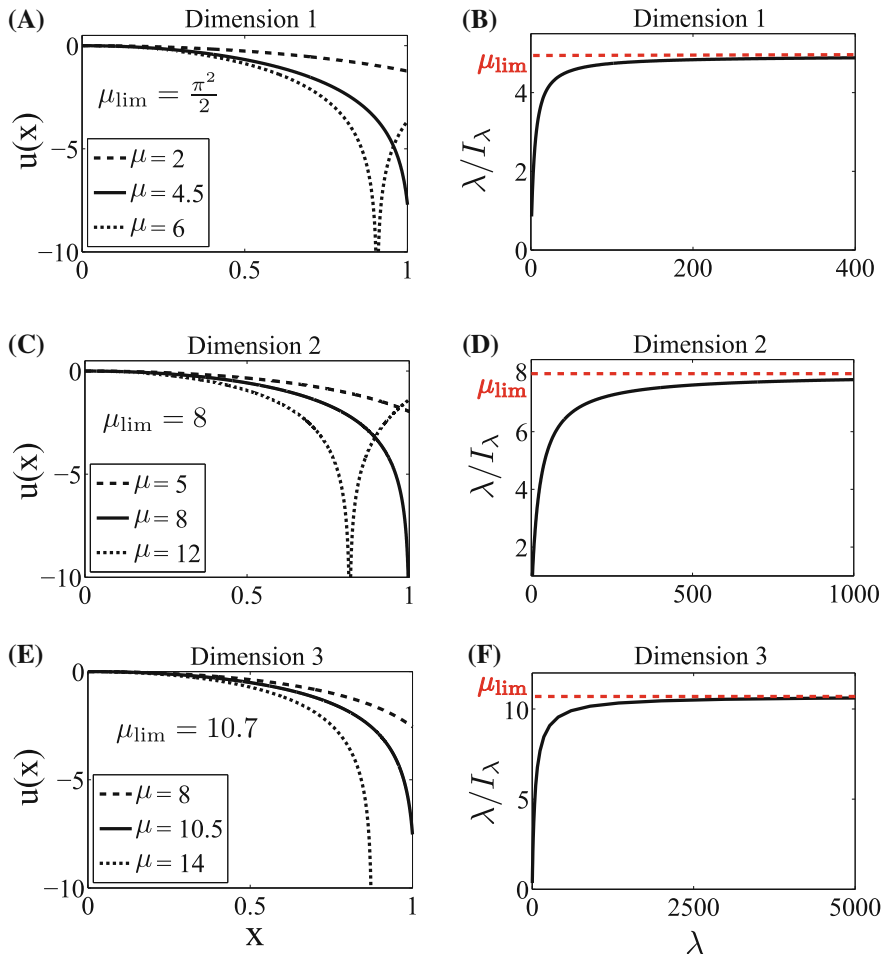


Fig. 10.4 Numerical solutions of the initial value problem (10.15). (A), (C), and (E) correspond to different profile values of λ in dimensions 1, 2, and 3, respectively. The dotted curves are solutions that blow-up for $x < 1$. (B), (D), and (F) are plots of the ratio λ/I_λ vs λ in dimensions 1, 2 and 3, respectively

The Potential Drop

The difference $u(0) - u(1)$ is the electric potential drop between the center and the boundary of the ball. In one dimension

$$|u_\lambda(1) - u_\lambda(0)| = \log \cos^2 \left(\sqrt{\frac{\lambda}{2I_\lambda}} \right), \quad (10.28)$$

where $\lambda/2I_\lambda \rightarrow \pi^2/4$ as $\lambda \rightarrow \infty$. In two dimensions

Fig. 10.5 Phase-plane solution of (10.20). The separatrix is shown in red, while the other trajectories are in blue

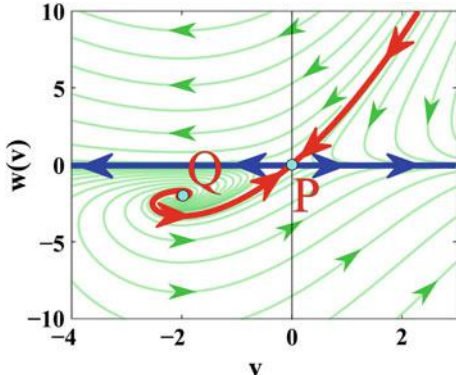
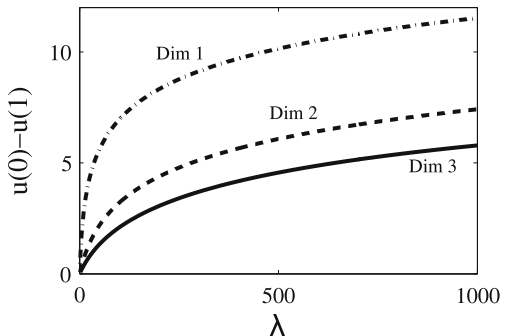


Fig. 10.6 Asymptotics of $u_\lambda(1) - u_\lambda(0)$ for dimensions 1, 2, and 3



$$|u_\lambda(1) - u_\lambda(0)| = 2 \log \left(\frac{8\pi}{\lambda + 8\pi} \right), \quad (10.29)$$

and in three dimensions, for $\lambda \gg 1$,

$$|u_\lambda(1) - u_\lambda(0)| = 2 \log[1 - f(\lambda)],$$

where the unknown function $f(\lambda)$ is increasing and $f(\lambda) \rightarrow 1$ as $\lambda \rightarrow \infty$. The different curves for dimensions 1, 2 and 3 are shown in Fig. 10.6. In all cases, the large λ asymptotics are dominated by the logarithmic behavior.

10.3.3 The Distribution of Voltage and Charge in a Dielectric Ball

The voltage and charge distributions in a dielectric ball can be estimated from the results of the previous sections by using the dimensional relation (10.12) in a ball of radius $R = 1\mu\text{m}$. Figure 10.7A shows the voltage drop for the total number of

charges in the ball $N = 10^2, 10^3$, and 10^4 . Even for 1000 charges, there is already a difference of a few millivolts between the center and the surface of the ball. Moreover, the density of charge is maximal near the boundary (Fig. 10.7B), leading to a large field $\mathbf{E} = -\nabla V$ close to the boundary (Fig. 10.7C). This is clearly seen in the plot of the cumulative density of charges (Fig. 10.7D)

$$Q(r) = N \frac{\int_0^r \exp \left\{ -\frac{ze\phi(r)}{kT} \right\} r^2 dr}{\int_0^R \exp \left\{ -\frac{ze\phi(r)}{kT} \right\} r^2 dr}. \quad (10.30)$$

In summary, when the total number of charges is sufficiently high, the charges accumulate near the surface. The field is only significant close to the surface and thus can trap a charged Brownian particle in a thin boundary layer. While outside the layer, the field is almost zero and charged particles experience no drift. This effect is discussed below.

10.3.4 Scaling Laws for the Maximal Number of Charges

Although the voltage drop in dimensionless variables $V(0) - V(1)$ is bounded as a function of the total number of charges, the maximal number of charges increases linearly with the radius R of the ball. Indeed, introducing the dimensionless radial variable $\zeta = r/R$ and $u_\lambda(r) = U_{\lambda/R}(\zeta)$, Eq. (10.10) becomes

$$U''_{\lambda/R}(\zeta) + \frac{2}{\zeta} U'_{\lambda/R}(\zeta) = - \frac{\lambda \exp \{-U_{\lambda/R}(\zeta)\}}{4\pi R \int_0^1 \exp \{-U_{\lambda/R}(\zeta)\} \zeta^2 d\zeta}, \quad (10.31)$$

with the initial conditions $U_{\lambda/R}(0) = U'_{\lambda/R}(0) = 0$. Solving with the new functions V_μ, W_μ , the initial value problems

$$\begin{aligned} V''_\mu(\zeta) + \frac{2}{\zeta} V'_\mu(\zeta) &= -\mu \exp \{-V_\mu(\zeta)\}, \quad V_\mu(0) = V'_\mu(0) = 0 \\ W'_\mu(\zeta) &= \zeta^2 \exp \{-V_\mu(\zeta)\}, \quad W_\mu(0) = 0 \end{aligned} \quad (10.32)$$

and noting that

$$u_\lambda(r) = V_\mu \left(\frac{r}{R} \right), \quad \lambda = 4\pi\mu RW(1), \quad (10.33)$$

we see that the total charge Q in a ball of radius R creates the same distribution as a charge Q/R in a ball of radius one, which can be stated as

$$Q(R) = RQ(1).$$

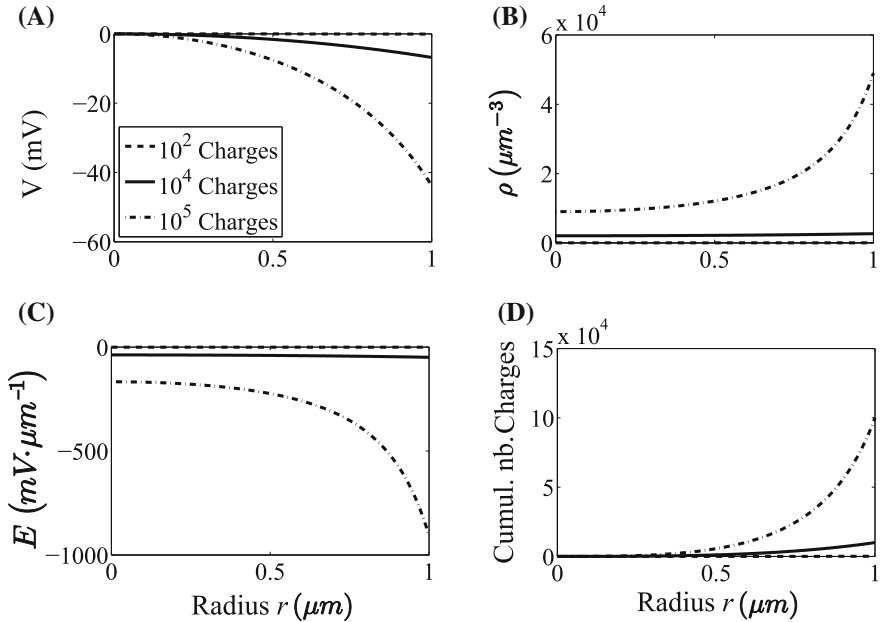


Fig. 10.7 Distribution of (A) the potential, (B) charge and the field (C) and cumulative density of charges (D) inside a dielectric ball. Parameters of simulations are given in Table 10.1

10.4 Ionic Flux in a Small Window at High Charge

Distributing charges close to the boundary in the large total charge regime has important consequences. The first consequence concerns the mean first passage time $\bar{\tau}(\mathbf{x})$ from $\mathbf{x} \in \Omega$ to a small absorbing window $\partial\Omega_a$ in the boundary. The function $\bar{\tau}(\mathbf{x})$ is the solution of the Pontryagin–Andronov–Vitt boundary value problem (1.25),

$$D \left[\Delta \bar{\tau}(\mathbf{x}) - \frac{ze}{kT} \nabla \bar{\tau}(\mathbf{x}) \cdot \nabla \phi(\mathbf{x}) \right] = -1 \quad \text{for } \mathbf{x} \in \Omega \quad (10.34)$$

$$\frac{\partial \bar{\tau}(\mathbf{x})}{\partial n} + \frac{ze}{kT} \bar{\tau}(\mathbf{x}) \frac{\partial \phi(\mathbf{x})}{\partial n} = 0 \quad \text{for } \mathbf{x} \in \partial\Omega_r \quad (10.35)$$

$$\bar{\tau}(\mathbf{x}) = 0 \text{ for } \mathbf{x} \in \partial\Omega_a, \quad (10.36)$$

where $\partial\Omega_r = \partial\Omega - \partial\Omega_a$ is the impermeable part of $\partial\Omega$. We consider the case of a large field $|\nabla\phi(\mathbf{x})| \gg 1$ near the boundary $|\mathbf{x}| = 1$. The profile of $\phi(\mathbf{x})$ is described in Sect. 10.3.2 (see Fig. 10.7). To study the solution of the problem (10.34)–(10.36), a neighborhood of $\partial\Omega_a$ is mapped smoothly into the upper half space with coordinates $\mathbf{X} = (x, y, z)$, where $z = 0$ is the image of the boundary, $\tilde{\tau}(\mathbf{X}) = \bar{\tau}(\mathbf{x})$, and outside a boundary layer near $\partial\Omega_a$

$$V = \frac{\partial\phi(\mathbf{x})}{\partial n} \Big|_{|\mathbf{x}|=1} = \text{const}, \quad \Phi(x, y) = \phi(\mathbf{x}) \Big|_{|\mathbf{x}|=1} = \text{const},$$

so that $\nabla_{x,y}\Phi(x, y) = 0$. The Pontryagin–Andronov–Vitt system (10.34)–(10.36) is converted into

$$\tilde{\tau}_{zz}(\mathbf{X}) - \frac{ze}{kT} \tilde{V} \tilde{\tau}_z(\mathbf{X}) + \Delta_{x,y} \tilde{\tau}(\mathbf{X}) = -\frac{1}{D}.$$

A regular expansion of $\tilde{\tau}(\mathbf{X})$ for large $\tilde{V} = \frac{\partial\phi}{\partial z}$ gives that to leading order $\tilde{\tau}(\mathbf{X})$ is a function of (x, y) and setting $T(x, y) = \tilde{\tau}(x, y, 0)$, we find that

$$\Delta_{x,y} T(x, y) = -\frac{1}{D}. \quad (10.37)$$

Thus the mean first passage time from $\mathbf{x} \in \Omega$ to $\partial\Omega_a$ is the sum of the mean first passage time from \mathbf{x} to $\partial\Omega$ and the mean first passage time to $\partial\Omega_a$ on the surface $\partial\Omega$. The mean first passage time to $\partial\Omega$ is negligible relative to that to $\partial\Omega_a$. This approximation means that to reach $\partial\Omega_a$ in a highly charged ball a charge is first transported by the field to the reflecting part $\partial\Omega_r$ of the sphere with overwhelming probability and then it finds $\partial\Omega_a$ by surface diffusion. Note that ions diffuse near the surface, not on it, so the diffusion coefficient is still that in the bulk and not the Saffman–Delbrück surface coefficient [Saffman and Delbrück (1975)].

10.5 Flow Through a Narrow Window at High Charge

A second consequence of the charge distribution is the control of flux by geometry. This sheds new light on the way voltage and current can be controlled in cellular microdomains, such as dendritic spines. The Poisson–Nernst–Planck model discussed above leads to new predictions concerning the electric current in a dendritic spine, which can be regulated even when voltage remains constant. Thus, we focus here on the spine-head geometry. The solution $T(x, y)$ of (10.37) is the mean first passage time of a Brownian motion on a sphere of radius R to an absorbing circle of small radius $a = R \sin \frac{\delta}{2}$, centered at the north-south axis near the south pole (see

(7.35)). It is given as (see Annotations 10.8 below)

$$T(x, y) = \frac{2R^2}{D} \log \frac{\sin \frac{\theta}{2}}{\sin \frac{\delta}{2}}, \quad (10.38)$$

where D is the diffusion coefficient and θ is the angle between x and the north pole. Thus

$$\bar{\tau}(x) = T(x, y). \quad (10.39)$$

The mean first passage time, averaged over the sphere with respect to a uniform distribution of x , is given by

$$\bar{\tau} = 2R^2 \left(\log \frac{1}{\delta} + O(1) \right) \text{ for } \delta \ll 1. \quad (10.40)$$

The mean first passage time for N independent charges is $\bar{\tau}_N = \bar{\tau}/N$ for $\delta \ll 1$. It follows that the electrical current through the small window is given by

$$J = \frac{ze}{\bar{\tau}_N} = \frac{QD}{2R^2 \left(\log \frac{R}{a} + O(1) \right)} \text{ for } a \ll R. \quad (10.41)$$

The ball represents here the dendritic spine-head and J is the current through the neck. Thus, once a current flows into a dielectric ball such as a spine-head, the excess of charges Q is first pushed toward the boundary, before diffusing to the entrance of the spine neck (small disk of size a). This result shows that the current J in a spine-head is governed by the spine geometry (formula (10.41)) and a key parameter is the radius a of the neck.

When there are no leaks and charge can escape the spine-head only through the absorbing end of the cylindrical neck, the same current that exits the spine-head and enters the cylinder at the window (spine neck) ends up at a bigger cylinder (the dendritic shaft). In this geometry the spine neck length does not affect or modulate the current.

10.6 Current in a Voltage-Clamped Dendritic Spine

A voltage-clamp is a condition under which the voltage is maintained constant. Some dendritic spines are synaptically interconnected, which is essential for neuronal communication. Although their functions are still unclear, they are involved in regulating synaptic transmission and plasticity (see Annotations 10.8). Most of the excitatory

connections occur not on the dendrite, but rather on spines and the reason for this is also unclear.

The spine shape, of a head connected to the dendritic shaft by a narrow cylinder, is quite intriguing. The analysis of the present model reveals that this geometry plays a key role: the model predicts that the spine-head geometry determines the voltage drop across the spine, while the current is determined by the two-dimensional diffusion of ions near the boundary surface and, specifically, by the mean time for the Brownian motion to find the entrance to the neck, as described in the previous chapters. In the neck, under voltage-clamp conditions, when a constant voltage drop between the head and the neck is maintained, the voltage-current relation follows Kirchhoff's resistance law. Thus the spine geometry defines both the capacitance and resistance in geometrical terms, a vision that complements previous studies (see Annotations 10.8).

Determining the voltage drop between the membrane of the spine-head and the dendrite, when a current is flowing from the head to the dendrite, remains a challenge, because cable theory cannot be applied in a system that cannot be approximated by a cable. The general scheme for modeling electro-diffusion in the spine is the Poisson–Nernst–Planck model in the head and a one-dimensional conduction of ions in the neck. The neck is considered to be an ionic conductor. Thus the steady-state Poisson–Nernst–Planck equations have to be solved in the sphere with boundary conditions implied by the compatibility condition and the flux through the neck is determined by the mean first passage time of ions from the head to the neck, as discussed above.

In the case of high charge Q the potential turns out to be practically flat throughout the ball with a sharp boundary layer with a large negative slope at the boundary. Thus, as a charge diffuses it is pushed strongly toward the membrane, so ionic motion is practically confined to motion on a surface. Due to spherical symmetry, the potential is constant on the boundary, so ionic motion is practically Brownian on a sphere. At high charge, ions interact in the bulk through the ambient potential that is determined from Poisson's equation in the ball. Therefore, neglecting memory effects, their motion can be approximated as free diffusion. The mean first passage time of an ion to the small opening of the neck on the surface, $\bar{\tau}$, is determined from the two-dimensional narrow escape time theory (see Chap. 7). Because the flux carried by a single ion is $q/\bar{\tau}$, where q is the ionic charge, the number of ions in the spine-head is $N = Q/q$ and the mean first passage time $\bar{\tau}_N$ of any of the N ions is given by $\bar{\tau}_N = \bar{\tau}/N$, hence the current through the neck is $I = Q/\bar{\tau}$, and due to charge conservation, it is independent of the length of the neck. If we consider the neck to be a parallel-plate capacitor carrying a steady current I , then the voltage drop across the neck is simply $V = I/G$, where G is the conductance of the neck (the reciprocal of resistance), given by

$$G = \frac{q^2 n D}{k T L^2},$$

where k is Boltzmann's constant, T is absolute temperature, L is the length of the conductor, n is the number of ions in the neck, q is the charge of an ion, and D is

the diffusion coefficient of the solution in the neck. This model is valid as long as the voltage is maintained in the spine-head, which is not usually the case. In general, resolving the $I - V$ conversion in a spine requires solving the full PNP equations within the specific geometry.

In the transient regime, the change in voltage drop between the spine-head and the dendritic shaft requires the solution of the time-dependent Poisson–Nernst–Planck equations. Another open question is to study the influence of the spine-head geometry on the distribution of charges. Computing the distribution of charges and the associated field in non-convex geometry is certainly the most challenging.

10.6.1 Appendix 1: Reverse Liouville–Gelfand–Bratú Equation

In this appendix, the Liouville equation (10.13) is solved analytically in one and two dimensions, and in the second part, the numerical method for computing the solution in three dimensions is described. Liouville's equation in the interval $[0, 1]$ is

$$-u''_\lambda(r) = \lambda \frac{e^{-u_\lambda(r)}}{\int_0^1 e^{-u_\lambda(r)} dr} \quad (10.42)$$

with initial conditions

$$u_\lambda(0) = 0, \quad u'_\lambda(0) = 0. \quad (10.43)$$

Integration and the initial conditions give

$$u'^2_\lambda(r) = \frac{2\lambda}{I_\lambda} [e^{-u_\lambda(r)} - 1], \quad (10.44)$$

where

$$I_\lambda = \int_0^1 e^{-u_\lambda(r)} dr. \quad (10.45)$$

A second integration gives

$$u_\lambda(r) = \log \cos^2 \sqrt{\frac{\lambda}{2I_\lambda}} r, \quad (10.46)$$

so

$$I_\lambda = \int_0^1 e^{-u_\lambda(r)} dr = \int_0^1 \frac{dr}{\cos^2 \sqrt{\frac{\lambda}{2I_\lambda}} r} = \frac{1}{\sqrt{\frac{\lambda}{2I_\lambda}}} \tan \sqrt{\frac{\lambda}{2I_\lambda}}. \quad (10.47)$$

Thus $I_\lambda > 0$ is the solution of the implicit equation

$$I_\lambda = \frac{2}{\lambda} \tan^2 \sqrt{\frac{\lambda}{2I_\lambda}}. \quad (10.48)$$

The graph of λ/I_λ versus λ is shown in Fig. 10.4. We have the limit $\lim_{\lambda \rightarrow \infty} \lambda/I_\lambda = \pi^2/2$, and specifically, $y_\lambda = \sqrt{\lambda/2I_\lambda} = \pi/2 - \pi^2/\lambda^2 + o(1/\lambda^2)$. The solution (10.46) is shown in Fig. 10.4 and is regular in the entire interval $0 \geq r < 1$ for all values of λ . The drop between the extreme points of the interval is

$$u_\lambda(1) - u_\lambda(0) = \log \cos^2 \sqrt{\frac{\lambda}{2I_\lambda}} \quad (10.49)$$

and becomes infinite as the total charge increases indefinitely. The two-dimensional case can be transformed into the one-dimensional case by the change of variables (see Annotations 10.8)

$$r = e^{-t}, \quad \tilde{u}(t) = u_\lambda(r) - 2t,$$

which reduces (10.13) to

$$-\tilde{u}_{tt}(t) = \frac{\lambda}{I_\lambda} e^{-\tilde{u}(t)+2t}. \quad (10.50)$$

Here $I_\lambda = 2\pi \int_0^1 e^{-u_\lambda(r)} r dr$ and $w(t) = \tilde{u}(t) + 2t$ satisfies the equation

$$-w_{tt}(t) = \lambda \frac{e^{-w(t)}}{I_\lambda}. \quad (10.51)$$

The initial conditions are now transformed to asymptotic conditions at infinity

$$\lim_{t \rightarrow \infty} (w(t) - 2t) = 0, \quad \lim_{t \rightarrow \infty} (\dot{w}(t) - 2) e^t = 0.$$

Integration of (10.51) gives

$$\frac{\dot{w}^2(t)}{2} = \lambda \frac{e^{-w(t)}}{I_\lambda} + 2, \quad (10.52)$$

whose solution is

$$w(t) = -\log \left(\frac{8}{(\lambda e^{2C+2t} - 1)^2} \right) - 2C - 2t. \quad (10.53)$$

The solution that satisfies the initial condition is

$$u_\lambda(r) = \log \left(1 - \frac{\lambda}{8I_\lambda} r^2 \right)^2. \quad (10.54)$$

Next,

$$I_\lambda = \int_0^1 e^{-u_\lambda(r)} 2\pi r dr = \int_0^1 \frac{2\pi r dr}{\left(1 - \frac{\lambda}{8I_\lambda} r^2 \right)^2} = \frac{8\pi}{8 - \lambda/I_\lambda} \quad (10.55)$$

and

$$I_\lambda = \pi + \frac{1}{8}\lambda, \quad \lim_{\lambda \rightarrow \infty} \frac{\lambda}{I_\lambda} = 8.$$

The plot of $\frac{\lambda}{I_\lambda}$ vs λ is shown in Fig. 10.4 and that of $|u_\lambda(1) - u_\lambda(0)|$ in Fig. 10.6. Thus the explicit solution is

$$\begin{aligned} u_\lambda(r) &= \log \left(1 - \frac{\lambda}{\lambda + 8\pi} r^2 \right)^2 \\ |u_\lambda(1) - u_\lambda(0)| &= 2 \log \left(1 - \frac{\lambda}{\lambda + 8\pi} \right). \end{aligned}$$

It follows that $u_\lambda(r)$ decreases smoothly and in the limit $\lambda \rightarrow \infty$, the solution blows up over the entire boundary.

10.6.2 Small λ Expansion of $u_\lambda(x)$

A regular expansion of the solution of (10.15) in powers of λ ,

$$u_\lambda(x) = u_0(x) + u_1(x)\lambda + u_2(x)\lambda^2 + o(\lambda^2), \quad (10.56)$$

gives that $u_0(x) = 0$ and that $u_1(x)$ is the solution of

$$-\Delta u_1(x) = \frac{1}{|\Omega|} \text{ for } x \in \Omega, \quad \frac{\partial u_1}{\partial n} = -\frac{1}{|\partial\Omega|} \text{ for } x \in \partial\Omega.$$

For $R = 1$,

$$u_1(r) = -\frac{r^2}{8\pi}, \quad (10.57)$$

which satisfies the initial condition $u_1(0) = 0$. It follows that $u_1(r) \leq 0$. Thus,

$$u_\lambda(r) = -\frac{\lambda r^2}{8\pi} + O(\lambda^2).$$

The second-order term $u_2(x)$ is the solution of

$$-\Delta u_2 = -\frac{u_1}{|\Omega|} \text{ for } x \in \Omega,$$

with $u_2(0) = 0$ and $u'_2(0) = 0$. For $R = 1$,

$$u_2(r) = -\frac{3r^4}{640\pi^2}, \quad (10.58)$$

hence

$$u_\lambda(r) = -\frac{\lambda r^2}{8\pi} - \frac{3\lambda^2 r^4}{640\pi^2} + O(\lambda^3) \text{ for } \lambda \ll 1.$$

10.6.3 Numerical Scheme for the Solution of (10.13)

The boundary value problem

$$\begin{aligned} v''(r) - \frac{2}{r}v'(r) &= -\lambda \exp\{-v(r)\} \text{ for } 0 \leq r \leq 1 \\ v'(1) &= -\frac{\lambda}{|S_3|}, \quad v'(0) = 0, \end{aligned} \quad (10.59)$$

where $S_3 = \partial B_3$ is the surface of the unit ball $B(3)$ solved as a Neumann problem. The relation between solutions $u_\lambda(r)$ and $v(r)$ is expressed by the shift

$$v(r) = u_\lambda(r) + \beta, \quad (10.60)$$

where the constant β is computed from the compatibility and the boundary condition of (10.59),

$$\lambda = -\oint_{\partial B_3} \frac{\partial v(x)}{\partial n} dS = -\lambda \int_{B_3} \exp\{-v(x)\} dx,$$

leading to

$$\int_{B_3} \exp\{-v(\mathbf{x})\} d\mathbf{x} = 1. \quad (10.61)$$

The relations (10.60) and (10.61) give that

$$\beta = \log I_\lambda,$$

where I_λ is defined for the three-dimensional case as $I_\lambda = \int_0^1 e^{-u_\lambda(r)} 4\pi r^2 dr$. The condition $u_\lambda(0) = 0$ in (10.13) links the value of β to the solution $v(r)$ by

$$\beta = v(0).$$

Thus the solution $u_\lambda(r)$ can be computed from $v(r)$ as

$$u(r) = v(r) - v(0).$$

The shift in relation (10.60) permits us to express the solution of a nonlinear elliptic parabolic partial differential equation, containing the integral of the solution over the domain, in terms of the solution of the Neumann problem (10.59).

The solution of (10.59) used here was constructed numerically by the one-dimensional finite elements method in both Matlab and Comsol for comparison. For the application to the different physical scenarios of Poisson–Nernst–Planck in a ball, an adaptative meshing was used to account for the stiff tangent in the region close to the boundary $r = R$. For example, for $R = 1\mu\text{m}$ the maximal element size taken was $5 \cdot 10^{-4}\mu\text{m}$. All numerical results in the ball B_3 (Figs. 10.3, 10.4, 10.6, and 10.7) were obtained by the scheme described here.

Table 10.1 Parameters

Parameter	Description	Value
z	Valence of ion	$z = 1$ (for sodium)
D	Diffusion coefficient	$D = 200\mu\text{m}^2/\text{sec}$
I_c	Injected current	$I \in [2; 30]\text{pA}$
I	Average Injected current	$I = 2.5\text{pA}$
Ω	Spine head	(volume $ \Omega = 1\mu\text{m}^3$)
a	Radius of spine neck	(typical) $a = 0.1\mu\text{m}$
L	Length of spine	(typical) $L = 1\mu\text{m}$
T	Temperature	$T = 300K$
E	Energy	$kT = 2.58 \times 10^{-2}\text{eV}$
e	Electron charge	$e = 1.6 \times 10^{-19}\text{C}$
ε	Dielectric constant	$\varepsilon = 80$

10.7 Steady Solution in a Ball with a Cusp-Shaped Funnel

Local boundary curvature is a key geometrical feature that controls charge distribution in the domain. Specifically, we study the effect of a narrow funnel attached to a sphere. In various media, such as air (e.g., the lightning rod), the manifestation of this effect is observed in Lebesgue's thorn, which is an inverted cusp singularity of the boundary, for which the solution of Laplace's equation blows-up inside the domain [Courant and Hilbert (1989), p. 304].

In the steady state, the particle density is given by

$$\rho(\mathbf{x}) = N \frac{\exp\left\{-\frac{ze\phi(\mathbf{x})}{kT}\right\}}{\int_{\Omega} \exp\left\{-\frac{ze\phi(\mathbf{x})}{kT}\right\} d\mathbf{x}}, \quad (10.62)$$

hence (10.5) gives Poisson equation

$$\Delta\phi(\mathbf{x}) = -\frac{zeN \exp\left\{-\frac{ze\phi(\mathbf{x})}{kT}\right\}}{\varepsilon\varepsilon_0 \int_{\Omega} \exp\left\{-\frac{ze\phi(\mathbf{x})}{kT}\right\} d\mathbf{x}} \quad (10.63)$$

and (10.6) gives the boundary condition

$$\frac{\partial\phi(\mathbf{x})}{\partial n} = -\frac{Q}{\varepsilon\varepsilon_0|\partial\Omega|}, \quad (10.64)$$

for $|\mathbf{x}| = R$, which is the compatibility condition, obtained by integrating Poisson's equation (10.5) over Ω . Changing variables to

$$u(\mathbf{x}) = \frac{ze\phi(\mathbf{x})}{kT}, \quad \lambda = \frac{(ze)^2 N}{\varepsilon\varepsilon_0 k T}, \quad (10.65)$$

Poisson's equation (10.63) becomes

$$\Delta u(\mathbf{x}) = -\frac{\lambda \exp\{-u(\mathbf{x})\}}{\int_{\Omega} \exp\{-u(\mathbf{x})\} d\mathbf{x}} \quad (10.66)$$

and the boundary condition (10.64) becomes

$$\frac{\partial u(\mathbf{x})}{\partial n} = -\frac{\lambda}{|\partial\Omega|} \text{ for } \mathbf{x} \in \partial\Omega. \quad (10.67)$$

The translation $\tilde{u} = u + \log \left(\lambda / \int_{\Omega} \exp\{v(x)\} dx \right)$ converts (10.66) into

$$\begin{aligned} -\Delta \tilde{u}(x) &= \exp\{-\tilde{u}(x)\} \text{ for } x \in \Omega \\ \frac{\partial \tilde{u}(x)}{\partial n} &= -\frac{\lambda}{|\partial\Omega|} \text{ for } x \in \partial\Omega. \end{aligned} \quad (10.68)$$

We consider a dimensionless planar domain Ω with a cusp-shaped funnel formed by two bounding circles A and B of dimensionless radii 1 (see Fig. 10.8 (left)). The opening of the funnel is $\varepsilon \ll 1$. We construct an asymptotic solution in this limit to the nonlinear boundary value problem (boundary value problem) (10.68) by first mapping the domain Ω conformally with the Möbius transformation of the two osculating circles A and B into concentric circles (see Fig. 10.8 (right)). To this end, we move the origin of the complex plane to the center of the osculating circle B and set

$$w = w(z) = \frac{z - \alpha}{1 - \alpha z}, \quad (10.69)$$

where

$$\alpha = -1 - \sqrt{\varepsilon} + O(\varepsilon). \quad (10.70)$$

The Möbius transformation (7.70) maps B into itself and Ω is mapped onto the domain $\Omega_w = w(\Omega)$ in Fig. 10.8 (right). The straits in Fig. 10.8 (left) are mapped onto the ring enclosed between the like-style arcs and the large disk is mapped onto the small red disk in Fig. 10.8 (right). The radius of the small disk and the elevation of its center above the real axis are $O(\sqrt{\varepsilon})$. The short black segment AB of length ε in Fig. 10.8 (left) is mapped onto the segment AB of length $2\sqrt{\varepsilon} + O(\varepsilon)$ in Fig. 10.8 (right). The mapping (10.69) (see Annotations 10.8) transforms the Poisson–Nernst–Planck equations as well and thus leads to a new non-linear effect.

Setting $u(z) = v(w)$ converts (10.66) to

$$\begin{aligned} \Delta_w v(w) &= -\frac{\exp\{-v(w)\}}{|w'(z)|^2} \\ &= -\frac{(4\varepsilon + O(\varepsilon^{3/2}))}{|w(1 - \sqrt{\varepsilon}) - 1 + O(\varepsilon)|^4} \exp\{-v(w)\} \quad \text{for } w \in \Omega_w. \end{aligned} \quad (10.71)$$

The boundary segment AB at the end of the cusp-shaped funnel in Fig. 10.8 (left) is denoted $\partial\Omega_{w,a}$. To determine the boundary conditions, we use the change of coordinates $w = Re^{i\theta} = X + iY$. At the end of the funnel, where $R \simeq 1$, we get

$$\frac{\partial u(z)}{\partial n_z} = -\frac{\partial v(w)}{\partial \theta} \Big|_{w=-1} \frac{\partial \theta}{\partial Y}, \quad (10.72)$$

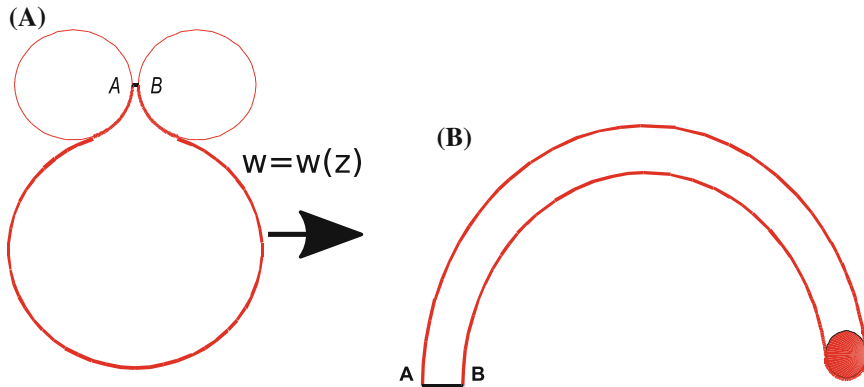


Fig. 10.8 Image $\Omega_w = w(\Omega)$ of the domain Ω (left) under the conformal mapping (7.70). The neck (left) is mapped onto the semi-annulus enclosed between the like-style arcs and the large disk in Ω is mapped onto the small red disk. The short black segment AB (left) (of length ε) is mapped onto the thick black segment AB (of length $2\sqrt{\varepsilon} + O(\varepsilon)$)

where

$$ie^{i\theta} \frac{\partial \theta}{\partial Y} = w'(z) = \frac{1 - \alpha^2}{(1 - \alpha z)^2}. \quad (10.73)$$

For $\theta = \pi$ (for $z = -1$), we obtain $\partial\theta/\partial Y = -2/\sqrt{\varepsilon}$ and the boundary condition at $\partial\Omega_{w,a}$ is

$$\frac{\partial v(w)}{\partial n} = -\frac{\lambda\sqrt{\varepsilon}}{2|\partial\Omega|} \text{ for } w \in \partial\Omega_{w,a}. \quad (10.74)$$

10.7.1 Reduced Equations in an Uncharged Cusp-Shaped Funnel

Approximating the banana-shaped domain Ω_w by a one-dimensional circular arc, we use a one-dimensional approximation of the solution in Ω_w . This approximation assumes that there are no non-neutralized charges on the surface of the cusp (Fig. 10.10A). The boundary condition for the approximate one-dimensional solution of (10.71) is zero at angle $\theta_{Lim} = c\sqrt{\varepsilon}$, where c is a constant (for details, see Sect. 8.4) and represents the solution inside the disk in Fig. 10.8 (left), away from the cusp. Thus, (10.71) in the conformal image Ω_w becomes the boundary value problem

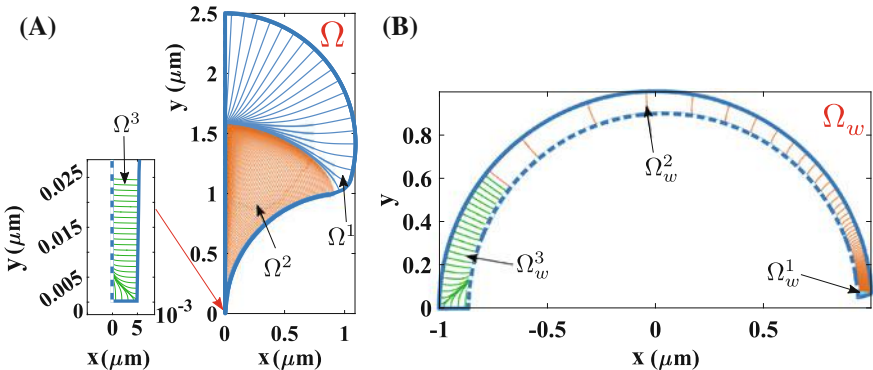


Fig. 10.9 Influence of the cusp on the field lines (orthogonal to the level lines). The field line inside the original **A.** and the mapped **B.** domain computed numerically from equation (10.68). The blue lines originate from the bulk, while the orange starts in the cusp. The domain Ω_w is subdivided into three regions: the region Ω_w^1 inside the funnel, the region Ω_w^2 connecting the end of the funnel to the bulk Ω_w^3

$$v'' + \frac{4\varepsilon}{|e^{i\theta} - 1 - e^{i\theta}\sqrt{\varepsilon}|^4} \exp\{-v(e^{i\theta})\} = 0 \quad (10.75)$$

$$v'(c\sqrt{\varepsilon}) = 0 \quad (10.76)$$

$$v'(\pi) = -\frac{\lambda\sqrt{\varepsilon}}{2|\partial\Omega|}.$$

The solution of (10.75) is shown in Fig. 10.10B-C in the two domains, Ω and Ω_w . To estimate the difference of potentials between the north pole N and the end of the funnel C ,

$$\tilde{\Delta}u = u(N) - u(C) = v(c\sqrt{\varepsilon}) - v(\pi), \quad (10.77)$$

we construct an asymptotic approximation to the solution of (10.76) in the limits $\varepsilon \rightarrow 0$ and $\lambda \rightarrow \infty$. We first construct the outer-solution in the form of a series in powers of ε , which is an approximation valid away from the boundary. In the limit of small ε , the first term in the series vanishes, exponential terms drop out, and the second-order term is

$$y_{\text{outer}}(\theta) = M\theta + M', \quad (10.78)$$

where M and M' are as yet undetermined constants. The outer solution cannot satisfy all boundary conditions, so a boundary layer correction is needed at the reflecting boundary at $\eta = c\sqrt{\varepsilon}$. Thus, we set $\eta = \sqrt{\varepsilon}\xi$ and expand

$$\frac{\varepsilon^2}{|e^{i\eta} - 1 - e^{i\eta}\sqrt{\varepsilon}|^4} = \frac{1}{(1 + \xi^2)^2} + O(\sqrt{\varepsilon}).$$

Writing the boundary layer solution as $y_{\text{bl}}(\eta) = Y(\xi)$, we obtain to leading order the boundary layer equation

$$Y''(\xi) + \frac{1}{4(1+\xi^2)^2} \exp\{-Y(\xi)\} = 0, \quad (10.79)$$

with $Y'(c) = 0$. The solution is decaying for large ξ and develops a singularity at finite ξ . However, a Taylor expansion near $\xi = 0$,

$$Y(\xi) = A + B_2\xi^2 + B_4\xi^4 + \dots, \quad (10.80)$$

gives in (10.79)

$$B_2 = -\frac{e^{-A}}{8}. \quad (10.81)$$

In general, the coefficients satisfy $B_k = O(e^{-A})$. For small ξ , we obtain the approximate solution of (10.79) by neglecting the ξ -dependence in the exponential. The approximate equation is

$$Y''(\xi) + \frac{e^{-A}}{4(1+\xi^2)^2} = 0 \quad (10.82)$$

and the solution is defined up to an additive constant. Setting $Y_{\text{appr}}(0) = 0$, which does not affect the potential difference, we find that

$$Y_{\text{appr}}(\xi) = -\frac{1}{8}\xi e^{-A} \arctan \xi. \quad (10.83)$$

It follows that the boundary layer solution at $c\sqrt{\varepsilon}$ is

$$y_{\text{bl}}(\theta) = A - \frac{\theta}{8\sqrt{\varepsilon}} e^{-A} \arctan\left(\frac{\theta}{\sqrt{\varepsilon}}\right). \quad (10.84)$$

The boundary layer near π is associated with the blow-up of the exponential term. An approximation of the solution can be obtained by freezing the power-law term in (10.76), for which the equation is for a generic parameter $b > 0$,

$$\begin{aligned} \frac{d^2}{d\theta^2} v + b \exp(-v) &= 0 \\ \frac{dv(0)}{d\theta} &= v(0) = 0. \end{aligned}$$

The solution is

$$v_b(\theta) = \log \left(\cos^2 \left(\frac{b}{2} \theta \right) \right). \quad (10.85)$$

Putting the outer and boundary layer solutions together gives the uniform asymptotic approximation

$$y_{\text{unif}}(\theta) = A - \frac{\theta}{8\sqrt{\varepsilon}} e^{-A} \arctan \left(\frac{\theta}{\sqrt{\varepsilon}} \right) + \log \left(\cos^2 \left(\frac{b}{2} \theta \right) \right), \quad (10.86)$$

where the parameters A and b are as yet undetermined constants. The condition at $c\sqrt{\varepsilon} \approx 0$ is satisfied, because

$$y'_{\text{unif}}(0) = 0.$$

The condition at $\theta = \pi$ gives that

$$y'_{\text{unif}}(\pi) = -\frac{\pi e^{-A}}{16\sqrt{\varepsilon}} - b \tan \left(\frac{b}{2} \pi \right) = -\frac{\lambda \sqrt{\varepsilon}}{2|\partial\Omega|}.$$

The compatibility condition for (10.68),

$$\lambda = \int_{\Omega} \exp\{-\tilde{u}(\mathbf{x})\} dS_{\mathbf{x}}, \quad (10.87)$$

gives in the conformal domain that

$$\lambda = \int_{w(\Omega)} \exp\{-\tilde{v}(w)\} \frac{dw}{|\phi'(\phi^{-1}(w))|} = 8\sqrt{\varepsilon} \int_{c\sqrt{\varepsilon}}^{\pi} \frac{\exp(-v(\theta))}{|e^{i\theta}(1-\sqrt{\varepsilon})-1|^4} d\theta. \quad (10.88)$$

Using the uniform solution (10.86) in the compatibility condition (10.88), we obtain the second condition

$$\begin{aligned} q\lambda &= 8\sqrt{\varepsilon} e^{-A} \int_{c\sqrt{\varepsilon}}^{\pi} \frac{1}{\cos^2 \left(\frac{b}{2} \theta \right)} \frac{\exp \left(e^{-A} \frac{\theta}{8\sqrt{\varepsilon}} \arctan \left(\frac{\theta}{\sqrt{\varepsilon}} \right) \right)}{|e^{i\theta}(1-\sqrt{\varepsilon})-1|^4} d\theta \\ &\approx \frac{8e^{-A}}{\varepsilon} \int_0^{\pi/\sqrt{\varepsilon}} \frac{1}{\cos^2 \left(\frac{b}{2}\sqrt{\varepsilon}\xi \right)} \frac{\exp \left(\frac{e^{-A}}{8} \xi \arctan \xi \right)}{|1+\xi^2|^2} d\xi, \end{aligned} \quad (10.89)$$

where we used the change of variable $\theta = \sqrt{\varepsilon}\xi$. Integrating by parts, we get

$$\lambda \approx \frac{8e^{-A}}{\varepsilon} \left(\frac{2}{b\sqrt{\varepsilon}} \tan\left(\frac{b}{2}\pi\right) \frac{\exp\left(\frac{e^{-A}}{8}\frac{\pi}{\sqrt{\varepsilon}}\frac{\pi}{2}\right)}{\left|1 + \left(\frac{\pi}{\sqrt{\varepsilon}}\right)^2\right|^2} - \int_0^{\pi/\sqrt{\varepsilon}} \frac{2}{b\sqrt{\varepsilon}} \tan\left(\frac{b}{2}\theta\right) \Psi(\theta) d\theta \right), \quad (10.90)$$

where

$$\Psi(\xi) = \frac{d}{d\xi} \left(\frac{\exp\left\{\frac{e^{-A}}{8}\xi \arctan \xi\right\}}{|1 + \xi^2|^2} \right). \quad (10.91)$$

Thus, it remains to solve the asymptotic equation

$$\lambda \approx 8e^{-A}\varepsilon^{1/2} \left[\frac{2}{b\pi^4} \tan\left(\frac{\pi b}{2}\right) \exp\left(\frac{\pi^2 e^{-A}}{16\sqrt{\varepsilon}}\right) + O\left(\log \left|\cos\left(\frac{\pi b}{2}\right)\right|\right) \right] \quad (10.92)$$

for A and b in the limit $\varepsilon \rightarrow 0$. We consider the limiting case where

$$\frac{e^{-A}}{\sqrt{\varepsilon}} = O(1) = C \text{ for } \lambda \rightarrow \infty, \quad (10.93)$$

for which condition (10.87) can be simplified and gives to leading order

$$b \tan\left(\frac{\pi b}{2}\right) = \frac{\lambda\sqrt{\varepsilon}}{2|\partial\Omega|}; \quad (10.94)$$

that is,

$$b \approx 1 - \frac{4}{\pi} \frac{|\partial\Omega|}{\lambda\sqrt{\varepsilon}}, \quad \tan\left(\frac{b}{2}\pi\right) \approx \frac{\lambda\sqrt{\varepsilon}}{2|\partial\Omega|}.$$

With condition (10.92), we get

$$\lambda \approx 8e^{-A}\varepsilon^{1/2} \left[\frac{2}{\pi^4} \frac{\lambda\sqrt{\varepsilon}}{2|\partial\Omega|} \exp\left\{\frac{\pi^2 e^{-A}}{16\sqrt{\varepsilon}}\right\} + O\left(\log \left|\cos\left(\frac{\pi b}{2}\right)\right|\right) \right]. \quad (10.95)$$

To leading order in large C , we obtain

$$\frac{\pi^4 |\partial\Omega|}{8\varepsilon^{3/2}} = C \exp\left(\frac{C\pi^2}{16}\right). \quad (10.96)$$

The solution is expressed in terms of the Lambert-W function,

$$\frac{C\pi^2}{16} = W\left(\frac{\pi^6|\partial\Omega|}{2^7\varepsilon^{3/2}}\right), \quad (10.97)$$

and for small ε , using the asymptotics of the Lambert function, as

$$\frac{C\pi^2}{16} = \log\left(\frac{\pi^6|\partial\Omega|}{2^7\varepsilon^{3/2}}\right) - \log\left[\log\left(\frac{\pi^6|\partial\Omega|}{2^7\varepsilon^{3/2}}\right)\right] + o(1), \quad (10.98)$$

so finally,

$$\begin{aligned} \frac{e^{-A}}{\sqrt{\varepsilon}} &= C \approx \frac{16}{\pi^2} \log\left(\frac{\pi^6|\partial\Omega|}{2^7\varepsilon^{3/2}}\right), \\ A &= \log\left(\frac{1}{\sqrt{\varepsilon}}\right) - \log\left[\frac{16}{\pi^2} \log\left(\frac{\pi^6|\partial\Omega|}{2^7\varepsilon^{3/2}}\right)\right]. \end{aligned}$$

It follows that a uniform asymptotic approximation (10.86) in the limits $\lambda \rightarrow \infty$ and $\varepsilon \rightarrow 0$ is given by

$$\begin{aligned} y_{\text{unif}}(\theta) &= \log\left(\frac{1}{\sqrt{\varepsilon}}\right) - \log\left[\frac{16}{\pi^2} \log\left(\frac{\pi^6|\partial\Omega|}{2^7\varepsilon^{3/2}}\right)\right] \\ &\quad - 2\theta \frac{1}{\pi^2} \log\left(\frac{\pi^6|\partial\Omega|}{2^7\varepsilon^{3/2}}\right) \arctan\left(\frac{\theta}{\sqrt{\varepsilon}}\right) + \log\left[\cos^2\left(\frac{1 - \frac{4}{\pi}\frac{|\partial\Omega|}{\lambda\sqrt{\varepsilon}}}{2}\right)\theta\right]. \end{aligned} \quad (10.99)$$

The uniform solution (10.99) is plotted for different values of ε and λ in Fig. 10.10 against the numerical simulations of (10.75), with the boundary conditions $v'(c\sqrt{\varepsilon}) = v'(0) = 0$. The simulations are run with COMSOL. We find that the asymptotic expansion is particularly good in the limit $\varepsilon \rightarrow 0$ and $\lambda \rightarrow \infty$ (Fig. 10.10A-D). However, for $\lambda = O(1)$ the log-term approximation in (10.99) is non-monotonic in θ . Finally, to further validate the uniform asymptotic expansion, we compared the numerical solutions of the full equation (10.77) in the initial domain Ω with the reduced Poisson–Nernst–Planck equation (10.68) with zero Neumann boundary conditions, except at the end of the funnel for the mapped domain Ω_w . The result is shown in Fig. 10.10A-C, showing good agreement between the one-dimensional Poisson–Nernst–Planck approximation in Ω_w and the numerical solution of the full equation. To compare the voltage at the north and south poles (at the end of the funnel), we use the two-dimensional analytical solution in the entire ball and the numerical solution of (10.68) (Fig. 10.10D). Interestingly, we find that the difference $u_N - u_S$, where u_N is the north pole and u_S is the end of the funnel, has a maximum with respect to λ .

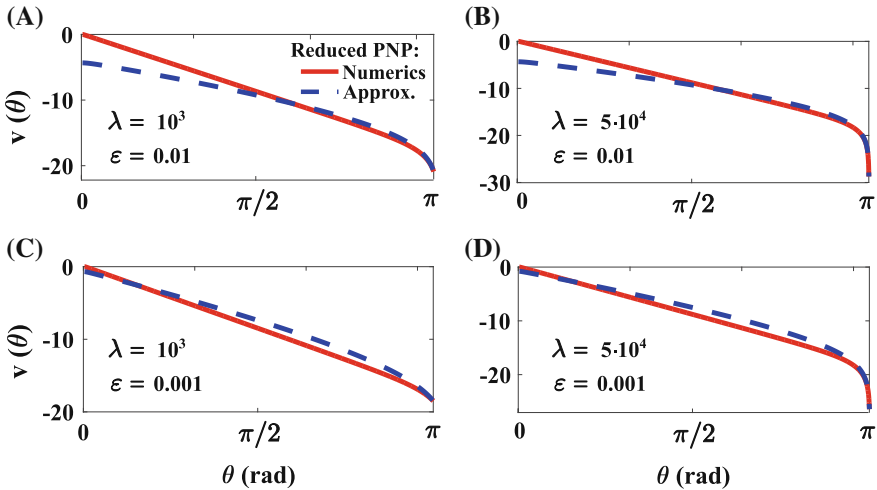


Fig. 10.10 One-dimensional Poisson–Nernst–Planck in the mapped banana-shaped domain. The asymptotic solution $y_{\text{unif}}(\theta)$ of (10.86) (blue dashed lines) is compared to the numerical solution of (10.75) (red line). The four panels **A–B–C–D** are obtained for different pairs of parameters (λ, ε)

10.7.2 Asymptotics of Voltage Between Funnel and Center

We can now compute the potential drop in (10.77) from (10.86). It is given by

$$\begin{aligned} \tilde{\Delta}_{SC}u &= u(S) - u(C) = -v(c\sqrt{\varepsilon}) + v(\pi) \\ &= -\log\left(\frac{\pi^6|\partial\Omega|}{2^7\varepsilon^{3/2}}\right) + 2\log\left(\frac{2|\partial\Omega|}{\lambda\varepsilon^{1/2}}\right) = \log\left(\frac{2^9|\partial\Omega|\sqrt{\varepsilon}}{\pi^6\lambda^2}\right). \end{aligned} \quad (10.100)$$

The potential difference $\tilde{\Delta}_{SC}u$ with respect to λ is shown in Fig. 10.10F (red line).

Next, we compare the potential drop (10.77) with the one between the center and the north pole. Numerical solution of the Poisson–Nernst–Planck equations shows that the voltage and charge distribution in a disk with a funnel do not differ from those of a disk in the upper sphere (Fig. 10.9). This result is compared next to the difference between the north pole and the center evaluated from the exact analytical expression derived for a disk.

The expression for the voltage in the two-dimensional disk of radius R is given by

$$u_{\lambda}^{2D}(x) = \log\left[1 - \frac{\lambda_D}{8\pi + \lambda_D}\left(\frac{r}{R}\right)^2\right]^2,$$

where λ_D is a parameter. We calibrate λ_D so that the solutions of the Poisson–Nernst–Planck equations in a disk with a funnel have the same total charge as a disk. The Neumann boundary conditions for the disk and the funnel are, respectively,

$$\frac{\partial u(\mathbf{x})}{\partial n} = -\frac{\lambda_D}{2\pi R}, \quad \frac{\partial u(\mathbf{x})}{\partial n} = -\frac{\lambda}{|\partial\Omega|}.$$

The calibration is

$$\lambda_D = \lambda \frac{2\pi R}{|\partial\Omega|}. \quad (10.101)$$

We compare in Fig. 10.10D the two-dimensional numerical solution of the Poisson–Nernst–Planck equation (10.68) in the domain Ω (blue line), with the analytical solution (10.101) in a disk with no cusp (dashed red). The numerical solution of the Poisson–Nernst–Planck equation (10.68) is plotted along the main axis $0y$ in the interval $[0, y_0]$ (where the point y_0 is defined by the condition $\nabla u(y_0) = 0$). In the range $[y_0, y_{cusp}]$, where y_{cusp} is the coordinate of the cusp, we compare the solution of (10.68) with the uniform solution y_{unif} of (10.86) in the funnel (dashed green). We conclude that in the cusp, the two-dimensional approximation in a disk is in very good agreement with the numerical solution of Eq. (10.68), confirming that the solution in the bulky head does not influence the one in the cusp (as already shown in Fig. 10.9). This result also confirms the validity of the analytical formula to predict the large λ asymptotics.

For a disk of radius R , the potential drop is given by

$$\tilde{\Delta}_{NC}u = u(N) - u(C) = \log\left(\frac{8\pi}{8\pi + \lambda_D}\right)^2. \quad (10.102)$$

The potential drop $\tilde{\Delta}_{NC}u$ is shown Fig. 10.10E (blue line). The two differences of potential $\tilde{\Delta}_{SC}u$ (10.102) and $\tilde{\Delta}_{NC}u$ (10.100) have the same asymptotic behavior in $\log 1/\lambda^2$ for large λ and the difference $u_N - u_S$ is of order $O(1)$. Two-dimensional numerical simulation shows that it may converge to zero as λ increases (Fig. 10.10F), containing a local maximum for a small value of λ . This maximum cannot be analyzed by the uniform expression (10.86), because it appears outside the domain where expression (10.86) was derived. This result is in agreement with the two-dimensional numerical simulations of (10.68) for the difference between u_N (north pole) and u_S (end of the funnel) (Fig. 10.10F). The potential drop calculated above is non-dimensionalized by the radius of curvatures R at the right and left of the funnel,

$$\varepsilon = \frac{\tilde{\varepsilon}}{R},$$

where $\tilde{\varepsilon}$ is the length of the absorbing arc AB . The non-dimensionalized volume and boundary measure are, respectively (Fig. 10.11),

$$|\Omega| = \frac{|\tilde{\Omega}|}{R^2}, \quad |\partial\Omega| = \frac{|\partial\tilde{\Omega}|}{R}.$$

In dimensional units (10.100) gives the potential drop in the dimensional disk with a funnel as

$$\tilde{\Delta}_{SC} u = u(S) - u(C) = \log \left(\frac{2^9 |\partial\tilde{\Omega}| \sqrt{R^{3/2} \tilde{\varepsilon}}}{\pi^6 \lambda^2} \right). \quad (10.103)$$

10.7.3 Poisson–Nernst–Planck Solutions in a 3D Cusp-Shaped Funnel

The three-dimensional Neumann boundary value problem (BVP) (10.68) in the cylindrical coordinates (r, z, ϕ) (Fig. 10.12A) is invariant along the axis of symmetry, so that $\tilde{u}(x)$ is independent of the angle ϕ in the domain Ω . Equation (10.68) in the domain Ω can be written as

$$\begin{aligned} \frac{\partial^2 u(r, z)}{\partial r^2} + \frac{1}{r} \frac{\partial u(r, z)}{\partial r} + \frac{\partial^2 u(r, z)}{\partial z^2} &= -\exp(-u(r, z)) \\ \frac{\partial u(r, z)}{\partial n} &= -\sigma, \end{aligned} \quad (10.104)$$

where r is the distance to the symmetry axis. The opening at the cusp funnel is a small segment $\overline{AB} = \varepsilon \ll 1$ (green line Fig. 10.8B), so the funnel constitutes a narrow passage. To remove the cusp singularity, we use the transformation to the rotated and translated coordinates, given by $\tilde{r} = r - 1 - \varepsilon/2$ and $\tilde{z} = -z + 1$. Setting $u(r, z) = \tilde{u}(\tilde{r}, \tilde{z})$, Eq. (10.104) becomes

$$\begin{aligned} \frac{\partial^2 \tilde{u}(\tilde{r}, \tilde{z})}{\partial \tilde{r}^2} + \frac{\partial^2 \tilde{u}(\tilde{r}, \tilde{z})}{\partial \tilde{z}^2} + \frac{1}{(\tilde{r} + 1 + \varepsilon/2)} \frac{\partial \tilde{u}(\tilde{r}, \tilde{z})}{\partial \tilde{r}} &= -\exp(-\tilde{u}(\tilde{r}, \tilde{z})) \\ \frac{\partial \tilde{u}(\tilde{r}, \tilde{z})}{\partial \tilde{n}} &= -\sigma. \end{aligned} \quad (10.105)$$

The asymptotic expansion of the solution $\tilde{u}(\tilde{r}, \tilde{z})$ for small ε is constructed as in Sect. 10.7, by mapping the cross section in the (\tilde{r}, \tilde{z}) -plane conformally into its image under the Möbius transformation

$$w(\xi) = \rho e^{i\theta} = \frac{\xi - \alpha}{1 - \alpha\xi}, \quad (10.106)$$

where

$$\alpha = -1 - \sqrt{\varepsilon} + O(\varepsilon), \quad (10.107)$$

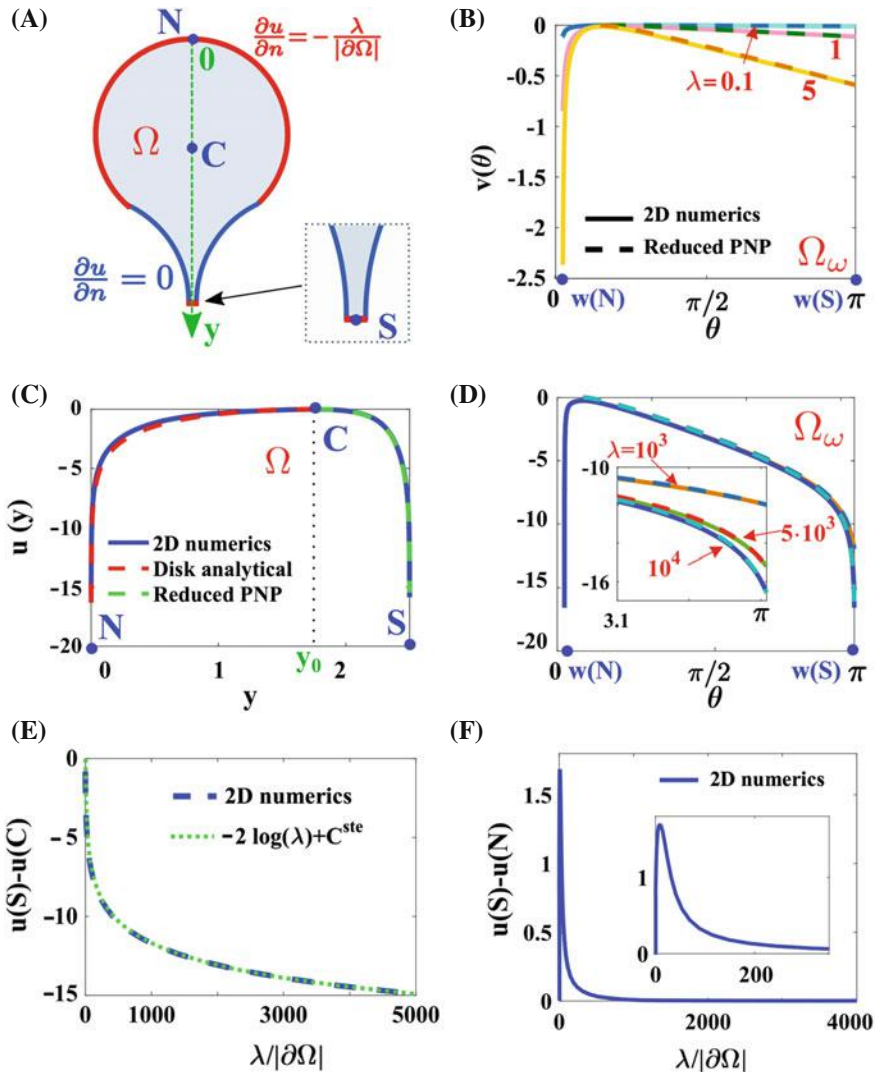


Fig. 10.11 Comparison of the numerical solutions of the full and reduced Poisson–Nernst–Planck equations (10.68) with zero Neumann boundary conditions, except at the end of the funnel. A. Schematic representation of the domain Ω with an uncharged cusp (blue). The letters N , S , and C refer to the north pole, the funnel tip, and the center of mass respectively. B–C Numerical solutions of (10.68) (solid) and the solutions of (10.71) in the funnel (dashed) in the mapped domain Ω_w . The solutions have been obtained for $\varepsilon = 0.01$. D. Comparison of (10.68) (blue) with the numerical solution (10.75) inside the funnel (dashed green) and (10.101) in the bulk (dashed red). E. Solution $u(S) - u(C)$ (dashed blue) obtained numerically from (10.100) and compared to the logarithmic function $-2 \log(\lambda)$ (green dotted). F. Two-dimensional numerical solutions of the difference $|u(N) - u(C)|$ vs λ . The inset in panel F. is a blowup showing a maximum for small λ

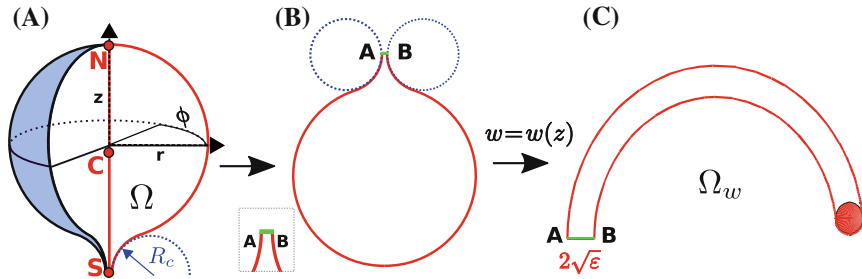


Fig. 10.12 Three-dimensional ball with a cusp-shaped funnel Ω_w , its cross-section and its image under the mapping (10.106). **A.** Domain Ω containing a funnel with curvature radius R_c , the north pole N , the funnel tip S , and the center of mass C . **B-C** The neck (**B**) is mapped onto the semi-annulus enclosed between the like-style arcs. The large disk in Ω is mapped onto the small red disk, while the short green segment AB (left) (of length ε) is mapped onto the thick green segment AB (of length $2\sqrt{\varepsilon} + O(\varepsilon)$)

and $\xi = \tilde{r} + i\tilde{z}$. In the dimensionless domain Ω , the parameter ε is also dimensionless and we define $\tilde{\varepsilon} = R_c\varepsilon$. The Möbius transformation maps the two osculating circles A and B (dashed blue) into concentric circles (see Fig. 10.8B-C). The Möbius transformation (10.106) maps the right circle B (dashed blue) into itself and Ω is mapped onto the banana-shaped domain $\Omega_w = w(\Omega)$ as shown in Fig. 10.12C.

The second-order derivative for $\tilde{u}(\xi) = v(w)$ is computed using (10.106) in (10.105) [Henricci (1997)]

$$\frac{\partial^2 \tilde{u}}{\partial \tilde{r}^2} + \frac{\partial^2 \tilde{u}}{\partial \tilde{z}^2} = |w'(\xi)|^2 \Delta_w v(w). \quad (10.108)$$

In the small ε limit, we have

$$|w'(\xi)|^2 = \frac{|(1 - \sqrt{\varepsilon})e^{i\theta} - 1 + O(\varepsilon)|^4}{4\varepsilon + O(\varepsilon^{3/2})}. \quad (10.109)$$

The three-dimensional BVP (10.105) differs from the two-dimensional one [Cartailler et al. (2016a)] by the extra first order radial derivative. In the small ε limit,

$$\tilde{r} + 1 + \varepsilon/2 = \frac{\varepsilon}{1 - \cos(\theta)} + O(\varepsilon^{3/2}). \quad (10.110)$$

Moreover,

$$\frac{\partial u(\tilde{r}, \tilde{z})}{\partial \tilde{r}} = \Re e (\nabla u(\xi)), \quad (10.111)$$

where $\Re e(\cdot)$ is the real part. Under the conformal mapping (10.106), the gradient from (10.111) transforms as follows [Henricci (1997)]

$$\nabla u(\xi) = \nabla_w v(w) \overline{w'(\xi)}. \quad (10.112)$$

Using polar coordinates (ρ, θ) in the mapped domain Ω_w ,

$$\overline{w'(\xi)} = w_1(\rho, \theta) + i w_2(\rho, \theta), \quad (10.113)$$

and (10.106), we find that

$$\begin{aligned} s\tilde{w}_1(\rho, \theta) &= \frac{1 - \alpha^2\rho^2 + 2\alpha\rho\cos(\theta)(1 + \alpha\rho\cos(\theta))}{1 - \alpha^2} \\ \tilde{w}_2(\rho, \theta) &= -2\alpha\rho\sin(\theta) \frac{1 + \alpha\rho\cos(\theta)}{1 - \alpha^2}. \end{aligned} \quad (10.114)$$

Hence,

$$\begin{aligned} \frac{\partial \tilde{u}(\tilde{r}, \tilde{z})}{\partial \tilde{r}} &= \frac{\partial \tilde{v}(\rho, \theta)}{\partial \rho} (\cos(\theta)\tilde{w}_1(\rho, \theta) - \sin(\theta)\tilde{w}_2(\rho, \theta)) \\ &\quad - \frac{1}{\rho} \frac{\partial \tilde{v}(\rho, \theta)}{\partial \theta} (\sin(\theta)\tilde{w}_1(\rho, \theta) + \cos(\theta)\tilde{w}_2(\rho, \theta)). \end{aligned} \quad (10.115)$$

Using (10.110) and (10.115), we get

$$\frac{1}{\tilde{r}} \frac{\partial \tilde{u}(\tilde{r}, \tilde{z})}{\partial \tilde{r}} = -\frac{\rho(1 - \cos(\theta))^2}{\varepsilon^{3/2}} \frac{\partial \tilde{v}(\rho, \theta z)}{\partial \rho} - \frac{\sin(\theta)(1 - \cos(\theta))}{\varepsilon} \frac{\partial \tilde{v}(\rho, \theta z)}{\partial \theta}. \quad (10.116)$$

Finally, using (10.108) in polar coordinates (ρ, θ) , (10.116) and (10.105) in Ω_w take the form

$$\begin{aligned} &\frac{|(1 - \sqrt{\varepsilon})e^{i\theta} - 1|^4}{4\varepsilon} \left(\frac{\partial^2 \tilde{v}(\rho, \theta)}{\partial \rho^2} + \frac{1}{\rho} \frac{\partial \tilde{v}(\rho, \theta)}{\partial \rho} + \frac{1}{\rho^2} \frac{\partial^2 \tilde{v}(\rho, \theta)}{\partial \theta^2} \right) \\ &- \frac{\rho(1 - \cos(\theta))^2}{\varepsilon^{3/2}} \frac{\partial \tilde{v}(\rho, \theta z)}{\partial \rho} - \frac{\sin(\theta)(1 - \cos(\theta))}{\varepsilon} \frac{\partial \tilde{v}(\rho, \theta z)}{\partial \theta} \\ &= -\exp\{-\tilde{v}(\rho, \theta)\} \\ \frac{\partial \tilde{v}(\rho, \theta)}{\partial n} &= -\frac{\sigma\sqrt{\varepsilon}}{1 - \cos(\theta)}. \end{aligned} \quad (10.117)$$

10.7.4 Asymptotic Analysis of the PNP Equations in a Cusp-Shaped Funnel

To analyze (10.117) in the limits of $\sigma \gg 1$, $\varepsilon \ll 1$, we partition Ω_w into two subregions and approximate the domain (Fig. 10.13A) by

$$A = \{(\rho, \theta) \in \Omega_w : |\theta - \sqrt{\varepsilon}| > \pi, |\rho - 1| \leq \sqrt{\varepsilon}\}$$

and denote the boundary arc $B = \{w = (1 - \sqrt{\varepsilon})e^{i\theta} : |\theta - \pi| \leq \sqrt{\varepsilon}\}$, (dashed red).

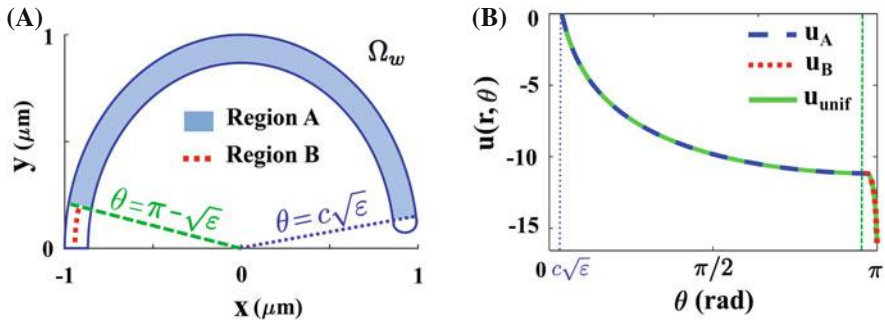


Fig. 10.13 Decomposition of Ω_w into A and B. **A.** Representation of A (blue) and B (dotted red). **B.** Solutions of (10.131) (dashed blue), (10.142) (red dots), and the uniform approximation u_{unif} (10.146) (green) for $r = 1 - \sqrt{\varepsilon}$

Construction of the solution $u_A(r, \theta)$ in Subregion A

To construct solution $u_A(r, \theta)$ in A, we use the estimate of the radial derivative $\partial/\partial r$ as $O(\sigma\sqrt{\varepsilon}) \rightarrow \infty$ as $\sigma\varepsilon^{3/2} = O(1)$, $\sigma \gg 1$, $\varepsilon \ll 1$. Under these conditions, the angular derivatives are negligible relative to the radial ones. The solution is expanded in powers of ε when the θ -derivative is negligible relative to the ρ derivative of Eq. (10.117) along the rays $\theta = \theta_0 = const$, for $\rho \in [1 - \sqrt{\varepsilon}, 1]$.

Setting $u_A(\rho, \theta_0) = v(\rho, \theta_0)$, Eq. (10.117) reduces to leading order in $\sigma\sqrt{\varepsilon}$ to

$$\begin{aligned} -e^{-u_A(\rho, \theta_0)} &= \frac{|(1 - \sqrt{\varepsilon})e^{i\theta_0} - 1|^4}{4\varepsilon} \left(\frac{\partial^2 u_A(\rho, \theta_0)}{\partial \rho^2} + \frac{1}{\rho} \frac{\partial u_A(\rho, \theta_0)}{\partial \rho} \right) \\ &\quad - \frac{\rho(1 - \cos(\theta_0))^2}{\varepsilon^{3/2}} \frac{\partial \bar{u}_A(\rho, \theta_0)}{\partial \rho} \end{aligned} \quad (10.118)$$

$$\frac{du_A(\rho, \theta_0)}{d\rho} \Big|_{\rho=1} = - \frac{\sqrt{\varepsilon}}{1 - \cos(\theta_0)}$$

$$\frac{du_A(\rho, \theta_0)}{d\rho} \Big|_{\rho=1-\sqrt{\varepsilon}} = 0.$$

For $\varepsilon \ll 1$, we can estimate $|\rho e^{i\theta_0}(1 - \sqrt{\varepsilon}) - 1|^4 = |e^{i\theta_0} - 1|^4 + O(\sqrt{\varepsilon})$, change to $\rho = \tilde{\rho}\sqrt{\varepsilon}$, and set $u_A(\rho, \theta_0) = v_A(\tilde{\rho}, \theta_0)$, to obtain from (10.118) to leading order in $\varepsilon \ll 1$

$$\frac{\partial^2 v_A(\tilde{\rho}, \theta_0)}{\partial \tilde{\rho}^2} - \sqrt{\varepsilon} \frac{\partial v_A(\tilde{\rho}, \theta_0)}{\partial \tilde{\rho}} \left(1 - \frac{4(1 - \cos(\theta_0))^2}{|e^{i\theta_0} - 1|^4} \right) = -\frac{4\varepsilon^2 e^{-v_A(\tilde{\rho}, \theta_0)}}{|e^{i\theta_0} - 1|^4}. \quad (10.119)$$

Setting

$$h(\theta_0) = \frac{4\varepsilon^2}{|e^{i\theta_0} - 1|^4} \quad (10.120)$$

and $\tilde{v}_A(\tilde{\rho}, \theta_0) = v_A(\tilde{\rho}, \theta_0) - \log(h(\theta_0))$, (10.119) is transformed into

$$\frac{\partial^2 \tilde{v}_A(\tilde{\rho}, \theta_0)}{\partial \tilde{\rho}^2} = -e^{-v_A(\tilde{\rho}, \theta_0)} + \sqrt{\varepsilon} \frac{\partial v_A(\tilde{\rho}, \theta_0)}{\partial \tilde{\rho}} \left(1 - \frac{(1 - \cos(\theta_0))^2}{|e^{i\theta_0} - 1|^4} \right). \quad (10.121)$$

Expanding in powers of ε (in the regime $\sigma\varepsilon^{3/2} = O(1)$),

$$\tilde{v}_A(\tilde{\rho}, \theta_0) = \tilde{v}_{A,0}(\tilde{\rho}, \theta_0) + \sqrt{\varepsilon} \tilde{v}_{A,1}(\tilde{\rho}, \theta_0) + O(\varepsilon), \quad (10.122)$$

we get in (10.121)

$$\begin{aligned} \frac{\partial^2 \tilde{v}_{A,0}(\tilde{\rho}, \theta_0)}{\partial \tilde{\rho}^2} &= -e^{-\tilde{v}_{A,0}(\tilde{\rho}, \theta_0)} & (10.123) \\ \frac{\partial \tilde{v}_{A,0}(\tilde{\rho}, \theta_0)}{\partial \tilde{\rho}} \Big|_{\tilde{\rho}=0} &= \frac{\sigma\varepsilon}{1 - \cos(\theta_0)} \\ \frac{\partial \tilde{v}_{A,0}(\tilde{\rho}, \theta_0)}{\partial \tilde{\rho}} \Big|_{\tilde{\rho}=1} &= 0. \end{aligned}$$

Direct integration of (10.123) gives [Cartailler et al. (2016a)]

$$\tilde{v}_{A,0}(\tilde{\rho}, \theta_0) = \log \left(2C_1(\theta_0)^2 \cos^2 \left(\frac{\tilde{\rho} + C_2(\theta_0)}{2C_1(\theta_0)} \right) \right), \quad (10.124)$$

where $C_1(\theta_0)$ and $C_2(\theta_0)$ are two constants that depend on θ_0 . To compute these constants, we differentiate (10.124),

$$\tilde{v}'_{A,0}(\tilde{\rho}, \theta_0) = \frac{-1}{C_1(\theta_0)} \tan \left(\frac{\tilde{\rho} + C_2(\theta_0)}{2C_1(\theta_0)} \right) \quad (10.125)$$

and apply the Neumann boundary condition at $\tilde{\rho} = 1$ in (10.123), to get

$$C_2(\theta_0) = -1. \quad (10.126)$$

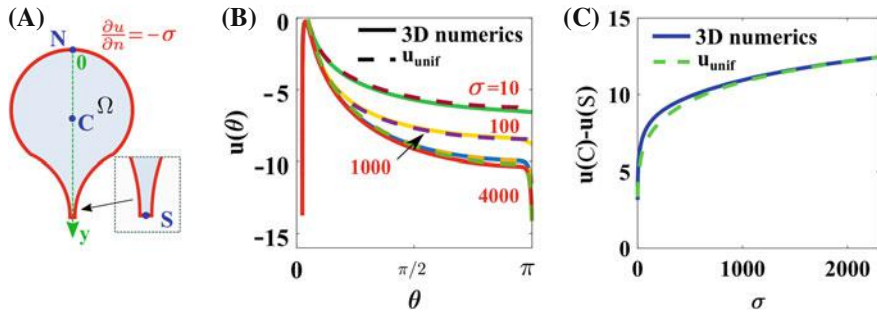


Fig. 10.14 PNP solution of (10.68) in a 3D domain with a cusp-shaped funnel. **A.** Representation of the domain Ω with a surface charge density σ , the north pole N , the funnel tip S , and the center of mass C , respectively. **B.** Numerical and analytical solutions of (10.68) (solid) and (10.146) (dashed), respectively, in the domain Ω_w for values $\sigma = 10, 100, 1000$, and 4000 for $\varepsilon = 0.01$. **C.** The difference $u(C) - u(S)$ computed numerically and analytically (solid blue) from (10.68) (dashed green) and (10.164), respectively

Using (10.126) and (10.125) and the boundary condition at $\tilde{\rho} = 0$ in (10.123), we find that C_1 is the solution of the transcendental equation,

$$\frac{\sigma \varepsilon C_1(\theta_0)}{(1 - \cos(\theta_0))} = \tan\left(\frac{1}{2C_1(\theta_0)}\right). \quad (10.127)$$

In the regime $\sigma = O(\varepsilon^{-3/2})$, we have

$$C_1(\theta_0) = \frac{2(1 - \cos(\theta_0)) + \sigma \varepsilon}{\pi \sigma \varepsilon} + O\left(\frac{1}{\sigma \varepsilon}\right). \quad (10.128)$$

Equations (10.124), (10.126), and (10.128) give in (10.124) the leading order

$$\begin{aligned} \tilde{v}_{A,0}(\tilde{\rho}, \theta_0) &= \log\left(2\left(\frac{2(1 - \cos(\theta_0)) + \sigma \varepsilon}{\pi \sigma \varepsilon}\right)^2\right) \\ &\quad + \log\left(\cos^2\left(\frac{\pi \sigma \varepsilon (\tilde{\rho} - 1)}{2(2(1 - \cos(\theta_0)) + \sigma \varepsilon)}\right)\right). \end{aligned} \quad (10.129)$$

Therefore, we conclude from (10.129), (10.122), and (10.120) that

$$\begin{aligned} v_A(\tilde{\rho}, \theta_0) &= \log\left(2\left(\frac{2(1 - \cos(\theta_0)) + \sigma \varepsilon}{\pi \sigma \varepsilon}\right)^2\right) + \log\left(\frac{4\varepsilon^2}{|e^{i\theta_0} - 1|^4}\right) \\ &\quad + \log\left(\cos^2\left(\frac{\pi \sigma \varepsilon (\tilde{\rho} - 1)}{2(2(1 - \cos(\theta_0)) + \sigma \varepsilon)}\right)\right) + O(\sqrt{\varepsilon}). \end{aligned} \quad (10.130)$$

In particular, the solution at $\rho = 1 - \sqrt{\varepsilon}$ is

$$u_A(1 - \sqrt{\varepsilon}, \theta_0) = \log \left(8 \left(\frac{2(1 - \cos(\theta_0)) + \sigma\varepsilon}{\pi\sigma|e^{i\theta_0} - 1|^2} \right)^2 \right) + O(\sqrt{\varepsilon}). \quad (10.131)$$

We note that the three-dimensional solution (10.131) is identical to the one obtained in a planar cusped-shaped domain (Sect. 10.7).

Asymptotics of $u_B(\theta)$ in B

The asymptotic solution $u_A(\rho, \theta)$ in A does not satisfy the boundary condition (10.117) at $\theta = \pi$. Indeed, $\partial u_A(\rho, \theta)/\partial\theta|_{\theta=\pi} = 0$, while the boundary condition (10.117) is $\partial v/\partial\theta|_{\theta=\pi} = -\sigma\sqrt{\varepsilon}/2 \gg 1$, thus a boundary layer should develop.

The boundary layer solution $u_B(\theta)$ is derived by taking into account the θ -derivatives in Eq. (10.117),

$$\frac{|(1 - \sqrt{\varepsilon})e^{i\theta} - 1|^4}{4\rho^2\varepsilon} \frac{\partial^2 u_B(\theta)}{\partial\theta^2} + \frac{\sin(\theta)(1 - \cos(\theta))}{\varepsilon} \frac{\partial \tilde{u}_B(\theta)}{\partial\theta} = -e^{-u_B(\theta)}. \quad (10.132)$$

For $\varepsilon \ll 1$, and $\rho = 1 - \sqrt{\varepsilon}$, we have

$$\frac{4\varepsilon}{|\rho e^{i\theta}(1 - \sqrt{\varepsilon}) - 1|^4} = \frac{\varepsilon}{4}, \quad (10.133)$$

which is constant. Using (10.133) in (10.132) and $\eta = \pi - \theta$, we define $u_B(\theta) = \tilde{u}_B(\eta)$, leading to

$$\frac{\partial^2 \tilde{u}_B(\eta)}{\partial\eta^2} - \frac{1}{4} \sin(\eta)(1 + \cos(\eta)) \frac{\partial \tilde{u}_B(\theta)}{\partial\eta} = -\frac{\varepsilon}{4} e^{-\tilde{u}_B(\eta)}. \quad (10.134)$$

Since $0 \leq \eta \leq \sqrt{\varepsilon}$, the first-order term in (10.134) reduces to

$$\frac{\partial^2 \tilde{u}_B(\eta)}{\partial\eta^2} - \frac{\eta}{2} \frac{\partial \tilde{u}_B(\theta)}{\partial\eta} = -\frac{\varepsilon}{4} e^{-\tilde{u}_B(\eta)}. \quad (10.135)$$

Setting $v(\eta) = u_B(\eta) - \log(4/\varepsilon)$ in (10.135) transforms it to

$$-\frac{\partial^2 \tilde{v}(\eta)}{\partial\eta^2} + \frac{\eta}{2} \frac{\partial \tilde{v}(\eta)}{\partial\eta} = e^{-\tilde{v}(\eta)}. \quad (10.136)$$

The boundary condition (10.117) reduces the equation to

$$-\frac{\partial^2 \tilde{v}(\eta)}{\partial\eta^2} = e^{-\tilde{v}(\eta)} + O(\lambda\varepsilon^2) \quad (10.137)$$

$$\left. \frac{\partial v(\eta)}{\partial\eta} \right|_{\eta=0} = \frac{\sigma\sqrt{\varepsilon}}{2}, \quad \left. \frac{\partial v(\eta)}{\partial\eta} \right|_{\eta=\sqrt{\varepsilon}} = 0.$$

The solution is

$$\tilde{v}(\eta) = \log \left(2\tilde{C}_1^2 \cos^2 \left(\frac{\eta + \tilde{C}_2}{2\tilde{C}_1} \right) \right), \quad (10.138)$$

where

$$\tilde{C}_2 = -\sqrt{\varepsilon}, \quad (10.139)$$

and \tilde{C}_1 is the solution of the transcendental equation

$$\frac{2\tilde{C}_1}{\sqrt{\varepsilon}} \arctan \left(\frac{\sigma\sqrt{\varepsilon}\tilde{C}_1}{2} \right) = 1. \quad (10.140)$$

For $\sigma \gg 1$, we have

$$\tilde{C}_1 = \frac{2}{\pi} \left(\frac{\sqrt{\varepsilon}}{2} + \frac{2}{\sigma\sqrt{\varepsilon}} \right) + O \left(\frac{1}{(\sigma\sqrt{\varepsilon})^3} \right). \quad (10.141)$$

Note that $\frac{\eta}{2} \frac{\partial \tilde{v}(\eta)}{\partial \eta}$ is small, thus justifying the simplifications.

We conclude from (10.139), (10.141), and (10.124) that for $\theta \in B$, the asymptotic solution is

$$u_B(\theta) = \log \cos^2 \frac{\pi}{2} \sqrt{\frac{(\theta - (\pi - \sqrt{\varepsilon}))^2}{\varepsilon}} \left(1 - \frac{4}{\sigma\varepsilon} \right) + C_0, \quad (10.142)$$

where C_0 is a matching constant found below.

A Uniform Approximation of $u(\rho, \theta)$ in Ω_w

To construct a uniform asymptotic approximation $u_{unif}(\rho, \theta)$ in the region $A \cup B$ (Fig. 10.14A) $u_A(\rho, \theta)$ is matched with $u_B(\rho, \theta)$ for $\theta = \pi - \sqrt{\varepsilon}$, leading to

$$C_0 = u_A(1 - \sqrt{\varepsilon}, \pi - \sqrt{\varepsilon}). \quad (10.143)$$

The analytical expression (10.131) for u_A gives

$$C_0 = \log \left(\frac{(4 + \sigma\varepsilon)^2}{2(\pi\sigma)^2} \right). \quad (10.144)$$

Thus,

$$u_B(\theta) = \log \cos^2 \frac{\pi}{2} \sqrt{\frac{(\theta - (\pi - \sqrt{\varepsilon}))^2}{\varepsilon}} \left(1 - \frac{4}{\sigma\varepsilon} \right) + \log \left(\frac{(4 + \sigma\varepsilon)^2}{2(\pi\sigma)^2} \right). \quad (10.145)$$

Consequently, using (10.131) and (10.145) the solution in the funnel domain is

$$u_{unif}(\rho, \theta) = \begin{cases} \log \left(8 \left(\frac{2(1 - \cos(\theta)) + \sigma\varepsilon}{\pi\sigma|e^{i\theta} - 1|^2} \right)^2 \right), & \text{for } \theta \in [0, \pi - \sqrt{\varepsilon}] \\ \log \cos^2 \frac{\pi}{2} \sqrt{\frac{(\theta - (\pi - \sqrt{\varepsilon}))^2}{\varepsilon}} \left(1 - \frac{4}{\sigma\varepsilon} \right) + \log \left(\frac{(4 + \sigma\varepsilon)^2}{2(\pi\sigma)^2} \right), & \text{for } \theta \in [\pi - \sqrt{\varepsilon}, \pi]. \end{cases} \quad (10.146)$$

The numerical solution of Eq. (10.68) in Ω_w and the approximation $u_{unif}(\rho, \theta)$ of (10.146) are shown in Fig. 10.14B.

10.7.5 The Potential Drop in Ω_w

The potential drop between the center of mass C and the tip of the funnel S (see Fig. 10.14A) is defined as

$$\tilde{\Delta}_{funnel}u = u(C) - u(S), \quad (10.147)$$

where

$$u(S) = u(1 - \sqrt{\varepsilon}, \pi) \quad \text{and} \quad u(C) = u(1 - \sqrt{\varepsilon}, c\sqrt{\varepsilon}), \quad (10.148)$$

where $u(r, \theta)$ is the solution of (10.68) and the geometric constant c is defined by the conformal mapping (10.106). To compute $\tilde{\Delta}_{funnel}u$, we use the two differences

$$\tilde{\Delta}u_A = u_A(1 - \sqrt{\varepsilon}, \pi) - u_A(1 - \sqrt{\varepsilon}, c\sqrt{\varepsilon}) \quad (10.149)$$

$$\tilde{\Delta}u_B = u_B(\pi) - u_B(\pi - \sqrt{\varepsilon}) \quad (10.150)$$

and

$$\tilde{\Delta}_{funnel} = \tilde{\Delta}u_A + \tilde{\Delta}u_B. \quad (10.151)$$

Equation (10.131) for $\rho = 1 - \sqrt{\varepsilon}$ and any θ_0 gives

$$u_A(1 - \sqrt{\varepsilon}, \theta_0) = -\log \frac{|e^{i\theta_0} - 1|^4}{8(1 - \sqrt{\varepsilon})^2} \left(\frac{\sigma\pi}{2(1 - \cos(\theta_0)) + \sigma\varepsilon} \right)^2 + O(\varepsilon). \quad (10.152)$$

At S (i.e., $\theta_0 = \pi$),

$$u_A(S) = -\log \frac{2\sigma^2\pi^2}{(4 + \sigma\varepsilon)^2} + 2\log(1 - \sqrt{\varepsilon}) + O(\varepsilon). \quad (10.153)$$

To estimate $u_A(C)$ (i.e., $\theta_0 = c\sqrt{\varepsilon}$), we note that for $\varepsilon \ll 1$ in (10.152),

$$|e^{i\theta_0} - 1|^4 = c^4\varepsilon^2 + O(\varepsilon^3), \quad (10.154)$$

and

$$2(1 - \cos(c\sqrt{\varepsilon})) + \sigma\varepsilon = \varepsilon(c^2 + \sigma) + O(\varepsilon^2). \quad (10.155)$$

Equations (10.154) and (10.155) imply that (10.152) reduces to

$$u_A(C) = -\log \frac{c^4}{8} \left(\frac{\sigma\pi}{c^2 + \sigma} \right)^2 + 2\log(1 - \sqrt{\varepsilon}) + O(\varepsilon). \quad (10.156)$$

For $\sigma \gg 1$,

$$u_A(C) = -\log \frac{\pi^2 c^4}{8} + 2\log(1 - \sqrt{\varepsilon}) + O\left(\varepsilon, \frac{1}{\sigma}\right), \quad (10.157)$$

hence

$$\tilde{\Delta}u_A = -\log \frac{2\sigma^2\pi^2}{(4 + \sigma\varepsilon)^2} + \log \frac{\pi^2 c^4}{8} + O\left(\varepsilon, \frac{1}{\sigma}\right). \quad (10.158)$$

The leading order solution of (10.158) is independent of σ , so

$$\tilde{\Delta}u_A \sim -\log \frac{2^4}{c^4\varepsilon^2}. \quad (10.159)$$

To estimate $\tilde{\Delta}u_B$, we note that (10.142) gives

$$u_B(\pi - \sqrt{\varepsilon}) = C_0 \quad (10.160)$$

$$u_B(\pi) = \log \sin^2\left(\frac{\pi}{\sigma\varepsilon}\right) + C_0. \quad (10.161)$$

Thus (10.160) and (10.161) give in (10.150),

$$\tilde{\Delta}u_B = \log \sin^2\left(\frac{\pi}{\sigma\varepsilon}\right). \quad (10.162)$$

Because (10.162) reduces to

$$\tilde{\Delta}u_B = -2\log\sigma + 2\log\frac{\pi}{\varepsilon} + O\left(\frac{1}{\sigma^2}\right), \quad (10.163)$$

Equations (10.158), (10.162), and (10.151) give the difference in the funnel as

$$\tilde{\Delta}u = \log \sin^2 \frac{\pi}{\sigma\varepsilon} - \log \frac{2\sigma^2\pi^2}{(4 + \sigma\varepsilon)^2} + \log \frac{\pi^2 c^4}{8} + O\left(\varepsilon, \frac{1}{\sigma}\right). \quad (10.164)$$

The results (10.159) and (10.163), found for $\sigma \gg 1$, lead to

$$\tilde{\Delta}u = -\log \sigma^2 + 2 \log \frac{\pi c^2}{4} + O\left(\frac{1}{\sigma}\right). \quad (10.165)$$

Equation (10.162) shows that for $\sigma \gg 1$, the potential drop in the cusp-shaped funnel is dominant in region B . Figure 10.14C compares (10.164) with the numerical solution of (10.68). Note that the distribution of the potential in a three-dimensional solid funnel is to leading order identical to that obtained inside a planar cusp [Cartailler et al. (2016a)].

For a constant surface charge density $\tilde{\sigma} \gg 1$, the voltage difference in dimensional units is given by

$$V(C) - V(S) = \frac{kT}{e} \left(\log \sin^2 \frac{kT\pi}{e\tilde{\varepsilon}\tilde{\sigma}} - 2 \log \frac{\sqrt{2} e\pi R_c \tilde{\sigma}}{4kT + e\tilde{\varepsilon}\tilde{\sigma}} + O(1) \right), \quad (10.166)$$

where the physical quantities are thermal energy kT , the elementary charge e of the electron ($1.602 \cdot 10^{-19} C$), the cusp-shaped funnel width at the base is $\tilde{\varepsilon}$, and its radius of curvature is R_c .

10.8 Annotations

The non-linear system of the Poisson–Nernst–Planck equations has been widely used to study properties of the electric field in local nanodomains such as ionic channels [Goldman (1943)], [Barcilon (1992)], [Barcilon et al. (1992)], [Schuss et al. (2001)], [Nadler et al. (2004)] and [Singer (2006)]. It was also used to simulate the rate of equilibration of ions between large reservoirs through narrow necks [Graf et al. (2000)], [Schuss et al. (2001)], and to study the effect of interacting ions in ionic channels [Taflia (2008)]. This equation is also known as the Liouville–Gelfand–Bratú-type equation [Frank–Kamenetskii (1955)] for the electric potential, normalized over the domain Ω with, however, two major differences [Cartailler et al. (2016a)]: first, the boundary condition on $\partial\Omega$ is Neumann, not Dirichlet, and second, there is a minus sign in the exponent. This equation is thus different from that of the Newtonian potential of a cluster of self-gravitating mass distribution [Chipot et al. (1997); Wolansky (1992a); Wolansky JDA (1992b)]. In addition, this equation should not be confused with the Poisson–Boltzmann equation, which is a model for two populations of negative and positive equivalent ions. The new asymptotic expansion for Poisson–Nernst–Planck in a entire ball and in a ball with a non-charged cusp-shaped funnel was developed in [Cartailler et al. (2016a)] and [Cartailler et al.

(2016b)], which also contains the computations of the voltage-drop inside an entirely charged funnel. The new method is based on matching solutions that blow up in finite time.

Considerable effort was dedicated to study the mathematics of diffusion in such structures [Holcman and Schuss (2011)], [Holcman and Schuss (2015)], but very little is known about their electro-diffusion properties, even experimentally, where almost no data are available at the nanometer resolution (see [Araya et al. (2007)], [Araya et al. (2006)], [Araya et al. Nov (2006)]). This high resolution is necessary to evaluate the change of voltage and whether or not electro-neutrality holds. Despite converging experimental efforts, the electrical properties of these structures remain unclear at the molecular level and a predictive theory based on mathematical physics is needed to interpret incoming data [Holcman and Yuste (2015)].

Diffusion in dendritic spines has been investigated in [Holcman and Schuss (2005a)] and in [Biess et al. (2007)], but little is known about the regulation of the electrical current since no experimental data are currently available about the voltage at a nanometer precision [Holcman and Yuste (2015)]. The solution $T(x, y)$ of (10.37) was given in [Singer et al. III (2006a)] and later in [Cheviakov et al. (2010)] and [Holcman and Schuss (2015)]. Some dendritic spines are synaptically connected [Holcman and Yuste (2015)]. Although their functions are still unclear, they are involved in regulating synaptic transmission and plasticity [Svoboda et al. (1996)], [Korkotian and Segal (1999)], [Bloodgood (2005)], [Araya et al. (2006)], [Araya et al. Nov (2006)], [Araya et al. (2007)], [Sheng et al. (2012)]. The view that spine geometry defines both the capacitance and resistance in geometrical terms complements previous studies [Qian (1989)], [Svoboda et al. (1996)], [Koch (1999)], [Segev and Rall (1988)]. The change of variables (10.19) was introduced in [Jacobsen (2002)].

Chapter 11

Reconstruction of Surface Diffusion from Projected Data

11.1 Projection of Diffusion from a Curve to a Line

The planar projections of short fragments of trajectories of particles (e.g., neuronal receptors) diffusing in the surface of a cell membrane are acquired by a confocal microscope to form a large data set. This and the next sections show how the data can be used to reconstruct the shape of the membrane surface and the physical properties of the receptor motion. A general method for the reconstruction of a two-dimensional surface from the statistics of planar projections of many independent trajectories of a diffusion process on the surface begins with determining the drift field and diffusion tensor of the stochastic dynamics from the projections. The latter represent physical interactions in the surface.

This reconstruction falls into a class of inverse problems that have been investigated in the context of extraction of shape from shading (see Annotations 11.3). In view of the irregularity of the stochastic trajectories, the reconstruction requires in practice a large set of data points. The reconstruction scheme is illustrated in Fig. 11.1.

11.1.1 Driftless Diffusion on a Curve

To clarify the geometric context of the reconstruction problem, we consider first the reconstruction of one-dimensional diffusion on a curve from its projection on a line. Given a sufficiently smooth curve $C = \{(x, f(x)) : a < x < b\}$, standard Brownian motion $X(t)$ on C is defined by the following Euler scheme. Assume that the Brownian motion $X(t) = (x(t), y(t))$ at time t is at the point $X = (x, y) \in C$ (Fig. 11.2). Define the tangent line at this point,

$$\ell = \{(\xi, \eta) : \eta = y + \tan \alpha(\xi - x), -\infty < \xi < \infty\}$$

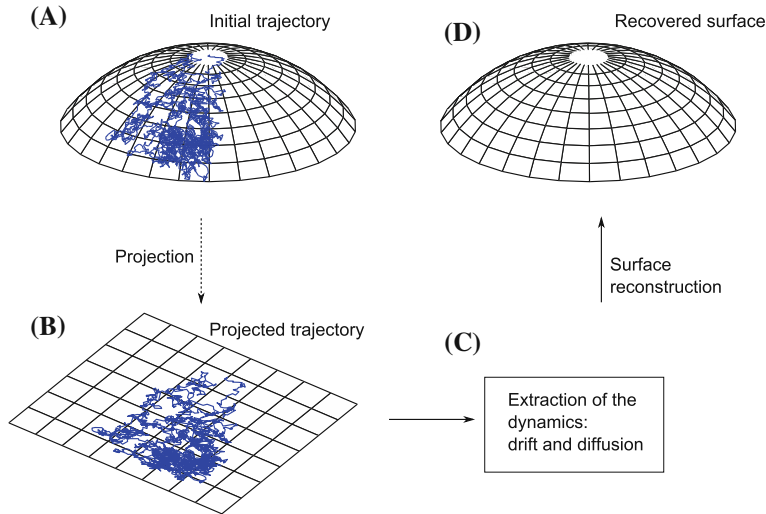


Fig. 11.1 Reconstruction of a surface from projected trajectories. (A) A trajectory of a diffusion process on the unknown surface Σ . (B) A planar projection of the trajectory. (C) Statistical estimates of the drift and the diffusion coefficients of the projected stochastic dynamics. (D) Reconstruction of Σ from the estimated coefficients

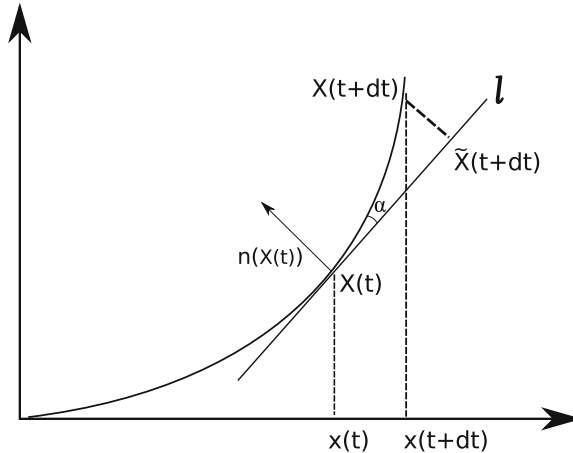


Fig. 11.2 Projection of a diffusion process $x(t)$ on a curve C onto the x -axis. Starting from a point $X(t)$ on C , the point $\tilde{X}(t + \Delta t)$ on the tangent line ℓ is defined by the projection of Euler's scheme for the dynamics (11.28) on ℓ . Then $\tilde{X}(t + \Delta t)$ is projected to the point $X(t + \Delta t)$ on C in the direction parallel to the normal $n(X(t))$. The projection $x(t + \Delta t)$ of the diffusion process on the x -axis is the x -component of $X(t + \Delta t)$

with $y = f(x)$, $\tan \alpha = f'(x)$. Standard Brownian motion $X(t + \Delta t)$ on C is defined as the orthogonal projection on C in the direction of the normal $n(X(t))$ of the point $\tilde{X}(t + \Delta t) = (\tilde{x}(t + \Delta t), \tilde{y}(t + \Delta t))$ on the tangent line ℓ , defined by

$$\tilde{x}(t + \Delta t) = x + \cos \alpha \sqrt{2} \Delta w, \quad \tilde{y}(t + \Delta t) = y + \sin \alpha \sqrt{2} \Delta w, \quad (11.1)$$

where $w(t)$ is standard Brownian motion in \mathbb{R} . The projection of the standard Brownian motion $X(t)$ on the x -axis is the coordinate $x(t)$ of $X(t)$.

A slight generalization of standard Brownian motion on C is the driftless diffusion process defined by the one-dimensional stochastic differential equation (in the Itô sense) [Schuss (2010b)] (11.28) with the diffusion coefficient $D(X)$. Equation (11.1) is then replaced by

$$\begin{aligned}\tilde{x}(t + \Delta t) &= x + \cos \alpha \sqrt{2D(X)} \Delta w \\ \tilde{y}(t + \Delta t) &= y + \sin \alpha \sqrt{2D(X)} \Delta w.\end{aligned}\quad (11.2)$$

The projection of $X(t)$ onto the x -axis is found from the normal projection $X(t + \Delta t)$ of $\tilde{X}(t + \Delta t)$ onto C that is determined by the equation

$$-\cot \alpha [\tilde{x}(t + \Delta t) - x(t + \Delta t)] = \tilde{y}(t + \Delta t) - y(t + \Delta t). \quad (11.3)$$

Setting $\Delta x = x(t + \Delta t) - x(t)$ and $\Delta f = f(x(t + \Delta t)) - f(x(t))$, we obtain the increment equation

$$\Delta x \cot \alpha + \Delta f = \frac{\sqrt{2D(X(t))} \Delta w}{\sin \alpha}. \quad (11.4)$$

The expansion

$$\Delta f = \tan \alpha \Delta x + \frac{1}{2} f''(x(t)) \Delta x^2 + o(\Delta x^2) \quad (11.5)$$

and (11.4) give

$$\Delta x (\cot \alpha + \tan \alpha) = \frac{\sqrt{2D(X(t))} \Delta w}{\sin \alpha} - \frac{1}{2} f''(x(t)) \Delta x^2 + \dots, \quad (11.6)$$

so neglecting powers of Δx higher than 2, solving the quadratic equation, and expanding in powers of Δw , we obtain

$$\Delta x = \frac{\sqrt{2D(x, f(x))}}{\sqrt{1 + f'^2(x)}} \Delta w - \frac{D(x, f(x)) f'(x(t)) f''(x)}{[1 + f'^2(x)]^2} \Delta w^2 + \dots \quad (11.7)$$

Replacing Δw^2 with Δt , we obtain for the projection $x(t)$ of the Brownian motion on C onto the x -axis

$$dx = a_{\text{geometric}}(x) dt + \sqrt{2D_{\text{effective}}(x)} dw, \quad (11.8)$$

where

$$a_{\text{geometric}}(x) = -\frac{D(x, f(x))f'(x)f''(x)}{\left[1 + f'^2(x)\right]^2} \quad (11.9)$$

and the effective diffusion coefficient, which depends on displacement, is given by

$$D_{\text{effective}}(x) = \frac{D(x, f(x))}{1 + f'^2(x)}. \quad (11.10)$$

We call $a_{\text{geometric}}(x)$ the geometric drift. Note that the Eqs. (11.9) and (11.10) recover both the original curve C and the diffusion coefficient $D(X)$ on C . Indeed, because $a_{\text{geometric}}(x)$ and $D_{\text{effective}}(x)$ are observed, we can recover $f(x)$ from the equation

$$\frac{a_{\text{geometric}}(x)}{D_{\text{effective}}(x)} = \frac{-f'(x)f''(x)}{1 + f'^2(x)} = \frac{1}{2} \log \left(\frac{1}{1 + f'^2(x)} \right)' . \quad (11.11)$$

When $D(x, f(x)) = D$ is constant, we have the simpler relation

$$a_{\text{geometric}}(x) = D'_{\text{effective}}(x). \quad (11.12)$$

Note that (11.11) is a second-order equation that defines $f(x)$ up to two constants of integration, e.g. $f(x_0)$ and $f'(x_0)$, where x_0 is a projected point. Because the projection line can be assumed to be a supporting line, x_0 can be chosen to be the point of contact and the line can be considered as the x -axis and $x_0 = 0$. Thus we can assume that the initial conditions for (11.11) are $f(0) = f'(0) = 0$. Now $D(X)$ is recovered from (11.9), (11.10) or (11.12) in the constant case. A statistical procedure for the calculation of the geometric drift $a_{\text{geometric}}(x)$ and the effective diffusion coefficient $D_{\text{effective}}(x)$ from projected trajectories is given below.

11.1.2 The Case of Diffusion with Drift

Consider a stochastic differential equation with drift on the curve C ,

$$dX = \mathbf{b}(X) dt + \sqrt{2D(X)} dW. \quad (11.13)$$

The drift vector $\mathbf{b}(X)$ is tangent to C , that is, $\mathbf{b}(X) = |\mathbf{b}(X)|(\cos \alpha, \sin \alpha)^T$ with $\tan \alpha = f'(x)$. Setting $b(x) = |\mathbf{b}(x, f(x))| \cos(\alpha)$, note that $\text{sign}[b(x)] = \text{sign}[\cos \alpha]$, so that $\mathbf{b}(X)$ can be recovered from $b(x)$ by the relations

$$\mathbf{b}(X) = \frac{b(x)}{\sqrt{1 + f'^2(x)}} \begin{pmatrix} 1 \\ f'(x) \end{pmatrix}. \quad (11.14)$$

Now, using (11.5) and (11.6), we find that the effective diffusion coefficient is (11.10) and that the drift of the projected motion on the x -axis is given by

$$a(x) = -\frac{D_{\text{effective}}(x)f'(x)f''(x)}{1+f'^2(x)} + \frac{b(x)}{\sqrt{1+f'^2(x)}}, \quad (11.15)$$

which is the sum of the geometric drift of Eq. 11.9 and the projection of the drift vector in (11.13).

Note that an additional equation is needed to recover the curve, drift, and effective diffusion coefficient from the projected data. The additional equation can be obtained by projecting trajectories of driftless diffusers from C to the x -axis, for example, by tracking inert particles on the curve. Indeed, inert particles do not interact with any force field on C , which makes them driftless, as in Sect. 11.1.1. Although inert particles may have a different diffusion coefficient, the shape of the curve remains unchanged. Thus C can be found from data collected for driftless particles, and the drift $b(X)$ and diffusion coefficient for particles with drift are then found from data collected from projections of their trajectories. Statistical estimates of the projected diffusion parameters and the reconstruction of the curve C are given in Appendix 11.1.4.

11.1.3 Reconstruction of a Parabola from Projected Diffusion Data

To reconstruct simulated diffusion with drift on a parabola $f(x) = \frac{1}{2}Ax^2$, we first reconstruct the curve from the projection on the x -axis of simulated driftless Brownian trajectories on the parabola. We then apply the procedure of Sect. 11.1.1 to compute the effective diffusion coefficient and the geometric drift, for which the analytical expressions are given by

$$D_{\text{effective}}(x) = \frac{D}{1+A^2x^2}, \quad a_{\text{geometric}}(x) = -\frac{DA^2x}{[1+A^2x^2]^2} \quad (11.16)$$

(see Eqs. (11.9), (11.10), and (11.12)). The reconstruction is presented in Fig. 11.3 with bin size $\Delta x = 0.1$, diffusion coefficient $D = 1$, and the parabola parameter $A = 10$. The analytical curve (red) overlaps with the sampled reconstructed points (black dots). A sample projected trajectory is shown in Fig. 11.3A. The geometric drift and effective diffusion coefficient are estimated in Appendix 11.1.4 below. The effective diffusion coefficient $D_{\text{effective}}(x)$ is estimated from Eq. (11.25) (see Fig. 11.3B) and the geometric drift $a_{\text{geometric}}(x)$ is estimated from (11.24) (Fig. 11.3C) and (11.26) (Fig. 11.3D) below. Next, we consider diffusion with drift on a parabola. Specifically, we consider (11.13) with the following two drifts.

1. Diffusion with constant drift along the parabola, that is,

$$\mathbf{b}(X) = \frac{B}{\sqrt{1 + A^2 X^2}} \begin{pmatrix} 1 \\ Ax \end{pmatrix}.$$

2. An OU process centered at the point $(x_0, 5x_0^2)$, given by

$$\mathbf{b}(X) = -\frac{C(x - x_0)}{\sqrt{1 + A^2 X^2}} \begin{pmatrix} 1 \\ Ax \end{pmatrix},$$

where C is a positive constant. The projection $x(t)$ on the x -axis is the solution of the stochastic differential equation

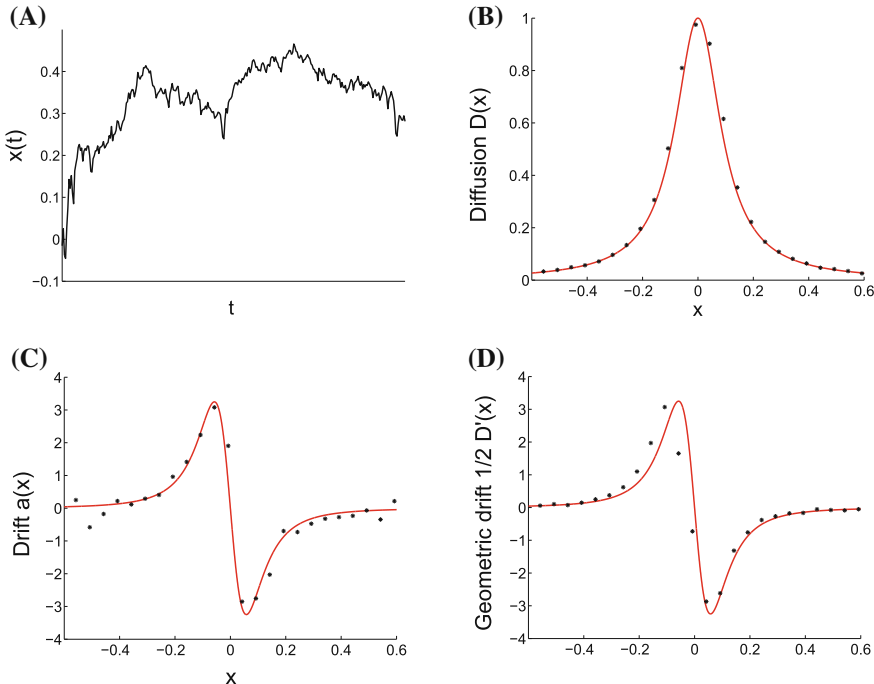


Fig. 11.3 Estimates of the effective diffusion coefficient and geometric drift of Brownian trajectories on the parabola $y = 5x^2$ from their projections on the x -axis. (A) Projection on the x -axis of a sampled Brownian trajectory on the parabola. (B) Comparison of the analytical expression (11.10) for $D_{\text{effective}}(x)$ (red) with the estimate computed from (11.25) (black dots) with 500 simulated Brownian trajectories and 300 grid points. (C) Comparison of the analytical expression (11.9) for $a_{\text{geometric}}(x)$ (red) and the estimate (11.24) (black dots). (D) Comparison of the geometric drift computed from (11.26) (black dots) with the estimated $D_{\text{effective}}(x)$ shown in (B) with the analytical $a_{\text{geometric}}(x)$ shown in red in (C). The simulation parameters are $\Delta t = 0.001$, $\Delta x = 0.05$

$$dx = \left[\frac{B}{\sqrt{1 + A^2 x^2}} - \frac{DA^2 x}{(1 + A^2 x^2)^2} \right] dt + \sqrt{\frac{2D}{1 + A^2 x^2}} dw \quad (11.17)$$

for diffusion with constant drift, and

$$dx = \left[-\frac{C(x - x_0)}{\sqrt{1 + A^2 x^2}} - \frac{DA^2 x}{(1 + A^2 x^2)^2} \right] dt + \sqrt{\frac{2D}{1 + A^2 x^2}} dw \quad (11.18)$$

for the OU process.

Figures 11.4 and 11.5 show the reconstruction of the diffusion and the drift for constant and linear drifts, respectively. Specifically, in both cases, we first estimate the diffusion coefficient and then evaluate the geometric drift by differentiating the coef-

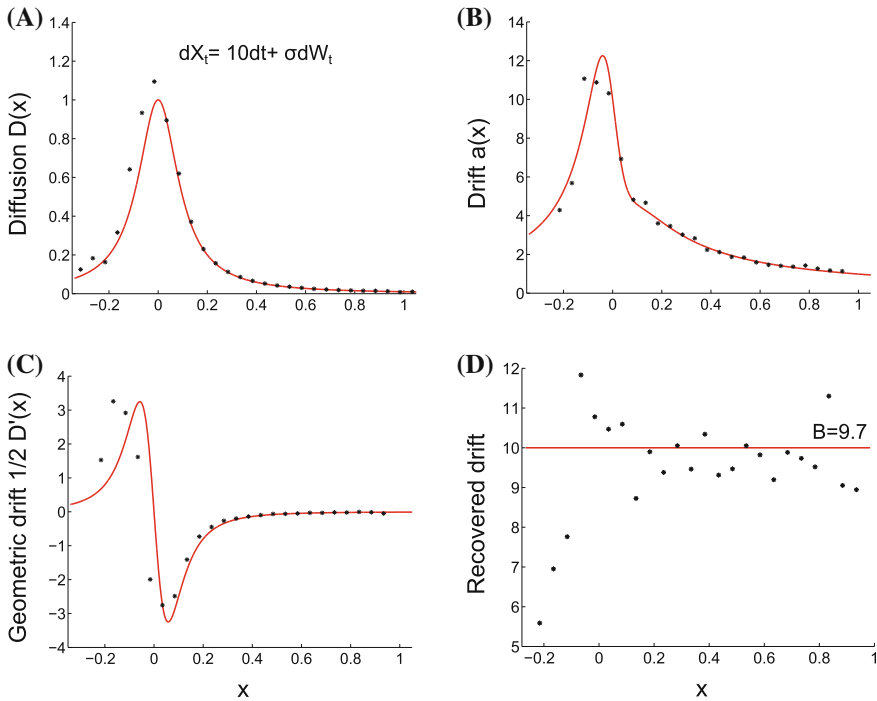


Fig. 11.4 Reconstruction of a diffusion process on a parabola in the case of constant drift. **(A)** The effective diffusion coefficient $D(X)$, calculated from (11.10) (red curve), is compared to the estimated diffusion coefficient (11.25) (black dots). **(B)** The effective drift estimated from formula (11.24) (black dots) and compared to the theoretical drift (red) computed from formula (11.17). The drift is the sum of two components, the first due to the projection on the parabola and the second one combines the constant drift and the curvature. **(C)** The estimate of the geometric drift is obtained by differentiating the diffusion coefficient with respect to the spatial variable (see (11.26)). **(D)** Extraction of the drift from (11.27) (black dots) and comparison with the theoretical constant drift (red line). We obtain $\tilde{B} = 9.7$. Initial Parameters: $dt = 0.0001$, $D = 1$, $B = 10$. Number of trajectories $N_t = 500$. Number of points per trajectory $N_s = 300$, $\Delta x = 0.05$

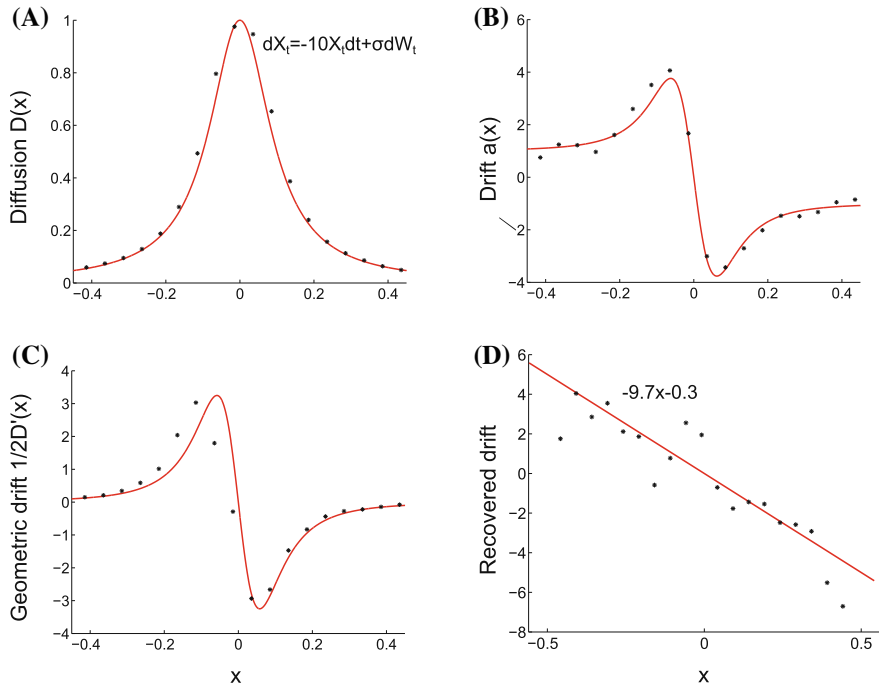


Fig. 11.5 Reconstruction of an OU process on a parabola See the legend of Fig. 11.4 for details

ficient of diffusion with respect to the spatial variable, as described in Eq. (11.15). The reconstruction of the diffusion coefficient in the former case is shown in Fig. 11.4A and of the drift in Fig. 11.4B. The derivative of the reconstructed diffusion coefficient with respect to the spatial variable is the estimated geometric drift and is shown in Fig. 11.4C. For constant drift $B = 10$ the estimate $B = 9.7$ is obtained by subtracting the geometric drift from the effective drift, as described in (11.27) (see Fig. 11.4D). The same method gives for linear drift with $C = 10$ and $x_0 = 0$ the values $C = 9.7$ and $x_0 = -0.03$ (see Fig. 11.5).

11.1.4 Appendix 2

To illustrate the theory developed above, we estimate first the geometric drift and effective diffusion coefficient. We study the projection of a simulated diffusion process $X(t)$ from a generic curve C into the x -axis, as described in Sect. 11.1.1. First, we generate N_t simulated Brownian trajectories $X(t)$ on the curve at times $t_n = n\Delta t$ ($n = 1, 2, \dots, N = t/\Delta t$) and sample their projections $(\tilde{x}_1, \dots, \tilde{x}_N)$ on a line (e.g., the x -axis) at these times, starting at the origin. The effective drift and diffusion coefficients of the projected trajectories are constructed from the approximations in the limit $\Delta t \rightarrow 0$ [Schuss (2010b)]

$$a_{\text{geometric}}(x) = \mathbb{E} \left[\frac{x(t + \Delta t) - x(t)}{\Delta t} \mid x(t) = x \right] + o(1) \quad (11.19)$$

$$D_{\text{effective}}(x) = \frac{1}{2} \mathbb{E} \left\{ \frac{[x(t + \Delta t) - x(t)]^2}{\Delta t} \mid x(t) = x \right\} + o(1), \quad (11.20)$$

where the expectation is replaced with sample averaging in the bins.

11.1.5 Reconstruction of Projected Stochastic Dynamics

We consider again the projected curve C . Given the approximate $a_{\text{geometric}}(x)$ and $D_{\text{effective}}(x)$, the curve is reconstructed at bin points. At points (x_1, \dots, x_M) the known values of the first and second derivatives of the function $y = f(x)$ (from the numerical integration of (11.11)) are denoted $f'^2(x_i) = f'_i$ and $f''(x_i) = f''_i$, respectively. To reconstruct the curve f , we use a linear approximation of the height $y_i = f(x_i)$ by $y_{i+1} - y_i = \Delta x f'_i$ and $y_i - y_{i-1} = \Delta x f'_{i-1}$. Fixing $y_1 = 0$ and summing these expressions, we obtain

$$2y_i = y_{i-1} + y_{i+1} + \Delta x(f'_{i-1} - f'_i) \text{ for } i = 2, \dots, M-1,$$

$$y_M = y_{M-1} + \Delta x f'_{M-1}.$$

Thus, we invert the linear system $\mathbf{a}\mathbf{y} = \mathbf{b}$, where

$$\mathbf{a} = \begin{pmatrix} 2 & -1 & & \dots & 0 \\ -1 & 2 & -1 & & \\ 0 & & \ddots & & \vdots \\ \vdots & & \ddots & 2 & -1 \\ 0 & \dots & 0 & -1 & 1 \end{pmatrix},$$

$\mathbf{y} = (y_1, \dots, y_M)^T$ and $\mathbf{b} = \Delta x (f'_1 - f'_2, \dots, f'_{M-1} - f'_M, f'_{M-1})^T$. The inverse matrix \mathbf{a} is

$$\mathbf{a}^{-1} = \begin{pmatrix} 1 & 1 & \dots & \dots & 1 \\ 1 & 2 & 2 & \dots & 2 \\ 1 & 2 & 3 & \dots & 3 \\ \vdots & & & & \vdots \\ 1 & 2 & \dots & M-1 & M \end{pmatrix}.$$

Figure 11.6A shows the reconstruction of the parabola $f(x) = x^2 + x$ for $x \in [0, 1]$ for $\Delta x = 0.05$ and $\Delta x = 0.1$. The precision of the reconstruction is given in terms of the sum of the squares of the errors,

$$(f, \Delta x) = \sum_{i=2}^M \left(f'_i - \frac{y_i - y_{i-1}}{\Delta x} \right)^2. \quad (11.21)$$

Figure 11.6B shows the small error, confirming the agreement between the input height f and the reconstructed curve y . Interestingly, $(f, \Delta x)$ varies linearly with the step size Δx .

The above reconstruction algorithm requires the knowledge of the sign of the derivative f'_i , which cannot be recovered from Eq. (11.10). To determine the sign of $f'(x)$, we use (11.12), because the sign of the geometric drift is that of $-f'(x)f''(x)$. Thus, if $\text{sign}[D'_{\text{effective}}(x_i)] = -\text{sign}[D'_{\text{effective}}(x_{i+1})]$, then there exists $x_i < \tilde{x} < x_{i+1}$ such that $f'(\tilde{x}) = 0$ or $f''(\tilde{x}) = 0$. But $f'(\tilde{x}) = 0$ implies that $D_{\text{effective}}(\tilde{x}) = D$ has a local maximum, which can be checked. Using this consideration we can determine whether $f'(x)$ changes sign in $[x_i, x_{i+1}]$ or not. Figure 11.6C shows the reconstruction algorithm in two cases. First, when the derivative does not change sign, the curve is reconstructed from the effective diffusion coefficient (black). Second, having estimated the effective diffusion coefficient and having computed its derivative, (11.12) captures the sign change, thereby allowing the correct reconstruction of the parabola (red).

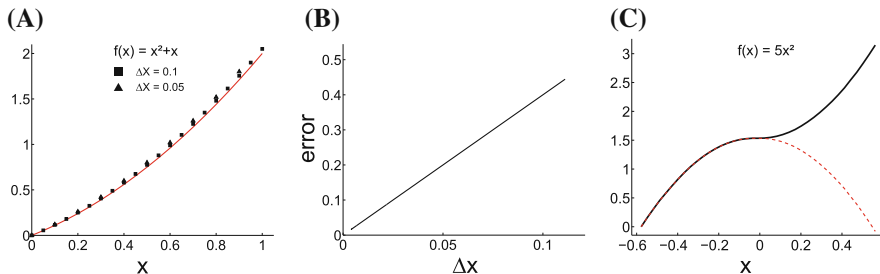


Fig. 11.6 Implementation of the reconstruction algorithm. (A) Reconstruction of the parabola $f(x) = x^2 + x$ (red) with the resolutions $\Delta x = 0.05$ and $\Delta x = 0.1$. (B) The estimation error $(f, \Delta x)$ vs bin size Δx . (C) Reconstruction of the parabola $f(x) = 5x^2$ from the effective diffusion coefficient assuming $f'(x) > 0$ (black), and with the sign of $f'(x)$ determined from the geometric drift (red). Both curves are normalized so that $f'(0) = 0$

Approximation Formulas for the Drift and Diffusion Coefficients

Starting with a sample of N_t projected trajectories $\{x^i(t_j), i = 1, 2, \dots, N_t, j = 1, 2, \dots, N_s\}$, where t_j are the sampling times, the dynamics (11.13) and the curve C are reconstructed by computing the effective drift and diffusion coefficients of the projected diffusion process. First, the range of the projected points on the line is partitioned into M bins of width Δx , centered at x_k , such that

$$x_1 - \frac{\Delta x}{2} < \min\{x^i(t_j), 1 \leq i \leq N_t, 1 \leq j \leq N_s\}$$

and

$$x_M + \frac{\Delta x}{2} > \max\{x^i(t_j), 1 \leq i \leq N_t, 1 \leq j \leq N_s\}.$$

The geometric drift and effective diffusion coefficient of the projected diffusion process are evaluated in each bin from the empirical versions of the formulas (see Annotations 11.3)

$$a_{\text{geometric}}(x) = \lim_{\Delta t \rightarrow 0} \frac{1}{\Delta t} \mathbb{E}[x(t + \Delta t) - x(t) | x(t) = x] \quad (11.22)$$

$$2D_{\text{effective}}(x) = \lim_{\Delta t \rightarrow 0} \frac{1}{\Delta t} \mathbb{E}[(x(t + \Delta t) - x(t))^2 | x(t) = x]. \quad (11.23)$$

The empirical version of (11.22) at each bin point x_k is

$$a_{\text{geometric}}(x_k) = \frac{1}{N_k} \sum_{i=1}^{N_t} \sum_{j=1, x^i(t_j) \in B(x_k, \Delta x/2)}^{N_s} \frac{x^i(t_{j+1}) - x^i(t_j)}{\Delta t}, \quad (11.24)$$

where $B(x_k, \Delta x/2)$ is the bin $[x_k - \Delta x, x_k + \Delta x]$.

The condition $x^i(t_j) \in B(x_k, \Delta x/2)$ in the summation means that $|x^i(t_j) - x_k| < \Delta x/2$. The points $x^i(t_j)$ and $x^i(t_{j+1})$ are sampled consecutively from the i th trajectory such that $x^i(t_j) \in B(x_k, \Delta x/2)$ and the number of points in $B(x_k, \Delta x/2)$ is N_k . Similarly, the empirical version of (11.23) at bin point x_k is

$$D_{\text{effective}}(x_k) = \frac{1}{N_k} \sum_{j=1}^{N_t} \sum_{j=1, \tilde{x}^i(t_j) \in B(x_k, \Delta x/2)}^{N_s} \frac{[x^i(t_{j+1}) - x^i(t_j)]^2}{2\Delta t}. \quad (11.25)$$

Once the effective diffusion coefficient is estimated empirically, the curve C can be reconstructed by solving the differential equation (11.11) over the sampling interval. In the case of a constant diffusion coefficient $D(X) = D$ the value of D is recovered from (11.10), and the geometric drift is then given by (11.9) as the empirical value

$$a_{\text{geometric}}(x_k) = \frac{1}{2} \frac{D_{\text{effective}}(x_k) - D_{\text{effective}}(x_{k-1})}{\Delta x}. \quad (11.26)$$

When the curve, the geometric drift, and the diffusion coefficients are known, the drift $b(X)$, described in (11.15), is found by combining (11.24), (11.25), and (11.26). The empirical projected drift $b(x)$ is recovered from (11.15) as

$$b(x_k) \approx \frac{a(x_k) - a_{\text{geometric}}(x)}{\sqrt{D(x_k)}}. \quad (11.27)$$

11.2 Reconstruction of a Surface from Planar Projections of Diffusion Trajectories

11.2.1 The Drift Field

As in the one-dimensional case, we begin with the driftless case. The model of an autonomous driftless diffusion process $X(t)$ on a smooth two-dimensional manifold $\Sigma \subset \mathbb{R}^3$ is the system of stochastic differential equations

$$dX(t) = \sqrt{2}\mathbf{B}(X(t)) dW(t), \quad (11.28)$$

where $W(t)$ is Brownian motion on Σ and $\mathbf{B}(X)$ is the noise matrix. The planar projection $Y(t)$ of $X(t)$ satisfies the stochastic differential equation

$$dY(t) = \mathbf{a}(Y(t)) dt + \sqrt{2}\tilde{\mathbf{B}}(Y(t)) d\tilde{W}(t), \quad (11.29)$$

where $\mathbf{a}(Y)$ and $\tilde{\mathbf{B}}(Y)$ are expressible in terms of the derivatives of Σ on the projection plane (e.g., a fixed plane Π tangent to Σ). Because Σ is unknown, $\mathbf{a}(Y)$ and $\tilde{\mathbf{B}}(Y)$ are the effective drift field and diffusion matrix observed in Π . Thus the first task is to obtain analytic expressions for these functions. Once explicit expressions for the effective drift field and diffusion tensor are found in terms of local surface properties, such as the mean curvature, the next task is the reconstruction of the surface. This step requires the solution of nonlinear partial differential equations that are derived below.

Consider first Brownian motion $X(t)$ on Σ and its planar projection. Assuming that Σ has the explicit representation $z = f(x, y)$, where $f(x, y)$ is a sufficiently smooth function defined in a planar domain \mathcal{D} in the (x, y) plane, we can assume that the (x, y) plane is tangent to Σ at the origin $\mathbf{0}$, that is, $\mathbf{0} \in \Sigma$ and the normal to Σ at $\mathbf{0}$ is the z -axis. We fix an orthonormal frame $(\mathbf{i}, \mathbf{j}, \mathbf{k})$, where \mathbf{k} is the unit vector in the direction of the z -axis. Thus

$$X(t) = x(t)\mathbf{i} + y(t)\mathbf{j} + z(t)\mathbf{k}, \quad z(t) = f(x(t), y(t)). \quad (11.30)$$

For a driftless diffusion $X(t)$ with a symmetric diffusion tensor $\sigma^{i,j}(X)$ on Σ with a tangent plane Π at $X(t) \in \Sigma$, we define the orthonormal frame

$$\begin{aligned} \tilde{\mathbf{x}} &= \frac{1}{\sqrt{1+f_x^2}} \begin{pmatrix} 1 \\ 0 \\ f_x \end{pmatrix}, \quad \mathbf{t}_y = \frac{1}{\sqrt{(1+f_x^2)(1+f_x^2+f_y^2)}} \begin{pmatrix} f_x f_y \\ -(1+f_x^2) \\ -f_y \end{pmatrix} \\ \mathbf{n} &= \frac{1}{\sqrt{1+f_x^2+f_y^2}} \begin{pmatrix} -f_x \\ -f_y \\ 1 \end{pmatrix}. \end{aligned} \quad (11.31)$$

The orthogonal projection $\tilde{X}(t + \Delta t) = \tilde{x}(t + \Delta t)\mathbf{i} + \tilde{y}(t + \Delta t)\mathbf{j} + \tilde{z}(t + \Delta t)\mathbf{k}$ on Π of the Brownian motion $X(t + \Delta t) \in \Sigma$ is given in terms of (11.31) by

$$\tilde{X}(t + \Delta t) = X(t) + \Delta u_1 \mathbf{i} + \Delta u_2 \mathbf{j} + \Delta u_3 \mathbf{k}, \quad (11.32)$$

where

$$\begin{aligned}\Delta u_1 &= \frac{1}{\sqrt{1 + f_x^2}} \left(\Delta s_1 + \frac{f_x f_y}{\sqrt{1 + f_x^2 + f_y^2}} \Delta s_2 \right) \\ \Delta u_2 &= - \frac{\sqrt{1 + f_x^2}}{\sqrt{1 + f_x^2 + f_y^2}} \Delta s_2 \\ \Delta u_3 &= \frac{1}{\sqrt{1 + f_x^2}} \left(f_x \Delta s_1 - \frac{f_y}{\sqrt{1 + f_x^2 + f_y^2}} \Delta s_2 \right)\end{aligned}$$

and

$$\begin{aligned}\Delta s_1 &= B_{1,1}(X(t)) \Delta w_1 + B_{1,2}(X(t)) \Delta w_2 \\ \Delta s_2 &= B_{2,1}(X(t)) \Delta w_1 + B_{2,2}(X(t)) \Delta w_2,\end{aligned} \quad (11.33)$$

with $w_1(t), w_2(t)$ independent standard Brownian motions in \mathbb{R} . The diffusion tensor $\sigma(X)$ is given in terms of the matrix $B(X)$ as

$$\sigma(X) = \frac{1}{2} B(X) B^T(X). \quad (11.34)$$

To regain $X(t + \Delta t)$, the point $\tilde{X}(t + \Delta t)$ is projected orthogonally back from Π to Σ to give

$$X(t + \Delta t) = \tilde{X}(t + \Delta t) + \theta(\Delta t) \mathbf{n}(X(t)), \quad (11.35)$$

where the parameter $\theta(\Delta t) \in \mathbb{R}$ is the solution of the equation

$$z(t + \Delta t) = f(x(t + \Delta t), y(t + \Delta t)) \quad (11.36)$$

with

$$\begin{cases} x(t + \Delta t) = x(t) \\ + \frac{1}{\sqrt{1 + f_x^2}} \left(\Delta s_1 + \frac{f_x f_y}{\sqrt{1 + f_x^2 + f_y^2}} \Delta s_2 \right) - \frac{\theta(\Delta t) f_x}{\sqrt{1 + f_x^2 + f_y^2}} \\ y(t + \Delta t) = y(t) \\ - \frac{\sqrt{1 + f_x^2}}{\sqrt{1 + f_x^2 + f_y^2}} \Delta s_2 - \frac{\theta(\Delta t) f_y}{\sqrt{1 + f_x^2 + f_y^2}} \\ z(t + \Delta t) = z(t) \\ + \frac{1}{\sqrt{1 + f_x^2}} \left(f_x \Delta s_1 - \frac{f_y}{\sqrt{1 + f_x^2 + f_y^2}} \Delta s_2 \right) + \frac{\theta(\Delta t)}{\sqrt{1 + f_x^2 + f_y^2}}, \end{cases} \quad (11.37)$$

where $\theta(\Delta t)$ is such that (see Annotations 11.3)

$$\begin{aligned} \theta(X) &= \lim_{\Delta t \rightarrow 0} \frac{\theta(\Delta t)}{\Delta t} \\ &= \frac{f_{xx}}{2(1 + f_x^2)} \left[\frac{\sigma_{1,1}(X)}{\sqrt{1 + f_x^2 + f_y^2}} + \frac{\sigma_{2,2}(X) f_x^2 f_y^2}{(1 + f_x^2 + f_y^2)^{3/2}} + \frac{2\sigma_{1,2}(X) f_x f_y}{1 + f_x^2 + f_y^2} \right] \\ &\quad - \frac{f_{xy}}{1 + f_x^2 + f_y^2} \left[\sigma_{1,2}(X) + \frac{\sigma_{2,2}(X) f_x f_y}{\sqrt{1 + f_x^2 + f_y^2}} \right] + \frac{f_{yy}}{2} \frac{\sigma_{2,2}(X)(1 + f_x^2)}{(1 + f_x^2 + f_y^2)^{3/2}}. \end{aligned} \quad (11.38)$$

In the isotropic case, $\mathbf{B}(X) = \mathbf{I}$, we obtain

$$\theta(X) = \frac{1}{2(1 + f_x^2 + f_y^2)^{3/2}} [(1 + f_y^2) f_{xx} - 2 f_x f_y f_{xy} + (1 + f_x^2) f_{yy}], \quad (11.39)$$

which is the mean curvature at the point X . Setting

$$\mathbf{C}(\mathbf{x}) = \begin{pmatrix} \frac{1}{\sqrt{1 + f_x^2(\mathbf{x})}} & \frac{f_x(\mathbf{x}) f_y(\mathbf{x})}{\sqrt{1 + f_x^2(\mathbf{x})} \sqrt{1 + f_x^2(\mathbf{x}) + f_y^2(\mathbf{x})}} \\ 0 & \frac{-\sqrt{1 + f_x^2(\mathbf{x})}}{\sqrt{1 + f_x^2(\mathbf{x}) + f_y^2(\mathbf{x})}} \end{pmatrix}, \quad (11.40)$$

we define

$$\tilde{\mathbf{B}}(X) = \mathbf{C}(\mathbf{x}) \mathbf{B}(X), \quad \tilde{\sigma}(X) = \frac{1}{2} \tilde{\mathbf{B}}(X) \tilde{\mathbf{B}}^T(\mathbf{x}). \quad (11.41)$$

To compute the observed drift $\mathbf{a}_{\text{geometric}}(\mathbf{x})$ and the observed effective diffusion tensor $\tilde{\sigma}(\mathbf{x}_k)$, we first partition the projection of the surface on the (x, y) plane into square bins $B(\mathbf{x}_k, \Delta x/2)$ of size Δx . The sampled points $\tilde{\mathbf{x}}_i^j = (\tilde{x}_i^j, \tilde{y}_i^j)$ are partitioned into the bins $B(\mathbf{x}_k, \Delta x/2)$. The generalization of (11.24) for the geometric drift $\mathbf{a}_{\text{geometric}}(\mathbf{x}) = (a_x(\mathbf{x}), a_y(\mathbf{x}))^T$ is

$$\begin{aligned} a_x(\mathbf{x}_k) &\approx \frac{1}{N_k} \sum_{j=1}^{N_t} \sum_{i=0, \tilde{\mathbf{x}}_i^j \in B(\mathbf{x}_k, \Delta x/2)}^{N_s-1} \left(\frac{\tilde{x}_{i+1}^j - \tilde{x}_i^j}{\Delta t} \right) \\ a_y(\mathbf{x}_k) &\approx \frac{1}{N_k} \sum_{j=1}^{N_t} \sum_{i=0, \tilde{\mathbf{x}}_i^j \in B(\mathbf{x}_k, \Delta x/2)}^{N_s-1} \left(\frac{\tilde{y}_{i+1}^j - \tilde{y}_i^j}{\Delta t} \right). \end{aligned} \quad (11.42)$$

The components of the effective diffusion tensor $\tilde{\sigma}(\mathbf{x}_k)$ (see (11.41)) is approximated by the empirical sums

$$\begin{aligned} \tilde{\sigma}_{xx}(\mathbf{x}_k) &\approx \frac{1}{N_k} \sum_{j=1}^{N_t} \sum_{i=0, \mathbf{x}_i \in B(\mathbf{x}_k, \Delta x/2)}^{N_s-1} \frac{(x_{i+1} - x_i)^2}{2\Delta t} \\ \tilde{\sigma}_{yy}(\mathbf{x}_k) &\approx \frac{1}{N_k} \sum_{j=1}^{N_t} \sum_{i=0, \mathbf{x}_i \in B(\mathbf{x}_k, \Delta x/2)}^{N_s-1} \frac{(y_{i+1} - y_i)^2}{2\Delta t} \\ \tilde{\sigma}_{xy}(\mathbf{x}_k) &\approx \frac{1}{N_k} \sum_{j=1}^{N_t} \sum_{i=0, \mathbf{x}_i \in B(\mathbf{x}_k, \Delta x/2)}^{N_s-1} \frac{(y_{i+1} - y_i)(x_{i+1} - x_i)}{2\Delta t}. \end{aligned} \quad (11.43)$$

Thus $\tilde{\sigma}(\mathbf{X})$ can be considered known (see, e.g., formula (11.20) for the estimate of $D_{\text{effective}}(\mathbf{x})$ in Appendix 11.1.4). Therefore the system in the (x, y) plane, which describes the projected driftless diffusion $\mathbf{z}(t) = f(\mathbf{x}(t), y(t))$ on Σ , is the planar diffusion $\mathbf{x}(t)$ process defined by the stochastic differential equation

$$d\mathbf{x} = \mathbf{a}_{\text{geometric}}(\mathbf{x}) dt + \tilde{\mathbf{B}}(\mathbf{x}, f(\mathbf{x})) d\mathbf{w}, \quad (11.44)$$

where

$$\mathbf{a}_{\text{geometric}}(\mathbf{x}) = - \frac{\nabla f(\mathbf{x})}{\sqrt{1 + |\nabla f(\mathbf{x})|^2}} \theta(\mathbf{x}, f(\mathbf{x})), \quad (11.45)$$

and $\mathbf{w}(t) = (w_1(t), w_2(t))^T$. If $\mathbf{B}(\mathbf{X}) = \sqrt{2D(\mathbf{X})}\mathbf{I}$, then

$$\theta(\mathbf{X}) = \frac{D(\mathbf{X})}{2(1 + f_x^2 + f_y^2)^{3/2}} [(1 + f_y^2)f_{xx} - 2f_x f_y f_{xy} + (1 + f_x^2)f_{yy}] \quad (11.46)$$

and (11.44) becomes

$$\begin{aligned} dx_t &= -D(\mathbf{X})f_x \left(\frac{(1+f_y^2)f_{xx} - 2f_x f_y f_{xy} + (1+f_x^2)f_{yy}}{2(1+|\nabla f|^2)^2} \right) dt \\ &\quad + \frac{\sqrt{2D(\mathbf{X})}}{\sqrt{1+f_x^2}} \left[dw_1 + \frac{f_x f_y}{\sqrt{1+|\nabla f|^2}} dw_2 \right] \\ dy_t &= -D(\mathbf{X})f_y \left(\frac{(1+f_y^2)f_{xx} - 2f_x f_y f_{xy} + (1+f_x^2)f_{yy}}{2(1+f_x^2+f_y^2)^2} \right) dt \\ &\quad - \frac{\sqrt{2D(\mathbf{X})(1+f_x^2)}}{\sqrt{1+|\nabla f|^2}} dw_2. \end{aligned} \tag{11.47}$$

The surface Σ and the diffusion tensor can be recovered from the observed projections. That is, when the dynamics on the surface Σ contains a drift field, that of the projected dynamics is split into a part that is due to the surface curvature and a part due to the original drift. Specifically, when $X(t)$ has a drift vector on Σ , $\beta(\mathbf{X}) = \beta_x \mathbf{i} + \beta_y \mathbf{j} + \beta_z \mathbf{k}$, such that $\beta_z(\mathbf{X}) = \beta_x(\mathbf{X})f_x(\mathbf{x}) + \beta_y(\mathbf{X})f_y(\mathbf{x})$, the stochastic equations of the projected diffusion contain an additional drift vector

$$d\mathbf{x} = \mathbf{a}(\mathbf{x}, f(\mathbf{x})) dt + \tilde{\mathbf{B}}(\mathbf{x}, f(\mathbf{x})) d\mathbf{w}, \tag{11.48}$$

where

$$\mathbf{a}(\mathbf{x}) = \mathbf{b}(\mathbf{x}) + \mathbf{a}_{\text{geometric}}(\mathbf{x}). \tag{11.49}$$

11.2.2 The Reconstruction Procedure

For an isotropic constant diffusion from the projection of a Brownian motion from Σ to the (x, y) plane and recover the function $z = f(x, y)$ and the diffusion coefficient D from the effective diffusion tensor

$$\begin{aligned} \tilde{\sigma}_{1,1} &= D \frac{1+f_y^2}{1+f_x^2+f_y^2} \\ \tilde{\sigma}_{1,2} &= -D \frac{f_x f_y}{1+f_x^2+f_y^2} \\ \tilde{\sigma}_{2,2} &= D \frac{1+f_x^2}{1+f_x^2+f_y^2}, \end{aligned} \tag{11.50}$$

given in (11.41). The system (11.50) of three algebraic equations for the unknowns D , f_x , and f_y can be solved explicitly and then Σ is recovered by integrating the gradient $\nabla f(x, y)$ and reduces to solving the new equation

$$\frac{\tilde{\sigma}_{2,2}}{\tilde{\sigma}_{1,1}} - 1 = f_x^2 - \frac{\tilde{\sigma}_{2,2}}{4\tilde{\sigma}_{1,1}} \left(-\frac{\tilde{\sigma}_{1,1}}{\tilde{\sigma}_{1,2}} f_x \pm \sqrt{\left(\frac{\tilde{\sigma}_{1,1}}{\tilde{\sigma}_{1,2}}\right)^2 f_x^2 - 4} \right)^2. \quad (11.51)$$

Before recovering the drift, we note that because

$$\boldsymbol{a}_{\text{geometric}}(\mathbf{x}) = -D \frac{(1 + f_y^2)f_{xx} - 2f_x f_y f_{xy} + (1 + f_x^2)f_{yy}}{2(1 + f_x^2 + f_y^2)^2} \begin{pmatrix} f_x \\ f_y \end{pmatrix}, \quad (11.52)$$

the level curves of $f(x, y)$ can be determined by integrating the geometric drift at any point in the planar projection of Σ . To recover an isotropic Brownian motion with constant diffusion coefficient on Σ from its planar projection, we determine the unknown drift $\boldsymbol{b}(\mathbf{x})$ by solving the system (11.49), where now the vector $\boldsymbol{a}(\mathbf{x})$ is the observed drift of the projected diffusion and thus can be considered known. Note that numerical reconstruction is not an easy task and attention should be paid to many details, as explained below (Fig. 11.7).

11.3 Annotations

The category of extraction shape from shading is described in [Berthold et al. (1986)]. Formulas (11.22) and (11.23) are given in (Karlin and Taylor, 1981, p. 159) and [Schuss (2010b)]. Formulas (11.38)–(11.40) are derived in [Hoze et al. (2013)].

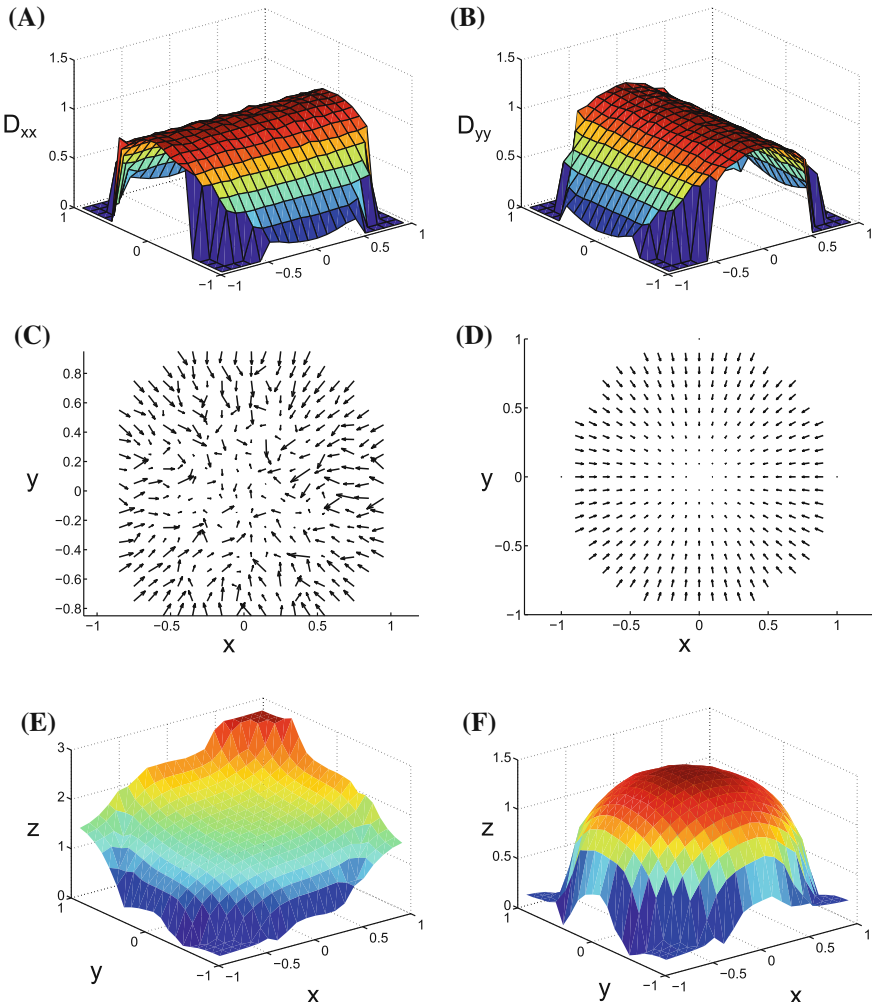


Fig. 11.7 Projection of spherical Brownian motion. (A) Diffusion coefficient D_{xx} reconstructed using equation (11.43). (B) Diffusion coefficient D_{yy} . (C) The drift field $\mathbf{a}(\mathbf{x}_k) = (a_x(\mathbf{x}_k), a_y(\mathbf{x}_k))^T$, reconstructed by formula (11.42). (D) The theoretical drift field of the projected Brownian motion on a sphere, obtained from Eq. (11.47). (E) Reconstruction of the sphere assuming $f_x \geq 0$ and $f_y \geq 0$. (F) Reconstruction of the sphere. The parameter values are $D = 1$, $dt = 0.00005$, number of trajectories $N_t = 9,000$, number of points per trajectory $N_s = 1,000$, $\Delta X = 0.1$

Chapter 12

Asymptotic Formulas in Molecular and Cellular Biology

12.1 Introduction

Critical biological processes, such as synaptic plasticity and transmission, activation of genes by transcription factors, or double-stranded DNA-break repair, are controlled by diffusion in structures that have both large and small spatial scales. These may be small binding sites inside or on the surface of a cell, or narrow passages between subcellular compartments. The great disparity in spatial scales is the key to controlling cell function by structure. This disparity poses analytical and numerical difficulties in extracting properties from experimental data, from biophysical models, and from Brownian dynamics simulation of diffusion in multi-scale structures. Some of these difficulties are resolved by the methods described in Chaps. 7 and 8, which are applied here to the analysis and simulations of subcellular processes and to the quantification of their biological functions.

The disparity between spatial scales in a biological cell structure leads to time-scale separation between molecular events in the cell and in its physiological response. Specifically, the time scale of diffusion at large is much shorter than that of diffusing into small and hidden targets in cells. This separation indicates that the conversion of molecular events into cellular response, which is a rare event (on the time scale of diffusion), is controlled by structure.

The resolution of the structure-function relationship in channels is more accurate than in cells due to the nano-scale resolution of channel structure. The coarser scale of structural resolution of cellular and subcellular compartments necessitates far more complex mathematical and biophysical models than channel models. The former can be expected to give much coarser functional information on cellular function than the latter for channel function. In order to produce manageable cell models many physical features have to be given up, for example, interactions between mobile particles, which are the determinants of channel conductance and selectivity. The structural model of the cell, which is by and large unknown, also has to be simplified. The functional information that can be extracted from the simplified models of cell structure calls for different analytical and simulation tools than in channels. To

address the structure-function question in cell models, this Chapter focuses on several examples of simplified structures of cellular microdomains, such as the structure of enzymatic active sites, confined chromatin structure, the transient structure during cell division, and the flow of genetic materials exchanged by diffusion; in particular, on the regulation of diffusion flux in synapses and dendritic spines of neurons, whose spatial structure has been extensively studied (see Annotations 12.5).

There are about 10^{11} neurons in the human brain, each containing about 10^3 synapses, which consist of pre- and post-synaptic terminals. In excitatory connections the latter can be a dendritic spine-like structure (Fig. 12.1A-B). There are also stand-alone spines that all in all can number about 10^5 in a hippocampal neuron. The function of synapses and dendritic spines is still unclear, though their morphological changes in cognitive pathology, such as in epilepsy and autism spectrum disorders, indicate that they may be involved in regulating the synaptic function. The structure-function approach in modeling and analyzing these structures can possibly be the key to bridging the gap between the molecular and the cellular scales.

Recognized more than one hundred years ago by Ramón y Cajal (see Annotations 12.5) dendritic spines are small terminal protrusions on neuronal dendrites and are considered to be the main locus of excitatory synaptic connections. The general spine geometry, as shown in Fig. 12.1 (right), consists of a relatively narrow cylindrical neck connected to a bulky head (the round part in the schematic Fig. 6.3). Indeed, spine shapes can fall into one of these categories. In addition, spine geometrical shapes correlate with their physiological functions. Change of spine morphology can be induced by synaptic potentiation protocols and indeed, intracellular signaling, such as calcium release from stores, alters the morphology of dendritic spines in cultured hippocampal neurons. These changes in geometry can affect the spine-dendrite communication. One of the first quantitative assessments of geometry was obtained by a direct measurement of diffusion through the spine neck. Concentration gradients between spines and shafts in rat CA1 pyramidal neurons were established by photo-bleaching and photo-release of fluorescein dextran in order to track the time course of re-equilibration. It was well approximated by a single exponential decay, with a time constant in the range of 20 to 100 msec. The role of the spine neck was further investigated experimentally with flash photolysis of caged calcium and theoretically, with the main conclusion that geometrical changes in the spine neck, such as the length or the radius, are key modulators of calcium dynamics in the process of spine-dendrite communication. The connection between the head and the neck is not only relevant to three-dimensional diffusion and also in the synaptic cleft (Fig. 12.2), but for two-dimensional surface diffusion. Indeed, synaptic transmission and plasticity involve the trafficking of receptors on cell membranes such as AMPA or NMDA glutamatergic receptors, which mediate the post-synaptic current [Smith et al. (2000)], [Adesnik, Nicoll, and England (2005)], [Chen et al. (2000)] and [Bredt and Nicoll (2003)].

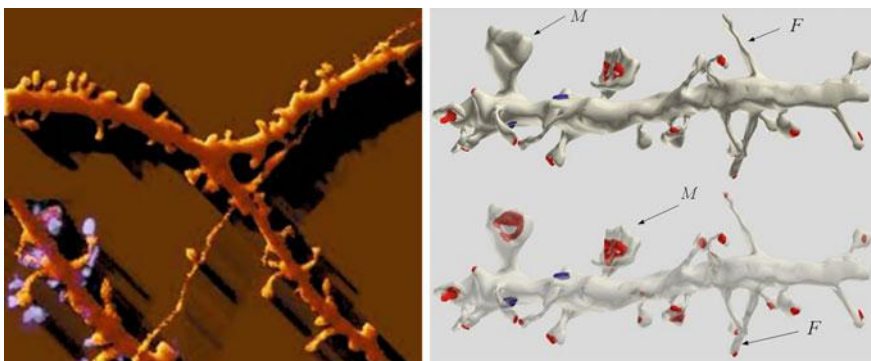
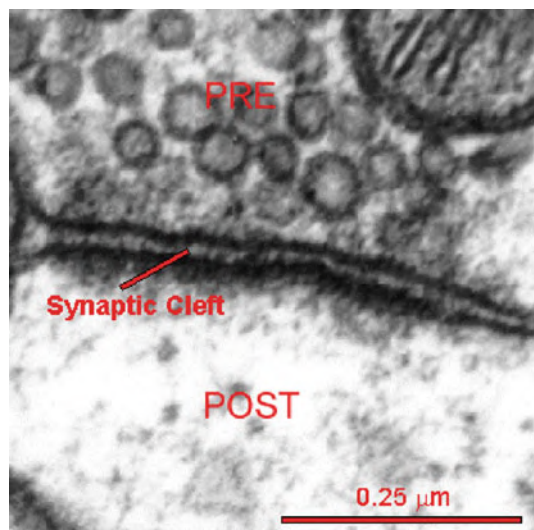


Fig. 12.1 Left: Spines on a dendrite. Right: Three-dimensional EM reconstruction of two dendrites from the hippocampus. The post-synaptic densities of excitatory synapses are marked red and of inhibitory synapses – blue. Filopodia (marked *F*) and mushroom spines (marked *M*) are clearly seen [Bourne and Harris (2008), with permission]

The number and type of receptors that shape the synaptic current can be regulated by spine geometry. Regulation of synaptic current by spine geometry was explored theoretically by using asymptotic expressions for the residence time and experimentally by monitoring the motion of AMPA receptors on the surface of mature neurons (see Annotations 12.5).

Fig. 12.2 Electron-microscopy of a synapse. Vesicles containing neurotransmitters can be seen inside the pre-synaptic terminal (marked Pre). The synaptic cleft separating pre- and post-synaptic membranes is 20–25 nm wide. Vesicles with neurotransmitters are clearly seen in this enlargement



12.2 From Molecular to Cellular Description

The asymptotic methods developed in Chaps. 7 and 8 describe how to bridge between physical models at the molecular scale and the micrometer scale, at which cells filter and convert molecular signals into cellular response. The latter defines cellular or subcellular function. The methods described here contributed to recent progress in quantifying analytically the control of diffusion flux into small absorbing targets or through narrow passages in cells. This case is especially important in molecular searches that are not directed at long distances by a field of force and the only flux control mechanism is the geometrical structure. We discuss here specific applications of the flux formulas in dendritic spines, in the case of synaptic transmission, for enzyme structure and hidden target sites, for diffusion in the confined chromatin structure in the context of DNA-repair, and the unilateral flow of genetic materials exchanged by diffusion during cell division.

The behavior of molecules is complex not only because of their individual structure, but also because they form clusters, interact, reflect, and so on. At this stage we only have access to certain sampled molecular trajectories, thus it is unclear how to reconstruct their dynamics from the statistics of the samples. In order to interpret molecular data, we adopt the widely accepted model of molecular motion as diffusion in a field of force. The force field may represent electric interactions with fixed or mobile charges, dielectric interactions with obstacles, such as lipid bilayers and other fixed cell components, hydrodynamical interactions with an ambient flow field, and so on. The task of molecular level model is to extract cellular level properties and infer from it cell function.

12.3 Flux Through Narrow Passages Identifies Cellular Compartments

The random movement of ions, proteins, and other particles in cells is traditionally described as Brownian motion, as mentioned above. The Brownian trajectories are reflected at the cell membrane and at other obstacles, but can be absorbed (terminated) at receptors and other binding sites or when they exit the cell (or a subcellular compartment) and enter another structure. Different compartments for Brownian trajectories are defined here by the probability density of the trajectories or the statistics of the time a trajectory spends at a point. As in segmentation of images (or other data, see Wikipedia), a histogram is computed from all points visited by a trajectory (or trajectories) and the peaks and valleys in the histogram are used to identify the compartments as clusters. By its very definition, the passage of a trajectory from one compartment to the other is a rare event. The rare events may be thermal activation over a potential barrier and/or traversing a narrow passage, such as a channel, a nano-pore, or a narrow neck.

The mean first passage time $\bar{\tau}$ of a Brownian trajectory from a compartment to an absorbing target or through a narrow passage is a fundamental concept in the description of rare events. Specifically, the probability density function of the time spent in a compartment prior to termination or escape from the compartment in the limit of small target is exponential for sufficiently long times,

$$p_{\bar{\tau}}(t) \sim \bar{\tau}^{-1} \exp\{-t/\bar{\tau}\}.$$

The exponential rate $\bar{\tau}^{-1}$ is therefore the flux into the absorbing target. In the case of crossing from one compartment to another through a narrow neck the crossing rate is $1/2\bar{\tau}$, where $\bar{\tau}$ is the mean first passage time to the stochastic separatrix between the compartments. The latter is the locus of initial points of a Brownian trajectory from which it ends up in one compartment or the other with equal probabilities [Schuss (2013)].

12.4 Examples of Asymptotic Formulas: Fluxes into Small Targets

In this section we provide models and applications in cell biology for the analytical approximations to the solution of mean first passage time discussed in Chaps. 7 and 8.

12.4.1 Formulas in Two Dimensions

The asymptotic formulas of the mean first passage time (6.1), when the domain Ω is in the plane and the absorbing boundary is a small sub-arc $\partial\Omega_a$ (of length a) of the boundary $\partial\Omega$, are not very intuitive. Thus, it is not very fruitful to guess what they should be, so exact computations are necessary. It is indeed hard to tell in advance how the geometry alters diffusion processes. The recipe we adopted in Chaps. 7 and 8 is to follow the analytical derivations that reveal how local and global structures, smooth or not, with and without local curvature controls the escape time. The local geometry of these escape problems are illustrated in Fig. 12.3.

- When $\partial\Omega_a$ is a sub-arc of a smooth boundary, the mean first passage time from any point x in Ω to $\partial\Omega_a$ is denoted $\bar{\tau}_{x \rightarrow \partial\Omega_a}$. For

$$\varepsilon = \frac{\pi |\partial\Omega_a|}{|\partial\Omega|} = \frac{\pi a}{|\partial\Omega|} \ll 1 \quad (12.1)$$

the mean first passage time is independent of x outside a small vicinity of $\partial\Omega_a$ (called a boundary layer). Thus for $x \in \Omega$, outside a boundary layer near $\partial\Omega_a$,

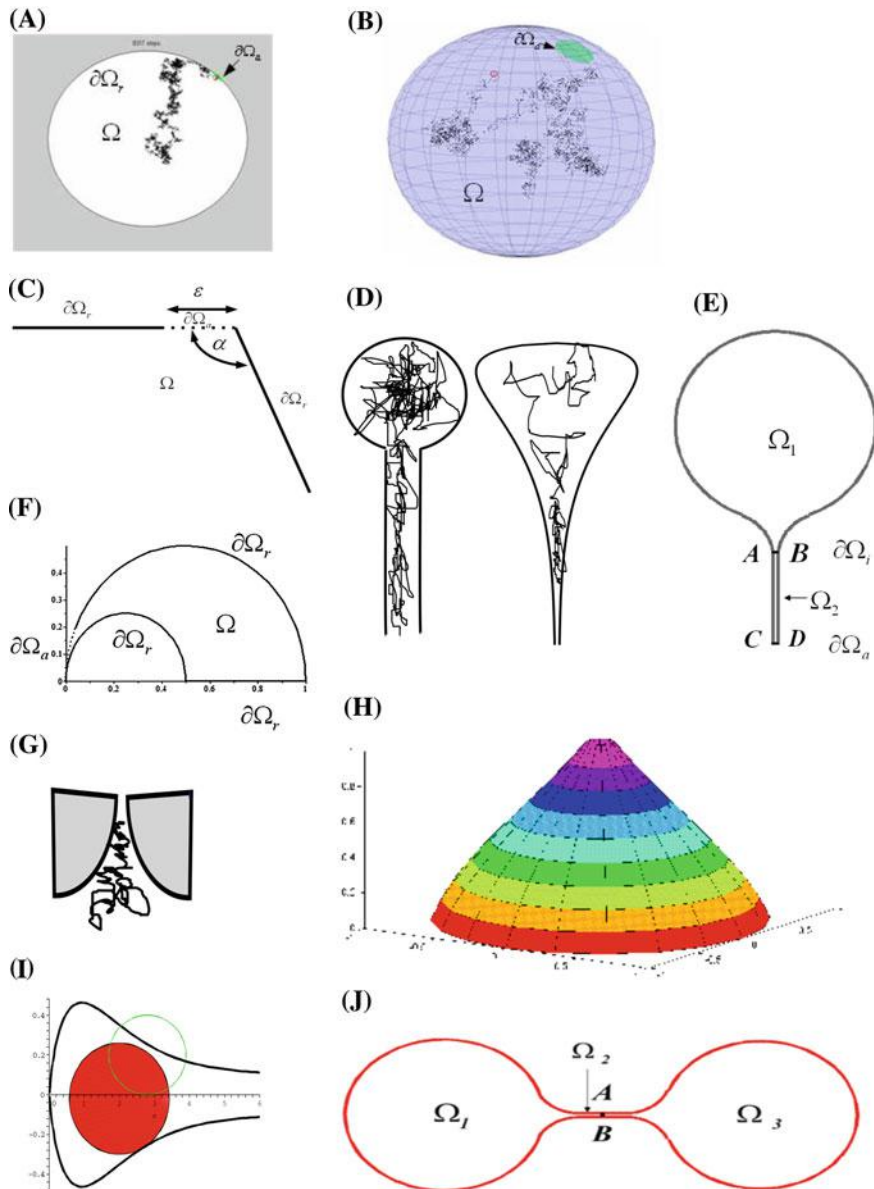


Fig. 12.3 Classification of narrow-escape-time formulas. (A) The absorbing boundary $\partial\Omega_a$ is a short arc (marked green) of the smooth boundary curve $\partial\Omega$. (B) $\partial\Omega_a$ is an absorbing disk arc (marked green) on a surface. (C) $\partial\Omega_a$ is a short arc at a corner arc (marked ε). (D) $\partial\Omega_a$ is an absorbing segment (resp. circle) at the end of a narrow strip (resp. cylinder) connected non-smoothly to the head in a planar (resp. surface of revolution) dendritic spine model. (E) $\partial\Omega_a$ is a short segment CD at the end of the narrow strip Ω_2 in the plane or a circle at the end of the narrow cylinder Ω_2 on a surface of revolution connected smoothly to the head. (F) $\partial\Omega_a$ is a short arc at a boundary cusp arc (marked ε). (G) $\partial\Omega_a$ is a narrow opening at the end of a cusp-like funnel. (H) $\partial\Omega_a$ is an opening at the end of a funnel of finite angle. (I) The narrow passage is formed by an obstacle. (J) A dumbbell-shaped domain

$$\bar{\tau}_{x \rightarrow \partial\Omega_a} = \frac{|\Omega|}{\pi D} \log \frac{1}{\varepsilon} + O(1), \quad (12.2)$$

where $O(1)$ depends on the initial distribution of x .

If Ω is a disc of radius R , then for x at the center of the disk (Fig. 12.3A),

$$\bar{\tau}_{x \rightarrow \partial\Omega_a} = \frac{R^2}{D} \left[\log \frac{R}{a} + 2 \log 2 + \frac{1}{4} + O(\varepsilon) \right], \quad (12.3)$$

and averaging with respect to a uniform distribution of x in the disk

$$\bar{\tau} = \frac{R^2}{D} \left[\log \frac{R}{a} + 2 \log 2 + \frac{1}{8} + O(\varepsilon) \right]. \quad (12.4)$$

The flux through a hole in a smooth wall on a flat membrane surface is regulated by the area $|\Omega|$ inside the wall, the diffusion coefficient D , and the aspect ratio ε (12.1). These formulae are used to estimate the residence time a receptor spends moving on the surface of a cell.

In the case of Brownian motion on a sphere of radius R , the mean first passage time to an absorbing circle centered on the north-south axis near the south pole with small radius $a = R \sin \delta/2$ is given by

$$\bar{\tau} = \frac{2R^2}{D} \log \frac{\sin \frac{\theta}{2}}{\sin \frac{\delta}{2}}, \quad (12.5)$$

where θ is the angle between x and the south-north axis of the sphere (Fig. 12.3B).

2. If the absorbing window is located at a corner of angle α , then

$$\bar{\tau} = \frac{|\Omega|_g}{D\alpha} \left[\log \frac{1}{\varepsilon} + O(1) \right], \quad (12.6)$$

where $|\Omega|_g$ is the surface area of the domain on the curved surface, calculated according to the Riemannian metric on the surface. Formula (12.6) indicates that control of flux is also regulated by the access to the absorbing window afforded by the angle of the corner leading to the window (Fig. 12.3C). This formula was obtained using a conformal map sending a corner to a flat line.

3. If the absorbing window is located at a cusp, then $\bar{\tau}$ grows algebraically, rather than logarithmically. Thus, in the domain bounded between two tangent circles, the expected lifetime is

$$\bar{\tau} = \frac{|\Omega|}{(d^{-1} - 1)D} \left(\frac{1}{\varepsilon} + O(1) \right), \quad (12.7)$$

where $d < 1$ is the ratio of the radii (Fig. 12.3F). Formula (12.7) indicates that a drastic reduction of flux can be achieved by inserting an obstacle that limits the

access to the absorbing window by forming a cusp-like passage. This formula was derived using the exponential conformal map.

4. When $\partial\Omega_a$ (of length a) is located at the end of a narrow neck with radius of curvature R_c , the mean first passage time is given in (Fig. 12.3G and I)

$$\bar{\tau} = \frac{|\Omega|}{4D\sqrt{2a/R_c}} (1 + O(1)) \text{ for } a \ll |\partial\Omega|. \quad (12.8)$$

This formula is derived by a new method that uses a Möbius transformation to resolve the cusp singularity. The boundary layer at the cusp is sent to a banana shaped domain. Asymptotic formulas for a general cusp with an arbitrary power law are not known. This formula was used to show that blocking the exit from a two-dimensional domain by a round obstacle creating locally the shape of a cusp increases the residence exponentially.

For a surface of revolution generated by rotating the curve about its axis of symmetry, we use the representation of the generating curve

$$y = r(x), \quad \Lambda < x < 0$$

where the x -axis is horizontal with $x = \Lambda$ at the absorbing end AB . We assume that the parts of the curve that generate the funnel have the form

$$\begin{aligned} r(x) &= O(\sqrt{|x|}) \text{ near } x = 0 \\ r(x) &= a + \frac{(x-\Lambda)^{1+\nu}}{\nu(1+\nu)\ell^\nu} (1 + o(1)) \text{ for } \nu > 0 \text{ near } x = \Lambda, \end{aligned} \quad (12.9)$$

where $a = \frac{1}{2}\overline{AB} = \varepsilon/2$ is the radius of the gap, and the constant ℓ has dimension of length. For $\nu = 1$ the parameter ℓ is the radius of curvature R_c at $x = \Lambda$. The mean first passage time from the head to the absorbing end AB is given by

$$\bar{\tau} \sim \frac{\mathcal{S}(\Lambda)}{2D} \frac{\left(\frac{\ell}{(1+\nu)a}\right)^{\nu/1+\nu}}{\sin \frac{\nu\pi}{1+\nu}}, \quad (12.10)$$

where \mathcal{S} is the entire unscaled area of the surface. In particular, for $\nu = 1$ the mean first passage time (12.10) reduces to

$$\bar{\tau} \sim \frac{\mathcal{S}}{4D\sqrt{a/2\ell}}. \quad (12.11)$$

5. When a bulky head is connected to an essentially one-dimensional strip (or cylinder) of small radius a and length L , as is the case for a neuronal spine membrane (Fig. 12.3D). The connection of the head to the neck can be at an angle or by a smooth funnel. The boundary of the domain reflects Brownian trajectories and

only the end of the cylinder $\partial\Omega_a$ absorbs them. The domain Ω_1 is connected to the cylinder at an interface $\partial\Omega_i$, which in this case is an interval AB . The mean first passage time from $x \in \Omega_1$ to $\partial\Omega_a$ is given by

$$\bar{\tau}_{x \rightarrow \partial\Omega_a} = \bar{\tau}_{x \rightarrow \partial\Omega_i} + \frac{L^2}{2D} + \frac{|\Omega_1|L}{|\partial\Omega_a|D}. \quad (12.12)$$

The flux dependence on the neck length is quite strong. This formula is derived using the additive property of the mean first passage time.

6. A dumbbell-shaped domain (of type (VI)) consists of two compartments Ω_1 and Ω_3 and a connecting neck Ω_2 that is effectively one-dimensional (Fig. 12.3J), or in a similar domain with a long neck. A Brownian trajectory that hits the segment AB in the center of the neck Ω_2 is equally likely to reach either compartment before the other; thus AB is the stochastic separatrix. Therefore the mean time to traverse the neck from compartment Ω_1 to compartment Ω_3 is asymptotically twice the mean first passage time $\bar{\tau}_{\Omega_1 \rightarrow SS}$. Neglecting, as we may, the mean residence time of a Brownian trajectory in Ω_2 relative to that in Ω_1 or in Ω_3 we can write the transition rates from Ω_1 to the Ω_3 and as

$$\lambda_{\Omega_1 \rightarrow \Omega_3} = \frac{1}{2\bar{\tau}_{\Omega_1 \rightarrow SS}}, \quad \lambda_{\Omega_3 \rightarrow \Omega_1} = \frac{1}{2\bar{\tau}_{\Omega_3 \rightarrow SS}}. \quad (12.13)$$

These rates can be found from explicit expressions for the flux into an absorbing window

$$\lambda_1 \sim \frac{1}{\bar{\tau}}, \quad (12.14)$$

where $\bar{\tau}$ is given in (12.12). Here $\bar{\tau}_{x \rightarrow \partial\Omega_i}$ is any one of the mean first passage times given above, depending on the geometry of Ω_1 with L half the length of the neck and with $SS = \partial\Omega_a$. The radii of curvature $R_{c,1}$ and $R_{c,3}$ at the two funnels may be different in Ω_1 and Ω_3 . The smallest positive eigenvalue λ of the Neumann problem for the Laplace equation in the dumbbell is to leading order $\lambda = -(\lambda_{\Omega_1 \rightarrow \Omega_3} + \lambda_{\Omega_3 \rightarrow \Omega_1})$. For example, if the solid dumbbell consists of two general heads connected smoothly to the neck by funnels (see (12.19)), the two rates are given by

$$\begin{aligned} \frac{1}{\lambda_{\Omega_1 \rightarrow \Omega_3}} &= \sqrt{2} \left[\left(\frac{R_{c,1}}{a} \right)^{3/2} \frac{|\Omega_1|}{R_{c,1} D} \right] (1 + o(1)) + \frac{L^2}{4D} + \frac{|\Omega_1|L}{\pi a^2 D} \\ \frac{1}{\lambda_{\Omega_3 \rightarrow \Omega_1}} &= \sqrt{2} \left[\left(\frac{R_{c,3}}{a} \right)^{3/2} \frac{|\Omega_3|}{R_{c,3} D} \right] (1 + o(1)) + \frac{L^2}{4D} + \frac{|\Omega_3|L}{\pi a^2 D}. \end{aligned} \quad (12.15)$$

Formulas (12.15) indicate that the unidirectional fluxes between the two compartments of a dumbbell-shaped domain can be controlled by the area (or surface area) of the two and by the type of obstacles to the access to the connecting neck. The equilibration rate in the dumbbell, λ , is thus controlled by the geometry.

7. The mean time to escape through N well-separated absorbing windows of lengths a_j at the ends of funnels with radii of curvature ℓ_j , respectively, in the boundary $\partial\Omega$ of a planar domain Ω is given by

$$\bar{\tau} = \frac{\pi|\Omega|}{2D \sum_{j=1}^N \sqrt{a_j/\ell_j}} (1 + o(1)) \quad \text{for } a_j/\ell_j \ll |\partial\Omega|. \quad (12.16)$$

The probability to escape through window i is given by

$$p_i = \frac{\sqrt{a_i/\ell_i}}{\sum_{j=1}^N \sqrt{a_j/\ell_j}}. \quad (12.17)$$

Formulas (12.16) and (12.17) are significant for diffusion in a network of compartments connected by narrow passages (e.g., on a membrane strewn with obstacles). The dependence of the mean first passage time $\bar{\tau}$ and of the transition probabilities p_i on the local geometrical properties of the compartments renders the effective diffusion tensor in the network position-dependent and can give rise to anisotropic diffusion.

12.4.2 Narrow Escape Formulas in Three-Dimensions

The results reviewed here were obtained by the same methods as in two dimensions: matched asymptotics, Green's function, and conformal mapping to resolve cusp singularities. In axial symmetry, three-dimensional problems reduce to two dimensions and thus the conformal transformation can be used here as well.

1. The mean first passage time to a circular absorbing window $\partial\Omega_a$ of small radius a centered at $\mathbf{0}$ on the boundary $\partial\Omega$ is given by

$$\bar{\tau}_{x \rightarrow \partial\Omega_a} = \frac{|\Omega|}{4aD \left[1 + \frac{L(\mathbf{0}) + N(\mathbf{0})}{2\pi} a \log a + o(a \log a) \right]}, \quad (12.18)$$

where $L(\mathbf{0})$ and $N(\mathbf{0})$ are the principal curvatures of the boundary at the center of $\partial\Omega_a$. This formula was derived using the second-order expansion of the Neumann–Green function at the pole.

2. The mean first passage time from the head of the solid of revolution, obtained by rotating the symmetric domain about its axis of symmetry, to a small absorbing window $\partial\Omega_a$ at the end of a funnel (Fig. 12.3H) is given by

$$\bar{\tau} = \frac{1}{\sqrt{2}} \left(\frac{R_c}{a} \right)^{3/2} \frac{|\Omega|}{R_c D} (1 + o(1)) \text{ for } a \ll R_c, \quad (12.19)$$

where the R_c is the radius of curvature of the rotated curve at the end of the funnel.

3. The mean first passage time from a point x in a bulky head Ω to an absorbing disk $\partial\Omega_a$ of small radius a at the end of a narrow neck of length L connected to the head at an interface $\partial\Omega_i$ is given by the connection formula (12.12). When the cylindrical neck is attached to the head at a right angle the interface $\partial\Omega_i$ is a circular disk and $\bar{\tau}_{x \rightarrow \partial\Omega_i}$ is given by (12.18). When the neck is attached smoothly through a funnel, $\bar{\tau}_{x \rightarrow \partial\Omega_i}$ is given by (12.19).
4. The mean time to escape through N well-separated absorbing circular windows of radii a_j at the ends of funnels with curvatures ℓ_j , respectively, is given by

$$\bar{\tau} = \frac{1}{\sqrt{2}} \frac{|\Omega|}{D \sum_{j=1}^N \ell_j \left(\frac{a_j}{\ell_j} \right)^{3/2}}. \quad (12.20)$$

The exit probability through window i is given by

$$p_i = \frac{a_i^{3/2} \ell_i^{-1/2}}{\sum_{j=1}^N a_j^{3/2} \ell_j^{-1/2}}. \quad (12.21)$$

5. The principal eigenvalue of the Laplace equation in a dumbbell-shaped structure is given in item (vi), and equations (12.13)–(12.15) above.
6. The leakage flux through a circular hole of small radius a centered at $\mathbf{0}$ in the reflecting boundary is given by

$$J_a = 4aDu_0(\mathbf{0}) + O\left(\frac{a^2}{|\Omega|^{2/3}} \log \frac{a}{|\Omega|^{1/3}}\right), \quad (12.22)$$

where $u_0(\mathbf{0})$ is the concentration of diffusers at the window in the same model without the absorbing window.

7. A ribbon is a two-dimensional manifold with a nontrivial topology and thus the classical narrow escape results do not apply. To model the Brownian search for a small target located between a membrane and a vesicle, the local geometry (Fig. 12.4) is approximated by two tangent balls of radii R_1 and R_2 ($R_1 \ll R_2$). The search target is a small band of width a ($a \ll 1$). The rotational symmetry of the domain reduces the geometry of the problem to a two-dimensional domain. The absorbing band becomes a segment ($\partial\Omega_a$) joining the two disks. The solution to the mean first passage time is

$$v(r, z) = \frac{|\Omega|}{4\pi\mathcal{D}a} \left(1 - 2Ra \left(\frac{r}{r^2 + z^2} \right)^2 \right), \quad (12.23)$$

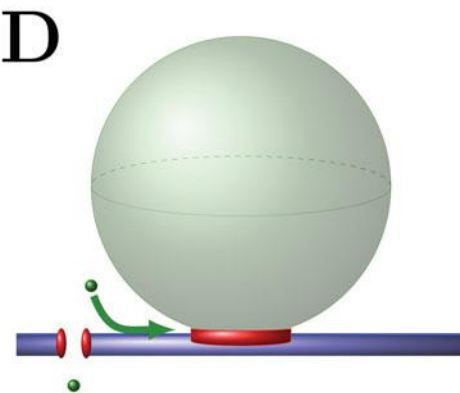
where $R = \frac{R_1 R_2}{R_2 - R_1}$. The Dire Strait Time is the mean first passage time $\bar{\tau}$ estimated for $x = 0$ in (12.23):

$$\bar{\tau} = \frac{|\Omega|}{4\pi\mathcal{D}a}. \quad (12.24)$$

This result is quite surprising compared to the narrow escape time: it does not depend on the curvature at the cusp and it diverges as $\frac{1}{a}$, which is the divergence obtained in the usual narrow escape problem for a small circular hole. Note that the surface area of the ribbon is $S_{rib}(a) = \sqrt{2Ra^{3/2}}$.

Fig. 12.4 Schematic cusp targets in cell biology characterized by the DST.

Model of particles searching for a cusp ribbon located between a ball and a flat surface



12.4.3 Cusp-Shaped Funnel: Hidden Targets Control Rates in \mathbb{R}^3

Active sites of a complex molecule, such as hemoglobin, penicillin-binding proteins, and many others, are often hidden inside the complex organization of α and β -sheet structures. A ligand, such β -lactam antibiotic, has to bind to a small site hidden inside the molecule and indeed, ligand recognition requires that strands be antiparallel in the active site area. This phenomenon was observed for large antibiotic molecules. In Figs. 12.5(2),(3) the penicillin-binding proteins are in closed and open conformations, respectively. In the closed conformation (Fig. 12.5 (2 and 3 Right)) the active site is blocked and unavailable for binding, while in the open state (Fig. 12.5 (2 and 3 Left)) the catalytic funnel reveals an elongated binding cleft, where the active site (red arrow) is hidden at the bottom.

The activation time for this case can be estimated from the funnel shape by the asymptotic formula (12.19).

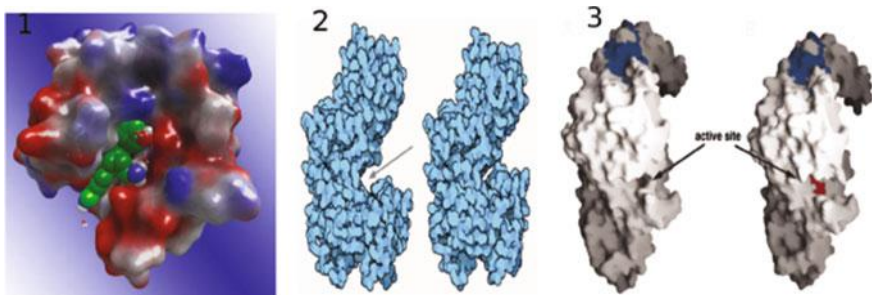


Fig. 12.5 (1) Complex molecule containing a hidden site. The domain Ω is the surrounding fluid, the absorbing boundary $\partial\Omega_a$ is the hidden target (marked green), and the reflecting boundary $\partial\Omega_r$ is the remaining surface of the molecule. (2) Hidden site. (3) Hidden active site

12.4.4 DNA Repair in a Confined Chromatin Structure in \mathbb{R}^2

A Brownian needle in a strip can model a messenger ribonucleic acid, a transcription factor, or a stiff DNA fragment moving in the very confined chromatin structure. For example, under severe stress, the DNA of the bacterium *Deinococcus radiodurans*, the most radioresistant organism, undergoes a phase transition in reorganizing the genome into tightly packed toroids (Fig. 12.6 (A,B,C)), which may facilitate DNA repair. Three-dimensional analysis reveals a complex network of double membranes that engulf the condensed DNA, suggesting that two-dimensional domains lying between parallel walls may play a significant role in DNA repair.

The diffusion of the needle is characterized by three diffusion coefficients: longitudinal along the axis D_X , transversal D_Y , and rotational D_r . For the diffusive motion of a needle confined to a planar strip, which is only slightly wider than the length of the needle, its turning around is a rare event (see Fig. 7.13). This is due to the narrow space around the vertical position of the needle in the strip. If the length of the needle l is only slightly smaller than the width of the strip $l_0 > l$, such that $\varepsilon = (l_0 - l)/l_0 \ll 1$, then the mean time for the needle to turn 180° is given by (Fig. 12.7)

$$\bar{\tau} = \frac{\pi \left(\frac{\pi}{2} - 1 \right)}{D_r \sqrt{l_0(l_0 - l)}} \sqrt{\frac{D_X}{D_r}} \left(1 + O \left(\sqrt{\frac{l_0 - l}{l_0}} \right) \right). \quad (12.25)$$

Formula (12.25) shows that when the free space between two planes decreases, the effective diffusion constant, proportional to the reciprocal of $\bar{\tau}$, experiences a second-order phase transition, characterized by a discontinuity of the derivative of the effective diffusion constant for the rotation (reciprocal of the mean first passage time (12.25)). Specifically, when the variable l reaches and exceeds the value $l = l_0$ the diffusion constant vanishes. This result explains the crucial role of the chromatin organization in maintaining the genome integrity during heavy radiation stress.

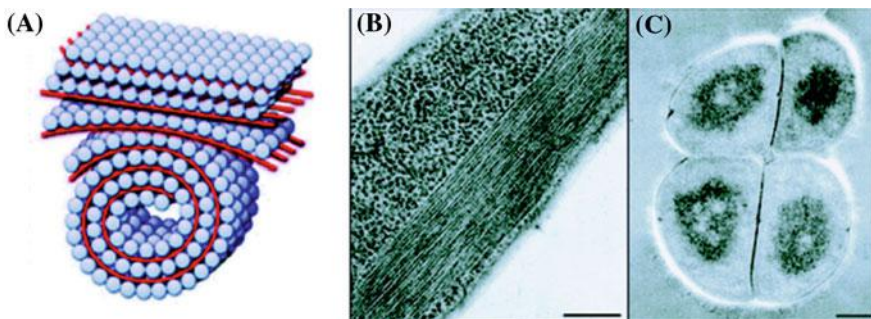


Fig. 12.6 (A) Two-dimensional stratification: the model depicts the toroidal morphology that acts as a structural template for growth of the DNA (DNA-binding protein) co-crystal. The DNA (red stripe) is localized in between the pseudo-hexagonal faces of the dodecameric symmetric proteins (blue spheres) [Minsky (2004)]. (B) Two-dimensional arrangement of DNA: formation of DNA–RecA “repairosome” assemblies in *E. coli* cells exposed to DNA-damaging agents. The ordered intracellular assembly is promoted by DNA molecular condensation and the structural features are modulated by the RecA proteins. Scale bar is 200 nm. (C) DNA packaging in the radioresistant bacteria *D. radiodurans*. The electron micrograph depicts the toroidal organization of its genome. Within this structure, the tight and ordered packaging of the DNA molecule may facilitate repair of double-stranded DNA breaks. Scale bar, 400 nm. The genomic reorganization in bacterial systems into tightly packed structures is proposed to restrict molecular diffusion

12.4.5 Asymmetric Dumbbell-Shaped Cell Division

An intermediate stage of a dividing cell consists of an asymmetric dumbbell shape with a relatively long connecting neck (Fig. 12.8). In this stage, some of the genetic material is delivered from the bigger (mother) to the smaller compartment (daughter). An open debate in this field is how the genetic material is selected. Specifically, the mean time to go from mother to daughter is given by $\tau_{M \rightarrow D} \sim 2\bar{\tau}_{M \rightarrow SS}$ and in the other direction by $\tau_{D \rightarrow M} \sim 2\bar{\tau}_{D \rightarrow SS}$ in the limit of a narrow neck. The transition rates given in (7.127) can differ by orders of magnitude as the geometry changes (see Annotations 12.5). The rate of equilibration between the two compartments can be found from the estimate of the second eigenvalue μ of the Neumann problem in the dumbbell-shaped domain, given by

$$\frac{1}{\mu} = \frac{1}{\tau_{D \rightarrow M}} + \frac{1}{\tau_{M \rightarrow D}}.$$

When the time scale of morphological changes in the shape of the dumbbell is slower than diffusion, the protein and genetic material transferred by diffusion from the mother to the daughter cell can be estimated from a reduced system of equations for the mass in the mother and daughter cells, M_M and M_D , respectively, given by

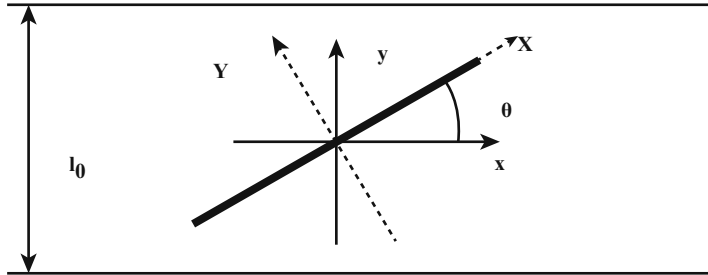


Fig. 12.7 Rod in strip. The strip width is l_0 and the needle length is $l < l_0$. The position of the needle is characterized by the angle θ and the fixed coordinates x, y of the center or in a rotating system of coordinates (X, Y, θ)

$$\begin{aligned}\dot{M}_D &= -\frac{M_D}{\tau_{M \rightarrow D}} + \frac{M_M}{\tau_{D \rightarrow M}} \\ \dot{M}_M &= -\frac{M_M}{\tau_{D \rightarrow M}} + \frac{M_D}{\tau_{M \rightarrow D}}\end{aligned}\tag{12.26}$$

with $M_M(0) = M_0$ and $M_D = 0$. The solution is

$$M_M(t) = M_0 \left(1 - \frac{\mu}{\tau_{D \rightarrow M}} \right) e^{-\mu t} + M_0 \frac{\mu}{\tau_{D \rightarrow M}}.\tag{12.27}$$

The mean transfer time from the mother to the daughter can be estimated with the following parameters [Gehlen et al. (2011)]: diffusion coefficient $D = 6.5 \times 10^{-3} \mu\text{m}^2/\text{s}$, a neck length $L = 0.1 \mu\text{m}$, a neck radius $a = 0.2 \mu\text{m}$, a mother radius of $R = 0.9 \mu\text{m}$ and a curvature of $R_c = 0.5 \mu\text{m}$, it is $\tau_{M \rightarrow D} = 5626\text{s}$, about an hour and a half.

As shown in Fig. 12.8, the connection geometry varies over time, which can change the flux drastically, as formulas (12.15) indicate. The small transfer rate may lead to an early separation between the mother and daughter cells, prior to reaching the steady state in (12.27). If steady state diffusion is reached before separation, the probability density function is uniform in the domain, rendering $M_M(\infty)$ and $M_D(\infty)$ proportional to the respective volumes. In the reduced model (12.26) the steady state masses are proportional to the fractions of the residence times in the two cells. In view of (12.15), these are proportional to the volumes to leading order in small neck radius. The reduced model can be used before steady state is reached. A simple consequence of (12.27) is that a Brownian simulation of the transferred material (messenger ribonucleic acid, soluble proteins, and so on) has to be run for times $t \gg 1/\mu$ to reach the steady state. Some transitions $M \rightarrow D$ and $D \rightarrow M$ have to occur in the simulation in order for a steady state to set in.

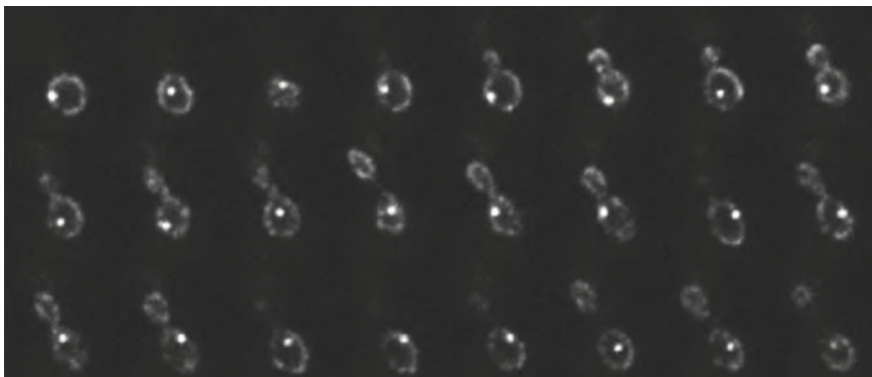


Fig. 12.8 Time-lapse images of mitotic cells: the dumbbell-shaped dividing cell seems to vary with time [Gehlen et al. (2011)]

12.5 Annotations

The discovery of dendritic spines was mentioned in 1909 by Ramón y Cajal in [Ramón y Cajal (1909)]. It is well known in the theory of ionic channels that structure is the main determinant of channel selectivity and gating [Hille (2001)] (see also R. MacKinnon's Nobel lecture [MacKinnon (2003)]). Traditionally, when the crystallographic structure of a channel is unknown, recordings of channel current-voltage characteristics are used to reconstruct the spatial organization of protein and ions that define the channel pore [Chen et al. (1997)], [Burger et al. (2007)]. But even when the crystallographic structure of a channel is known, the determination of the function of different channel components, such as gating, ionic selectivity, and channel conductances from the molecular structure is only partially known [Chen et al. (1999)], [Boda et al. (2007)].

A possible approach for an answer relies on either solving the Poisson–Nernst–Planck equations [Eisenberg and Chen (1993)] or Brownian or molecular dynamics simulations of the joint diffusive motion of protein and ions as well as the computation of the time-dependent electric field (see for example [Aboud et al. (2003)]).

The results mentioned in Sect. 12.4.5 can explain some experimental findings reported in [Gehlen et al. (2011)]. The regulation of diffusion flux has been demonstrated not only between mother and daughter cell during division but also for synapses and dendritic spines of neurons, whose spatial structures have been extensively studied (see for example [Harris and Stevens (1988)] and [Bourne and Harris (2008)]).

What makes the clusters, be it membranes, obstacles, or forces, is an active field of forces, observed in experimental live cell images by super-resolution microscopy [Manley et al. (2008)], [Huang et al. (2010)]. Formula (12.2) was derived in [Ward and Keller (1993)] and [Holcman and Schuss (2004)] (the paper predicted the potential wells discovered in [Hoze et al. (2012)]). The mean first passage time

(12.7) is given in [Holcman and Schuss (2012a)], [Holcman and Schuss (2015)] and (12.8) – in [Holcman and Schuss (2012a)] and [Holcman and Schuss (2015)]. Equation (12.8) is a key modulation for trafficking of receptors and channels on the surface of a neuron [Kerchner and Nicoll (2008)], (Borgdorff and Choquet, 2002), [Ashby et al. (2006)] (12.12) – in [Holcman and Schuss (2012a)], (12.15) - in [Holcman and Schuss (2012a)], (12.18)- in [Singer et al. (2008)], (12.19) – in [Holcman and Schuss (2012a)], (7.127)–(12.15) - in [Holcman and Schuss (2012a)] and (12.22) – in [Singer et al. (2008)].

The splitting probability to find the ribbon before exit is computed in [Guerrier and Holcman (2015)]. This ribbon asymptotic result is used to estimate the release probability of a vesicle (ball) driven by few ions sampled from a very large number located in the synaptic bulk. A new hybrid model based on discret Markov chain and continuum (mass-action law) equations is presented in [Guerrier and Holcman (2016)].

The asymptotic formula for narrow escape time [Holcman and Schuss (2014c)] is also referred to as the dire strait time (when escape occurs at a cusp-shaped boundary) [Holcman and Schuss (2012a)] (see the recent monographs [Holcman and Schuss (2015)] and [Holcman and Schuss (2016)] for recent applications in cellular biology. Other applications of the NET to immunology are described in [Delgado et al. (2014)]).

In Figs. 12.5(2),(3) the penicillin-binding proteins are in closed and open conformations, respectively [Macheboeuf et al. (2005)]. When the site can switch between an active and inactive state, the effective rate constant can be estimated from the gated narrow escape theory of [Reingruber and Holcman (2009)].

Figure 12.6 is given in [Minsky (2004)]. The three-dimensional case – in [Lieber et al. (2009)], (12.25) - in [Holcman and Schuss BN (2012b)]. The phase transition indicated by (12.25) was reported experimentally several times [Lieber et al. (2009)], (Minsky, 2004) and [Levin-Zaidman et al. (2003)]. It should be associated with the high probability of DNA repair by preventing the broken DNA strand to drift apart or become misaligned by turning around. A recent report [(Gehlen et al., 2011)] proposes that diffusion through the connecting neck is the main determinant of the delivery rate and of the selection of fast-diffusing particles during the transient regime, before steady state is reached. Indeed, the present analysis confirms that in the absence of any active mechanism, the control of the delivery process can be realized by a drastic slowdown of the back flow from the daughter to the mother cell by an asymmetry in the curvature of the connecting neck in the smaller compartment, as described in the asymptotic formulas (7.127)–(12.15) for the mean residence times $\bar{\tau}$ in the compartments.

Bibliography

- Aboud, S., M. Saraniti, and R.S. Eisenberg. 2003. Issues in modeling ion transport in biological channels: self-consistent particle-based simulations. *Journal of Computational Electronics* 2: 239–243.
- Abramowitz, M., and I. Stegun. 1972. *Handbook of Mathematical Functions with Formulas, Graphs, and Mathematical Tables*. NY: Dover Publications.
- Adesnik, H., R.A. Nicoll, and P.M. England. 2005. Photoinactivation of native AMPA receptors reveals their real-time trafficking. *Neuron* 48 (6): 977–985.
- Alberts, B., D. Bray, J. Lewis, M. Raff, K. Roberts, and J.D. Watson. 1994. *Molecular Biology of the Cell*. NY: Garland.
- Alberts, P., R. Rudge, T. Irinopoulou, L. Danglot, C. Gauthier-Rouviere, and T. Galli. 2006. Cdc42 and actin control polarized expression of TI-VAMP vesicles to neuronal growth cones and their fusion with the plasma membrane. *Molecular Biology of the Cell* 17: 1194–1203.
- Amitai, A., and D. Holcman. 2017a. Encounter time of two loci governed by polymer decondensation and local chromatin interaction. [arXiv:1707.02908](https://arxiv.org/abs/1707.02908).
- Amitai, A., and D. Holcman. 2017b. Polymer physics of nuclear organization and function. *Physics Reports*.
- Anderson, J., I. Lampl, I. Reichova, M. Carandini, and D. Ferster. 2000. Stimulus dependence of two-state fluctuations of membrane potential in cat visual cortex. *Nature Neuroscience* 3 (6): 617–621.
- Araya, R., K.B. Eisenthal, and R. Yuste. 2006. Dendritic spines linearize the summation of excitatory potentials. *Proceedings of the National Academy of Sciences of the United States of America* 103 (49): 18799–18804.
- Araya, R., J. Jiang, K.B. Eisenthal, and R. Yuste. 2006. The spine neck filters membrane potentials. *Proceedings of the National Academy of Sciences of the United States of America* 103 (47): 17961–17966.
- Araya, R., V. Nikolenko, K.B. Eisenthal, and R. Yuste. 2007. Sodium channels amplify spine potentials. *Proceedings of the National Academy of Sciences of the United States of America* 24, 104 (30): 12347–12352.
- Ashby, M.C., S.R. Maier, A. Nishimune, and J.M. Henley. 2006. Lateral diffusion drives constitutive exchange of AMPA receptors at dendritic spines and is regulated by spine morphology. *Journal of Neuroscience* 26: 7046.
- Aubin, T. 1998. *Some Nonlinear Problems in Riemannian Geometry*. NY: Springer.
- Balian, R., and C. Bloch. 1972. Distribution of eigenfrequencies for the wave equation in a finite domain: III. eigenfrequency density oscillations. *Annals of Physics* 69: 76–160.

- Barcilon, V. 1992. Ion flow through narrow membrane channels: Part I. *SIAM Journal on Applied Mathematics* 52 (5): 1391–1404.
- Barcilon, V., D.P. Chen, and R.S. Eisenberg. 1992. Ion flow through narrow membrane channels: Part II. *SIAM Journal on Applied Mathematics* 52 (5): 1405–1425.
- Belch, A.C., and M. Berkowitz. 1985. Molecular dynamics simulations of tips2 water restricted by a spherical hydrophobic boundary. *Chemical Physics Letters* 113: 278–282.
- Bender, C.M., and S.A. Orszag. 1978. *Advanced Mathematical Methods for Scientists and Engineers*. New York: McGraw-Hill.
- Bénichou, O., and R. Voituriez. 2008. Narrow-escape time problem: Time needed for a particle to exit a confining domain through a small window. *Physical Review Letters* 100: 168105.
- Ben-Jacob, E., D. Bergman, and Z. Schuss. 1982. Thermal fluctuations and the lifetime of the nonequilibrium steady-state in a hysteretic Josephson junction. *Physical Review B, Rapid Communications* 25: 519–522.
- Ben-Jacob, E., D. Bergman, B.J. Matkowsky, and Z. Schuss. 1982. Lifetime of oscillatory steady-states. *Physical Review A* 26: 805–2816.
- Ben-Jacob, E., D.J. Bergman, Y. Imry, B.J. Matkowsky, and Z. Schuss. 1983. Thermal activation from the fluxoid and the voltage states of dc SQUIDS. *Journal of Applied Physics* 54: 6533–6542.
- Berezhkovskii, A.M., and A.V. Barzykin. 2012. Search for a small hole in a cavity wall by intermittent bulk and surface diffusion. *The Journal of Chemical Physics* 136 (5): 054115.
- Berezhkovskii, A.M., A.V. Barzykin, and VYu. Zitserman. 2009. Escape from cavity through narrow tunnel. *The Journal of Chemical Physics* 130: 245104.
- Berezhkovskii, A.M., Y.A. Makhnovskii, M.I. Monine, VYu. Zitserman, and S.Y. Shvartsman. 2004. Boundary homogenization for trapping by patchy surfaces. *The Journal of Chemical Physics* 121 (22): 11390–11394.
- Berg, H.C., and E.M. Purcell. 1977. Physics of chemoreception. *Biophysical Journal* 20: 193–219.
- Berkowitz, M., and J.A. McCammon. 1982. Molecular dynamics with stochastic boundary conditions. *Chemical Physics Letters* 90: 215–217.
- Berne, B.J., and R. Pecora. 1976. *Dynamic Light Scattering with Applications to Chemistry, Biology, and Physics*. New York: Wiley-Interscience.
- Berry, M.V., and C.J. Howls. 1994. High orders of the Weyl expansion for quantum billiards: Resurgence of periodic orbits, and the Stokes phenomenon. *Proceedings of the Royal Society of London A* 447: 525–555.
- Berry, R.S., S. Rice, and J. Ross. 2000. *Physical Chemistry*, 2nd ed. Oxford: Oxford University Press.
- Berthold, K., P. Horn, and M.J. Brooks. 1986. The variational approach to shape from shading. *Computer Vision, Graphics, and Image Processing* 33: 174–208.
- Bezanilla, F. 2008. How membrane proteins sense voltage. *Nature Reviews Molecular Cell Biology* 9: 323–32.
- Bloodgood, B.L., and B.L. Sabatini. 2005. Neuronal activity regulates diffusion across the neck of dendritic spines. *Science* 310 (5749): 866–869.
- Biess, A., E. Korkotian, and D. Holcman. 2007. Diffusion in a dendritic spine: The role of geometry. *Physical Review E, Statistical, Nonlinear, and Soft Matter Physics* 76 (1): 021922.
- Biess, A., E. Korkotian, and D. Holcman. 2011. Barriers to diffusion in dendrites and estimation of calcium spread following synaptic inputs. *PloS Computational Biology* 7 (10): e1002182.
- Bobrovsky, B.Z., and Z. Schuss. 1982. A singular perturbation method for the computation of the mean first passage time in a nonlinear filter. *SIAM Journal on Applied Mathematics* 42 (1): 174–187.
- Bobrovsky, B.Z., and O. Zeitouni. 1992. Some results on the problem of exit from a domain. *Stochastic Processes and their Applications* 41 (2): 241–256.
- Boda, D., W. Nonner, M. Valisko, D. Henderson, R.S. Eisenberg, and D. Gillespie. 2007. Steric selectivity in na channels arising from protein polarization and mobile side chains. *Biophysical Journal* 93: 1960–1980.

- Borgdorff, A.J., and D. Choquet. 2002. Regulation of AMPA receptor lateral movements. *Nature* 417: 649–653.
- Bourne, J.N., and K.M. Harris. 2008. Balancing structure and function at hippocampal dendritic spines. *Annual Review of Neuroscience* 31: 47–67.
- Bredt, D.S., and R.A. Nicoll. 2003. AMPA receptor trafficking at excitatory synapses. *Neuron* 40 (2): 361–379.
- Bressloff, P.C., and J. Newby. 2013. Stochastic models of intracellular transport. *Reviews of Modern Physics* 85: 135–196.
- Brooks III, C.L., and M. Karplus. 1983. Deformable stochastic boundaries in molecular dynamics. *The Journal of Chemical Physics* 79: 6312.
- Burger, M., R.S. Eisenberg, and H.W. Engl. 2007. Inverse problems related to ion channel selectivity. *SIAM Journal on Applied Mathematics* 67 (4): 960–989.
- Büttiker, M., E.P. Harris, and R. Landauer. 1979. Thermal activation in extremely underdamped Josephson-junction circuits. *Physical Review B* 28: 1268.
- Callaghan, P.T. 1991. *Principles of Nuclear Magnetic Resonance Microscopy*. NY: Oxford University Press.
- Cartailler, J., Z. Schuss, and D. Holcman. 2016. Analysis of the Poisson–Nernst–Planck equation in a ball for modeling the voltage-current relation in neurobiological microdomains. *Physica D. Nonlinear Phenomena*. <https://doi.org/10.1016/j.physd.2016.09.001>
- Cartailler, J., Z. Schuss, and D. Holcman. 2017. Geometrical effects on nonlinear electrodiffusion in cell physiology. *Journal of Nonlinear Science* 1–30.
- Chandrasekhar, S. 1943. Stochastic problems in physics and astronomy. *Reviews of Modern Physics* 15: 2–89.
- Chen, D.P., J. Lear, and R.S. Eisenberg. 1997. Permeation through an open channel: Poisson–Nernst–Planck theory of a synthetic ionic channel. *Biophysical Journal* 72: 97–116.
- Chen, D.P., L. Xu, A. Tripathy, G. Meissner, and R.S. Eisenberg. 1999. Selectivity and permeation in calcium release channel of cardiac muscle: Alkali metal ions. *Biophysical Journal* 76: 1346–1366.
- Chen, L., D.M. Chetkovich, R.S. Petralia, N.T. Sweeney, Y. Kawasaki, R.J. Wenthold, D.S. Bredt, and R.A. Nicoll. 2000. Stargazin regulates synaptic targeting of AMPA receptors by two distinct mechanisms. *Nature* 408 (6815): 936–943.
- Chen, W., and M.J. Ward. 2011. The stability and dynamics of localized spot patterns in the two-dimensional Gray Scott model. *SIAM Journal on Applied Dynamical Systems* 10 (2): 582–666.
- Chen, W., R. Erban, and S.J. Chapman. 2014. From Brownian dynamics to Markov chain: An ion channel example. *SIAM Journal of Applied Mathematics* 74 (1): 208–235.
- Cheviakov, A., M.J. Ward, and R. Straube. 2010. An asymptotic analysis of the mean first passage time for narrow escape problems: Part II: The sphere. *SIAM Multiscale Modeling and Simulation* 8 (3): 836–870.
- Cheviakov, A.F., and M.J. Ward. 2011. Optimizing the principal eigenvalue of the Laplacian in a sphere with interior traps. *Mathematical and Computer Modelling* 53: 1394–1409.
- Cheviakov, A.F., and D. Zawada. 2013. Narrow-escape problem for the unit sphere: Homogenization limit, optimal arrangements of large numbers of traps, and the n(2) conjecture. *Physical Review E, Statistical, Nonlinear, and Soft Matter Physics* 87 (4): 042118.
- Chipot, M., I. Shafrir, and G. Wolansky. 1997. On the solutions of Liouville systems. *Journal of Differential Equations* 140: 59–105. (Erratum *ibid* 178: 130 (2002)).
- Choquet, D. 2010. Fast AMPAR trafficking for a high-frequency synaptic transmission. *European Journal of Neuroscience* 32: 250–260.
- Christiano, R., and P. Silvestrini. 1988. Decay of the running state in Josephson junctions: Preliminary experimental results. *Physics Letters A* 133 (2): 347.
- Cohen, J., and R. Lewis. 1967. Ray method for the asymptotic solution of the diffusion equation. *Journal of the Institute of Mathematics and its Applications* 3: 266–290.
- Cohen, J.K., F. Hagin, and J.B. Keller. 1972. Short time asymptotic expansion of solutions of parabolic equations. *Journal of Mathematical Analysis and Applications* 38: 82–91.

- Colin de Verdière, Y. 1973. Spectre du Laplacien et longueurs des géodésiques périodiques I, *Composito Mathematica* 27 (1): 83–106. *Spectre du Laplacien et longueurs des géodésiques périodiques II*, *Composito Mathematica* 27 (2): 159–184.
- Coombs, D., R. Straube, and M. Ward. 2009. Diffusion on a sphere with localized traps: Mean first passage time, eigenvalue asymptotics, and Fekete points. *SIAM Journal on Applied Mathematics* 70 (1): 302–322.
- Coffey, W.T., Yu.P. Kalmykov, and J.T. Waldron. 2004. *The Langevin Equation: With Applications to Stochastic Problems in Physics, Chemistry and Electrical Engineering*, vol. 14, 2nd ed. Contemporary Chemical Physics. New York: World Scientific.
- Courant, R., and D. Hilbert. 1989. *Methods of Mathematical Physics*. New York: Wiley-Interscience.
- Crank, J. 1980. *The Mathematics of Diffusion*, 2nd ed. Oxford: Oxford University Press.
- Cossart, R., D. Aronov, and R. Yuste. 2003. Attractor dynamics of network UP states in the neocortex. *Nature* 423: 283–288.
- Physical Review E 89: 030101(R).
- Multiscale Modeling Simulation 14 (2): 772–798.
- Dao Duc, K., P. Parutto, X. Chen, J. Epzstein, A. Konnerth, and D. Holcman. 2015. Synaptic dynamics and neuronal network connectivity are reflected in the distribution of times in Up states. *Frontiers in Computational Neuroscience*. <https://doi.org/10.3389/fncom.2015.00096>.
- Day, M.V. 1992. Conditional exits for small noise diffusions. *The Annals of Probability* 20: 1385–1419.
- Day, M.V. 1989. Boundary local time and small parameter exit problems with characteristic boundaries. *SIAM Journal on Mathematical Analysis* 20: 222–248.
- Day, M.V. 1990a. Large deviations results for the exit problem with characteristic boundary. *Journal of Mathematical Analysis and Applications* 147: 134–153.
- Day, M.V. 1990b. Some phenomena of the characteristic boundary exit problem. In *Diffusion Processes and Related Problems in Analysis*, ed. Diffusion Processes, and Related Problems. Basel: Birkhäuser.
- Day, M.V. 1994. Cycling and skewing of exit measures for planar systems. *Stochastics* 48: 227–247.
- Delgado, M.J., M. Ward, and D. Coombs. 2014. Conditional mean first passage times to small traps in a 3-D domain with a sticky boundary: Applications to T cell searching behaviour in lymph nodes. *SIAM Journal on Multiscale Analysis and Simulation*.
- Dembo, A., and O. Zeitouni. 1993. *Large Deviations Techniques and Applications*. Boston: Jones and Bartlett.
- Dent, E.W., and F.B. Gertler. 2003. Cytoskeletal dynamics and transport in growth cone motility and axon guidance. *Neuron* 40: 209–227.
- De Finetti, B. 1993. *Theory of Probability*, 3rd ed. New York: Wiley.
- Deuschel, J.D., and D.W. Stroock. 1989. *Large Deviations*. Boston: Academic Press.
- Devinatz, A., and A. Friedman. 1977. The asymptotic behavior of the principal eigenvalue of singularly perturbed degenerate elliptic operators. *Illinois Journal of Mathematics* 21 (4): 852–870.
- Devinatz, A., and A. Friedman. 1978. The asymptotic behavior of the solution of a singularly perturbed Dirichlet problem. *Indiana University Mathematics Journal* 27 (3): 527–537.
- Doob, J.L. 1953. *Stochastic Processes*. New York: Wiley.
- Doob, J.L. 1994. *Measure Theory*. New York: Springer.
- Doucet, A., N.D. Freitas, and N. Gordon. 2001. *Sequential Monte-Carlo Methods in Practice*. Berlin: Springer.
- Dvoretzky, A., P. Erdős, and S. Kakutani. 1961. Nonincreasing everywhere of the Brownian motion process, In *Proceedings of the Fourth Berkeley Symposium on Mathematical Statistics and Probability II*, University of California Press, Bekeley.
- Dygas, M.M., B.J. Matkowsky, and Z. Schuss. 1986. A singular perturbation approach to non-Markovian escape rate problems. *SIAM Journal on Applied Mathematics* 46 (2): 265–298.

- Dynkin, E.B., T. Kovary, and D.E. Brown. 2006. *Theory of Markov Processes*. NY: Dover Publications.
- Earnshaw, B.A., and P.C. Bressloff. 2006. A biophysical model of AMPA receptor trafficking and its regulation during LTP/LTD. *The Journal of Neuroscience* 26: 12362–12373.
- Edidin, M., S.C. Kuo, and M.P. Sheetz. 1991. Lateral movements of membrane glycoproteins restricted by dynamic cytoplasmic barriers. *Science* 254: 1379–1382.
- Einstein, A. 1956. *Investigations on the Theory of the Brownian Movement*. (transl.) New York: Dover.
- Eisenberg, R.S. 1998. Ionic channels in biological membranes. Electrostatic analysis of a natural nanotube. *Contemporary Physics* 39 (6): 447–466.
- Eisenberg, R.S. 1999. From structure to function in open ionic channels. *Journal of Membrane Biology* 171: 1–24.
- Eisenberg, R.S., and D.P. Chen. 1993. Charges, currents, and potentials in ionic channels of one conformation. *Biophysical Journal* 64: 1405–1421.
- Eisenberg, R.S., M.M. Klosek, and Z. Schuss. 1995. Diffusion as a chemical reaction: Stochastic trajectories between fixed concentrations. *Journal of Chemical Physics* 102 (4): 1767–1780.
- Eisinger, J., J. Flores, and W.P. Petersen. 1986. A milling crowd model for local and long-range obstructed lateral diffusion. Mobility of excimeric probes in the membrane of intact erythrocytes. *Biophysical Journal* 49: 987–1001.
- Eliezer, S., and Z. Schuss. 1979. Stochastic (white noise) analysis of resonant absorption in laser generated plasma. *Physics Letters A* 70 (4): 307–310.
- Ellis, R.S. 1985. *Entropy, Large Deviations and Statistical Mechanics*. New York: Springer.
- Erchova, I., G. Kreck, U. Heinemann, and A.V.M. Herz. 2004. Dynamics of rat entorhinal cortex layer II and III cells: Characteristics of membrane potential resonance at rest predict oscillation properties near threshold. *Journal of Physiology* 560: 89–110.
- Ethier, S.N., and T.G. Kurtz. 2005. *Markov Processes: Characterization and Convergence*, 2nd ed. Wiley Series in Probability and Statistics. New York: Wiley.
- Fabrikant, V.I. 1989. *Applications of Potential Theory in Mechanics*. Dordrecht: Kluwer.
- Fabrikant, V.I. 1991. *Mixed Boundary Value Problems of Potential Theory and Their Applications in Engineering*. Dordrecht: Kluwer.
- Faierman, M. 1995. Eigenvalue asymptotics for a non-selfadjoint elliptic problem involving an indefinite weight. *Rocky Mountain Journal of Mathematics* 25 (1): 179–187.
- Farr, G.A., L.G. Zhang, and P. Tattersall. 2005. Parvoviral virions deploy a capsid-tethered lipolytic enzyme to breach the endosomal membrane during cell entry. *Proceedings of the National Academy of Sciences of the United States of America* 102: 17148–17153.
- Frank-Kamenetskii, D.A. 1955. *Diffusion and Heat Exchange in Chemical Kinetics*. Princeton: Princeton University Press.
- Freche, D., U. Pannasch, N. Rouach, and D. Holcman. 2011. Synapse geometry and receptor dynamics modulate synaptic strength. *PLoS One* 6 (10): e25122.
- Fresche, D., C.Y. Lee, N. Rouach, and D. Holcman. 2013. Synaptic transmission in neurological disorders dissected by a quantitative approach. *Communicative and Integrative Biology* 5 (5): 1–5.
- Feller, W. 1954. Diffusion processes in one dimension. *Transactions of the American Mathematical Society* 77 (1): 1–31.
- Feller, W. 1968. *An Introduction to Probability Theory and Its Applications*, vol. I, II, 3rd ed. New York: Wiley.
- Fichera, G. 1960. On a unified theory of boundary problems for elliptic-parabolic equations of second order. In: Proceedings of a Symposium on Boundary value problems in differential equations, University of Wisconsin Press, Madison.
- Freidlin, M. 2002. *Markov Processes and Differential Equations*. Boston: Birkhäuser.
- Freidlin, M. 2004. Some remarks on the Smoluchowski-Kramers approximation. *Journal of Statistical Physics* 117 (3/4): 617–654.

- Freidlin, M.A. 1985. *Functional Integration and Partial Differential Equations*. Princeton: Princeton University Press.
- Freidlin, M.A., and A.D. Wentzell. 1984. *Random Perturbations of Dynamical Systems*. New York: Springer.
- Gandolfi, A., A. Gerardi, and F. Marchetti. 1985. Diffusion-controlled reactions in two dimensions. *Acta Applicandae Mathematicae* 4: 139–159.
- Gantmacher, F.R. 1998. *The Theory of Matrices*. Providence: American Mathematical Society.
- Garabedian, P.R. 1964. *Partial Differential Equations*. NY: Wiley.
- Gardiner, C.W. 1985. *Handbook of Stochastic Methods*, 2nd ed. New York: Springer.
- Gehlen, L.R., S. Nagai, K. Shimada, P. Meister, A. Taddei, and S.M. Gasser. 2011. Nuclear geometry and rapid mitosis ensure asymmetric episome segregation in yeast. *Current Biology* 21 (1): 25–33.
- Gihman, I.I., and A.V. Skorohod. 1972. *Stochastic Differential Equations*. Berlin: Springer.
- Gihman, I.I., and A.V. Skorohod. 1975. *The Theory of Stochastic Processes*, vol. I, II, III. Berlin: Springer.
- Gilbarg, D., and N.S. Trudinger. 2001. *Elliptic Partial Differential Equations of Second-Order*. NY: Springer.
- Gillespie, D.T. 1976. A general method for numerically simulating the stochastic time evolution of coupled chemical reactions. *Journal of Computational Physics* 22 (4): 403–434.
- Girsanov, I.V. 1960. On transforming a certain class of stochastic processes by absolutely continuous substitution of measures. *Theory of Probability and Its Applications* 5: 285–301.
- Glasstone, S., K.J. Laidler, and H. Eyring. 1941. *The Theory of Rate Processes*. New York: McGraw-Hill.
- Graf, P., A. Nitzan, M.G. Kurnikova, and R. Coalson. 2000. A dynamic lattice Monte Carlo model of ion transport in inhomogeneous dielectric environments: Method and implementation. *The Journal of Physical Chemistry B* 104: 12324–12338.
- Graham, R., and T. Tel. 1985. Weak-noise limit of Fokker-Planck models and nondifferentiable potentials for dissipative dynamical systems. *Physical Review A* 31: 1109.
- Graham, B.P., K. Lauchlan, and D.R. McLean. 2006. Dynamics of outgrowth in a continuum model of neurite elongation. *Journal of Computational Neuroscience* 20: 43–60.
- Greiner, P. 1971. An asymptotic expansion for the heat equation. *Archive for Rational Mechanics and Analysis* 41 (3): 163–218.
- Grigoriev, I.V., Y.A. Makhnovskii, A.M. Berezhkovskii, and V.Y. Zitserman. 2002. Kinetics of escape through a small hole. *The Journal of Chemical Physics* 116 (22): 9574–9577.
- Gobet, E. 2001. Euler schemes and half-space approximation for the simulation of diffusion in a domain. *ESAIM: Probability and Statistics* 5: 261–297.
- Goldman, D.E. 1943. Potential, impedance, and rectification in membranes. *The Journal of General Physiology* 27 (1): 37–60.
- Goodrich, F.C. 1954. Random walk with semiadsorbing barrier. *The Journal of Chemical Physics* 22: 588–594.
- Gordon, C., D. Webb, and S. Wolpert. 1992. Isospectral plane domains and surfaces via Riemannian orbifolds. *Inventiones Mathematicae* 110: 1–22, (English transl.) One cannot hear the shape of a drum. *Bulletin of the American Mathematical Society* 27: 134–138.
- Grote, F.R., and J.T. Hynes. 1980. The stable states picture of chemical reactions II: Rate constants for condensed and gas phase reaction models. *The Journal of Chemical Physics* 73: 2715–2732.
- Grote, F.R., and J.T. Hynes. 1981a. Reactive modes in condensed phase reactions. *The Journal of Chemical Physics* 74: 4465–4475.
- Grote, F.R., and J.T. Hynes. 1981b. Saddle point model for atom transfer reactions in solution. *The Journal of Chemical Physics* 75: 2191–2198.
- Guerrier, C., and D. Holcman. 2015. Search time for a small ribbon and application to vesicular release at neuronal synapses. *Multiscale Modeling and Simulation* 13 (4): 1173–1193.
- Guerrier, C., and D. Holcman. 2016. Hybrid Markov-mass action law model for cell activation by rare binding events: Application to calcium induced vesicular release at neuronal synapses. *Scientific Reports* 6: 35506. <https://doi.org/10.1038/srep35506>.

- Guerrier, C., E. Korkotian, and D. Holcman. 2015. Calcium dynamics in neuronal microdomains: Modeling, stochastic simulations, and data analysis. *Encyclopedia of Computational Neuroscience*, 486–516. New York: Springer.
- Guillemin, V., and R. Melrose. 1979. The Poisson summation formula for manifolds with boundary. *Advances in Mathematics* 32: 204–232.
- Gutzwiller, M.C. 1990. *Chaos in Classical and Quantum Mechanics*. NY: Springer.
- Hagan, P.S., C.R. Doering, and C.D. Levermore. 1987. Bistability driven by weakly colored Gaussian noise: The Fokker-Planck boundary layer and mean first-passage times. *Physical Review Letters* 59: 2129–2132.
- Hagan, P.S., C.R. Doering, and C.D. Levermore. 1989a. The distribution of exit times for weakly colored noise. *Journal of Statistical Physics* 54 (5/6): 1321–1352.
- Hagan, P.S., C.R. Doering, and C.D. Levermore. 1989b. Mean exit times for particles driven by weakly colored noise. *SIAM Journal on Applied Mathematics* 49 (5): 1480–1513.
- Hahn, T.T., B. Sakmann, and M.R. Mehta. 2007. Differential responses of hippocampal subfields > to cortical up-down states. *Proceedings of the National Academy of Sciences of the United States of America* 104 (12): 5169–5174.
- Hale, J.K. 1969. *Ordinary Differential Equations*. New York: Wiley.
- Hammele, M., and W. Zimmermann. 2003. Modeling oscillatory microtubule polymerization. *Physical Review E, Statistical, Nonlinear, and Soft Matter Physics* 67: 021903.
- Han, W., Y.K. Ng, D. Axelrod, and E.S. Levitan. 1999. Neuropeptide release by efficient recruitment of diffusing cytoplasmic secretory vesicles. *Proceedings of the National Academy of Sciences of the United States of America* 96: 14577–14582.
- Hänggi, P. 1993. *Activated Barrier Crossing: Applications in Physics, Chemistry and Biology*. Singapore: World Scientific.
- Hänggi, P., and P. Talkner. 1995. *New Trends in Kramers' Reaction Rate Theory*. Dordrecht: Kluwer.
- Hänggi, P., P. Talkner, and M. Borkovec. 1990. 50 years after Kramers. *Reviews of Modern Physics* 62: 251–341.
- Harris, K.M., and J.K. Stevens. 1988. Dendritic spines of rat cerebellar Purkinje cells: Serial electron microscopy with reference to their biophysical characteristics. *The Journal of Neuroscience* 12: 4455–4469.
- Henricci, P. 1997. *Applied and Computational Complex Analysis Volume I: Power Series Integration Conformal Mapping Location of Zero*, vol. 1. Wiley-Blackwell.
- Hentschel, H.G., and A. Fine. 1994. Instabilities in cellular dendritic morphogenesis. *Physical Review Letters* 3: 3592–3595.
- Hida, T. 1980. *Brownian Motion*. New York: Springer.
- Hille, B. 2001. *Ionic Channels of Excitable Membranes*, 3rd ed. Sunderland: Sinauer.
- Hille, E. 1976. *Analytic Function Theory*, vol. 1. NY: Chelsea Publishing Company.
- Holcman, D. 2007. Modeling viral and DNA trafficking in the cytoplasm of a cell. *Journal of Statistical Physics* 127: 471–494.
- Holcman, D., and Z. Schuss. 2004. Escape through a small opening: Receptor trafficking in a synaptic membrane. *Journal of Statistical Physics* 117 (5/6): 191–230.
- Holcman, D., and Z. Schuss. 2005a. Stochastic chemical reactions in micro-domains. *Journal of Chemical Physics* 122: 1.
- Holcman, D., and Z. Schuss. 2005b. Stochastic chemical reactions in microdomains. *Journal of Chemical Physics* 122: 114710.
- Holcman, D., and Z. Schuss. 2008a. Diffusion escape through a cluster of small absorbing windows. *Journal of Physics A: Mathematical and Theoretical* 41: 155001.
- Holcman, D., and Z. Schuss. 2008b. Diffusion through a cluster of small windows and flux regulation in microdomains. *Physics Letters A* 372: 3768–3772.
- Holcman, D., and Z. Schuss. 2011. Diffusion laws in dendritic spines. *The Journal of Mathematical Neuroscience* 1 (10): 1–14.
- Holcman, D., and Z. Schuss. 2012a. Brownian motion in dire straits. *SIAM Journal on Multiscale Modeling and Simulation* 10 (4): 1204–1231.

- Holcman, D., and Z. Schuss. 2012b. Brownian needle in dire straits: Stochastic motion of a rod in very confined narrow domains. *Physical Review E* 85: 010103(R).
- Holcman, D., and Z. Schuss. 2013. Control of flux by narrow passages and hidden targets in cellular biology. *Reports on Progress in Physics* 76 (7): 074601.
- Holcman, D., and Z. Schuss. 2014a. The narrow escape problem. *SIAM Review* 56 (2): 213–257.
- Holcman, D., and Z. Schuss. 2014b. Oscillatory survival probability and eigenvalues of the non-self-adjoint Fokker-Planck operator. *Multiscale Modeling Simulation* 12 (3): 1294–1308.
- Holcman, D., and Z. Schuss. 2014c. Time scale of diffusion in molecular and cellular biology. *Journal of Physics A: Mathematical and Theoretical* 47 (17): 173001.
- Holcman, D., and Z. Schuss. 2015. *Stochastic Narrow Escape in Molecular and Cellular Biology: Analysis and Applications*. NY: Springer.
- Holcman, D., and Z. Schuss. 2016. 100 years after Smoluchowski: stochastic processes in cell biology. *Journal of Physics A* (in press).
- Holcman, D., Z. Schuss, and E. Korkotian. 2004. Calcium dynamics in dendritic spines and spine motility. *Biophysical Journal* 87: 81–91.
- Holcman, D., and A. Triller. 2006. Modeling synaptic dynamics and receptor trafficking. *Biophysical Journal* 91 (7): 2405–2415.
- Holcman, D., and M. Tsodyks. 2006. The emergence of up and down states in cortical networks. *PLOS Computational Biology* 2 (3): e23.
- Holcman, D., and I. Kupka. 2010. Some questions in computational cellular biology. *Journal of Fixed Point Theory and Applications* 7 (1): 67–83.
- Holcman, D., and R. Yuste. 2015. Poisson Nernst Planck equations for a dendritic spine, from the new nanophysiology: Regulation of ionic flow in neuronal subcompartments. *Nature Reviews Neuroscience* 16: 685–692. <https://doi.org/10.1038/nrn4022>.
- Holcman, D., E. Korkotian, and M. Segal. 2005. Calcium dynamics in dendritic spines, modeling and experiments. *Cell Calcium* 37: 467–475.
- Holcman, D., A. Marchewka, and Z. Schuss. 2005. Survival probability of diffusion with trapping in cellular neurobiology. *Physical Review E, Statistical, Nonlinear, and Soft Matter Physics* 72 (3): 031910.
- Holcman, D., N. Hoze, and Z. Schuss. 2011. Narrow escape through a funnel and effective diffusion on a crowded membrane. *Physical Review E* 84: 021906.
- Holcman, D., K. Dao Duc, E. Byrne, A. Jones, and K. Burrage. 2014. Successful delivery of PTEN in the cytoplasm escaping from micro RNA degradation. *Journal of Mathematical Biology*. <https://doi.org/10.1007/s00285-014-0782-y>.
- Holmes, M.H. 2013. *Introduction to Perturbation Methods*, vol. 20. Texts in Applied Mathematics. Berlin: Springer.
- Honerkamp, J. 1994. *Stochastic Dynamical Systems: Concepts, Numerical Methods, Data Analysis*. New York: VCH.
- Hotulainen, P., and C.C. Hoogenraad. 2010. Actin in dendritic spines: connecting dynamics to function. *The Journal of Cell Biology* 189 (4): 619–629.
- Hoze, N., and D. Holcman. 2014. Residence times of receptors in dendritic spines analyzed by stochastic simulations in empirical domains. *Biophysical Journal* 107 (12): 3008–3017.
- Hoze, N., Z. Schuss, and D. Holcman. 2013. Reconstruction of surface and stochastic dynamics from a planar projection of trajectories. *SIAM Journal on Imaging Sciences* 6 (4): 2430–2449.
- Hoze, N., D. Nair, E. Hosy, C. Sieben, S. Manley, A. Herrmann, J.B. Sibarita, D. Choquet, and D. Holcman. 2012. Heterogeneity of AMPA receptor trafficking and molecular interactions revealed by superresolution analysis of live cell imaging. *Proceedings of the National Academy of Sciences of the United States of America* 109 (42): 17052–17057.
- Huang, Q., R. Opitz, E.W. Knapp, and A. Herrmann. 2002. Protonation and stability of the globular domain of influenza virus hemagglutinin. *Biophysical Journal* 82 (2): 1050–1058.
- Huang, B., H. Babcock, and X. Zhuang. 2010. Breaking the diffraction barrier: Super-resolution imaging of cells. *Cell* 143: 1047–1058.

- Im, B., S. Seefeld, and B. Roux. 2000. A grand canonical Monte-Carlo-Brownian dynamics algorithm for simulating ion channels. *Biophysical Journal* 79: 788–801.
- Izhikevich, E.M. 2005. *Dynamical Systems in Neuroscience*. NY: Springer.
- Jackson, J.D. 1998. *Classical Electrodynamics*, 3rd ed. NY: Wiley.
- Jacobsen, J., and K. Schmitt. 2002. The Liouville Bratu Gelfand problem for radial operators. *Journal of Differential Equations* 184: 283–298.
- Jazwinski, A.H. 2007. *Stochastic Processes and Filtering Theory*. NY: Dover Books on Electrical Engineering.
- John, F. 1982. *Partial Differential Equations*, vol. 1, 4th ed., Applied Mathematical Sciences NY: Springer.
- Kac, M. 1966. Can one hear the shape of a drum? *The American Mathematical Monthly* 73 (4), part II, 1–23.
- Kamienomostskaya, S. 1952. On equations of elliptic type and parabolic type with a small parameter in the highest derivative. *Matematicheskii Sbornik* 31 (73): 703–708.
- Kamienomostskaya, S. 1955. The first boundary value problem for elliptic equations containing a small parameter. *Izvestiya Akademii Nauk SSR* 27 (6): 360–935.
- Kamin, S. 1978. On elliptic perturbation of a first order operator with a singular point of attracting type. *Indiana University Mathematics Journal* 27 (6): 935–951.
- Kandel, E.R., J.H. Schwartz, and T.M. Jessell. 2000. *Principles of Neural Science*, 4th ed. New York: McGraw-Hill.
- Karatzas, I., and S.E. Shreve. 1991. *Brownian Motions and Stochastic Calculus*, vol. 113, 2nd ed. Graduate Texts in Mathematics. New York: Springer.
- Karlin, S., and H.M. Taylor. 1975. *A First Course in Stochastic Processes*, vol. I, 2nd ed. New York: Academic Press.
- Karlin, S., and H.M. Taylor. 1981. *A Second Course in Stochastic Processes*, vol. II, 2nd ed. New York: Academic Press.
- Katz, A. 1985. *Reliability of Elastic Structures Driven by Random Loads*. PhD. diss.: Department of Mathematics, Tel-Aviv University, Israel.
- Katz, A., and Z. Schuss. 1985. Reliability of elastic structures driven by random loads. *SIAM Journal on Applied Mathematics*. 45 (3): 383–402.
- Keller, J.B. 1962. Geometrical theory of diffraction. *Journal of the Optical Society of America* 52: 116–130.
- Keller, J.B., and D.W. McLaughlin. 1975. The Feynman integral. *American Mathematical Monthly* 82 (5): 451–576.
- Kellogg, O.D. 1954. *Foundations of Potential Theory*. NY: Dover Publications.
- Kerchner, G.A., and R.A. Nicoll. 2008. Silent synapses and the emergence of a postsynaptic mechanism for LTP. *Nature Reviews Neuroscience* 9 (11): 813–825.
- Kevorkian, J., and J.D. Cole. 1985. *Perturbation Methods in Applied Mathematics*. Applied Mathematical Sciences. Berlin: Springer.
- Khasminskii, R.Z., and A.M. Il'in. 1964. On equations of Brownian motion. *Theory of Probability and Its Applications* 9: 421–444.
- Kim, S., and I. Oppenheim. 1972. Molecular theory of Brownian motion in external fields. *Physica* 57: 469–482.
- Klosek-Dygas, M.M., B.J. Matkowsky, and Z. Schuss. 1988a. Colored noise in dynamical systems. *SIAM Journal on Applied Mathematics* 48 (2): 425–441.
- Klosek-Dygas, M.M., B.J. Matkowsky, and Z. Schuss. 1988b. A first passage time approach to stochastic stability of nonlinear oscillators. *Physics Letters A* 130 (1): 11–18.
- Klosek-Dygas, M.M., B.J. Matkowsky, and Z. Schuss. 1988c. Stochastic stability of nonlinear oscillators. *SIAM Journal on Applied Mathematics* 48 (5): 1115–1127.
- Klosek, M.M. 1995. Half-range expansions for analysis for Langevin dynamics in the high friction limit with a singular boundary condition: Non-characteristic case. *Journal of Statistical Physics* 79 (1/2): 313–345.

- Klosek, M.M., and P.S. Hagan. 1998. Colored noise and a characteristic level crossing problem. *Journal of Mathematical Physics* 39: 931–953.
- Kleinert, H. 1994. *Path Integrals in Quantum Mechanics, Statistics, and Polymer Physics*. New York: World Scientific.
- Kleinrock, L., and 1975, 1976. *Queueing Systems*, vol. I. II. New York: Wiley.
- Kloeden, P.E. 2002. The systematic derivation of higher order numerical schemes for stochastic differential equations. *Milan Journal of Mathematics* 70: 187–207.
- Kloeden, P.E., and E. Platen. 1992. *Numerical Solution of Stochastic Differential Equations*. New York: Springer.
- Knerr, C., M. Mangel, B.J. Matkowsky, and Z. Schuss. 1984. Solution of Kramers-Moyal equations for problems in chemical physics. *The Journal of Chemical Physics* 81: 1285–1293.
- Knerr, C., B.J. Matkowsky, Z. Schuss, and C. Tier. 1984. An asymptotic theory of large deviations for Markov jump processes. *SIAM Journal on Applied Mathematics* 45: 1006–1102.
- Knerr, C., B.J. Matkowsky, Z. Schuss, and C. Tier. 1985. An asymptotic theory of large deviations for Markov jump processes. *SIAM Journal on Applied Mathematics* 45: 1006–1028.
- Knerr, C., B.J. Matkowsky, Z. Schuss, and C. Tier. 1986a. Asymptotic analysis of a state dependent M/G/1 queueing system. *SIAM Journal on Applied Mathematics* 46 (3): 483–505.
- Knerr, C., B.J. Matkowsky, Z. Schuss, and C. Tier. 1986b. Boundary behavior of diffusion approximations to Markov jump processes. *Journal of Statistical Physics* 45: 245–266.
- Knerr, C., B.J. Matkowsky, Z. Schuss, and C. Tier. 1986c. On the performance of state dependent single server queues. *SIAM Journal on Applied Mathematics* 46 (4): 657–697.
- Knerr, C., B.J. Matkowsky, Z. Schuss, and C. Tier. 1986d. A singular perturbations approach to first passage times for Markov jump processes. *Journal of Statistical Physics* 42: 169–184.
- Knerr, C., B.J. Matkowsky, Z. Schuss, and C. Tier. 1986e. System crash in finite capacity M/G/1 queue. *Communications in Statistics. Stochastic Models* 2 (2): 171–201.
- Koch, C. 1999. *Biophysics of Computation*. NY: Oxford University Press.
- Kochubey, O., X. Lou, and R. Schneggenburger. 2011. Regulation of transmitter release by Ca^{2+} and synaptotagmin: insights from a large cns synapse. *Trends in Neuroscience* 34 (5): 237–246.
- Kolokolnikov, T., M. Titcombe, and M.J. Ward. 2005. Optimizing the fundamental Neumann eigenvalue for the Laplacian in a domain with small traps. *European Journal of Applied Mathematics* 16: 161–200.
- Korkotian, E., and M. Segal. 1999. Release of calcium from stores alters the morphology of dendritic spines in cultured hippocampal neurons. *Proceedings of the National Academy of Sciences of the United States of America* 96 (21): 12068–12072.
- Korkotian, E., and M. Segal. 2001. Spike-associated fast contraction of dendritic spines in cultured hippocampal neurons. *Neuron* 30 (3): 751–758.
- Korkotian, E., D. Holzman, and M. Segal. 2004. Dynamic regulation of spine-dendrite coupling in cultured hippocampal neurons. *European Journal of Neuroscience* 20 (10): 2649–2663.
- Kramers, H.A. 1940. Brownian motion in field of force and diffusion model of chemical reaction. *Physica* 7: 284–304.
- Kubo, R. 1957. Statistical-mechanical theory of irreversible processes I. *Journal of the Physical Society of Japan* 12: 570–586.
- Kupferman, R., M. Kaiser, Z. Schuss, and E. Ben-Jacob. 1992. A WKB study of fluctuations and activation in nonequilibrium dissipative steady-states. *Physical Review A* 45 (2): 745–756.
- Kushner, H.J. 1982. A cautionary note on the use of singular perturbation methods for small-noise models. *Stochastics* 6: 116–120.
- Kushner, H.J., and G. Yin. 2003. *Stochastic Approximation Algorithms and Applications*, revised, 2nd ed. Berlin: Springer.
- Kuznetsov, Y.A. 2004. *Elements of Applied Bifurcation Theory*, vol. 112, 3rd ed. Applied Mathematical Sciences. NY: Springer.
- Kusumi, A., Y. Sako, and M. Yamamoto. 1993. Confined lateral diffusion of membrane receptors as studied by single particle tracking (nanovid microscopy). Effects of calcium-induced differentiation in cultured epithelial cells. *Biophysical Journal* 65: 2021–2040.

- Kusumi, A., C. Nakada, K. Ritchie, K. Murase, K. Suzuki, H. Murakoshi, R.S. Kasai, J. Kondo, and T. Fujiwara. 2005. Paradigm shift of the plasma membrane concept from the two-dimensional continuum fluid to the partitioned fluid: High-speed single-molecule tracking of membrane molecules. *Annual Review of Biophysics and Biomolecular Structure* 34: 351–378.
- Lagache, T., and D. Holcman. 2017. Extended narrow escape with many windows for analyzing viral entry into the cell nucleus. *Journal of Statistical Physics* 166 (2): 244–266.
- Lagache, T., C. Sieben, T. Meyer, A. Herrmann, and D. Holcman. 2017. Stochastic model of acidification, activation of hemagglutinin and escape of influenza viruses from an endosome. *Frontiers in Physics* 5: 25.
- Levin-Zaidman, S., J. Englander, E. Shimoni, A.K. Sharma, K.W. Minton, and A. Minsky. 2003. *Science* 299 (5604): 254–256.
- Lewis, R.M., and J.B. Keller. 1964. Asymptotic methods for partial differential equations: the reduced wave equation and Maxwell's equations, NYU Research Report no. EM-194, NYU.
- Lieber, A., A. Leis, A. Kushmaro, A. Minsky, and O. Medalia. 2009. Chromatin organization and radio resistance in the bacterium *gemmae obscuriglobus*. *Journal of Bacteriology* 191 (5): 1439–1445.
- Lindsay, A.E., A.J. Bernoff, and M.J. Ward. 2017. First passage statistics for the capture of a brownian particle by a structured spherical target with multiple surface traps. *Multiscale Modeling Simulation* 15 (1): 74–109.
- Ludwig, D. 1975. Persistence of dynamical systems under random perturbations. *SIAM Review* 17 (4): 605–640.
- Lurie, A.I. 1964. *Three-Dimensional Problems of the Theory of Elasticity*. NY: Interscience Publishers.
- Macheboeuf, P., A.M. Di Guilmi, V. Job, T. Vernet, O. Dideberg, and A. Dessen. 2005. Active site restructuring regulates ligand recognition in class A penicillin-binding proteins. *Proceedings of the National Academy of Sciences of the United States of America* 102 (3): 577–582.
- MacKinnon, R. 2003. Potassium channels and the atomic basis of selective ion conduction, In *Nobel Lecture*. http://www.nobelprize.org/nobel_prizes/chemistry/laureates/2003/mackinnon-lecture.html.
- Maier, R., and D.L. Stein. 1993a. Effect of focusing and caustics on exit phenomena in systems lacking detailed balance. *Physical Review Letters* 71: 1783–1786.
- Maier, R., and D.L. Stein. 1993b. Escape problem for irreversible systems. *Physical Review E* 48: 931–938.
- Maier, R., and D.L. Stein. 1996a. Oscillatory behavior of the rate of escape through an unstable limit cycle. *Physical Review Letters* 77: 4860–4863.
- Maier, R., and D.L. Stein. 1996b. A scaling theory of bifurcation in the symmetric weak-noise escape problem. *Journal of Statistical Physics* 83: 291–357.
- Maier, R., and D.L. Stein. 1997. Limiting exit location distributions in the stochastic exit problem. *SIAM Journal on Applied Mathematics* 57: 752–790.
- Maier, R., D.G. Luchinsky, R. Mannella, P.V.E. McClintock, and D.L. Stein. 1997. Experiments on critical phenomena in a noisy exit problem. *Physical Review Letters* 79: 3109–3112.
- Malinow, R., and R.C. Malenka. 2002. AMPA receptor trafficking and synaptic plasticity. *Annual Review of Neuroscience* 25: 103.
- Mandl, P. 1968. *Analytical Treatment of One-Dimensional Markov Processes*. New York: Springer.
- Mangel, M., and D. Ludwig. 1977. Probability of extinction in a stochastic competition. *SIAM Journal on Applied Mathematics* 33 (2): 256.
- Manley, S., J.M. Gillette, G.H. Patterson, H. Shroff, H.F. Hess, E. Betzig, and J. Lippincott-Schwartz. 2008. High-density mapping of single-molecule trajectories with photoactivated localization microscopy. *Nature Methods* 5: 155–157.
- Mannella, R. 1999. Absorbing boundaries and optimal stopping in a stochastic differential equation. *Physics Letters A* 254 (5): 257–262.
- Mannella, R. 2002. Integration of stochastic differential equations on a computer. *International Journal of Modern Physics C* 13 (9): 1177–1194.

- Marchewka, A., and Z. Schuss. 2000. Path integral approach to the Schrödinger current. *Physical Review A* 61: 052107.
- Marshall, T.W., and E.J. Watson. 1985. A drop of ink falls from my pen... it comes to earth, I know not when. *Journal of Physics A* 18: 3531–3559.
- Matkowsky, B.J., and Z. Schuss. 1976. On the problem of exit. *Bulletin of the American Mathematical Society* 82 (2): 321–324.
- Matkowsky, B.J., and Z. Schuss. 1977. The exit problem for randomly perturbed dynamical systems. *SIAM Journal on Applied Mathematics* 33: 365–382.
- Matkowsky, B.J., and Z. Schuss. 1981. Eigenvalues of the Fokker-Planck operator and the approach to equilibrium in potential fields. *SIAM Journal on Applied Mathematics* 40: 242–252.
- Matkowsky, B.J., and Z. Schuss. 1982. Diffusion across characteristic boundaries. *SIAM Journal on Applied Mathematics* 42 (4): 822–834.
- Matkowsky, B.J., Z. Schuss, and C. Tier. 1983. Diffusion across characteristic boundaries with critical points. *SIAM Journal on Applied Mathematics* 43: 673–695.
- Matkowsky, B.J., Z. Schuss, and C. Tier. 1984. Uniform expansion of the transition rate in Kramers problem. *Journal of Statistical Physics* 35 (3,4): 443–456.
- Matkowsky, B.J., Z. Schuss, C. Knessl, C. Tier, and M. Mangel. 1984. Asymptotic solution of the Kramers-Moyal equation and first-passage times for Markov jump processes. *Physical Review A* 29: 3359–3369.
- Meyer, R.E. 1980. Exponential asymptotics. *SIAM Review* 22 (2): 213–224.
- Mazur, P., and I. Oppenheim. 1970. Molecular theory of Brownian motion. *Physica* 50: 241–258.
- McKean Jr., H.P. 1969. *Stochastic Integrals*. New York: Academic Press.
- McLean, D.R., and B.P. Graham. 2006. Stability in a mathematical model of neurite elongation. *Mathematical Medicine and Biology* 23: 101–17.
- Mel'nikov, V.I., and S.V. Meshkov. 1986. Theory of activated rate processes: Exact solution of the Kramers problem. *The Journal of Chemical Physics* 85: 1018–1027.
- Meraldi, P., V.M. Draviam, and P.K. Sorger. 2004. Timing and checkpoints in the regulation of Mitotic progression. *Developmental Cell* 7: 45–60.
- Miller, W.H. 1974. Quantum-mechanical transition state theory and a new semiclassical model for reaction rate constants. *The Journal of Chemical Physics* 61: 1823–1834.
- Minsky, A. 2004. Information content and complexity in the high-order organization of DNA. *Annual Review of Biophysics and Biomolecular Structure* 33: 317–342.
- Monine, M.I., and J.M. Haugh. 2005. Reactions on cell membranes: Comparison of continuum theory and Brownian dynamics simulations. *Journal of Chemical Physics* 123: 074908.
- Mori, H. 1965. Transport, collective motion, and Brownian motion. *Progress of Theoretical Physics* 33: 423–454.
- Musiela, M., and M. Rutkowski. 1997. *Martingale Methods in Financial Modeling*, vol. 36, 2nd ed., Applications of Mathematics New York: Springer.
- Nadler, B., T. Naeh, and Z. Schuss. 2002. The stationary arrival process of diffusing particles from a continuum to an absorbing boundary is Poissonian. *SIAM Journal on Applied Mathematics* 62 (2): 433–447.
- Nadler, B., T. Naeh, and Z. Schuss. 2003. Connecting a discrete ionic simulation to a continuum. *SIAM Journal on Applied Mathematics* 63 (3): 850–873.
- Nadler, B., Z. Schuss, A. Singer, and R.S. Eisenberg. 2004. Ionic diffusion through confined geometries: from Langevin equations to partial differential equations. *Journal of Physics: Condensed Matter* 16: S2153–S2165.
- Naeh, T. 2001. *Simulation of Ionic Solutions*. PhD diss., Department of Mathematics. Tel-Aviv University, Israel.
- Naeh, T., M.M. Klosek, B.J. Matkowsky, and Z. Schuss. 1990. Direct approach to the exit problem. *SIAM Journal on Applied Mathematics* 50: 595–627.
- Natanson, I.P. 1961. *Theory of Functions of a Real Variable*. New York: Ungar.
- Nesse, W.H., C.A. Negro, and P.C. Bressloff. 2008. Oscillation regularity in noise-driven excitable systems with multi-time-scale adaptation. *Physical Review Letters* 101 (8): 088101.

- Nevel'son, M.B., and R.Z. Has'minski. 1976. *Stochastic Approximation and Recursive Estimation*, translated by Israel Program for Scientific Translations and B. AMS, Providence, RI: Silver.
- Newpher, T.M., and M.D. Ehlers. 2009. Spine microdomains for postsynaptic signaling and plasticity. *Trends in Cell Biology* 5: 218–227.
- Nitzan, A. 2006. *Chemical Dynamics in Condensed Phases Relaxation, Transfer and Reactions in Condensed Molecular Systems.*, Graduate Texts New York: Oxford University Press.
- Nitzan, A., and Z. Schuss. 1993. Multidimensional barrier crossing. In *Activated Barrier Crossings*, ed. G.R. Fleming, and P. Hänggi. Singapore: World Scientific.
- Noble, B. 1988. *Methods Based on the Wiener-Hopf Technique For The Solution of Partial Differential Equations*. Providence: AMS/Chelsea.
- Nonner, W., and R.S. Eisenberg. 1998. Ion permeation and glutamate residues linked by Poisson-Nernst-Planck theory in L-type calcium channels. *Biophysical Journal* 75: 1287–1305.
- Nonner, W., D.P. Chen, and R.S. Eisenberg. 1998. Anomalous mole fraction effect, electrostatics, and binding in ionic channels. *Biophysical Journal* 74: 2327–2334.
- Nonner, W., L. Catacuzzeno, and R.S. Eisenberg. 2000. Binding and selectivity in l-type ca channels: A mean spherical approximation. *Biophysical Journal* 79: 1976–1992.
- Nonner, W., D. Gillespie, D. Henderson, and R.S. Eisenberg. 2001. Ion accumulation in a biological calcium channel: Effects of solvent and confining pressure. *The Journal of Physical Chemistry B* 105: 6427–6436.
- Nyquist, H. 1928. Thermal agitation of electric charge in conductors. *Physical Review* 32: 110–113.
- Olver, F.W.J. 1974. *Asymptotics and Special Functions*. New York: Academic Press.
- O'Malley Jr., R.E. 1991. *Singular Perturbation Methods for Ordinary Differential Equations*. New York: Springer.
- Ozawa, S. 1980. *Proceedings of the Japan Academy* 56: 459.
- Oshanin, G., M. Tamm, and O. Vasilyev. 2010. Narrow-escape times for diffusion in microdomains with a particle-surface affinity: mean-field results. *The Journal of Chemical Physics* 132 (23): 35101.
- Papa, M., and M. Segal. 1996. Morphological plasticity in dendritic spines of cultured hippocampal neurons. *Neuroscience* 71 (4): 1005–1011.
- Pfenninger, K.H., L. Laurino, D. Peretti, X. Wang, S. Rosso, G. Morfini, A. Caceres, and S. Quiroga. 2003. Regulation of membrane expansion at the nerve growth cone. *Journal of Cell Science* 116: 1209–1217.
- Pontryagin, L.S., A.A. Andronov, and A.A. Vitt. 1933. On the statistical treatment of dynamical systems. *Journal of Experimental and Theoretical Physics (Russian)* 3: 165–180. (English transl.) Noise. *Nonlinear Dynamics* 1: 329–340.
- Popov, I.Yu. 1992. Extension theory and localization of resonances for domains of trap type. *Mathematics of the USSR-Sbornik* 71 (1): 209–234.
- Prochiantz, A. 1995. Neuronal polarity: Giving neurons heads and tails. *Neuron* 15: 743–746.
- Qian, N., and T.J. Sejnowski. 1989. An electro-diffusion model for computing membrane potentials and ionic concentrations in branching dendrites, spines and axons. *Biological Cybernetics* 62: 1–15.
- Ramón y Cajal, S. 1909. Les nouvelles idées sur la structure du système nerveux chez l'homme et chez les vertébrés, (transl.) L. Azouly, Malaine, Paris, France. New ideas on the structure of the nervous system of man and vertebrates, (transl.) N. & N.L. Swanson, MIT Press, Cambridge, MA 1991.
- Rayleigh, J.W.S. 1945. *The Theory of Sound*, vol. 2, 2nd ed. NY: Dover.
- Redner, S. 2001. *A Guide to First Passage Processes*. Cambridge: Cambridge University Press.
- Reingruber, J., and D. Holcman. 2009. The gated narrow escape time for molecular signaling. *Physical Review Letters* 103: 148102.
- Reingruber, J., and D. Holcman. 2010. Narrow escape for a stochastically gated Brownian ligand. *Journal of Physics: Condensed Matter* 22 (6): 065103.
- Reingruber, J., and D. Holcman. 2011a. Transcription factor search for a DNA promoter in a three-state model. *Physical Review E* 84 (2): 020901.

- Reingruber, J., and D. Holcman. 2011b. The narrow escape problem in a flat cylindrical microdomain with application to diffusion in the synaptic cleft. *Multiscale Modeling and Simulation* 9 (2): 793–816.
- Reingruber, J., E. Abad, and D. Holcman. 2009. Narrow escape time to a structured target located at the boundary of a microdomain. *The Journal of Chemical Physics* 130: 094909.
- Reingruber, J., J. Pahlberg, M.L. Woodruff, A.P. Sampath, G.L. Fain, and D. Holcman. 2013. Detection of single photons by toad and mouse rods. *Proceedings of the National Academy of Sciences* 110 (48): 19378–19383.
- Renner, M., D. Choquet, and A. Triller. 2009. Control of the postsynaptic membrane viscosity. *The Journal of Neuroscience* 29 (9): 2926–2937.
- Rieder, C.L., A. Schultz, R. Cole, and G. Sluder. 1994. Anaphase onset in vertebrate somatic cells is controlled by a checkpoint that monitors sister kinetochore attachment to the spindle. *Journal of Cell Biology* 127 (5): 1301–1310.
- Risken, H. 1996. *The Fokker-Planck Equation: Methods of Solutions and Applications*, 2nd ed. New York: Springer.
- Rouse, P.E. 1953. A theory of the linear viscoelastic properties of dilute solutions of coiling polymers. *The Journal of Chemical Physics* 21: 1272–1280.
- Rubinstein, I. 1990. *Electro-Diffusion of Ions.*, Studies in Applied and Numerical Mathematics Philadelphia: SIAM Publications.
- Ryter, D., and H. Meyr. 1978. Theory of phase tracking systems of arbitrary order. *IEEE Transactions on Information Theory* IT-24: 1–7.
- Saffman, P.G. 1976. Brownian motion in thin sheets of viscous fluid. *Journal of Fluid Mechanics* 73 (4): 593–602.
- Saffman, P.G., and M. Delbrück. 1975. Brownian motion in biological membranes. *Proceedings of the National Academy of Sciences* 72: 3111–3113.
- Sakai, T., M. Ohuchi, M. Imai, T. Mizuno, K. Kawasaki, K. Kuroda, and S. Yamashina. 2006. Dual wavelength imaging allows analysis of membrane fusion of influenza virus inside cells. *Journal of Virology* 80 (4): 2013–2018.
- Saxton, M.J. 1993. Lateral diffusion in an archipelago. *Single-particle diffusion*. *Biophysical Journal* 64: 1766–1780.
- Saxton, M.J. 1995. Single-particle tracking: Effects of corrals. *Biophysical Journal* 69: 389–398.
- Saxton, M.J., and K. Jacobson. 1997. Single-particle tracking: Applications to membrane dynamics. *Annual Review of Biophysics and Biomolecular Structure* 26: 373–399.
- Schumaker, M. 2002. Boundary conditions and trajectories of diffusion processes. *The Journal of Chemical Physics* 117: 2469–2473.
- Schuss, Z. 1980a. Singular perturbation methods for stochastic differential equations of mathematical physics. *SIAM Review* 22: 116–155.
- Schuss, Z. 1980b. *Theory and Applications of Stochastic Differential Equations*. NY: Wiley.
- Schuss, Z. 2010a. Equilibrium and recrossings of the transition state: what can be learned from diffusion? *Journal of Physical Chemistry C* 114 (48): 20320–20334.
- Schuss, Z. 2010b. *Theory and Applications of Stochastic Processes, and Analytical Approach*, vol. 170. Applied Mathematical Sciences NY: Springer.
- Schuss, Z. 2012. *Noisy Nonlinear Filtering and Optimal Phase Tracking*, vol. 180. Applied Mathematical Sciences. NY: Springer.
- Schuss, Z. 2013. *Brownian Dynamics at Boundaries and Interfaces in Physics, Chemistry, and Biology*. Applied Mathematical Sciences. NY: Springer.
- Schuss, Z., and B.J. Matkowsky. 1979. The exit problem: A new approach to diffusion across potential barriers. *SIAM Journal on Applied Mathematics* 35 (3): 604–623.
- Schuss, Z., and A. Spivak. 1998. Where is the exit point? *Chemical Physics* 235: 227–242.
- Schuss, Z., and A. Spivak. 2002. The exit distribution on the stochastic separatrix in Kramers' exit problem. *SIAM Journal on Applied Mathematics* 62 (5): 1698–1711.
- Schuss, Z., and A. Spivak. 2005. On recovering the shape of a domain from the trace of the heat kernel. *SIAM Journal on Applied Mathematics* 66 (1): 339–360.

- Schuss, Z., B. Nadler, and R.S. Eisenberg. 2001. Derivation of PNP equations in bath and channel from a molecular model. *Physical Review E* 64 (2–3): 036116–1–036116–14.
- Schuss, Z., A. Singer, and D. Holcman. 2007. The narrow escape problem for diffusion in cellular microdomains. *Proceedings of the National Academy of Sciences of the United States of America* 104: 16098–16103.
- Seckler, B.D., and J.B. Keller. 1959. Geometrical theory of diffraction in inhomogeneous media. *The Journal of Acoustical Society of America* 31: 192–205.
- Segev, I., and W. Rall. 1988. Computational study of an excitable dendritic spine. *Journal of Neurophysiology* 60 (6): 499–523.
- Seisenberger, G., M.U. Ried, T. Endress, H. Brüning, M. Hallek, and Bräuchle. 2001. Real-time single-molecule imaging of the infection pathway of an adeno-associated virus. *Science* 294 (5548): 1929–1932.
- Sheetz, M.P. 1993. Glycoprotein motility and dynamic domains in fluid plasma membranes. *Annual Review of Biophysics and Biomolecular Structure* 22: 417–431.
- Sheng, M., B. Sabatini, and T. Sudhof (eds.). 2012. *The Synapse*. Cold Spring Harbor: Cold Spring Harbor Laboratory Press.
- Shukron, O., and D. Holcman. 2017. Statistics of randomly cross-linked polymer models to interpret chromatin conformation capture data. *Physical Review E* 96 (1): 012503.
- Smith, G.A., L. Pomeranz, S.P. Gross, and L.W. Enquist. 2004. Local modulation of plus-end transport targets herpesvirus entry and egress in sensory axons. *Proceedings of the National Academy of Sciences of the United States of America* 45: 16034–16039.
- Shi, S.H., Y. Hayashi, R.S. Petralia, S.H. Zaman, R.J. Wenthold, K. Svoboda, and R. Malinow. 1999. Rapid spine delivery and redistribution of AMPA receptors after synaptic NMDA receptor activation. *Science* 284 (5421): 1811–1816.
- Silbergleit, A., I. Mandel, and I. Nemenman. 2003. Potential and field singularity at a surface point charge. *Journal of Mathematical Physics* 44 (10): 4460–4466.
- Singer, A. 2006. *Diffusion theory of ion permeation through protein channels of biological membranes*. PhD diss.: Department of Mathematics, Tel-Aviv University.
- Singer, A., and Z. Schuss. 2006. Activation through a narrow opening. *Physical Review E (Rapid Communications)* 74: 020103(R).
- Singer, A., and Z. Schuss. 2007. Activation through a narrow opening. *SIAM Journal on Applied Mathematics* 68 (1): 98–108.
- Singer, A., Z. Schuss, and D. Holcman. 2006a. Narrow escape, Part III: Non-smooth domains and Riemann surfaces. *Journal of Statistical Physics* 122 (3): 491–509.
- Singer, A., Z. Schuss, and D. Holcman. 2006b. Narrow escape, Part II: The circular disk. *Journal of Statistical Physics* 122 (3): 465–489.
- Singer, A., Z. Schuss, and D. Holcman. 2008. Narrow escape and leakage of Brownian particles. *Physical Review E* 78: 051111.
- Singer, A., Z. Schuss, D. Holcman, and R.S. Eisenberg. 2006. Narrow escape. Part I. *Journal of Statistical Physics* 122 (3): 437–463.
- Singer, A., Z. Schuss, A. Osipov, and D. Holcman. 2008. Partially reflected diffusion. *SIAM Journal on Applied Mathematics* 68: 844–868.
- Sjöstrand, J. 2009. *Spectral properties of non-self-adjoint operators*, Lecture notes Journées Équations aux Dérivées Partielles, Évian, Juin 8–12.
- Smith, T.C., and J.R. Howe. 2000. Concentration-dependent substrate behavior of native AMPA receptors. *Nature Neuroscience* 3: 922–927.
- Sneddon, I.N. 1966. *Mixed Boundary Value Problems in Potential Theory*. NY: Wiley.
- Snyder, D.L. 1969. *The State Variable Approach to Continuous Estimation*. Cambridge: The M.I.T. Press.
- Sodeik, B. 2000. Mechanisms of viral transport in the cytoplasm. *Trends in Microbiology* 8: 465–472.
- Stensby, J. 1997. *Phase-Locked Loops, Theory and Applications*. NY: CRC Press.

- Stewartson, K., and R.T. Waechter. 1971. On hearing the shape of a drum: Further results. *Proceedings of the Cambridge Philosophical Society* 69: 353–363.
- Suzuki, K., and M.P. Sheetz. 2001. Binding of cross-linked glycosylphosphatidyl-inositol-anchored proteins to discrete actin-associated sites and cholesterol-dependent domains. *Biophysical Journal* 81: 2181–2189.
- Südhof, T.C. 2008. Neuroligins and neurexins link synaptic function to cognitive disease. *Nature* 455 (7215): 903–911.
- Svoboda, K., D.W. Tank, and W. Denk. 1996. Direct measurement of coupling between dendritic spines and shafts. *Science* 272 (5262): 716–719.
- Tafnia, A. 2008. *Diffusion of interacting particles in confined domains and applications to biology, PhD dissertation, Faculty of Mathematics, The Weizmann Institute of Science*. Israel: Rehovot.
- Tafnia, A., and D. Holcman. 2007. Dwell time of a molecule in a microdomain. *The Journal of Chemical Physics* 126 (23): 234107.
- Tafnia, A., and D. Holcman. 2011. Estimating the synaptic current in a multiconductance AMPA receptor model. *Biophysical Journal* 101 (4): 781–792.
- Tang, A.H., H. Chen, T.P. Li, S.R. Metzbower, H.D. MacGillavry, and T.A. Blanpied. 2016. A trans-synaptic nanocolumn aligns neurotransmitter release to receptors. *Nature* 536 (7615): 210–4.
- Tardin, C., L. Cognet, C. Bats, B. Lounis, and D. Choquet. 2003. Direct imaging of lateral movements of AMPA receptors inside synapses. *The EMBO Journal* 22: 4656–4665.
- Tier, C., and J.B. Keller. 1978. Asymptotic analysis of diffusion equations in population genetics. *SIAM Journal on Applied Mathematics* 34 (3): 549–576.
- Toresson, H., and S.G.N. Grant. 2005. Dynamic distribution of endoplasmic reticulum in hippocampal neuron dendritic spines. *European Journal of Neuroscience* 22: 1793–1798.
- Triller, A., and D. Choquet. 2003. The role of receptor diffusion in the organization of the postsynaptic membrane. *Nature Reviews Neuroscience* 4: 1251–1265.
- Tsaneva, K., A. Burgo, T. Galli, and D. Holcman. 2009. Quantifying neurite growth mediated by interactions between secretory vesicles, microtubules and actin networks. *Biophysical Journal* 96 (3): 840–857.
- Tsodyks, M.V., and H. Markram. 1997. The neural code between neocortical pyramidal neurons depends on neurotransmitter release probability. *Proceedings of the National Academy of Sciences of the United States of America* 94 (2): 719–723. (Erratum in: *Proceedings of the National Academy of Sciences of the United States of America* 94 (10): 5495).
- Uhlenbeck, G.E., and L.S. Ornstein. 1930. On the theory of the Brownian motion. *Physical Review* 36: 823–841.
- Usmani, R.A. 1994. Inversion of a tridiagonal jacobi matrix. *Linear Algebra and its Applications* 212–213: 413–414.
- Vakeroudis, S., M. Yor, and D. Holcman. 2011. The mean first rotation time of a planar polymer. *Journal of Statistical Physics* 143 (6): 1074–1095.
- Verechtaguina, T., I.M. Sokolov, and L. Schimansky-Geier. 2006. First passage > time densities in resonate-and-fire models. *Physical Review E, Statistical, Nonlinear, and Soft Matter Physics* 73: 031108.
- Verechtaguina, T., I.M. Sokolov, and L. Schimansky-Geier. 2007. Interspike interval densities of resonate and fire neurons. *Biosystems* 89 (1–3): 63–68.
- Viterbi, A. 1967. *Principles of Coherent Communication*. NY: McGraw-Hill Inc.
- Volfovsky, N., H. Parnas, M. Segal, and E. Korkotian. 1999. Geometry of dendritic spines affects calcium dynamics in hippocampal neurons: Theory and experiments. *Journal of Neurophysiology* 82 (1): 450–462.
- von Helmholtz, H.L.F. 1860. Theorie der Luftschnüngungen in Röhren mit offenen Enden. *Crelle Bn.* 57: 1–72.
- Whittaker, G.R., M. Kann, and A. Helenius. 2000. Viral entry into the nucleus. *Annual Review of Cell and Developmental Biology* 16: 627–651.
- Wang, Y., R. Austin, and E. Cox. 2006. Single molecule measurements of repressor protein 1D diffusion on DNA. *Physical Review Letters* 97: 048302.

- Ward, M.J., and E. Van De Velde. 1992. The onset of thermal runaway in partially insulated or cooled reactors. *IMA Journal of Applied Mathematics* 48: 53–85.
- Ward, M.J., and J.B. Keller. 1993. Strong localized perturbations of eigenvalue problems. *SIAM Journal on Applied Mathematics* 53: 770–798.
- Ward, M.J., W.D. Henshaw, and J.B. Keller. 1993. Summing logarithmic expansions for singularly perturbed eigenvalue problems. *SIAM Journal on Applied Mathematics* 53: 799–828.
- Ward, M.J., S. Pillay, A. Peirce, and T. Kolokolnikov. 2010. An asymptotic analysis of the mean first passage time for narrow escape problems: Part I: Two-dimensional domains. *SIAM Journal on Multiscale Modeling and Simulation* 8 (3): 803–835.
- Wilmott, P.J., and Dewynne, and S. Howison. 1994. *Option Pricing: Mathematical Models and Computation*. Oxford: Oxford Financial Press.
- Wolansky, G. 1992a. On steady distributions of self-attracting clusters under fiction and Juttuations. *Archive for Rational Mechanics and Analysis* 119: 355–391.
- Wolansky, G. 1992b. On the evolution of self-interacting clusters and applications to semi-linear equations with exponential nonlinearity. *J. d'Analyse Mathematics* 59: 251–272.
- Yu, A.W., G.P. Agrawal, and R. Roy. 1989. Power spectra and spatial pattern dynamics of a ring laser. *Journal of Statistical Physics* 54: 1223.
- Zakharenko, S., and S. Popov. 1998. Dynamics of axonal microtubules regulate the topology of new membrane insertion into the growing neurites. *The Journal of Cell Biology* 143: 1077–1086.
- Zauderer, E. 1989. *Partial Differential Equations of Applied Mathematics*, 2nd ed. NY: Wiley-Interscience.
- Zelditch, S. 2000. Spectral determination of analytic bi-axisymmetric plane domains'. *Geometric and Functional Analysis* 10: 628–677.
- Zwanzig, R. 1990. Diffusion-controlled ligand binding to spheres covered by receptors: An effective medium treatment. *Proceedings of the National Academy of Sciences of the United States of America* 87: 5856–5857.
- Zwanzig, R., and A. Szabo. 1991. Time dependent rate of diffusion-influenced ligand binding to receptors on cell surfaces. *Biophysical Journal* 60: 671–678.

Index

A

Absorbing boundary, 201, 211, 213, 214, 216, 229, 234, 238, 248, 261, 283, 290, 292, 293

Absorption, 26, 50

Absorption flux density, 93

Absorption rate, 7

Activation, 406

Activation rate, 285–287

Activation rate through a narrow opening, 279

Activation through a narrow opening, 279

Active binding site, 256

Adjoint operator, 281

Adjoint problem, 125

Alberts, B., 199, 309

α -amino-3-hydroxy-5-methyl-4-isoxazolepropionic acid (AMPA) receptors (AMPAR), 254, 303, 305, 307

Amplitude modulated, 45

Andronov-Vitt-Pontryagin equation, 76

Anisotropic diffusion, 240, 242, 255

Arrhenius formula, 279

Arrhenius kinetics, 285, 286

Asymptotic expansion, 17, 30, 32, 36, 39, 44, 63, 74, 77, 78, 81, 82, 206, 210, 215, 267, 291

B

Backward Kolmogorov equation, 40

Backward Kolmogorov operator, 22, 76

Barzykin, A.V., 254

Bats, C., 255

Belch, A.C. and M. Berkowitz, 113

Bender, C.M. and S.A. Orszag, 48

Bénichou, O., 253

Ben-Jacob, E., D. Bergman, B.J. Matkowsky and Z. Schuss, 97

Ben-Jacob, E., D.J. Bergman, Y. Imry, B.J. Matkowsky and Z. Schuss, 113

Berezhkovskii, A.M., 253, 254

Berkowitz, M. and J.A. McCammon, 113

Bernoulli's equation, 80, 122

Berry, R.S., S. Rice and J. Ross, 112

Biess, A., 200, 254

Bi-orthogonal eigenfunction of the FPO, 281

Bi-orthonormal system, 127

Bobrovsky, B.Z., 72, 94

Bobrovsky, B.Z. and O. Zeitouni, 96

Bobrovsky, B.Z. and Z. Schuss, 94–96

Boda, D., 200

Borgdorff, A.J., 200, 255

Borkovec, M., 255

Bottleneck, 223, 229, 233, 236–238, 254, 295

Boundary behavior, 113

Boundary conditions, 20, 22, 27, 31, 40, 44, 67, 70, 79, 81, 113

Boundary layer, 16, 20, 29, 31–33, 35, 36, 39–41, 52, 57–63, 65, 70, 78, 79, 81, 97, 202, 208, 216, 229, 236, 241, 248, 255, 279, 292–294

Boundary layer equation, 77

Boundary value problem, 203, 229, 235, 236, 258, 282, 283, 291

Bourne, J.N., 200

Bray, D., 199, 309

Brooks, C.L., III and M. Karplus, 113

Brown, E., 200

Brownian dynamics, 307

Brownian dynamics simulations, 250, 251

Brownian motion, 26, 66, 67, 191, 205, 211, 212, 216, 223, 230, 232, 237, 239, 252, 405

Brownian needle in a planar strip, 241, 244

Brownian needle in dire straits, 240

Burger, M., 199

Büttiker, M., E.P. Harris and R. Landauer, 96

C

Carrier frequency, 45, 70

Cellular biology, 403

Center of curvature, 246

Channel gating, 199

Characteristic equations, 83, 89, 92

Chen, D.P., 199, 200

Cheviakov, A., 253, 308, 309

Choquet, D., 200, 254, 255

Christiano, R. and P. Silvestrini, 97

Coffey, W.T., Yu.P. Kalmykov, and J.T. Wall-dron, 113

Cognet, L., 255

Conditioning, 288

Conformal mapping, 209–211, 213, 223–225, 246, 247, 291

Co-normal reflection, 241

Conservation law, 50

Convergence, 17, 97, 112

Coombs, D., 253

Courant, R. and D. Hilbert, 51, 53

Curvature, 295

Curvature parameter, 223

Cycle slip, 46, 48

D

Day, M.V, 95, 96

Dembo, A. and O. Zeitouni, 52, 65, 94

Dendrite, 303, 308

Dendritic shaft, 301

Dendritic spine, 308

Denk, W., 200

Density of time spent at a point, 284

Depressing synapses, 130

Detector, 47

Devinatz, A. and A. Friedman, 97

Diffusion approximation to a Markovian jump process, 253

Diffusion coefficient, 18, 22

Diffusion equation, 252

Diffusion matrix, 56, 61, 66, 89

Diffusion of a Brownian needle, 241, 242

Diffusion of a stiff rod, 240, 242, 244, 290

Diffusion on a membrane with obstacles, 250, 252, 253, 255, 256

Diffusion process, 44, 108

Diffusion with obstacles, 250, 253–255

Dirichlet boundary condition, 238

Drift, 26, 28, 30, 32–34, 74–76, 83

Drift equation, 68

Drift vector, 40, 60, 61, 66

Dumbbell-shaped domain, 238–240, 255

Dygas, M.M., B.J. Matkowsky and Z. Schuss, 112

Dynamical system, 18, 19, 49, 94, 96

E

Edidin, M., 255

Effective diffusion coefficient, 240, 250, 252–255

Ehlers, M.D., 200

Eigenfunction expansion, 279

Eigenfunction of the reduced problem, 278, 309

Eigenfunctions, 8

Eigenvalue, 24, 44, 50, 54, 67, 70, 73, 74, 83, 240, 281

Eigenvalue of the reduced problem, 275

Eigenvalues of a Markov chain, 238

Eikonal equation, 51–54, 57, 61, 64, 66, 68, 78, 82, 83, 86, 88, 91, 103, 107, 109, 110, 112, 138

Eikonal function, 53, 69, 82, 103, 110

Eisenberg, R.S., 112, 199, 200, 253

Eisinger, J., 255

Ellis, R.S, 52

Engl, H.W., 199

Equation of motion, 47

Equilibrium, 97, 102, 113

Escape of MBM through a narrow window, 280

Escape time, 252, 253

Euler, 13

Exit density, 51, 61, 63, 66, 68, 70, 93–95

Exit points, 147

Exit probability, 18, 21, 30, 31, 35

Exit problem, 17, 20, 33, 51, 94

Exit time, 44, 48

Exponentially distributed FPT, 237, 239, 240, 252

Exponentially distributed inter-arrival times, 239

F

Fabrikant, V.I., 199

Flores, J., 255

Fluctuations, 102, 108, 112
 Flux of eigenfunction of the FPO, 275
 FM, 45, 47, 71
 Fokker–Planck equation, 27, 40, 50, 56, 62, 67, 81, 82, 89, 109
 Force field, 12
 Free Brownian motion, 201, 250
 Freidlin, M, 52, 112
 Freidlin, M.A. and A.D. Wentzell, 52, 94, 110
 Frequency deviation, 45
 Frequency estimation error, 71–73
 Frequency modulated, 45, 47, 70, 71
 Fresche,D, 199
 Fujiwara, T., 255
 Functional, 95
 Funnel, 202, 223, 230, 232, 237–240, 254, 290, 291, 294, 295

G

Gamma function, 13
 Gandolfi, A., 253
 Gantmacher, F.R, 54, 84
 Garabedian, P.R., 206, 257
 Gardiner, C.W, 94
 Gaussian white noise, 280
 Generalized Langevin equation, 112
 Gerardi, A., 253
 Gillespie, D., 200
 Graham, R. and T. Tel, 110
 Grant, S.G.N., 309
 Green’s formula, 235
 Green’s function, 22, 30, 40
 Grigoriev, I.V., 253
 Grote, F.R. and J.T. Hynes, 112

H

Hagan, P.S., C.R. Doering and C.D. Levermore, 113
 Hamilton–Jacobi equation, 51, 103
 Hänggi, P., 94, 96, 113, 255
 Harris, K.M., 200
 Helmholtz integral equation, 204, 257, 262, 265, 308
 Helmholtz, H.L.F. von, 257, 265, 308
 Helmholtz lemma, 265, 266
 Henderson, D., 200
 Henshaw, W.D., 253
 Hermite polynomials, 126
 Herrmann, A., 200, 256
 Higher-order asymptotics of the mean first passage time, 265, 267

Hille, B., 97, 112, 199, 212, 418
 Histogram, 9
 Hitting time, 141
 Holcman, D., 199, 200, 210, 211, 251, 253–255, 309
 Hopf system, 128
 Hoze, N., 251, 254, 255
 Huang, Q., 200, 256

I

Im, B., S. Seefeld and B. Roux, 113
 Im, W., 200
 Initial condition, 249, 280
 Instantaneous re-injected, 7
 Internal layer, 30, 31, 33, 37, 55, 89
 Ion exchanger, 303
 Ion pump, 301, 303, 304
 Itô equation, 242
 Itô, K., 241, 242

J

Jackson, J.D., 257
 Jacobian, 154
 Jacobson, K., 255
 Jessell, T.M., 199
 Josephson junction, 97
 Jump process, 113

K

Kamienomostskaya, S, 97
 Kamin, S, 97
 Kandel, E.R., 199
 Karlin, S. and H.M. Taylor, 113
 Kasai, R.S., 255
 Katz, A., 95–97
 Katz, A., Z. Schuss, 96
 Keller, J.B., 253, 309
 Kellogg, O.D., 261
 Kevorkian, J. and J.D. Cole, 48
 Kim, S. and I. Oppenheim, 112
 Klosek, M.M., 113
 Klosek, M.M., and P.S. Hagan, 113
 Klosek, M.M., B. J. Matkowsky and Z. Schuss, 51
 Knapp, E.W., 200, 256
 Kolokolnikov, T., 253
 Kondo, J., 255
 Korkotian, E., 200
 Kramers’ formula, 285, 287
 Kramers, H.A., 44, 94, 96, 113, 285, 287
 Kubo, R., 112

Kuo, S.C., 255
 Kupferman, R., M. Kaiser, Z. Schuss and E. Ben-Jacob, 112, 113
 Kupka, I., 200
 Kushmaro, A., 200
 Kusumi, A., 255

L

Lagache, T., 200
 Langevin's equation, 65–67, 97, 113, 307
 Laplace integral, 92
 Laplace method, 12
 Laplace-Beltrami operator, 201, 205, 211, 213
 Large deviations, 18
 Large deviations theory, 52, 65, 94, 95
 Last passage time, 48
 Leakage, 274, 301, 302
 Leakage flux, 275
 Lear, J., 199
 Leis, A., 200
 Lewis, J., 199, 309
 Lieber, A., 200
 Lifetime, 108
 Lifetime of a trajectory, 201
 Loss of lock, 47, 48, 70–72, 76
 Lounis, B., 255
 Lurie, A.I., 308

M

MacKinnon, R., 199
 Maier, R. and D.L. Stein, 96
 Maier, R., D.G. Luchinsky, R. Mannella, P.V.E. McClintock and D.L. Stein, 96
 Majewska, A., 200
 Makhnovskii, Y.A., 253, 254
 Mandel, I., 308
 Mandl, P., 113
 Mangel, M. and D. Ludwig, 94, 96
 Marchetti, F., 253
 Markov chain model, 287, 289
 Markovian jump process, 239, 240, 252
 Markov process, 239, 287
 Marshall, T.W. and E.J. Watson, 113
 Matching condition, 248, 293
 Mathematical Brownian motion, 26
 Matkowsky, B.J. and Z. Schuss, 48, 60
 Matkowsky, B.J., Z. Schuss and C. Tier, 66, 69, 96
 Mazur, P. and I. Oppenheim, 112
 Mean exit time, 252

Mean first passage time, 17–19, 21, 22, 25, 26, 32, 37, 40, 41, 43, 48, 49, 51, 65–67, 69, 70, 76, 77, 191, 212, 213, 216, 225, 230, 231, 234, 236–239, 242–244, 250, 253, 262, 265, 290, 294, 307

Mean inter-arrival time, 307
 Mean time spent at a point, 283
 Mean time spent in a domain, 289
 Mean time spent in a well, 287
 Mean time to lose lock, 47, 48, 72
 Medalia, O., 200
 Meissner, G., 199
 Mel'nikov, V.I. and S.V. Meshkov, 94, 96
 MFPT, 48, 76, 77
 MFPT to a bottleneck, 223
 MFPT to an elliptic absorbing window, 267, 284, 285, 308
 MFPT to the boundary of a square, 251
 Minsky, A., 200
 Mixed boundary value problem, 201, 214, 229, 234, 237, 238, 252, 267, 275, 276, 279
 Möbius transformation, 224, 291
 Modulation, 45, 46, 70
 Modulation index, 45
 Mori, H., 112
 MTLL, 47, 48
 Murakoshi, H., 255
 Murase, K., 255

N

Nadler, B., T. Naeh and Z. Schuss, 113
 Naeh, T., 113
 Nakada, C., 255
 Narrow escape problem, 199, 201, 257, 275, 307
 Narrow escape time, 191, 199, 201, 202, 204, 208, 211, 214–216, 223, 233, 238, 250, 251, 253, 255, 256, 279, 288, 295
 Narrow neck, 202, 225, 228, 229, 232, 233, 235–241, 247, 250, 255, 290, 294, 295, 303, 308
 Nemenman, I., 308
 NET from a composite domain, 233, 238, 254, 295
 NET from a domain with a long neck, 239, 254
 NET from domains with corners, 208, 209, 253, 286
 NET from domains with cusps, 202, 210, 211, 232, 253, 286, 295

- NET on a surface of revolution, 234, 290
NET on the sphere, 211, 213
NET solid funnel-shaped domain, 240
Neumann function, 203, 204, 206, 209, 235, 257, 258, 261, 282–284, 286, 309
Neumann problem, 239, 240
Neumann–Dirichlet boundary conditions, 237, 238, 252, 267, 291
Neuron, 250, 255
Neuronal cleft, 199, 305
Neuronal dendrite, 255
Neuronal membrane, 254
Neuronal spine neck, 303
Neuronal synapse, 301, 305
Neurotransmitter (NT), 303
Newpher, T.M., 200
Nitzan, A. and Z. Schuss, 96
N-methyl-D-aspartate, 303, 305
Nonequilibrium, 97, 98, 101–103, 108, 111
Nonlinear system, 45
Nonner, W., 200
Nonner, W., D. Gillespie, D. Henderson and R.S. Eisenberg, 112
Nonner, W., D.P. Chen and R.S. Eisenberg, 112
Nonner, W., L. Catacuzzeno and R.S. Eisenberg, 112
Nonner, W., R.S. Eisenberg, 112
Non-self-adjoint operators, 127
Normal form, 132
Normalized eigenfunction of the FPO, 281
- O**
O’Malley, R.E., Jr, 48
Opitz, R., 200, 256
Ordinary Differential Equation (ODE), 74
Ornstein–Uhlenbeck process, 26, 27
Outer expansion, 16, 29–31, 33, 39, 59, 78
Overdamped Langevin’s equation, 44, 65
- P**
Petersen, W.P., 255
Phase estimation error, 71
Phase-locked loop, 70, 72, 90
Phase-locked loop second-order, 70–72, 80, 90, 92
Phase modulated, 45
Phase slip, 71
Phase tracker, 46–48, 71
Poisson equation, 213, 255
Popov, I.Yu., 257, 265, 267, 284
Post-synaptic density, 302, 303, 305, 306
- Potential, 12
Potential barrier, 32, 33, 36, 41, 43, 44, 65, 66, 103, 232, 238, 255, 285, 288
Potential well, 238, 255, 279, 287–289
Principal curvatures, 258, 259, 266, 276
Principal eigenvalue, 8
Principal eigenvalue in a domain with a bottleneck, 237
Principal eigenvalue in a dumbbell-shaped domain, 239, 255
Principal eigenvalue of the mixed problem in a domain with a bottleneck, 238
Principal eigenvalue of the mixed problem in a domain with a narrow neck, 238
Principal eigenvalue of the Neumann problem in a domain with a bottleneck, 238
Principal eigenvalue of the Neumann–Dirichlet problem, 237, 238, 252, 267
Probability density function, 242
Protein channel, 112
- R**
RADAR, 47
Radius of curvature, 223, 236, 239, 245
Raff, M., 199, 309
Random trajectory, 17, 49, 94
Random walk, 240, 252
Rate, 22
Rayleigh, J.W.S., 191, 199, 308
Recurrent process, 15
Reflected trajectories, 201
Reflecting boundary, 191, 201, 202, 205, 209, 216, 225, 238, 248, 250, 252, 253, 261, 279, 280, 292, 293
Reflection at a curved boundary, 243, 245
Regular expansion of eigenvalues, 275
Renewal equation, 289
Renner, M., 254, 255
Risken, H., 94, 113
Ritchie, K., 255
R. Nicoll, 200
Roberts, K., 199, 309
Ross, J., 200
Roux, B., 200
Ryter, D. and H. Meyr, 95, 97
- S**
Saddle point, 71, 73–76, 84, 86–88, 91, 93, 94
Sako, Y., 255
Saxton, M.J., 255

- Schumaker, M., 113
 Schuss, Z., 44, 48, 54, 65, 72, 84, 94–96,
 112, 199, 210, 211, 234, 251–255,
 289, 309
 Schuss, Z. and A. Spivak, 96
 Schuss, Z., B. Nadler and R.S. Eisenberg,
 112
 Schwartz, J.H., 199
 Seefeld, S., 200
 Segal, M., 200
 Separatrix, 71, 74, 75, 84, 86, 88, 91, 93–95
 Sheetz, M.P., 255
 Signal tracker, 46
 Silbergleit, A., 308
 Simulations, 71, 72, 95–97, 113
 Singer, A., 113, 199, 210, 211, 253
 Small jumps, 141
 Small parameter, 12
 Smoluchowski equation, 279, 307
 Sneddon, I., 51, 53
 SNR, 72
 Snyder, D.L., 72
 Source of trajectories, 302, 304, 305
 Spine head, 301, 308
 Spine neck, 301
 Stability, 96, 97
 Stable equilibrium, 18, 69, 99, 101, 104, 111
 Stable focus, 131
 Stable point, 47, 48, 71, 73, 76, 78
 Stable trajectory, 74
 State-dependent diffusion, 244
 Stationary density, 275, 279
 Stationary process, 108
 Steady-state, 6, 7, 7, 97, 101–104, 106, 108,
 109, 111, 113
 Stensby, J., 72
 Stevens, J.K., 200
 Stochastic differential equation, 19, 94
 Stochastic dynamics, 98
 Stochastic separatrix, 239, 241
 Straube, R., 253, 308, 309
 Super-resolution, 418
 Suzuki, K., 255
 Svoboda, K., 200
 Synapses, 404
 Synaptic cleft, 302, 303, 305–307, 309
 Synaptic vesicles, 303
- T**
 Taflia, A., 199
 Talkner, P., 255
 Tank, D.W., 200
 Tardin, C., 255
 Telegraph process, 239
- Terminated trajectories, 287
 Titcombe, M., 253
 Toresson, H., 309
 Total population, 7, 41, 42
 Tracking loop, 47
 Trafficking, 404
 Trajectory, 6, 7, 7, 19–23, 25, 26, 28, 32, 43,
 44, 50, 51, 53, 55, 60, 63, 66, 67, 83,
 84, 95, 97, 109, 113
 Transition PDF, 239
 Transport equation, 55–57, 68, 82, 88, 89,
 91, 92, 103, 105, 121
 Tripathy, A., 199
 Turnaround time, 240, 241, 244, 256
- U**
 Underdamped Langevin's equation, 97, 98
 Uniform asymptotic, 14, 39, 49
 Uniform asymptotic construction, 14, 49
 Uniform expansion, 16, 17, 33, 59, 62, 63,
 101
 Unstable equilibrium, 30, 100, 101, 110, 111
 Unstable point, 47, 48, 83
- V**
 Valisko, M., 200
 Van DeVelde, E., 253
 Viterbi, A.J., 72, 96
 Voituriez, R., 253
- W**
 Ward, M.J., 253, 308, 309
 Watson, J.D., 199, 309
 White noise, 19, 46, 280
 Wilmott, P., 96
 WKB, 40, 51, 56, 65, 82, 89, 92, 102
 WKB construction, 40
- X**
 Xu, L., 199
- Y**
 Yamamoto, M., 255
 Yu, A.W., G.P. Agrawal and R. Roy, 113
 Yuste, R., 200
- Z**
 Zitserman, V.Yu., 253, 254